

Prevalence of Earth-size Planets Orbiting Sun-like Stars

By

Erik Ardeshir Petigura

A dissertation submitted in partial satisfaction of the

requirements for the degree of

Doctor of Philosophy

in

Astrophysics

in the

Graduate Division

of the

University of California, Berkeley

Committee in charge:

Professor Geoffrey Marcy, Chair

Professor Eugene Chiang

Professor Michael Manga

Professor Eliot Quataert

Spring 2015

Prevalence of Earth-size Planets Orbiting Sun-like Stars

Copyright 2015  
by  
Erik Ardeshir Petigura

## Abstract

## Prevalence of Earth-size Planets Orbiting Sun-like Stars

by

Erik Ardeshir Petigura

Doctor of Philosophy in Astrophysics

University of California, Berkeley

Professor Geoffrey Marcy, Chair

In this thesis, I explore two topics in exoplanet science. The first is the prevalence of Earth-size planets in the Milky Way Galaxy. To determine the occurrence of planets having different sizes, orbital periods, and other properties, I conducted a survey of extrasolar planets using data collected by NASA's *Kepler Space Telescope*. This project involved writing new algorithms to analyze *Kepler* data, finding planets, and conducting follow-up work using ground-based telescopes. I found that most stars have at least one planet at or within Earth's orbit and that 26% of Sun-like stars have an Earth-size planet with an orbital period of 100 days or less.

The second topic is the connection between the properties of planets and their host stars. The precise characterization of exoplanet hosts helps to bring planet properties like mass, size, and equilibrium temperature into sharper focus and probes the physical processes that form planets. I studied the abundance of carbon and oxygen in over 1000 nearby stars using optical spectra taken by the California Planet Search. I found a large range in the relative abundance of carbon and oxygen in this sample, including a handful of carbon-rich stars. I also developed a new technique called SpecMatch for extracting fundamental stellar parameters from optical spectra. SpecMatch is particularly applicable to the relatively faint planet-hosting stars discovered by *Kepler*.

For Alana.

# Contents

<b>List of Figures</b>	<b>v</b>
<b>List of Tables</b>	<b>viii</b>
<b>Acknowledgments</b>	<b>xi</b>
<b>1 Introduction</b>	<b>1</b>
1.1 Exoplanets: A Brief History . . . . .	2
1.2 Exoplanet Demographics . . . . .	4
1.3 Precision Characterization of Stars . . . . .	6
<b>2 Identification and Removal of Noise Modes in <i>Kepler</i> Photometry</b>	<b>8</b>
2.1 Introduction . . . . .	8
2.2 Instrumental Noise in <i>Kepler</i> Photometry . . . . .	9
2.3 Identification of Photometric Modes . . . . .	12
2.3.1 PCA on Ensemble Photometry . . . . .	12
2.3.2 PCA implementation . . . . .	14
2.3.3 Interpretation of Photometric Modes . . . . .	16
2.4 Calibrated Photometry . . . . .	16
2.4.1 Removal of Modes . . . . .	16
2.4.2 Performance . . . . .	19
2.4.3 Comparison to PDC . . . . .	19
2.5 Conclusions . . . . .	21
<b>3 A Plateau in the Planet Population Below Twice the Size of Earth</b>	<b>24</b>
3.1 Introduction . . . . .	25
3.2 The Best12k Stellar Sample . . . . .	26
3.3 Planet Search Pipeline . . . . .	29
3.3.1 Photometric Calibration . . . . .	29
3.3.2 Grid-based Transit Search . . . . .	29
3.3.3 Data Validation . . . . .	31
3.4 Small Planets Found by TERRA . . . . .	33
3.5 Completeness of Planet Catalog . . . . .	36

3.6	Occurrence of Small Planets . . . . .	38
3.7	Comparison of TERRA and Batalha et al. (2012) Planet Catalogs . . . . .	41
3.7.1	Candidates in Common . . . . .	41
3.7.2	TERRA Candidates Not in Batalha et al. (2012) Catalog . . . . .	45
3.7.3	Batalha et al. (2012) Candidates Not in TERRA catalog . . . . .	45
3.8	Occurrence with Planet Multiplicity Included . . . . .	46
3.9	Discussion . . . . .	48
3.9.1	TERRA . . . . .	48
3.9.2	Planet Occurrence . . . . .	52
3.9.3	Interpretation . . . . .	52
<b>4</b>	<b>The Prevalence of Earth-Size Planets Orbiting Sun-Like Stars</b>	<b>68</b>
4.1	Planet Survey . . . . .	68
4.2	Planet Occurrence . . . . .	70
4.2.1	Planet Occurrence and Orbital Period . . . . .	70
4.2.2	Planet Occurrence and Stellar Light Intensity . . . . .	72
4.3	Interpretation . . . . .	72
4.3.1	Earth-Size Planets with Year-Long Orbital Periods . . . . .	72
4.3.2	Earth-Size Planets in the Habitable Zone . . . . .	74
4.4	Conclusions . . . . .	75
<b>5</b>	<b>Supporting Information for Prevalence of Earth-size Planets Orbiting Sun-like Stars</b>	<b>81</b>
5.1	The Best42k Stellar Sample . . . . .	82
5.2	Planet Search Photometric Pipeline . . . . .	85
5.2.1	Time-domain pre-processing of raw <i>Kepler</i> Photometry . . . . .	85
5.2.2	Grid-based transit search . . . . .	85
5.3	Data Validation . . . . .	87
5.3.1	Machine Triage . . . . .	90
5.3.2	Manual Triage . . . . .	90
5.4	KOIs That Fail Data Validation . . . . .	93
5.5	Removal of Astrophysical False Positives . . . . .	95
5.6	Planet Radius Refinement . . . . .	100
5.7	Completeness . . . . .	100
5.8	Planet Occurrence . . . . .	104
5.8.1	Occurrence of Earth-Size Planets on Year-Long Orbits . . . . .	104
5.8.2	Planet Occurrence in the Habitable Zone . . . . .	104
5.8.3	Occurrence Including Planets in Multi-planet Systems . . . . .	111
5.8.4	Correction due to False Positives . . . . .	111

<b>6</b>	<b>Carbon and Oxygen in Nearby Stars: Keys to Protoplanetary Disk Chemistry</b>	<b>136</b>
6.1	Introduction . . . . .	136
6.2	Observations . . . . .	137
6.2.1	Stellar Sample . . . . .	137
6.2.2	Spectra . . . . .	137
6.3	Spectroscopic Analysis . . . . .	138
6.3.1	Line Synthesis . . . . .	138
6.3.2	Atomic Parameters . . . . .	138
6.3.3	Telluric Rejection . . . . .	139
6.3.4	Iodine Removal . . . . .	143
6.3.5	Fitting Abundances . . . . .	146
6.4	Results . . . . .	146
6.4.1	Carbon and Oxygen Abundances . . . . .	146
6.4.2	Random Errors . . . . .	149
6.4.3	Nickel Systematics . . . . .	152
6.4.4	Comparison with Literature . . . . .	152
6.4.5	Abundance Trends in the Thin and Thick Disks . . . . .	154
6.4.6	Exoplanets . . . . .	154
6.4.7	$N_C/N_O$ . . . . .	158
6.4.8	WASP-12 . . . . .	161
6.5	Conclusion . . . . .	162
<b>7</b>	<b>SpecMatch: Accurate Stellar Characterization with Optical Spectra</b>	<b>201</b>
7.1	Introduction . . . . .	201
7.2	SpecMatch . . . . .	203
7.2.1	Reduction and Calibration of Target Spectra . . . . .	203
7.2.2	Comparison to Library Spectra . . . . .	204
7.2.3	Stellar Parameters from Linear Combinations of Spectra . . . . .	206
7.2.4	Measuring the Instrumental Profile with Telluric Lines . . . . .	206
7.2.5	Polishing the Parameters by Forward Modeling . . . . .	209
7.2.6	Calibrating Effective Temperature and Metallicity to Valenti & Fischer (2005) . . . . .	209
7.2.7	Calibrating Surface Gravities to Huber et al. (2013) . . . . .	210
7.3	Reliability of SpecMatch Parameters . . . . .	212
7.3.1	Photon-Limited Errors . . . . .	212
7.3.2	Systematic Errors . . . . .	215
7.3.3	Summary . . . . .	217
7.4	Conclusions . . . . .	217
7.5	Appendix . . . . .	224
	<b>Bibliography</b>	<b>244</b>

# List of Figures

1.1	Known extrasolar planets before and after the launch of <i>Kepler</i> . . . . .	5
2.1	Representative <i>Kepler</i> photometry . . . . .	10
2.2	Correlation across <i>Kepler</i> light curves . . . . .	13
2.3	TERRA principle components . . . . .	15
2.4	Light curve systematics across the <i>Kepler</i> field of view . . . . .	17
2.5	TERRA calibrated photometry . . . . .	18
2.6	PDC calibrated photometry . . . . .	22
2.7	Comparison of TERRA and PDC . . . . .	23
3.1	Effective temperatures and surface gravities of stellar sample . . . . .	27
3.2	Brightness and photometric variability of stellar sample . . . . .	28
3.3	SNR periodogram of KIC-3120904 photometry . . . . .	31
3.4	SNR periodogram of KIC-5094751 photometry . . . . .	32
3.5	Distribution of the highest SNR peak for each star in the Best12k sample . . . . .	33
3.6	SNR periodogram of KIC-7592977 photometry . . . . .	34
3.7	TERRA planet candidates . . . . .	36
3.8	TERRA planet candidates listed in other catalogs . . . . .	37
3.9	Completeness from injection and recovery experiments . . . . .	39
3.10	Planet occurrence using TERRA planet candidates . . . . .	42
3.11	Planet size distribution . . . . .	43
3.12	Planet orbital period distribution . . . . .	44
3.13	Phase-folded photometry of KIC-8280511 . . . . .	46
3.14	KOIs missed by TERRA . . . . .	47
3.15	Planet occurrence including Batalha et al. (2012) candidates . . . . .	49
3.16	Planet radius distribution including Batalha et al. (2012) candidates . . . . .	50
3.17	Transits of TERRA planet candidates, not in <a href="#">Batalha et al. (2012)</a> . . . . .	66
3.18	Transits of TERRA planet candidates, not in <a href="#">Batalha et al. (2012)</a> . . . . .	67
4.1	Detected planets and survey completeness . . . . .	76
4.2	Planet occurrence . . . . .	77
4.3	Distributions of planet sizes and orbital periods . . . . .	78
4.4	Detected planets and stellar light intensity . . . . .	79

4.5	Cumulative distribution of small planets . . . . .	80
5.1	Effective temperatures and surface gravities of stellar sample . . . . .	83
5.2	Brightness and photometric variability of stellar sample . . . . .	84
5.3	DV summary plots for KIC-5709725 . . . . .	88
5.4	DV summary plots for KIC-1570270 . . . . .	91
5.5	DV summary plots for KIC-1724842 . . . . .	92
5.6	Four KOIs that fail manual vetting . . . . .	94
5.7	DV summary plots for KIC-8879427 . . . . .	97
5.8	DV summary plots eKOI KIC-2166206 . . . . .	98
5.9	Sizes and orbital periods of TERRA planet candidates . . . . .	99
5.10	Results of injection and recovery experiments . . . . .	102
5.11	Completeness computed over small bins in $P$ and $R_P$ . . . . .	103
5.12	Cumulative occurrence of 2–4 $R_{\oplus}$ planets with increasing orbital period . . . . .	105
5.13	Cumulative occurrence of 1–2 $R_{\oplus}$ planets with increasing orbital period . . . . .	106
5.14	Cumulative occurrence of 1–2 $R_{\oplus}$ planets with decreasing stellar light intensity . . . . .	108
5.15	Phase folded photometry for ten Earth-size habitable zone candidates . . . . .	109
5.16	Survey completeness for small planets in the habitable zone . . . . .	110
5.17	Planet occurrence including multi-planet systems . . . . .	112
6.1	Solar spectrum in the vicinity of the [OI] line at 6300.312 Å . . . . .	140
6.2	Solar spectrum in the vicinity of the CI line at 6587.625 Å . . . . .	142
6.3	The [OI]/NiI blend in the NSO spectrum. . . . .	142
6.4	The CI line in the NSO spectrum . . . . .	143
6.5	Sample spectra of stars with low and high carbon and oxygen abundances . . . . .	144
6.6	Two spectra of HIP 92922 in the star’s rest frame . . . . .	145
6.7	HD 148284 spectrum with iodine contamination . . . . .	147
6.8	Oxygen abundances from spectra taken with and without the iodine cell . . . . .	148
6.9	Systematic trends of [O/H] and [C/H] with temperature . . . . .	150
6.10	Distributions of [O/H], [C/H], and [Fe/H] . . . . .	151
6.11	Statistical uncertainties in derived abundances . . . . .	153
6.12	Comparison to <a href="#">Bensby et al. (2005)</a> and <a href="#">Luck &amp; Heiter (2006)</a> . . . . .	155
6.13	Carbon and oxygen abundance versus iron abundance . . . . .	156
6.14	[C/Fe] and [O/Fe] versus iron abundance . . . . .	157
6.15	Planet occurrence as a function of oxygen, carbon, and iron abundance . . . . .	159
6.16	$N_C/N_O$ as a function of iron abundance . . . . .	161
7.1	Spectrum of HD 209458 around the O <sub>2</sub> telluric band . . . . .	207
7.2	Spectrum of KOI-2 around the O <sub>2</sub> telluric band . . . . .	208
7.3	Width of telluric lines as a function of HIRES decker . . . . .	208
7.4	Comparison to <a href="#">Valenti &amp; Fischer (2005)</a> effective temperatures . . . . .	211
7.5	Comparison to <a href="#">Valenti &amp; Fischer (2005)</a> metallicities . . . . .	212
7.6	Comparison to <a href="#">Huber et al. (2013)</a> surface gravities . . . . .	213

---

7.7	Statistical uncertainties for stellar parameters . . . . .	214
7.8	Comparison to <a href="#">Huber et al. (2013)</a> . . . . .	220
7.9	Comparison to <a href="#">Torres et al. (2012)</a> . . . . .	221
7.10	Comparison to <a href="#">Albrecht et al. (2012)</a> . . . . .	222
7.11	Comparison to <a href="#">Valenti &amp; Fischer (2005)</a> . . . . .	223
7.12	Spectrum of KOI-1 . . . . .	224
7.13	Spectrum of KOI-1 . . . . .	225
7.14	Spectrum of KOI-1 . . . . .	226
7.15	Spectrum of KOI-1 . . . . .	227
7.16	Spectrum of KOI-1 . . . . .	228

# List of Tables

2.1	Comparison of fits to KIC-8144222 photometry. . . . .	20
2.2	Comparison of TERRA and PDC cotrending performance for 100 stars. . . . .	21
3.1	Cuts used during data validation . . . . .	34
3.2	Planet candidates identified with TERRA . . . . .	54
3.2	Planet candidates identified with TERRA . . . . .	55
3.2	Planet candidates identified with TERRA . . . . .	56
3.2	Planet candidates identified with TERRA . . . . .	57
3.2	Planet candidates identified with TERRA . . . . .	58
3.3	New candidates identified with TERRA . . . . .	59
3.3	New candidates identified with TERRA . . . . .	60
3.4	Union of <a href="#">Batalha et al. (2012)</a> and TERRA planet candidate catalogs . . . . .	61
3.4	Union of <a href="#">Batalha et al. (2012)</a> and TERRA planet candidate catalogs . . . . .	62
3.4	Union of <a href="#">Batalha et al. (2012)</a> and TERRA planet candidate catalogs . . . . .	63
3.4	Union of <a href="#">Batalha et al. (2012)</a> and TERRA planet candidate catalogs . . . . .	64
3.4	Union of <a href="#">Batalha et al. (2012)</a> and TERRA planet candidate catalogs . . . . .	65
4.1	Occurrence of Small Planets the Habitable Zone . . . . .	76
5.1	TERRA Grid Search Parameters . . . . .	86
5.2	Properties of 836 eKOIs . . . . .	114
5.2	Properties of 836 eKOIs . . . . .	115
5.2	Properties of 836 eKOIs . . . . .	116
5.2	Properties of 836 eKOIs . . . . .	117
5.2	Properties of 836 eKOIs . . . . .	118
5.2	Properties of 836 eKOIs . . . . .	119
5.2	Properties of 836 eKOIs . . . . .	120
5.2	Properties of 836 eKOIs . . . . .	121
5.2	Properties of 836 eKOIs . . . . .	122
5.2	Properties of 836 eKOIs . . . . .	123
5.2	Properties of 836 eKOIs . . . . .	124
5.2	Properties of 836 eKOIs . . . . .	125
5.2	Properties of 836 eKOIs . . . . .	126

---

5.2	Properties of 836 eKOIs . . . . .	127
5.2	Properties of 836 eKOIs . . . . .	128
5.2	Properties of 836 eKOIs . . . . .	129
5.2	Properties of 836 eKOIs . . . . .	130
5.2	Properties of 836 eKOIs . . . . .	131
5.2	Properties of 836 eKOIs . . . . .	132
5.2	Properties of 836 eKOIs . . . . .	133
5.2	Properties of 836 eKOIs . . . . .	134
5.3	Spectroscopic properties of 13 eKOIs (added in proof) . . . . .	135
6.1	Adopted solar atmospheric parameters . . . . .	140
6.2	Atomic parameters from fitting the NSO atlas . . . . .	141
6.3	Summary of Derived Abundances. . . . .	152
6.4	Best fit parameters to abundance trends. . . . .	158
6.5	Statistical abundance properties of stars with planets. . . . .	160
6.6	Stellar Data. . . . .	163
6.6	Stellar Data. . . . .	164
6.6	Stellar Data. . . . .	165
6.6	Stellar Data. . . . .	166
6.6	Stellar Data. . . . .	167
6.6	Stellar Data. . . . .	168
6.6	Stellar Data. . . . .	169
6.6	Stellar Data. . . . .	170
6.6	Stellar Data. . . . .	171
6.6	Stellar Data. . . . .	172
6.6	Stellar Data. . . . .	173
6.6	Stellar Data. . . . .	174
6.6	Stellar Data. . . . .	175
6.6	Stellar Data. . . . .	176
6.6	Stellar Data. . . . .	177
6.6	Stellar Data. . . . .	178
6.6	Stellar Data. . . . .	179
6.6	Stellar Data. . . . .	180
6.6	Stellar Data. . . . .	181
6.6	Stellar Data. . . . .	182
6.6	Stellar Data. . . . .	183
6.6	Stellar Data. . . . .	184
6.6	Stellar Data. . . . .	185
6.6	Stellar Data. . . . .	186
6.6	Stellar Data. . . . .	187
6.6	Stellar Data. . . . .	188
6.6	Stellar Data. . . . .	189

6.6	Stellar Data. . . . .	190
6.6	Stellar Data. . . . .	191
6.6	Stellar Data. . . . .	192
6.6	Stellar Data. . . . .	193
6.6	Stellar Data. . . . .	194
6.6	Stellar Data. . . . .	195
6.6	Stellar Data. . . . .	196
6.6	Stellar Data. . . . .	197
6.6	Stellar Data. . . . .	198
6.6	Stellar Data. . . . .	199
6.6	Stellar Data. . . . .	200
7.1	Parameters for Model Spectra in C05 Library . . . . .	205
7.2	SpecMatch Wavelength Segments . . . . .	205
7.3	Parameters of Template Spectra Used for Wavelength Calibration . . . . .	207
7.4	Median photon-limited errors as a function of SNR . . . . .	215
7.5	SpecMatch Systematic Uncertainties . . . . .	218
7.6	SpecMatch/ Huber et al. (2013) Comparison . . . . .	229
7.6	SpecMatch/ Huber et al. (2013) Comparison . . . . .	230
7.7	SpecMatch/ Torres et al. (2012) Comparison . . . . .	231
7.7	SpecMatch/ Torres et al. (2012) Comparison . . . . .	232
7.8	SpecMatch/ Valenti & Fischer (2005) Comparison . . . . .	233
7.8	SpecMatch/ Valenti & Fischer (2005) Comparison . . . . .	234
7.8	SpecMatch/ Valenti & Fischer (2005) Comparison . . . . .	235
7.8	SpecMatch/ Valenti & Fischer (2005) Comparison . . . . .	236
7.8	SpecMatch/ Valenti & Fischer (2005) Comparison . . . . .	237
7.8	SpecMatch/ Valenti & Fischer (2005) Comparison . . . . .	238
7.8	SpecMatch/ Valenti & Fischer (2005) Comparison . . . . .	239
7.8	SpecMatch/ Valenti & Fischer (2005) Comparison . . . . .	240
7.8	SpecMatch/ Valenti & Fischer (2005) Comparison . . . . .	241
7.9	SpecMatch/ Albrecht et al. (2012) Comparison . . . . .	242
7.9	SpecMatch/ Albrecht et al. (2012) Comparison . . . . .	243

# Acknowledgments

As my stint as an Berkeley Astronomy Grad comes to a close, I've enjoyed the chance to reflect on the last five years. This thesis would not have been possible without a vast network of people who helped me along the way. Thank you for helping me to pursue my dreams.

I'd like to acknowledge the support I've received from the US taxpayers. I've enjoyed financial support from the National Science Foundation and the University of California, Berkeley. My thesis depended heavily on data from the Keck Observatory, *Kepler Space Telescope*, and the NERSC supercomputing center. All of these institutions receive public support, and I'm grateful to live in a society that values the pursuit of knowledge for its own sake.

Geoff Marcy, my PhD adviser, deserves special recognition. Geoff: as a young kid, I dreamed of being a scientist, but I never thought I'd get to work with one of the most brilliant, creative, and inspiring scientists on the planet Earth. I am so grateful for the extraordinary effort you took to guide me as a student and launch my career, even if it meant Skype meetings at midnight. You showed me what it takes to be a good scientist. As I step out of the nest and try to strike out my own, I know I'll depend on the many pearls of wisdom you gave me during our time together. "Data is precious and doesn't grow on trees." "If a project isn't exciting and fun, don't do it!" I feel so lucky to have you as a mentor, colleague, and friend.

I've also had the good fortune to have a number of other mentors. Particle physicist Yury Kolomoisky took me under his wing when I was a freshman at Cal and gave me my first taste of real scientific research. Andrew Howard generously hosted me for a year at the University of Hawaii, which proved to be one of the most exciting years of my life. Eugene Chiang poured his heart into improving the graduate student experience and into his classes, each of which was a masterpiece. Eugene: thanks for holding me to a high standard, and inspiring me to do better. I'll miss our lively discussions on the BART. Peter Nugent taught me nearly everything I know about high-performance computing and always made time to help me with my software. Eliot Quataert and Michael Manga served on my qual and thesis committees (along with Geoff and Eugene) and helped guide me toward finishing my dissertation.

I had the good fortune of starting my PhD as *Kepler Space Telescope* began beaming its precious photometry back to Earth. The *Kepler Mission* was a monumental and heroic accomplishment that began before I was born. There are hundreds of scientists and engineers

at NASA and Ball Aerospace who poured years of their lives into making *Kepler* a reality. A few who I'd like to single out are Bill Borucki, David Koch, Natalie Batalha, Jon Jenkins, and Doug Caldwell. Thank you.

Nearly every chapter in this thesis benefited directly from data collected at the Keck Observatory. Thinking back to my high school years, when I would squint to see Saturn's rings with my 80 mm refractor, it's remarkable that only a few years later, I'd observe at one of the largest telescopes in the world. I'm grateful for the hard work of the telescope operators, support astronomers, and other staff that keep the mighty Keck telescope running. While in Hawaii, I had the privilege of meeting many people of Hawaiian descent. In our conversations, I was able to glimpse the powerful connection many feel to the land of their ancestors. The summit of Mauna Kea has profound cultural significance and deserves respect. I am deeply grateful that we astronomers have been treated as guests on the mountain.

It's been a joy to work in a department with so many wonderful colleagues. Thanks to all the staff that kept the department humming along and helped me focus on my research. Thanks in particular to Bill Boyd, Nina Ruymaker, Rayna Helgens, Barb Hoversten, and especially Dexter Stewart. Dexter: every time I see you, I leave with a smile on my face. Through my nine years at Berkeley, it meant so much to know that you cared about my well-being.

A big shout out to my fellow BADGrads. Graduate school is filled with hard work and uncertainty, and having you all there made navigating the uncertain waters easier. Thanks for all your support, and thanks also for making grad school so fun. The rest of my cohort deserves special recognition: Casey Stark, Garrett "Karto" Keating, and Francesca Fornasini. When I first met you five years ago in Eugene's radiation class, I couldn't have guessed that you would soon turn into some of my closest friends. I'll especially cherish all the delicious home-cooked meals we shared.

I've also had the privilege of working alongside the other fantastic astronomers in the Marcy group: Howard Isaacson, Lauren Weiss, Lea Hirsch, and Rea Kolbl. Thanks for your willingness to help me with my research—you all feel more like family than co-workers. Some of my fondest memories of grad school are the group pizza lunches in the courtyard of HFA.

Finally, I'm grateful to have an amazing family which is a limitless fountain of love, support, and encouragement. Mom and Dad, thanks for renting those Cosmos laserdiscs all those years ago. I think that got the ball rolling. Thanks for supporting my dreams. Ryan, I'm lucky to have a brother who I know is rooting for me to succeed. I really appreciate your quirky humor, your sense of adventure, and your reminders to come out and play basketball. And, of course, there's Alana. Getting a PhD involved its fair share of frustration and you bore the brunt of my emotional pain. You helped soften the pain of setbacks and amplified the joy of my successes, all while wrestling with the demands of medical school. You're an amazing woman, and I couldn't have done it with you.

## 1

# Introduction

*“There are 400 billion stars in the Milky Way Galaxy. Of this immense multitude, could it be that our humdrum Sun is the only one with an inhabited planet? Maybe... Or, here and there, peppered across space, orbiting other suns, maybe there are worlds something like our own, on which other beings gaze up and wonder as we do about who else lives in the dark.”*

– Carl Sagan, *Pale Blue Dot*

Our species has, for a long time, looked up at the night sky and wondered if there are other worlds like our own out there among the stars. Until recently, this question was relegated to the realm of philosophy and metaphysics given the limitations of our eyes and telescopes. Today, we live in a privileged time. Over the past twenty years, we have discovered thousands of planets around other stars. Their existence proves that the processes that form planets are not unique to the Solar System and that the real estate for life may be plentiful throughout the Universe.

Over the past five years, I have been fortunate to play a part in the rapidly growing field of extrasolar planet science. My thesis consists of two major themes: (i) the prevalence of planets in the Milky Way and (ii) the precise characterization of stars with planets. In Chapter 1, I give a brief historical review of exoplanet discoveries and provide some background for the rest of my thesis. I measured the occurrence of planets by analyzing data collected by NASA’s *Kepler Space Telescope*. This survey involved constructing my own photometric pipeline to remove instrumental systematics from *Kepler* photometry (Chapter 2). I analyzed *Kepler* data to measure the occurrence of planets out to Mercury’s orbit (Chapter 3), which I later extended to include Earth-like orbits (Chapters 4 and 5). I also worked on two projects involving the precision characterization of planet-hosting stars. I studied carbon and oxygen in nearby stars with an eye toward finding carbon-rich stars (Chapter 6). In Chapter 7, I present a new tool called SpecMatch for extracting fundamental stellar properties from high-resolution optical spectra with an emphasis on faint stars, where existing techniques are challenged.

## 1.1 Exoplanets: A Brief History

The study of extrasolar planets touches on some of the core questions that define us as a species: “Are there other Earths?” “Is there life among the stars?” and “Are there other beings that revel at the miracle of life and ponder their own origins?” These questions were debated by the philosophers of ancient Greece. Some, like Democritus (c. 460 – c. 370 BC) and Epicurus (341 – 270 BC), thought that there were other planets like Earth. Epicurus wrote, “There are infinite worlds both like and unlike this world of ours . . . We must believe in all worlds there are living creatures and plants and other things we see in this world” (Seager & Lissauer 2010). The idea that there might be a plurality of worlds was also considered, but rejected, by Plato (c. 420 – c. 348 BC) and Aristotle (384 – 332 BC). Platonic and Aristotelian philosophy had a profound influence on Western thought, while only fragments of Democritus’ and Epicurus’ work survive today (Billings 2013).

Astronomical techniques capable of detecting extrasolar planets emerged in the second half of the twentieth century. In 1952, Otto Struve wrote a two-page paper outlining two techniques that could detect planets around other stars (Struve 1952). The first technique involves looking for the slight wobble of a star as it is tugged by an unseen planetary companion. The wobble of a star can be detected by Doppler shifts in the star’s spectral lines over a planet’s orbital period. This technique is called the radial velocity (RV) or Doppler technique. For circular orbits seen edge on, the line of sight velocity of a planet hosting star is:

$$v_{\star} = \frac{M_p}{M_{\star}} v_p,$$

where  $M_p$  and  $M_{\star}$  are the masses of the planet and host star and  $v_p$  is the orbital velocity of the planet. For inclined orbits, we replace  $M_p$  by  $M_p \sin i$  where  $i$  is the orbital inclination.<sup>1</sup>

Struve also noted that planets that happen to pass in front of their host stars as seen from Earth would dim their stellar hosts once per orbit. A transiting planet dims its host star by an amount equal to the fraction of the stellar disk blocked:

$$\frac{\Delta F}{F} = \left( \frac{R_p}{R_{\star}} \right)^2,$$

where  $R_p$  and  $R_{\star}$  are the planet and star radii, respectively. As a point of reference, Jupiter dims the Sun by 1%, while the Earth blocks only 0.01% of the Sun’s light. The radial velocity and transit techniques have enabled the vast majority of exoplanet discoveries to date.

Doppler searches for extrasolar planets began in earnest the early 1980s (Campbell 1983; Marcy 1983; Mayor & Maurice 1985; Latham 1985). Latham et al. (1989) reported a substellar object orbiting HD 114762 with  $M \sin i = 11 M_J$ , on the dividing line between brown dwarf and giant planet.<sup>2</sup> Wolszczan & Frail (1992) made the first unambiguous detection of planet-mass objects outside the Solar System. They found two planets weighing 2.8 and

<sup>1</sup> $i = 90^\circ$  for edge on orbits and  $0^\circ$  for face on orbits.

<sup>2</sup>Objects more massive than  $13 M_J$  are considered brown dwarfs because they fuse Deuterium

3.4 Earth-masses orbiting the millisecond pulsar PSR B1257+12.<sup>3</sup> In 1995, [Mayor & Queloz](#) announced 51 Pegasi b, a Jupiter-mass planet orbiting the star 51 Pegasi with a 4.2 day orbital period. This discovery ushered in a torrent of planets discovered with the radial velocity technique. Within months of the 51 Pegasi b discovery, two more giant planets were announced around 70 Virginis ([Marcy & Butler 1996](#)) and 47 Ursae Majoris ([Butler & Marcy 1996](#)). By 2000, RVs had uncovered roughly a dozen planets and by 2010, that number had grown to around 300 ([Han et al. 2014](#)).

Detecting extrasolar planets by the transit method also began to receive serious consideration in 1980s. [Borucki & Summers \(1984\)](#) concluded that, while it was possible to detect the transits of giant planets from the ground, Earth-size planets required a dedicated space-born mission. In 1984, Borucki began a thirty-year effort to design, fund, build, and fly a telescope called *Kepler*, which today has discovered roughly 4000 of the 5000 exoplanets known.

In late 1999, eleven extrasolar planets had been discovered with RVs, but none had been observed transiting their host stars ([Charbonneau et al. 2000](#)). Shortly after the RV discovery of HD 209458b, [Henry et al. \(2000\)](#) and [Charbonneau et al. \(2000\)](#) observed the periodic dimming of HD 209458 due to the occultation by a Jupiter-sized companion. The discovery of a transiting planet was a significant milestone for the exoplanet field. The observations helped dispel doubts that the radial velocity detections were face on binary stars or coherent stellar pulsations. HD 209458b was the first planet with a measured radius and the fact that the orbit was edge on meant the  $M \sin i \approx M$ . Knowing a planet’s mass and radius together helps constrain its bulk composition and structure.

HD 209458b invigorated efforts to detect planets by the transit technique. Starting in the early 2000s, many groups started ground-based transit surveys.<sup>4</sup> These surveys are strongly biased toward detecting close-in planets. Assuming random orbital inclinations, the probability that an extrasolar planet will transit, as seen from earth is  $P_T = R_\star/a$ , where  $R_\star$  is the stellar radius and  $a$  is the planet-star orbital separation. For the Earth and the Sun,  $P_T = R_\odot/1 \text{ AU} = 1/200$ . Ground-based transit surveys must also contend with photometric noise due to differential extinction, scintillation, and flat-fielding errors ([Winn 2010](#)). Photometric precision improves dramatically when using space-based facilities. As an example, the original ground-based [Charbonneau et al. \(2000\)](#) observations of HD 209458b achieved photometric precision of  $\approx 3$  ppt per minute. [Brown et al. \(2001\)](#) observed the same planet using the *Hubble Space Telescope* and achieved photometric precision of  $\approx 0.11$  ppt per minute, sufficient to detect Earth-sized planets. These observations strengthened the case for a dedicated space-based mission to search for Earth-size extrasolar planets. After

<sup>3</sup>The PSR B1257+12 discoveries were a strange twist of fate. PSR B1257+12 was the third millisecond pulsar discovered and its associated planets suggested that planets around pulsars might be common. However, today, we know of roughly 300 millisecond pulsars, and only one other pulsar planet: PSR B1620-26b. Given current pulsar timing precision, we could easily detect Earth-analog planets around all of them. (Scott Ransom, priv. communication 2015).

<sup>4</sup>A few of the more prolific ground-based surveys are OGLE ([Udalski et al. 2002](#)), TrES ([Alonso et al. 2004](#)), XO ([McCullough et al. 2005](#)), HAT ([Bakos et al. 2007](#)), and SuperWASP ([Pollacco et al. 2006](#)).

four attempts beginning in 1992, the *Kepler Space Telescope* was approved in December 2001 (Borucki et al. 2003).

On March 7, 2009, *Kepler* lifted off from Cape Canaveral, Florida into an Earth-trailing orbit. From December 2009 to May 2013, *Kepler* took a picture of a  $10^\circ \times 10^\circ$  region of the sky in the constellation Cygnus every thirty minutes. On the ground, these images were converted into brightness measurements of  $\sim 150,000$  stars. *Kepler* has completely transformed our knowledge of planets outside the Solar System. The left panel of Figure 1.1 shows known planets when *Kepler* was launched. We see a large population of giant planets with orbital periods of a year and longer, a number of hot Jupiters, which are favored by selection effects, and a small number of close-in planets the size of Neptune ( $4 R_\oplus$ ) and smaller. The right panel of Figure 1.1 includes planets found in the first year of *Kepler* photometry (Batalha et al. 2013). Planets with sizes between Earth and Neptune are common around other stars, while absent in our own Solar System.

## 1.2 Exoplanet Demographics

Once it became clear that other stars had planets, the natural next question is “what fraction of stars have planets?” The emerging field of exoplanet demographics parallels the work of Hertzsprung, Russell, and others a century ago. Just as the HR diagram shaped our understanding of stellar physics, the prevalence of planets with different sizes, orbital distances, and other properties is shaping our understanding of planet formation and evolution.

The key measured quantity in exoplanet demography is planet occurrence,  $f_p$ , which is simply

$$f_p = \frac{N_p}{N_\star},$$

the number of planets divided by the number of stars. However, all planet surveys contain biases and selection effects, which require careful attention.

Prior to *Kepler*, RV surveys probed giant planet occurrence out to  $\sim 10$ -year orbits as well the occurrence of smaller planets on close-in orbits. Cumming et al. (2008) found that 10.5% of Sun-like stars have a giant planet with an orbital period less than 5.5 years (Jupiter has a 12-year orbit). While these “exo-Jupiters” are reminiscent of the giant planets in our own solar system, they are often found on highly elliptical orbits in contrast to the nearly circular orbits of the Solar System planets. Hot Jupiters, while easy to detect, are relatively rare. Marcy et al. (2005) found an occurrence of  $1.2 \pm 0.1\%$  for hot Jupiters ( $P \lesssim 12$  d). Through intense monitoring of restricted stellar samples, Howard et al. (2010) and Mayor et al. (2011) found that close-in ( $P < 50$  d) planet occurrence rises steeply toward small planet sizes. Roughly 15% of GK stars have a 3-10  $M_E$  planet with  $P < 50$  d.

One way in which planet occurrence ties in with planet formation is through planet population synthesis modeling. These models attempt to capture the important aspects of planet formation physics to produce synthetic populations of planets that can be compared with observations. One such study is that of Ida & Lin (2008) who predicted that planets

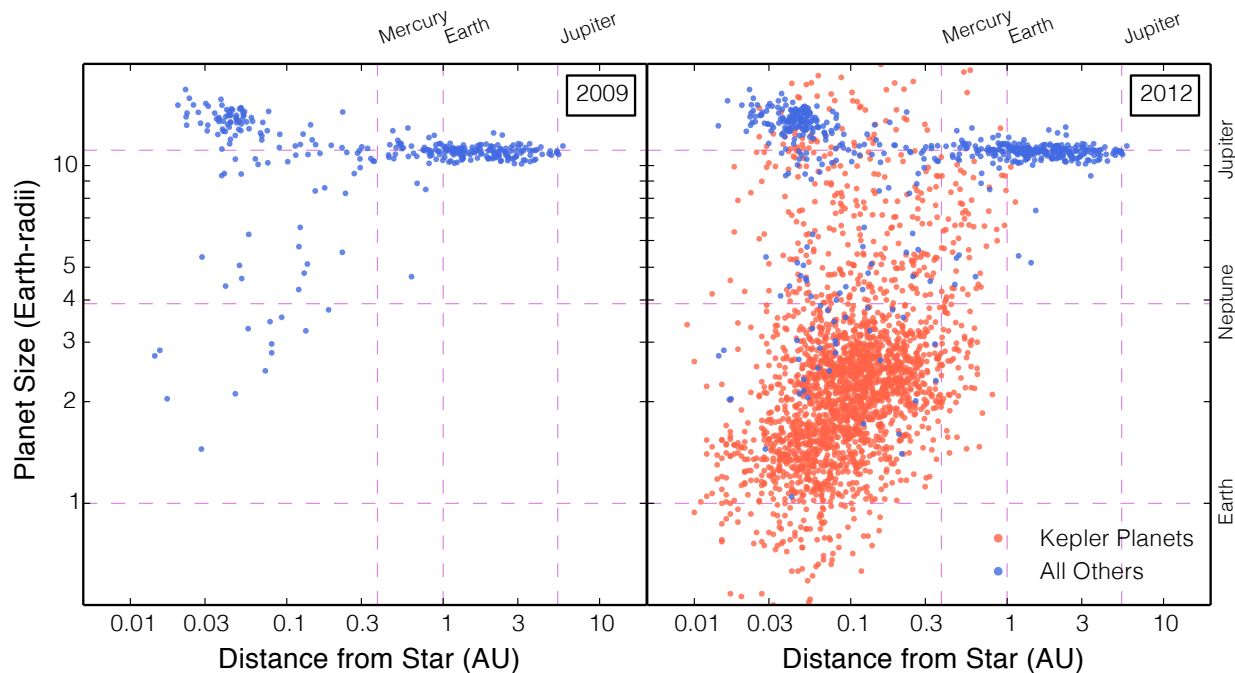


Figure 1.1: *Kepler* has ushered in a paradigm shift in our understanding of extrasolar planets. The left panel shows the sizes and orbital distances of planets known prior to the launch of *Kepler* in 2009. Most planets in this figure were discovered using the Doppler technique. When only planet mass is known, planet size is estimated according to the [Weiss et al. \(2013\)](#) mass-radius relationship. Two distinct populations of planets are visible. Long-period giant planets (many of which are on eccentric orbits) and close-in “hot Jupiters” (which have inflated radii due to poorly understood processes). By 2012, this picture had changed dramatically with the analysis of just over one year of *Kepler* data ([Batalha et al. 2013](#)). Planets closer than 1 AU between the size of Earth and Neptune are a common outcome of planet formation, yet are absent in our own solar system.

between 1 and 30  $M_E$  and  $P < 1$  year should be extremely rare. However, the RV surveys of Howard et al. (2010), Mayor et al. (2011) and the *Kepler*-based surveys of Howard et al. (2012), Fressin et al. (2013), and Petigura et al. (2013a) showed that sub-Neptune-size planets are very common. The migration models have since been modified to more closely match the observed distribution of planets (Mordasini et al. 2012).

### 1.3 Precision Characterization of Stars

Another component of my thesis involves the precise characterization of stars with extrasolar planets. Planet formation is believed to occur early in a star’s lifetime. Millimeter observations of young stars show that gas disks dissipate within roughly 10 Myr (Haisch et al. 2001). Gas giant planets are thought to form during this time frame. In order to understand planet formation, we would like to observe planets during the process of formation. However, detecting planets around young stars is challenging due to high activity levels which hamper transit and RV methods. However, the composition of the host star offers a window into the protoplanetary disk from which planets form.

Stellar metallicity is thought to be a good tracer of the amount of solids available in a protoplanetary disk. There is a well-established correlation between giant planet occurrence and host star metallicity (Gonzalez 1997; Santos et al. 2004; Fischer & Valenti 2005). However, smaller planets are found around stars having a wide range of metallicities. This new trend was observed among the RV-detected planets (Mayor et al. 2011) and (Buchhave et al. 2012). The spectra taken during the course of RV planet detection surveys are valuable in probing the connection between planet and host star.

In Chapter 6, I study the carbon and oxygen abundances of over 1000 stars from the California Planet Search (Marcy et al. 2008). I find that planet-hosting stars have a wide range of carbon and oxygen abundances. Of particular interest are planets around stars with carbon to oxygen ratios approaching unity. Terrestrial planets in carbon-rich environments are thought to have radically different compositions compared to planets that form in environments with  $C/O < 1$  (Kuchner & Seager 2005; Bond et al. 2010).

Another reason for studying host star properties is that in many cases, our understanding of planet properties is limited by our imperfect knowledge of the host star. In fitting a transit profile, we measure the planet-star radius ratio,  $R_P/R_*$ , not on the physical size of the planet itself. Most stars in the *Kepler* field have photometrically determined stellar radii which are uncertain at the 35% level (Brown et al. 2011; Batalha et al. 2013; Burke et al. 2014). Large uncertainties in planet size can hide features in the properties of large ensembles of planets. For example, any sharp features in the planet radius distribution that would indicate an important size scale for planet formation are smeared by planet radius errors.

Extracting stellar parameters for *Kepler* host stars presented new challenges compared to similar efforts for nearby stars. Stars in the *Kepler* field are typically  $\sim 1$  kpc from Earth. A Sun-like star at 1 kpc has  $V = 14.7$ . Traditional spectroscopic methods often utilize high SNR spectra. For example, Valenti & Fischer (2005) analyzed Keck HIRES spectra with

---

SNR/pixel  $> 200$ . However, obtaining a SNR/pixel = 100 spectrum of a  $V = 14.7$  star would take 2.5 hours with HIRES and is impractical for large samples of stars. In order to work with fainter stars, I developed a new tool called SpecMatch that fits large swaths of spectra containing thousands of lines. SpecMatch is able to accurately constrain fundamental stellar properties even for low SNR spectra. SpecMatch will enable measurements of stellar radii good to 5% for large samples of *Kepler* planet hosts.

## 2

# Identification and Removal of Noise Modes in *Kepler* Photometry

A version of this chapter was previously published in the *Publications of the Astronomical Society of the Pacific* (Erik A. Petigura & Geoffrey W. Marcy, 2012, PASP 124, 1073).

We present the Transiting Exoearth Robust Reduction Algorithm (TERRA) — a novel framework for identifying and removing instrumental noise in *Kepler* photometry. We identify instrumental noise modes by finding common trends in a large ensemble of light curves drawn from the entire *Kepler* field of view. Strategically, these noise modes can be optimized to reveal transits having a specified range of timescales. For *Kepler* target stars of low photometric noise, TERRA produces ensemble-calibrated photometry having 33 ppm RMS scatter in 12-hour bins, rendering individual transits of earth-size planets around sun-like stars detectable as  $\sim 3\sigma$  signals.

## 2.1 Introduction

The *Kepler* Mission is ushering in a new era of exoplanet science. Landmark discoveries include *Kepler*-10b, a rocky planet (Batalha et al. 2011); the *Kepler*-11 system of six transiting planets (Lissauer et al. 2011); earth-sized *Kepler*-20e and 20f (Fressin et al. 2012); KOI-961b, c, and d – all smaller than earth (Muirhead et al. 2012); and *Kepler*-16b a circumbinary planet (Doyle et al. 2011). While *Kepler* has revealed exciting individual systems, the mission’s legacy will be the first statistical sample of planets extending down to earth size and out to 1 AU. *Kepler* is the first instrument capable of answering “How common are earths?” — A question that dates to antiquity.

Planet candidates are detected by a sophisticated pipeline developed by the *Kepler* team Science Operations Center. In brief, systematic effects in the photometry are suppressed by the Pre-search Data Conditioning (PDC) module, the output of which is fed into the Transiting Planet Search (TPS) module. For further information, see Jenkins et al. (2010a).

The *Kepler* mission was designed to study astrophysical phenomena with a wide range of timescales, which include 1-hour transits of hot Jupiters, 10-hour transits of planets at 1 AU, and weeklong spot modulation patterns. The PDC module is charged with removing instrumental noise while preserving signals with a vast range of timescales. We review sources of instrumental errors in § 2.2, highlighting the effects that are most relevant to transit detection.

The *Kepler* team has released candidate planets based on the first 4 and 16 months of data (Borucki et al. 2011; Batalha et al. 2012). Many of the candidates have additional followup observations from the ground and space aimed at ruling out false positive scenarios. In addition, statistical arguments suggest that 90-95% of all candidates and that  $\sim 98\%$  of candidates in multi-candidate systems are bonafide planets (Morton & Johnson 2011; Lissauer et al. 2012).

While *Kepler's* false positive rate is low, its completeness is largely uncharacterized. If the completeness decreases substantially with smaller planet size or longer orbital periods, the interpretations regarding occurrence drawn from the Borucki et al. (2011) and Batalha et al. (2012) catalogs will be incorrect. Hunting for the smallest planets, including earth-sized planets in the habitable zone, will require exquisite suppression of systematic effects. Without optimal detrending, systematic noise will prevent the detection of the smallest planets, possibly the habitable-zone earth-sized planets, which is the main goal of the *Kepler* mission. Therefore, it is essential for independent groups to develop pipelines that compliment both PDC and TPS. An early example of an outside group successfully identifying new planet candidates is the Planet Hunters project (Fischer et al. 2011; Lintott et al. 2012), which uses citizen scientists to visually inspect light curves. In addition, existing pipelines from the HAT ground-based search (Huang et al. 2012) and the *CoRoT* space mission (Ofir & Dreizler 2012) have been brought to bear on the *Kepler* dataset yielding  $\sim 100$  new planet candidates.

We present the Transiting Exoearth Robust Reduction Algorithm (TERRA) — a framework for identifying and removing systematic noise. We identify systematic noise terms by searching for photometric trends common to a large ensemble of stars. Our implementation is tuned toward finding trends with transit-length timescales.

## 2.2 Instrumental Noise in *Kepler* Photometry

The *Kepler* spacecraft makes photometric observations of  $\sim 156,000$  targets. Long cadence photometry is computed by summing all the photoelectrons within a predefined target aperture during a 29.4 minute integration. The *Kepler* team makes this “Simple Aperture Photometry” available to the scientific community (Fraquelli & Thompson 2012). Simple aperture photometry contains many sources of noise other than Poisson shot noise. We illustrate several noise sources in Figure 2.1, where we show the normalized photometry ( $\delta F$ ) of KIC-8144222 ( $Kp = 12.4$ ).  $\delta F = (F - \bar{F})/\bar{F}$  where  $F$  is the simple aperture photometry.

The dominant systematic effect on multi-quarter timescales is “differential velocity aber-

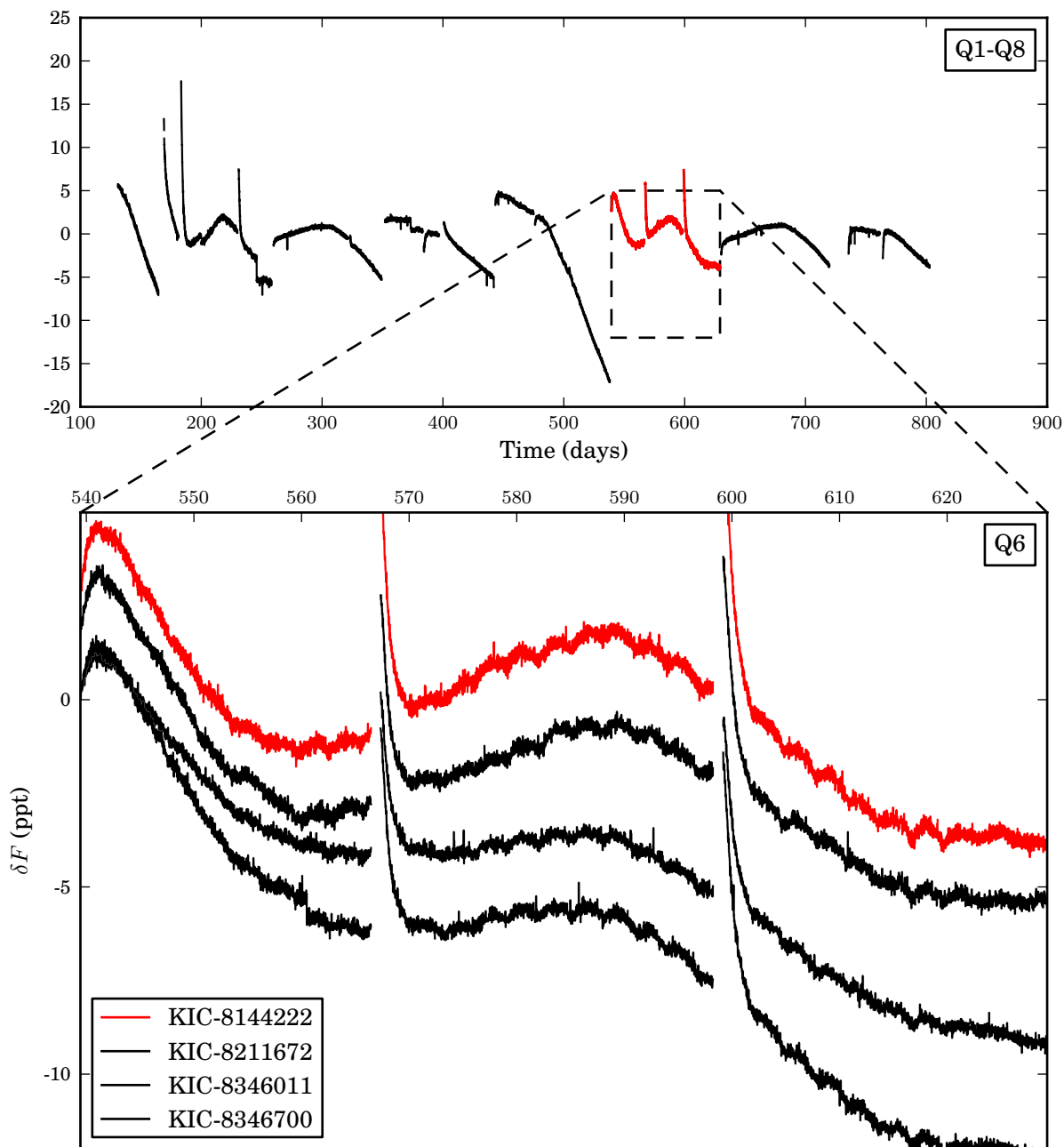


Figure 2.1: Top: Normalized flux from KIC-8144222 ( $K_p = 12.4$ ,  $CDPP_{12} = 35.4$  ppm) from Quarter 1 through 8 (Q1-Q8). Bottom: Detail of Q6 photometry showing KIC-8144222 along with three stars of similar brightness, noise level, and location on the FOV ( $12.0 < K_p < 13.0$ ,  $CDPP_{12} < 40$  ppm,  $mod.out = 16.1$ ). Much of the variability is common to the 4 stars and therefore instrumental in origin. The two spikes are due to thermal settling events, and the three-day ripples are due to onboard momentum management.

ration” (Van Cleve & Caldwell 2009). As *Kepler* orbits the sun, its velocity relative to the *Kepler* field changes. When the spacecraft approaches the *Kepler* field, stars on the extremities of the field move toward the center. Stellar PSFs move over *Kepler* apertures by  $\sim 1$  arcsecond resulting in a  $\sim 1\%$  effect over 1-year timescales.

We show a detailed view of KIC-8144222 photometry from Quarter 6 (Q6) in Figure 2.1. The decaying exponential shapes are caused by thermal settling after data downlinks. Each month, *Kepler* rotates to orient its antenna toward earth. Since *Kepler* is not a uniformly colored sphere, changing the spacecraft orientation with respect to the sun changes its overall temperature. After data downlink, *Kepler* takes several days to return to its equilibrium temperature (Jeffrey Smith, private communication, 2012). KIC-8144222 photometry also shows a  $\sim 0.1\%$  effect with a 3-day period due to thermal coupling of telescope optics to the reaction wheels. We explore this 3-day cycle in depth in § 2.3.3.

Since all of the previously mentioned noise sources are coherent on timescales longer than one cadence (29.4 minutes), the RMS of binned photometry does not decrease as  $1/\sqrt{N}$ , where  $N$  is the number of measurements per bin. In order to describe the noise on different timescales, the *Kepler* team computes quantities called CDPP3, CDPP6, and CDPP12 which are measures of the photometric scatter in 3, 6, and 12-hour bins. KIC-8144222 has CDPP12 35.4 ppm and is a low-noise star (bottom 10 percentile). For a more complete description of noise in *Kepler* data see Christiansen et al. (2011).

As a comparison, we selected stars which were similar to KIC-8144222 in position on the Field of View (FOV), noise level, and brightness (mod.out = 16.1, CDPP12 < 40 ppm,  $12.0 < Kp < 13.0$ ). From this 13-star sample, we randomly selected 3 stars and show their light curves in Figure 2.1. The photometry from the comparison stars is strikingly similar to the KIC-8144222 photometry. Since much of the variability is correlated, it must be due to the state of the *Kepler* spacecraft. Common trends among stars can be identified and removed. The *Kepler* team calls this “cotrending,” a term we adopt.

Correlated noise with timescales between 1 and 10 hours can mimic planetary transits and requires careful treatment. To illustrate the transit-scale correlations among a large sample of stars, we show a correlation matrix constructed from 200 Q6 light curves in Figure 2.2. The *Kepler* photometer is an array of 42 CCDs arranged in 21 modules (Fraquelli & Thompson 2012). We organized the rows and columns of the correlation matrix by module. We constructed the correlation matrix using the following steps:

1. We randomly selected 10 light curves from each of the 20 total modules<sup>1</sup> from stars with the following properties:  $12.5 < Kp < 13.5$  and CDPP12 < 40 ppm.
2. To highlight transit-scale correlations, we subtracted a best fit spline from the photometry. The knots of the spline are fixed at 10-day intervals so that we remove trends  $\gtrsim 10$  days.
3. We normalized each light curve so that its median absolute deviation (MAD) is unity.

---

<sup>1</sup>Module 3 failed during Q4 (Christiansen et al. 2011).

4. We evaluated the pairwise correlation (Pearson-R) between all 200 stars.

The correlation matrix shows that stars in some modules (e.g. module 2) correlate strongly with other stars in the same module. However, other modules (e.g. module 12) shows little inter-module correlation. Finally, the large off-diagonal correlations show that stars in some modules correlate strongly with stars in different modules.

## 2.3 Identification of Photometric Modes

We have shown that there is significant high-frequency ( $\lesssim 10$  days) systematic noise in *Kepler* photometry. In order to recover the smallest planets, this noise must be carefully characterized and removed. We isolate systematic noise by finding common trends in a large ensemble of stars. This is an extension of differential photometry, widely used by ground-based transit surveys to calibrate out the time-variable effects of the earth's atmosphere. We find these trends using Principle Component Analysis (PCA). This is similar to the Sys-Rem, TFA, and PDC algorithms (Tamuz et al. 2005; Kovács et al. 2005; Twicken et al. 2010), but our implementation is different. We briefly review PCA in the context of cotrending a large ensemble of light curves.

### 2.3.1 PCA on Ensemble Photometry

Consider an ensemble of  $N$  light curves each with  $M$  photometric measurements. We can think of the ensemble as a collection of  $N$  vectors in an  $M$ -dimensional space. Each light curve  $\delta F$  can be written as a linear combination of  $M$  basis vectors that span the space,

$$\begin{aligned} \delta F_1 &= a_{1,1}V_1 + \dots + a_{1,M}V_M \\ &\vdots \\ \delta F_N &= a_{N,1}V_1 + \dots + a_{N,M}V_M \end{aligned} \tag{2.1}$$

where each of the  $V_j$  basis vectors is the same length as the original photometric time series. Equation 2.1 can be written more compactly as

$$\mathbf{D} = \mathbf{A}\mathbf{V}$$

where

$$\mathbf{D} = \begin{pmatrix} \delta F_1 \\ \vdots \\ \delta F_N \end{pmatrix}, \mathbf{A} = \begin{pmatrix} a_{1,1} & \dots & a_{1,M} \\ \vdots & \ddots & \vdots \\ a_{N,1} & \dots & a_{N,M} \end{pmatrix}, \mathbf{V} = \begin{pmatrix} V_1 \\ \vdots \\ V_M \end{pmatrix}$$

Singular Value Decomposition (SVD) simultaneously solves for the basis vectors  $\mathbf{V}$  and the coefficient matrix  $\mathbf{A}$  because it decomposes any matrix  $\mathbf{D}$  into

$$\mathbf{D} = \mathbf{U}\mathbf{S}\mathbf{V}^\top.$$

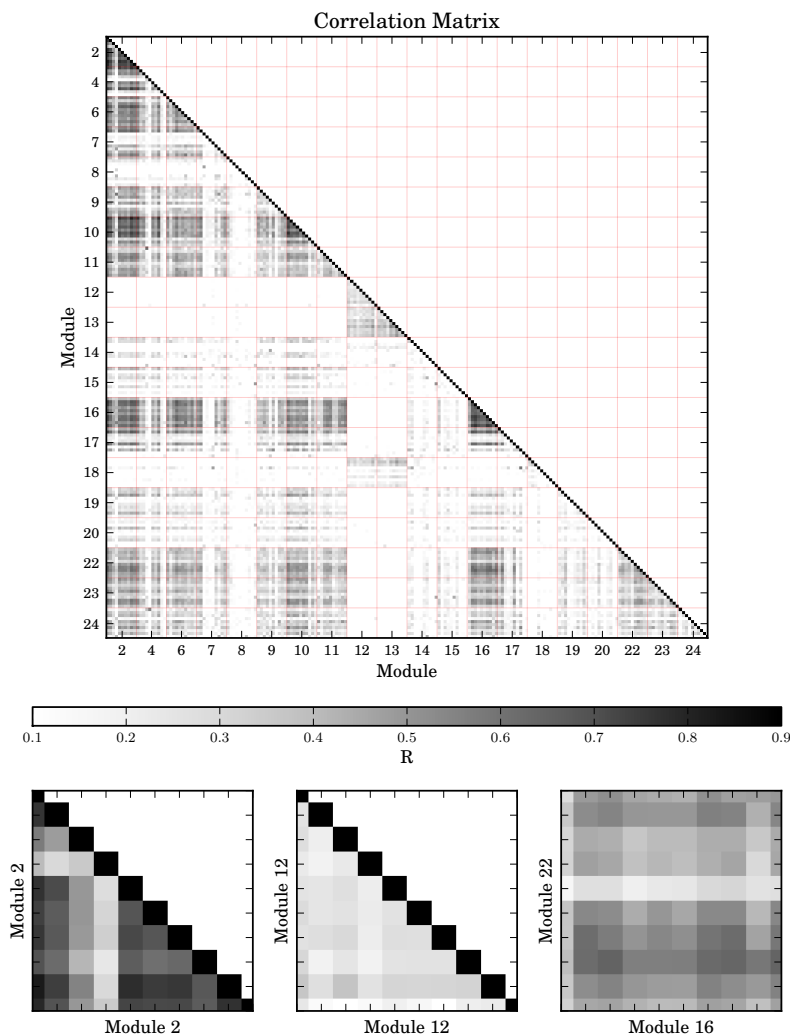


Figure 2.2: Top: Correlation matrix constructed from 200 Q6 light curves. The correlation (R-value) between two stars is represented by the gray scale, which ranges from 0.1 to 0.9. The diagonal elements have  $R = 1$ . The stars are ordered according to module and the red lines delineate one module from another. We enlarge several  $10 \times 10$  regions in the lower panels. Stars in some modules (such as module 2) are highly correlated, while other modules (such as module 12) show little correlation. The module 22 - module 16 correlation matrix is an example of significant inter-module correlation. We observed the same patterns in a correlation matrix constructed from  $\sim 1200$  stars, but we show the 200-star correlation matrix so that individual elements are discernible as pixels.

$\mathbf{V}$  is an  $M \times M$  matrix where the columns are the eigenvectors of  $\mathbf{D}^\top \mathbf{D}$  or “principle components,” and the diagonal elements of  $\mathbf{S}$  are the corresponding eigenvalues. The eigenvalues  $\{s_{1,1}, \dots, s_{M,M}\}$  describe the extent to which each of the principle components capture variability in the ensemble and are ordered from high to low. The columns of  $\mathbf{U}$  are the eigenvectors of  $\mathbf{D}\mathbf{D}^\top$ . Both  $\mathbf{U}$  and  $\mathbf{V}$  are unitary matrices, i.e.  $\mathbf{U}\mathbf{U}^\top = \mathbf{I}$  and  $\mathbf{V}\mathbf{V}^\top = \mathbf{I}$ .

As we saw in § 2.2, stars show common photometric trends due to changes in the state of the *Kepler* spacecraft. The most significant principle components will correspond to these common trends. If we identify the first  $N_{Mode}$  principle components as instrumental noise modes, we can remove them via

$$\delta F_{i,cal} = \delta F_i - \sum_{j=1}^{N_{Mode}} a_{i,j} V_j \quad (2.2)$$

where  $\delta F_{cal}$  is an ensemble-calibrated light curve. However since the collection of  $\{V_1, \dots, V_M\}$  spans the space, the higher principle components describe astrophysical variability, shot noise, and exoplanet transits. We must be careful not to remove too many components because we would be removing the signals of interest.

### 2.3.2 PCA implementation

We construct a large reference ensemble of light curves  $\{\delta F_1, \dots, \delta F_N\}$  of 1000 stars ( $12.5 < Kp < 13.5$ ,  $CDPP12 < 40$  ppm) drawn randomly from the entire FOV. Before performing SVD, we remove thermal settling events and trends  $\gtrsim 10$  days as described in § 2.2. Since SVD finds the eigenvectors of  $\mathbf{D}^\top \mathbf{D}$  it is susceptible to outliers as is any least squares estimator. We perform a robust SVD that relies on iterative outlier rejection following these steps:

1. Find principle components and weights for light curve ensemble.
2. The  $i^{\text{th}}$  light curve is considered an outlier if any of the mode weights  $(a_{i,1}, \dots, a_{i,4})$  differ significantly from the typical mode weight in the ensemble. We consider  $a_{i,j}$  to be significantly different from the ensemble if

$$\frac{|a_{i,j} - \text{med}(a_j)|}{\text{MAD}(a_j)} > 10$$

where  $\text{med}(a_j)$  and  $\text{MAD}(a_j)$  are the median value and the median absolute deviation of all the  $a_j$  mode weights.

3. Remove outlier light curves from the ensemble.
4. Repeat until no outliers remain.

For our 1000-star sample we identified and removed 51 stars from our ensemble. These stars tended to have high amplitude intrinsic astrophysical variability, i.e. due to spots and flares. We plot the four most significant TERRA principle components in Figure 2.3 and offer some physical interpretations of the mechanisms behind these modes in the following section.

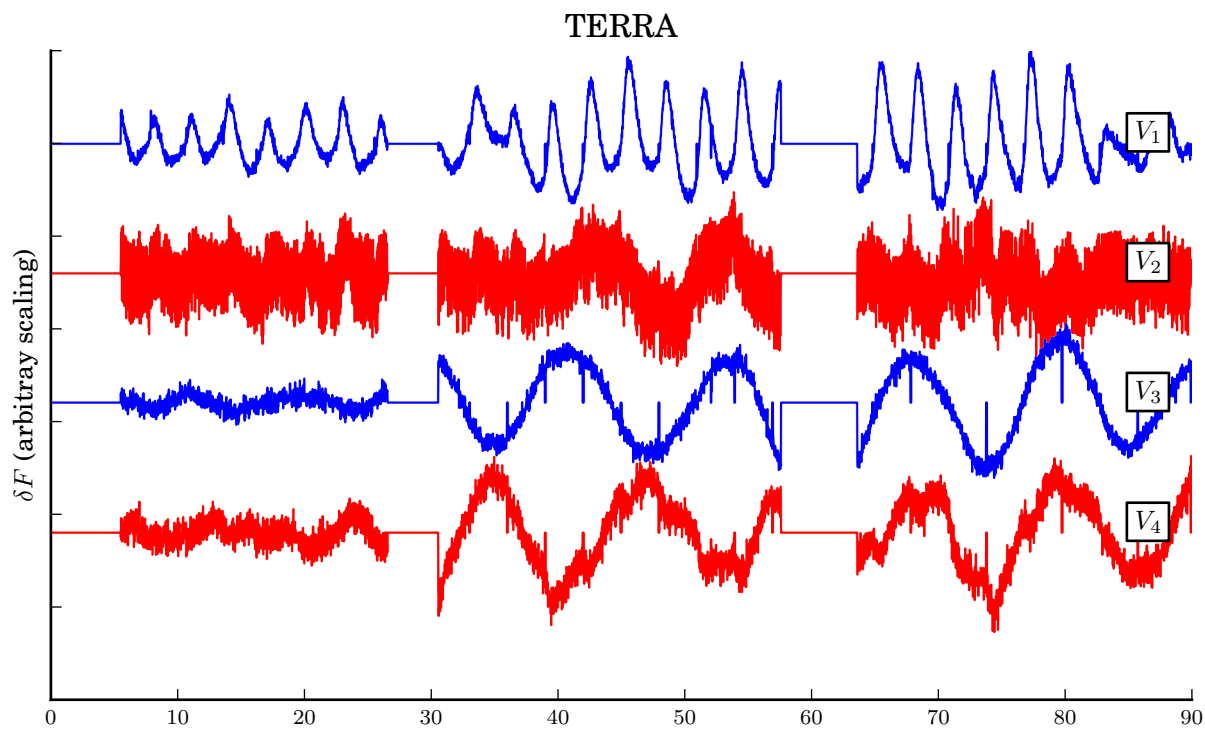


Figure 2.3: Top: The first four TERRA principle components in our 1000-light curve ensemble plotted in order of significance.  $V_1$  has a 3-day periodicity and is due to changes in the thermal state of the spacecraft caused by a 3-day momentum management cycle.  $V_2$  has a high frequency component ( $P = 1.68$  hours) that could be due to a 20 minute thermal cycle from an onboard heater aliased with the 29.4 minute observing cadence alias of a 20-minute thermal cycle driven by an onboard heater.

### 2.3.3 Interpretation of Photometric Modes

In this section, we associate the variability captured in the principle components to changes in the state of the *Kepler* spacecraft that couple to photometry. The three-day cycle isolated in our first principle component is due to a well-known, three-day momentum management cycle on the spacecraft (Christiansen et al. 2011). To keep a fixed position angle, *Kepler* must counteract external torques by spinning up reaction wheels. These reaction wheels have frictional losses which leak a small amount of heat into the spacecraft, which changes the PSF width and shape of the stars.

We can gain a more detailed understanding of this effect, by examining how the mode weights for each reference star corresponding to  $V_1$ , i.e.  $\{a_{1,1}, \dots, a_{N,1}\}$ , vary across the FOV. We display the RA and Dec positions of our 1000-star sample in Figure 2.4 and color-code the points with the value of  $a_i$ . The  $a_1$  and  $a_2$  mode weights show remarkable spatial correlation across the FOV. That  $a_1$  is positive in the center of the FOV and negative at the edges of the FOV means the systematic photometric errors in these two regions respond to the momentum cycle in an anticorrelated sense. The telescope is focused such that the PSF is sharpest at intermediate distances from the center of the FOV. Since stars in the center and on the extreme edges have the blurriest PSFs (Van Cleve & Caldwell 2009), they respond most strongly to the momentum cycle.

The mechanism behind the variability seen in  $V_2$  is less clear.  $V_2$  includes a high frequency component with a period of 1.68 hours. The *Kepler* team has also noticed this periodicity in the pixel scale (Douglas Caldwell, private communication, 2012). A possible explanation is thermal coupling of the telescope optics to a heater that turns off and on with a  $\sim 20$  minute period. The 1.68 hour variability would be an alias of this higher frequency with the observing cadence of 29.4 minutes. The gradient in  $a_2$  across the FOV suggests the heater is coupled to the telescope optics in a tip/tilt rather than piston sense.

The higher-order components  $a_3$  and  $a_4$  do not show significant spatial correlation, which suggests that  $V_3$  and  $V_4$  are not due to changes in the local PSF. Since  $V_3$  and  $V_4$  have a  $\sim 10$ -day timescale, they could be the high frequency component of the differential velocity aberration trend that was not removed by our 10-day spline.

## 2.4 Calibrated Photometry

### 2.4.1 Removal of Modes

After determining which of the  $N_{Mode}$  principle components correspond to noise modes, we can remove them according to Equation 2.2. In Figure 2.5, we show fits to KIC-8144222 Q6 photometry using different combinations of TERRA principle components. We achieve uniform residuals using only 2 of our modes as we show quantitatively below. The simplicity of our model buys some insurance against overfitting.

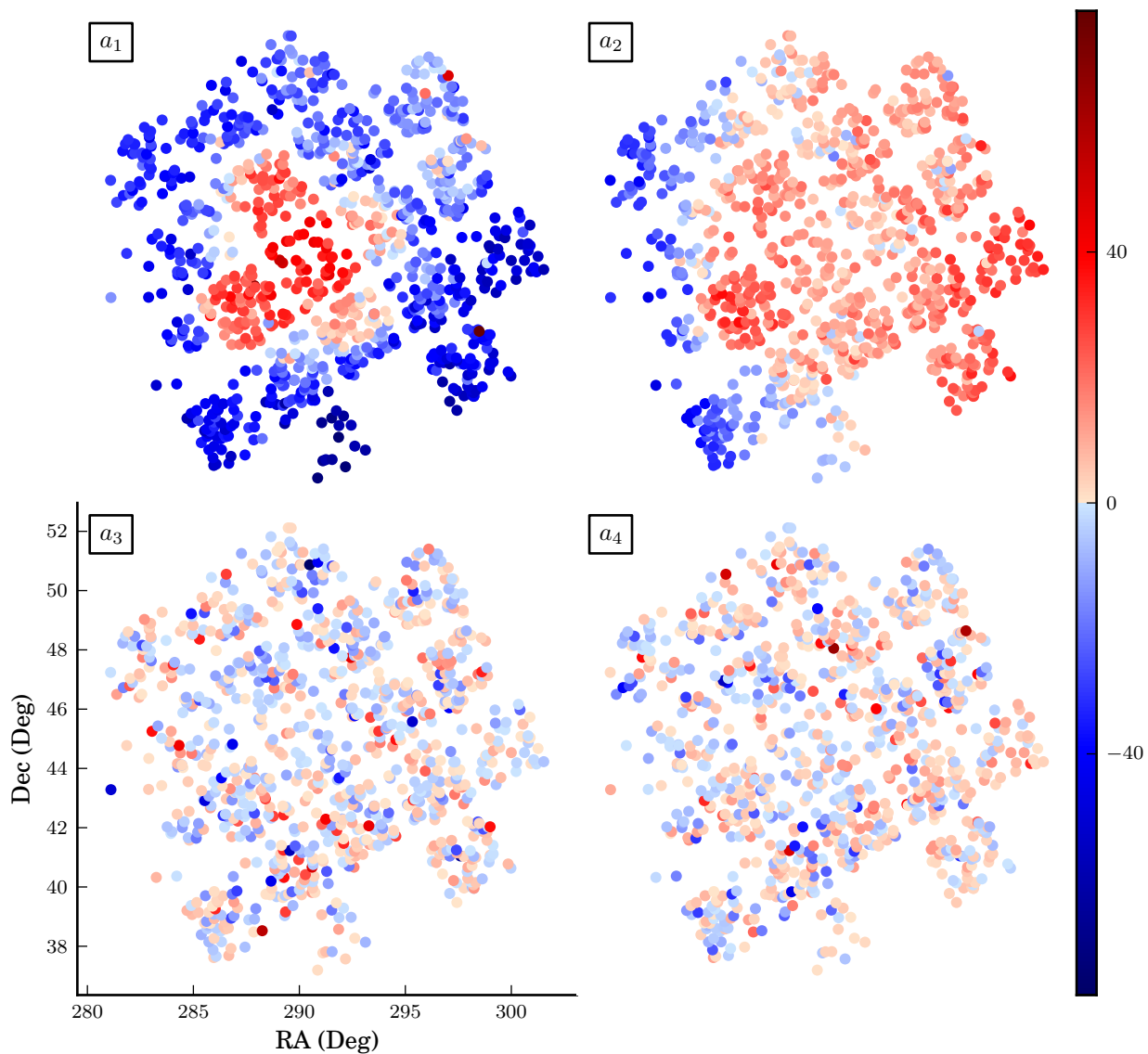


Figure 2.4: The RA and Dec positions of our 1000-star ensemble. The points are color-coded by  $a_i$ , the weights for mode  $V_i$ . Negative values are shown in blue and positive values are shown in red. The fact that the sign and magnitude of  $a_1$  depends on distance from the center of the FOV supports the idea that the variability captured by  $V_1$  is due to PSF breathing of the telescope which is driven by the three-day momentum management cycle. The gradient in  $a_2$  could be due to the thermal coupling of an onboard heater to the optics in a tip/tilt sense. Mode weights  $a_3$  and  $a_4$  show no spatial correlation and do not seem to depend on changes in the PSF width.

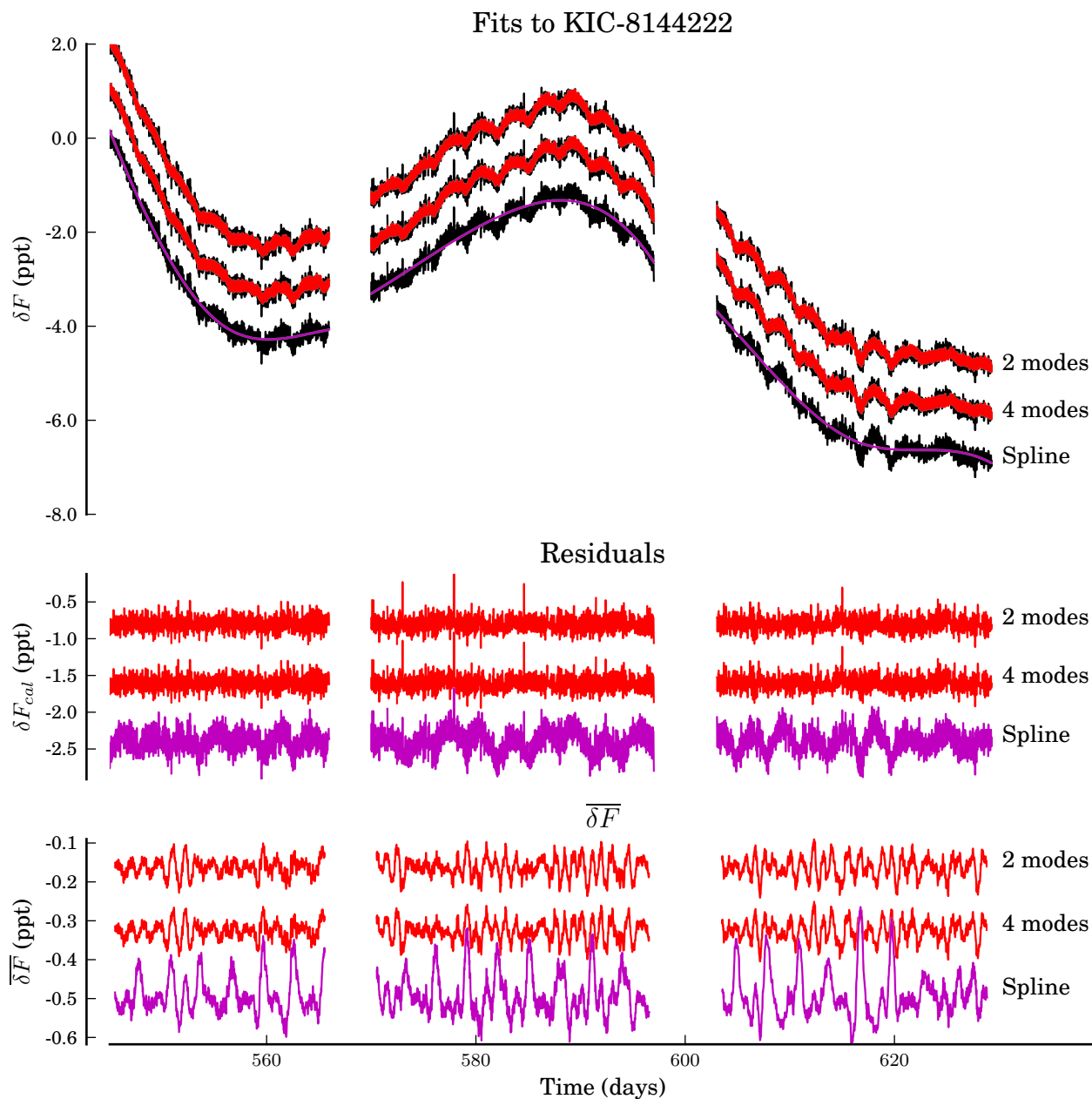


Figure 2.5: Least squares fits using TERRA principle components to KIC-8144222 Q6 photometry. The bottom panel shows 12-hour  $\overline{\delta F}$  where smaller scatter implies greater sensitivity to small transits. We show the spline fit (magenta) as a baseline since it incorporates no ensemble-based cotrending information. The  $\overline{\delta F}$  using spline detrending shows large spikes at the momentum cycle cusps, which are suppressed in the TERRA cotrending. Using our robust modes, we are able to produce a clean, calibrated light curve using only two modes. Decreased model complexity helps guard against overfitting.

### 2.4.2 Performance

For each of the residuals in Figure 2.5, we computed the mean depth  $\overline{\delta F}(t_i)$  of a putative 12-hour transit centered at  $t_i$  for every cadence in Q6. The distribution of  $\overline{\delta F}$  due to noise determines the minimum transit depth that can be detected by a transit search algorithm.  $\overline{\delta F}$  is computed by

$$\overline{\delta F}(t_i) = [\delta F * g](t_i)$$

where ‘\*’ denotes convolution and  $g$  is the following kernel

$$g(t_i) = \frac{1}{N_T} \left[ \underbrace{\frac{1}{2}, \dots, \frac{1}{2}}_{\text{length} = N_T}, \underbrace{-1, \dots, -1}_{\text{length} = N_T}, \underbrace{\frac{1}{2}, \dots, \frac{1}{2}}_{\text{length} = N_T} \right].$$

where  $N_T$  is 24. For each of the cotrending schemes, we computed the following statistics describing the distribution of  $\overline{\delta F}$ : standard deviation ( $\sigma$ ), 90 percentile (90 %), and 99 percentile (99 %). The standard deviation is roughly equivalent to CDPP12. Since transit search algorithms key off on peaks in  $\overline{\delta F}$ , the percentile statistics are more appropriate figures of merit. We list these statistics for KIC-8144222 in Table 2.1. Ensemble-calibrated photometry produced tighter distributions in  $\overline{\delta F}$  than the spline baseline.

### 2.4.3 Comparison to PDC

In this section, we offer some simple comparisons between TERRA and the PDC implementation of Twicken et al. (2010). This paper represents our efforts to improve upon that algorithm. The *Kepler* PDC pipeline has evolved beyond that presented in Twicken et al. (2010) culminating with PDC-MAP (Stumpe et al. 2012; Smith et al. 2012). We feel that the Twicken et al. (2010) algorithm is an important touchstone for comparison given that the most recent release of planets (Batalha et al. 2012) was based on photometry that was largely processed with the Twicken et al. (2010) algorithm.

We assess cotrending performance in the context of transit detectability. We note that PDC outputs are not directly used in transit detection. PDC light curves are subject to additional detrending (mostly of low frequency content) before the transiting planet search is run (Tenenbaum et al. 2010).

In Figure 2.6, we show fits to the KIC-8144222 photometry using 4 TERRA modes and the PDC algorithm. While PDC flattens photometry collected during the thermal transients, it injects high frequency noise into regions that are featureless in the TERRA-calibrated photometry. For KIC-8144222, the RMS scatter in the 12-hour  $\overline{\delta F}$  distribution is 24 ppm for TERRA processed photometry and 36 ppm for PDC processed photometry.

Using 4 TERRA modes, we cotrend 100 stars selected at random from our 1000-star reference ensemble. We then compute 3, 6, and 12-hour  $\overline{\delta F}$  from TERRA and PDC calibrated light curves. We then calculate the difference between the  $\sigma$ , 90%, and 99% statistics for TERRA and PDC cotrending. We show the distribution of these differences for the 12-hour

Table 2.1: Comparison of fits to KIC-8144222 photometry.

Cotrending	$\sigma$	90 %	99 %
2 PMs	24	28	53
4 PMs	24	28	53
Spline	53	66	146

Note. — Standard deviation, 90 percentile, and 99 percentile (in ppm) of the  $\overline{\delta F}$  distributions for KIC-8144222 using different cotrending schemes. The spline fit is included as a baseline since it incorporates no ensemble-based cotrending information. In computing  $\overline{\delta F}$ , we have assumed a 12-hour transit duration. All cotrending approaches yield tighter  $\overline{\delta F}$  distributions than the spline baseline.

Table 2.2: Comparison of TERRA and PDC cotrending performance for 100 stars.

Transit Width (hours)	$\sigma$		90%		99%	
	TERRA	PDC	TERRA	PDC	TERRA	PDC
3	58	60	68	76	129	141
6	43	45	50	57	97	105
12	33	37	39	47	76	88

Note. — A comparison of the  $\overline{\delta F}$  distributions using TERRA and PDC cotrending of 100 stars drawn randomly from our 1000-star sample. We have assumed a range of transit widths. We show the median values of the standard deviation, 90 percentile, and 99 percentile (in ppm) of the  $\overline{\delta F}$  distributions. For these 100 stars, TERRA yields tighter distributions of  $\overline{\delta F}$ . The improvement ranges from 8 to 12 ppm in the 99 % statistic.

$\overline{\delta F}$  in Figure 2.7. The median improvement in  $\sigma$ , 90%, and 99% using TERRA cotrending is 2.8, 6.6, and 8.7 ppm. We tabulate the median values of the  $\sigma$ , 90%, and 99% statistics in Table 2.2.

We believe that these comparisons are representative of the stars from which we constructed our reference ensemble ( $12.5 < Kp < 13.5$  and  $CDPP12 < 40$  ppm). These bright, low-noise stars are the most amenable to exoearth detection. Our comparisons do not pertain to stars with different brightness or noise level.

## 2.5 Conclusions

TERRA is a new technique for using ensemble photometry to self-calibrate instrumental systematics in *Kepler* light curves. We construct a simple noise model by running a high-pass filter and removing thermal settling events before computing principle components. For a typical  $12.5 < Kp < 13.5$  and  $CDPP12 < 40$  ppm star, TERRA produces ensemble-calibrated photometry with 33 ppm RMS scatter in 12 hour bins. With this noise level, a 100 ppm transit from an exoearth will be detected at  $\sim 3\sigma$  per transit.

A potential drawback of removing thermal settling events is discarding photometry that contains a transit. Thermal settling events amounted to 14% of the valid cadences in Q1-Q8 photometry. Since signal to noise grows as the square root of the number of transits, removing 14% of the photometry results in a 7% reduction in the signal to noise of a given transit. The completeness of the survey may decrease slightly, since some borderline transits will remain below threshold. One further complication arises due to the fact that gaps due

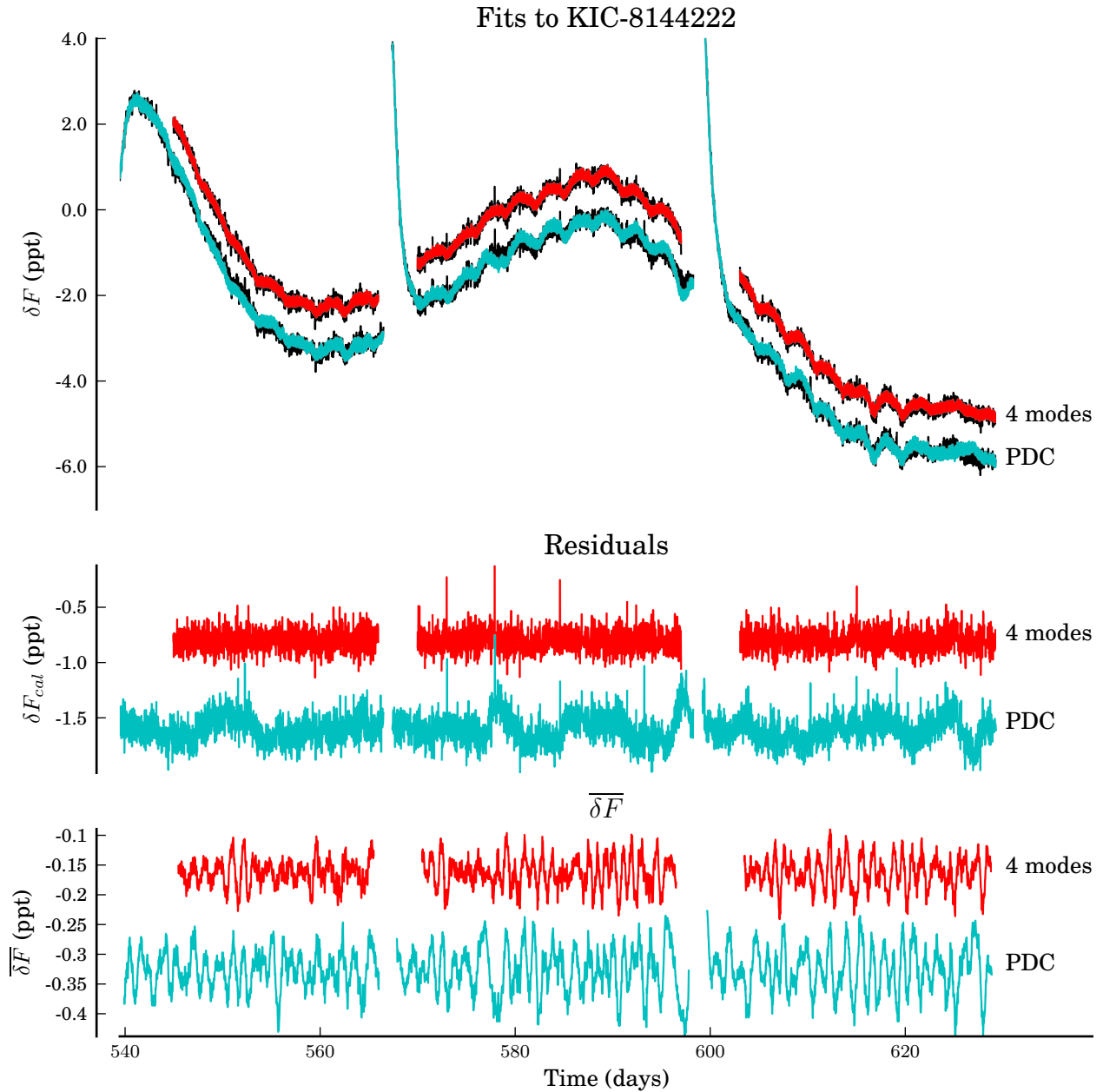


Figure 2.6: Same as Figure 2.5 except we compare fits using the 4 TERRA modes, with the PDC processed photometry. The bottom panel shows 12-hour  $\overline{\delta F}$  where smaller scatter implies greater sensitivity to small transits. The RMS scatter in the 12-hour  $\overline{\delta F}$  distribution is 24 ppm for TERRA processed photometry and 36 ppm for PDC processed photometry.

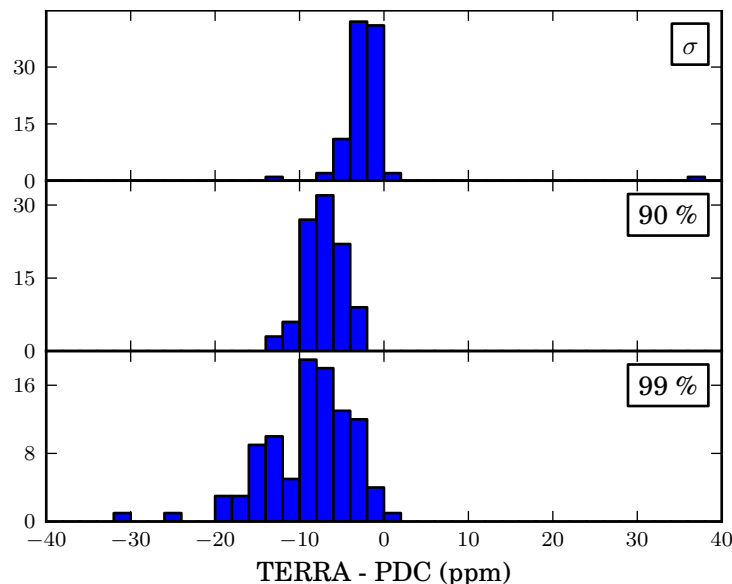


Figure 2.7: We computed the standard deviation, 90 percentile, and 99 percentile (in ppm) of 12-hour  $\overline{\delta F}$  for 100 light curves using TERRA and PDC cotrending. The histograms show the difference of the TERRA and PDC statistics. Negative values mean a tighter  $\overline{\delta F}$  distribution using our cotrending and hence a lower noise floor in a transit search.

to thermal settling occur on regular (monthly) intervals. Given the right epoch, a planet with a period that is a multiple of  $\sim 30$  days may repeatedly transit during a gap. Thus, removing gaps amounts to a more significant reduction of survey completeness for specific regions in period-epoch space.

Ensemble-based cotrending is most effective when the timescales in the ensemble are matched to the signal of interest. We are skeptical that a “one size fits all” approach exists and we encourage those who wish to get the most out of *Kepler* data to tune their cotrending to the timescale of their signals of interest.

## 3

# A Plateau in the Planet Population Below Twice the Size of Earth

A version of this chapter was previously published in the *Astrophysical Journal* (Erik A. Petigura, Geoffrey W. Marcy, & Andrew W. Howard, 2013, ApJ 770, 69).

We carry out an independent search of *Kepler* photometry for small transiting planets with sizes 0.5–8.0 times that of Earth and orbital periods between 5 and 50 days, with the goal of measuring the fraction of stars harboring such planets. We use a new transit search algorithm, TERRA, optimized to detect small planets around photometrically quiet stars. We restrict our stellar sample to include the 12,000 stars having the lowest photometric noise in the *Kepler* survey, thereby maximizing the detectability of Earth-size planets. We report 129 planet candidates having radii less than  $6 R_{\oplus}$  found in 3 years of *Kepler* photometry (quarters 1–12). Forty-seven of these candidates are not in [Batalha et al. \(2012\)](#), which only analyzed photometry from quarters 1–6. We gather Keck HIRES spectra for the majority of these targets leading to precise stellar radii and hence precise planet radii. We make a detailed measurement of the completeness of our planet search. We inject synthetic dimmings from mock transiting planets into the actual *Kepler* photometry. We then analyze that injected photometry with our TERRA pipeline to assess our detection completeness for planets of different sizes and orbital periods. We compute the occurrence of planets as a function of planet radius and period, correcting for the detection completeness as well as the geometric probability of transit,  $R_{\star}/a$ . The resulting distribution of planet sizes exhibits a power law rise in occurrence from  $5.7 R_{\oplus}$  down to  $2 R_{\oplus}$ , as found in [Howard et al. \(2012\)](#). That rise clearly ends at  $2 R_{\oplus}$ . The occurrence of planets is consistent with constant from  $2 R_{\oplus}$  toward  $1 R_{\oplus}$ . This unexpected plateau in planet occurrence at  $2 R_{\oplus}$  suggests distinct planet formation processes for planets above and below  $2 R_{\oplus}$ . We find that  $15.1^{+1.8}_{-2.7}\%$  of solar type stars—roughly one in six—has a  $1\text{--}2 R_{\oplus}$  planet with  $P = 5\text{--}50$  days.

## 3.1 Introduction

The *Kepler* Mission has discovered an extraordinary sample of more than 2300 planets with radii ranging from larger than Jupiter to smaller than Earth (Borucki et al. 2011; Batalha et al. 2012). Cleanly measuring and debiasing this distribution will be one of *Kepler*'s great legacies. Howard et al. (2012), H12 hereafter, took a key step, showing that the planet radius distribution increases substantially with decreasing planet size down to at least  $2 R_{\oplus}$ . While the distribution of planets of all periods and radii contains a wealth of information, we choose to focus on the smallest planets. Currently, only *Kepler* is able to make quantitative statements about the occurrence of planets down to  $1 R_{\oplus}$ .

The occurrence distributions in H12 were based on planet candidates<sup>1</sup> detected in the first four months of *Kepler* photometry (Borucki et al. 2011). These planet candidates were detected by a sophisticated pipeline developed by the *Kepler* team Science Operations Center (Twicken et al. 2010; Jenkins et al. 2010a).<sup>2</sup> Understanding pipeline completeness, the fraction of planets missed by the pipeline as a function of size and period, is a key component to measuring planet occurrence. Pipeline completeness can be assessed by injecting mock dimmings into photometry and measuring the rate at which injected signals are found. The completeness of the official *Kepler* pipeline has yet to be measured in this manner. This was the key reason why H12 were cautious interpreting planet occurrence under  $2 R_{\oplus}$ .

In this work, we focus on determining the occurrence of small planets. To maximize our sensitivity to small planets, we restrict our stellar sample to include only the 12,000 stars having the lowest photometric noise in the *Kepler* survey. We comb through quarters 1–12 (Q1–Q12) — 3 years of *Kepler* photometry — with a new algorithm, TERRA, optimized to detect low signal-to-noise transit events. We determine TERRA's sensitivity to planets of different periods and radii by injecting synthetic transits into *Kepler* photometry and measuring the recovery rate as a function of planet period and radius.

We describe our selection of 12,000 low-noise targets in Section 3.2. We comb their photometry for exoplanet transits with TERRA, introduced in Section 5.2. We report candidates found with TERRA (Section 3.4), which we combine with our measurement of pipeline completeness (Section 3.5) to produce debiased measurements of planet occurrence (Section 3.6). We offer some comparisons between TERRA planet candidates and those from Batalha et al. (2012) in Section 3.7 as well as occurrence measured using both catalogs in Section 3.8. We offer some interpretations of the constant occurrence rate for planets smaller than  $2 R_{\oplus}$  in Section 3.9.

---

<sup>1</sup>The term “planet candidate” is used because a handful of astrophysical phenomena can mimic a transiting planet. However, Morton & Johnson (2011), Morton (2012), and Fressin et al. (2013) have shown that the false positive rate among *Kepler* candidates is low, generally between 5% and 15%.

<sup>2</sup>Since H12, Batalha et al. (2012) added many candidates, bringing the number of public KOIs to  $> 2300$ . In addition, the *Kepler* team planet search pipeline has continued to evolve (Smith et al. 2012; Stumpe et al. 2012).

## 3.2 The Best12k Stellar Sample

We restrict our study to the best 12,000 solar type stars from the perspective of detecting transits by Earth-size planets, hereafter, the “Best12k” sample. For the smallest planets, uncertainty in the occurrence distribution stems largely from pipeline incompleteness due to the low signal-to-noise ratio (SNR) of an Earth-size transit.

Our initial sample begins with the 102,835 stars that were observed during every quarter from Q1–Q9.<sup>3</sup> From this sample, following H12, we select 73,757 “solar subset” stars that are solar-type G and K having  $T_{\text{eff}} = 4100\text{--}6100$  K and  $\log g = 4.0\text{--}4.9$  (cgs).  $T_{\text{eff}}$  and  $\log g$  values are present in the *Kepler* Input Catalog (KIC; Brown et al. 2011) which is available online.<sup>4</sup> Figure 3.1 shows the KIC-based  $T_{\text{eff}}$  and  $\log g$  values as well as the solar subset. KIC stellar parameters have large uncertainties:  $\sigma(\log g) \sim 0.4$  dex and  $\sigma(T_{\text{eff}}) \sim 200$  K (Brown et al. 2011). As we will discuss in Section 3.4, we determine stellar parameters for the majority of TERRA planet candidates spectroscopically. For the remaining cases, we use stellar parameters that were determined photometrically, but incorporated a main sequence prior (Batalha et al. 2012). After refining the stellar parameters, we find that 10 of the 129 TERRA planet candidates fall outside of the  $T_{\text{eff}} = 4100\text{--}6100$  K and  $\log g = 4.0\text{--}4.9$  (cgs) solar subset.

From the 73,757 stars that pass our cuts on  $\log g$  and  $T_{\text{eff}}$ , we choose the 12,000 lowest noise stars. *Kepler* target stars have a wide range of noise properties, and there are several ways of quantifying photometric noise. The *Kepler* team computes quantities called CDPP3, CDPP6, and CDPP12, which are measures of the photometric scatter in 3, 6, and 12 hour bins (Jenkins et al. 2010a). Since CDPP varies by quarter, we adopt the maximum 6-hour CDPP over Q1–Q9 as our nominal noise metric. We use the maximum noise level (as opposed to median or mean) because a single quarter of noisy photometry can set a high noise floor for planet detection. One may circumvent this problem by removing noisy regions of photometry, which is a planned upgrade to TERRA. Figure 3.2 shows the distribution of  $\max(\text{CDPP6})$  among the 73,757 stars considered for our sample.

In choosing our sample, we wanted to include stars amenable to the detection of planets as small as  $1 R_{\oplus}$ . We picked the 12,000 quietest stars based on preliminary completeness estimates. The noisiest star in the Best12k sample has  $\max(\text{CDPP6})$  of 79.2 ppm. We estimated that the  $\sim 100$  ppm transit of an Earth-size planet would be detected at  $\text{SNR}_{\text{CDPP}} \sim 1.25$ .<sup>5</sup> Given that Q1–Q12 contains roughly 1000 days of photometry, we expected to detect a 5-day planet at  $\text{SNR}_{\text{CDPP}} \sim 1.25 \times \sqrt{1000/5} \sim 18$  (a strong detection) and to detect a 50-day planet at  $\text{SNR}_{\text{CDPP}} \sim 1.25 \times \sqrt{1000/50} \sim 5.6$  (a marginal detection). In our detailed study of completeness, described in Section 3.5, we find that TERRA recovers most planets down to  $1 R_{\oplus}$  having  $P = 5\text{--}50$  days.

<sup>3</sup>We ran TERRA on Q1–Q12 photometry, but we selected the Best12k sample before Q10–Q12 were available.

<sup>4</sup><http://archive.stsci.edu/Kepler/kic.html>

<sup>5</sup> $\text{SNR}_{\text{CDPP}}$ , the expected SNR using the  $\max(\text{CDPP6})$  metric, is different from the SNR introduced in Section 3.3.2.  $\text{SNR}_{\text{CDPP}}$  is more similar to the SNR computed by the *Kepler* team, which adopts  $\text{SNR}_{\text{CDPP}} > 7.1$  as their detection threshold.

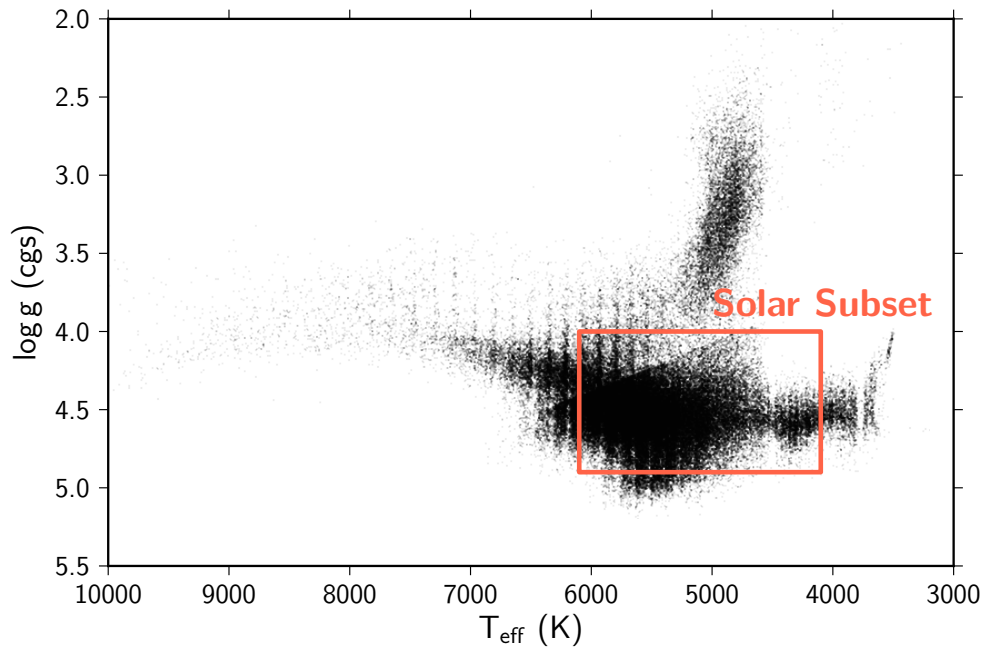


Figure 3.1: *Kepler* target stars observed every quarter from Q1–Q9. The rectangle marks the “solar subset” of stars with  $T_{\text{eff}} = 4100\text{--}6100$  K and  $\log g = 4.0\text{--}4.9$  (cgs).

We draw stars from the H12 solar subset for two reasons. First, we may compare our planet occurrence to that of H12 without the complication of varying occurrence with different stellar types. We recognize that subtle differences may exist between the H12 and Best12k stellar sample. One such difference is that the Best12k is noise-limited, while the H12 sample is magnitude-limited. H12 included bright stars with high photometric variability, which are presumably young and/or active stars. Planet formation efficiency could depend on stellar age. Planets may be less common around older stars that formed before the metallicity of the Galaxy was enriched to current levels. This work assesses planet occurrence for a set of stars that are systematically selected to be 3–10 Gyr old by virtue of their reduced magnetic activity.

The second reason for adopting the H12 solar subset is a practical consideration of our completeness study. As shown in Section 3.5, we parameterize pipeline efficiency as a function of  $P$  and  $R_P$ . Because M-dwarfs have smaller radii than G-dwarfs, an Earth-size planet dims an M-dwarf more substantially and should be easier for TERRA to detect. Thus, measuring completeness as a function of  $P$ ,  $R_P$ , and  $R_*$  (or perhaps  $P$  and  $R_P/R_*$ ) is appropriate when analyzing stars of significantly different sizes. Such extensions are beyond the scope of this paper, and we consider stars with  $R_* \sim R_\odot$ .

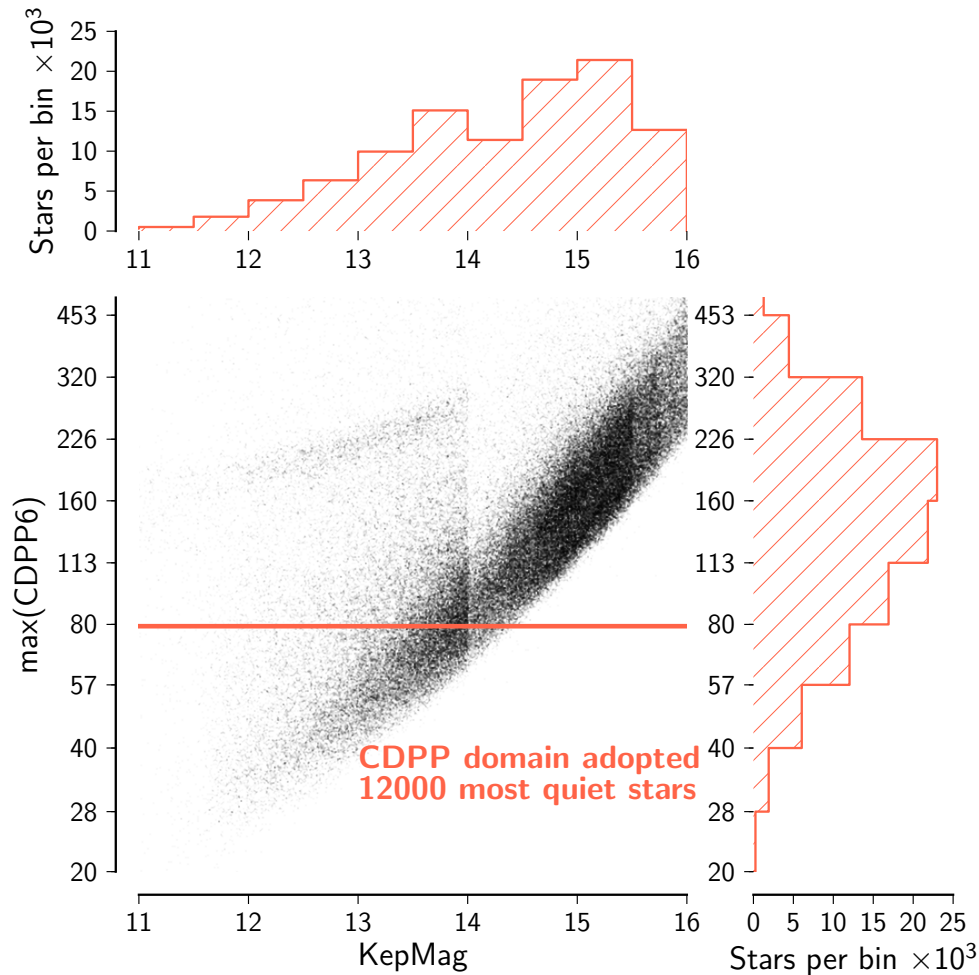


Figure 3.2: Stellar photometric noise level plotted against *Kepler* magnitude. Noise level is the maximum value of CDPP6 over Q1–Q9. Of the 73,757 stars that pass our cuts on  $T_{\text{eff}}$  and  $\log g$ , we select the 12,000 most quiet stars. The line shows  $\max(\text{CDPP6}) = 79.2$  ppm, corresponding to the noisiest star in the Best12k sample, well below the median value of 143 ppm.

### 3.3 Planet Search Pipeline

Identifying the smallest transiting planets in *Kepler* photometry requires a sophisticated automated pipeline. Our pipeline is called “TERRA” and consists of three major components. First, TERRA calibrates photometry in the time domain. Then, TERRA combs the calibrated photometry for periodic, box-shaped signals by evaluating the signal-to-noise ratio (SNR) over a finely-spaced grid in transit period ( $P$ ), epoch ( $t_0$ ) and duration ( $\Delta T$ ). Finally, TERRA fits promising signals with a [Mandel & Agol \(2002\)](#) transit model and rejects signals that are not consistent with an exoplanet transit. We review the calibration component in Section 3.3.1, but refer the reader to [Petigura & Marcy \(2012\)](#) for a detailed description. We present, for the first time, the grid-search and light curve fitting components in Sections 3.3.2 and 3.3.3.

#### 3.3.1 Photometric Calibration

We briefly review the major time domain components of TERRA; for a more complete description, please refer to [Petigura & Marcy \(2012\)](#). We begin with *Kepler* “simple aperture long cadence photometry,” which we downloaded from the Mikulski Archive for Space Telescopes (MAST). This photometry is the total photoelectrons accumulated within a pre-defined target aperture over a 29.4 minute interval ([Fraquelli & Thompson 2012](#)). We remove thermal settling events manually and cosmic rays using a median filter. Next, we remove photometric trends longer than 10 days with a high-pass filter. Finally, we identify photometric modes shared by a large ensemble of stars with using a robust principal components analysis. The optimum linear combination of the four most significant modes is removed from each light curve individually.

#### 3.3.2 Grid-based Transit Search

We then search for periodic, box-shaped signals in ensemble-calibrated photometry. Such a search involves evaluating the SNR over a finely sampled grid in period ( $P$ ), epoch ( $t_0$ ), and duration ( $\Delta T$ ), i.e.

$$\text{SNR} = \text{SNR}(P, t_0, \Delta T). \quad (3.1)$$

Our approach is similar to the widely-used BLS algorithm of [Kovács et al. \(2002\)](#) as well as to the TPS component of the *Kepler* pipeline ([Jenkins et al. 2010b](#)). BLS, TPS, and TERRA are all variants of a “matched filter” (North 1943). The way in which such an algorithm searches through  $P$ ,  $t_0$ , and  $\Delta T$  is up to the programmer. We choose to search first through  $\Delta T$  (outer loop), then  $P$ , and finally,  $t_0$  (inner loop).

For computational simplicity, we consider transit durations that are integer numbers of long cadence measurements. Since we search for transits with  $P = 5\text{--}50$  days, we try  $\Delta T = [3, 5, 7, 10, 14, 18]$  long cadence measurements, which span the range of expected transit durations, 1.5 to 8.8 hours, for G and K dwarf stars.

After choosing  $\Delta T$ , we compute the mean depth,  $\overline{\delta F}(t_i)$ , of a putative transit with duration =  $\Delta T$  centered at  $t_i$  for each cadence.  $\overline{\delta F}$  is computed via

$$\overline{\delta F}(t_i) = \sum_j F(t_{i-j})G_j \quad (3.2)$$

where  $F(t_i)$  is the median-normalized stellar flux at time  $t_i$  and  $G_j$  is the  $j$ th element of the following kernel

$$\mathbf{G} = \frac{1}{\Delta T} \left[ \underbrace{\frac{1}{2}, \dots, \frac{1}{2}}_{\Delta T}, \underbrace{-1, \dots, -1}_{\Delta T}, \underbrace{\frac{1}{2}, \dots, \frac{1}{2}}_{\Delta T} \right]. \quad (3.3)$$

As an example, if  $\Delta T = 3$ ,

$$\mathbf{G} = \frac{1}{3} \left[ \frac{1}{2}, \frac{1}{2}, \frac{1}{2}, -1, -1, -1, \frac{1}{2}, \frac{1}{2}, \frac{1}{2} \right]. \quad (3.4)$$

We search over a finely sampled grid of trial periods from 5–50 days and epochs ranging from  $t_{\text{start}}$  to  $t_{\text{start}} + P$ , where  $t_{\text{start}}$  is the time of the first photometric observation. For a given  $(P, t_0, \Delta T)$  there are  $N_T$  putative transits with depths  $\overline{\delta F}_i$ , for  $i = 0, 1, \dots, N_T - 1$ . For each  $(P, t_0, \Delta T)$  triple, we compute SNR from

$$\text{SNR} = \frac{\sqrt{N_T}}{\sigma} \text{mean}(\overline{\delta F}_i), \quad (3.5)$$

where  $\sigma$  is a robust estimate (median absolute deviation) of the noise in bins of length  $\Delta T$ .

For computational efficiency, we employ the ‘‘Fast Folding Algorithm’’ (FFA) of [Staelin \(1969\)](#) as implemented in [Petigura & Marcy \(2013; in prep.\)](#). Let  $P_{\text{cad},0}$  be a trial period that is an integer number of long cadence measurements, e.g.  $P_{\text{cad},0} = 1000$  implies  $P = 1000 \times 29.4 \text{ min} = 20.43 \text{ days}$ . Let  $N_{\text{cad}} = 51413$  be the length of the Q1-Q12 time series measured in long cadences. Leveraging the FFA, we compute SNR at the following periods:

$$P_{\text{cad},i} = P_{\text{cad},0} + \frac{i}{M-1}; \quad i = 0, 1, \dots, M-1 \quad (3.6)$$

where  $M = N_{\text{cad}}/P_{\text{cad},0}$  rounded up to the nearest power of two. In our search from 5–50 days,  $P_{\text{cad},0}$  ranges from 245–2445, and we evaluate SNR at  $\sim 10^5$  different periods. At each  $P_{\text{cad},i}$  we evaluate SNR for  $P_{\text{cad},0}$  different starting epochs. All told, for each star, we evaluate SNR at  $\sim 10^9$  different combinations of  $P$ ,  $t_0$ , and  $\Delta T$ .

Due to runtime and memory constraints, we store only one SNR value for each of the trial periods. TERRA stores the maximum SNR at that period for all  $\Delta T$  and  $t_0$ . We refer to this one-dimensional distribution of SNR as the ‘‘SNR periodogram,’’ and we show the KIC-3120904 SNR periodogram in [Figure 3.3](#) as an example. Because we search over many  $\Delta T$  and  $t_0$  at each trial period, fluctuations often give rise SNR  $\sim 8$  events and set the detectability floor in the SNR periodogram. For KIC-3120904, a star not listed in the [Batalha et al. \(2012\)](#) planet catalog, we see a SNR peak of 16.6, which rises clearly above stochastic background.

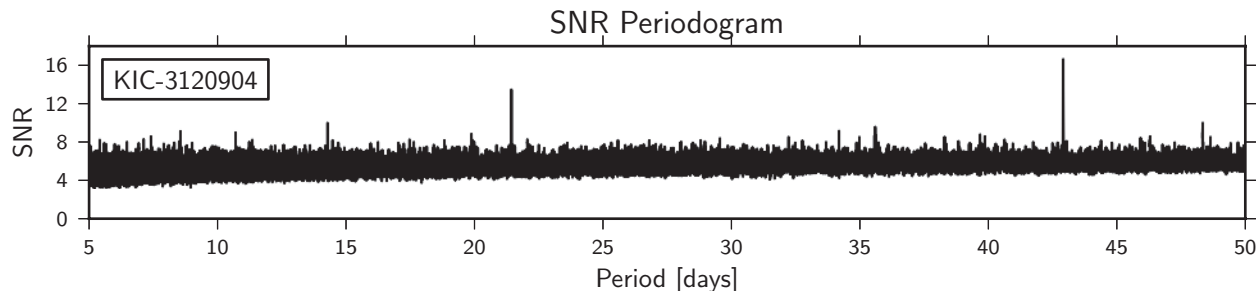


Figure 3.3: SNR periodogram of KIC-3120904 photometry. We evaluate SNR over a finely-spaced, three-dimensional grid of  $P$ ,  $t_0$ , and  $\Delta T$ . We store the maximum SNR for each trial period, resulting in a one-dimensional distribution of SNR. A planet candidate (not in [Batalha et al. 2012](#)) produces a SNR peak of 16.6 at  $P = 42.9$  days, which rises clearly above the detection floor of  $\text{SNR} \sim 8$ .

If the maximum SNR in the SNR periodogram exceeds 12, we pass that particular  $(P, t_0, \Delta T)$  on to the “data validation” (DV) step, described in the following section, for additional vetting. We chose 12 as our SNR threshold by trial and error. Note that the median absolute deviation of many samples drawn from a Gaussian distribution is 0.67 times the standard deviation, i.e.  $\sigma_{\text{MAD}} = 0.67\sigma_{\text{STD}}$ . Therefore, **TERRA**  $\text{SNR} = 12$  corresponds roughly to  $\text{SNR} = 8$  in a BLS or TPS search.

Since **TERRA** only passes the  $(P, t_0, \Delta T)$  triple with the highest SNR on to DV, **TERRA** does not detect additional planets with lower SNR due to either smaller size or longer orbital period. As an example of **TERRA**’s insensitivity to small candidates in multi-candidate systems, we show the **TERRA** SNR periodogram for KIC-5094751 in Figure 3.4. [Batalha et al. \(2012\)](#) lists two candidates belonging to KIC-5094751: KOI-123.01 and KOI-123.02 with  $P = 6.48$  and 21.22 days, respectively. Although the SNR periodogram shows two sets of peaks coming from two distinct candidates, **TERRA** only identifies the first peak. Automated identification of multi-candidate systems is a planned upgrade for **TERRA**. Another caveat is that **TERRA** assumes strict periodicity and struggles to detect low SNR transits with significant transit timing variations, i.e. variations longer than the transit duration.

### 3.3.3 Data Validation

If the SNR periodogram has a maximum SNR peak  $> 12$ , we flag the corresponding  $(P, t_0, \Delta T)$  for additional vetting. Following the language of the official *Kepler* pipeline, we refer to these triples as “threshold crossing events” (TCEs), since they have high photometric SNR, but are not necessarily consistent with an exoplanet transit. **TERRA** vets the TCEs in a step called “data validation,” again following the nomenclature of the official *Kepler* pipeline. Data validation (DV), as implemented in the official *Kepler* pipeline, is described in [Jenkins et al. \(2010a\)](#). We emphasize that **TERRA** DV does not depend on the DV component of the *Kepler* team pipeline.

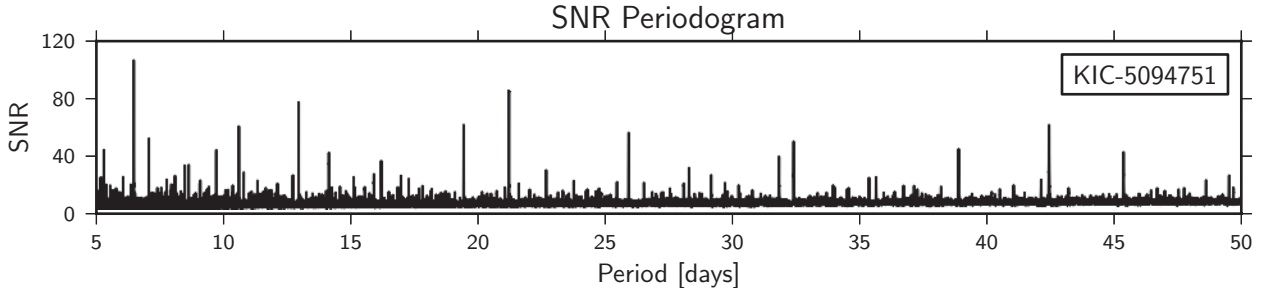


Figure 3.4: SNR periodogram of KIC-5094751 photometry, demonstrating TERRA’s insensitivity to lower SNR candidates in multi-candidate systems. [Batalha et al. \(2012\)](#) lists two planets belonging to KIC-5094751, KOI-123.01 and KOI-123.02 with  $P = 6.48$  and 21.22 days, respectively. TERRA detected KOI-123.01 with a period of 6.48 days (highest SNR peak). Sub-harmonics belonging to KOI-123.01 are visible at  $[2, 3, \dots] \times P = [13.0, 19.4, \dots]$  days. A second set of SNR peaks due to KOI-123.02 ( $P = 21.2$  days) is visible at  $[0.5, 2, \dots] \times P = [10.6, 42.4, \dots]$  days. Had we removed the transit due to KOI-123.01, KOI-123.02 would be easily detectable due its high SNR of  $\sim 80$ . TERRA does not yet include multi-candidate logic and is thus blind to lower SNR candidates in multi-candidate systems.

We show the distribution of maximum SNR for each Best12k star in Figure 3.5. Among the Best12k stars, 738 have a maximum SNR peak exceeding 12. Adopting  $\text{SNR} = 12$  as our threshold balances two competing needs: the desire to recover small planets (low SNR) and the desire to remove as many non-transit events as possible before DV (high SNR). As discussed below, only 129 out of all 738 events with  $\text{SNR} > 12$  are consistent with an exoplanet transit, with noise being responsible for the remaining 609. As shown in Figure 3.5, that number grows rapidly as we lower the SNR threshold. For example, the number of TCEs grows to 3055 with a SNR threshold of 10, dramatically increasing the burden on the DV component.

A substantial number (347) of TCEs are due to harmonics or subharmonics of TCEs outside of the  $P = 5\text{--}50$  day range and are discarded. In order to pass DV, a TCE must also pass a suite of four diagnostic metrics. The metrics are designed to test whether a light curve is consistent with an exoplanet transit. We describe the four metrics in Table 3.1 along with the criteria the TCE must satisfy in order pass DV. The metrics and cuts were determined by trial and error. We recognize that the TERRA DV metrics and cuts are not optimal and discard a small number of compelling exoplanet candidates, as discussed in Section 3.7.3. However, since we measure TERRA’s completeness by injection and recovery of synthetic transits, the sub-optimal nature of our metrics and cuts is incorporated into our completeness corrections.

Our suite of automated cuts removes all but 145 TCEs. We perform a final round of manual vetting and remove 16 additional TCEs, leaving 129 planet candidates. Most TCEs that we remove manually come from stars with highly non-stationary photometric noise properties. Some stars have small regions of photometry that exceed typical noise levels by

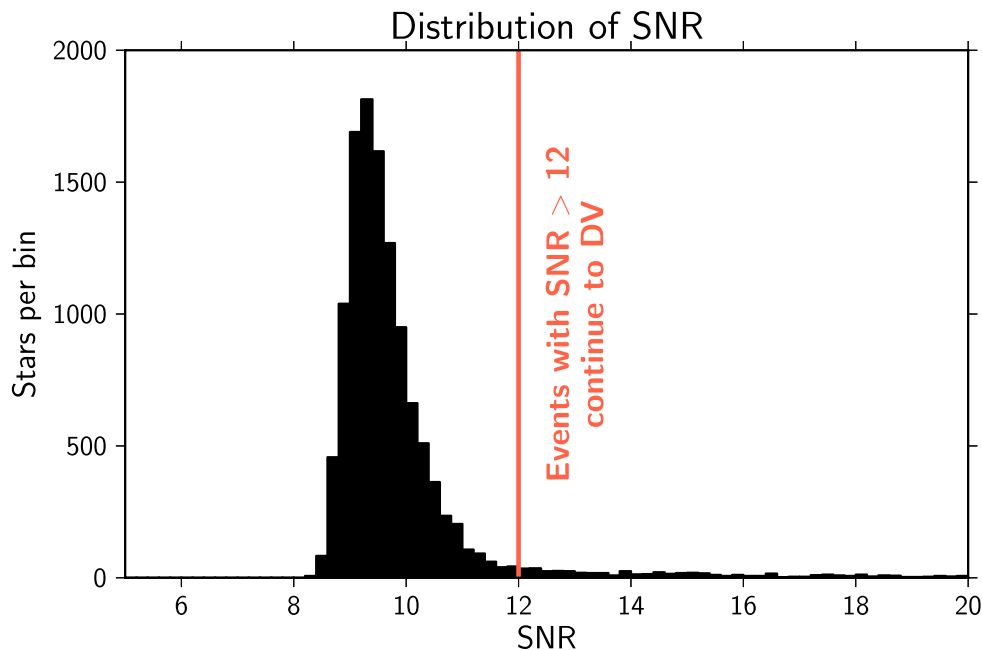


Figure 3.5: Distribution of the highest SNR peak for each star in the Best12k sample. We show SNR = 5–20 to highlight the distribution of low SNR events. The 738 stars with SNR > 12 are labeled “threshold crossing events” (TCEs) and are subjected to additional scrutiny in the “data validation” component of TERRA.

a factor of 3. We show the SNR periodogram for one such star, KIC-7592977, in Figure 3.6. Our definition of SNR (Equation 3.5) incorporates a single measure of photometric scatter based on the median absolute deviation, which is insensitive to short bursts of high photometric variability. In such stars, fluctuations readily produce SNR  $\sim 12$  events and raise the detectability floor to SNR  $\sim 12$ , up from SNR  $\sim 8$  in most stars. We also visually inspect phase-folded light curves for coherent out-of-transit variability, not caught by our automated cuts, and for evidence of a secondary eclipse.

### 3.4 Small Planets Found by TERRA

Out of the 12,000 stars in the Best12k sample, TERRA detected 129 planet candidates achieving SNR > 12 that passed our suite of DV cuts as well as visual inspection. Table 3.2 lists the 129 planet candidates. We derive planet radii using  $R_P/R_\star$  (from Mandel-Agol model fits) and  $R_\star$  from spectroscopy (when available) or broadband photometry.

We obtained spectra for 100 of the 129 stars using HIRES (Vogt et al. 1994) at the Keck I telescope with standard configuration of the California Planet Survey (Marcy et al. 2008). These spectra have resolution of  $\sim 50,000$ , at a signal-to-noise of 45 per pixel at 5500 Å.

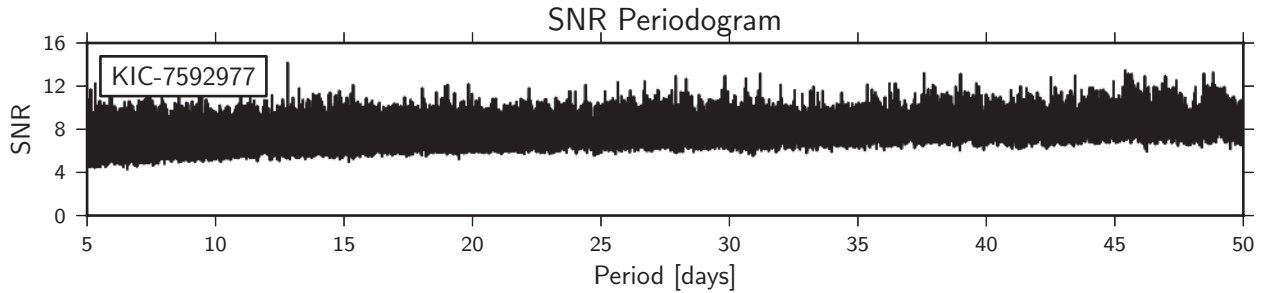


Figure 3.6: SNR periodogram of KIC-7592977, which passed the automated DV cuts, but was removed manually. KIC-7592977 photometry exhibited short bursts of high photometric scatter, which raised the noise floor to  $\text{SNR} \sim 12$ , up from  $\text{SNR} \sim 8$  as in most stars.

Table 3.1: Cuts used during data validation

name	description	value
<code>s2n_out_on_in</code>	Compelling transits have flat out-of-transit light curves. For a TCE with $(P, t_0, \Delta T)$ , we remove the transit region from the light curve and evaluate the SNR of all other $(P', t'_0, \Delta T')$ triples where $P = P'$ and $\Delta T = \Delta T'$ . <code>s2n_out_on_in</code> is the ratio of the two highest SNR events.	$< 0.7$
<code>med_on_mean</code>	Since the our definition of SNR (Equation 3.5) depends on the arithmetic mean of individual transit depths, outliers occasionally produce high SNR TCEs. For each TCE, we compute a robust SNR,	$> 1.0$
	$\text{medSNR} = \frac{\sqrt{N_T}}{\sigma} \text{median}(\overline{\delta F}_i).$	
	<code>med_on_mean</code> is <code>medSNR</code> divided by SNR as defined in Equation 3.5.	
<code>autor</code>	We compute the circular autocorrelation of the phase-folded light curve. <code>autor</code> is the ratio of the highest autocorrelation peak (at 0 lag) to the second highest peak and is sensitive to out-of-transit variability.	$> 1.6$
<code>taur</code>	We fit the phase-folded light curve with a Mandel & Agol (2002) model. <code>taur</code> is the ratio of the best fit transit duration to the maximum duration given the KIC stellar parameters and assuming a circular orbit.	$< 2.0$

We determine stellar parameters using a routine called `SpecMatch` (Howard et al. 2013, in prep). In brief, `SpecMatch` compares a stellar spectrum to a library of  $\sim 800$  spectra with  $T_{\text{eff}} = 3500\text{--}7500$  K and  $\log g = 2.0\text{--}5.0$  (determined from LTE spectral modeling). Once the target spectrum and library spectrum are placed on the same wavelength scale, we compute  $\chi^2$ , the sum of the squares of the pixel-by-pixel differences in normalized intensity. The weighted mean of the ten spectra with the lowest  $\chi^2$  values is taken as the final value for the effective temperature, stellar surface gravity, and metallicity. We estimate `SpecMatch`-derived stellar radii are uncertain to 10% RMS, based on tests of stars having known radii from high resolution spectroscopy and asteroseismology.

For 27 stars where spectra are not available, we adopt the photometrically-derived stellar parameters of Batalha et al. (2012). These parameters are taken from the KIC (Brown et al. 2011), but then modified so that they lie on the Yonsei-Yale stellar evolution models of Demarque et al. (2004). The resulting stellar radii have uncertainties of 35% (rms), but can be incorrect by a factor of 2 or more. As an extreme example, the interpretations of the three planets in the KOI-961 system (Muirhead et al. 2012) changed dramatically when HRES spectra showed the star to be an M5 dwarf ( $0.2 R_{\odot}$  as opposed to  $0.6 R_{\odot}$  listed in the KIC). We could not obtain spectra for two stars, KIC-7345248 and KIC-8429668, which were not present in Batalha et al. (2012). We determine stellar parameters for these stars by fitting the KIC photometry to Yonsei-Yale stellar models. We adopt 35% fractional errors on photometrically-derived stellar radii.

Once we determine  $P$  and  $t_0$ , we fit a Mandel & Agol (2002) model to the phase-folded photometry. Such a model has three free parameters:  $R_P/R_{\star}$ , the planet to stellar radius ratio;  $\tau$ , the time for the planet to travel a distance  $R_{\star}$  during transit; and  $b$ , the impact parameter. In this work,  $R_P/R_{\star}$  is the parameter of interest. However,  $b$  and  $R_P/R_{\star}$  are covariant, i.e. a transit with  $b$  approaching unity only traverses the limb of the star, and thus produces a shallower transit depth. In order to account for this covariance, best fit parameters were computed via Markov Chain Monte Carlo. We find that the fractional uncertainty on  $R_P/R_{\star}$ ,  $\frac{\sigma(R_P/R_{\star})}{R_P/R_{\star}}$  can be as high as 10%, but is generally less than 5%. Therefore, the error on  $R_P$  due to covariance with  $b$  is secondary to the uncertainty on  $R_{\star}$ .

We show the distribution of TERRA candidates in Figure 3.7 over the two-dimensional domain of planet radius and orbital period. Our 129 candidates range in size from  $6.83 R_{\oplus}$  to  $0.48 R_{\oplus}$  (smaller than Mars). The median TERRA candidate size is  $1.58 R_{\oplus}$ . In Figure 3.8, we show the substantial overlap between the TERRA planet sample and those produced by the *Kepler* team. TERRA recovers 82 candidates listed in Batalha et al. (2012). We discuss the significant overlap between the two works in detail in Section 3.7. As of August 8th, 2012, 10 of our TERRA candidates were listed as false positives in an internal database of *Kepler* planet candidates maintained by Jason Rowe (Jason Rowe, 2012, private communication) and are shown as blue crosses in Figure 3.8. We do not include these 10 candidates in our subsequent calculation of occurrence. Table 3.2 lists the KIC identifier, best fit transit parameters, stellar parameters, planet radius, and *Kepler* team false positive designation of all 129 candidates revealed by the TERRA algorithm. The best fit transit parameters include orbital period,  $P$ ; time of transit center,  $t_0$ ; planet to star radius ratio,  $R_P/R_{\star}$ ; time for

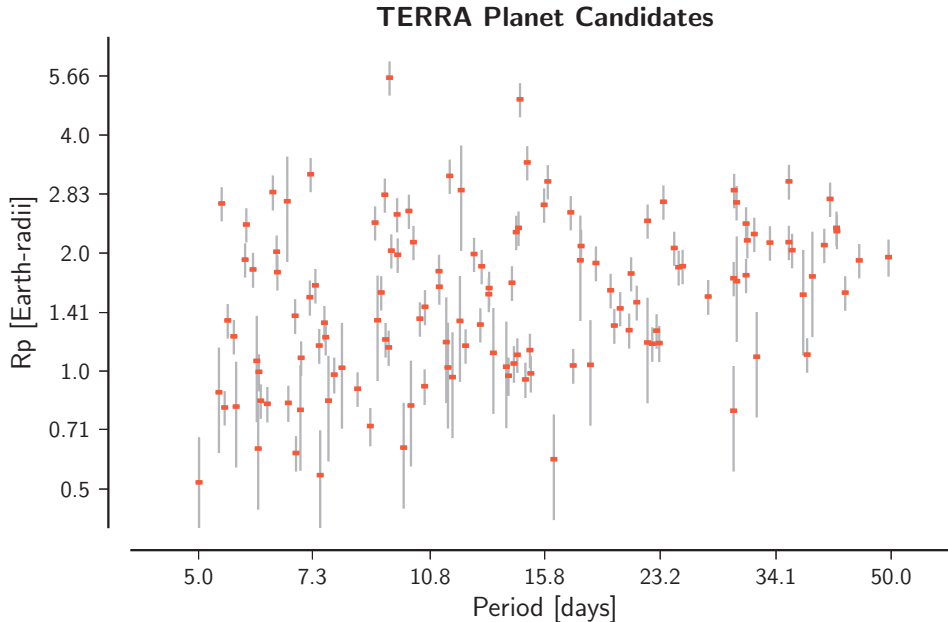


Figure 3.7: Periods and radii of 129 planet candidates detected by **TERRA**. Errors on  $R_P$  are computed via  $\frac{\sigma(R_P)}{R_P} = \sqrt{\left(\frac{\sigma(R_\star)}{R_\star}\right)^2 + \left(\frac{\sigma(R_P/R_\star)}{R_P/R_\star}\right)^2}$ , where  $R_P/R_\star$  is the radius ratio. The error in  $R_P$  stems largely from the uncertainty in stellar radii. We adopt  $\frac{\sigma(R_\star)}{R_\star} = 10\%$  for the 100 stars with spectroscopically determined  $R_\star$  and  $\frac{\sigma(R_\star)}{R_\star} = 35\%$  for the remaining stars with  $R_\star$  determined from photometry. Using MCMC, we find the uncertainty in  $R_P/R_\star$  is generally  $< 5\%$  and thus a minor component of the overall error budget.

planet to cross  $R_\star$  during transit,  $\tau$ ; and impact parameter,  $b$ . We list the following stellar properties: effective temperature,  $T_{\text{eff}}$ ; surface gravity,  $\log g$ ; and stellar radius,  $R_\star$ .

### 3.5 Completeness of Planet Catalog

When measuring the distribution of planets as a function of  $P$  and  $R_P$ , understanding the number of missed planets is as important as finding planets themselves. H12 accounted for completeness in a rough sense based on signal-to-noise considerations. For each star in their sample, they estimated the SNR over a range of  $P$  and  $R_P$  using CDPP as an estimate of the photometric noise on transit-length timescales. H12 chose to accept only planets with  $\text{SNR} > 10$  in a single quarter of photometry for stars brighter than  $K_p = 15$ . This metric used CDPP and was a reasonable pass on the data, particularly when the pipeline completeness was unknown. Determining expected SNR from CDPP does not incorporate the real noise characteristics of the photometry, but instead approximates noise

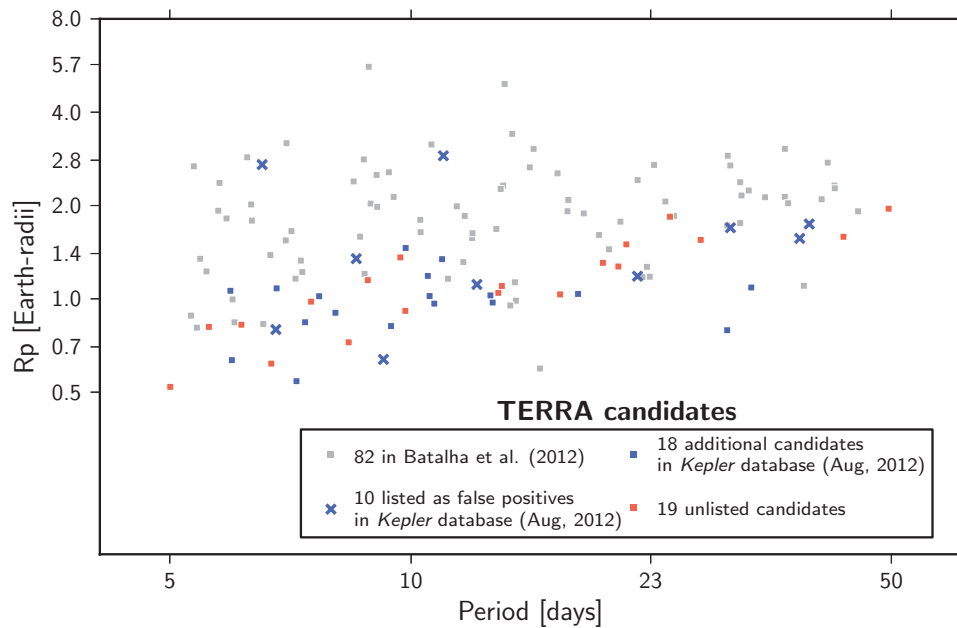


Figure 3.8: Periods and radii of all 129 TERRA planet candidates. The gray points show candidates that were listed in [Batalha et al. \(2012\)](#). The blue crosses represent candidates deemed false positives by the *Kepler* team as of August 8, 2012 (Jason Rowe, private communication 2012). These false positives are removed from our sample prior to computing occurrence. Eighteen additional candidates were listed in the same *Kepler* team database. Red points show 19 unlisted TERRA candidates.

on transit timescales as stationary (CDDP assumed to be constant over a quarter) and Gaussian distributed. Moreover, identifying small transiting planets with transit depths comparable to the noise requires a complex, multistage pipeline. Even if the integrated SNR is above some nominal threshold, the possibility of missed planets remains a concern.

We characterize the completeness of our pipeline by performing an extensive suite of injection and recovery experiments. We inject mock transits into raw photometry, run this photometry through the same pipeline used to detect planets, and measure the recovery rate. This simple, albeit brute force, technique captures the idiosyncrasies of the TERRA pipeline that are missed by simple signal-to-noise considerations.

We perform 10,000 injection and recovery experiments using the following steps:

1. We select a star randomly from the Best12k sample.
2. We draw  $(P, R_P)$  randomly from log-uniform distributions over 5–50 days and 0.5–16.0  $R_\oplus$ .
3. We draw impact parameter and orbital phase randomly from uniform distributions ranging from 0 to 1.
4. We generate a [Mandel & Agol \(2002\)](#) model.
5. We inject it into the “simple aperture photometry” of the selected star.

We then run the calibration, grid-based search, and data validation components of TERRA (Sections 3.3.1, 3.3.2, and 3.3.3) on this photometry and calculate the planet recovery rate. We do not, however, perform the visual inspection described in Section 3.3.3. An injected transit is considered recovered if the following two criteria are met: (1) The highest SNR peak passes all DV cuts and (2) the output period and epoch are consistent with the injected period and epoch to within 0.01 and 0.1 days, respectively.

Figure 6.12 shows the distribution of recovered simulations as a function of period and radius. Nearly all simulated planets with  $R_P > 1.4 R_\oplus$  are recovered, compared to almost none with  $R_P < 0.7 R_\oplus$ . Pipeline completeness is determined in small bins in  $(P, R_P)$ -space by dividing the number of successfully recovered transits by the total number of injected transits in a bin-by-bin basis. This ratio is TERRA’s recovery rate of putative planets within the Best12k sample. Thus, our quoted completeness estimates only pertain to the low photometric noise Best12k sample. Had we selected an even more rarified sample, e.g. the “Best6k,” the region of high completeness would extend down toward smaller planets.

## 3.6 Occurrence of Small Planets

Following H12, we define planet occurrence,  $f$ , as the fraction of a defined population of stars having planets within a domain of planet radius and period, including all orbital inclinations. TERRA, however, is only sensitive to one candidate (highest SNR) per system,

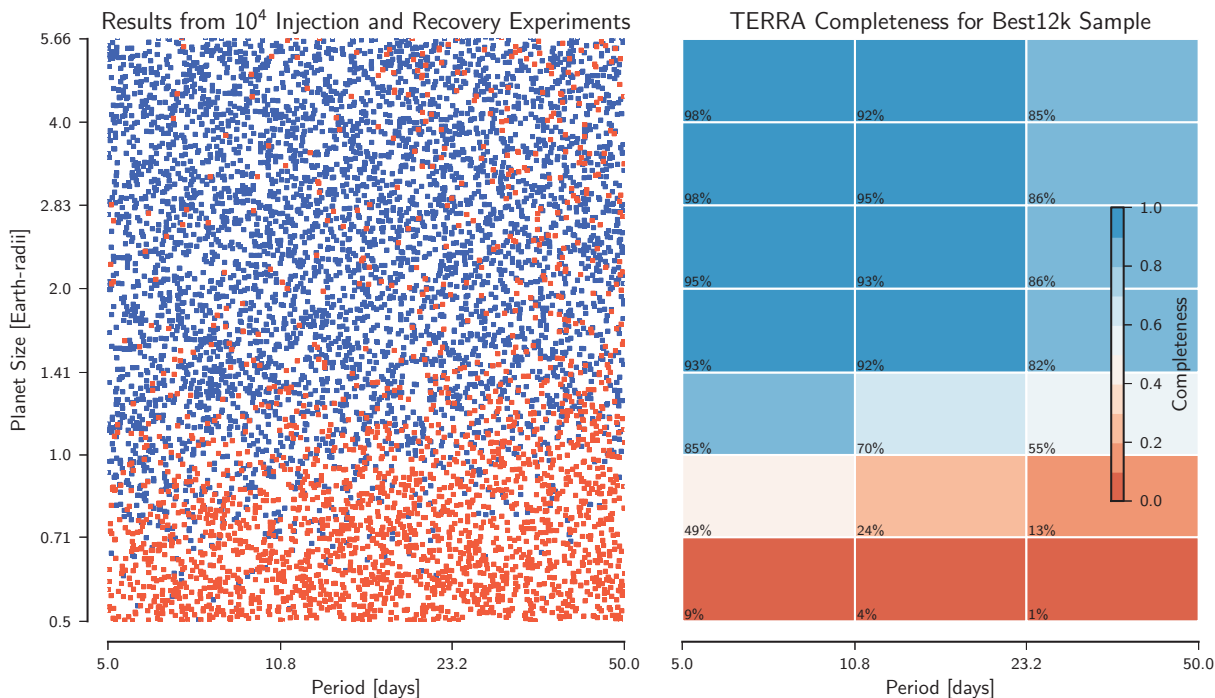


Figure 3.9: Results from the injection and recovery of 10,000 synthetic transit signals into actual photometry of randomly selected stars from our Best12k stellar sample. Each point represents the planet radius and orbital period of a mock transiting planet. The blue points represent signals that passed the DV post-analysis and where **TERRA** recovers the correct period and epoch. Signals that did not pass DV and/or were not successfully recovered, are shown as red points. Pipeline completeness is simply the number of blue points divided by the total number of points in each bin. The figure shows that for planet sizes above  $1.0 R_{\oplus}$ , our pipeline discovers over 50% of the injected planets, and presumably accomplishes a similar success rate for actual transiting planets. The completeness for planets larger than  $1 R_{\oplus}$  is thus high enough to compute planet occurrence for such small planets, with only moderate completeness corrections needed (less than a factor of 2). Note that we are measuring the recovery rate of putative planets in the Best12k sample with **TERRA**. Had we selected a lower noise stellar sample, for example the “Best6k,” the region of high completeness would extend to even small radii.

so we report occurrence as the fraction of stars with *one or more* planets with  $P = 5\text{--}50$  days. Our occurrence measurements apply to the Best12k sample of low-noise, solar-type stars described in Section 3.2.

In computing planet occurrence in the Best12k sample, we follow the prescription in H12 with minor modifications. Notably, we have accurate measures of detection completeness described in the previous section. In contrast, H12 estimated completeness based on the presumed signal-to-noise of the transit signal, suffering both from approximate characterization of photometric noise using CDPP and from poor knowledge of the efficiency of the planet-finding algorithm for all periods and sizes.

For each  $P\text{--}R_P$  bin, we count the number of planet candidates,  $n_{\text{pl,cell}}$ . Each planet that transits represents many that do not transit given the orientation of their orbital planes with respect to *Kepler's* line of sight. Assuming random orbital alignment, each observed planet represents  $a/R_\star$  total planets when non-transiting geometries are considered. For each cell, we compute the number of augmented planets,  $n_{\text{pl,aug,cell}} = \sum_i a_i/R_{\star,i}$ , which accounts for planets with non-transiting geometries. We then use Kepler's 3<sup>rd</sup> law together with  $P$  and  $M_\star$  to compute  $a/R_\star$  assuming a circular orbit.<sup>6</sup>

To compute occurrence, we divide the number of stars with planets in a particular cell by the number of stars amenable to the detection of a planet in a given cell,  $n_{\star,\text{amen}}$ . This number is just  $N_\star = 12,000$  times the completeness, computed in our Monte Carlo study. The debiased fraction of stars with planets per  $P\text{--}R_P$  bin,  $f_{\text{cell}}$ , is given by  $f_{\text{cell}} = n_{\text{pl,aug,cell}}/n_{\star,\text{amen}}$ . We show  $f_{\text{cell}}$  on the  $P\text{--}R_P$  plane in Figure 3.10 as a color scale. We also compute  $d^2 f_{\text{cell}}/d \log P/d \log R_P$ , i.e. planet occurrence divided by the logarithmic area of each cell, which is a measure of occurrence which does not depend on bin size. We annotate each  $P\text{--}R_P$  bin of Figure 3.10 with the corresponding value of  $n_{\text{pl,cell}}$ ,  $n_{\text{pl,aug,cell}}$ ,  $f_{\text{cell}}$ , and  $d^2 f_{\text{cell}}/d \log P/d \log R_P$ .

Due to the small number of planets in each cell, errors due to counting statistics alone are significant. We compute Poisson errors on  $n_{\text{pl,cell}}$  for each cell. Errors on  $n_{\text{pl,aug,cell}}$ ,  $f_{\text{cell}}$ , and  $d^2 f_{\text{cell}}/d \log P/d \log R_P$  include only the Poisson errors from  $n_{\text{pl,cell}}$ . There is also shot noise associated with the Monte Carlo completeness correction due to the finite number of simulated planets in each  $P\text{--}R_P$  cell, but such errors are small compared to errors on  $n_{\text{pl,cell}}$ . The orbital alignment correction,  $a/R_\star$ , is also uncertain due to imperfect knowledge of stellar radii and orbital separations. We do not include such errors in our occurrence estimates.

Of particular interest is the distribution of planet occurrence with  $R_P$  for all periods. We marginalize over  $P$  by summing occurrence over all period bins from 5 to 50 days. The distribution of radii shown in Figure 3.11 shows a rapid rise in occurrence from  $8.0$  to  $2.8 R_\oplus$ . H12 also observed a rising occurrence of planets down to  $2.0 R_\oplus$ , which they modeled as a power law. *Planet occurrence is consistent with a flat distribution from  $2.8$  to  $1.0 R_\oplus$ , ruling out a continuation of a power law increase in occurrence for planets smaller than  $2.0 R_\oplus$ . We find  $15.1^{+1.8}_{-2.7}\%$  of Sun-like stars harbor a  $1.0\text{--}2.0 R_\oplus$  planet with  $P = 5\text{--}50$  days.*

<sup>6</sup>H12 determined  $a/R_\star$  directly from light curve fits, but found little change when computing occurrence from  $a/R_\star$  using Kepler's third law.

Including larger planets, we find that  $24.8_{-3.4}^{+2.1}\%$  of stars harbor a planet larger than Earth with  $P = 5\text{--}50$  days. Occurrence values assuming a 100% efficient pipeline are shown as gray bars in Figure 3.11. The red bars show the magnitude of our completeness correction. Even though TERRA detects many planets smaller than  $1.0 R_{\oplus}$ , we do not report occurrence for planets smaller than Earth since pipeline completeness drops abruptly below 50%.

We show planet occurrence as a function of orbital period in Figure 3.12. In computing this second marginal distribution, we include radii larger than  $1 R_{\oplus}$  so that corrections due to incompleteness are small. Again, as in Figure 3.11, gray bars represent uncorrected occurrence values while red bars show our correction to account for planets that TERRA missed. Planet occurrence rises as orbital period increases from 5.0 to 10.8 days. Above 10.8 days, planet occurrence is nearly constant per logarithmic period bin with a slight indication of a continued rise. This leveling off of the distribution was noted by H12, who considered  $R_P > 2.0 R_{\oplus}$ . We fit the distribution of orbital periods for  $R_P > 1.0 R_{\oplus}$  with two power laws of the form

$$\frac{df}{d \log P} = k_P P^{\alpha}, \quad (3.7)$$

where  $\alpha$  and  $k_P$  are free parameters. We find best fit values of  $k_P = 0.185_{-0.035}^{+0.043}$ ,  $\alpha = 0.16 \pm 0.07$  for  $P = 5\text{--}10.8$  days and  $k_P = 8.4_{-0.8}^{+0.9} \times 10^{-3}$ ,  $\alpha = 1.35 \pm 0.05$  for  $P = 10.8\text{--}50$  days. We note that  $k_P$  and  $\alpha$  are strongly covariant. Extrapolating the latter fit speculatively to  $P > 50$  days, we find  $41.7_{-5.9}^{+6.8}\%$  of Sun-like stars host a planet  $1 R_{\oplus}$  or larger with  $P = 50\text{--}500$  days.

## 3.7 Comparison of TERRA and Batalha et al. (2012) Planet Catalogs

Here, we compare our candidates to those of Batalha et al. (2012). Candidates were deemed in common if their periods agree to within 0.01 days. We list the union of the TERRA and Batalha et al. (2012) catalogs in Table 3.4. Eighty-two candidates appear in both catalogs (Section 3.7.1), 47 appear in this work only (Section 3.7.2), and 33 appear in Batalha et al. (2012) only (Section 3.7.3). We discuss the significant overlap between the two catalogs and explain why some candidates were detected by one pipeline but not the other.

### 3.7.1 Candidates in Common

Eighty-two of our candidates appear in the Batalha et al. (2012) catalog. We show these candidates in  $P$ - $R_P$  space in Figure 3.8 as grey points. TERRA detected no new candidates with  $R_P > 2 R_{\oplus}$ . This agreement in detected planets having  $R_P > 2 R_{\oplus}$  demonstrates high completeness for such planets in both pipelines for this sample of quiet stars. This is not very surprising since candidates with  $R_P > 2 R_{\oplus}$  have high SNR, e.g. min, median, and max SNR = 19.3, 71.5, and 435 respectively.

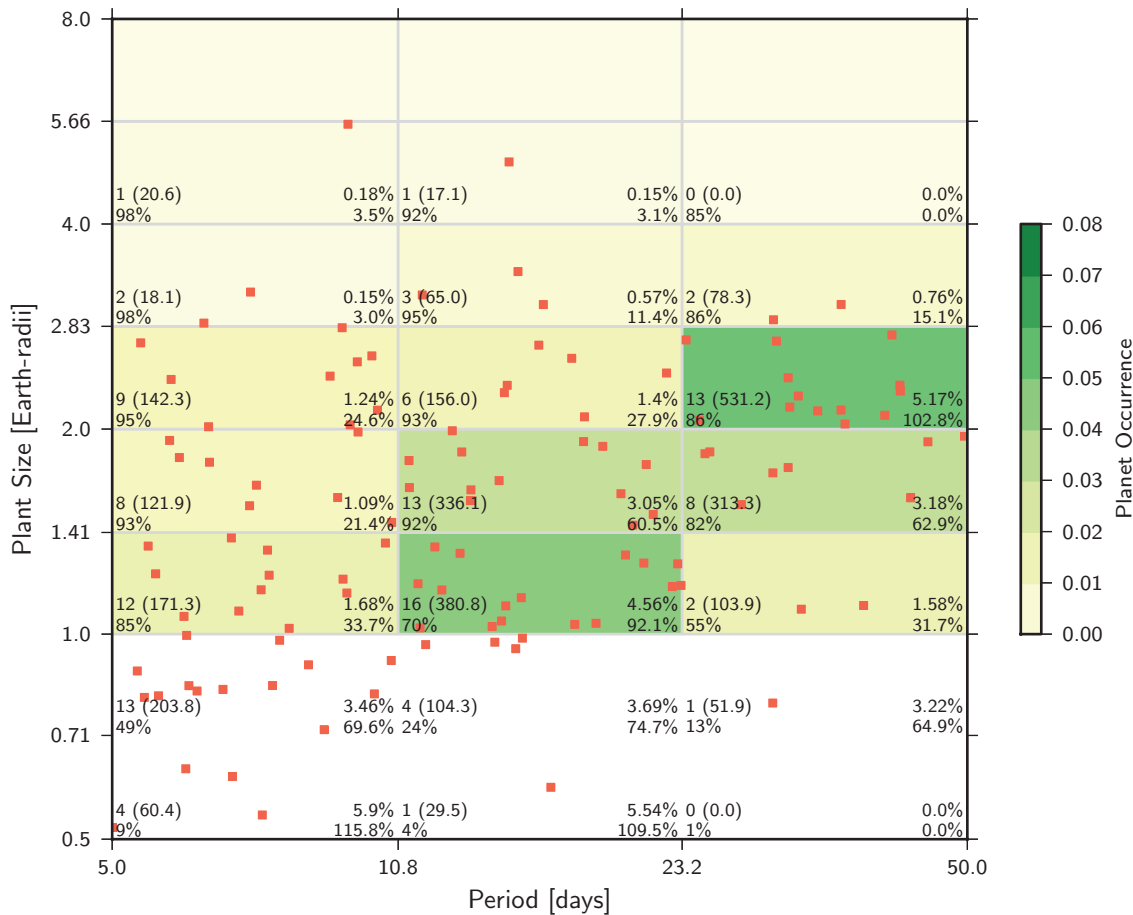


Figure 3.10: Planet occurrence as a function of orbital period and planet radius for  $P = 5\text{--}50$  days and  $R_P = 0.5\text{--}8 R_{\oplus}$ . **TERRA** planet candidates are shown as red points. Cell occurrence,  $f_{\text{cell}}$ , is given by the color scale. We quote the following information for each cell: Top left—number of planets (number of augmented planets); lower left—completeness; top right—fractional planet occurrence,  $f_{\text{cell}}$ ; bottom right—normalized planet occurrence,  $d^2 f_{\text{cell}}/d \log P/d \log R_P$ . We do not color cells where the completeness is less than 50% (i.e. the completeness correction is larger than a factor of 2).

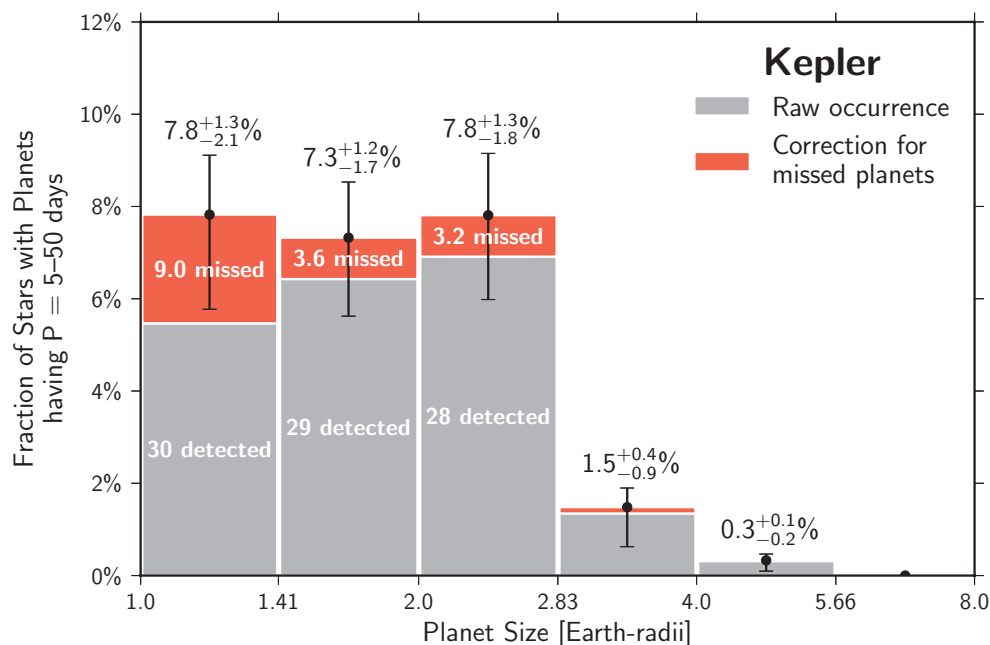


Figure 3.11: Distribution of planet occurrence for  $R_P$  ranging from 1.0 to 8.0  $R_\oplus$ . We quote the fraction of Sun-like stars harboring a planet with  $P = 5\text{--}50$  days for each  $R_P$  bin. We observe a rapid rise in planet occurrence from 8.0 down to 2.8  $R_\oplus$ , as seen in H12. Below 2.8  $R_\oplus$ , the occurrence distribution is consistent with flat. This result rules out a power law increase in planet occurrence toward smaller radii. Adding up the two smallest radius bins, we find  $15.1^{+1.8\%}_{-2.7\%}$  of Sun-like stars harbor a 1.0–2.0  $R_\oplus$  planet within  $\sim 0.25$  AU. To compute occurrence as a function of  $R_P$ , we simply sum occurrence rates for all period bins shown in Figure 3.10. Errors due to counting statistics are computed by adding errors from each of the three period bins in quadrature. The gray portion of the histogram shows occurrence values before correcting for missed planets due to pipeline incompleteness. Our correction to account for missed planets is shown in red, and is determined by the injection and recovery of synthetic transits described in Section 3.5. We do not show occurrence values where the completeness is  $< 50\%$ .

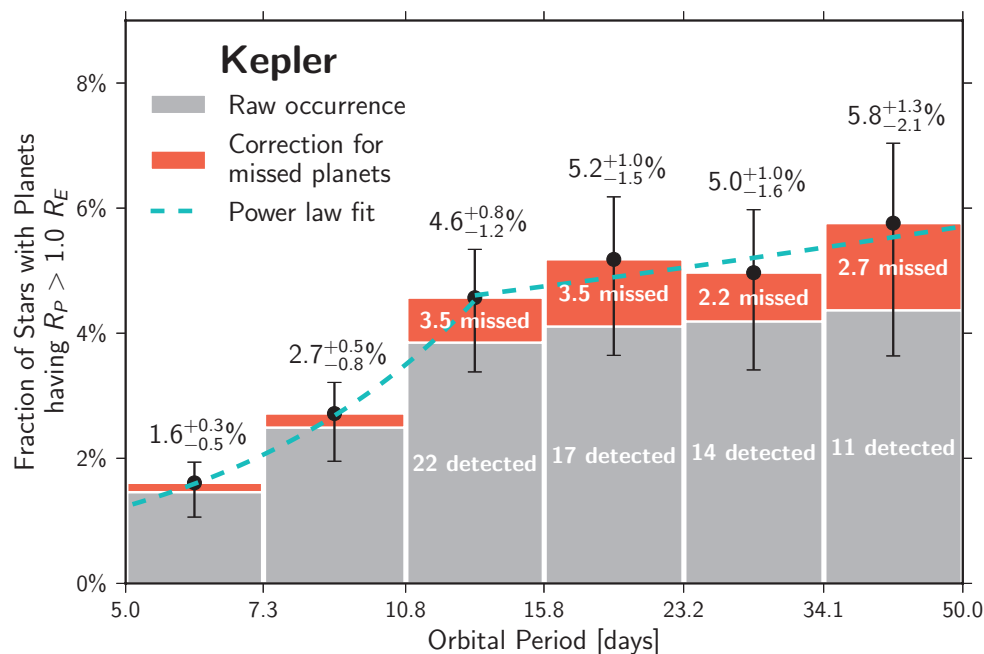


Figure 3.12: Distribution of planet occurrence for different orbital periods ranging from 5 to 50 days. We quote the fraction of Sun-like stars with a planet Earth-size or larger as a function of orbital period. We observe a gradual rise in occurrence from 5.0 to 10.8  $R_{\oplus}$  followed by a leveling off for longer orbital periods. H12 observed a similar leveling off in their analysis which included planets larger than 2  $R_{\oplus}$ . We fit the domains above and below 10.8  $R_{\oplus}$  separately with power laws,  $df/d\log P = k_P P^{\alpha}$ . We find best fit values of  $k_P = 0.185^{+0.043}_{-0.035}$ ,  $\alpha = 0.16 \pm 0.07$  for  $P = 5\text{--}10.8$  days and  $k_P = 8.4^{+0.9}_{-0.8} \times 10^{-3}$ ,  $\alpha = 1.35 \pm 0.05$  for  $P = 10.8\text{--}50$  days. Speculatively, we extrapolate the latter power law fit another decade in period and estimate  $41.7^{+6.8}_{-5.9}\%$  of Sun-like stars harbor a planet Earth-size or larger with  $P = 50\text{--}500$  days. As in Figure 3.11, the gray portion of the histogram shows uncorrected occurrence while the red region shows our correction for pipeline incompleteness. Note that the number of detected planets decreases as  $P$  increases from 10.8 to 50 days, while occurrence remains nearly constant. At longer periods, the geometric transit probability is lower, and each detected planet counts more toward  $df/d\log P$ .

Radii for the 82 planets in common were fairly consistent between [Batalha et al. \(2012\)](#) and this work. The two exceptions were KIC-8242434 and KIC-8631504. Using `SpecMatch`, we find stellar radii of 0.68 and 0.72  $R_{\odot}$ , respectively, down from 1.86 and 1.80  $R_{\odot}$  in [Batalha et al. \(2012\)](#). The revised planet radii are smaller by over a factor of two. Radii for the other planets in common were consistent to  $\sim 20\%$ .

### 3.7.2 TERRA Candidates Not in [Batalha et al. \(2012\)](#) Catalog

TERRA revealed 47 planet candidates that did not appear in [Batalha et al. \(2012\)](#). Such candidates are colored blue and red in Figure 3.8. Many of these new detections likely stem from the fact that we use twice the photometry that was available to [Batalha et al. \(2012\)](#). To get a sense of how additional photometry improves the planet yield of the *Kepler* pipeline beyond [Batalha et al. \(2012\)](#), we compared the TERRA candidates to the *Kepler* team KOI list dated August 8, 2012 (Jason Rowe, private communication). The 28 candidates in common between the August 8, 2012 *Kepler* team sample and this work are colored blue in Figure 3.8. Of these 28 candidates, 10 are listed as false positives and denoted as crosses in Figure 3.8.

We announce 37 new planet candidates with respect to [Batalha et al. \(2012\)](#) that were not listed as false positives in the *Kepler* team sample. These 37 candidates, all with  $R_P \lesssim 2 R_{\oplus}$ , are a subset of those listed in Table 3.2. As a convenience, we show this subset in Table 3.3. We remind the reader that all photometry used in this work is publicly available. We hope that interested readers will fold the photometry on the ephemeris in Table 3.2 and assess critically whether a planet interpretation is correct. As a quick reference, we have included plots of the transits of the 37 new candidates from Table 3.3 in the appendix (Figures 3.17 and 3.18). We do not claim that our additional candidates bring pipeline completeness to unity for planets with  $R_P \lesssim 2 R_{\oplus}$ . As shown in Section 3.5, our planet sample suffers from significant incompleteness in the same  $P$ - $R_P$  space where most of the new candidates emerged.

### 3.7.3 [Batalha et al. \(2012\)](#) Candidates Not in TERRA catalog

There are 33 planet candidates in the [Batalha et al. \(2012\)](#) catalog from Best12k stars that TERRA missed. Of these, 28 are multi-candidate systems where one component was identified by TERRA. TERRA is currently insensitive to multiple planet systems (as described in Section 3.3.2). TERRA missed the remaining 5 [Batalha et al. \(2012\)](#) candidates for the following reasons:

- 2581.01 : A bug in the pipeline prevented successful photometric calibration (Section 3.3.1). This bug affected 19 out of 12,000 stars in the Best12k sample.
- 70.01, 111.01, 119.01 : Failed one of the automated DV cuts (`taur`, `med_on_mean`, and `taur`, respectively). We examined these three light curves in the fashion described in Section 3.3.3, and we determined these light curves were consistent with an exoplanet transit. The fact that DV is discarding compelling transit signals decreases TERRA's

overall completeness. Computing DV metrics and choosing the optimum cuts is an art. There is room for improvement here.

- KOI-1151.01 : Period misidentified in [Batalha et al. \(2012\)](#). In [Batalha et al. \(2012\)](#) KOI-1151.01 is listed with with a  $P = 5.22$  days. TERRA found a candidate with  $P = 10.43$  days. Figure 3.13 shows phase-folded photometry with the TERRA ephemeris. A period of 5.22 days would imply dimmings in regions where the light curve is flat.

We plot the 33 total candidates listed in [Batalha et al. \(2012\)](#), but not found by TERRA in Figure 3.14. We highlight the 5 missed candidates that cannot be explained by the fact that they are a lower SNR candidate in a multi-candidate system. TERRA is blind to planets in systems with another planet with higher SNR. Figure 3.14 shows that most of these missed planets occur at  $R_P < 1.4 R_\oplus$ .

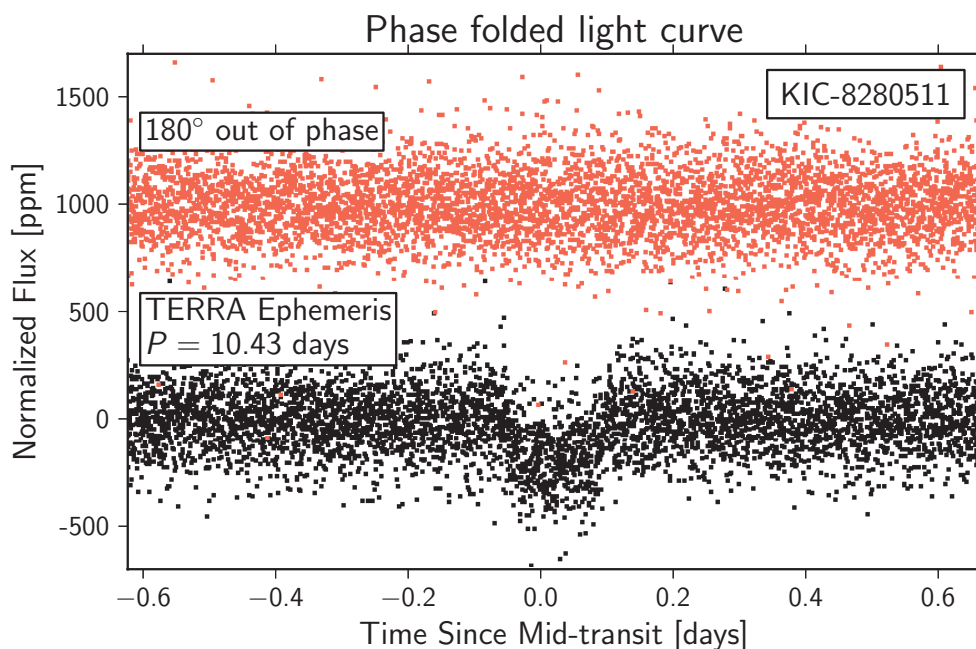


Figure 3.13: Phase-folded photometry of KIC-8280511 folded on the correct 10.43 day period found by TERRA. KOI-1151.01 is listed with  $P = 5.22$  days in [Batalha et al. \(2012\)](#). If the transit was truly on the 5.22 day period, we should see a transit of equal depth 180 degrees out of phase. KOI-1151.01 is listed in [Batalha et al. \(2012\)](#) with half its true period.

### 3.8 Occurrence with Planet Multiplicity Included

While the TERRA planet occurrence measurement benefits from well-characterized completeness, it does not include the contribution of multis to overall planet occurrence. As

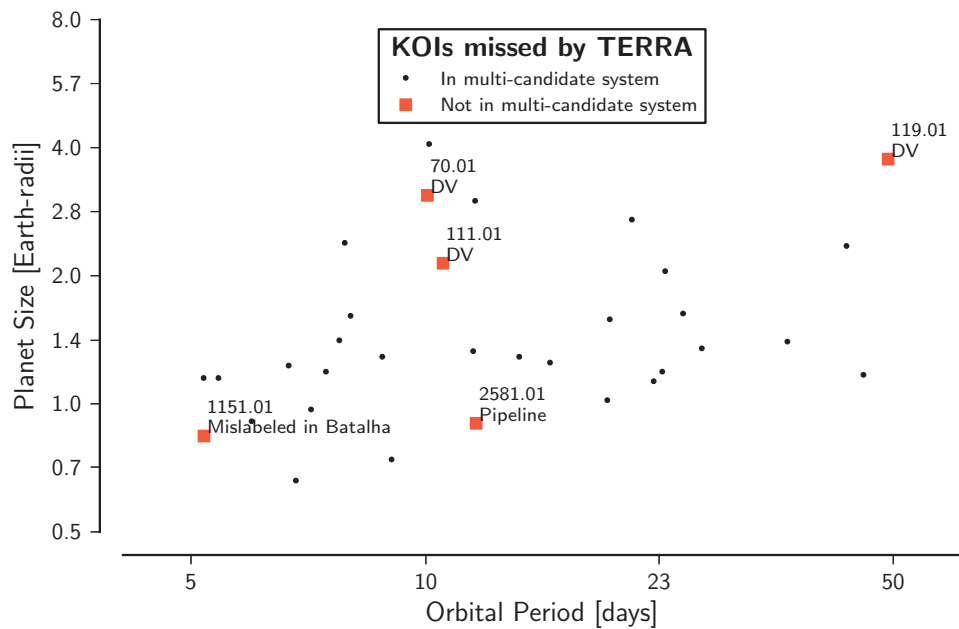


Figure 3.14:  $P$  and  $R_P$  for the 33 candidates present in [Batalha et al. \(2012\)](#) but not found by TERRA. The small symbols show the candidates in multi-planet systems. TERRA is blind to such candidates. The 5 larger symbols show the other failure modes of TERRA: 2581.01 failed due to a pipeline bug; 70.01, 111.01, and 119.01 did not pass DV; and TERRA missed KOI-1151.01 because it is listed in [Batalha et al. \(2012\)](#) with the incorrect period. Most of the missed planets have  $R_P < 1.4 R_{\oplus}$ .

discussed in Sections 3.3.2 and 3.7.3, TERRA only detects the highest SNR candidate for a given star. Here, we present planet occurrence including multis from Batalha et al. (2012). Thus, the occurrence within a bin,  $f$ , in this section should be interpreted as the *average number of planets* per star with  $P = 5\text{--}50$  days. The additional planets from Batalha et al. (2012) raise the occurrence values somewhat over those of the previous section. However, the rise and plateau structure remains the same.

We compute  $f_{\text{cell}}$  from the 32 candidates present in Batalha et al. (2012), but not found by TERRA (mislabelled KOI-1151.01 was not included). For clarity, we refer to this separate occurrence calculation as  $f_{\text{cell,Batalha}}$ . Because the completeness of the *Kepler* pipeline is unknown, we apply no completeness correction. This assumption of 100% completeness is certainly an overestimate, but we believe that the sensitivity of the *Kepler* pipeline to multis is nearly complete for  $R_P > 1.4 R_{\oplus}$ . TERRA has  $> 80\%$  completeness for  $R_P > 1.4 R_{\oplus}$  because planets in that size range with  $P = 5\text{--}50$  days around Best12k stars have high SNR. The *Kepler* pipeline should also be detecting these high SNR candidates. Also, once a KOI is found, the *Kepler* team reprocesses the light curve for additional transits (Jason Rowe, private communication). Due to this additional scrutiny, we believe that the *Kepler* completeness for multis is higher than for singles, all else being equal.

We then add  $f_{\text{cell,Batalha}}$  to  $f_{\text{cell}}$  computed in the previous section. We show occurrence computed using TERRA and Batalha et al. (2012) planets as a function of  $P$  and  $R_P$  in Figure 3.15 and as a function of only  $R_P$  in Figure 3.16. The 32 additional planets from Batalha et al. (2012) do not change the overall shape of the occurrence distribution: rising from 4.0 to 2.8  $R_{\oplus}$  and consistent with flat from 2.8 down to 1.0  $R_{\oplus}$ .

H12 fit occurrence for  $R_P > 2 R_{\oplus}$  with a power law,

$$\frac{df}{d \log R_P} = k_R R_P^{\alpha}, \quad (3.8)$$

finding  $\alpha = -1.92 \pm 0.11$  and  $k_R = 2.9_{-0.4}^{+0.5}$  (Section 3.1 of H12). As a point of comparison, we plot the H12 power law over our combined occurrence distribution in Figure 3.16. The fit agrees qualitatively for  $R_P > 2 R_{\oplus}$ , but not within errors. We expect the H12 fit to be  $\sim 25\%$  higher than our occurrence measurements since H12 included planets with  $P < 50$  days (not  $P = 5\text{--}50$  days). Additional discrepancies could stem from different characterizations of completeness, reliance on photometric versus spectroscopic measurements of  $R_{\star}$ , and magnitude-limited, rather than noise-limited, samples.

## 3.9 Discussion

### 3.9.1 TERRA

We implement in this work a new pipeline for the detection of transiting planets in *Kepler* photometry and apply it to a sample of 12,000 G and K-type dwarfs stars chosen to be among the most photometrically quiet of the *Kepler* target stars. These low noise stars offer the

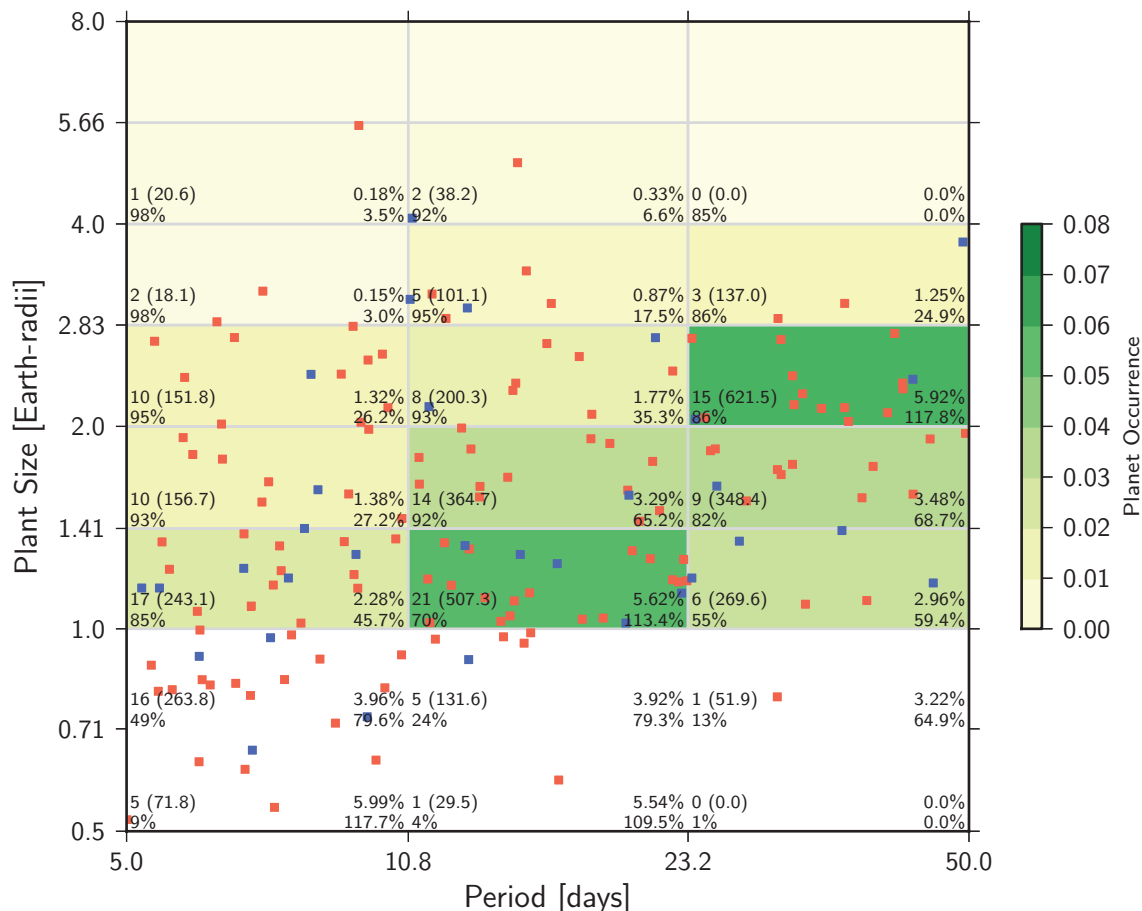


Figure 3.15: As in Figure 3.10, red points show 119 TERRA-detected planets. Blue points represent additional planets from Batalha et al. (2012). Most (28 out of 32) of these new candidates are planets in multi-candidate systems where TERRA successfully identifies the higher SNR candidate. We apply no completeness correction to these new planets, and we believe this is appropriate for  $R_P > 1.4 R_{\oplus}$ . We quote the following occurrence information for each cell: Top left—number of planets (number of augmented planets), lower left—completeness, top right—fractional planet occurrence  $f_{\text{cell}}$ , bottom right—normalized planet occurrence  $d^2 f_{\text{cell}} / (d \log P / d \log R_P)$ . We do not color cells where the completeness is less than 50% (i.e. the completeness correction is larger than a factor of 2). The planet counts and occurrence values are for the combined TERRA and Batalha et al. (2012) sample. The completeness values are the same as in Figure 3.10.

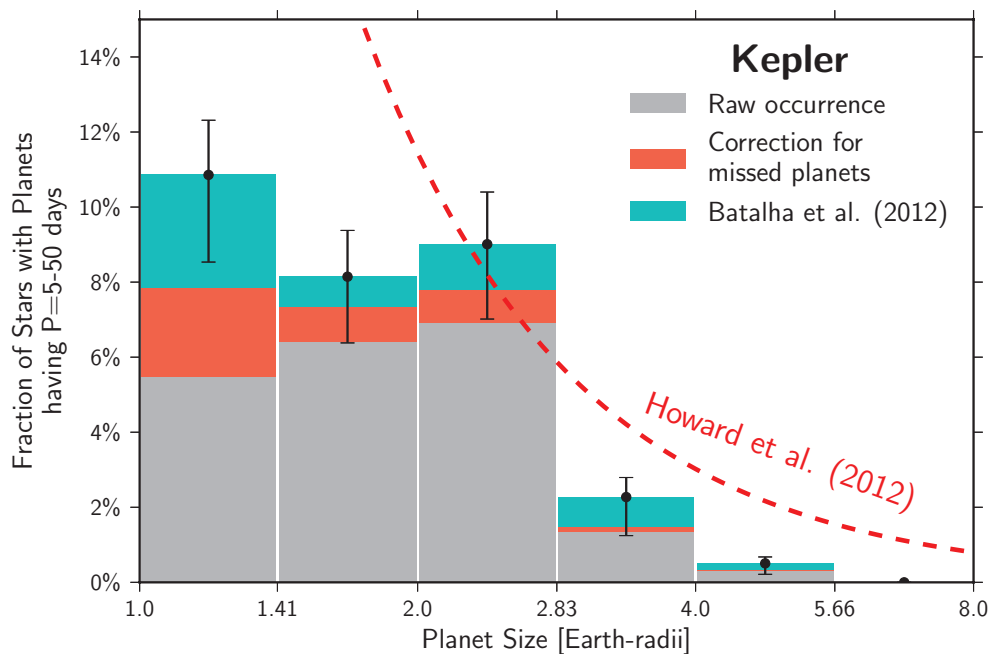


Figure 3.16: Same as Figure 3.11 with inclusion of planets in multi planet systems. The blue regions represent the additional contribution to planet occurrence from the [Batalha et al. \(2012\)](#) planets. The addition of these new planets does not change the overall shape of the distribution. The dashed line is the power law fit to the planet size distribution in H12. The fit agrees qualitatively for  $R_P > 2 R_{\oplus}$ , but not within errors. We expect the H12 fit to be  $\sim 25\%$  higher than our occurrence measurements since H12 included planets with  $P < 50$  days (not  $P = 5\text{--}50$  days). Additional discrepancies between occurrence in H12 and this work could stem from different characterizations of completeness, reliance on photometric versus spectroscopic measurements of  $R_{\star}$ , and magnitude-limited, rather than noise-limited, samples.

best chance for the detection of small, Earth-size planets in the *Kepler* field and will one day be among the stars from which  $\eta_{\oplus}$ —the fraction of Sun-like stars bearing Earth-size planets in habitable zone orbits—is estimated. In this work, we focus on the close-in planets having orbital periods of 5–50 days and semi-major axes  $\lesssim 0.25$  AU. Earth-size planets with these characteristics are statistically at the margins of detectability with the current  $\sim 3$  years of photometry in *Kepler* quarters Q1–Q12.

Our TERRA pipeline has two key features that enable confident measurement of the occurrence of close-in planets approaching Earth size. First, TERRA calibrates the *Kepler* photometry and searches for transit signals independent of the results from the *Kepler* Mission’s official pipeline. In some cases, TERRA calibration achieves superior noise suppression compared to the Pre-search Data Conditioning (PDC) module of the official *Kepler* pipeline (Petigura & Marcy 2012). The transit search algorithm in TERRA is efficient at detecting low SNR transits in the calibrated light curves. This algorithm successfully rediscovers 82 of 86 stars bearing planets in Batalha et al. (2012). Recall that the current version of TERRA only detects the highest SNR transit signal in each system. Thus, additional planets orbiting known hosts are not reported here. We report the occurrence of stars having one or more planets, not the mean number of planets per star as in H12 and elsewhere. Our pipeline also detects 37 planets not found in Batalha et al. (2012) (19 of which were not in the catalog of the *Kepler* team as of August 8<sup>th</sup>, 2012), albeit with the benefit of 6 quarters of additional photometry for TERRA to search.

The second crucial feature of TERRA is that we have characterized its detection completeness via the injection and recovery of synthetic transits in real *Kepler* light curves from the Best12k sample. *This completeness study is crucial to our occurrence calculations because it allows us to statistically correct for incompleteness variations across the  $P$ – $R_P$  plane.* While the *Kepler* Project has initiated a completeness study of the official pipeline (Christiansen et al. 2012), TERRA is the only pipeline for *Kepler* photometry whose detection completeness has been calibrated by injection and recovery tests. Prior to TERRA, occurrence calculations required one to *assume* that the *Kepler* planet detections were complete down to some SNR limit, or to estimate completeness based on SNR alone without empirical tests of the performance of the algorithms in the pipeline. For example, H12 made cuts in stellar brightness ( $Kp < 15$ ) and transit SNR ( $> 10$  in a single quarter of photometry) and restricted their search to planets larger than  $2 R_{\oplus}$  with orbital periods shorter than 50 days. These conservative cuts on the planet and star catalogs were driven by the unknown completeness of the official *Kepler* pipeline at low SNR. H12 applied two statistical corrections to convert their distribution of detected planets into an occurrence distribution. They corrected for non-transiting planets with a geometric  $a/R_{\star}$  correction. They also computed the number of stars amenable to the detection (at SNR  $> 10$  in a single quarter) of each planet and considered only that number of stars in the occurrence calculation. H12 had no empirical way to determine the actual detection efficiency of the algorithms in the pipeline. Here, we apply the geometric  $a/R_{\star}$  correction and correct for pipeline completeness across the  $P$ – $R_P$  plane by explicit tests of the TERRA pipeline efficiency, which naturally incorporates an SNR threshold correction as in H12.

### 3.9.2 Planet Occurrence

H12 found that for close-in planets, the planet radius function rises steeply from Jupiter size to  $2 R_{\oplus}$ . For smaller planets of  $\sim 1\text{--}2 R_{\oplus}$ , occurrence was approximately constant in logarithmic  $R_P$  bins, but H12 were skeptical of the result below  $2 R_{\oplus}$  because of unknown pipeline completeness and the small number statistics near  $1 R_{\oplus}$  in the [Borucki et al. \(2011\)](#) planet catalog. In this work, we strongly confirm the power law rise in occurrence from 4 to  $2 R_{\oplus}$  using a superior assessment of completeness and nine times more photometry than in H12. Using TERRA, we can empirically and confidently compute occurrence down to  $1 R_{\oplus}$ . Our key result is the plateau of planet occurrence for the size range  $1\text{--}2.8 R_{\oplus}$  for planets having orbital periods 5–50 days around Sun-like stars. In that size range of  $1\text{--}2.8 R_{\oplus}$ , 23% of stars have a planet orbiting with periods between 5 and 50 days. Including the multiple planets within each system, we find 0.28 planets per star within the size range  $1\text{--}2.8 R_{\oplus}$  and with periods between 5–50 days. These results apply, of course, to the *Kepler* field, with its still unknown distribution of masses, ages, and metallicities in the Galactic disk.

As shown in [Figure 3.10](#), TERRA detects many sub-Earth size planets ( $< 1.0 R_{\oplus}$ ). These sub-Earths appear in regions of low completeness, and, provocatively, may represent just the tip of the iceberg. A rich population of sub-Earths may await discovery given more photometry and continued pipeline improvements. With 8 years of total photometry in an extended *Kepler* mission (compared to 3 years here), the computational machinery of TERRA—including its light curve calibration, transit search, and completeness calibration—will enable a measurement of  $\eta_{\oplus}$  for habitable zone orbits.

### 3.9.3 Interpretation

We are not the first to note the huge population of close-in planets smaller or less massive than Neptune. Using Doppler surveys, [Howard et al. \(2010\)](#) and [Mayor et al. \(2011\)](#) showed that the planet mass function rises steeply with decreasing mass, at least for close-in planets. In *Kepler* data, the excess of close-in, small planets was obvious in the initial planet catalogs released by the *Kepler* Project ([Borucki et al. 2011](#); [Borucki et al. 2011](#)). H12 characterized the occurrence distribution of these small planets as a function of their size, orbital period, and host star temperature. These occurrence measurements, based on official *Kepler* planet catalogs, were refined and extended by [Youdin \(2011\)](#), [Traub \(2012\)](#), [Dong & Zhu \(2012\)](#), [Beaugé & Nesvorný \(2013\)](#), and others. Our contribution here shows a clear plateau in occurrence in the  $1\text{--}2.8 R_{\oplus}$  size range and certified by an independent search of *Kepler* photometry using a pipeline calibrated by injection and recovery tests. The onset of the plateau at  $\sim 2.8 R_{\oplus}$  suggests that there is a preferred size scale for the formation of close-in planets.

H12 and [Youdin \(2011\)](#) noted falling planet occurrence for periods shorter than  $\sim 7$  days. We also observe declining planet occurrence for short orbital periods, but find that the transition occurs closer to  $\sim 10$  days. We consider our period distribution to be in qualitative agreement with those of H12 and [Youdin \(2011\)](#). Planet formation and/or migration seems

to discourage very close-in planets ( $P \lesssim 10$  days).

Close-in, small planets are now the most abundant planets detected by current transit and Doppler searches, yet they are absent from the solar system. The solar system is devoid of planets between 1 and  $3.88 R_{\oplus}$  (Earth and Neptune) and planets with periods less than Mercury’s ( $P < 88.0$  days). The formation mechanisms and possible subsequent migration of such planets are hotly debated. The population synthesis models of [Ida & Lin \(2010\)](#) and [Mordasini et al. \(2012\)](#) suggest that they form near or beyond the ice line and then migrate quiescently in the protoplanetary disk. These models follow the growth and migration of planets over a wide range of parameters (from Jupiter mass down to Earth mass orbiting at distances out to  $\sim 10$  AU) and they predict “deserts” of planet occurrence that are not detected.

More recently, [Hansen & Murray \(2012\)](#) and [Chiang & Laughlin \(2012\)](#) have argued for the *in situ* formation of close-in planets of Neptune size and smaller. In these models, close-in rocky planets of a few Earth masses form from protoplanetary disks more massive than the minimum mass solar nebula. Multiple planets per disk form commonly in these models and accretion is fast ( $\sim 10^5$  years) and efficient due to the short dynamical timescales of close-in orbits. The rocky cores form before the protoplanetary disk has dissipated, accreting nebular gas that adds typically  $\sim 3\%$  to the mass of the planet ([Chiang & Laughlin 2012](#)). But the small amounts of gas can significantly swell the radii of these otherwise rocky planets. For example, [Adams et al. \(2008\)](#) found that adding a H/He gas envelope equivalent to 0.2–20% of the mass of a solid  $5 M_E$  planet increases the radius 8–110% above the gas-free value.

We find the *in situ* model plausible because it naturally explains the large number of close, sub-Neptune-size planets, the high rate of planet multiplicity and nearly co-planar and circular orbits ([Lissauer et al. 2011](#); [Fang & Margot 2012](#)), and does not require tuning of planet migration models. Our result of a plateau in the planet size distribution for 1– $2.8 R_{\oplus}$  with a sharp falloff in occurrence for larger planets along with decreasing occurrence for  $P \lesssim 10$  days are two significant observed properties of planets around Sun-like stars that must be reproduced by models that form planets *in situ* or otherwise and by associated population synthesis models.

The *in situ* model seems supported by the sheer large occurrence of sub-Neptune-size planets within 0.25 AU. It seems unlikely that all such planets form beyond the snow line at  $\sim 2$  AU, which would require inward migration to within 0.25 AU, but not all the way into the star. Such models of formation beyond the snow line seem to require fine tuning of migration and parking mechanisms, as well as the tuning of available water or gas beyond 2 AU, while avoiding runaway gas accretion toward Jupiter masses. Still, *in situ* formation seems to require higher densities than those normally assumed in a minimum mass solar nebula ([Chiang & Laughlin 2012](#)) in order to form the sub-Neptune planets before removal of the gas. If this *in situ* model is correct, we expect these sub-Neptune-size planets to be composed of rock plus H and He, rather than rock plus water ([Chiang & Laughlin 2012](#)). Thus, a test of the *in situ* mode of formation involves spectroscopic measurements of the chemical composition of the close-in sub-Neptunes.

Table 3.2: Planet candidates identified with TERRA

KIC	Light Curve Fit								Stellar Parameters				source <sup>b</sup>	FP	B12	
	$P$ (d)	$t_0^a$ (d)	$\frac{R_P}{R_\star}$ (%)	$\sigma(\frac{R_P}{R_\star})$	$\tau$ (hrs)	$\sigma(\tau)$	$b$	$\sigma(b)$	$T_{\text{eff}}$ (K)	$\log g$ (cgs)	$R_\star$ ( $R_\odot$ )	$R_P$ ( $R_\oplus$ )				$\sigma(R_P)$
2142522	13.323	67.043	0.98	0.34	2.32	0.51	< 0.85		6046	4.40	1.04	1.11	0.39	P1	Y	N
2307415	13.122	66.396	1.26	0.13	1.90	0.12	< 0.52		6133	4.38	1.14	1.57	0.16	S	N	Y
2441495	12.493	71.457	2.38	0.24	1.13	0.03	< 0.47		5192	4.56	0.76	1.99	0.20	S	N	Y
2444412	14.911	74.337	3.38	0.34	4.24	0.31	0.93	0.01	5551	4.47	0.92	3.41	0.34	S	N	Y
2571238	9.287	68.984	2.90	0.29	3.72	0.38	0.90	0.03	5544	4.50	0.89	2.82	0.28	S	N	Y
2853446	7.373	70.613	1.39	0.14	0.74	0.06	< 0.70		5969	4.37	1.10	1.65	0.17	S	N	Y
3098810	40.811	75.673	1.98	0.20	1.45	0.12	< 0.70		6071	4.31	1.27	2.75	0.28	S	N	Y
3120904	42.915	72.866	1.15	0.12	2.96	0.36	< 0.66		6151	4.31	1.26	1.59	0.16	S		N
3342794	14.172	75.591	1.40	0.14	1.31	0.13	< 0.55		5900	4.35	1.10	1.68	0.17	S	N	Y
3442055	29.619	66.681	1.57	0.16	2.48	0.15	< 0.57		5624	4.41	1.01	1.72	0.17	S	N	Y
3531558	24.994	71.674	1.49	0.15	2.93	0.12	< 0.53		5808	4.35	1.14	1.85	0.19	S	N	Y
3545135	8.483	65.973	0.81	0.08	1.44	0.10	< 0.57		5794	4.40	1.02	0.90	0.09	S	N	N
3835670	14.558	78.084	2.86	0.29	3.89	0.22	0.31	0.19	5722	4.14	1.58	4.93	0.49	S	N	Y
3839488	11.131	67.370	1.36	0.14	1.97	0.11	< 0.50		5991	4.36	1.11	1.64	0.17	S	N	Y
3852655	11.629	65.817	0.85	0.30	1.49	0.23	< 0.79		5822	4.36	1.05	0.97	0.34	P1	N	N
3942670	33.416	70.911	1.48	0.15	3.99	0.24	< 0.63		6012	4.28	1.32	2.13	0.21	S	N	Y
4043190	6.401	69.883	1.07	0.11	1.35	0.08	< 0.65		5302	3.83	2.45	2.86	0.29	S	N	Y
4049901	16.291	65.115	0.64	0.23	1.72	0.16	< 0.68		5250	4.48	0.85	0.60	0.21	P1	N	Y
4548011	6.284	66.198	0.60	0.06	2.23	0.64	< 0.49		5991	4.30	1.26	0.83	0.09	S		N
4644604	14.486	64.550	2.03	0.21	1.49	0.15	< 0.59		5739	4.34	1.04	2.32	0.23	S	N	Y
4770174	6.096	67.600	0.57	0.20	3.08	0.44	< 0.75		6013	4.44	1.01	0.63	0.22	P1	N	N
4827723	7.239	68.024	1.63	0.17	2.20	0.37	0.70	0.12	5392	4.52	0.87	1.54	0.16	S	N	Y
4914423	15.965	75.182	2.17	0.22	3.14	0.28	0.71	0.06	5904	4.27	1.29	3.05	0.31	S	N	Y
4914566	22.241	77.736	0.83	0.29	3.76	0.36	< 0.73		5974	4.22	1.31	1.18	0.41	P1	Y	N
5009743	41.699	102.563	1.94	0.20	2.87	0.30	< 0.70		5937	4.35	1.09	2.32	0.23	S	N	Y
5042210	12.147	64.535	0.81	0.08	3.22	0.21	< 0.56		6007	4.27	1.31	1.16	0.12	S	N	Y
5094751	6.482	68.943	1.69	0.17	2.51	0.31	0.69	0.13	5929	4.37	1.10	2.02	0.20	S	N	Y
5096590	29.610	70.332	1.00	0.35	2.60	0.20	< 0.67		5623	4.63	0.73	0.79	0.28	P1		N

Table 3.2 (cont'd): Planet candidates identified with TERRA

KIC	Light Curve Fit								Stellar Parameters					source <sup>b</sup>	FP	B12
	$P$ (d)	$t_0^a$ (d)	$\frac{R_P}{R_\star}$ (%)	$\sigma(\frac{R_P}{R_\star})$	$\tau$ (hrs)	$\sigma(\tau)$	$b$	$\sigma(b)$	$T_{\text{eff}}$ (K)	$\log g$ (cgs)	$R_\star$ ( $R_\odot$ )	$R_P$ ( $R_\oplus$ )	$\sigma(R_P)$			
5121511	30.996	93.790	2.35	0.24	1.40	0.06	< 0.47		5217	4.53	0.84	2.15	0.22	S	N	Y
5308537	14.265	76.217	0.76	0.08	1.92	0.53	< 0.87		5831	4.29	1.26	1.05	0.11	S		N
5561278	20.310	79.826	1.16	0.12	2.73	0.15	< 0.47		6161	4.38	1.14	1.45	0.15	S	N	Y
5613330	23.449	69.031	1.68	0.17	4.44	0.28	< 0.25	0.22	6080	4.20	1.48	2.70	0.27	S	N	Y
5652893	14.010	65.959	1.15	0.13	1.98	0.49	< 0.85		5150	4.55	0.78	0.97	0.11	S	N	N
5702939	18.398	77.934	1.09	0.38	2.45	0.27	< 0.54		5634	4.47	0.87	1.04	0.36	P1	N	N
5735762	9.674	68.009	2.73	0.27	1.61	0.06	< 0.47		5195	4.53	0.84	2.51	0.25	S	N	Y
5866724	5.860	65.040	1.65	0.17	2.01	0.05	< 0.22	0.14	6109	4.29	1.31	2.37	0.24	S	N	Y
5959719	6.738	66.327	0.99	0.10	1.30	0.21	< 0.76		5166	4.56	0.77	0.83	0.09	S	N	Y
6071903	24.308	87.054	2.28	0.23	1.29	0.05	< 0.27		5296	4.55	0.83	2.06	0.21	S	N	Y
6197215	10.613	68.691	1.23	0.13	0.48	0.06	< 0.80		5933	4.39	1.09	1.46	0.15	S	N	N
6289257	19.675	69.903	1.33	0.13	1.96	0.21	< 0.35	0.27	6023	4.36	1.11	1.61	0.16	S	N	Y
6291837	35.596	84.942	2.45	0.25	3.18	0.42	< 0.71		6165	4.38	1.14	3.05	0.31	S	N	Y
6356692	11.392	74.555	0.66	0.23	2.74	0.31	< 0.73		5420	4.03	1.64	1.19	0.42	P1	N	N
6365156	10.214	73.050	1.57	0.16	2.83	0.09	< 0.42		5852	4.28	1.25	2.13	0.21	S	N	Y
6442340	13.137	76.973	1.38	0.14	2.41	0.13	< 0.55		5764	4.38	1.08	1.63	0.16	S	N	Y
6521045	12.816	68.772	1.37	0.14	3.42	0.34	< 0.40	0.19	5874	4.29	1.24	1.85	0.19	S	N	Y
6523351	6.067	69.128	0.72	0.25	1.02	0.20	< 0.89		5489	4.15	1.35	1.06	0.37	P1		N
6605493	9.310	69.379	0.99	0.10	1.80	0.16	< 0.62		5805	4.36	1.12	1.20	0.12	S	N	Y
6607357	7.700	67.390	0.85	0.30	2.72	0.45	< 0.55	0.22	5592	4.51	0.91	0.84	0.29	P1	N	N
6707835	22.248	84.881	2.25	0.23	1.97	0.07	< 0.43		5619	4.44	0.99	2.42	0.24	S	N	Y
6716545	13.910	75.855	0.84	0.30	3.29	0.68	< 0.85		6044	4.30	1.12	1.03	0.36	P1	N	N
6803202	21.061	76.591	1.58	0.16	2.64	0.08	< 0.36		5719	4.40	1.03	1.77	0.18	S	N	Y
6851425	11.120	72.744	2.29	0.23	1.71	0.12	< 0.62		5071	4.59	0.72	1.80	0.18	S	N	Y
6922710	23.127	78.663	1.01	0.11	2.57	0.47	< 0.78		5929	4.40	1.07	1.18	0.12	S	N	Y
7021534	9.066	68.147	1.42	0.50	0.81	0.05	< 0.55		5848	4.55	0.87	1.35	0.47	P1	Y	N
7033671	9.490	66.961	1.48	0.15	1.81	0.09	< 0.46		5679	4.29	1.26	2.03	0.20	S	N	Y
7211221	5.621	69.903	1.21	0.12	1.23	0.11	< 0.53		5634	4.44	0.93	1.23	0.12	S	N	Y

Table 3.2 (cont'd): Planet candidates identified with TERRA

KIC	Light Curve Fit								Stellar Parameters					source <sup>b</sup>	FP	B12
	$P$ (d)	$t_0^a$ (d)	$\frac{R_P}{R_\star}$ (%)	$\sigma(\frac{R_P}{R_\star})$	$\tau$ (hrs)	$\sigma(\tau)$	$b$	$\sigma(b)$	$T_{\text{eff}}$ (K)	$\log g$ (cgs)	$R_\star$ ( $R_\odot$ )	$R_P$ ( $R_\oplus$ )	$\sigma(R_P)$			
7219825	17.233	68.084	2.06	0.21	2.27	0.13	< 0.22		6089	4.36	1.13	2.54	0.25	S	N	Y
7345248	5.665	69.338	0.63	0.22	2.81	0.43	< 0.61		5656	4.27	1.19	0.81	0.29	P2		N
7419318	18.736	73.153	2.13	0.22	1.47	0.11	< 0.61		5187	4.54	0.81	1.89	0.19	S	N	Y
7466863	11.971	68.173	1.83	0.64	0.98	0.03	< 0.39		6035	4.12	1.45	2.89	1.01	P1	Y	N
7582689	11.921	70.475	0.75	0.26	5.84	1.24	< 0.95		6022	4.04	1.64	1.34	0.47	P1		N
7668663	6.498	69.012	1.44	0.15	1.85	0.34	< 0.79	0.09	5725	4.33	1.14	1.79	0.18	S	N	Y
7700622	35.585	86.426	2.83	0.28	1.99	0.10	< 0.46		4787	4.62	0.69	2.13	0.21	S	N	Y
7762723	9.887	72.539	0.73	0.26	2.21	0.39	< 0.65		5501	4.58	0.80	0.64	0.22	P1	Y	N
7810483	29.921	79.024	1.71	0.60	1.58	0.11	< 0.58		5893	4.52	0.91	1.70	0.59	P1	Y	N
7906739	7.015	69.903	0.90	0.31	2.43	0.32	< 0.68		5652	4.53	0.81	0.80	0.28	P1	Y	N
7906892	8.849	72.797	0.58	0.07	8.03	3.69	< 0.89	0.12	6095	4.35	1.14	0.72	0.08	S		N
7918652	11.456	69.316	0.79	0.28	2.45	0.47	< 0.81		5809	4.25	1.19	1.02	0.36	P1	N	N
8008067	15.771	70.584	2.22	0.22	3.32	0.31	< 0.67	0.08	5594	4.37	1.10	2.66	0.27	S	N	Y
8009496	38.476	83.567	1.88	0.66	1.72	0.14	< 0.70		5833	4.54	0.85	1.74	0.61	P1	Y	N
8073705	10.601	65.967	0.75	0.08	2.29	0.36	< 0.80		6086	4.36	1.12	0.91	0.10	S		N
8077137	15.090	78.772	0.78	0.08	2.47	0.65	< 0.85		6179	4.37	1.16	0.99	0.10	S	N	Y
8081187	37.323	85.828	1.67	0.59	3.58	0.39	< 0.62		6030	4.55	0.86	1.57	0.55	P1	Y	N
8087812	27.211	65.360	1.01	0.10	5.01	0.57	< 0.67		5985	4.17	1.41	1.55	0.16	S		N
8242434	44.964	77.565	2.58	0.26	2.58	0.15	< 0.31	0.22	4692	4.63	0.68	1.92	0.19	S	N	Y
8280511	10.435	67.826	1.37	0.14	1.70	0.12	< 0.58		5522	4.45	0.91	1.36	0.14	S		N
8323753	6.714	67.308	1.97	0.69	1.33	0.05	< 0.52		5817	4.23	1.26	2.71	0.95	P1	Y	N
8349582	11.523	64.959	2.14	0.22	2.41	0.21	< 0.61	0.09	5668	4.23	1.35	3.15	0.32	S	N	Y
8429668	5.007	67.696	0.73	0.26	1.66	0.47	< 0.62	0.29	5034	4.63	0.65	0.52	0.18	P2		N
8480285	29.667	92.687	2.43	0.25	4.72	0.42	< 0.48	0.14	5960	4.36	1.09	2.89	0.29	S	N	Y
8494617	22.923	66.640	1.06	0.11	3.72	0.36	< 0.50		5905	4.36	1.10	1.27	0.13	S	N	Y
8560804	31.976	66.803	0.99	0.35	4.96	0.48	< 0.65		5878	4.44	1.01	1.09	0.38	P1	N	N
8611832	22.597	73.431	1.08	0.11	3.15	0.17	< 0.58		5577	4.37	0.99	1.17	0.12	S	N	Y
8628758	14.374	71.204	1.99	0.20	4.76	0.68	< 0.91		5773	4.40	1.04	2.26	0.23	S	N	Y

Table 3.2 (cont'd): Planet candidates identified with TERRA

KIC	Light Curve Fit								Stellar Parameters					source <sup>b</sup>	FP	B12
	$P$ (d)	$t_0^a$ (d)	$\frac{R_P}{R_\star}$ (%)	$\sigma(\frac{R_P}{R_\star})$	$\tau$ (hrs)	$\sigma(\tau)$	$b$	$\sigma(b)$	$T_{\text{eff}}$ (K)	$\log g$ (cgs)	$R_\star$ ( $R_\odot$ )	$R_P$ ( $R_\oplus$ )	$\sigma(R_P)$			
8631504	14.820	66.409	1.20	0.12	2.02	0.25	< 0.63		4828	4.60	0.72	0.95	0.10	S	N	Y
8644365	19.917	72.354	1.07	0.11	3.37	0.55	< 0.85		6054	4.39	1.12	1.31	0.13	S		N
8804455	7.597	64.958	1.14	0.12	2.55	0.47	< 0.74	0.11	5715	4.38	1.07	1.33	0.14	S	N	Y
8805348	29.907	78.383	2.36	0.24	3.20	0.39	< 0.66	0.12	5739	4.34	1.05	2.69	0.27	S	N	Y
8822366	30.864	65.012	1.41	0.14	4.16	0.20	< 0.62		6089	4.35	1.14	1.76	0.18	S	N	Y
8827575	10.129	68.997	0.84	0.30	1.94	0.18	< 0.63		5284	4.45	0.89	0.82	0.29	P1		N
8866102	17.834	114.225	1.66	0.17	2.28	0.06	< 0.39		6178	4.37	1.15	2.08	0.21	S	N	Y
8962094	30.865	75.052	2.09	0.21	1.37	0.10	< 0.61		5739	4.34	1.04	2.38	0.24	S	N	Y
8972058	8.991	69.746	2.01	0.20	2.10	0.11	< 0.52		5979	4.38	1.09	2.39	0.24	S	N	Y
9006186	5.453	67.152	0.85	0.09	1.07	0.08	< 0.61		5404	4.53	0.87	0.81	0.08	S	N	Y
9086251	6.892	64.632	0.87	0.09	0.93	0.10	< 0.68		6044	4.22	1.45	1.38	0.14	S	N	Y
9139084	5.836	67.853	2.07	0.21	1.06	0.03	< 0.41		5411	4.53	0.85	1.92	0.19	S	N	Y
9226339	21.461	65.230	1.10	0.11	1.66	0.16	< 0.70		5807	4.28	1.25	1.50	0.15	S		N
9288237	7.491	68.329	0.52	0.18	3.01	0.73	< 0.84		5946	4.44	0.96	0.54	0.19	P1		N
9491832	49.565	103.693	1.14	0.12	6.43	1.49	< 0.74	0.25	5821	4.15	1.57	1.95	0.21	S		N
9549648	5.992	69.883	1.46	0.15	1.80	0.45	< 0.89	0.06	6165	4.38	1.14	1.82	0.19	S	N	Y
9704384	5.509	65.285	1.35	0.14	1.85	0.26	< 0.75		5448	4.50	0.91	1.35	0.14	S	N	Y
9716028	17.373	71.258	0.82	0.08	2.46	0.27	< 0.73		6119	4.37	1.15	1.03	0.11	S		N
9717943	6.110	69.903	0.72	0.08	1.80	0.87	< 0.79	0.20	5968	4.30	1.27	1.00	0.11	S	N	Y
9886361	7.031	67.464	0.88	0.09	3.04	0.21	< 0.42		6090	4.39	1.13	1.08	0.11	S	N	N
10055126	9.176	71.722	1.33	0.13	2.43	0.24	< 0.48		5905	4.36	1.10	1.59	0.16	S	N	Y
10130039	12.758	66.961	1.19	0.12	2.19	0.07	< 0.38		5828	4.42	1.01	1.31	0.13	S	N	Y
10136549	9.693	65.809	1.14	0.12	3.44	0.44	< 0.57	0.20	5684	4.13	1.59	1.98	0.20	S	N	Y
10212441	15.044	66.211	0.95	0.10	2.97	0.24	< 0.57		5939	4.35	1.09	1.13	0.11	S	N	Y
10593535	20.925	67.900	0.93	0.10	3.63	0.59	< 0.81		5822	4.28	1.25	1.27	0.13	S		N
10722485	7.849	67.907	0.87	0.09	2.61	0.51	< 0.87		5682	4.36	1.03	0.98	0.10	S		N
10917433	6.912	65.190	0.51	0.05	2.03	0.57	< 0.87		5680	4.33	1.12	0.62	0.06	S		N
11086270	31.720	75.821	1.90	0.19	3.35	0.40	< 0.70	0.14	5960	4.37	1.08	2.24	0.22	S	N	Y

Table 3.2 (cont'd): Planet candidates identified with TERRA

KIC	Light Curve Fit							Stellar Parameters					source <sup>b</sup>	FP	B12	
	$P$ (d)	$t_0^a$ (d)	$\frac{R_P}{R_\star}$ (%)	$\sigma(\frac{R_P}{R_\star})$	$\tau$ (hrs)	$\sigma(\tau)$	$b$	$\sigma(b)$	$T_{\text{eff}}$ (K)	$\log g$ (cgs)	$R_\star$ ( $R_\odot$ )	$R_P$ ( $R_\oplus$ )				$\sigma(R_P)$
11121752	7.630	70.087	1.00	0.10	1.56	0.23	< 0.75		6045	4.36	1.12	1.22	0.12	S	N	Y
11133306	41.746	101.657	1.90	0.19	2.32	0.15	0.27	0.22	5953	4.37	1.10	2.27	0.23	S	N	Y
11241912	14.427	71.857	0.95	0.10	2.40	0.18	< 0.59		5931	4.40	1.07	1.10	0.11	S		N
11250587	7.257	67.028	1.95	0.20	2.41	0.05	< 0.40		5853	4.18	1.49	3.18	0.32	S	N	Y
11253711	17.791	82.259	1.86	0.65	1.29	0.09	< 0.57		5816	4.48	0.95	1.92	0.67	P1	N	Y
11295426	5.399	69.065	1.89	0.19	2.78	0.20	0.80	0.05	5793	4.25	1.30	2.68	0.27	S	N	Y
11402995	10.061	71.959	2.00	0.20	2.42	0.19	< 0.62		5709	4.30	1.18	2.56	0.26	S	N	Y
11554435	9.434	73.119	5.69	0.57	1.29	0.02	< 0.43		5536	4.52	0.90	5.60	0.56	S	N	Y
11560897	35.968	71.667	1.46	0.15	1.47	0.11	< 0.45		5832	4.27	1.28	2.03	0.21	S	N	Y
11612280	9.406	70.699	0.80	0.08	3.02	0.54	< 0.77		5857	4.24	1.32	1.15	0.12	S		N
11771430	40.031	81.863	1.39	0.14	2.25	0.14	< 0.57		5850	4.23	1.38	2.10	0.21	S	N	Y
11774991	37.815	74.112	1.45	0.15	2.37	0.21	< 0.65		4710	4.62	0.70	1.10	0.11	S	N	Y
12254909	5.350	66.872	0.84	0.29	2.26	0.14	< 0.60		5987	4.46	0.96	0.88	0.31	P1	N	Y
12301181	6.147	67.867	1.04	0.11	1.45	0.07	< 0.40		4997	4.60	0.74	0.84	0.09	S	N	Y
12416661	8.053	67.968	0.63	0.22	2.93	0.37	< 0.59		6091	4.12	1.47	1.02	0.36	P1		N
12454461	7.467	69.392	0.84	0.09	1.83	0.20	< 0.71		6048	4.31	1.27	1.16	0.12	S	N	Y
12737015	24.669	69.616	1.05	0.11	4.94	0.49	< 0.69		6045	4.15	1.60	1.84	0.19	S		N

Note. — Orbital period,  $P$ ; time of transit center,  $t_0$ ; planet-to-star radius ratio,  $R_P/R_\star$ ; the time for the planet to travel  $R_\star$  during transit,  $\tau$ ; and transit impact parameter,  $b$  are all determined from the [Mandel & Agol \(2002\)](#) light curve fit. By default, stellar parameters  $R_\star$ ,  $T_{\text{eff}}$ , and  $\log g$  come from SpecMatch. If SpecMatch parameters do not exist, parameters are taken from the corrected KIC values, described in Section 3.4. The FP column lists whether a candidate was designated a false positive by the *Kepler* team (‘Y’–yes, ‘N’–no, ‘ ’–no designation). The B12 column lists whether a candidate was present in [Batalha et al. \(2012\)](#).

<sup>a</sup>Time of transit center (BJD-2454900).

<sup>b</sup>Source of stellar parameters: ‘S’–SpecMatch-derived parameters using Keck HIRES spectra, ‘P1’–photometrically-derived parameters from [Batalha et al. \(2012\)](#), ‘P2’–photometrically-derived parameters computed by the authors. See Section 3.4 for more details.

Table 3.3: New candidates identified with TERRA

KIC	Light Curve Fit								Stellar Parameters					source <sup>b</sup>
	$P$ (d)	$t_0^a$ (d)	$\frac{R_P}{R_\star}$ (%)	$\sigma(\frac{R_P}{R_\star})$	$\tau$ (hrs)	$\sigma(\tau)$	$b$	$\sigma(b)$	$T_{\text{eff}}$ (K)	$\log g$ (cgs)	$R_\star$ ( $R_\odot$ )	$R_P$ ( $R_\oplus$ )	$\sigma(R_P)$	
3120904	42.915	72.866	1.15	0.12	2.96	0.36	< 0.66		6151	4.31	1.26	1.59	0.16	S
3545135	8.483	65.973	0.81	0.08	1.44	0.10	< 0.57		5794	4.40	1.02	0.90	0.09	S
3852655	11.629	65.817	0.85	0.30	1.49	0.23	< 0.79		5822	4.36	1.05	0.97	0.34	P1
4548011	6.284	66.198	0.60	0.06	2.23	0.64	< 0.49		5991	4.30	1.26	0.83	0.09	S
4770174	6.096	67.600	0.57	0.20	3.08	0.44	< 0.75		6013	4.44	1.01	0.63	0.22	P1
5096590	29.610	70.332	1.00	0.35	2.60	0.20	< 0.67		5623	4.63	0.73	0.79	0.28	P1
5308537	14.265	76.217	0.76	0.08	1.92	0.53	< 0.87		5831	4.29	1.26	1.05	0.11	S
5652893	14.010	65.959	1.15	0.13	1.98	0.49	< 0.85		5150	4.55	0.78	0.97	0.11	S
5702939	18.398	77.934	1.09	0.38	2.45	0.27	< 0.54		5634	4.47	0.87	1.04	0.36	P1
6197215	10.613	68.691	1.23	0.13	0.48	0.06	< 0.80		5933	4.39	1.09	1.46	0.15	S
6356692	11.392	74.555	0.66	0.23	2.74	0.31	< 0.73		5420	4.03	1.64	1.19	0.42	P1
6523351	6.067	69.128	0.72	0.25	1.02	0.20	< 0.89		5489	4.15	1.35	1.06	0.37	P1
6607357	7.700	67.390	0.85	0.30	2.72	0.45	0.55	0.22	5592	4.51	0.91	0.84	0.29	P1
6716545	13.910	75.855	0.84	0.30	3.29	0.68	< 0.85		6044	4.30	1.12	1.03	0.36	P1
7345248	5.665	69.338	0.63	0.22	2.81	0.43	< 0.61		5656	4.27	1.19	0.81	0.29	P2
7582689	11.921	70.475	0.75	0.26	5.84	1.24	< 0.95		6022	4.04	1.64	1.34	0.47	P1
7906892	8.849	72.797	0.58	0.07	8.03	3.69	0.89	0.12	6095	4.35	1.14	0.72	0.08	S
7918652	11.456	69.316	0.79	0.28	2.45	0.47	< 0.81		5809	4.25	1.19	1.02	0.36	P1
8073705	10.601	65.967	0.75	0.08	2.29	0.36	< 0.80		6086	4.36	1.12	0.91	0.10	S
8087812	27.211	65.360	1.01	0.10	5.01	0.57	< 0.67		5985	4.17	1.41	1.55	0.16	S
8280511	10.435	67.826	1.37	0.14	1.70	0.12	< 0.58		5522	4.45	0.91	1.36	0.14	S
8429668	5.007	67.696	0.73	0.26	1.66	0.47	0.62	0.29	5034	4.63	0.65	0.52	0.18	P2
8560804	31.976	66.803	0.99	0.35	4.96	0.48	< 0.65		5878	4.44	1.01	1.09	0.38	P1
8644365	19.917	72.354	1.07	0.11	3.37	0.55	< 0.85		6054	4.39	1.12	1.31	0.13	S
8827575	10.129	68.997	0.84	0.30	1.94	0.18	< 0.63		5284	4.45	0.89	0.82	0.29	P1
9226339	21.461	65.230	1.10	0.11	1.66	0.16	< 0.70		5807	4.28	1.25	1.50	0.15	S
9288237	7.491	68.329	0.52	0.18	3.01	0.73	< 0.84		5946	4.44	0.96	0.54	0.19	P1
9491832	49.565	103.693	1.14	0.12	6.43	1.49	0.74	0.25	5821	4.15	1.57	1.95	0.21	S

Table 3.3 (cont'd): New candidates identified with TERRA

KIC	Light Curve Fit							Stellar Parameters					source <sup>b</sup>	
	$P$ (d)	$t_0^a$ (d)	$\frac{R_P}{R_\star}$ (%)	$\sigma(\frac{R_P}{R_\star})$	$\tau$ (hrs)	$\sigma(\tau)$	$b$	$\sigma(b)$	$T_{\text{eff}}$ (K)	$\log g$ (cgs)	$R_\star$ ( $R_\odot$ )	$R_P$ ( $R_\oplus$ )		$\sigma(R_P)$
9716028	17.373	71.258	0.82	0.08	2.46	0.27	< 0.73		6119	4.37	1.15	1.03	0.11	S
9886361	7.031	67.464	0.88	0.09	3.04	0.21	< 0.42		6090	4.39	1.13	1.08	0.11	S
10593535	20.925	67.900	0.93	0.10	3.63	0.59	< 0.81		5822	4.28	1.25	1.27	0.13	S
10722485	7.849	67.907	0.87	0.09	2.61	0.51	< 0.87		5682	4.36	1.03	0.98	0.10	S
10917433	6.912	65.190	0.51	0.05	2.03	0.57	< 0.87		5680	4.33	1.12	0.62	0.06	S
11241912	14.427	71.857	0.95	0.10	2.40	0.18	< 0.59		5931	4.40	1.07	1.10	0.11	S
11612280	9.406	70.699	0.80	0.08	3.02	0.54	< 0.77		5857	4.24	1.32	1.15	0.12	S
12416661	8.053	67.968	0.63	0.22	2.93	0.37	< 0.59		6091	4.12	1.47	1.02	0.36	P1
12737015	24.669	69.616	1.05	0.11	4.94	0.49	< 0.69		6045	4.15	1.60	1.84	0.19	S

Note. — The 37 TERRA candidates not in [Batalha et al. \(2012\)](#) and not listed as false positives by the *Kepler* team. The column definitions are the same as in Table 3.2

Table 3.4: Union of Batalha et al. (2012) and TERRA planet candidate catalogs

KIC	Batalha			TERRA	
	KOI	$P$	$R_P$	$P$	$R_P$
2142522				13.32	1.11
2307415	2053.01	13.12	1.65	13.12	1.57
2441495	166.01	12.49	2.70	12.49	1.99
2444412	103.01	14.91	2.97	14.91	3.41
2571238	84.01	9.29	2.53	9.29	2.82
2853446	1118.01	7.37	2.52	7.37	1.65
3098810	1878.01	40.81	3.24	40.81	2.75
3120904				42.91	1.59
3342794	2278.01	14.17	1.99	14.17	1.68
3442055	1218.01	29.62	2.22	29.62	1.72
3531558	118.01	24.99	1.41	24.99	1.85
3545135				8.48	0.90
3835670	149.01	14.56	5.50	14.56	4.93
3839488	1216.01	11.13	1.57	11.13	1.64
3852655				11.63	0.97
3942670	392.02	12.61	1.33		
3942670	392.01	33.42	2.27	33.42	2.13
4043190	1220.01	6.40	1.95	6.40	2.86
4049901	2295.01	16.29	0.63	16.29	0.60
4548011				6.28	0.83
4644604	628.01	14.49	1.87	14.49	2.32
4770174				6.10	0.63
4827723	632.01	7.24	1.46	7.24	1.54
4914423	108.01	15.97	2.94	15.97	3.05
4914566				22.24	1.18
5009743	1609.01	41.70	2.34	41.70	2.32
5042210	2462.01	12.15	1.37	12.15	1.16
5094751	123.01	6.48	2.64	6.48	2.02
5094751	123.02	21.22	2.71		
5096590				29.61	0.79
5121511	640.01	31.00	2.43	31.00	2.15
5308537				14.27	1.05
5446285	142.01	10.92	4.08		
5561278	1621.01	20.31	2.48	20.31	1.45
5613330	649.01	23.45	2.31	23.45	2.70
5652893				14.01	0.97
5702939				18.40	1.04
5735762	148.02	9.67	3.14	9.67	2.51
5735762	148.03	42.90	2.35		

Table 3.4 (cont'd): Union of [Batalha et al. \(2012\)](#) and TERRA planet candidate catalogs

KIC	Batalha			TERRA	
	KOI	$P$	$R_P$	$P$	$R_P$
5866724	85.01	5.86	2.35	5.86	2.37
5866724	85.03	8.13	1.41		
5959719	2498.01	6.74	0.78	6.74	0.83
6061773	2001.01	8.28	2.39		
6071903	306.01	24.31	2.28	24.31	2.06
6197215				10.61	1.46
6289257	307.02	5.21	1.15		
6289257	307.01	19.67	1.80	19.67	1.61
6291837	308.01	35.60	3.15	35.60	3.05
6356692				11.39	1.19
6365156	662.01	10.21	2.05	10.21	2.13
6442340	664.02	7.78	1.19		
6442340	664.01	13.14	1.83	13.14	1.63
6442340	664.03	23.44	1.19		
6521045	41.02	6.89	1.23		
6521045	41.01	12.82	2.08	12.82	1.85
6521045	41.03	35.33	1.40		
6523351				6.07	1.06
6605493	2559.01	9.31	0.99	9.31	1.20
6607357				7.70	0.84
6678383	111.01	11.43	2.14		
6678383	111.02	23.67	2.05		
6707835	666.01	22.25	2.56	22.25	2.42
6716545				13.91	1.03
6803202	177.01	21.06	1.84	21.06	1.77
6850504	70.04	6.10	0.91		
6850504	70.01	10.85	3.09		
6850504	70.05	19.58	1.02		
6851425	163.01	11.12	2.27	11.12	1.80
6922710	2087.01	23.13	1.54	23.13	1.18
7021534				9.07	1.35
7033671	670.01	9.49	1.92	9.49	2.03
7211221	1379.01	5.62	1.06	5.62	1.23
7219825	238.01	17.23	2.40	17.23	2.54
7219825	238.02	26.69	1.35		
7345248				5.66	0.81
7419318	313.02	8.44	1.61		
7419318	313.01	18.74	2.20	18.74	1.89
7466863				11.97	2.89

Table 3.4 (cont'd): Union of [Batalha et al. \(2012\)](#) and TERRA planet candidate catalogs

KIC	Batalha			TERRA	
	KOI	$P$	$R_P$	$P$	$R_P$
7582689				11.92	1.34
7668663	1898.01	6.50	1.50	6.50	1.79
7700622	315.01	35.59	2.14	35.59	2.13
7762723				9.89	0.64
7810483				29.92	1.70
7906739				7.01	0.80
7906892				8.85	0.72
7918652				11.46	1.02
8008067	316.01	15.77	2.72	15.77	2.66
8009496				38.48	1.74
8073705				10.60	0.91
8077137	274.01	15.09	1.12	15.09	0.99
8077137	274.02	22.80	1.13		
8081187				37.32	1.57
8087812				27.21	1.55
8242434	1726.01	44.96	5.25	44.96	1.92
8280511	1151.01	5.22	0.84		
8280511	1151.02	7.41	0.97		
8280511				10.44	1.36
8323753				6.71	2.71
8349582	122.01	11.52	2.78	11.52	3.15
8429668				5.01	0.52
8480285	691.02	16.23	1.25		
8480285	691.01	29.67	2.92	29.67	2.89
8494617	2389.01	22.92	1.45	22.92	1.27
8554498	5.02	7.05	0.66		
8560804				31.98	1.09
8611832	2414.01	22.60	1.03	22.60	1.17
8611832	2414.02	45.35	1.17		
8628758	1279.02	9.65	0.74		
8628758	1279.01	14.37	1.31	14.37	2.26
8631504	2503.01	14.82	2.41	14.82	0.95
8644365				19.92	1.31
8804455	2159.01	7.60	1.01	7.60	1.33
8805348	695.01	29.91	2.51	29.91	2.69
8822366	1282.01	30.86	3.00	30.86	1.76
8827575				10.13	0.82
8866102	42.01	17.83	2.71	17.83	2.08
8962094	700.02	9.36	1.29		

Table 3.4 (cont'd): Union of Batalha et al. (2012) and TERRA planet candidate catalogs

KIC	Batalha			TERRA	
	KOI	$P$	$R_P$	$P$	$R_P$
8962094	700.03	14.67	1.29		
8962094	700.01	30.86	2.28	30.87	2.38
8972058	159.01	8.99	2.70	8.99	2.39
9006186	2169.01	5.45	1.02	5.45	0.81
9086251	2367.01	6.89	1.17	6.89	1.38
9139084	323.01	5.84	2.17	5.84	1.92
9226339				21.46	1.50
9288237				7.49	0.54
9471974	119.01	49.18	3.76		
9491832				49.57	1.95
9549648	1886.01	5.99	2.45	5.99	1.82
9704384	1913.01	5.51	1.40	5.51	1.35
9716028				17.37	1.03
9717943	2273.01	6.11	1.02	6.11	1.00
9886361				7.03	1.08
10055126	1608.01	9.18	1.81	9.18	1.59
10055126	1608.02	19.74	1.58		
10130039	1909.02	5.47	1.15		
10130039	1909.01	12.76	1.52	12.76	1.31
10130039	1909.03	25.10	1.63		
10136549	1929.01	9.69	2.00	9.69	1.98
10212441	2342.01	15.04	1.22	15.04	1.13
10593535				20.92	1.27
10722485				7.85	0.98
10917433				6.91	0.62
11086270	124.01	12.69	3.00		
11086270	124.02	31.72	3.58	31.72	2.24
11121752	2333.02	7.63	1.63	7.63	1.22
11133306	276.01	41.75	2.49	41.75	2.27
11241912				14.43	1.10
11250587	107.01	7.26	3.09	7.26	3.18
11253711	1972.01	17.79	1.93	17.79	1.92
11295426	246.01	5.40	2.53	5.40	2.68
11402995	173.01	10.06	2.48	10.06	2.56
11554435	63.01	9.43	6.30	9.43	5.60
11560897	2365.01	35.97	1.59	35.97	2.03
11612280				9.41	1.15
11771430	2582.01	40.03	1.98	40.03	2.10
11774991	2173.01	37.82	1.24	37.82	1.10

Table 3.4 (cont'd): Union of [Batalha et al. \(2012\)](#) and TERRA planet candidate catalogs

KIC	Batalha			TERRA	
	KOI	$P$	$R_P$	$P$	$R_P$
11818872	2581.01	12.74	0.90		
12254909	2372.01	5.35	1.11	5.35	0.88
12301181	2059.01	6.15	0.59	6.15	0.84
12416661				8.05	1.02
12454461	2463.01	7.47	1.07	7.47	1.16
12737015				24.67	1.84

Note. — All [Batalha et al. \(2012\)](#) candidates with  $P = 5$ –50 days belonging to stars in the Best12k sample are included. Candidates are considered equal if they belong to the same star and the periods in each catalog agree to better than 0.01 days. Eighty-two candidates appear in both catalogs, 33 appear in [Batalha et al. \(2012\)](#) only, and 47 appear in this work only (although 10 were listed as false positives by the *Kepler* team). Differences in  $R_P$  between the two catalogs stem from different values of  $R_*$ . Most TERRA planet candidates have SpecMatch-derived stellar parameters which are more accurate than [Batalha et al. \(2012\)](#) parameters, which were derived from KIC broadband photometry.

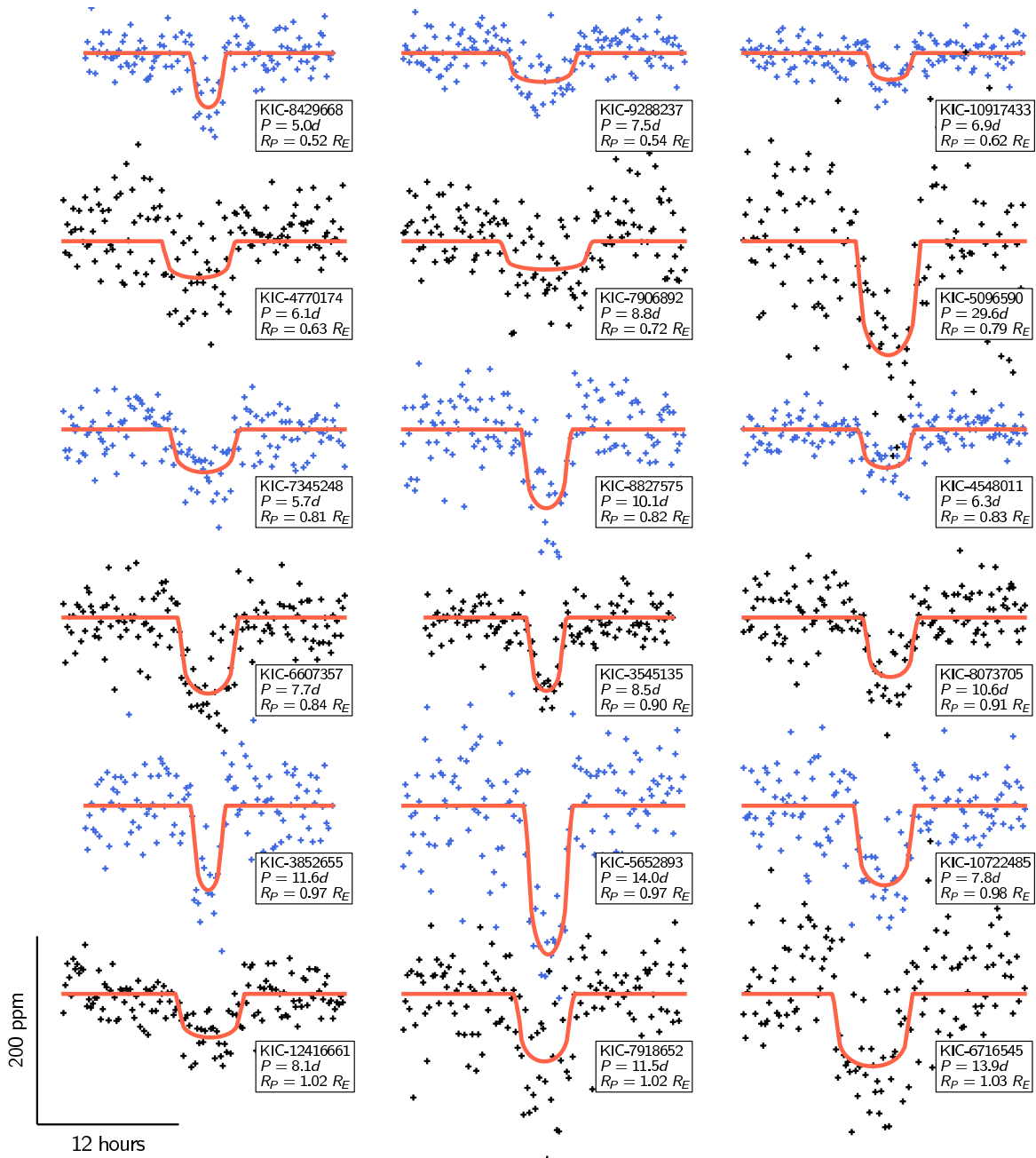


Figure 3.17: Phase-folded photometry for 18 of the 37 TERRA planet candidates, not in [Batalha et al. \(2012\)](#), ordered according to size. For clarity, we show median photometric measurements in 10 min bins. The red lines are the best-fitting [Mandel & Agol \(2002\)](#) model.

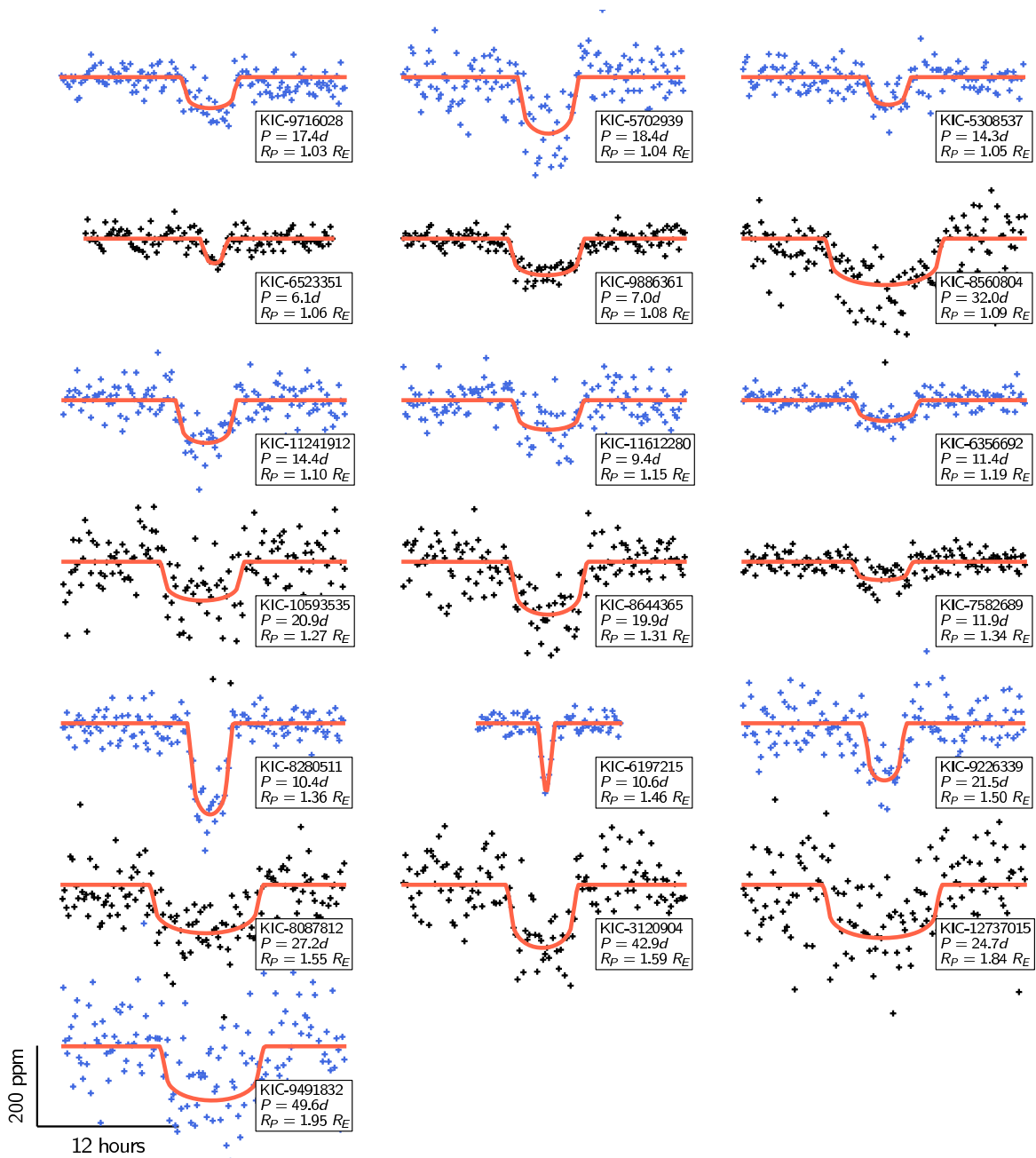


Figure 3.18: Same as Figure 3.17, but showing the remaining 19 of the 37 TERRA planet candidates, not in Batalha et al. (2012).

## 4

# The Prevalence of Earth-Size Planets Orbiting Sun-Like Stars

A version of this chapter was previously published in the *Proceedings of the National Academy of Science* (Erik A. Petigura, Andrew W. Howard, & Geoffrey W. Marcy, 2013, PNAS 110, 19273).

NASA’s *Kepler* mission was launched in 2009 to search for planets that transit (cross in front of) their host stars [Borucki et al. \(2010\)](#); [Koch et al. \(2010\)](#); [Borucki et al. \(2011\)](#); [Batalha et al. \(2012\)](#). The resulting dimming of the host stars is detectable by measuring their brightness, and *Kepler* monitored the brightness of 150,000 stars every 30 minutes for four years. To date, this exoplanet survey has detected more than 3000 planet candidates [Batalha et al. \(2012\)](#).

The most easily detectable planets in the *Kepler* survey are those that are relatively large and orbit close to their host stars, especially those stars having lower intrinsic brightness fluctuations (noise). These large, close-in worlds dominate the list of known exoplanets. But the *Kepler* brightness measurements can be analyzed and debiased to reveal the diversity of planets, including smaller ones, in our Milky Way Galaxy [Howard et al. \(2012\)](#); [Petigura et al. \(2013b\)](#); [Fressin et al. \(2013\)](#). These previous studies showed that small planets approaching Earth-size are the most common, but only for planets orbiting *close* to their host stars. Here, we extend the planet survey to *Kepler*’s most important domain – Earth-size planets orbiting far enough from Sun-like stars to receive a similar intensity of light energy as Earth.

## 4.1 Planet Survey

We performed an independent search of *Kepler* photometry for transiting planets with the goal of measuring the underlying occurrence distribution of planets as a function of orbital period,  $P$ , and planet radius,  $R_P$ . We restricted our survey to a set of Sun-like stars (“GK-type”) that are the most amenable to the detection of Earth-size planets. We

define GK-type stars as those with surface temperatures  $T_{\text{eff}} = 4100\text{--}6100$  K and gravities  $\log g = 4.0\text{--}4.9$  (cgs) [Pinsonneault et al. \(2012\)](#). Our search for planets was further restricted to the brightest Sun-like stars observed by *Kepler* ( $Kp = 10\text{--}15$  mag). These 42557 stars (“Best42k”) have the lowest photometric noise making them amenable to the detection of Earth-size planets. When a planet crosses in front of its star, it causes a fractional dimming that is proportional to the fraction of the stellar disk blocked,  $\delta F = (R_P/R_\star)^2$ , where  $R_\star$  is the radius of the star. As viewed by a distant observer, the Earth dims the Sun by  $\sim 100$  parts per million (ppm) lasting 12 hours every 365 days.

We searched for transiting planets in *Kepler* brightness measurements using our custom-built TERRA software package described in previous work [Petigura & Marcy \(2012\)](#); [Petigura et al. \(2013b\)](#) and in the Supporting Information (SI). In brief, TERRA conditions *Kepler* photometry in the time-domain, removing outliers, long timescale variability ( $> 10$  day), and systematic errors common to a large number of stars. TERRA then searches for transit signals by evaluating the signal-to-noise ratio (SNR) of prospective transits over a finely-spaced three-dimensional grid of orbital period,  $P$ , time of transit,  $t_0$ , and transit duration,  $\Delta T$ . This grid-based search extends over the orbital period range 0.5–400 days.

TERRA produced a list of “Threshold Crossing Events” (TCEs) that meet the key criterion of a photometric dimming signal-to-noise ratio,  $\text{SNR} > 12$ . Unfortunately, an unwieldy 16227 TCEs met this criterion, many of which are inconsistent with the periodic dimming profile from a true transiting planet. Further vetting was performed by automatically assessing which light curves were consistent with theoretical models of transiting planets [Mandel & Agol \(2002\)](#). We also visually inspected each TCE light curve, retaining only those exhibiting a consistent, periodic, box-shaped dimming, and rejecting those caused by single epoch outliers, correlated noise, and other data anomalies. The vetting process was applied homogeneously to all TCEs and is described in further detail in the SI.

To assess our vetting accuracy, we evaluated the 235 Kepler Objects of Interest (KOIs) among Best42k stars having  $P > 50$  days which had been found by the *Kepler* Project and identified as planet “candidates” in the official Exoplanet Archive.<sup>1</sup> Among them, we found four whose light curves are not consistent with being planets. These four KOIs (364.01, 2224.02, 2311.01, and 2474.01) have long periods and small radii (see SI). This exercise suggests that our vetting process is robust, and that careful scrutiny of the light curves of small planets in long period orbits is useful to identify false positives.

Vetting of our TCEs produced a list of 836 eKOIs, which are analogous to KOIs produced by the *Kepler* Project. Each light curve is consistent with an astrophysical transit, but could be due to an eclipsing binary (EB), either in the background or gravitationally bound, instead of a transiting planet. If an EB resides within the software aperture of a *Kepler* target star (within  $\sim 10$  arcsec), the dimming of the EB can masquerade as a planet transit when diluted by the bright target star. We rejected as likely EBs any eKOIs with these characteristics: radii larger than  $20 R_\oplus$ , observed secondary eclipse, or astrometric motion of the target star in and out of transit (SI). This rejection of EBs left 603 eKOIs in our catalog.

<sup>1</sup>URL:exoplanetarchive.ipac.caltech.edu (accessed 19 September 2013)

*Kepler* photometry can be used to measure  $R_P/R_\star$  with high precision, but the extraction of planet radii is compromised by poorly known radii of the host stars [Brown et al. \(2011\)](#). To determine  $R_\star$  and  $T_{\text{eff}}$ , we acquired high-resolution spectra of 274 eKOIs using HIRES spectrometer on the 10-m Keck I telescope. Notably, we obtained spectra of all 62 eKOIs that have  $P > 100$  days. For these stars, the  $\sim 35\%$  errors in  $R_\star$  were reduced to  $\sim 10\%$  by matching spectra to standards.

To measure planet occurrence, one must not only detect planets but also assess what fraction of planets were missed. Missed planets are of two types, those whose orbital planes are so tilted as to avoid dimming the star and those whose transits were not detected in the photometry by TERRA. Both effects can be quantified to establish a statistical correction factor. The first correction can be computed as the geometrical probability that an orbital plane is viewed edge-on enough (from Earth) so that the planet transits the star. This probability is,  $P_T = R_\star/a$ , where  $a$  is the semi-major axis of the orbit.

The second correction is computed by the injection and recovery of synthetic (mock) planet-caused dimmings into real *Kepler* photometry. We injected 40,000 transit-like synthetic dimmings having randomly selected planetary and orbital properties into the actual photometry of our Best42k star sample, with stars selected at random. We measured survey completeness,  $C(P, R_P)$ , in small bins of  $(P, R_P)$ , determining the fraction of injected synthetic planets that were “discovered” by TERRA (SI). [Fig. 4.1](#) shows the 603 detected planets and the survey completeness,  $C$ , color-coded as a function of  $P$  and  $R_P$ .

The survey completeness for small planets is a complicated function of  $P$  and  $R_P$ . It decreases with increasing  $P$  and decreasing  $R_P$  as expected due to fewer transits and less dimming, respectively. It is dangerous to replace this injection and recovery assessment with noise models to determine  $C$ . Such models are not sensitive to the absolute normalization of  $C$ , only providing relative completeness. Models also may not capture the complexities of a multistage transit-finding pipeline that is challenged by correlated, non-stationary, and non-Gaussian noise. Measuring the occurrence of small planets with long periods requires injection and recovery of synthetic transits to determine the absolute detectability of the small signals buried in noise.

## 4.2 Planet Occurrence

We define planet occurrence,  $f$ , to be the fraction of stars having a planet within a specified range of orbital period, size, and perhaps other criteria. We report planet occurrence as a function of planet size and orbital period,  $f(P, R_P)$  and as a function of planet size and the stellar light intensity (flux) incident on the planet,  $f(F_P, R_P)$ .

### 4.2.1 Planet Occurrence and Orbital Period

We computed  $f(P, R_P)$  in a  $6 \times 4$  grid of  $P$  and  $R_P$  shown in [Fig. 4.2](#). We start by first counting the number of detected planets,  $n_{\text{cell}}$ , in each  $P$ - $R_P$  cell. Then we computed

$f(P, R_P)$  by making statistical corrections for planets missed because of non-transiting orbital inclinations and because of the completeness factor,  $C$ . The first correction augments each detected transiting planet by  $1/P_T = a/R_*$ , where  $P_T$  is the geometric transit probability, to account for planets missed in inclined orbits. Accounting for the completeness,  $C$ , the occurrence in a cell is  $f(P, R_P) = 1/n_* \sum_i a_i / (R_{*,i} C_i)$ , where  $n_* = 42,557$  stars and the sum is over all detected planets within that cell. Uncertainties in the statistical corrections for  $a/R_*$  and for completeness may cause errors in the final occurrence rates of  $\sim 10\%$ . Such errors will be smaller than the Poisson uncertainties in the occurrence of Earth-size planets in long period orbits.

Fig. 4.2 shows the occurrence of planets,  $f(P, R_P)$ , within the  $P$ - $R_P$  plane. Each cell is color-coded to indicate the final planet occurrence: the fraction of stars having a planet with radius and orbital period corresponding to that cell (after correction for both completeness factors). For example,  $7.7 \pm 1.3\%$  of Sun-like stars have a planet with periods between 25 and 50 days and sizes between 1 and  $2 R_\oplus$ .

We compute the distribution of planet sizes, including all orbital periods  $P = 5$ –100 days, by summing  $f(P, R_P)$  over all periods. The resulting planet size distribution is shown in Fig 4.3a. Planets with orbital periods of 5–100 days have a characteristic shape to their size distribution (Fig 3b). Jupiter-sized planets ( $11 R_\oplus$ ) are rare, but the occurrence of planets rises steadily with decreasing size down to about  $2 R_\oplus$ . The distribution is nearly flat (equal numbers of planets per log  $R_P$  interval) for 1–2  $R_\oplus$  planets. *We find that  $26 \pm 3\%$  of Sun-like stars harbor an Earth-size planet (1–2  $R_\oplus$ ) with  $P = 5$ –100 days, compared to  $1.6 \pm 0.4\%$  occurrence of Jupiter-size planets (8–16  $R_\oplus$ ).*

We also computed the distribution of orbital periods, including all planet sizes, by summing each period interval of  $f(P, R_P)$  over all planet radii. As shown in Fig. 4.3b, the occurrence of planets larger than Earth rises from  $8.9 \pm 0.7\%$  in the  $P = 6.25$ –12.5 day domain to  $13.7 \pm 1.2\%$  in the  $P = 12.5$ –25 day interval and is consistent with constant for larger periods. This rise and plateau feature was observed for  $\gtrsim 2 R_\oplus$  planets in earlier work Youdin (2011); Howard et al. (2012).

Two effects lead to minor corrections to our occurrence estimates. First, some planets in multi-transiting systems are missed by TERRA. Second, a small number of eKOIs are false detections. These two effects are small, and they provide corrections to our occurrence statistics with opposite signs. To illustrate their impact, we consider the small and long period ( $P > 50$  days) planets that are the focus of this study.

TERRA detects the highest SNR transiting planet per system, so additional transiting planets that cause lower SNR transits are not included in our occurrence measurement. Using the *Kepler* Project catalog (Exoplanet Archive), we counted the number of planets within the same cells in  $P$  and  $R_P$  as Fig. 4.2, noting those that did not yield the highest SNR in the system. Inclusion of these second and third transiting planets boosts the total number of planets per cell (and hence the occurrence) by 21–28% over the  $P = 50$ –400,  $R_P = 1$ –4  $R_\oplus$  domain (SI).

Even with our careful vetting of eKOIs, the light curves of some false positives scenarios are indistinguishable from planets. Fressin et al. Fressin et al. (2013) simulated the con-

tamination of a previous KOI [Batalha et al. \(2012\)](#) sample by false positives that were not removed by the *Kepler* Project vetting process. They determined that the largest source of false positives for Earth-size planets are physically bound stars with a transiting Neptune-size planet with an overall false positive rate of 8.8–12.3%. As we have shown (Fig. 4.2), the occurrence of Neptune-size planets is nearly constant as a function of orbital period, in  $\log P$  intervals. Thus, this false positive rate is also nearly constant in period. Therefore, we adopt a 10% false positive rate for planets having  $P = 50$ –400 days and  $R_P = 1$ –2  $R_{\oplus}$ . Planet occurrence, shown in Figs 4.2 and 4.3, has not been adjusted to account for false positives or planet multiplicity. The quoted errors reflect only binomial counting uncertainties. Note that for Earth-size planets in the 50–100 day and 100–200 day period bins, planet occurrence is  $5.8 \pm 1.8\%$  and  $3.2 \pm 1.6\%$ , respectively. Corrections due to false positives or planet multiplicity are smaller than fractional uncertainties due to small number statistics.

### 4.2.2 Planet Occurrence and Stellar Light Intensity

The amount of light energy a planet receives from its host star depends on the luminosity of the star ( $L_{\star}$ ) and the planet-star separation ( $a$ ). Stellar light flux,  $F_P$ , is given by  $F_P = L_{\star}/4\pi a^2$ . The intensity of sunlight on Earth is  $F_{\oplus} = 1.36 \text{ kW m}^{-2}$ . We compute  $L_{\star}$  using  $L_{\star} = 4\pi R_{\star}^2 \sigma T_{\text{eff}}^4$  where  $\sigma = 5.670 \times 10^{-8} \text{ W m}^{-2} \text{ K}^{-4}$  is the Stefan-Boltzmann constant. The dominant uncertainty in  $F_P$  is due to  $R_{\star}$ . Using spectroscopic stellar parameters, we determine  $F_P$  to 25% accuracy, and to 80% accuracy using photometric parameters. We obtained spectra for all 62 stars hosting planets with  $P > 100$  days, allowing more accurate light intensity measurements.

Fig. 4.4 shows the two-dimensional domain of stellar light flux incident on our 603 detected planets, along with planet size. The planets in our sample receive a wide range of flux from their host stars, ranging from 0.5 to 700  $F_{\oplus}$ . We highlight the 10 small ( $R_P = 1$ –2  $R_{\oplus}$ ) planets that receive stellar flux comparable to Earth,  $F_P = 0.25$ –4  $F_{\oplus}$ .

Since only two 1–2  $R_{\oplus}$  planets have  $F_P < 1 F_{\oplus}$ , we measure planet occurrence in the domain, 1–2  $R_{\oplus}$  and 1–4  $F_{\oplus}$ . *Correcting for survey completeness we find that  $11 \pm 4\%$  of Sun-like stars have a  $R_P = 1$ –2  $R_{\oplus}$  planet that receives between 1 and 4 times the incident flux as the Earth (SI).*

## 4.3 Interpretation

### 4.3.1 Earth-Size Planets with Year-Long Orbital Periods

Detections of Earth-size planets having orbital periods of  $P = 200$ –400 days are expected to be rare in this survey. Low survey completeness ( $C \approx 10\%$ ) and low transit probability ( $P_T = 0.5\%$ ) imply that only a few such planets would be expected, even if they are intrinsically

common. Indeed, we did not detect any such planets with **TERRA**.<sup>2</sup> We can place an upper limit on their occurrence:  $f < 12\%$  with 95% confidence using binomial statistics. We would have detected one or two such planets if their occurrence were higher than 12%.

However, one may estimate the occurrence of 1–2  $R_{\oplus}$  planets with periods of 200–400 days by a modest extrapolation of planet occurrence with  $P$ . Fig. 4.5 shows the fraction of stars with 1–2  $R_{\oplus}$  planets, whose orbital period is less than a maximum period,  $P$ , on the horizontal axis. This cumulative period distribution shows that 20.4% of Sun-like stars harbor a 1–2  $R_{\oplus}$  planet with an orbital period,  $P < 50$  days. Similarly, 26.2% of Sun-like stars harbor a 1–2  $R_{\oplus}$  planet with a period less than 100 days. The linear increase in cumulative occurrence implies constant planet occurrence per  $\log P$  interval. Extrapolating the cumulative period distribution predicts  $5.7^{+1.7}_{-2.2}\%$  occurrence of Earth-size (1–2  $R_{\oplus}$ ) planets with orbital periods of  $\sim 1$  year ( $P = 200\text{--}400$  days). The details of our extrapolation technique are explained in the SI. *Extrapolation based on detected planets with  $P < 200$  days predicts that  $5.7^{+1.7}_{-2.2}\%$  of Sun-like stars have an Earth-size planet on an Earth-like orbit ( $P = 200\text{--}400$  days).*

Naturally, such an extrapolation carries less weight than a direct measurement. However, the loss of *Kepler*'s second reaction wheel in May 2013 ended observations shortly after the completion of the nominal 3.5 year mission. We cannot count on any additional *Kepler* data to improve the low completeness to Eartha analog planets beyond what is reported here. Indeed, low survey sensitivity to Earth analogs was the primary reason behind a four-year extension to the *Kepler* mission. Modest extrapolation is required to understand the prevalence of Earth-size planets with Earth-like orbits around Sun-like stars.

We offer empirical and theoretical justification for extrapolation out to 400 days. As shown in Fig. 4.2, the prevalence of small planets as a function of  $\log P$  is remarkably uniform. To test the reliability of our extrapolation into a region of low completeness, we used the same technique to estimate occurrence in more complete regions of phase space and compared the results with our measured occurrence values.

Again, assuming uniform occurrence per  $\log P$  interval, extrapolating the occurrence of 2–4  $R_{\oplus}$  planets from 50–200 day orbits out to 400 days predicts  $6.4^{+0.5}_{-1.2}\%$  occurrence of planets in the domain of  $R_P = 1\text{--}2 R_{\oplus}$  and  $P = 200\text{--}400$  days. The extrapolation is consistent with the measured value of  $5.0 \pm 2.1\%$  to within 1  $\sigma$  uncertainty. Furthermore, extrapolation based on 1–2  $R_{\oplus}$  planets with  $P = 12.5\text{--}50$  days predicts  $6.5^{+0.9}_{-1.7}\%$  occurrence within the  $R_P = 50\text{--}100$  day bin. Again, the measured value of  $5.8 \pm 1.6\%$  agrees to better than 1  $\sigma$ .

While planet size is governed by non-linear processes such as runaway gas accretion [Ida et al. \(2013\)](#), which favors certain planet sizes over others, no such non-linear processes occur as a function of orbital period in the range, 200–400 days. Extrapolation out to orbital periods of 200–400 days, while dangerous, seems unlikely to be unrealistic by more than factors of two.

<sup>2</sup>Although the radii of three planets (KIC-4478142, KIC-8644545, and KIC-10593626) have 1  $\sigma$  confidence intervals that extend into the  $P = 200\text{--}400$  day  $R_P = 1\text{--}2 R_{\oplus}$  domain.

### 4.3.2 Earth-Size Planets in the Habitable Zone

While the details of planetary habitability are debated and depend on planet-specific properties as well as the stochastic nature of planet formation Seager (2013), the “habitable zone” (HZ) is traditionally defined as the set of planetary orbits that permit liquid water on the surface. The precise inner and outer edges of the HZ depend on details of the model Kasting et al. (1993); Kopparapu et al. (2013); Zsom et al. (2013); Pierrehumbert & Gaidos (2011). For solar analog stars, Zsom et al. (2013) estimated that the inner edge of the HZ could reside as close as 0.38 AU, for planets having either a reduced greenhouse effect due to low humidity or a high reflectivity Zsom et al. (2013). Pierrehumbert and Gaidos (2011) estimated that the outer edge of the HZ may extend up to 10 AU for planets that are kept warm by efficient greenhouse warming with an H<sub>2</sub> atmosphere Pierrehumbert & Gaidos (2011).

A planet’s ability to retain surface liquid water depends, in large part, on the energy received from its host star. We consider a planet to reside in the HZ if it is bathed in a similar level of starlight as Earth. One may adopt  $F_P = 0.25\text{--}4 F_\oplus$  as a simple definition of the HZ, which corresponds orbital separations of 0.5 to 2.0 AU for solar analog stars. This definition is more conservative than the range of published HZ boundaries that extend from 0.38 AU to 10 AU Zsom et al. (2013); Pierrehumbert & Gaidos (2011). This HZ includes Venus (0.7 AU) and Mars (1.5 AU) which do not currently have surface liquid water. However, Venus may have had liquid water in its past, and there is strong geomorphological evidence of liquid water earlier in Mars’ history Seager (2013).

Previously, we showed that  $11 \pm 4\%$  of stars harbor a planet having an  $R_P = 1\text{--}2 R_\oplus$  and  $F_P = 1\text{--}4 F_\oplus$ . Using the definition of  $F_P$  and Kepler’s third law,  $F_P$  is proportional to  $P^{-4/3}$ . Therefore, uniform occurrence in  $\log P$  translates to uniform occurrence in  $\log F_P$ . We find that the occurrence of  $1\text{--}2 R_\oplus$  planets is constant per  $\log F_P$  interval for  $F_P = 100\text{--}1 F_\oplus$ . If one were to adopt  $F_P = 0.25\text{--}4 F_\oplus$  as the HZ and extrapolate from the  $F_P = 1\text{--}4 F_\oplus$  domain, then occurrence of HZ Earth-size planets is 22% for Sun-like stars.

One may adopt alternative definitions of both the properties of Earth-size planets and the domain of the HZ. We showed previously that the occurrence of planets is approximately constant as a function of both  $R_P$  (for  $R_P < 2.8 R_\oplus$ ) and  $P$  (in logarithmic intervals). Thus, the occurrence of planets in this domain is proportional to a logarithmic area in the  $R_P\text{--}F_P$  parameter space being considered. For example, the occurrence of planets of size  $1.0\text{--}1.4 R_\oplus$  in orbits that receive  $0.25\text{--}1.0 F_\oplus$  in stellar flux is  $22\%/4 = 5.5\%$ . We offer a number of estimates for the prevalence of Earth-size planets in the HZ based different published definitions of the HZ in Table 4.1.

Cooler, M dwarf stars also have a high occurrence of Earth-size planets. Based on the *Kepler* planet catalog, Dressing et al. Dressing & Charbonneau (2013) found that  $15_{-6}^{+15}\%$  of early M dwarfs have an Earth-size planet ( $0.5\text{--}1.4 R_\oplus$ ) in the HZ using a conservative definition of  $0.5\text{--}1.1 F_\oplus$  Kasting et al. (1993), and three times that value when the HZ is expanded to  $0.25\text{--}1.5 F_\oplus$  Kopparapu (2013). This result is consistent with a Doppler survey that found that  $41_{-13}^{+54}\%$  of nearby M dwarfs have planets with masses  $1\text{--}10$  Earth masses

( $M_{\oplus}$ ) in the HZ [Bonfils et al. \(2013\)](#). Thus, Earth-size planets appear to be common in the HZs of a range of stellar types.

## 4.4 Conclusions

Using *Kepler* photometry of Sun-like stars (GK-type), we have measured the prevalence of planets having different orbital periods and sizes, down to the size of the Earth and out to orbital periods of one year. We gathered Keck spectra of all host stars of planets having periods greater than 100 days to accurately determine their radii. The detection of planets with periods longer than 100 days is challenging, and we have characterized our sensitivity to such planets by using injection and recovery of synthetic planets in the photometry. After correcting for orbital tilt and detection completeness, we find that  $26 \pm 3\%$  of Sun-like stars have an Earth-size ( $1\text{--}2 R_{\oplus}$ ) planet with  $P = 5\text{--}100$  days. We also find that  $11 \pm 4\%$  of Sun-like stars harbor an Earth-size planet that receives nearly Earth-levels of stellar energy ( $F_P = 1\text{--}4 F_{\oplus}$ ).

We have shown that small planets far outnumber large ones. Only  $1.6 \pm 0.4\%$  of Sun-like stars harbor a Jupiter-size ( $8\text{--}16 R_{\oplus}$ ) planet with  $P = 5\text{--}100$  days compared to  $23 \pm 3\%$  occurrence of Earth-size planets. This pattern supports the core accretion scenario in which planets form by the accumulation of solids first and gas later in the protoplanetary disk [Levy & Lunine \(1993\)](#); [Pollack et al. \(1996\)](#); [Ida et al. \(2013\)](#); [Mordasini et al. \(2012\)](#). The details of this family of models are hotly debated, including the movement of material within the disk, the timescale for planet formation, and the amount of gas accretion in small planets. Our measurement of a constant occurrence of  $1\text{--}2.8 R_{\oplus}$  planets per  $\log P$  interval establishes an important observational constraint for these models.

The occurrence of Earth-size planets is constant with decreasing stellar light intensity from  $100 F_{\oplus}$  down to  $1 F_{\oplus}$ . If one were to assume that this pattern continues down to  $0.25 F_{\oplus}$ , then the occurrence of planets having flux levels of  $1\text{--}0.25 F_{\oplus}$  is also  $11 \pm 4\%$ .

Earth-size planets are common in the *Kepler* field. If the stars in the *Kepler* field are representative of stars in the solar neighborhood, then Earth-size planets are common around nearby Sun-like stars. If one were to adopt a  $22\%$  occurrence rate of Earth-size planets in habitable zones of Sun-like stars, then the nearest such planet is expected to orbit a star that is less than 12 light-years from Earth and can be seen by the unaided eye. Future instrumentation to image and take spectra of these Earths need only observe a few dozen nearby stars to detect a sample of Earth-size planets residing in the habitable zones of their host stars.

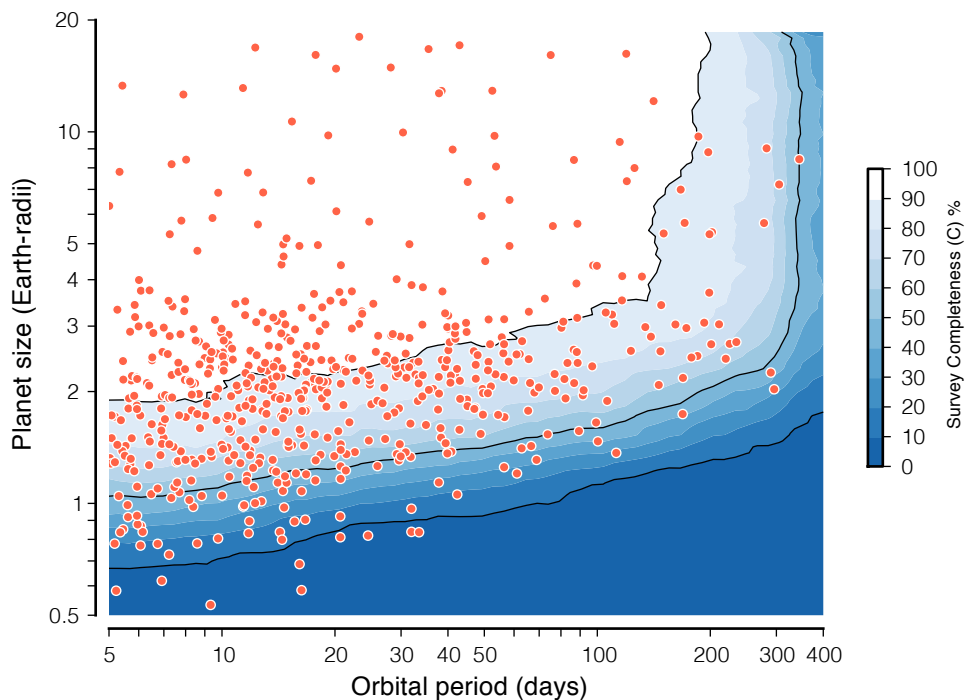


Figure 4.1: Two-dimensional domain of orbital period and planet size, on a logarithmic scale. Red circles show the 603 detected planets in our survey of 42,557 bright, Sun-like stars ( $Kp = 10\text{--}15$  mag, GK spectral type). The color scale shows survey completeness measured by injection and recovery of synthetic planets into real photometry. Dark regions represent  $(P, R_P)$  with low completeness,  $C$ , where significant corrections for missed planets must be made to compute occurrence. The most common planets *detected* have orbital  $P < 20$  days and  $R_P \approx 1\text{--}3 R_\oplus$  (at middle-left of graph). But their detectability is favored by orbital tilt and detection completeness,  $C$ , that favors detection of such close-in, large planets.

Table 4.1: Occurrence of Small Planets the Habitable Zone

HZ Definition	$a_{\text{inner}}$	$a_{\text{outer}}$	$F_{P,\text{inner}}$	$F_{P,\text{outer}}$	$f_{\text{HZ}}$
Simple	0.5	2	4	0.25	22%
Kasting (1993)	0.95	1.37	1.11	0.53	5.8%
Kopparapu et al. (2013)	0.99	1.70	1.02	0.35	8.6%
Zsom et al. (2013)	0.38	...	6.92	...	26%
Pierrehumbert & Gaidos (2011)	...	10	...	0.01	$\sim 50\%^*$

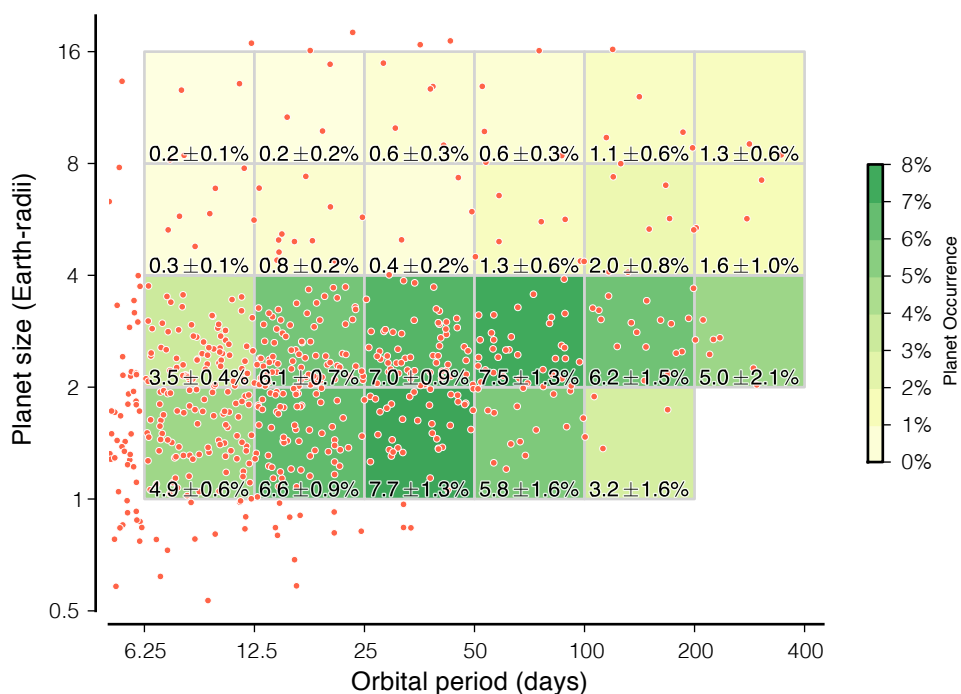


Figure 4.2: Planet occurrence,  $f(P, R_P)$ , as a function of orbital period and planet radius for  $P = 6.25\text{--}400$  days and  $R_P = 0.5\text{--}16 R_\oplus$ . As in Fig. 4.1, detected planets are shown as red circles. Each cell spans a factor of two in orbital period and planet size. Planet occurrence in a cell is given by  $f(P, R_P) = 1/n_\star \sum_i a_i / (R_{\star,i} C_i)$  where the sum is over all detected planets within each cell. Here,  $a_i / R_i$  is the number of non-transiting planets (for each detected planet) due to large tilt of the orbital plane,  $C_i = C(P_i, R_{P,i})$  is the detection completeness factor, and  $n_\star = 42,557$  stars in the Best42k sample. Cells are colored according to planet occurrence within the cell. We quote planet occurrence within each cell. We do not color cells where the completeness is less than 25%. Among the small planets, 1–2 and 2–4  $R_\oplus$ , planet occurrence is constant (within a factor of two level) over the entire range of orbital period. This uniformity supports mild extrapolation into the  $P = 200\text{--}400$  day,  $R_P = 1\text{--}2 R_\oplus$  domain.

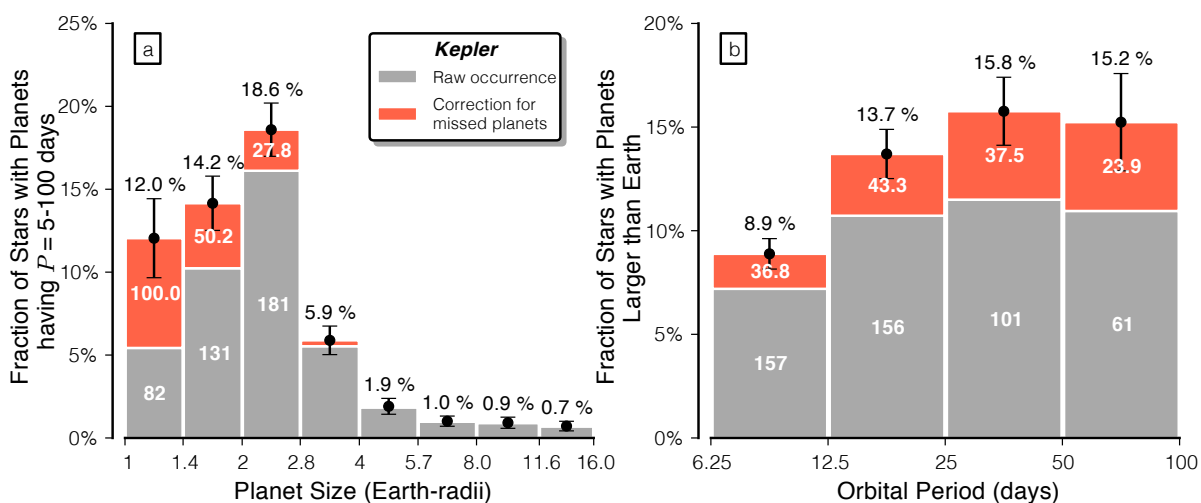


Figure 4.3: The measured distributions of planet sizes and orbital periods for  $R_P > 1 R_\oplus$  and  $P = 5\text{--}100$  days. Heights of the bars represent the fraction of Sun-like stars harboring a planet within a given  $P$  or  $R_P$  domain. The gray portion of the bars show planet occurrence without correction for survey completeness, i.e. for  $C = 1$ . The red region shows the correction to account for missed planets,  $1/C$ . Bars are annotated to reflect the number of planets detected (gray bars) and missed (red bars). The occurrence of planets of different sizes rises by a factor of 10 from Jupiter-size to Earth-sized planets. The occurrence of planets with different orbital periods is constant, within 15%, between 12.5 and 100 days. Due to the small number of detected planets with  $R_P = 1\text{--}2 R_\oplus$  and  $P > 100$  days (four detected planets), we do not include  $P > 100$  days in these marginalized distributions.

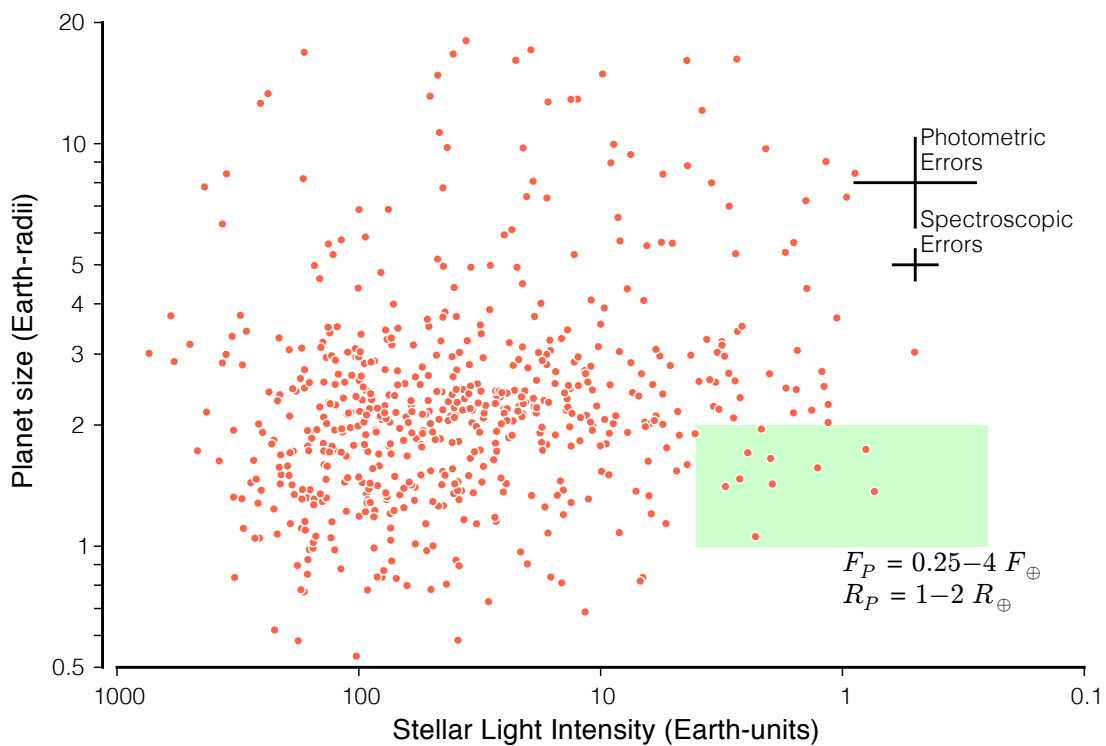


Figure 4.4: The detected planets (dots) in a two-dimensional domain similar to Figures 4.1 and 4.2. Here, the two-dimensional domain has orbital period replaced by stellar light intensity, “incident flux,” hitting the planet. The highlighted region shows the 10 Earth-size planets that receive a incident stellar flux comparable to the Earth: flux =  $0.25-4.0 \times$  the flux received by Earth from the Sun. Our uncertainties on stellar flux and planet radii are indicated at top right.

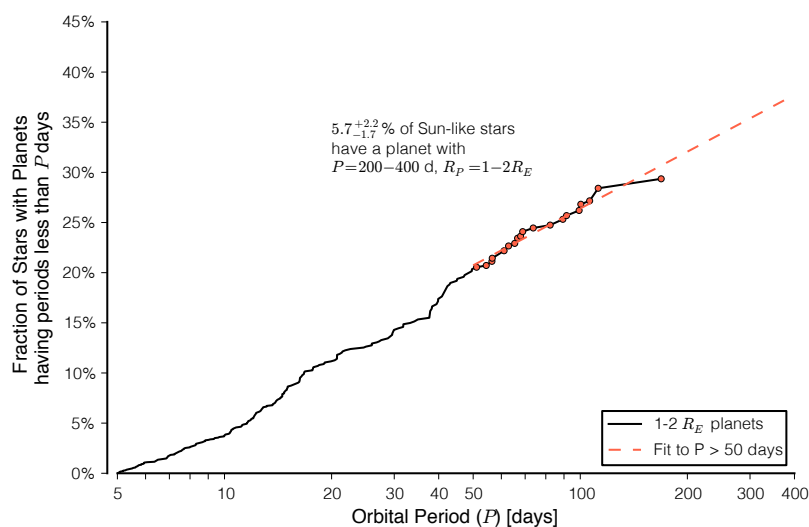


Figure 4.5: The fraction of stars having nearly Earth-size planets ( $1-2 R_{\oplus}$ ) with any orbital period up to a maximum period,  $P$ , on the horizontal axis. Only planets of nearly Earth-size ( $1-2 R_{\oplus}$ ) are included. This cumulative distribution reaches 20.2% at  $P = 50$  days, meaning 20.4% of Sun-like stars harbor a  $1-2 R_{\oplus}$  planet with an orbital period,  $P < 50$  days. Similarly, 26.2% of Sun-like stars harbor a  $1-2 R_{\oplus}$  planet with a period of  $P < 100$  days. The linear increase in this cumulative quantity corresponds to planet occurrence that is constant in equal intervals of  $\log P$ . One may perform a modest extrapolation into the  $P = 200-400$  day range, equivalent to assuming constant occurrence per  $\log P$  interval, using all planets with  $P > 50$  days. Such an extrapolation predicts that  $5.7^{+1.7}_{-2.2}\%$  of Sun-like stars have a planet with size,  $1-2 R_{\oplus}$ , with an orbital period between  $P = 200-400$  days.

## 5

# Supporting Information for Prevalence of Earth-size Planets Orbiting Sun-like Stars

A version of this chapter was previously published in the *Proceedings of the National Academy of Science* (Erik A. Petigura, Andrew W. Howard, & Geoffrey W. Marcy, 2013, PNAS 110, 19273).

In this supplement to “The Prevalence of Earth-size Planets Orbiting Sun-Like Stars” by Petigura et al., we elaborate on the technical details of our analysis. In Section 5.1, we define our sample of 42,557 Sun-like stars that are amenable to the detection of small planets — the “Best42k” stellar sample. In Section 5.2, we describe the algorithmic components of TERRA, our custom pipeline that we used to find transiting planets within *Kepler* photometry. Section 5.3 describes “data validation,” how we prune the large number of “Threshold Crossing Events” into a list of 836 eKOIs, analogous to KOIs from the *Kepler* Project. Section 5.4 shows four KOIs in the current online Exoplanet Archive [Akeson et al. \(2013\)](#) that failed the data validation step. Section 5.5 describes the procedure by which we remove astrophysical false positives from our list of eKOIs. Section 5.6 describes how we refine our initial estimate of planet radii using spectra of the eKOIs coupled with MCMC-based light curve fitting. Section 5.7 contains a description of the fundamental component of this study: measuring the completeness of our planet search by injecting synthetic transit light curves, caused by planets of all sizes and orbital periods, directly into the *Kepler* photometry, and analyzing the photometry with our pipeline to determine the fraction of planets detected. In Section 5.8 we provide details describing our calculation of planet occurrence and discuss the effects of multiplanet systems and false positives.

## 5.1 The Best42k Stellar Sample

We restrict our planet search to Sun-like stars with well-determined photometric properties and low photometric noise. We select stars having revised *Kepler* Input Catalog (KIC) parameters. Effective temperatures are based on the Pinsonneault et al. [Pinsonneault et al. \(2012\)](#) revisions to the KIC effective temperatures. Surface gravities are based on fits to Yonsei-Yale stellar evolution models [Yi et al. \(2001\)](#) assuming  $[\text{Fe}/\text{H}] = -0.2$ . Further details regarding isochrone fitting can be found in Batalha et al. [Batalha et al. \(2012\)](#); Burke et al., submitted; and Rowe et al., in prep. These revised stellar parameters are tabulated on the Exoplanet Archive with the `prov_prim` flag set to “Pinsonneault.” Out of the 188,329 stars observed at some point during Q1–Q15, we selected stars that:

1. Have revised KIC stellar properties. (155,046 stars),
2.  $Kp = 10\text{--}15$  mag (98,471 stars),
3.  $T_{\text{eff}} = 4100\text{--}6100$  K (63,915 stars), and
4.  $\log g = 4.0\text{--}4.9$  (cgs) (42,557 stars).

Figure [5.1](#) shows the position of the 155,046 stars with revised stellar properties along with the “solar subset” corresponding to G and K dwarfs. Figure [5.2](#) shows the distribution of brightness and noise level of the Best42k stellar sample.

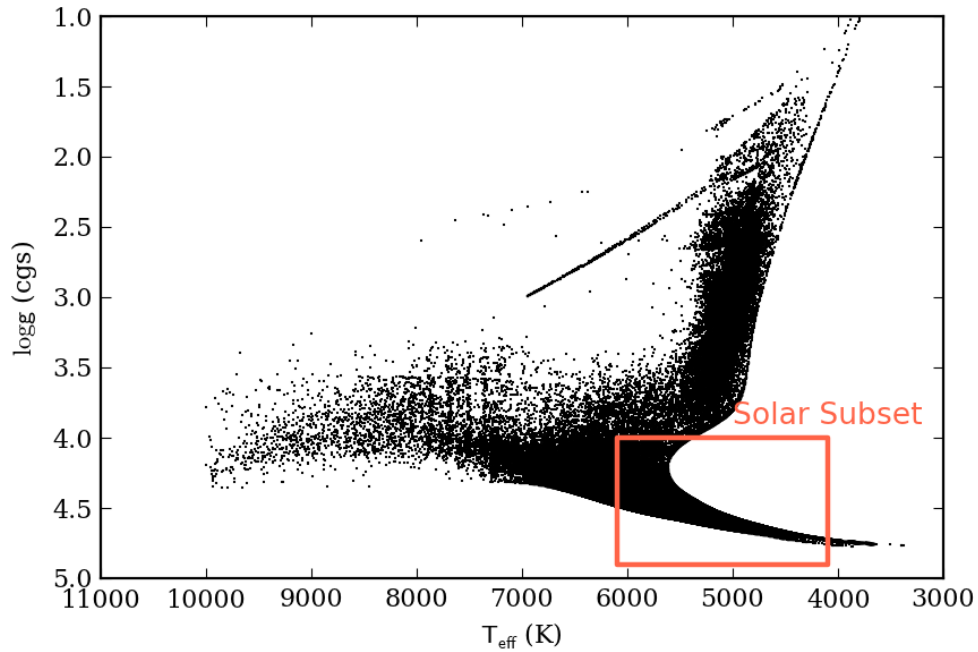


Figure 5.1: Distribution of 155,046 stars with revised photometric stellar parameters. The Best42k sample of 42000 stars is made up of Solar-type stars with  $T_{\text{eff}} = 4100\text{--}6100$  K,  $\log g = 4.0\text{--}4.9$  (cgs), and  $\text{Kepmag} = 10\text{--}15$  (brighter half of targets).

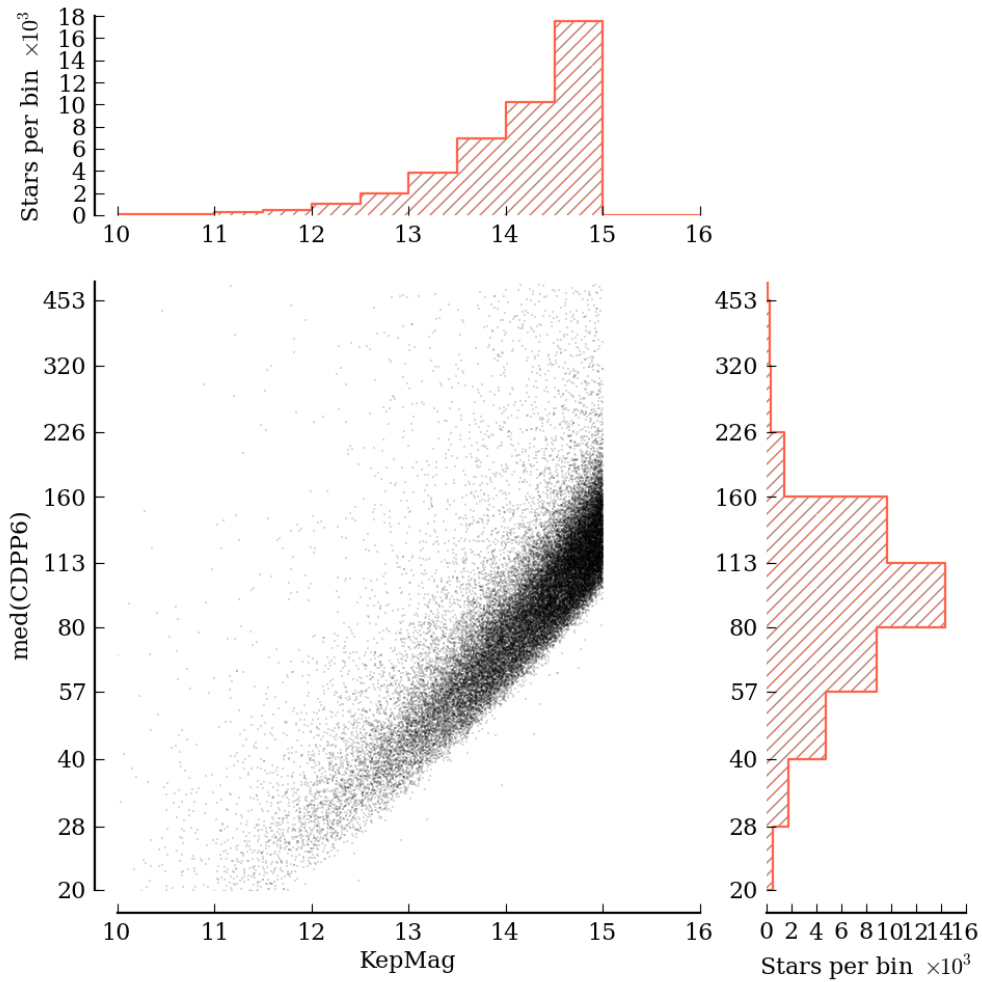


Figure 5.2: Distribution of photometric noise (median quarterly 6 hour CDPP) and brightness  $K_p$  for the 42,557 stars in the Best42k stellar sample.

## 5.2 Planet Search Photometric Pipeline

We search for planet candidates in the Best42k stellar sample using the TERRA pipeline described in detail in Petigura & Marcy (2012) and in Petigura, Marcy, and Howard (2013; P13, hereafter) Petigura & Marcy (2012); Petigura et al. (2013b). We review the major components of TERRA below, noting the changes since P13.

### 5.2.1 Time-domain pre-processing of raw *Kepler* Photometry

TERRA begins by conditioning the photometry in the time-domain. TERRA first searches for single cadence outliers, mostly due to cosmic rays. TERRA also searches for abrupt drops in the raw photometry known as Sudden Pixel Sensitivity Drops (SPSDs) discussed by Stumpe et al. Stumpe et al. (2012). SPSPDs are particularly challenging since they mimic transit ingress, and aggressive attempts to remove them run the risk of removing real transits. TERRA removes the largest SPSPDs, but they remain a source of non-astrophysical false positives that we remove during manual triage (Section 5.3.2).

TERRA also removes trends longer than  $\sim 10$  days. In P13, this high-pass filtering was implemented by fitting a spline to the raw photometry with the knots of the spline separated by 10 days. But in this work we employ high-pass filtering using Gaussian Process regression Rasmussen & Williams (2006), which gives finer control over the timescales removed. We adopt a squared exponential kernel with a 5-day correlation length. After this high-pass filter, TERRA identifies systematic noise modes via principle components analysis on large number of stars.

### 5.2.2 Grid-based transit search

We search for periodic box-shaped dimmings by evaluating the signal-to-noise ratio (SNR) of a putative transit over a finely-spaced grid of period,  $P$ ; epoch,  $t_0$ ; and transit duration,  $\Delta T$ . In P13, we searched over a period range,  $P = 5\text{--}50$  days, and over transit durations ranging from 1.5–8.8 hr. But in this work, we extend our search in orbital period to  $P = 0.5\text{--}400$  days. Since we search over nearly three decades in orbital period, and because transit duration is proportional to  $P^{1/3}$ , we let the range of trial transit durations vary with period. We break our period range into 10 equal logarithmic intervals. Then, using photometrically determined parameters for each star, namely  $M_\star$  and  $R_\star$ , we compute an approximate, expected transit duration ( $\Delta T_{\text{circ}}$ ) for the simple case of circular orbits with impact parameter,  $b = 1$ . However, we actually search over  $\Delta T = 0.5\text{--}1.5 \Delta T_{\text{circ}}$  to account for a range of impact parameters and orbital eccentricities and for mis-characterized  $M_\star$  and  $R_\star$ . As an example, Table 5.2.2 shows our trial  $\Delta T$  for a star with solar mass and radius.

Table 5.1: **TERRA** Grid Search Parameters

$P_1$ days	$P_2$ days	Trial Transit Duration ( $\Delta T$ ) long cadence measurements
5.0	7.7	[3, 4, 5, 7, 9, 11]
7.7	12.0	[4, 5, 7, 9, 13]
12.0	18.6	[4, 5, 7, 9, 13, 15]
18.6	28.9	[5, 7, 9, 12, 16, 17]
28.9	44.7	[6, 8, 11, 14, 19, 20]
44.7	69.3	[7, 9, 12, 16, 22, 23]
69.3	107.4	[8, 11, 14, 19, 25, 26]
107.4	166.5	[9, 12, 16, 21, 28, 31]
166.5	258.1	[10, 13, 18, 24, 31, 35]
258.1	400.0	[12, 16, 21, 28, 38, 41]

## 5.3 Data Validation

If TERRA detects a  $(P, t_0, \Delta T)$  with  $\text{SNR} > 12$ , we flag the light curve for additional scrutiny. While the grid-based component of TERRA is well-matched to exoplanet transits, there are other phenomena that can produce  $\text{SNR} > 12$  events and contaminate our planet sample. We distinguish between two classes of contaminants: “astrophysical false positives” such as diluted eclipsing binaries (EBs), and “non-astrophysical false positives” such as noise that can mimic a transit. We establish a series of quality control measures called “Data Validation” (DV), designed to remove formally strong dimmings (i.e.  $\text{SNR} > 12$ ) found by the blind photometric pipeline that are not consistent with an astrophysical transit. DV consists of two steps:

1. *Machine triage*: Select potential transits by automated cuts.
2. *Manual triage*: Manually remove light curves that are inconsistent with a Keplerian transit.

Manual triage is accomplished by inspection of DV summary plots which contain numerous useful diagnostics necessary to warrant planet status. The diagnostics permit a multi-faceted evaluation of the integrity (as a potential planet candidate) of a given dimming identified by the photometric pipeline. Figure 5.3 shows a sample DV report, this for KIC-5709725 that passed examination.

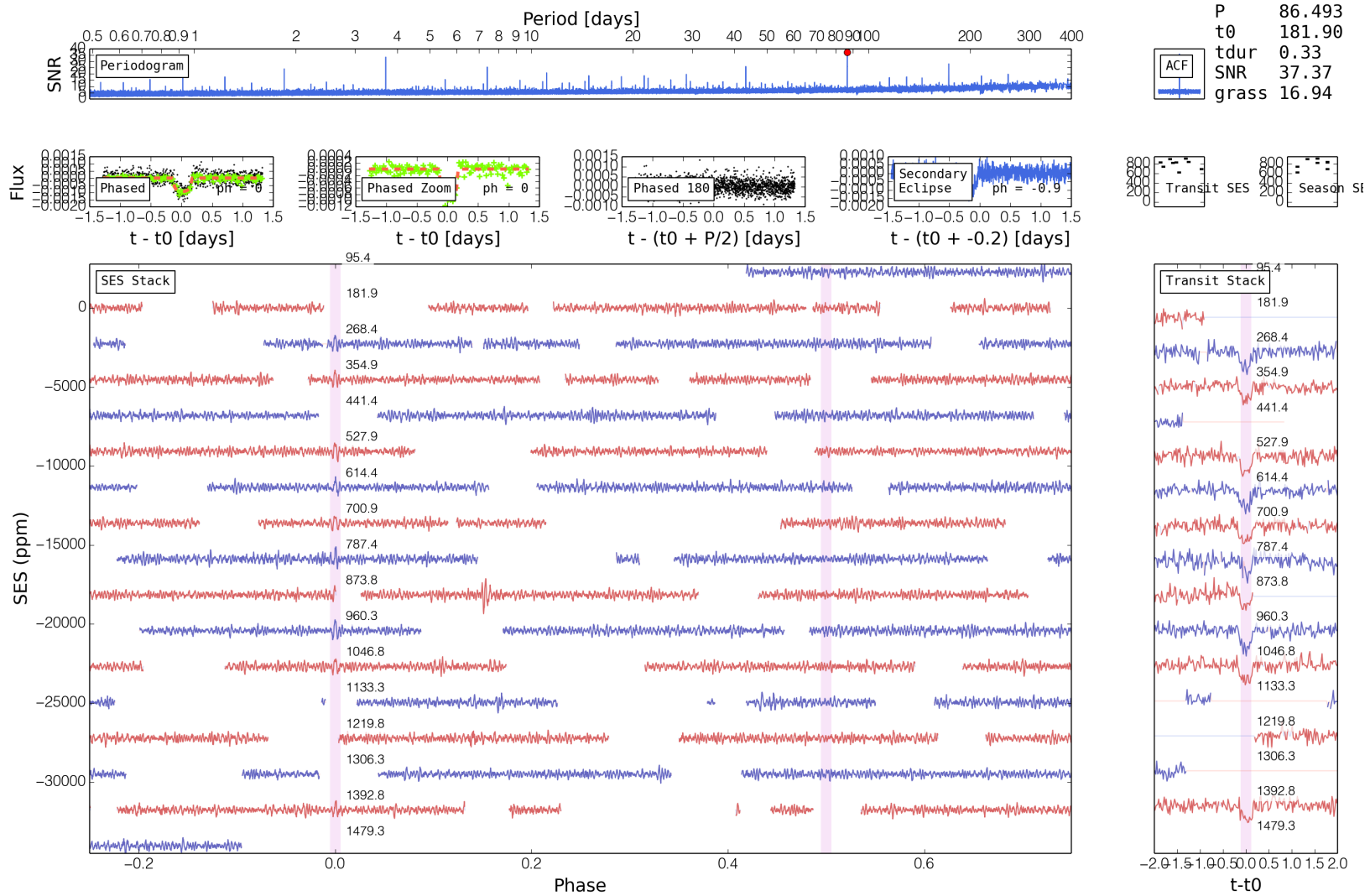


Figure 5.3: (Continued on the following page)

Figure 5.3: DV summary plots for KIC-5709725. Top row: SNR “periodogram” of box-car photometric search for transiting planets, ranging from 0.5 to 400 days. The red dot shows the  $P$  and SNR of the most significant peak in the periodogram at  $P = 86.5$  days (also found by the *Kepler* Project as KOI-555.02). Also visible is a second set of peaks corresponding to KOI-555.01 at  $P = 3.702$  days. **TERRA** does not search for more than one planet per system. Moreover, KOI-555.01 would be excluded from our planet sample since  $P < 5$  days. The autocorrelation function, “ACF”, plot at upper right shows the circular auto-correlation function from the phase folded photometry, used to identify secondary eclipses and correlated noise in the photometry. Second row: at left “Phase” shows the phase-folded photometry, where black points represent detrended photometry near the time of transit, green symbols show median flux over 30 min bins, and the dashed line shows the best-fitting Mandel-Agol transit model [Mandel & Agol \(2002\)](#). At second from left, “Phased Zoom” shows a zoomed y-axis to highlight the transit itself. For this TCE, the transit model is a good match to the photometry. At third from left, “Phased 180” shows phase folded photometry  $180^\circ$  in orbital phase from transit center. At fourth from left, “Secondary eclipse” shows how **TERRA** notches out the putative transit and searches for secondary eclipses. We show the photometry folded on the second most significant dimming. For KIC-5709725, this phase is  $0.9^\circ$  relative to the primary transit, so close in phase that the primary transit is still visible. This transit does not show signs of a secondary eclipse. Transit SES — transit single event statistic as a function of transit number. Conceptually, SES is the depth of the transit in ppm, as described by Petigura and Marcy [Petigura & Marcy \(2012\)](#). “Season SES” shows the SES statistic grouped according to season. Bottom row: At left, “SES stack” shows SES for the entire light curve, split on the best-fitting transit period and stacked so that transit number increases downward. Compelling transits appear as a sequence of SES peaks at phase =  $0^\circ$ . “Transit stack” shows for TCEs with fewer than 20 transits a plot of the **TERRA**-calibrated photometry of each transit (transit number increases downward).

The product of the DV quality control is a list of “eKOIs,” for which most instrumental events identified preliminarily and erroneously by the photometric pipeline have been rejected. The resulting planet candidates are analogous to the KOIs *Kepler* Project. Astrophysically plausible causes (i.e. transiting planets and background eclipsing binaries) are retained among our eKOIs. We address astrophysical false positives in Section 5.5.

### 5.3.1 Machine Triage

Prior to the identification of final eKOIs, we carry out machine triage to identify a set of “Threshold Crossing Events” (TCEs) that can be classified by a human in a reasonable amount of time. TCE status requires a  $\text{SNR} > 12$ ; however, we find that 16227 light curves (out of the 42000 target stars) meet this criterion. Outliers and correlated noise are responsible for the majority of  $\text{SNR} > 12$  events. We show set of diagnostic plots for such an outlier in Figure 5.4. Here, an uncorrected sudden pixel sensitivity dropoff at  $t = 365.3$  days, raises the noise floor to  $\text{SNR} \sim 15$  for  $P \lesssim 100$  days. Its contribution to SNR is averaged down for shorter periods.

We flag such outliers by comparing the most significant period,  $P_{\text{max}}$ , to nearby periods. We call the ratio of the maximum SNR to the median of the next tallest five peaks between  $[P_{\text{max}}/1.4, P_{\text{max}} \times 1.4]$  the `s2n_on_grass` statistic. We require `s2n_on_grass`  $> 1.2$  for TCE status. After that cut, 3438 TCEs remain. We also require  $P_{\text{max}} > 5$  d, which leaves 2184 TCEs.

### 5.3.2 Manual Triage

The sample of 2184 TCEs has a significant degree of contamination from non-astrophysical false positives. In P13, we relied on aggressive automatic cuts that removed nearly all of the non-astrophysical false positives (final sample was  $\sim 90\%$  pure). However, by comparing our sample to that of Batalha et al. [Batalha et al. \(2012\)](#), we found that these automatic cuts were removing a handful of compelling planet candidates.

In this work, we aim for higher completeness and rely more heavily on visual inspection of light curves. We assess whether a TCE is due to a string of three or more transits or instead caused by outlier(s) such as SPSDs. Figure 5.5 shows an example of a light curve that passed machine triage, but was removed manually. During manual triage, we do not attempt to distinguish between planets and astrophysical false positives. The end product is a list of 836 eKOIs, which are analogous to KOIs produced by the *Kepler* Project in that they are highly likely to be astrophysical in origin but false positives have not been ruled out.

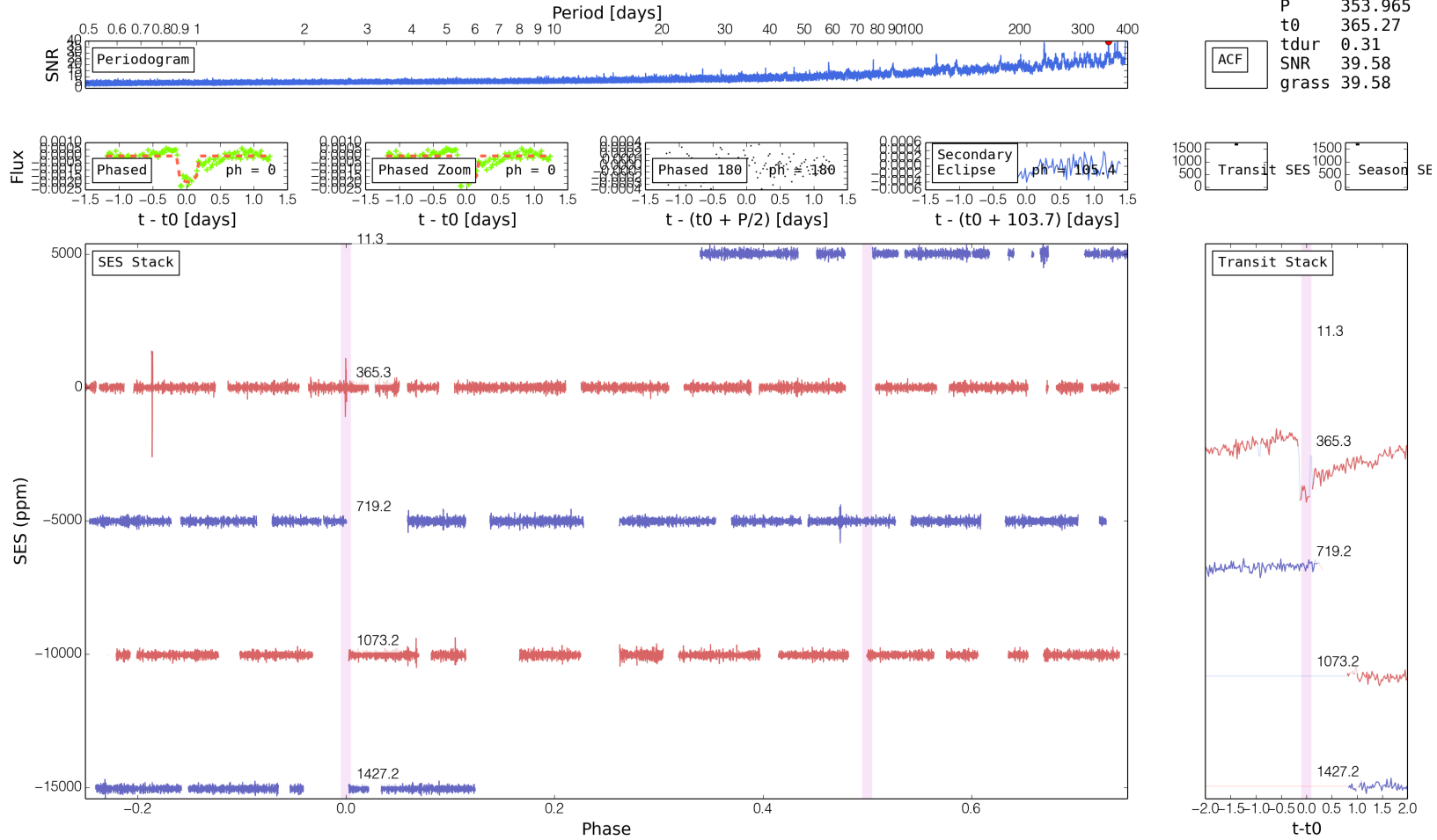


Figure 5.4: DV summary plots (defined in Figure 5.3) for KIC-1570270 showing a non-astrophysical false positive removed in the machine triage step. Here, an uncorrected SPSD at  $t = 365.3$  days resulted in a  $\text{SNR} \sim 40$  event with  $P = 353.965$  days, seen in the SNR periodogram. SES stack plot shows this high SNR TCE is due to a single spike in SES due to the SPSD.  $P = 353.965$  days is favored over nearby periods because the anomaly aligns with gaps in the photometry. We flag cases like this with our  $\text{s2n\_on\_grass}$  statistic. We find several nearby peaks with nearly equal SNR. For KIC-1570270,  $\text{s2n\_on\_grass}$  is less than our threshold of 1.2 and does not pass machine triage.

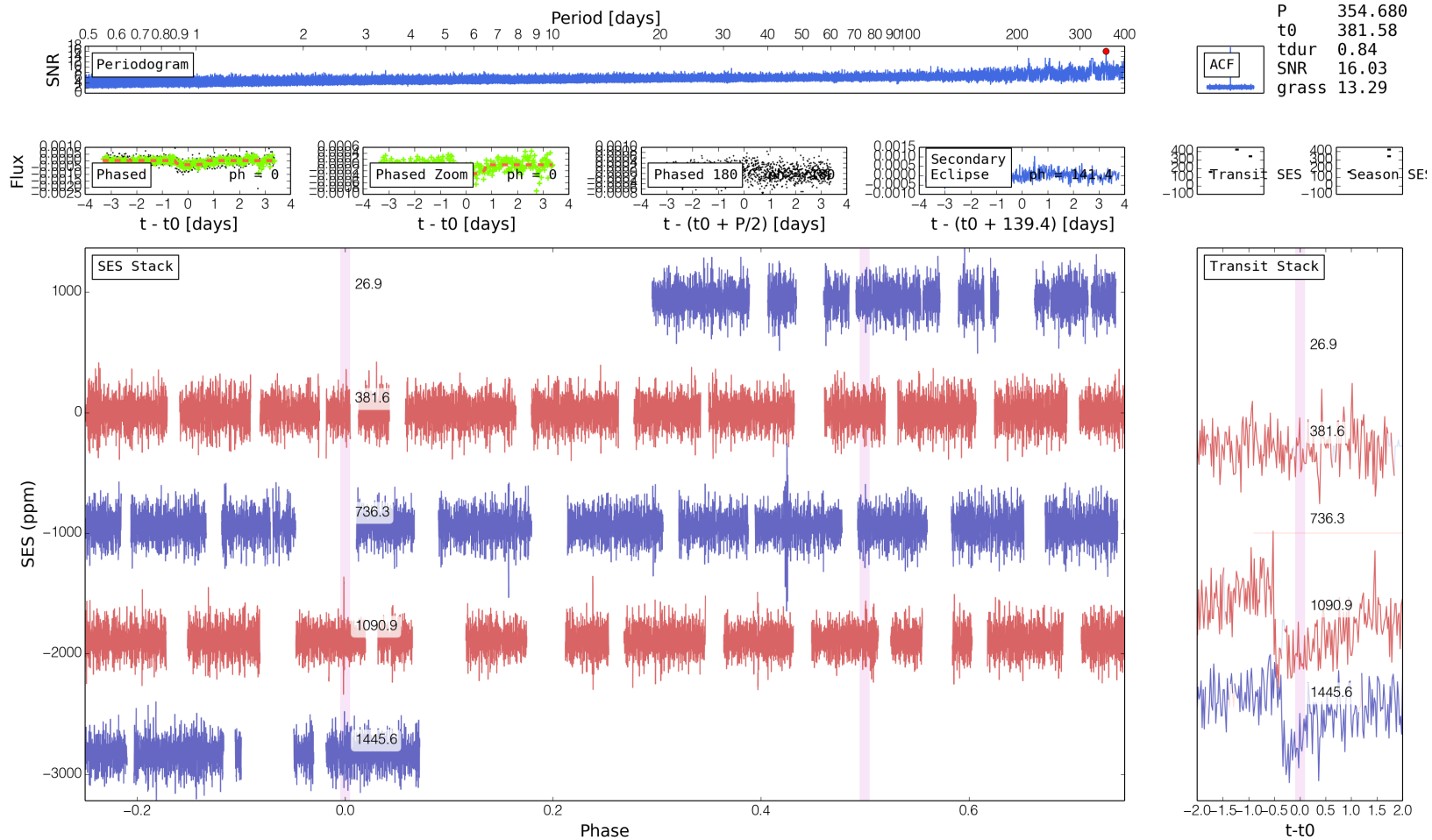


Figure 5.5: DV summary plots (defined in Figure 5.3) for the KIC-1724842 TCE at  $P = 354.680$  days that we removed during the manual triage. This photometry contains two pixel sensitivity drops spaced by 354.680 days. These two data anomalies combine to produce  $\text{SNR} = 16.035$  event, which is substantially higher than the background (“grass” = 13.294) Since  $\text{s2n\_on\_grass} = 1.206 > 1.2$ , this event passed our TERRA software-based triage. However, such data anomalies are easily identified by eye.

## 5.4 KOIs That Fail Data Validation

As a cross-check of our DV quality control methods, we performed the same inspection on 235 KOIs that had been identified by the *Kepler* Project and which appear currently in the online Exoplanet Archive [Akeson et al. \(2013\)](#). These KOIs have periods longer than 50 days, representative of long period transiting planets that enjoy a reduced number transits (compared to short-period planets) during the 4-year lifetime of the *Kepler* mission. We found four KOIs, 2311.01, 2474.01, 364.01, and 2224.01, that are not consistent with an astrophysical transit. We show the raw light curves around the published ephemerides in [Figure 5.6](#). All four have  $R_P \leq 2.04 R_\oplus$ , and three have  $P \geq 173$  days. Due to the small number of KOIs near the habitable zone, inclusion of these KOIs would bias occurrence measurements upward by a large amount. Vetting all 3000 KOIs in the Exoplanet Archive requires a substantial effort, and is beyond the scope of this paper. However, these four KOIs are a reminder than detailed, expert, and visual vetting of DV diagnostics existing KOIs is useful.

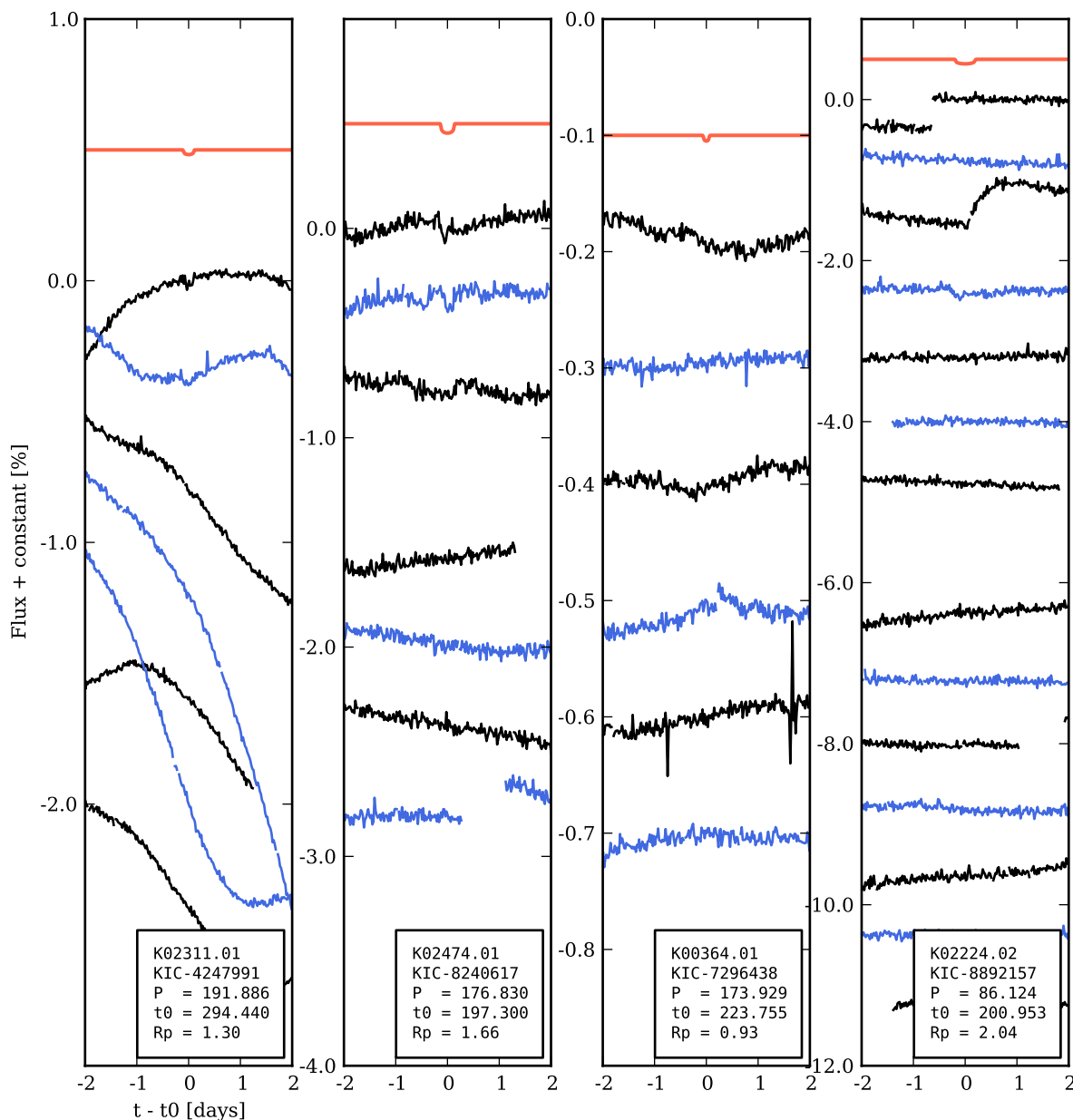


Figure 5.6: Four small KOIs with long orbital periods that fail our manual vetting. We show 4-day chunks of raw photometry (“SAP\_FLUX” in fits table) around the supposed transits. Transit number increases downward. We alternate the use of black and blue lines for clarity. The red lines show a Mandel Agol light curve model synthesized according to the published transit parameters.

## 5.5 Removal of Astrophysical False Positives

We take great care to cleanse our sample of false positives (FPs). Some transits are so deep ( $\delta F \gtrsim 10\%$ ) that they can only be caused by an EB. However, if an EB is close enough to a *Kepler* target star, the dimming of the EB can be diluted to the point where it resembles a planetary transit. For each eKOI, we assess four indicators of EB status. Here, we list the indicators along with the number of eKOIs removed from our planet sample due to each cut:

1. *Radius too large (115)*. We consider any transit where the best fit planet radius is larger than  $20 R_{\oplus}$  to be stellar. Planets are generally smaller than  $1.5 R_{\text{J}} = 16 R_{\oplus}$  especially for  $P > 5$  days, where planets are less inflated. Our cut at  $20 R_{\oplus}$  allows some margin of safety to account for mis-characterized stellar radii.
2. *Secondary eclipse (44)*. The expected equilibrium temperature for a planet with  $P > 5$  days is too small to produce a detectable secondary eclipse. Therefore, the presence of a secondary eclipse indicates the eclipsing body is stellar. We search for secondary eclipses by masking out the primary transit and searching for additional transits at the same period. If an eKOI, such as KIC-8879427 shown in Figure 5.7, has a secondary eclipse, we designate it an EB.
3. *Variable depth transits (27)*. Since *Kepler* photometric apertures are typically two or three pixels (8 or 12 arcsec) on a side, light from neighboring stars can contribute to the overall photometry. A faint EB, when diluted with the target star's light, can produce a dimming that looks like a planetary transit. If the angular separation between the two stars is large enough, the EB will contribute a different amount of light at each *Kepler* orientation. For eKOIs like KIC-2166206 shown in Figure 5.8, the contribution of a nearby EB results in a season-dependent transit depths. Since the target apertures are defined to include nearly all ( $\gtrsim 90\%$ ) of the light from the target star, variations between quarters produce a negligible effect on transits associated with the target star, i.e. fractional changes of  $\lesssim 1\%$ .
4. *Centroid offset (31)*. *Kepler* project DV reports exist for nearly all (609/650) of the eKOIs that survive the previous cuts and are available on the Exoplanet Archive. We inspect the transit astronomy diagnostics Bryson et al. (2013) for significant motion of the transit photocenter in and out of transit. eKOIs with significant motion are designated false positives.

We remove a small number of eKOIs (11) with V-shaped transits. Since planets are so much smaller than their host stars, ingress/egress durations are short compared to the duration of the transit, i.e. planetary transits are box-shaped. Stellar eclipses tend to be V-shaped. Limb-darkening, the 30-minute integration time, and the possibility of grazing incidence blur this distinction. We assessed transit shape visually rather than using more detailed approaches based on light curve fitting and models of Galactic structure Torres et al.

(2011); Morton (2012). Only 1.3% of eKOIs are removed in this way and are a small effect compared to other uncertainties in our occurrence measurements.

We also remove five eKOIs with large TTVs. Since TERRA's light curve fitting assumes constant period, fits are biased toward smaller planet radii in the presence of transit timing variations  $\gtrsim \Delta T$ . If the resulting error is  $\gtrsim 25\%$ , we remove that eKOI. While these eKOIs are likely planets, our constant period model results in a significant bias in derived planet radii. Given the small number of eKOIs with such large TTVs, our decision to remove them has small effect on our statistical results based off of hundreds of planets.

We compute planet occurrence from the 603 eKOIs that survive the above cuts. We show the distribution of TERRA candidates and FPs on the  $P-R_p$  plane in Figure 5.9. All 836 eKOIs are listed in Table 5.2. For each eKOI, Table 5.2 lists KIC identifier, transit ephemeris, FP designation, Mandel-Agol fit parameters, adopted host star parameters, and size. We also crossed checked our eKOIs against the catalog *Kepler* team KOIs accessed from the NASA Exoplanet Archive Akesson et al. (2013) on 13 September 2013. If the *Kepler* Project KOI number exists for an eKOI, we include it in Table 5.2.

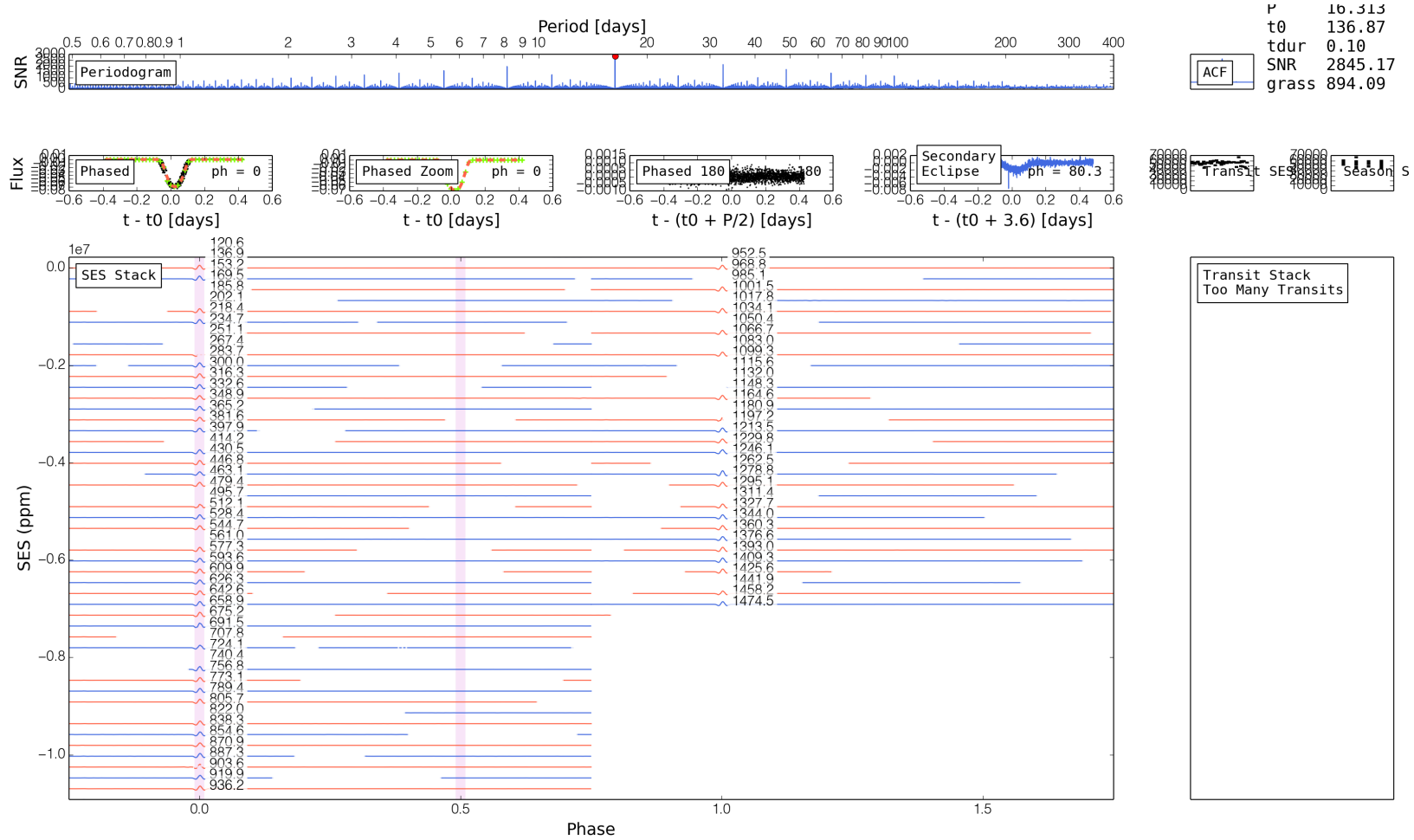


Figure 5.7: DV summary plots (defined in Figure 5.3) for eKOI KIC-8879427 ( $P = 16.313$ ). The “Secondary Eclipse” plot shows the second most significant dimming at  $P = 16.313$ , offset from the primary transit in phase by  $80.3^\circ$ . The ratio of the primary to secondary eclipses ( $\delta F_{pri} = 0.07$ ;  $\delta F_{sec} = 0.002$ ) along with the effective temperature of the primary ( $T_{eff} = 5995$  K) imply the transiting object is 2343 K – too high to be consistent with a planet with  $P = 16.313$  days orbital period.

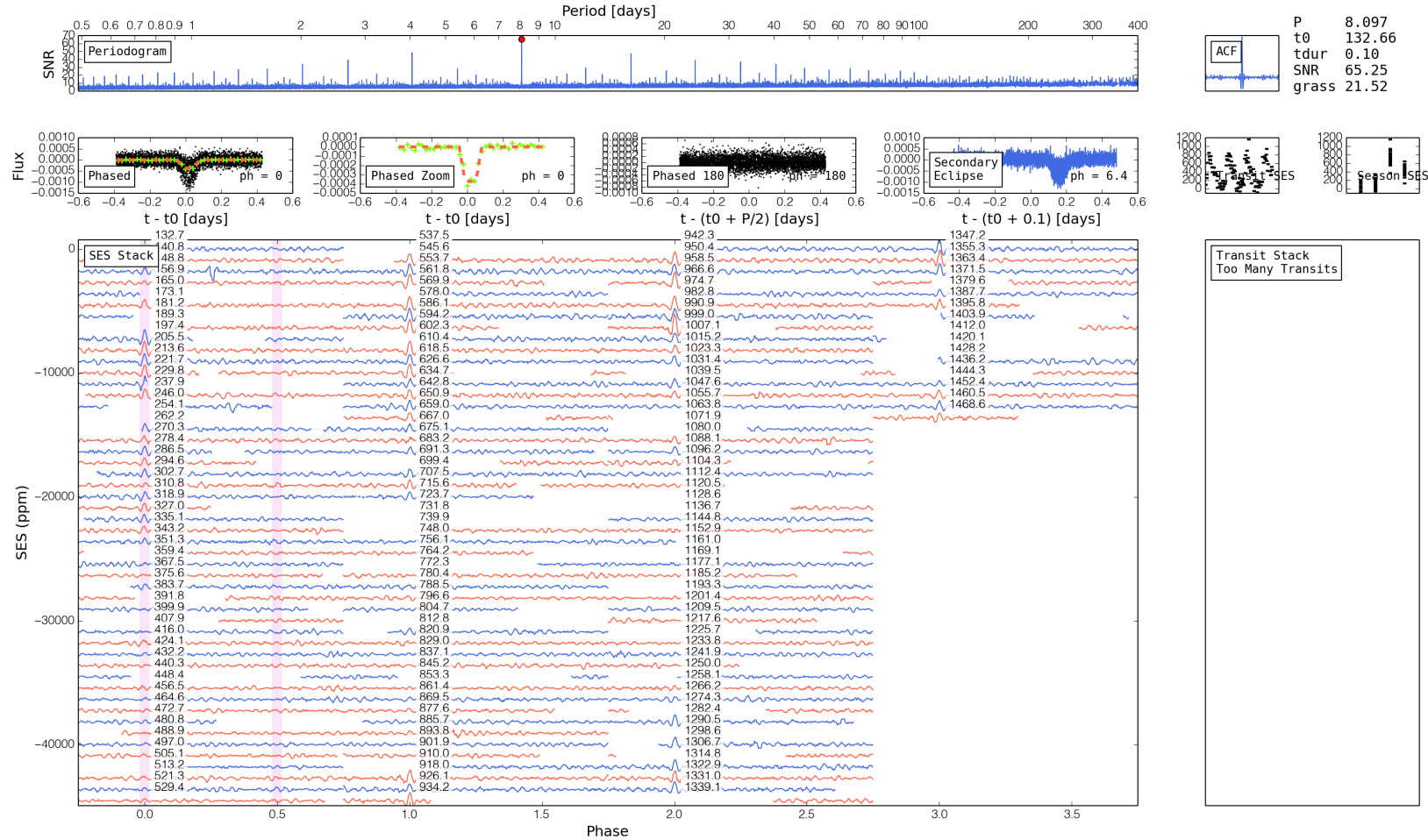


Figure 5.8: DV summary plots (defined in Figure 5.3) for eKOI KIC-2166206 with season-dependent transit depths. Season SES plot shows that the transit depths vary significantly for different observing seasons. Since the apparent dimming is a strong function of the orientation of the spacecraft, the dimming is likely not associated with KIC-2166206, but rather an EB displaced from the target by several arc seconds.

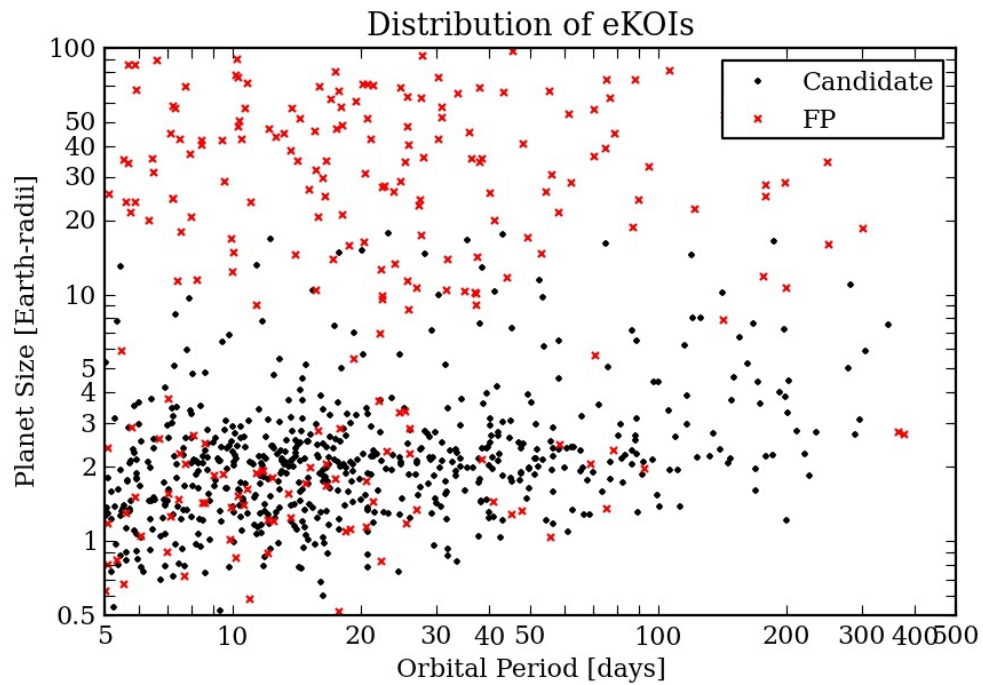


Figure 5.9: Distribution of TERRA planet candidates as a function of planet size and period. Candidates are labeled as black points; FPs are labeled as red Xs.

## 5.6 Planet Radius Refinement

We fit the phase folded transit photometry of each eKOI with a Mandel-Agol model [Mandel & Agol \(2002\)](#). That model has three free parameters:  $R_P/R_*$ , the planet to star radius ratio,  $\tau$ , the time for the planet travel a distance  $R_*$  during during transit; and  $b$ , the impact parameter. Following P13, we account for the covariance among the three parameters using an MCMC exploration of the parameter posteriors. The error on  $R_P/R_*$  in Table 5.2 incorporates the covariance with  $\tau$  and  $b$ .

Because photometry alone only provides the  $R_P/R_*$ , knowledge of the planet population depends heavily on our characterization of their stellar hosts. We obtained spectra of 274 eKOIs with HIRES on the Keck I telescope using the standard configuration of the California Planet Survey (Marcy et al. 2008). These spectra have resolution of  $\sim 50,000$  and SNR of  $\sim 45/\text{pixel}$  at  $5500 \text{ \AA}$ . We obtained spectra for all 62 eKOIs with  $P > 100$  days.

We determine stellar parameters using a routine called `SpecMatch` (Petigura et al., in prep). `SpecMatch` compares a target stellar spectrum to a library of  $\sim 800$  spectra from stars that span the HR diagram ( $T_{\text{eff}} = 3500\text{--}7500 \text{ K}$ ;  $\log g = 2.0\text{--}5.0$ ). Parameters for the library stars are determined from LTE spectral modeling. Once the target spectrum and library spectrum are placed on the same wavelength scale, we compute  $\chi^2$ , the sum of the squares of the pixel-by-pixel differences in normalized intensity. The weighted mean of the ten spectra with the lowest  $\chi^2$  values is taken as the final value for the effective temperature, stellar surface gravity, and metallicity. We estimate `SpecMatch`-derived stellar radii are uncertain to 10% RMS, based on tests of stars having known radii from high resolution spectroscopy and asteroseismology.

## 5.7 Completeness

When measuring planet occurrence, understanding the number of missed planets is as important as the planet catalog itself. We measure TERRA’s planet finding efficiency as a function of  $P$  and  $R_P$  using the injection/recovery framework developed for P13. We briefly review the key aspects of our pipeline completeness study; for more detail, please see P13. We generate 40,000 synthetic light curves according to the following steps:

1. Select a star randomly from the Best42k sample,
2. draw  $(P, R_P)$  randomly from log-uniform distributions over 5–400 d and  $0.5\text{--}16 R_{\oplus}$ ,
3. draw impact parameter and orbital phase randomly from uniform distributions over 0–1,
4. synthesize a Mandel-Agol model [Mandel & Agol \(2002\)](#), and
5. inject the model into the “simple aperture photometry” of a random Best42k star.

We process the synthetic photometry with the calibration, grid-based search, and DV components of TERRA. We consider a synthetic light curve successfully recovered if the injected  $(P, t_0)$  agree with the recovered  $(P, t_0)$  to 0.1 days. Figure 5.10 shows the distribution of recovered simulations as a function of injected planet size and orbital period.

Pipeline completeness is determined in small bins in  $(P, R_P)$ -space by dividing the number of successfully recovered transits by the total number of injected transits on a bin-by-bin basis. This ratio is TERRA’s recovery rate of putative planets within the Best42k sample. Pipeline completeness is higher among a more rarefied sample of low noise stars. However, a smaller sample of stars yields fewer planets.

We show survey completeness for a dense grid of  $P$  and  $R_P$  cells in Figure 5.11. Completeness falls toward smaller  $R_P$  and longer  $P$ . Above  $2 R_\oplus$ , completeness is greater than 50% even for the longest periods searched (except for the  $R_P = 2\text{--}2.8 R_\oplus$ ,  $P = 283\text{--}400$  days bin). Completeness falls precipitously toward smaller planet sizes; very few simulated planets smaller than Earth are recovered. Compared to a  $1 R_\oplus$  planet, a  $2 R_\oplus$  planet produces a transit with 4 times the SNR and is much easier to detect. For planets larger than  $2 R_\oplus$ , we note a gradual drop in completeness toward longer periods, that steepens at  $\sim 300$  days. Above  $\sim 300$  days, the probability that a two or more transits land in data gaps becomes appreciable, and the completeness falls off more rapidly.

Measuring completeness by injection and recovery captures the vagaries in planet search pipeline. Real and synthetic transits are treated the same way, up until the manual triage section. Recall from Section 5.3.2 that 836 of 2184 TCEs pass machine triage. We perform no such manual inspection of TCEs from the injection and recovery simulations. A potential concern is that a planet may pass machine triage, but is accidentally thrown out in manual triage. Such a planet would be missing from our planet catalog, but not properly accounted in the occurrence measurement by lower completeness. However, because our  $\text{SNR} > 12$  threshold for TCE status is high, distinguishing non-astrophysical false positives and eKOIs is easy. Therefore, we consider it unlikely that they are cut during the manual triage stage, and do not expect the lack of manual vetting of the injected TCEs to bias our completeness measurements.

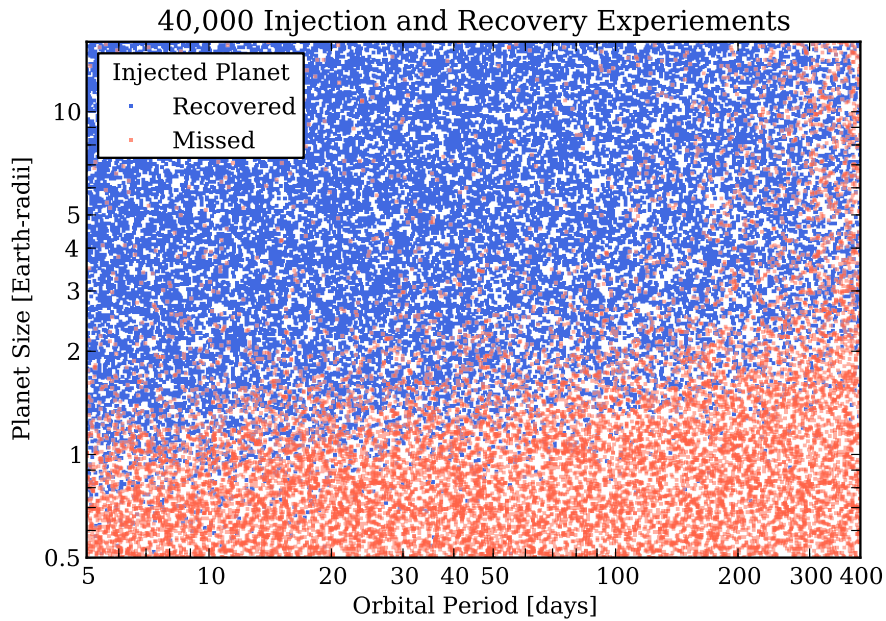


Figure 5.10:  $P$  and  $R_P$  of 40,000 injected planets color coded by whether they were recovered by TERRA. Completeness over a small range in  $P$ – $R_P$  is computed by dividing the number of successfully recovered transits (blue points) by the total number of injected transits (blue and red points). For planets larger than  $2 R_{\oplus}$ , completeness is  $> 50\%$  out to 400 d. Completeness rapidly falls over  $1$ – $2 R_{\oplus}$  and is  $\lesssim 10\%$  for planets smaller than  $1 R_{\oplus}$ .

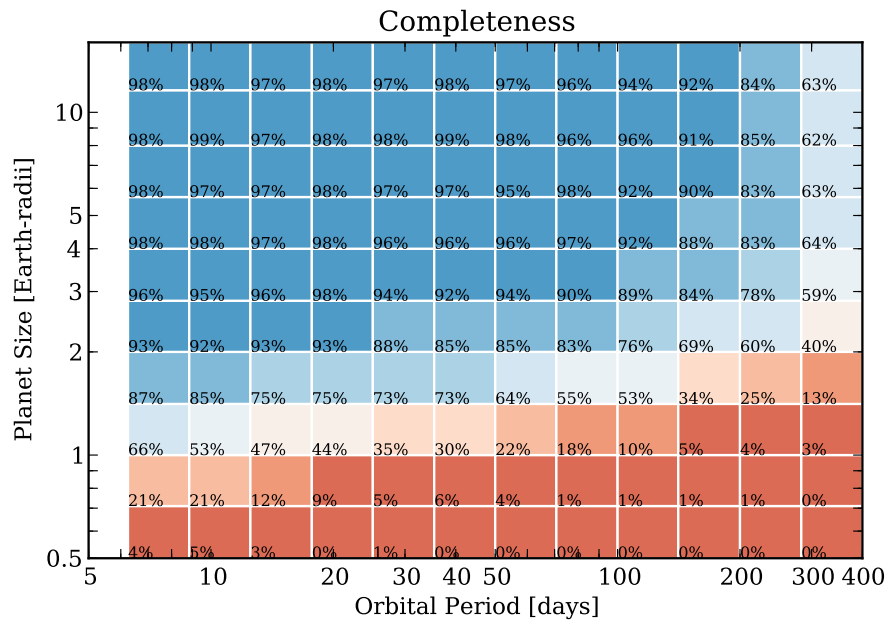


Figure 5.11: Completeness computed over small bins in  $P$  and  $R_P$ .

## 5.8 Planet Occurrence

Here, we expand on the key planet occurrence results presented in the main text. We describe our method for extrapolation into the  $R_P = 1\text{--}2 R_\oplus$ ,  $P = 200\text{--}400$  day domain. We give additional details regarding our measurement of the prevalence of Earth-size planets in the HZ. We also discuss two minor corrections to our occurrence measurements due to planets in multiplanet systems and false positives (FPs).

### 5.8.1 Occurrence of Earth-Size Planets on Year-Long Orbits

In the main text, we reported  $5.7_{-2.2}^{+1.7}\%$  occurrence of planets with  $R_P = 1\text{--}2 R_\oplus$  and  $P = 200\text{--}400$  days based on extrapolation from shorter periods. The use of such extrapolation is supported by uniform planet occurrence per  $\log P$  interval. Cumulative Planet Occurrence (CPO) is helpful to understand the detailed shape of the planet period distribution. If planet occurrence is constant per  $\log P$  interval, CPO is a linear function in  $\log P$ . The slope of the CPO conveys planet occurrence: the higher the planet occurrence, the steeper the slope of the CPO.

Figure 5.12 shows CPO for  $R_P = 2\text{--}4 R_\oplus$  planets. Planet occurrence increases with period from 5 days up to  $\sim 10$  days, and is consistent with uniform for larger periods. This change in the planet period distribution was noted in previous work Youdin (2011); Howard et al. (2012); Dong & Zhu (2012). We fit a line to the CPO from 50–200 days and extrapolate into the 200–400 day range. The extrapolation predicts  $6.4_{-1.2}^{+0.5}\%$  occurrence, which agrees with our measured value of  $5.0 \pm 2.1\%$  to 1  $\sigma$ . We estimate errors on our extrapolation by fitting subsets of the CPO that span half the original period range. We fit 100 subsections ranging from  $P = 50\text{--}100$  days up to  $P = 100\text{--}200$  days.

We also compare occurrence in the  $P = 50\text{--}100$  day,  $R_P = 1\text{--}2 R_\oplus$  domain based on extrapolation to our measured value. Figure 5.13 shows the CPO for  $R_P = 1\text{--}2 R_\oplus$  planets. We fit the CPO from  $P = 12.5\text{--}50$  days. This fit predicts an occurrence of  $6.5_{-1.7}^{+0.9}\%$  in the 50–100 day range, in good agreement with our measured value of  $5.8 \pm 1.6\%$ . The uniformity in the occurrence of small planets as a function of period, lends support to the same kind of modest extrapolation into the  $R_P = 1\text{--}2 R_\oplus$ ,  $P = 200\text{--}400$  day domain.

### 5.8.2 Planet Occurrence in the Habitable Zone

We consider a planet to reside in the habitable zone if it receives a similar amount of light flux,  $F_P$ , from its host star as does the Earth. As described in the main text, we consider the most recent theoretical work on habitability of planets following the seminal work by Kasting Kasting et al. (1993); Seager (2013); Kopparapu et al. (2013); Zsom et al. (2013); Pierrehumbert & Gaidos (2011).

We adopt an inner edge of the HZ at 0.5 AU for a Sun-like star where a planet would receive four times the light flux that Earth does. This inner edge is slightly more conservative than that found by Zsom et al. Zsom et al. (2013). The outer edge of the HZ less well

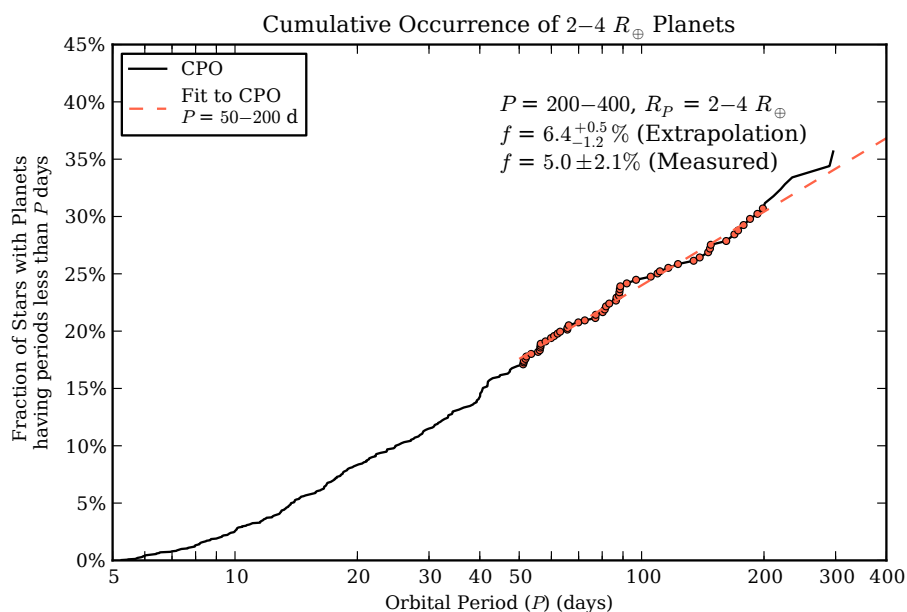


Figure 5.12: The fraction of stars having 2–4  $R_{\oplus}$  planets with any orbital period up to a maximum period,  $P$ , on the horizontal axis. This is the Cumulative Planet Occurrence (CPO). A linear increase in CPO corresponds to planet occurrence that is constant in equal intervals of  $\log P$ . The CPO steepens from 5 to  $\sim 10$  days, corresponding to increasing planet occurrence in the 5–10 day range. For  $P \gtrsim 10$  days, the CPO has a constant slope, reflecting uniform planet occurrence per  $\log P$  interval. Planet occurrence in the  $R_p = 2\text{--}4 R_{\oplus}$ ,  $P = 200\text{--}400$  day domain is predicted to be  $6.4^{+0.5}_{-1.2}\%$  by extrapolation from shorter periods, which is consistent with our measured value of  $5.0 \pm 2.1\%$ .

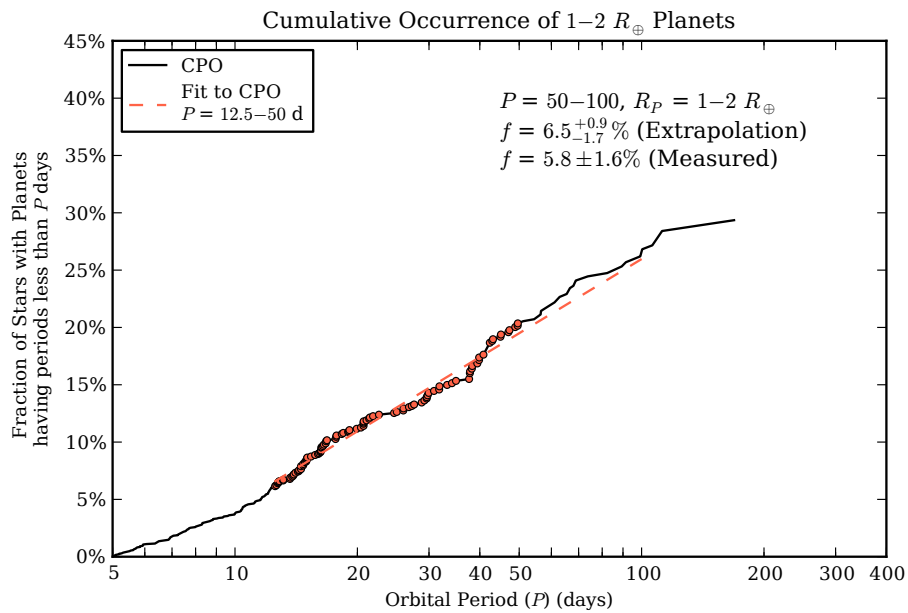


Figure 5.13: Same as Figure 5.12, but showing the CPO for  $1-2 R_{\oplus}$  planets. Planet occurrence in the  $R_P = 1-2 R_{\oplus}$ ,  $P = 50-100$  day bin is predicted to be  $6.5^{+0.9}_{-1.7}\%$  by extrapolation from shorter periods, which is consistent with our measured value of  $5.8 \pm 1.6\%$ .

understood. Kasting found the outer edge to be at 1.7 AU [Kasting et al. \(1993\)](#); Pierrehumbert and Gaidos [Pierrehumbert & Gaidos \(2011\)](#) found it could extend to 10 AU for planets with thick H<sub>2</sub> atmospheres. Here, we adopt an intermediate value of 2 AU for solar analogs where the stellar flux is 1/4 that incident on the Earth. This outer edge is consistent with the presence of liquid water on Mars in its past. Mars might still have liquid water today, if it were more massive. Thus following the theory of planetary habitability, we adopt a habitable zone for stars in general based on stellar flux between 4x and 1/4 the solar flux falling on the Earth:  $F_P = 0.25\text{--}4 F_\oplus$ .

The stellar light flux hitting a planet,  $F_P$ , depends linearly on stellar luminosity,  $L_\star$ , and inversely as the square of the distance between the planet and the star. Stellar luminosity,  $L_\star$ , is given by:

$$L_\star = 4\pi R_\star^2 \sigma T_{\text{eff}}^4,$$

where  $\sigma = 5.670 \times 10^{-8} \text{ W m}^{-2} \text{ K}^{-4}$  is the Stefan-Boltzmann constant. In our study, the stellar radii and temperatures,  $T_{\text{eff}}$ , are computed two ways. We obtained high SNR spectra with high spectral resolution using the Keck Observatory HIRES spectrometer for all of the 62 stars that host planets with periods over 100 days, approaching the HZ. For those 62 stars, we performed a `SpecMatch` analysis [Petigura et al. \(2013b\)](#) to determine  $T_{\text{eff}}$  and the surface gravity,  $\log g$ , and metallicity,  $[\text{Fe}/\text{H}]$ . These stellar values were matched to stellar evolution models (Yonsei-Yale) to yield the radii and masses of the stars. The resulting values of stellar radii are uncertain by 10%, as determined by calibrations with nearby stars having parallaxes and hence having more accurately determined stellar radii. The values of  $T_{\text{eff}}$  are accurate to within 2%. Thus, summing the fractional errors in quadrature, the resulting stellar luminosities for the 62 stars (having  $P > 100$  days) are measured but carry uncertainties of 25%. For those stars without Keck spectra, we adopted photometric stellar radius and mass, for which the stellar radii are in error by 35% and the  $T_{\text{eff}}$  values are uncertain by 4%, giving errors in luminosity of 80%. We estimated the star-planet separation ( $a$ ) using  $P$ ,  $M_\star$ , and Kepler's third law. The stellar light flux falling on a planet is now easily calculated from  $F_P \propto L_\star / a^2$ . In what follows, we quote the flux falling on a planet relative to that falling on the Earth.

We find 10 planets having radii 1–2  $R_\oplus$  that fall within the stellar incident flux domain of the habitable zone, 0.25–4  $F_\oplus$ . As a reference, we plot their phase folded light curves in [Figure 5.15](#) along with the KIC identifier, period, radius, and stellar light flux. To compute the prevalence of such planets within the HZ, we apply the usual geometric correction for orbital tilts too large to cause transits, augmenting the counting of each transiting planet by  $a/R_\star$  total planets. We compute  $F_P$  for each synthetic planet in our completeness measurement study. [Figure 5.16](#) shows stellar flux level and radii of the 10 habitable zone planets, having size 1–2  $R_\oplus$ , along with the synthetic HZ planets from our completeness study. Because the number of synthetic trials is small for  $F_P < 1 F_\oplus$ , we compute occurrence using the 8 planets with  $F_P = 1\text{--}4 F_\oplus$ . We find  $11 \pm 4\%$  of Sun-like stars have a  $R_P = 1\text{--}2 R_\oplus$  planet that receives  $F_P = 1\text{--}4 F_\oplus$  light energy from their host star.

We account for the entire HZ (extending out to 0.25  $F_\oplus$ ) by extrapolating occurrence in  $F_P$ , assuming constant planet occurrence per  $\log P$  interval. [Figure 5.14](#) shows the CPO as a

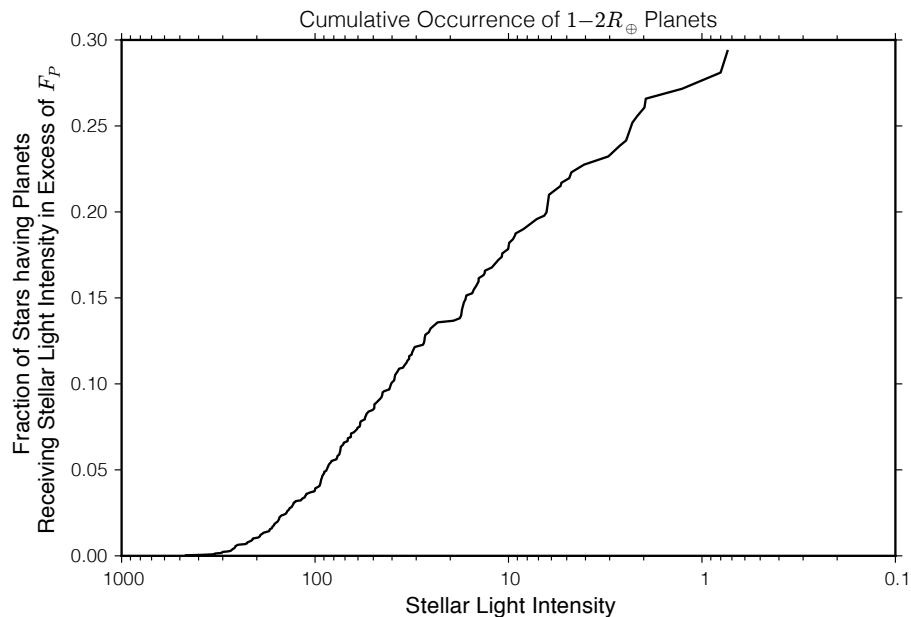


Figure 5.14: Same as Figure 5.12, but showing the CPO for 1–2  $R_{\oplus}$  planets as a function of decreasing flux. Planet occurrence is constant over a wide range of incident flux values,  $F_P = 100\text{--}4 F_{\oplus}$ , which supports extrapolation to the outer edge of our adopted HZ,  $F_P = 0.25 F_{\oplus}$ .

function of  $F_P$ . Planet occurrence is constant from  $\sim 100 F_{\oplus}$  down to  $\sim 4 F_{\oplus}$ , beyond which, small number fluctuations are significant. Assuming the occurrence of planets is constant in  $\log F_P$  implies that the same number of 1–2  $R_{\oplus}$  planets have incident fluxes of 1–0.25  $F_{\oplus}$  as have fluxes of 1–4  $F_{\oplus}$  where we computed directly the occurrence of planets to be 11%. Thus,  $22 \pm 8\%$  of Sun-like stars have a  $R_P = 1\text{--}2 R_{\oplus}$  planet within our adopted habitable zone with fluxes of 0.25–4.0  $F_{\oplus}$ .

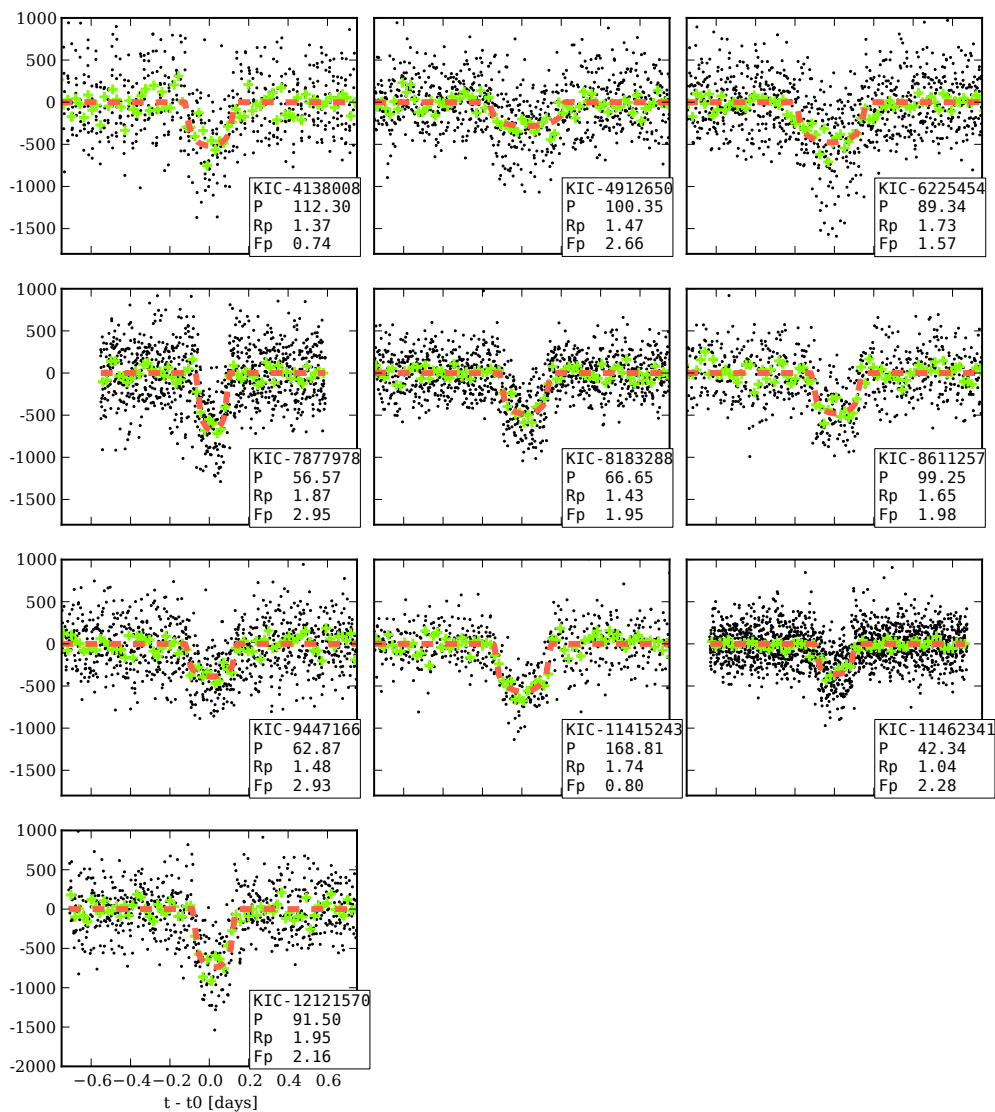


Figure 5.15: Phase folded photometry for ten Earth-size HZ candidates. Black point shows **TERRA**-calibrated photometry folded on the best fit ephemeris listed in Table 5.2. The green symbols show the median flux value in 30-minute bins. The red dashed lines shows the best-fit Mandel-Agol model. We have annotated each plot with the KIC identifier, period, planet size (Earth-radii), incident flux level (relative to Earth). All measurements of planet size and incident flux are based on spectra taken with the Keck 10 m telescope. Spectra for KIC-6225454, KIC-7877978, KIC-9447166, and KIC-11462341 were obtained during peer-review and were added in proof (see Table 5.3).

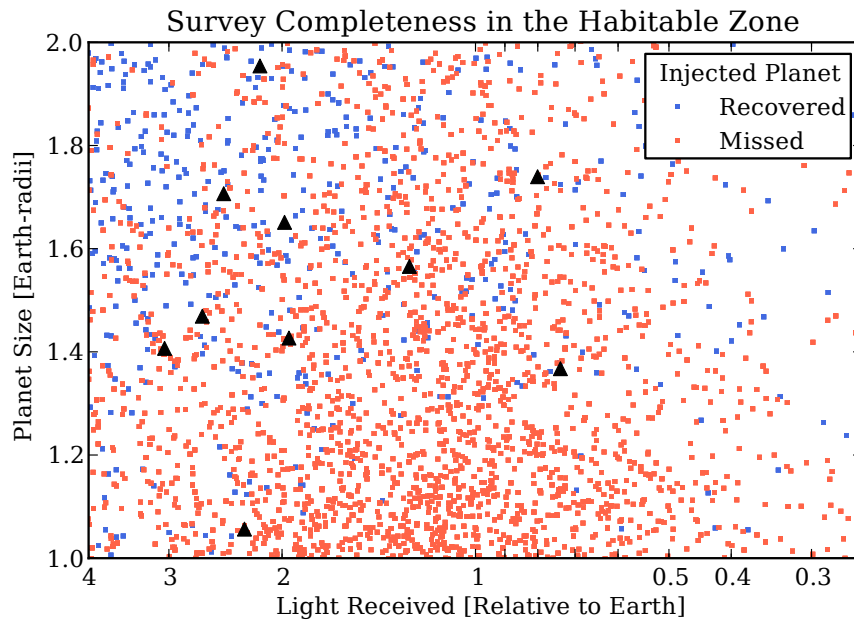


Figure 5.16: Ten small ( $R_P = 1\text{--}2 R_\oplus$ ) planets (black triangles) fall within our adopted habitable zone of  $F_P = 1/4\text{--}4 F_\oplus$ . We also plot the injected planets over this same domain. Survey completeness  $C$  is computed locally for each planet by dividing the number of injected planets that were recovered by the total number of injected planets in a small box centered on the real planet.

### 5.8.3 Occurrence Including Planets in Multi-planet Systems

For systems harboring more than one planet, **TERRA** only detects the planet with highest SNR, i.e. the most significant planet. The actual rate of planet occurrence is higher than we report when the missed planets in these multi-transiting systems is included. (Note that this correction only applies to multi-transiting system and not all multi-planet systems.) We estimate the size of this effect using the Q12 sample of KOIs from the *Kepler* project, which includes stars with multiple planets. We selected the 1190 “candidates” with well-determined periods ( $\sigma(P) < 0.1$  days) that orbit stars in the Best42k. In order to make a fair comparison between our planet sample and the Q12 sample, we computed the SNR of each of the 1190 candidates using **TERRA**. We excluded 82 KOIs with  $\text{SNR} < 12$ , i.e. candidates that would have been deemed sub-significant by **TERRA**.

For each planet in a multi-transiting system, we rank order each candidate by its “Relative SNR” defined as:

$$\text{Relative SNR} = \delta F \sqrt{\frac{\Delta T}{P}}.$$

Figure 5.17 shows the distribution of Q12 candidates in the Best42k as points on the  $P$ – $R_P$  plane. We highlight points corresponding to the most significant planet. We assess the boost in planet counts due to multi-transiting systems for different domains in  $P$  and  $R_P$ . For  $P > 50$  days and  $R_P < 4 R_\oplus$ , this multi-boost factor ranges from 21 to 28%, neglecting bins with fewer than 8 detected planets that suffer from small number fluctuations. Had we included additional planets, our occurrence measurements would rise by  $\sim 25\%$ , which is comparable to or slightly smaller than the fractional occurrence error for small planets in long-period orbits.

### 5.8.4 Correction due to False Positives

As discussed earlier, the sample of eKOIs is polluted by astrophysical false positives. Like the *Kepler* team, we do our best to identify and remove transits that are clearly due to eclipsing binaries, but cannot remove all eclipsing binary configurations. Thus, our sample, as well as those produced by the Kepler team, still contain a false positive component.

Fressin et al. (2013) addressed the contamination of the February 2012 *Kepler* Project sample of KOIs Batalha et al. (2012) by FPs that were not removed by the *Kepler* Project vetting process. FPs include background eclipsing binaries, physically associated eclipsing binaries (hierarchical triples), and physically associated stars, which themselves have a transiting planet. We consider the last scenario to be a FP because even though the transiting object is a planet, the radius is at least 1.4 times larger (1.4 corresponds stars of equal brightness). Fressin et al. (2013) added FPs to the Batalha et al (2012) sample of KOIs according to models of galactic structure, stellar binarity, and assumptions about the distributions of planets. Simulated FPs that would exhibit a detectable secondary eclipse or a significant centroid offset were removed, assuming the Kepler Project vetting process catches these FPs.

Fressin et al. (2013) found an overall FP rate of  $8.8 \pm 1.9\%$  for 1.25–2.0  $R_\oplus$  planets and

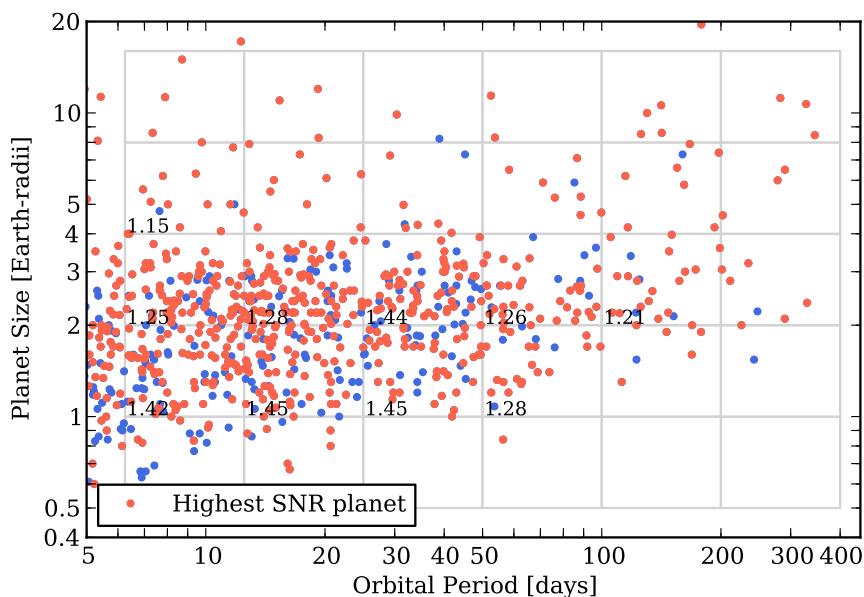


Figure 5.17: Distribution of  $P$  and  $R_P$  for *Kepler* team candidates from the Q12 catalog. We include planets with TERRA SNR  $> 12$  and well-determined orbital periods ( $\sigma(P) < 0.1$  days) that around “Best42k” stars. Planets that are either single or are the most significant planet in a multi-planet system are shown in red. Blue points correspond to additional planets in multi planet systems. For each cell with 10 or more planets, we compute the boost in planet counts due to multiplanet systems, the total number of planets divide by the number of most significant planets. For planets smaller than  $4 R_{\oplus}$  and  $P$  50 days, the boost ranges from 21–28%. Thus, including multis, we expect  $\sim 25\%$  higher occurrence.

$12.3 \pm 3.0\%$  for  $0.8\text{--}1.25 R_{\oplus}$  planets. Again, note that this fractional occurrence correction is small compared to our reported errors for small planets in long-period orbits. Stars with bound companions with transiting planets are the dominant fraction of FPs for small planets (76% for  $1.25\text{--}2.0 R_{\oplus}$  planets and 66% for  $0.8\text{--}1.25 R_{\oplus}$  planets). FPs of this type are very difficult to identify. A Sun-like star with  $V = 14.7$  mag (typical for our sample) is 1 kpc away. The binary star separation distribution peaks at 50 AU [Raghavan et al. \(2010\)](#) or 0.05 arcsec assuming a face-on orbit. Detecting companions separated by 0.05 arcsec is near the limits of current ground-based AO. Even if a companion was detected, we still wouldn't know which star harbored the transiting planet.

We adopt a 10% FP rate for planets having  $P = 50\text{--}400$  days and  $R_P = 1\text{--}2 R_{\oplus}$ . Adopting a false positive rate that is constant with period is justified because the occurrence of Neptune-sized planets is approximately constant with period, as shown in the main text. In the context of the occurrence of Earth-size planets with  $P = 200\text{--}400$  days ( $5.7^{+1.7}_{-2.2}\%$ ) and Earth-size planets in the HZ ( $22 \pm 8\%$ ), FPs contribute 10% fractional uncertainty and are secondary compared to statistical uncertainty.

Table 5.2: Properties of 836 eKOIs

KIC	KOI	$P$ days	$t_0$ days	Disp.	$p$ %	$\sigma(p)$	$T_{\text{eff}}$ K	$\log g$ cgs	$R_{\star}$ $R_{\odot}$	$\sigma(R_{\star})$	Prov.	$R_P$ $R_{\oplus}$	$\sigma(R_P)$	$F_P$ $F_{\oplus}$
1026032		8.460	133.78	R	40.6	0.09	6044	4.5	0.95	0.29	P	42.12	12.64	159.7
1026957	958.01	21.762	144.77	P	3.1	0.42	4861	4.6	0.72	0.07	SM	2.46	0.41	13.4
1571511	362.01	14.023	135.52	SE	12.8	0.00	6055	4.4	1.04	0.31	P	14.46	4.34	98.7
1718189	993.01	21.854	144.32	P	1.7	0.10	5827	4.5	0.88	0.26	P	1.65	0.50	34.6
1849702	2538.01	39.833	155.62	P	1.7	0.37	5023	4.6	0.73	0.07	SM	1.37	0.33	7.1
1872821	2351.01	10.274	134.64	P	1.8	0.11	5706	4.6	0.85	0.25	P	1.69	0.52	82.7
2141783	2201.01	116.521	144.14	P	2.5	0.37	6063	4.2	1.53	0.15	SM	4.09	0.74	10.9
2164169	1029.01	32.312	133.88	P	2.3	0.07	5975	4.5	0.96	0.29	P	2.39	0.72	26.5
2166206	1028.01	8.097	132.66	VD	1.8	0.09	6014	4.2	1.41	0.42	P	2.75	0.83	364.7
2304320	2033.01	16.541	133.94	P	1.8	0.09	5061	4.6	0.75	0.07	SM	1.43	0.16	24.6
2305255		24.567	155.97	P	2.1	0.05	5980	4.5	0.98	0.29	P	2.21	0.66	40.3
2306740		10.307	138.75	R	54.7	0.13	5932	4.2	1.26	0.38	P	75.44	22.63	208.0
2309719	1020.01	54.357	164.06	R	16.0	0.40	6159	4.3	1.34	0.13	SM	23.41	2.41	25.6
2438264	440.01	15.907	146.12	P	2.8	0.12	5070	4.6	0.77	0.08	SM	2.35	0.25	26.0
2441495	166.01	12.493	138.46	P	2.4	0.05	5208	4.6	0.77	0.08	SM	2.05	0.21	41.8
2444412	103.01	14.911	141.34	P	2.8	0.14	5554	4.5	0.92	0.09	SM	2.79	0.31	55.2
2449431	2009.01	86.752	170.29	P	2.1	0.16	5578	4.4	0.94	0.09	SM	2.11	0.27	5.9
2557816	488.01	9.379	138.93	P	2.6	0.15	5770	4.5	0.91	0.27	P	2.56	0.78	114.4
2571238	84.01	9.287	135.99	P	2.4	0.03	5523	4.5	0.89	0.09	SM	2.31	0.23	96.9
2576692		87.877	194.10	R	74.9	5.10	5801	4.5	0.87	0.26	P	71.11	21.88	5.3
2580872		15.927	145.55	R	71.9	0.70	5434	4.5	0.88	0.26	P	68.76	20.64	44.7
2695110	400.01	44.189	165.80	VD	9.4	0.88	6089	4.4	1.03	0.31	P	10.60	3.33	21.4
2715135	1024.01	5.748	133.31	P	2.4	0.11	4302	4.7	0.56	0.17	P	1.50	0.45	35.1
2716979		8.832	137.72	P	0.8	0.05	6098	4.3	1.22	0.37	P	1.05	0.32	257.8
2837111	1110.01	8.735	135.09	P	1.6	0.07	5948	4.5	0.93	0.28	P	1.59	0.48	139.3
2854698	986.01	8.187	138.05	P	2.2	0.10	5475	4.5	0.91	0.09	SM	2.15	0.24	107.9
2985767	2032.01	14.080	139.97	P	1.2	0.06	5530	4.5	0.86	0.26	P	1.14	0.35	52.9
2987027	197.01	17.276	133.84	P	9.2	0.10	4945	4.6	0.74	0.07	SM	7.39	0.74	20.2
2990873	2335.01	16.224	136.01	P	1.5	0.12	5555	4.5	0.93	0.09	SM	1.54	0.20	50.4
3002478	2380.01	6.357	135.48	P	1.5	0.08	5951	4.5	0.92	0.28	P	1.51	0.46	209.7
3003991		7.245	131.86	R	27.9	0.22	5532	4.6	0.80	0.24	P	24.35	7.31	107.9
3098194		30.477	136.97	R	71.4	1.67	5484	4.4	0.96	0.29	P	74.64	22.46	23.3
3098197	3362.01	30.477	136.97	R	41.9	0.69	5962	4.5	0.92	0.28	P	42.08	12.64	26.1
3102024		13.783	139.48	R	67.3	0.36	5353	4.6	0.77	0.23	P	56.71	17.02	39.1
3102384	273.01	10.574	132.78	P	1.6	0.04	5672	4.4	1.12	0.11	SM	1.94	0.20	125.9
3109930	1112.01	37.811	158.36	P	2.0	0.08	6099	4.5	1.01	0.30	P	2.19	0.66	25.2
3116412	1115.01	12.992	136.33	P	1.5	0.07	5760	4.2	1.31	0.13	SM	2.09	0.23	139.7
3120308	3380.01	10.266	136.50	C	1.5	0.13	5706	4.5	0.93	0.28	P	1.54	0.48	102.4
3120320		10.266	136.50	R	48.0	2.27	5903	4.5	0.93	0.28	P	48.78	14.81	111.7
3120904	3277.01	42.915	139.87	P	1.2	0.08	6152	4.3	1.23	0.12	SM	1.58	0.19	30.5
3128552	2055.01	8.679	133.04	P	2.1	0.10	5748	4.6	0.86	0.26	P	1.97	0.60	108.3

Table 5.2 (cont'd): Properties of 836 eKOIs

KIC	KOI	$P$ days	$t_0$ days	Disp.	$p$ %	$\sigma(p)$	$T_{\text{eff}}$ K	$\log g$ cgs	$R_{\star}$ $R_{\odot}$	$\sigma(R_{\star})$	Prov.	$R_P$ $R_{\oplus}$	$\sigma(R_P)$	$F_P$ $F_{\oplus}$
3128793	1786.01	24.679	137.78	P	8.3	0.07	4669	4.7	0.64	0.19	P	5.73	1.72	8.3
3217264	401.01	29.199	156.24	P	4.1	0.05	5363	4.5	0.89	0.09	SM	4.01	0.40	17.7
3218908	1108.01	18.925	149.49	P	2.4	0.13	5546	4.6	0.81	0.24	P	2.08	0.64	30.5
3219037	3395.01	10.005	136.78	P	1.0	0.09	5948	4.5	0.97	0.29	P	1.05	0.33	130.5
3223433	4548.01	61.079	132.53	P	1.4	0.33	5518	4.6	0.80	0.24	P	1.20	0.46	6.2
3230753	2928.01	17.734	143.92	P	1.4	0.08	5250	4.6	0.78	0.23	P	1.15	0.35	27.1
3230787		17.734	143.92	R	59.4	1.75	5905	4.4	1.00	0.30	P	64.98	19.59	63.3
3231341	1102.01	12.334	137.58	P	2.0	0.12	6005	4.2	1.38	0.14	SM	3.08	0.36	194.1
3236705	3343.01	83.264	194.26	P	2.3	0.32	5965	4.5	0.94	0.28	P	2.39	0.79	7.1
3239671	2066.01	147.976	263.08	P	3.4	0.33	5573	4.4	0.91	0.09	SM	3.42	0.47	2.7
3323289		33.693	158.87	R	67.2	0.03	5401	4.4	0.89	0.27	P	65.36	19.61	16.8
3323887	377.01	19.273	143.96	TTV	8.0	1.60	5780	4.4	1.06	0.11	SM	9.32	2.07	56.7
3326377	1830.02	198.711	156.52	P	4.3	0.19	5180	4.6	0.79	0.08	SM	3.69	0.40	1.1
3337425	1114.01	7.048	132.72	P	1.5	0.08	5721	4.4	1.03	0.31	P	1.69	0.51	210.5
3342467	3278.01	88.181	209.16	P	3.0	0.27	5414	4.6	0.77	0.23	P	2.56	0.80	3.4
3342592	402.01	17.177	136.19	SE	13.6	0.05	6004	4.5	0.94	0.28	P	13.90	4.17	59.2
3353050	384.01	5.080	133.80	P	1.4	0.04	6156	4.4	1.14	0.11	SM	1.73	0.18	465.0
3433668	3415.01	15.022	143.71	P	1.0	0.09	5823	4.2	1.37	0.14	SM	1.47	0.20	136.8
3442055	1218.01	29.619	133.70	P	1.6	0.06	5624	4.4	1.01	0.10	SM	1.80	0.19	27.2
3446746	385.01	13.145	135.41	P	1.9	0.12	5412	4.5	0.91	0.09	SM	1.85	0.22	57.9
3448130	2043.01	78.546	144.08	C	2.2	0.16	6005	4.5	0.94	0.28	P	2.28	0.70	7.8
3531558	118.01	24.994	138.66	P	1.5	0.07	5807	4.3	1.14	0.11	SM	1.85	0.20	46.0
3534118	3641.01	178.420	218.19	R	20.3	3.12	6079	4.3	1.15	0.11	SM	25.41	4.66	4.0
3539231	4626.01	91.954	183.13	P	1.7	0.16	5971	4.3	1.11	0.33	P	2.02	0.64	8.9
3541946	624.01	17.790	146.86	P	2.7	0.05	5576	4.5	0.90	0.09	SM	2.65	0.27	41.2
3547760	4535.01	9.848	136.80	V	1.2	0.09	5339	4.6	0.80	0.24	P	1.05	0.33	65.4
3548044	2194.02	67.968	163.57	P	1.7	0.12	5725	4.3	1.04	0.10	SM	1.99	0.24	10.8
3559935	492.01	29.913	134.86	P	2.7	0.07	5465	4.4	0.95	0.28	P	2.81	0.85	23.0
3632089	3308.01	31.777	136.82	P	1.5	0.08	5683	4.4	1.02	0.31	P	1.64	0.50	27.7
3642741	242.01	7.258	138.36	P	5.7	0.11	5546	4.5	0.86	0.26	P	5.30	1.59	127.8
3655332	1179.01	15.066	140.67	R	23.5	1.24	5818	4.4	0.98	0.30	P	25.25	7.69	73.1
3657176	2903.01	17.417	141.09	C	1.7	0.10	5887	4.5	0.97	0.29	P	1.84	0.56	59.9
3728701	2536.01	51.131	137.17	P	1.9	0.19	6054	4.4	1.12	0.33	P	2.28	0.72	20.4
3732035	3966.01	138.946	153.91	P	2.3	0.22	6014	4.4	1.11	0.11	SM	2.81	0.38	5.2
3745690	442.01	13.541	144.59	P	2.0	0.13	5768	4.4	0.99	0.10	SM	2.16	0.26	81.5
3747817	4103.01	184.778	217.35	P	2.9	0.27	5275	4.6	0.78	0.08	SM	2.49	0.34	1.2
3749134	1212.01	11.301	134.94	P	1.6	0.15	5916	4.4	0.98	0.29	P	1.66	0.52	111.1
3756264	3108.01	7.363	136.87	P	2.0	0.18	5853	4.5	0.89	0.27	P	1.93	0.60	153.2
3757588		24.090	154.27	SE	13.1	0.49	5386	4.4	0.89	0.27	P	12.79	3.87	26.2
3761319		16.249	143.94	P	1.8	0.11	5758	4.4	0.95	0.29	P	1.91	0.58	60.4
3833007	443.01	16.218	147.59	P	2.6	0.10	5891	4.5	0.90	0.27	P	2.52	0.76	55.8

Table 5.2 (cont'd): Properties of 836 eKOIs

KIC	KOI	$P$ days	$t_0$ days	Disp.	$p$ %	$\sigma(p)$	$T_{\text{eff}}$ K	$\log g$ cgs	$R_{\star}$ $R_{\odot}$	$\sigma(R_{\star})$	Prov.	$R_P$ $R_{\oplus}$	$\sigma(R_P)$	$F_P$ $F_{\oplus}$
3835670	149.01	14.557	145.10	P	2.9	0.08	5724	4.1	1.59	0.16	SM	4.98	0.52	152.5
3847138	444.01	11.723	142.16	P	2.0	0.07	5551	4.4	0.93	0.09	SM	2.06	0.22	80.6
3848966	3389.01	29.766	155.58	P	1.4	0.11	6025	4.5	0.97	0.29	P	1.44	0.45	31.0
3852655	3002.01	11.629	132.82	P	0.9	0.06	5716	4.3	1.16	0.12	SM	1.15	0.14	129.2
3858917	3294.01	25.950	180.86	SE	9.8	0.13	5565	4.6	0.81	0.24	P	8.61	2.59	20.4
3858949	995.01	25.952	154.89	SE	2.8	0.03	5341	4.6	0.75	0.23	P	2.28	0.68	15.7
3858988	3388.01	25.953	154.85	SE	2.5	0.03	5738	4.3	1.06	0.32	P	2.86	0.86	39.7
3859079	1199.01	53.529	147.86	P	3.1	0.23	4767	4.6	0.66	0.20	P	2.23	0.69	3.4
3938073		31.024	158.87	R	45.5	0.04	6007	4.3	1.16	0.35	P	57.63	17.29	42.2
3939150	1215.01	17.324	142.12	P	1.4	0.11	6034	4.3	1.34	0.13	SM	2.12	0.27	111.9
3942670	392.01	33.420	137.85	P	1.5	0.03	5989	4.3	1.29	0.13	SM	2.10	0.22	41.8
3962872	4539.01	25.954	148.82	P	1.1	0.04	6055	4.4	1.05	0.32	P	1.26	0.38	44.7
3966801	494.01	25.696	137.40	P	3.4	0.22	5055	4.7	0.69	0.21	P	2.56	0.79	11.3
3969687	2904.01	16.358	141.26	P	1.0	0.09	6049	4.1	1.60	0.16	SM	1.77	0.24	162.7
3970233	604.01	8.255	133.15	SE	12.4	0.00	5354	4.5	0.84	0.25	P	11.41	3.42	94.2
4035640	1881.01	28.267	140.93	P	3.1	0.07	5257	4.5	0.82	0.25	P	2.83	0.85	16.7
4043190	1220.01	6.401	136.89	P	1.1	0.06	5296	3.8	2.50	0.25	SM	3.01	0.34	737.3
4043443	231.01	119.839	161.88	P	10.4	1.40	4604	4.7	0.65	0.06	SM	7.37	1.23	1.0
4049901	2295.01	16.291	132.10	P	0.6	0.04	5430	4.5	0.83	0.08	SM	0.58	0.07	38.9
4075064		61.423	161.24	R	69.0	3.93	4945	4.7	0.67	0.20	P	50.13	15.31	3.1
4076976		9.761	133.68	P	1.0	0.04	4960	4.6	0.71	0.21	P	0.80	0.24	43.4
4077526	1336.01	10.218	136.89	P	2.1	0.12	6082	4.4	1.09	0.33	P	2.46	0.75	168.3
4077901	2239.01	12.110	140.73	C	1.0	0.07	5516	4.5	0.83	0.25	P	0.92	0.28	58.7
4138008	4742.01	112.303	230.45	P	2.2	0.28	4402	4.7	0.57	0.06	SM	1.37	0.22	0.7
4165473	550.01	13.023	139.46	P	2.2	0.09	5627	4.5	0.98	0.10	SM	2.39	0.26	74.5
4172013	2386.01	16.270	145.12	P	2.0	0.15	5877	4.5	0.89	0.27	P	1.94	0.60	54.3
4178389	185.01	23.211	134.39	P	18.2	0.67	5927	4.5	0.91	0.27	P	18.02	5.45	36.0
4242147	1934.01	28.783	132.33	P	2.7	0.10	4569	4.7	0.59	0.18	P	1.76	0.53	5.3
4247092	403.01	21.056	150.11	P	2.8	0.15	6160	4.4	1.13	0.11	SM	3.48	0.40	69.0
4249725	222.01	6.313	132.66	P	3.3	0.07	4533	4.7	0.59	0.18	P	2.11	0.63	39.7
4252322	396.01	14.591	137.09	P	3.2	0.09	5922	4.2	1.34	0.40	P	4.62	1.39	145.2
4254466	2134.01	42.300	168.80	P	2.2	0.08	5718	4.4	0.97	0.29	P	2.30	0.70	17.2
4262581	2122.01	37.646	161.47	P	1.9	0.14	5778	4.5	0.88	0.27	P	1.79	0.55	16.7
4263529	3358.01	10.104	132.92	P	3.0	0.11	5520	4.5	0.84	0.25	P	2.74	0.83	77.9
4270253	551.01	11.637	132.31	P	2.2	0.11	5841	4.5	0.88	0.26	P	2.11	0.64	81.6
4276716	1619.01	20.665	132.02	P	1.0	0.12	4882	4.6	0.71	0.07	SM	0.81	0.12	14.5
4281895		9.544	137.78	R	27.1	0.09	5608	4.4	0.97	0.29	P	28.67	8.60	118.7
4352168		10.644	134.94	R	63.2	0.18	5374	4.5	0.81	0.24	P	55.84	16.75	62.3
4376644	397.01	27.677	146.14	V	15.0	1.39	6059	4.5	0.96	0.29	P	15.77	4.95	33.9
4454934	2245.01	33.470	140.16	P	1.8	0.11	5900	4.3	1.12	0.34	P	2.18	0.67	34.0
4474462	4452.01	12.858	141.85	P	1.0	0.10	6050	4.2	1.40	0.42	P	1.58	0.50	197.3

Table 5.2 (cont'd): Properties of 836 eKOIs

KIC	KOI	$P$ days	$t_0$ days	Disp.	$p$ %	$\sigma(p)$	$T_{\text{eff}}$ K	$\log g$ cgs	$R_{\star}$ $R_{\odot}$	$\sigma(R_{\star})$	Prov.	$R_P$ $R_{\oplus}$	$\sigma(R_P)$	$F_P$ $F_{\oplus}$
4478142		219.909	329.43	P	2.5	0.34	5699	4.5	0.89	0.27	P	2.45	0.80	1.6
4544907	2024.01	46.878	137.66	P	2.3	0.08	5839	4.4	1.04	0.31	P	2.57	0.78	18.2
4551663	2576.01	12.077	140.48	C	1.4	0.18	5376	4.5	0.87	0.26	P	1.34	0.43	61.3
4552729	2691.01	97.447	204.83	P	6.2	0.99	4704	4.6	0.65	0.19	P	4.37	1.49	1.4
4563268	627.01	7.752	137.42	P	1.8	0.06	5999	4.2	1.45	0.14	SM	2.85	0.30	366.6
4633570	446.01	16.709	141.34	P	2.6	0.07	4629	4.7	0.63	0.19	P	1.77	0.53	13.3
4639868	1326.01	53.099	136.01	TTV	14.5	1.75	5467	4.4	0.95	0.09	SM	15.04	2.35	10.9
4644604	628.01	14.486	131.55	P	2.0	0.06	5783	4.3	1.05	0.11	SM	2.31	0.24	88.5
4644952	1805.01	6.941	137.56	P	2.7	0.13	5529	4.5	0.88	0.09	SM	2.56	0.29	139.6
4676964	3069.01	43.103	140.13	P	1.7	0.17	5637	4.4	1.02	0.31	P	1.91	0.60	17.8
4679314		7.697	133.27	VD	0.8	0.03	5747	4.6	0.86	0.26	P	0.74	0.22	127.1
4753988		7.304	135.03	R	52.5	1.85	6039	4.5	0.95	0.28	P	54.38	16.43	193.0
4773155		25.705	156.64	R	65.3	0.13	5606	4.5	0.89	0.27	P	63.31	18.99	26.3
4813563	1959.01	36.516	151.29	P	2.7	0.10	4869	4.6	0.69	0.21	P	2.03	0.61	6.6
4815520	367.01	31.578	145.65	P	4.2	0.08	5688	4.4	1.08	0.11	SM	4.98	0.51	28.6
4820550	3823.01	202.121	292.04	P	5.7	0.65	5796	4.5	0.87	0.26	P	5.37	1.72	1.7
4827723	632.01	7.239	135.03	P	1.5	0.02	5398	4.5	0.87	0.09	SM	1.44	0.15	114.5
4833421	232.01	12.466	134.00	P	4.6	0.12	6063	4.4	1.12	0.11	SM	5.63	0.58	133.6
4841374	633.01	161.472	170.62	P	2.7	0.18	5758	4.4	1.03	0.10	SM	3.03	0.37	3.3
4847534	499.01	9.669	135.86	P	1.9	0.07	5214	4.5	0.80	0.24	P	1.68	0.51	63.1
4847832		30.960	139.44	R	60.5	0.12	5186	4.5	0.79	0.24	P	52.29	15.69	13.1
4857058	3061.01	7.329	132.10	P	1.3	0.11	5062	4.6	0.75	0.22	P	1.03	0.32	73.8
4860678	1602.01	9.977	137.25	P	1.5	0.13	5813	4.5	0.87	0.26	P	1.44	0.45	96.9
4860932	1600.01	12.366	137.89	VD	1.8	0.08	6059	4.5	0.96	0.29	P	1.85	0.56	98.9
4912650		100.348	152.82	P	1.7	0.19	5180	4.5	0.80	0.08	SM	1.47	0.22	2.7
4932442	1665.01	6.934	137.07	P	1.0	0.07	5869	4.2	1.43	0.14	SM	1.63	0.20	377.9
4948730		23.029	139.87	SE	2.2	0.18	5876	4.4	0.98	0.29	P	2.38	0.74	42.4
4949751	404.01	31.805	154.58	V	9.9	0.45	5956	4.5	0.92	0.28	P	9.94	3.01	24.5
4951877	501.01	24.796	145.53	P	2.2	0.07	5750	4.5	0.90	0.27	P	2.14	0.65	30.3
4989057	1923.01	7.234	137.70	P	2.0	0.13	5416	4.5	0.88	0.09	SM	1.92	0.23	116.8
5003117	405.01	37.610	153.11	SE	14.8	0.04	5576	4.5	0.88	0.26	P	14.24	4.27	15.3
5025294		5.463	134.29	SE	7.3	2.53	5978	4.5	0.95	0.28	P	7.50	3.45	277.5
5035972	406.01	49.266	141.93	SE	14.7	0.34	5848	4.4	1.04	0.31	P	16.68	5.02	17.0
5042210	2462.01	12.146	131.57	P	0.8	0.02	5995	4.3	1.33	0.13	SM	1.11	0.12	172.7
5088591	1801.01	14.532	140.73	P	3.5	0.11	5331	4.5	0.86	0.26	P	3.24	0.98	45.8
5091614		21.142	138.40	R	40.3	0.14	6077	4.5	0.97	0.29	P	42.47	12.74	49.5
5095082	4320.01	20.658	145.63	P	0.9	0.07	5520	4.4	0.96	0.29	P	0.92	0.29	39.6
5096590	3093.01	29.610	137.34	P	1.0	0.07	5818	4.3	1.17	0.12	SM	1.31	0.16	38.5
5098444	637.01	26.949	151.03	SE	13.8	0.09	4918	4.6	0.70	0.21	P	10.57	3.17	10.5
5103942	1668.01	10.102	131.82	P	2.2	0.16	6090	4.5	0.97	0.29	P	2.28	0.70	133.3
5113822	638.01	23.640	149.00	P	3.1	0.35	5685	4.4	0.97	0.10	SM	3.24	0.49	35.6

Table 5.2 (cont'd): Properties of 836 eKOIs

KIC	KOI	$P$ days	$t_0$ days	Disp.	$p$ %	$\sigma(p)$	$T_{\text{eff}}$ K	$\log g$ cgs	$R_*$ $R_{\odot}$	$\sigma(R_*)$	Prov.	$R_P$ $R_{\oplus}$	$\sigma(R_P)$	$F_P$ $F_{\oplus}$
5121511	640.01	30.997	160.79	P	2.4	0.06	5216	4.5	0.84	0.08	SM	2.18	0.22	13.9
5128673	2698.01	87.974	168.29	P	3.0	0.20	5845	4.3	1.20	0.12	SM	3.91	0.47	9.7
5131180	641.01	14.852	133.43	C	3.0	0.15	4240	4.7	0.55	0.17	P	1.78	0.54	9.1
5193077	3492.01	22.296	146.43	C	0.9	0.05	5785	4.5	0.87	0.26	P	0.85	0.26	32.2
5199426		78.603	144.00	R	35.8	3.87	5946	4.4	0.99	0.30	P	38.86	12.39	8.7
5213404	3468.01	20.706	139.95	P	1.2	0.12	5793	4.4	0.98	0.29	P	1.26	0.40	46.8
5217586	1592.01	26.069	143.12	P	2.5	0.03	5614	4.4	1.02	0.31	P	2.83	0.85	34.9
5254230		7.036	137.95	SE	4.2	1.39	5369	4.5	0.89	0.27	P	4.04	1.81	131.6
5266937		5.917	132.90	R	62.5	0.04	5655	4.4	0.99	0.30	P	67.70	20.31	241.5
5272233	2711.01	9.024	133.56	P	1.4	0.08	5823	4.3	1.16	0.12	SM	1.72	0.20	186.6
5282051	502.01	5.910	135.68	C	1.4	0.05	5546	4.4	1.02	0.30	P	1.53	0.46	240.6
5299459	1576.01	10.416	132.64	P	2.6	0.04	5489	4.4	0.99	0.10	SM	2.84	0.29	94.9
5301750	1589.01	8.726	138.77	P	2.0	0.07	6094	4.4	1.11	0.11	SM	2.38	0.25	212.2
5303346	3275.01	37.325	143.04	SE	11.5	0.21	5297	4.6	0.79	0.24	P	9.90	2.97	10.5
5308537	4409.01	14.265	143.22	P	0.8	0.07	5896	4.4	0.98	0.29	P	0.84	0.26	80.2
5340644	503.01	8.222	131.84	P	3.5	0.16	4272	4.7	0.56	0.17	P	2.13	0.65	21.0
5351250	408.01	7.382	136.17	P	3.5	0.11	5554	4.5	0.89	0.09	SM	3.39	0.36	131.9
5360082	3768.01	11.354	133.27	SE	12.7	0.07	4723	4.6	0.65	0.20	P	9.00	2.70	25.4
5374403	2556.01	40.837	152.84	P	1.4	0.08	5523	4.5	0.91	0.09	SM	1.38	0.16	14.3
5375194	1825.01	13.523	142.18	P	2.3	0.06	5337	4.6	0.81	0.08	SM	2.05	0.21	42.7
5393558		10.217	137.25	R	62.5	0.61	5888	4.2	1.30	0.39	P	88.98	26.71	219.5
5431027	4558.01	8.823	136.89	P	1.1	0.11	5596	4.3	1.08	0.33	P	1.32	0.42	164.3
5438757	1601.01	10.351	133.72	P	1.5	0.04	5727	4.6	0.85	0.26	P	1.41	0.43	83.7
5443604	2713.01	21.391	141.30	VD	2.2	0.33	4896	4.7	0.66	0.20	P	1.58	0.53	12.0
5444548	409.01	13.249	139.77	P	2.4	0.12	5796	4.4	1.12	0.11	SM	2.95	0.33	102.9
5446285	142.01	10.922	134.76	TTV	0.1	0.36	5423	4.5	0.90	0.09	SM	0.05	0.36	70.1
5461440	504.01	40.606	158.67	P	2.4	0.19	5579	4.6	0.81	0.24	P	2.11	0.66	11.4
5474613	1599.01	20.409	140.11	P	1.6	0.08	5762	4.5	0.92	0.28	P	1.57	0.48	41.3
5478055	411.01	15.852	142.52	VD	2.2	0.07	5982	4.3	1.16	0.35	P	2.84	0.86	101.9
5480640	2707.01	58.033	138.77	P	2.7	0.15	5610	4.6	0.82	0.25	P	2.41	0.74	7.4
5481148	2701.01	22.024	135.19	C	3.8	0.13	5836	4.5	0.92	0.27	P	3.75	1.13	37.9
5520547	2990.01	11.200	137.52	P	1.4	0.08	6055	4.5	0.95	0.29	P	1.48	0.45	111.3
5526527	1838.01	16.737	143.14	P	3.1	0.09	4565	4.7	0.61	0.18	P	2.09	0.63	12.1
5526717	1677.01	52.069	178.16	P	2.2	0.16	5717	4.6	0.85	0.25	P	2.06	0.64	9.6
5530882	1680.01	5.083	132.94	C	0.9	0.06	5709	4.6	0.85	0.25	P	0.81	0.25	212.3
5535280		74.987	146.12	R	41.0	4.19	5950	4.5	0.92	0.28	P	40.99	12.99	7.8
5546277	3797.01	7.500	137.40	SE	2.4	0.05	5809	4.5	0.87	0.26	P	2.29	0.69	141.6
5546761	2160.01	17.671	131.57	P	1.6	0.09	5807	4.5	0.87	0.26	P	1.53	0.47	45.0
5553624		25.762	150.56	R	52.8	0.94	5545	4.5	0.84	0.25	P	48.14	14.47	22.2
5562784	608.01	25.337	142.24	VD	5.1	0.05	4502	4.7	0.60	0.18	P	3.33	1.00	6.4
5563300	3309.01	71.053	134.76	V	7.3	0.98	5272	4.5	0.83	0.25	P	6.66	2.18	5.0

Table 5.2 (cont'd): Properties of 836 eKOIs

KIC	KOI	$P$ days	$t_0$ days	Disp.	$p$ %	$\sigma(p)$	$T_{\text{eff}}$ K	$\log g$ cgs	$R_{\star}$ $R_{\odot}$	$\sigma(R_{\star})$	Prov.	$R_P$ $R_{\oplus}$	$\sigma(R_P)$	$F_P$ $F_{\oplus}$
5640085	448.01	10.139	137.91	P	3.3	0.19	4616	4.6	0.66	0.07	SM	2.36	0.28	26.9
5652010		14.641	140.32	P	1.0	0.10	5399	4.4	0.90	0.27	P	0.97	0.31	52.4
5686174	610.01	14.282	137.99	P	3.2	0.27	4207	4.7	0.55	0.16	P	1.91	0.59	9.2
5700330		53.220	181.70	P	7.4	0.04	5883	4.3	1.21	0.36	P	9.76	2.93	20.9
5702939	3000.01	18.398	144.94	C	1.1	0.04	5606	4.4	0.99	0.10	SM	1.18	0.13	52.0
5706966	1908.01	12.551	137.27	P	2.1	0.12	4350	4.7	0.57	0.17	P	1.28	0.39	13.3
5709725	555.02	86.493	181.90	P	2.9	0.21	5246	4.5	0.83	0.08	SM	2.59	0.32	3.5
5728139	206.01	5.334	131.98	P	6.3	0.05	6043	4.3	1.14	0.34	P	7.81	2.34	434.7
5731312		7.946	135.11	R	48.1	0.82	4938	4.6	0.71	0.21	P	37.10	11.15	55.2
5735762	148.02	9.674	135.01	P	2.8	0.03	5189	4.5	0.84	0.08	SM	2.53	0.26	64.4
5738496	556.01	9.502	137.66	SE	1.9	0.09	5921	4.5	0.91	0.27	P	1.92	0.58	118.0
5768816	3288.01	47.987	160.67	P	2.4	0.06	5613	4.4	0.96	0.29	P	2.51	0.75	13.6
5770074	1928.01	63.040	169.11	P	2.4	0.13	5804	4.4	1.06	0.11	SM	2.73	0.31	11.6
5771719	190.01	12.265	139.30	P	10.9	0.05	5538	4.1	1.42	0.42	P	16.86	5.06	168.3
5774349	557.01	15.656	139.48	P	3.5	0.11	5147	4.5	0.78	0.23	P	2.94	0.89	30.6
5780930	3412.01	16.753	131.59	P	1.7	0.07	4683	4.6	0.64	0.19	P	1.20	0.36	14.3
5781192		9.460	138.34	R	69.2	0.81	5539	4.6	0.80	0.24	P	60.63	18.20	76.5
5786676	650.01	11.955	142.87	P	2.6	0.10	5064	4.6	0.76	0.08	SM	2.18	0.23	37.2
5791986	413.01	15.229	146.10	P	3.1	0.09	5439	4.6	0.81	0.24	P	2.74	0.83	39.4
5794570	2675.01	5.448	132.49	P	2.3	0.16	5693	4.5	0.95	0.10	SM	2.42	0.29	235.4
5796675	652.01	16.081	134.52	P	5.4	0.10	5305	4.5	0.83	0.08	SM	4.93	0.50	34.4
5807769	2614.01	7.990	132.27	P	1.3	0.09	5948	4.5	0.92	0.27	P	1.31	0.40	152.9
5812960	507.01	18.492	136.52	P	3.7	0.10	5290	4.5	0.84	0.25	P	3.37	1.02	31.2
5819801	4686.01	11.831	138.25	P	0.6	0.04	5522	4.1	1.44	0.43	P	0.90	0.27	179.5
5866099	1055.01	36.977	133.64	SE	6.3	0.37	5571	4.1	1.39	0.42	P	9.58	2.93	37.9
5872150	414.01	20.355	134.64	SE	14.3	0.02	6041	4.4	1.05	0.31	P	16.28	4.88	60.8
5903749	3029.01	18.976	134.84	P	1.8	0.12	5421	4.4	0.92	0.28	P	1.82	0.56	38.7
5906426	2377.01	13.903	143.53	P	1.8	0.18	5229	4.5	0.81	0.24	P	1.56	0.49	41.0
5940165	2031.01	9.304	140.36	P	3.8	0.54	4452	4.7	0.59	0.18	P	2.44	0.81	22.7
5941160	654.01	8.595	137.25	P	1.7	0.08	5662	4.5	0.93	0.09	SM	1.74	0.19	126.5
5953297	2733.01	5.620	132.94	P	1.3	0.04	4809	4.6	0.67	0.20	P	0.92	0.28	73.2
5959719	2498.01	6.738	133.31	P	0.9	0.11	5153	4.6	0.78	0.08	SM	0.78	0.12	92.0
5959753	226.01	8.309	138.11	P	2.6	0.07	5241	4.6	0.73	0.22	P	2.09	0.63	63.8
5966322	303.01	60.928	173.38	P	2.5	0.06	5560	4.4	0.93	0.09	SM	2.52	0.26	9.1
5972334	191.01	15.359	132.39	P	10.9	0.07	5417	4.5	0.90	0.09	SM	10.66	1.07	46.4
5978361	558.01	9.178	136.39	P	2.6	0.13	5505	4.6	0.80	0.24	P	2.23	0.68	78.1
5992270	1855.01	58.430	168.31	C	5.7	1.55	4386	4.7	0.58	0.17	P	3.61	1.46	1.8
6029130		12.592	134.74	R	74.6	10.82	5289	4.6	0.74	0.22	P	60.37	20.12	38.9
6034945	1683.01	9.115	133.98	P	1.7	0.10	5919	4.4	1.01	0.30	P	1.85	0.57	156.6
6037187	1061.01	41.806	142.81	P	2.1	0.13	5899	4.5	0.97	0.29	P	2.22	0.68	18.9
6037581	1916.02	9.600	136.58	P	1.6	0.08	5865	4.4	1.12	0.11	SM	1.94	0.22	163.0

Table 5.2 (cont'd): Properties of 836 eKOIs

KIC	KOI	$P$ days	$t_0$ days	Disp.	$p$ %	$\sigma(p)$	$T_{\text{eff}}$ K	$\log g$ cgs	$R_{\star}$ $R_{\odot}$	$\sigma(R_{\star})$	Prov.	$R_P$ $R_{\oplus}$	$\sigma(R_P)$	$F_P$ $F_{\oplus}$
6046540	200.01	7.341	134.35	P	8.2	0.05	5940	4.5	0.91	0.27	P	8.18	2.46	169.7
6058816	3500.01	73.750	188.54	P	1.4	0.09	6093	4.5	0.99	0.30	P	1.53	0.47	9.9
6072593	3070.01	5.076	133.90	C	1.0	0.10	5914	4.3	1.12	0.34	P	1.23	0.39	423.2
6119141	2343.01	29.073	136.97	P	1.9	0.10	5781	4.4	1.06	0.32	P	2.20	0.67	34.7
6124512	2627.01	8.384	134.41	P	0.9	0.06	5469	4.4	0.95	0.28	P	0.98	0.30	125.8
6131659		17.528	144.57	R	57.0	0.10	5088	4.6	0.76	0.23	P	46.91	14.07	24.0
6137704	3605.01	178.274	255.32	R	28.5	2.79	5195	4.5	0.80	0.24	P	24.76	7.81	1.3
6142862	2336.01	5.335	133.43	C	1.4	0.11	4423	4.7	0.58	0.18	P	0.87	0.27	45.6
6146418		22.446	149.15	SE	7.5	0.09	6077	4.3	1.20	0.36	P	9.79	2.94	70.7
6146838		27.467	143.67	R	23.6	0.04	5600	4.4	0.94	0.28	P	24.23	7.27	27.0
6147573		25.837	137.36	R	40.4	0.73	5695	4.5	0.91	0.27	P	40.31	12.12	28.8
6152974	216.01	20.172	141.22	P	7.1	0.35	5187	4.5	0.79	0.24	P	6.11	1.86	23.3
6184894		7.203	135.21	P	3.8	0.10	5485	4.5	0.85	0.26	P	3.51	1.06	122.8
6185476	227.01	17.706	135.97	TTV	0.9	0.15	5491	4.4	1.28	0.13	SM	1.29	0.24	70.3
6185711	169.01	11.702	139.42	VD	2.0	0.05	5814	4.5	0.88	0.26	P	1.95	0.59	79.0
6209677	1750.01	7.769	138.05	P	1.3	0.06	5799	4.5	0.94	0.28	P	1.38	0.42	159.1
6225454		89.338	218.54	P	2.4	0.58	4549	4.7	0.61	0.18	P	1.57	0.61	1.3
6266741	508.01	7.930	137.81	P	2.6	0.09	5614	4.3	1.15	0.34	P	3.29	0.99	213.7
6267535	660.01	6.080	134.13	P	1.6	0.09	5317	3.9	2.10	0.21	SM	3.74	0.43	598.8
6289650	415.01	166.790	245.14	P	6.4	0.33	5663	4.4	1.01	0.10	SM	6.99	0.79	2.9
6305192	219.01	8.025	132.47	P	5.3	0.08	6006	4.2	1.45	0.15	SM	8.42	0.85	352.7
6307062		75.377	167.11	R	88.5	6.03	5416	4.6	0.77	0.23	P	74.67	22.97	4.2
6307063		376.891	317.87	SE	3.3	1.29	5872	4.4	1.11	0.11	SM	4.01	1.62	1.2
6307083	2050.01	75.378	167.11	SE	1.7	0.09	5047	4.6	0.74	0.22	P	1.38	0.42	3.2
6342333	2065.01	80.232	162.39	P	3.1	0.40	5655	4.5	0.88	0.26	P	2.97	0.97	5.7
6346809	2775.01	17.578	137.72	P	2.1	0.14	5681	4.4	0.94	0.28	P	2.16	0.67	51.2
6347299	661.01	14.401	131.80	P	1.8	0.05	5789	4.4	1.10	0.11	SM	2.19	0.23	90.4
6351097	2618.01	12.491	136.33	C	1.3	0.11	5771	4.5	0.95	0.28	P	1.30	0.41	84.6
6356692	2948.01	11.391	141.57	P	0.6	0.04	5561	4.2	1.39	0.14	SM	0.98	0.12	160.1
6359798	1121.01	14.154	140.69	R	36.4	0.37	5855	4.4	1.07	0.11	SM	42.44	4.27	89.7
6364582	3456.01	30.861	200.05	P	1.2	0.02	6012	4.4	1.09	0.33	P	1.37	0.41	37.6
6383821	1238.01	27.072	139.11	P	2.2	0.10	5611	4.5	0.86	0.26	P	2.05	0.62	23.0
6421188		16.434	136.29	R	20.0	0.05	5948	4.3	1.14	0.34	P	24.80	7.44	91.7
6428794	4054.01	169.135	201.82	P	2.5	0.28	5172	4.5	0.81	0.08	SM	2.18	0.33	1.3
6432345	2757.01	234.639	172.62	P	2.8	0.27	5421	4.5	0.89	0.09	SM	2.72	0.38	1.2
6442340	664.01	13.137	143.96	P	1.5	0.08	5717	4.4	1.07	0.11	SM	1.74	0.20	93.5
6449552		20.149	135.82	R	69.7	0.05	5524	4.4	0.92	0.28	P	69.89	20.97	37.7
6468138	1826.01	134.250	182.74	P	2.7	0.17	5807	4.4	1.03	0.10	SM	2.98	0.35	4.2
6468938		7.217	135.45	R	40.1	1.17	6068	4.2	1.30	0.39	P	57.03	17.19	374.4
6471021	372.01	125.630	253.34	P	7.9	0.11	5614	4.4	0.93	0.09	SM	7.99	0.81	3.5
6500206	2451.01	13.375	142.40	P	2.2	0.19	5315	4.5	0.86	0.26	P	2.02	0.63	50.6

Table 5.2 (cont'd): Properties of 836 eKOIs

KIC	KOI	$P$ days	$t_0$ days	Disp.	$p$ %	$\sigma(p)$	$T_{\text{eff}}$ K	$\log g$ cgs	$R_{\star}$ $R_{\odot}$	$\sigma(R_{\star})$	Prov.	$R_P$ $R_{\oplus}$	$\sigma(R_P)$	$F_P$ $F_{\oplus}$
6501635	560.01	23.675	131.92	P	2.8	0.10	5277	4.6	0.74	0.22	P	2.28	0.69	16.4
6504534		28.162	143.73	P	19.5	0.23	4909	4.6	0.70	0.21	P	14.90	4.47	9.8
6508221	416.01	18.208	149.43	P	3.6	0.02	5085	4.6	0.74	0.07	SM	2.91	0.29	21.8
6521045	41.01	12.816	135.78	P	1.3	0.02	5889	4.3	1.20	0.12	SM	1.77	0.18	129.0
6522750		17.446	135.74	R	78.4	1.15	5802	4.5	0.94	0.28	P	80.07	24.05	53.5
6523351	3117.01	6.067	136.13	P	0.8	0.09	5544	4.5	0.90	0.09	SM	0.77	0.12	168.5
6525209	3479.01	75.132	200.78	P	18.7	0.09	5421	4.6	0.79	0.24	P	16.10	4.83	4.4
6541920	157.03	31.995	154.17	P	3.4	0.08	5801	4.4	1.06	0.11	SM	3.87	0.40	28.8
6584273	3287.01	51.110	143.79	P	2.0	0.20	5979	4.5	0.93	0.28	P	1.98	0.63	13.4
6587002	612.02	47.428	169.13	P	2.7	0.12	5124	4.5	0.80	0.08	SM	2.36	0.26	7.0
6594972		10.819	132.98	R	81.9	1.43	5957	4.4	1.01	0.30	P	89.89	27.01	125.9
6607357	2838.01	7.700	134.39	P	0.9	0.10	5731	4.3	1.15	0.12	SM	1.07	0.16	217.5
6613006	1223.01	7.389	133.94	SE	11.7	0.02	5858	4.5	0.89	0.27	P	11.36	3.41	152.8
6634112		9.942	133.86	V	18.8	0.34	5253	4.5	0.82	0.25	P	16.90	5.08	66.9
6634133	2262.01	9.942	133.86	VD	1.7	0.09	5123	4.5	0.77	0.23	P	1.41	0.43	54.2
6665223	1232.01	119.414	232.62	P	17.3	2.12	5317	4.5	0.86	0.09	SM	16.22	2.57	2.7
6665512	2005.01	6.921	135.64	P	2.2	0.12	4559	4.7	0.61	0.18	P	1.45	0.44	38.9
6665695	561.01	5.379	131.96	P	2.0	0.10	5072	4.6	0.76	0.08	SM	1.67	0.19	112.9
6685609	665.01	5.868	135.13	P	2.0	0.09	5923	4.2	1.45	0.15	SM	3.17	0.35	500.2
6692833	1244.01	10.805	134.09	C	1.6	0.16	6075	4.5	0.96	0.29	P	1.71	0.54	119.6
6694186		5.554	135.17	R	34.3	0.02	5458	4.4	0.94	0.28	P	35.13	10.54	212.9
6705137	2609.01	5.597	131.88	C	1.3	0.12	5799	4.5	0.88	0.26	P	1.24	0.39	213.3
6707835	666.01	22.248	151.88	P	2.3	0.08	5615	4.4	0.99	0.10	SM	2.45	0.26	37.0
6751874	2282.01	6.892	132.47	P	1.5	0.16	6054	4.5	0.96	0.29	P	1.57	0.50	213.4
6752002	4184.01	6.080	136.89	P	1.1	0.15	4936	4.6	0.71	0.21	P	0.87	0.28	78.9
6761777	4571.01	47.312	146.33	P	1.7	0.11	6005	4.4	1.00	0.30	P	1.81	0.55	17.6
6762829	1740.01	18.795	138.66	SE	15.2	0.00	5898	4.5	0.95	0.29	P	15.77	4.73	52.6
6786037	564.01	21.057	150.84	P	2.3	0.10	5951	4.5	0.92	0.28	P	2.29	0.69	42.7
6803202	177.01	21.061	143.59	P	1.6	0.07	5711	4.4	1.04	0.10	SM	1.84	0.20	48.3
6838050	512.01	6.510	133.86	P	2.3	0.13	5488	4.4	0.96	0.29	P	2.43	0.74	181.9
6841577		15.537	140.28	R	45.8	0.05	5741	4.5	0.92	0.27	P	45.67	13.70	57.9
6842682	2649.01	7.561	135.64	P	1.4	0.10	5820	4.5	0.88	0.26	P	1.29	0.40	141.3
6846911	2477.01	14.026	135.19	P	2.0	0.18	5911	4.4	1.09	0.33	P	2.36	0.74	102.7
6850504	70.01	10.854	138.62	P	3.5	0.05	5506	4.5	0.90	0.09	SM	3.44	0.35	77.5
6851425	163.01	11.120	139.75	P	2.3	0.04	5079	4.6	0.73	0.07	SM	1.81	0.18	41.1
6864893	2375.01	40.880	163.41	SE	1.8	0.14	5441	4.6	0.78	0.23	P	1.49	0.46	9.7
6871071	2220.02	5.028	134.11	P	1.3	0.08	6023	4.5	0.97	0.29	P	1.32	0.41	329.6
6879865	417.01	19.193	138.60	P	10.1	2.64	5867	4.5	0.89	0.27	P	9.78	3.89	43.1
6922203	2578.01	13.331	133.76	P	2.3	0.22	5992	4.4	1.06	0.32	P	2.66	0.83	107.0
6924203	1370.01	6.883	135.27	P	2.0	0.12	5704	4.6	0.84	0.25	P	1.80	0.55	140.2
6934986	2294.01	131.488	177.49	P	2.7	0.72	5755	4.2	1.39	0.14	SM	4.08	1.16	6.6

Table 5.2 (cont'd): Properties of 836 eKOIs

KIC	KOI	$P$ days	$t_0$ days	Disp.	$p$ %	$\sigma(p)$	$T_{\text{eff}}$ K	$\log g$ cgs	$R_{\star}$ $R_{\odot}$	$\sigma(R_{\star})$	Prov.	$R_P$ $R_{\oplus}$	$\sigma(R_P)$	$F_P$ $F_{\oplus}$
6936977		36.473	159.77	R	41.3	0.41	5468	4.6	0.79	0.24	P	35.43	10.63	11.6
6947164	3531.01	70.584	190.48	R	53.3	2.39	5976	4.5	0.93	0.28	P	53.78	16.31	8.7
6960445	669.01	5.074	136.05	VD	2.4	0.03	5633	4.5	0.91	0.27	P	2.39	0.72	241.1
6960913	1361.01	59.878	151.19	P	3.5	0.22	4338	4.7	0.57	0.06	SM	2.14	0.26	1.6
6964159	3129.01	25.503	139.36	C	1.3	0.12	5806	4.5	0.87	0.26	P	1.27	0.40	27.7
7019524	2877.01	5.309	134.27	P	1.0	0.11	5883	4.5	0.93	0.28	P	1.05	0.33	268.9
7046804	205.01	11.720	142.18	P	9.3	0.10	5210	4.6	0.77	0.23	P	7.77	2.33	44.9
7047207	2494.01	19.119	138.44	P	1.4	0.07	5999	4.5	0.97	0.29	P	1.50	0.46	55.4
7047299		35.882	165.55	R	43.8	2.50	5885	4.5	0.90	0.27	P	42.81	13.07	19.2
7090524	2920.01	6.740	132.29	P	1.1	0.12	5707	4.5	0.90	0.27	P	1.10	0.35	166.3
7091432	3353.01	11.555	134.13	P	1.7	0.19	5140	4.5	0.77	0.23	P	1.42	0.46	45.4
7098355	454.01	29.007	141.57	P	2.8	0.40	5258	4.6	0.77	0.23	P	2.32	0.77	13.8
7101828	455.01	47.878	145.35	VD	2.2	0.10	4257	4.7	0.55	0.17	P	1.34	0.41	2.0
7103919	4310.01	10.777	140.28	P	1.3	0.10	5483	4.4	0.96	0.29	P	1.35	0.42	93.1
7105574		20.726	143.20	R	49.8	0.25	6031	4.5	0.94	0.28	P	51.33	15.40	47.4
7107802	2420.01	10.417	137.46	P	1.4	0.14	5813	4.5	0.88	0.26	P	1.30	0.41	92.0
7115785	672.02	41.749	153.85	P	2.9	0.04	5543	4.5	0.90	0.09	SM	2.87	0.29	12.9
7124026	2275.01	15.744	145.61	P	1.1	0.03	6088	4.5	0.97	0.29	P	1.20	0.36	74.3
7133294	4473.01	13.648	132.23	P	0.8	0.08	5791	4.1	1.45	0.43	P	1.31	0.41	171.9
7211221	1379.01	5.621	136.91	P	1.2	0.09	5634	4.4	0.93	0.09	SM	1.24	0.15	224.7
7219906		35.089	153.42	SE	11.3	0.45	5556	4.6	0.81	0.24	P	9.93	3.00	13.6
7269974	456.01	13.700	144.08	P	3.2	0.05	5889	4.5	0.92	0.28	P	3.16	0.95	73.1
7286173	1862.01	56.435	151.41	P	2.3	0.16	5537	4.4	1.06	0.11	SM	2.68	0.33	11.5
7286911	2180.01	11.555	138.21	P	2.0	0.12	5630	4.6	0.83	0.25	P	1.83	0.56	65.3
7289317	2450.01	16.832	140.52	P	1.8	0.19	5784	4.5	0.93	0.28	P	1.79	0.57	55.2
7289577	1974.01	109.441	198.00	P	3.4	0.78	5403	4.5	0.87	0.09	SM	3.22	0.81	3.2
7336754		12.155	133.76	R	41.3	1.68	5798	4.4	0.99	0.30	P	44.79	13.56	98.3
7353970	3574.01	198.445	155.60	R	30.6	0.41	5421	4.5	0.91	0.09	SM	30.35	3.06	1.5
7357531	1368.01	251.068	230.00	V	11.8	1.69	5710	4.3	1.17	0.12	SM	14.96	2.62	2.1
7368664	614.01	12.875	144.28	P	7.0	0.70	5889	4.5	0.90	0.27	P	6.87	2.17	75.5
7376490	3586.01	5.877	136.42	R	19.1	0.11	5802	4.3	1.12	0.34	P	23.40	7.02	332.1
7382313	2392.01	7.427	133.11	P	1.3	0.09	5810	4.4	0.99	0.30	P	1.42	0.44	189.0
7386827	1704.01	10.419	137.74	P	2.4	0.09	5637	4.4	1.03	0.31	P	2.68	0.81	121.7
7428316	2809.01	7.126	137.46	C	1.3	0.15	6077	4.5	0.96	0.29	P	1.36	0.44	209.6
7445445	567.01	10.688	137.87	P	2.5	0.09	5817	4.5	0.89	0.27	P	2.44	0.74	93.4
7446631	2598.01	29.226	143.98	P	1.2	0.08	6018	4.5	1.00	0.30	P	1.36	0.42	33.6
7447200	676.01	7.973	131.72	P	5.1	0.02	4503	4.7	0.63	0.06	SM	3.54	0.35	31.5
7455981	3096.01	14.454	135.48	P	0.8	0.04	5642	4.5	0.93	0.28	P	0.80	0.24	63.2
7456001	1517.01	40.069	151.80	P	2.9	0.12	6062	4.4	1.03	0.31	P	3.20	0.97	23.9
7504328	458.01	53.719	154.36	P	6.3	1.10	5832	4.3	1.17	0.35	P	8.06	2.79	19.0
7534267	3147.01	39.440	169.21	P	1.5	0.11	5764	4.6	0.86	0.26	P	1.45	0.45	14.7

Table 5.2 (cont'd): Properties of 836 eKOIs

KIC	KOI	$P$ days	$t_0$ days	Disp.	$p$ %	$\sigma(p)$	$T_{\text{eff}}$ K	$\log g$ cgs	$R_*$ $R_{\odot}$	$\sigma(R_*)$	Prov.	$R_P$ $R_{\oplus}$	$\sigma(R_P)$	$F_P$ $F_{\oplus}$
7602070	514.01	11.756	140.81	SE	2.2	0.05	5656	4.6	0.83	0.25	P	1.96	0.59	65.3
7624297		18.020	148.66	R	57.7	0.55	5366	4.6	0.76	0.23	P	47.77	14.34	26.3
7626506	150.01	8.409	134.00	P	2.8	0.06	5535	4.4	0.97	0.10	SM	2.94	0.30	136.3
7630229	683.01	278.128	177.53	P	5.0	0.43	5834	4.4	1.04	0.10	SM	5.68	0.75	1.6
7668663	1898.01	6.498	136.01	P	1.3	0.07	5726	4.3	1.15	0.11	SM	1.63	0.19	272.5
7700622	315.01	35.582	153.48	P	2.7	0.08	4780	4.6	0.69	0.07	SM	2.02	0.21	6.2
7742408		33.498	163.76	P	1.1	0.05	4802	4.6	0.67	0.20	P	0.84	0.25	6.7
7743464		55.249	164.98	R	61.7	2.72	6013	4.5	0.94	0.28	P	63.42	19.23	12.7
7747425	1952.01	8.010	135.33	P	1.5	0.07	5998	4.4	1.01	0.30	P	1.71	0.52	192.8
7750419	1708.01	32.774	151.45	P	2.3	0.22	5890	4.5	0.90	0.27	P	2.22	0.70	21.8
7768451	1527.01	192.669	162.88	P	3.2	0.30	5405	4.5	0.88	0.09	SM	3.06	0.42	1.5
7779077	1842.01	16.842	137.99	P	2.6	0.07	5526	4.4	0.95	0.29	P	2.65	0.80	51.6
7802136	1449.01	10.980	137.15	R	22.1	0.12	6010	4.5	0.98	0.30	P	23.72	7.12	120.3
7812179	515.01	17.794	134.03	SE	3.4	0.24	5467	4.6	0.79	0.24	P	2.94	0.91	30.2
7813039	3787.01	141.734	167.39	V	4.0	0.74	5611	4.5	0.94	0.09	SM	4.07	0.86	2.9
7826659	2686.01	211.032	279.14	P	4.1	0.21	4662	4.6	0.67	0.07	SM	3.03	0.34	0.5
7830637	1454.01	121.599	211.47	R	21.1	0.18	6076	4.5	0.96	0.29	P	22.21	6.66	4.8
7833305	4528.01	8.312	139.66	P	0.8	0.09	5437	4.0	1.53	0.46	P	1.31	0.42	304.5
7840044	516.01	13.542	144.02	VD	1.5	0.24	5891	4.4	1.01	0.30	P	1.61	0.55	92.6
7841925	1499.01	14.164	140.58	P	2.6	0.12	5437	4.4	0.92	0.28	P	2.63	0.80	58.4
7866914	3971.01	366.020	182.66	SE	4.0	1.15	6082	4.5	0.99	0.30	P	4.38	1.81	1.2
7870032	1818.01	16.877	138.64	P	2.8	0.16	5497	4.5	0.88	0.09	SM	2.64	0.30	40.8
7877978	2760.01	56.573	146.59	P	2.5	0.35	4588	4.7	0.62	0.19	P	1.71	0.56	2.5
7906671	3018.01	45.117	157.01	VD	1.7	0.12	5559	4.4	1.00	0.30	P	1.87	0.58	15.7
7906739	2165.01	7.014	136.93	VD	0.9	0.04	5951	4.5	0.93	0.28	P	0.93	0.28	189.1
7906882	686.01	52.514	171.68	P	11.7	0.14	5589	4.4	1.01	0.10	SM	12.90	1.30	12.5
7918652	2984.01	11.455	136.33	P	0.8	0.08	6116	4.4	1.15	0.11	SM	0.99	0.14	154.6
7938499		7.227	143.40	P	1.2	0.04	4387	4.7	0.58	0.17	P	0.73	0.22	29.1
7941200	92.01	65.705	137.44	P	2.5	0.14	5800	4.3	1.23	0.12	SM	3.28	0.38	14.5
7949593	4759.01	17.768	146.61	P	1.1	0.09	6027	4.4	1.08	0.32	P	1.31	0.41	76.9
7971389		13.175	136.46	R	39.2	0.89	6077	4.4	1.03	0.31	P	43.98	13.23	106.7
7975727	418.01	22.418	150.39	SE	10.2	0.13	5352	4.5	0.88	0.26	P	9.76	2.93	27.1
7977197	459.01	19.446	150.66	P	3.3	0.32	5833	4.4	0.98	0.29	P	3.51	1.11	51.3
7987749		17.031	145.55	R	41.0	0.45	5574	4.1	1.37	0.41	P	61.03	18.32	104.0
7989422	2151.01	7.478	133.41	VD	0.9	0.05	6012	4.2	1.35	0.41	P	1.33	0.41	374.8
8008067		15.771	137.60	P	2.1	0.07	5594	4.4	1.10	0.11	SM	2.52	0.27	69.1
8008206	569.01	20.729	143.98	P	2.5	0.24	5174	4.5	0.78	0.23	P	2.10	0.66	21.2
8009496	1869.01	38.477	150.58	VD	2.1	0.06	6097	4.5	0.97	0.29	P	2.17	0.66	22.6
8009500		38.476	150.58	R	38.5	0.09	5329	4.5	0.85	0.25	P	35.61	10.68	12.2
8017703	518.01	13.982	140.03	P	2.9	0.04	4917	4.6	0.69	0.07	SM	2.20	0.22	24.3
8022244	519.01	11.903	142.63	P	2.5	0.13	6027	4.5	0.95	0.28	P	2.58	0.78	99.5

Table 5.2 (cont'd): Properties of 836 eKOIs

KIC	KOI	$P$ days	$t_0$ days	Disp.	$p$ %	$\sigma(p)$	$T_{\text{eff}}$ K	$\log g$ cgs	$R_*$ $R_{\odot}$	$\sigma(R_*)$	Prov.	$R_P$ $R_{\oplus}$	$\sigma(R_P)$	$F_P$ $F_{\oplus}$
8022489	2674.01	197.511	272.38	P	5.3	0.09	5756	4.2	1.52	0.15	SM	8.81	0.89	4.4
8023317		16.579	146.73	R	20.2	0.29	5862	4.1	1.59	0.48	P	34.85	10.47	161.4
8041216	237.01	8.508	134.78	P	2.3	0.08	5767	4.4	1.08	0.11	SM	2.74	0.29	167.7
8043638	460.01	17.588	140.89	P	3.4	0.06	5520	4.4	0.98	0.30	P	3.66	1.10	52.1
8044608	3523.01	106.176	234.62	R	55.2	2.76	6095	4.3	1.27	0.38	P	76.57	23.29	10.0
8074805	2670.01	170.866	186.05	P	3.7	0.35	5987	4.2	1.41	0.14	SM	5.69	0.78	5.6
8087812	4343.01	27.211	132.37	P	1.0	0.09	6014	4.2	1.40	0.42	P	1.49	0.47	71.0
8095441	2743.01	11.874	140.24	P	1.4	0.14	5530	4.5	0.88	0.09	SM	1.35	0.19	68.0
8099138	2338.01	66.184	141.63	P	2.1	0.24	5899	4.5	0.90	0.27	P	2.11	0.68	8.7
8107225	235.01	5.633	133.82	P	2.3	0.08	5127	4.6	0.70	0.21	P	1.80	0.54	93.8
8107380	162.01	14.006	142.22	P	2.4	0.03	5795	4.3	1.17	0.12	SM	3.10	0.31	103.3
8121328	3486.01	19.072	145.63	P	1.2	0.08	5430	4.0	1.53	0.46	P	1.99	0.61	100.8
8127586	1752.01	16.610	147.57	C	1.8	0.08	6043	4.4	1.05	0.32	P	2.04	0.62	80.5
8127607	1919.01	16.609	147.61	VD	2.2	0.23	5225	4.6	0.75	0.22	P	1.79	0.57	26.7
8142787	4005.01	178.146	210.10	P	2.6	0.24	5431	4.5	0.88	0.09	SM	2.47	0.34	1.7
8142942	1985.01	5.756	133.90	P	2.8	0.24	4931	4.6	0.72	0.07	SM	2.20	0.29	83.7
8160953	1858.01	116.331	173.71	P	3.9	0.15	5354	4.5	0.83	0.08	SM	3.52	0.38	2.6
8168187	2209.01	18.302	142.89	P	1.4	0.14	5744	4.5	0.86	0.26	P	1.35	0.42	40.5
8183288	3255.01	66.650	171.19	P	2.1	0.13	4550	4.7	0.64	0.06	SM	1.43	0.17	2.0
8193178	572.01	10.640	137.21	P	2.1	0.09	6166	4.4	1.14	0.11	SM	2.61	0.28	174.4
8197343	1746.01	11.791	134.56	P	1.9	0.14	5965	4.5	0.93	0.28	P	1.89	0.59	93.6
8210721		22.673	138.15	R	23.9	0.23	5584	4.3	1.05	0.32	P	27.39	8.22	43.5
8218379	1920.01	16.571	133.90	P	2.4	0.07	5488	4.6	0.79	0.24	P	2.03	0.61	34.0
8219673	419.01	20.132	149.13	P	14.5	0.35	5986	4.5	0.93	0.28	P	14.80	4.45	47.2
8223328	1767.01	35.516	165.94	P	11.4	0.17	5719	4.2	1.34	0.40	P	16.70	5.02	40.7
8226050	1910.01	34.270	147.02	P	2.4	0.09	5299	4.5	0.84	0.25	P	2.21	0.67	13.7
8233802	3302.01	69.379	154.19	VD	2.3	0.26	5803	4.5	0.88	0.27	P	2.19	0.70	7.5
8242434	1726.01	44.963	144.57	P	2.6	0.07	4684	4.6	0.68	0.07	SM	1.90	0.20	4.1
8247770	2569.01	8.282	136.25	P	1.0	0.12	5650	4.4	1.03	0.31	P	1.15	0.37	167.1
8260234	2085.01	5.715	132.12	P	1.5	0.07	5237	4.5	0.81	0.24	P	1.32	0.40	136.2
8260902	2144.01	38.671	157.63	P	2.2	0.08	5420	4.0	1.54	0.46	P	3.72	1.12	39.5
8265218	522.01	12.830	144.28	P	3.3	0.22	5897	4.5	0.90	0.27	P	3.27	1.00	76.4
8280511		10.435	134.82	P	1.6	0.11	5489	4.5	0.88	0.09	SM	1.58	0.19	82.3
8301878	3301.01	20.711	140.89	P	1.2	0.12	5613	4.5	0.91	0.27	P	1.16	0.37	36.8
8313667	1145.01	30.587	132.29	P	1.9	0.05	5943	4.4	1.10	0.11	SM	2.32	0.24	36.4
8321314	2293.01	15.034	144.98	P	1.7	0.14	5451	4.4	0.93	0.28	P	1.76	0.55	55.0
8323753	175.01	6.714	134.31	VD	1.9	0.06	6075	4.3	1.27	0.38	P	2.63	0.79	395.8
8326342	2680.01	14.408	142.03	P	5.1	1.17	5474	4.6	0.79	0.24	P	4.39	1.66	40.4
8332986	1137.01	302.374	309.16	V	15.8	3.62	5330	4.5	0.83	0.08	SM	14.26	3.57	0.8
8344004	573.01	5.996	136.54	P	2.4	0.07	6010	4.3	1.12	0.34	P	2.99	0.90	354.1
8349399	4763.01	56.449	170.58	P	1.0	0.13	5980	4.4	1.10	0.33	P	1.25	0.41	17.0

Table 5.2 (cont'd): Properties of 836 eKOIs

KIC	KOI	$P$ days	$t_0$ days	Disp.	$p$ %	$\sigma(p)$	$T_{\text{eff}}$ K	$\log g$ cgs	$R_{\star}$ $R_{\odot}$	$\sigma(R_{\star})$	Prov.	$R_P$ $R_{\oplus}$	$\sigma(R_P)$	$F_P$ $F_{\oplus}$
8349582	122.01	11.523	131.98	P	2.3	0.06	5695	4.3	1.26	0.13	SM	3.21	0.33	140.9
8352537	420.01	6.010	132.02	P	5.3	0.18	4860	4.6	0.69	0.21	P	3.99	1.21	71.9
8355239	574.01	20.135	151.23	P	3.0	0.13	5217	4.6	0.72	0.22	P	2.33	0.71	19.0
8358008		10.065	135.25	SE	16.2	0.06	5260	4.5	0.83	0.25	P	14.65	4.40	66.9
8358012	2929.01	10.065	135.25	P	1.7	0.20	5387	4.6	0.76	0.23	P	1.40	0.45	58.5
8364115		7.736	137.99	SE	2.0	0.02	5953	4.5	0.93	0.28	P	2.06	0.62	164.4
8364119		7.736	137.99	R	75.2	3.52	5661	4.6	0.83	0.25	P	68.40	20.77	114.6
8374580	615.01	176.240	192.51	V	10.3	1.26	5565	4.2	1.39	0.14	SM	15.52	2.46	4.1
8378922		43.263	150.39	R	79.1	2.22	5676	4.4	1.03	0.31	P	89.15	26.86	18.6
8409295	3404.01	82.299	211.96	P	1.8	0.32	6049	4.5	0.95	0.29	P	1.92	0.66	7.7
8429668	4449.01	5.008	134.68	C	0.8	0.08	5306	4.6	0.75	0.22	P	0.62	0.20	136.8
8453211	236.01	5.777	131.53	VD	2.8	1.41	5578	4.3	1.05	0.31	P	3.21	1.88	268.6
8460600	1730.01	6.352	134.21	SE	23.6	0.11	5163	4.5	0.77	0.23	P	19.88	5.96	101.0
8474898	576.01	199.441	240.87	V	8.8	1.18	5650	4.3	1.26	0.13	SM	12.11	2.02	3.1
8481129	2402.01	16.302	133.78	P	1.5	0.10	4763	4.6	0.66	0.20	P	1.08	0.33	16.5
8491277	234.01	9.614	132.19	P	2.6	0.09	5940	4.4	1.09	0.33	P	3.10	0.94	172.3
8509781		70.334	198.96	R	21.1	2.17	6074	4.2	1.37	0.41	P	31.58	10.01	19.9
8543278		7.549	135.03	SE	23.9	1.88	5159	4.6	0.71	0.21	P	18.48	5.73	65.4
8547429	2658.01	11.660	140.65	P	1.2	0.09	6009	4.5	0.94	0.28	P	1.19	0.37	99.7
8552719	1792.01	88.407	176.28	P	3.8	0.08	5288	4.6	0.77	0.23	P	3.16	0.95	3.2
8559863		22.470	143.28	R	32.5	0.13	5375	4.6	0.76	0.23	P	27.01	8.10	19.8
8560940	3450.01	31.971	133.88	P	1.0	0.08	5852	4.5	0.89	0.27	P	0.97	0.30	21.4
8564587	1270.01	5.729	132.82	P	2.7	0.13	5289	4.6	0.74	0.22	P	2.14	0.65	110.4
8564674	2022.01	5.930	135.50	P	1.8	0.04	5936	4.5	0.91	0.27	P	1.83	0.55	224.8
8565266	578.01	6.412	137.80	P	3.1	0.05	5990	4.4	1.10	0.33	P	3.75	1.13	309.1
8572936		27.796	146.73	R	84.1	0.89	6003	4.4	1.01	0.30	P	92.45	27.75	36.6
8573193	4337.01	8.185	134.56	P	1.0	0.11	5981	4.5	0.93	0.28	P	1.02	0.33	154.3
8580438		6.496	135.48	R	29.8	0.02	5504	4.4	0.96	0.29	P	31.31	9.39	187.0
8583696	1275.01	50.285	167.66	P	3.4	0.16	5907	4.3	1.20	0.12	SM	4.49	0.50	21.0
8591693	2123.01	29.455	154.19	P	2.2	0.18	6030	4.5	0.95	0.28	P	2.24	0.70	29.9
8611257	2931.01	99.250	148.55	P	2.1	0.32	4995	4.6	0.72	0.07	SM	1.65	0.30	2.0
8611781	2185.01	76.964	192.28	P	1.9	0.21	5887	4.4	1.08	0.32	P	2.23	0.71	10.4
8611832	2414.01	22.597	140.44	P	1.3	0.08	5587	4.4	0.98	0.10	SM	1.37	0.16	39.0
8618226		5.882	131.76	R	66.4	3.00	6044	4.3	1.12	0.34	P	81.07	24.59	366.2
8621348	461.01	11.344	138.83	VD	2.1	0.07	5643	4.6	0.83	0.25	P	1.91	0.58	67.4
8625732	4701.01	31.971	133.92	P	0.9	0.07	5597	4.6	0.82	0.25	P	0.84	0.26	16.1
8625925	580.01	6.521	136.58	P	2.6	0.19	5795	4.5	0.87	0.26	P	2.47	0.76	167.7
8628758	1279.01	14.374	138.21	P	1.7	0.04	5771	4.4	1.06	0.11	SM	1.94	0.20	85.4
8644288	137.02	14.859	143.02	P	5.2	0.07	5424	4.5	0.91	0.09	SM	5.17	0.52	47.3
8644365	3384.02	19.916	139.36	P	1.1	0.07	6049	4.4	1.12	0.11	SM	1.34	0.16	67.7
8644545		295.963	138.91	P	1.9	0.28	5507	4.4	0.95	0.10	SM	2.03	0.36	1.1

Table 5.2 (cont'd): Properties of 836 eKOIs

KIC	KOI	$P$ days	$t_0$ days	Disp.	$p$ %	$\sigma(p)$	$T_{\text{eff}}$ K	$\log g$ cgs	$R_*$ $R_\odot$	$\sigma(R_*)$	Prov.	$R_P$ $R_\oplus$	$\sigma(R_P)$	$F_P$ $F_\oplus$
8652999	1953.01	15.161	136.54	VD	1.7	0.20	5892	4.3	1.17	0.35	P	2.22	0.71	105.9
8681734	2340.01	7.685	137.64	P	1.6	0.10	5621	4.4	0.97	0.29	P	1.73	0.53	161.2
8686097	374.01	172.699	236.95	P	2.6	0.17	5706	4.3	1.04	0.10	SM	2.96	0.36	3.1
8692861	172.01	13.722	137.85	P	2.2	0.06	5603	4.4	0.98	0.10	SM	2.38	0.25	75.0
8733497	3527.01	76.818	188.13	R	56.7	7.31	5692	4.6	0.84	0.25	P	52.08	17.00	5.6
8742590	1281.01	49.478	141.83	P	2.2	0.15	5773	4.5	0.86	0.26	P	2.03	0.63	11.0
8746295	2475.01	6.856	136.03	P	1.4	0.27	5691	4.5	0.85	0.26	P	1.35	0.47	144.3
8751933	1257.01	86.648	173.79	P	7.8	0.22	5472	4.4	0.99	0.10	SM	8.40	0.87	5.5
8802165	694.01	17.421	131.98	P	2.8	0.02	5702	4.4	1.05	0.11	SM	3.16	0.32	59.5
8804283	1276.01	22.790	138.68	P	2.4	0.19	5594	4.6	0.82	0.24	P	2.14	0.66	25.1
8804455	2159.01	7.597	131.96	P	1.0	0.04	5714	4.4	1.07	0.11	SM	1.14	0.13	191.9
8804845	2039.01	5.426	135.86	P	1.6	0.17	5597	4.6	0.82	0.25	P	1.38	0.44	171.1
8806072	1273.01	40.058	169.93	P	3.3	0.11	5633	4.6	0.83	0.25	P	2.95	0.89	12.4
8822216	581.01	6.997	133.94	P	3.3	0.07	5653	4.6	0.83	0.25	P	2.97	0.89	129.6
8826168	1850.01	11.551	134.90	P	1.9	0.09	5905	4.4	1.08	0.11	SM	2.24	0.25	124.8
8827575	3052.02	15.611	144.85	P	1.0	0.05	5386	4.5	0.82	0.08	SM	0.89	0.10	38.5
8832512	1821.01	9.977	131.76	P	2.9	0.13	5487	4.4	0.94	0.28	P	2.95	0.90	100.1
8848271	1256.01	9.992	137.44	SE	10.1	0.08	5855	4.3	1.11	0.33	P	12.21	3.67	164.8
8869680	696.01	7.034	131.96	C	1.2	0.06	5964	4.4	1.09	0.33	P	1.49	0.45	266.4
8879427		16.313	136.87	R	27.3	0.19	5995	4.5	0.99	0.30	P	29.48	8.85	71.6
8890783	464.01	58.363	138.19	P	6.7	0.13	5490	4.5	0.90	0.27	P	6.56	1.97	8.5
8939211		27.078	137.15	SE	1.3	0.02	5984	4.5	0.99	0.30	P	1.36	0.41	35.9
8949247	1387.01	23.800	152.56	R	24.7	0.17	5918	4.5	0.96	0.29	P	26.04	7.81	39.7
8950568	2038.01	8.306	139.73	P	1.8	0.06	5438	4.5	0.89	0.09	SM	1.78	0.19	105.1
8962094	700.01	30.864	142.08	P	2.2	0.11	5785	4.3	1.05	0.11	SM	2.53	0.28	32.3
8972058	159.01	8.991	136.74	P	2.1	0.15	5964	4.4	1.09	0.11	SM	2.46	0.30	187.7
8973000		28.028	148.78	R	40.7	0.09	5407	4.6	0.80	0.24	P	35.68	10.70	17.0
8984706		10.135	137.50	R	71.6	0.76	5914	4.1	1.50	0.45	P	117.22	35.19	289.6
9002278	701.01	18.164	144.47	P	2.8	0.06	4968	4.6	0.70	0.07	SM	2.14	0.22	18.5
9006186	2169.01	5.453	134.15	P	0.9	0.06	5395	4.5	0.87	0.09	SM	0.85	0.10	163.2
9006449	1413.01	12.646	138.60	P	1.3	0.03	5630	4.4	0.94	0.28	P	1.33	0.40	76.4
9020160	582.01	5.945	134.80	P	2.7	0.13	5236	4.6	0.73	0.22	P	2.16	0.66	99.2
9025971	3680.01	141.243	256.20	P	10.3	0.10	5710	4.4	1.07	0.11	SM	12.10	1.22	3.8
9031703	4520.01	9.334	137.62	P	0.9	0.05	5490	4.1	1.47	0.44	P	1.38	0.42	253.2
9042357	1993.01	16.004	146.39	P	2.3	0.22	5367	4.6	0.78	0.23	P	1.98	0.62	32.7
9086154	4060.01	225.257	225.00	P	1.9	0.19	5795	4.3	1.27	0.13	SM	2.69	0.37	3.0
9101496	1915.01	6.562	132.61	P	1.5	0.08	5873	4.1	1.74	0.17	SM	2.87	0.33	580.6
9116075		24.498	154.70	P	1.3	0.21	4570	4.7	0.60	0.18	P	0.82	0.28	6.9
9119458	525.01	11.531	139.11	P	2.8	0.15	5738	4.3	1.14	0.34	P	3.50	1.07	134.1
9119568	3087.01	5.548	133.96	C	0.8	0.05	5257	4.5	0.87	0.09	SM	0.75	0.09	148.0
9139084	323.01	5.836	134.86	P	2.1	0.05	5403	4.5	0.85	0.08	SM	1.95	0.20	149.1

Table 5.2 (cont'd): Properties of 836 eKOIs

KIC	KOI	$P$ days	$t_0$ days	Disp.	$p$ %	$\sigma(p)$	$T_{\text{eff}}$ K	$\log g$ cgs	$R_{\star}$ $R_{\odot}$	$\sigma(R_{\star})$	Prov.	$R_P$ $R_{\oplus}$	$\sigma(R_P)$	$F_P$ $F_{\oplus}$
9146018	584.01	9.927	135.97	P	2.8	0.10	5464	4.5	0.93	0.09	SM	2.88	0.30	86.2
9150827	1408.01	14.534	145.43	P	2.1	0.10	4252	4.7	0.48	0.05	SM	1.08	0.12	8.4
9164836	213.01	48.119	170.85	R	38.9	0.87	6031	4.5	0.95	0.28	P	40.21	12.10	15.5
9177629	2522.01	5.604	133.84	P	1.2	0.12	4849	4.6	0.75	0.08	SM	0.99	0.14	86.6
9226339	3477.01	21.461	132.25	P	1.0	0.06	5995	4.3	1.24	0.37	P	1.36	0.41	77.4
9266285		5.614	132.57	R	36.8	0.04	4452	4.7	0.59	0.18	P	23.67	7.10	44.4
9266431	704.01	18.396	148.35	P	2.8	0.15	5313	4.6	0.80	0.08	SM	2.43	0.27	27.2
9283156	2657.01	5.224	132.84	P	0.6	0.04	5422	4.5	0.84	0.08	SM	0.58	0.07	178.3
9284741		20.729	141.24	R	79.2	1.63	5265	4.5	0.83	0.25	P	71.55	21.52	25.6
9334893	2298.01	16.667	141.77	P	1.2	0.07	4922	4.6	0.70	0.21	P	0.90	0.28	20.1
9353182		10.476	136.54	R	31.6	0.01	6100	4.3	1.24	0.37	P	42.72	12.82	210.7
9353314	1900.01	5.185	131.88	P	2.0	0.16	4451	4.7	0.59	0.18	P	1.29	0.40	49.4
9364290	2374.01	5.262	136.35	P	1.3	0.09	5622	4.4	1.00	0.30	P	1.44	0.44	279.8
9364609	2137.01	14.974	141.50	P	1.6	0.11	5332	4.5	0.83	0.08	SM	1.43	0.17	40.1
9394762		77.136	166.60	P	2.2	0.30	5688	4.6	0.84	0.25	P	2.01	0.66	5.5
9412445	3970.01	10.186	132.55	C	1.5	0.03	4168	4.7	0.54	0.16	P	0.86	0.26	13.7
9412462		10.187	132.53	R	77.7	0.77	5540	4.5	0.91	0.27	P	77.02	23.12	91.9
9412760	1977.01	9.387	137.40	P	2.0	0.18	4346	4.7	0.60	0.06	SM	1.34	0.18	19.3
9425139		305.071	294.06	P	5.9	0.33	5642	4.4	1.12	0.11	SM	7.22	0.83	1.4
9447166	3296.01	62.868	166.04	P	1.9	0.26	4838	4.6	0.68	0.20	P	1.41	0.46	3.0
9455325	1813.01	9.768	139.46	P	2.2	0.06	5369	4.5	0.85	0.09	SM	2.03	0.21	74.5
9458343	2246.01	11.895	132.90	P	1.3	0.12	5650	4.4	0.97	0.10	SM	1.39	0.19	90.9
9471974	119.01	49.184	141.91	P	3.8	0.06	5642	4.2	1.44	0.14	SM	5.93	0.60	25.0
9472000	2082.01	31.589	155.62	P	1.7	0.10	5875	4.2	1.50	0.15	SM	2.79	0.32	54.7
9489953	3238.01	58.345	169.84	P	3.4	1.36	5861	4.2	1.33	0.40	P	4.93	2.48	22.2
9491832	4226.01	49.565	170.68	P	1.0	0.05	5641	4.1	1.53	0.46	P	1.73	0.53	31.5
9509343	4346.01	6.392	135.64	P	1.3	0.12	5390	4.4	0.89	0.27	P	1.27	0.40	153.6
9514372	4242.01	145.787	215.04	P	2.1	0.29	5574	4.4	0.93	0.09	SM	2.08	0.36	2.8
9520838	1866.01	105.304	207.18	P	3.4	0.26	5530	4.5	0.87	0.09	SM	3.26	0.41	3.6
9527915	165.01	13.222	139.56	P	2.7	0.06	5214	4.6	0.78	0.08	SM	2.28	0.23	39.2
9549471		15.714	132.08	SE	8.9	0.79	5818	4.4	0.97	0.29	P	9.41	2.95	67.2
9549472		15.714	132.10	R	28.9	0.40	5842	4.4	1.01	0.30	P	31.93	9.59	73.8
9570741	586.01	15.780	144.41	P	2.3	0.12	5934	4.5	0.91	0.27	P	2.24	0.68	60.8
9571186	3313.01	34.953	163.53	P	2.2	0.17	4805	4.6	0.67	0.20	P	1.63	0.50	6.4
9573539	180.01	10.046	139.13	P	2.4	0.16	5561	4.5	0.94	0.09	SM	2.49	0.29	95.9
9576197		7.964	136.19	R	23.8	0.02	5311	4.5	0.79	0.24	P	20.57	6.17	85.1
9578686	709.01	21.385	136.01	P	2.4	0.10	5343	4.5	0.86	0.09	SM	2.26	0.25	27.3
9583881	467.01	18.009	146.43	P	5.2	0.14	5803	4.5	0.88	0.26	P	4.96	1.49	44.7
9589524	468.01	22.185	152.39	P	4.4	0.11	5132	4.5	0.77	0.23	P	3.72	1.12	18.8
9597058	1819.01	12.057	135.43	P	2.1	0.06	5368	4.5	0.84	0.08	SM	1.91	0.20	54.5
9597345	711.01	44.700	174.81	P	2.6	0.04	5556	4.4	1.08	0.11	SM	3.06	0.31	16.1

Table 5.2 (cont'd): Properties of 836 eKOIs

KIC	KOI	$P$ days	$t_0$ days	Disp.	$p$ %	$\sigma(p)$	$T_{\text{eff}}$ K	$\log g$ cgs	$R_{\star}$ $R_{\odot}$	$\sigma(R_{\star})$	Prov.	$R_P$ $R_{\oplus}$	$\sigma(R_P)$	$F_P$ $F_{\oplus}$
9607164	587.01	14.035	143.53	P	2.6	0.10	5290	4.5	0.84	0.25	P	2.42	0.73	45.3
9631762	588.01	10.356	134.25	P	2.5	0.16	4678	4.6	0.64	0.19	P	1.72	0.53	26.9
9631995	22.01	7.892	137.79	P	9.1	0.01	5789	4.3	1.26	0.13	SM	12.60	1.26	255.2
9632895	1451.01	27.322	132.43	R	25.3	0.01	5662	4.6	0.83	0.25	P	22.97	6.89	21.3
9635606	2535.01	48.889	153.83	P	2.0	0.11	4930	4.6	0.71	0.21	P	1.54	0.47	4.9
9636569	527.01	10.636	139.79	VD	1.5	0.09	5897	4.5	0.90	0.27	P	1.46	0.45	98.7
9651234	1938.01	96.914	187.11	P	2.8	0.22	5170	4.6	0.77	0.08	SM	2.34	0.30	2.6
9661979	2132.01	69.895	160.67	P	2.2	0.23	5584	4.5	0.84	0.25	P	2.05	0.65	6.0
9662811	1854.01	43.034	137.70	P	2.1	0.09	5548	4.5	0.91	0.09	SM	2.14	0.23	13.1
9663113	179.01	20.740	142.79	P	2.9	0.03	6230	4.3	1.38	0.14	SM	4.38	0.44	100.6
9673173		21.294	147.10	R	50.4	0.32	6024	4.2	1.27	0.38	P	69.92	20.98	83.0
9704384	1913.01	5.509	132.31	P	1.3	0.07	5448	4.5	0.92	0.09	SM	1.34	0.15	185.0
9714358		6.474	134.39	R	44.9	0.37	5057	4.6	0.75	0.22	P	36.56	10.97	86.7
9718066	2287.01	16.092	142.52	P	1.0	0.09	4470	4.7	0.62	0.06	SM	0.69	0.09	11.6
9729691	1751.01	8.689	133.66	P	3.2	0.14	5165	4.5	0.79	0.24	P	2.73	0.83	69.3
9735426	1849.01	8.088	138.74	P	2.8	0.06	5170	4.6	0.71	0.21	P	2.16	0.65	60.4
9758089	1871.01	92.728	177.47	C	3.0	0.15	4569	4.7	0.66	0.07	SM	2.15	0.24	1.3
9762519		7.515	138.09	R	43.4	4.33	5709	4.5	0.89	0.27	P	42.11	13.31	141.2
9765975	1520.01	18.458	138.17	P	2.1	0.06	5372	4.5	0.83	0.25	P	1.92	0.58	31.6
9783760	3487.01	89.738	205.28	R	29.3	5.05	5859	4.5	0.89	0.27	P	28.43	9.83	5.5
9815053	2923.01	5.839	136.89	P	1.5	0.08	5262	4.6	0.76	0.23	P	1.22	0.37	112.7
9818462	1521.01	25.943	156.18	P	2.2	0.07	5136	4.5	0.77	0.23	P	1.89	0.57	15.4
9821078		8.429	132.29	R	65.1	0.11	4246	4.7	0.55	0.17	P	39.20	11.76	19.5
9838468	2943.01	54.411	175.40	P	1.3	0.11	5750	4.3	1.23	0.12	SM	1.73	0.23	17.4
9846086	617.01	37.864	160.75	P	13.2	0.48	5781	4.5	0.88	0.26	P	12.70	3.84	16.5
9849884	4516.01	5.357	131.63	P	0.8	0.09	6093	4.5	0.99	0.30	P	0.84	0.27	326.5
9850893	1523.01	8.481	135.82	VD	1.6	0.05	5263	4.5	0.83	0.25	P	1.44	0.44	84.0
9851271	2003.01	8.480	135.86	P	1.8	0.04	5881	4.4	1.07	0.32	P	2.10	0.63	193.4
9851662	2483.01	15.054	135.54	P	1.4	0.15	5520	4.4	0.96	0.29	P	1.42	0.45	60.6
9873254	717.01	14.707	131.68	P	1.5	0.06	5641	4.4	1.08	0.11	SM	1.77	0.19	75.0
9886661	1606.01	5.083	133.23	P	1.5	0.05	5403	4.5	0.89	0.09	SM	1.50	0.16	194.3
9895006	1717.01	10.561	133.76	P	1.5	0.19	5440	4.4	0.93	0.28	P	1.56	0.50	87.6
9910828		8.480	135.88	P	1.4	0.09	5504	4.5	0.82	0.25	P	1.28	0.39	92.5
9941387		27.660	141.26	R	76.3	2.62	5298	4.6	0.75	0.22	P	62.16	18.77	13.9
9941859	528.01	9.577	138.38	P	2.7	0.26	5675	4.3	1.05	0.32	P	3.12	0.98	143.5
9957627	592.01	39.753	135.72	P	2.1	0.08	6090	4.4	1.06	0.32	P	2.43	0.74	26.3
9958962	593.01	9.998	131.80	P	2.3	0.10	5964	4.5	0.92	0.28	P	2.32	0.70	116.1
9962455	2748.01	23.198	142.65	P	1.5	0.11	5426	4.0	1.88	0.19	SM	3.04	0.38	98.7
9962595		11.375	142.44	P	15.3	0.21	5264	4.5	0.79	0.24	P	13.12	3.94	50.8
9963009		40.070	153.01	R	21.4	0.02	5795	4.3	1.11	0.33	P	25.89	7.77	24.9
9963524	720.01	5.691	134.21	P	3.3	0.04	5246	4.6	0.80	0.08	SM	2.90	0.29	125.0

Table 5.2 (cont'd): Properties of 836 eKOIs

KIC	KOI	$P$ days	$t_0$ days	Disp.	$p$ %	$\sigma(p)$	$T_{\text{eff}}$ K	$\log g$ cgs	$R_{\star}$ $R_{\odot}$	$\sigma(R_{\star})$	Prov.	$R_P$ $R_{\oplus}$	$\sigma(R_P)$	$F_P$ $F_{\oplus}$
9964801	721.01	13.724	139.48	P	1.8	0.19	5819	4.3	1.22	0.12	SM	2.33	0.34	115.9
9967884	425.01	5.428	131.76	P	13.6	0.83	5866	4.5	0.90	0.27	P	13.31	4.08	237.7
9973109	2018.01	27.496	133.27	P	2.2	0.16	5707	4.4	1.03	0.31	P	2.50	0.77	34.6
9991621	3382.01	18.925	145.55	VD	1.1	0.05	5456	4.4	0.93	0.28	P	1.14	0.35	41.0
9993683		29.940	145.08	P	1.5	0.12	5241	4.5	0.82	0.25	P	1.34	0.41	15.1
10004738	1598.01	56.477	143.81	P	3.2	0.34	5816	4.5	0.90	0.27	P	3.13	1.00	10.2
10006581	1595.01	40.110	142.08	P	2.6	0.16	5965	4.5	0.93	0.28	P	2.58	0.79	18.4
10016874	426.01	16.302	139.54	P	2.7	0.10	6059	4.3	1.14	0.34	P	3.36	1.02	97.9
10019643	471.01	21.347	150.39	P	2.4	0.15	5732	4.6	0.85	0.26	P	2.27	0.69	32.1
10022908	1586.01	6.991	135.48	P	2.2	0.13	4735	4.7	0.63	0.19	P	1.50	0.46	44.0
10024701	2002.01	14.375	139.05	P	1.5	0.10	5935	4.4	1.06	0.11	SM	1.72	0.21	91.8
10028792	1574.01	114.737	165.14	P	6.6	0.16	5802	4.3	1.30	0.13	SM	9.39	0.97	7.5
10031885	329.01	8.590	132.02	SE	1.4	0.02	6035	4.5	0.95	0.28	P	1.44	0.43	154.6
10031907	3828.01	8.590	132.02	SE	2.8	0.02	5632	4.6	0.83	0.25	P	2.50	0.75	97.7
10031918	4894.01	8.590	131.96	P	1.0	0.08	4944	4.6	0.71	0.21	P	0.78	0.24	50.3
10033279	1604.01	72.492	139.77	P	3.1	0.17	5812	4.4	1.04	0.31	P	3.56	1.09	10.0
10053138		11.773	138.79	P	0.9	0.07	5703	4.6	0.85	0.26	P	0.83	0.26	70.0
10063208	4292.01	9.328	132.90	P	0.6	0.04	5780	4.5	0.87	0.26	P	0.53	0.16	102.5
10064256	2849.01	5.960	135.01	P	1.0	0.08	5301	4.6	0.78	0.23	P	0.88	0.27	118.7
10098844	2964.01	47.449	173.46	P	1.8	0.06	6008	4.3	1.11	0.11	SM	2.17	0.23	22.0
10122255	1086.01	27.665	144.88	P	2.1	0.10	6057	4.4	1.05	0.32	P	2.38	0.72	41.1
10134152	2056.01	39.314	154.93	P	2.2	0.14	6060	4.5	0.96	0.29	P	2.33	0.71	21.0
10136549	1929.01	9.693	132.80	P	1.2	0.08	5681	4.1	1.60	0.16	SM	2.01	0.24	259.7
10154388	991.01	12.062	138.23	P	1.8	0.11	5541	4.4	0.91	0.09	SM	1.80	0.21	74.1
10155434	473.01	12.706	142.50	P	2.6	0.13	5541	4.6	0.80	0.24	P	2.30	0.70	51.6
10158418	1784.01	5.007	135.03	P	5.6	0.20	5956	4.4	1.04	0.10	SM	6.32	0.67	366.5
10187159	1870.01	7.964	136.82	P	2.6	0.16	5101	4.6	0.76	0.23	P	2.15	0.66	70.3
10189542		24.615	142.53	P	1.6	0.24	5645	4.5	0.85	0.26	P	1.48	0.49	25.8
10189546	427.01	24.615	142.51	C	3.6	0.12	5462	4.5	0.85	0.26	P	3.35	1.01	23.9
10190075	3007.01	11.192	138.03	P	1.3	0.15	5879	4.5	0.89	0.27	P	1.28	0.41	89.7
10198109		17.919	146.39	R	31.5	0.01	5971	4.0	1.66	0.50	P	57.15	17.15	166.4
10215422		24.847	154.11	R	75.0	1.44	5615	4.6	0.84	0.25	P	68.60	20.62	24.1
10252275	3130.01	14.863	143.00	P	1.3	0.11	5141	4.5	0.78	0.23	P	1.14	0.35	32.6
10266615	530.01	10.940	137.48	P	2.2	0.16	5720	4.6	0.85	0.25	P	2.08	0.64	77.1
10268809		24.709	138.99	R	25.0	0.81	6058	4.4	1.03	0.31	P	27.97	8.44	45.4
10274244		13.684	135.21	R	43.4	0.10	5453	4.5	0.83	0.25	P	39.18	11.75	48.3
10285631	331.01	18.684	133.47	P	1.9	0.11	5689	4.4	1.04	0.10	SM	2.12	0.25	53.0
10289119	2390.01	16.104	135.05	P	1.0	0.04	6077	4.2	1.42	0.14	SM	1.58	0.17	135.1
10290666	332.01	5.458	133.88	P	1.5	0.09	5720	4.2	1.34	0.13	SM	2.15	0.25	426.3
10292238	3526.01	143.116	245.53	R	59.4	7.13	5687	4.6	0.84	0.25	P	54.43	17.59	2.4
10319590		21.321	132.74	SE	0.2	0.15	5738	4.4	1.04	0.31	P	0.22	0.18	49.9

Table 5.2 (cont'd): Properties of 836 eKOIs

KIC	KOI	$P$ days	$t_0$ days	Disp.	$p$ %	$\sigma(p)$	$T_{\text{eff}}$ K	$\log g$ cgs	$R_{\star}$ $R_{\odot}$	$\sigma(R_{\star})$	Prov.	$R_P$ $R_{\oplus}$	$\sigma(R_P)$	$F_P$ $F_{\oplus}$
10328393	1905.01	7.626	136.03	P	1.7	0.09	4954	4.6	0.72	0.07	SM	1.30	0.15	58.8
10330495		18.060	138.60	R	22.4	0.04	5333	4.5	0.86	0.26	P	21.10	6.33	35.0
10336951	2401.01	38.229	166.02	P	2.3	0.41	4625	4.7	0.63	0.19	P	1.59	0.56	4.4
10337517	1165.01	7.054	136.37	P	2.1	0.16	5357	4.5	0.86	0.09	SM	1.96	0.24	117.7
10345862		58.289	152.46	R	22.3	0.05	5374	4.4	0.89	0.27	P	21.59	6.48	7.9
10353968	618.01	9.071	132.98	P	2.8	0.04	5591	4.5	0.86	0.26	P	2.65	0.79	97.7
10384798	1997.01	38.506	158.30	P	2.4	0.11	6019	4.5	0.94	0.28	P	2.43	0.74	20.6
10404582	2147.01	37.865	134.37	P	2.0	0.21	5867	4.5	0.89	0.27	P	1.97	0.63	17.5
10420279		45.434	172.95	R	86.1	1.56	5665	4.4	1.03	0.31	P	96.75	29.08	17.2
10426656	1161.01	6.057	135.92	P	1.9	0.07	5294	4.5	0.84	0.25	P	1.72	0.52	139.7
10453588	2484.01	68.887	160.30	P	1.1	0.10	5739	4.3	1.07	0.11	SM	1.31	0.18	11.2
10480915	2040.01	19.586	132.37	P	2.2	0.27	5623	4.4	1.01	0.10	SM	2.42	0.38	47.3
10482160	1170.01	7.344	137.31	P	2.3	0.26	5805	4.5	0.87	0.26	P	2.22	0.71	145.1
10483644		5.111	133.31	R	24.5	0.52	6056	4.5	0.96	0.29	P	25.60	7.70	319.1
10490960		5.682	133.64	R	67.0	0.16	5871	4.3	1.17	0.35	P	85.36	25.61	386.4
10513530	533.01	16.550	138.58	P	2.6	0.16	5335	4.5	0.87	0.26	P	2.45	0.75	39.6
10514429	1614.01	20.720	143.28	P	1.1	0.09	5899	4.3	1.13	0.34	P	1.39	0.43	65.1
10514430	263.01	20.720	143.28	P	1.2	0.08	5855	4.3	1.13	0.11	SM	1.44	0.17	61.9
10545066	337.01	19.783	138.15	P	1.9	0.13	5751	4.3	1.13	0.11	SM	2.30	0.28	60.9
10554999	534.01	6.400	135.64	P	2.6	0.15	5283	4.6	0.74	0.22	P	2.07	0.63	94.4
10577994	475.01	8.181	135.78	P	2.5	0.04	5236	4.5	0.79	0.24	P	2.14	0.64	78.1
10586208	1308.01	23.585	145.94	P	1.9	0.04	5647	4.2	1.56	0.16	SM	3.29	0.34	73.4
10586744	4892.01	21.376	143.63	P	1.0	0.06	6035	4.3	1.17	0.35	P	1.23	0.38	71.5
10593626	87.01	289.862	133.70	P	2.2	0.16	5567	4.4	0.93	0.09	SM	2.25	0.28	1.1
10599206	476.01	18.428	141.59	P	2.4	0.11	5139	4.5	0.78	0.23	P	2.05	0.62	24.4
10600955	2227.01	65.650	173.30	P	2.2	0.26	5819	4.4	1.01	0.30	P	2.44	0.79	10.8
10616679	429.01	8.600	138.13	P	5.3	0.09	5254	4.5	0.82	0.25	P	4.78	1.44	81.1
10656823	598.01	8.308	137.93	P	2.4	0.11	5292	4.6	0.74	0.22	P	1.96	0.59	67.8
10657406	1837.01	34.174	137.78	P	2.2	0.08	5166	4.6	0.80	0.08	SM	1.94	0.21	10.8
10666242	198.01	87.242	153.35	V	17.7	2.25	5731	4.6	0.85	0.26	P	16.47	5.36	4.9
10674871	2068.01	41.889	171.99	P	3.0	0.30	5939	4.5	0.92	0.27	P	3.00	0.95	16.7
10676014	1797.01	16.782	139.79	P	2.8	0.13	4925	4.6	0.74	0.07	SM	2.26	0.25	20.9
10709622	2108.01	51.329	177.67	P	2.5	0.17	6096	4.4	1.13	0.34	P	3.13	0.96	21.1
10717241	430.01	12.376	142.28	P	4.1	0.57	4286	4.7	0.56	0.17	P	2.50	0.83	12.4
10724369	1302.01	55.638	131.94	P	2.8	0.33	5906	4.5	0.90	0.27	P	2.80	0.90	11.0
10753734		19.407	149.80	R	66.4	0.32	5655	4.6	0.83	0.25	P	60.25	18.08	33.4
10779233	1989.01	201.111	187.60	P	2.5	0.22	5647	4.4	0.98	0.10	SM	2.68	0.36	2.0
10793172	2871.01	12.100	143.04	P	1.4	0.16	5678	4.6	0.84	0.25	P	1.25	0.40	65.2
10794242		7.144	137.80	R	41.6	0.02	5645	4.4	0.99	0.30	P	44.73	13.42	184.2
10798331	2373.01	147.281	148.80	P	2.1	0.18	5712	4.4	1.13	0.11	SM	2.57	0.34	3.9
10798605	3390.01	56.049	159.16	R	33.5	0.95	5243	4.5	0.82	0.25	P	29.90	9.01	6.6

Table 5.2 (cont'd): Properties of 836 eKOIs

KIC	KOI	$P$ days	$t_0$ days	Disp.	$p$ %	$\sigma(p)$	$T_{\text{eff}}$ K	$\log g$ cgs	$R_{\star}$ $R_{\odot}$	$\sigma(R_{\star})$	Prov.	$R_P$ $R_{\oplus}$	$\sigma(R_P)$	$F_P$ $F_{\oplus}$
10798838	3449.01	62.127	172.07	R	27.7	1.52	5381	4.4	0.89	0.27	P	26.89	8.20	7.3
10810838	174.01	56.355	144.83	P	2.9	0.19	4752	4.6	0.68	0.07	SM	2.19	0.26	3.2
10843590	431.01	18.870	140.97	P	3.1	0.11	5417	4.4	0.91	0.27	P	3.03	0.92	38.4
10845188	3602.01	249.357	279.64	R	26.0	2.36	5982	4.4	1.10	0.33	P	31.09	9.75	2.3
10858832	432.01	5.263	132.25	P	3.1	0.21	6045	4.5	1.00	0.30	P	3.32	1.02	334.2
10867062	1303.01	34.302	143.53	P	2.4	0.07	5506	4.1	1.46	0.44	P	3.82	1.15	44.0
10873260	535.01	5.853	136.07	P	3.1	0.09	6021	4.4	1.00	0.30	P	3.42	1.03	291.7
10875245	117.01	14.749	138.79	P	2.2	0.17	5807	4.3	1.28	0.13	SM	3.03	0.39	111.2
10878263		7.171	133.64	P	2.6	0.06	5450	4.5	0.89	0.09	SM	2.52	0.26	125.2
10880507	2936.01	6.480	132.86	P	1.2	0.15	5690	4.6	0.84	0.25	P	1.06	0.35	150.6
10908248	3146.01	39.855	154.85	P	1.2	0.08	5902	4.4	1.08	0.33	P	1.36	0.42	25.3
10917433	3248.01	6.912	132.19	P	0.5	0.06	5767	4.4	1.05	0.11	SM	0.62	0.09	223.1
10917681	1963.01	12.896	136.84	P	1.9	0.17	6074	4.5	0.97	0.29	P	2.03	0.64	95.3
10925104	156.03	11.776	142.71	P	3.3	0.04	4587	4.7	0.66	0.07	SM	2.35	0.24	21.3
10933561	291.01	31.518	153.64	P	1.7	0.03	5727	4.3	1.24	0.12	SM	2.33	0.24	36.5
10934674	477.01	16.543	136.56	P	2.5	0.07	5088	4.6	0.75	0.23	P	2.01	0.61	25.8
10936427		14.361	131.67	R	62.4	0.50	5333	4.6	0.76	0.23	P	51.48	15.45	34.9
10964440	1310.01	19.130	139.42	P	2.0	0.13	6045	4.5	0.96	0.29	P	2.13	0.65	54.6
10965008		81.170	178.59	P	3.2	0.19	5808	4.5	0.87	0.26	P	3.08	0.94	5.9
10965963		6.640	132.76	R	66.5	1.47	6056	4.3	1.20	0.36	P	87.02	26.18	357.2
10973814	1307.01	44.852	172.48	P	2.6	0.12	5783	4.4	1.00	0.30	P	2.89	0.88	17.5
10977671		199.038	180.22	P	1.4	0.24	5161	3.5	3.38	0.34	SM	5.30	1.02	12.9
10990917	1643.01	11.046	136.41	P	1.8	0.13	6072	4.4	1.03	0.31	P	2.02	0.62	135.9
11015108	344.01	39.309	132.02	P	3.2	0.14	5581	4.4	0.92	0.09	SM	3.25	0.35	16.2
11015323	479.01	34.189	159.20	P	3.0	0.08	5516	4.5	0.91	0.09	SM	3.03	0.31	18.1
11017901	1800.01	7.794	137.27	P	6.0	0.35	5540	4.5	0.88	0.09	SM	5.77	0.67	118.2
11037335	1435.01	40.716	146.55	P	2.2	0.03	5993	4.5	0.93	0.28	P	2.21	0.66	18.4
11045383	1645.01	41.166	158.93	P	10.3	1.24	5199	4.5	0.79	0.24	P	8.96	2.89	9.1
11069176	2007.01	15.379	143.38	P	1.3	0.12	6063	4.4	1.05	0.32	P	1.43	0.45	89.8
11075279	1431.01	345.158	318.30	P	7.8	0.16	5495	4.4	0.99	0.10	SM	8.44	0.86	0.9
11100383	346.01	12.925	132.00	P	2.9	0.15	5104	4.6	0.76	0.08	SM	2.39	0.27	35.2
11124436	4442.01	13.948	132.76	P	1.1	0.08	5964	4.4	1.03	0.31	P	1.22	0.38	93.9
11125797		12.254	143.69	P	1.2	0.11	5444	4.6	0.79	0.24	P	1.00	0.31	49.3
11147814	3334.01	95.177	224.61	R	42.5	5.07	4538	4.7	0.61	0.18	P	28.18	9.10	1.1
11153121	1647.01	14.971	134.49	P	1.6	0.07	5741	4.4	1.13	0.11	SM	1.92	0.21	84.8
11177543	1648.01	38.326	142.10	P	1.8	0.11	5333	4.6	0.75	0.23	P	1.50	0.46	9.2
11177676		47.032	175.44	P	2.0	0.07	5586	4.6	0.81	0.24	P	1.80	0.54	9.5
11192998	481.01	7.650	133.72	P	2.8	0.06	5429	4.6	0.78	0.23	P	2.39	0.72	89.4
11193263	1438.01	6.911	136.64	P	1.3	0.06	5767	4.2	1.32	0.13	SM	1.94	0.21	329.8
11194032	348.01	28.511	158.87	P	3.8	0.04	4686	4.6	0.68	0.07	SM	2.86	0.29	7.5
11250587	107.01	7.257	134.02	P	2.0	0.07	5883	4.3	1.29	0.13	SM	2.82	0.30	303.0

Table 5.2 (cont'd): Properties of 836 eKOIs

KIC	KOI	$P$ days	$t_0$ days	Disp.	$p$ %	$\sigma(p)$	$T_{\text{eff}}$ K	$\log g$ cgs	$R_{\star}$ $R_{\odot}$	$\sigma(R_{\star})$	Prov.	$R_P$ $R_{\oplus}$	$\sigma(R_P)$	$F_P$ $F_{\oplus}$
11253711	1972.01	17.791	149.25	P	1.9	0.18	6074	4.5	0.97	0.29	P	2.03	0.64	62.4
11253827	2672.01	88.516	182.66	P	5.6	0.26	5569	4.5	0.93	0.09	SM	5.66	0.62	5.1
11255231	3003.01	13.655	137.52	C	1.2	0.08	6058	4.5	0.97	0.29	P	1.29	0.40	87.7
11288051	241.01	13.821	131.80	P	2.5	0.09	4987	4.6	0.70	0.07	SM	1.93	0.21	26.9
11297236	1857.01	88.642	145.49	P	2.4	0.15	5657	4.5	0.92	0.09	SM	2.39	0.28	5.5
11305996	3256.01	55.699	152.72	C	2.0	0.31	4238	4.7	0.55	0.17	P	1.17	0.40	1.6
11337833	1651.01	51.300	153.54	P	2.3	0.28	6026	4.5	0.94	0.28	P	2.40	0.78	14.1
11358389	2163.01	10.665	132.00	P	1.5	0.06	5983	4.4	1.01	0.30	P	1.71	0.52	132.1
11360805	2422.01	26.784	140.75	P	1.9	0.13	5412	4.4	0.91	0.27	P	1.86	0.57	24.0
11361646	330.01	7.974	134.68	P	1.9	0.06	5969	4.4	1.10	0.11	SM	2.30	0.24	216.9
11391018	189.01	30.361	148.08	P	13.1	0.01	4905	4.6	0.70	0.21	P	9.96	2.99	8.8
11392618	1623.01	110.919	174.24	P	2.0	0.10	5606	4.2	1.39	0.14	SM	3.04	0.34	8.4
11394027	349.01	14.387	141.69	P	2.3	0.13	5725	4.4	1.14	0.11	SM	2.87	0.33	89.0
11395587	350.01	12.990	138.28	P	1.9	0.11	5786	4.4	1.04	0.10	SM	2.12	0.25	93.0
11402995	173.01	10.061	138.97	P	2.0	0.03	5707	4.3	1.19	0.12	SM	2.55	0.26	160.2
11403389	2482.01	45.090	133.58	P	1.9	0.13	5753	4.6	0.86	0.26	P	1.83	0.56	12.2
11413812	1885.01	5.654	131.72	P	1.9	0.13	5973	4.5	0.93	0.28	P	1.92	0.59	250.1
11415243	4036.01	168.814	211.45	P	2.3	0.23	4794	4.6	0.70	0.07	SM	1.74	0.25	0.8
11449844	125.01	38.479	151.86	P	13.9	0.01	5486	4.5	0.85	0.26	P	12.89	3.87	13.3
11450414	1992.01	12.798	133.66	P	1.7	0.07	6069	4.5	0.96	0.29	P	1.79	0.54	94.8
11461844	2356.01	13.681	139.23	P	1.2	0.07	6055	4.5	0.96	0.29	P	1.23	0.37	85.9
11462341	2124.01	42.337	158.28	P	1.8	0.08	4252	4.7	0.55	0.17	P	1.06	0.32	2.3
11495458	2318.01	10.459	137.64	P	1.7	0.13	4702	4.6	0.65	0.19	P	1.18	0.37	27.4
11498128	2296.01	106.252	135.72	P	1.8	0.14	5673	4.4	0.95	0.10	SM	1.89	0.24	4.7
11502172		25.432	135.62	R	32.6	0.11	5787	4.4	0.96	0.29	P	34.11	10.23	33.8
11506235		20.413	140.01	R	30.2	0.10	5908	4.5	0.94	0.28	P	30.94	9.28	45.5
11519226		22.161	148.47	SE	10.4	2.41	5938	4.5	0.91	0.27	P	10.39	3.93	38.8
11521048	540.01	25.703	143.40	VD	11.4	0.50	5569	4.5	0.88	0.26	P	10.89	3.30	24.9
11521793	352.01	27.083	137.64	P	1.8	0.06	5855	4.3	1.21	0.12	SM	2.42	0.26	47.6
11554435	63.01	9.434	140.11	P	5.9	0.18	5551	4.5	0.91	0.09	SM	5.86	0.61	94.0
11601584	1831.01	51.810	182.96	P	2.9	0.11	5192	4.5	0.84	0.08	SM	2.68	0.29	6.8
11614617	1990.01	24.757	142.08	P	2.0	0.07	6088	4.5	0.97	0.29	P	2.09	0.63	40.3
11619964		10.369	132.72	R	46.4	1.41	5899	4.4	1.00	0.30	P	50.45	15.21	127.7
11623629	365.01	81.737	211.69	P	2.3	0.09	5465	4.5	0.85	0.09	SM	2.16	0.23	4.8
11651712	3363.01	14.532	140.48	P	1.7	0.12	5996	4.5	0.94	0.28	P	1.70	0.52	73.6
11656302	434.01	22.265	150.82	SE	13.5	0.05	5700	4.6	0.85	0.26	P	12.57	3.77	29.9
11656721	541.01	13.646	139.40	P	2.4	0.10	5536	4.6	0.80	0.24	P	2.07	0.63	46.6
11656918	1945.01	62.139	161.14	P	2.9	0.21	5434	4.6	0.81	0.24	P	2.52	0.78	6.1
11657614	3370.02	5.942	133.80	P	1.5	0.11	4870	4.6	0.69	0.21	P	1.11	0.34	73.9
11662184	2791.01	27.572	145.41	P	1.7	0.08	6046	4.5	0.95	0.29	P	1.72	0.52	33.2
11669239	542.01	41.886	136.80	P	2.5	0.10	5731	4.4	1.04	0.31	P	2.77	0.84	20.0

Table 5.2 (cont'd): Properties of 836 eKOIs

KIC	KOI	$P$ days	$t_0$ days	Disp.	$p$ %	$\sigma(p)$	$T_{\text{eff}}$ K	$\log g$ cgs	$R_{\star}$ $R_{\odot}$	$\sigma(R_{\star})$	Prov.	$R_P$ $R_{\oplus}$	$\sigma(R_P)$	$F_P$ $F_{\oplus}$
11671579	4510.01	5.176	133.78	P	0.9	0.08	5557	4.6	0.81	0.24	P	0.78	0.24	173.6
11702948	1465.01	9.771	135.60	P	7.2	0.05	5811	4.5	0.88	0.26	P	6.86	2.06	99.9
11709124	435.01	20.550	137.85	P	3.4	0.07	5706	4.4	0.99	0.10	SM	3.71	0.38	44.9
11718144	2310.01	16.458	134.04	P	2.0	0.12	5808	4.5	0.87	0.26	P	1.92	0.59	49.5
11724210		5.746	132.04	R	19.3	0.20	5971	4.4	1.02	0.31	P	21.50	6.45	303.2
11754430	3403.01	39.817	166.68	P	1.5	0.11	5715	4.1	1.80	0.18	SM	2.98	0.36	47.8
11760231	1841.01	49.608	138.42	P	2.3	0.09	5151	4.6	0.79	0.08	SM	1.98	0.21	6.5
11764462	1531.01	5.699	136.58	P	1.2	0.04	5738	4.4	0.99	0.10	SM	1.27	0.13	259.2
11769146		282.962	350.44	R	67.9	5.69	5966	4.5	0.93	0.28	P	68.67	21.39	1.4
11769689	4551.01	14.719	135.62	P	1.1	0.07	6078	4.5	1.00	0.30	P	1.18	0.36	86.7
11769890	1980.01	122.884	165.45	P	2.6	0.35	5413	4.5	0.89	0.09	SM	2.57	0.43	2.8
11773022	620.01	45.156	159.12	P	7.1	0.01	6023	4.5	0.94	0.28	P	7.33	2.20	16.7
11773328	1906.01	8.710	134.64	P	2.8	0.15	5380	4.6	0.77	0.23	P	2.37	0.72	71.1
11774991	2173.01	37.815	141.11	P	1.5	0.05	4705	4.6	0.69	0.07	SM	1.14	0.12	5.4
11802615	296.01	28.863	149.62	P	2.2	0.10	5754	4.4	1.01	0.10	SM	2.43	0.27	31.3
11812199		37.321	135.41	SE	10.7	0.28	5878	4.5	0.91	0.27	P	10.53	3.17	18.6
11818607	2467.01	5.057	134.39	P	1.3	0.14	5885	4.5	0.90	0.27	P	1.28	0.41	261.2
11818872	2581.01	12.737	136.01	P	1.0	0.09	5424	4.5	0.91	0.09	SM	1.01	0.13	58.4
11824222	437.01	15.841	145.47	R	20.7	2.53	5189	4.6	0.76	0.23	P	17.17	5.56	29.1
11858541		5.674	135.74	R	29.1	0.22	5585	4.3	1.07	0.32	P	33.96	10.19	287.2
11869052	120.01	20.546	137.91	TTV	1.5	0.17	5619	4.2	1.20	0.36	P	1.94	0.63	65.7
11875734	1828.01	99.747	208.40	P	3.4	0.23	5638	4.2	1.18	0.35	P	4.36	1.34	7.8
11906217		37.910	162.47	R	45.7	1.72	4772	4.6	0.66	0.20	P	33.02	9.98	5.4
11909686	1483.01	185.937	288.87	P	10.0	2.65	5861	4.5	0.89	0.27	P	9.71	3.89	2.1
11922778	3408.01	65.427	176.32	P	1.7	0.17	6010	4.5	0.94	0.28	P	1.78	0.56	10.0
11955499	1512.01	9.042	137.87	C	2.4	0.07	5118	4.6	0.70	0.21	P	1.86	0.56	49.0
12055539	3261.01	12.271	137.58	P	1.4	0.10	6066	4.5	0.96	0.29	P	1.48	0.46	100.1
12058204	2218.01	5.535	132.76	P	1.5	0.05	5803	4.5	0.87	0.26	P	1.43	0.43	211.2
12061222	484.01	17.205	140.65	P	3.0	0.05	5254	4.6	0.73	0.22	P	2.40	0.72	24.4
12071037	2388.01	6.096	135.11	C	1.0	0.03	5901	4.4	0.99	0.30	P	1.06	0.32	257.4
12105785		31.953	142.69	SE	15.9	0.21	5508	4.6	0.80	0.24	P	13.81	4.15	14.5
12106929	359.01	5.937	135.97	P	1.8	0.04	5954	4.5	0.92	0.28	P	1.79	0.54	229.3
12107008	4297.01	5.937	135.93	P	1.0	0.05	5480	4.5	0.86	0.26	P	0.93	0.28	162.4
12116489	547.01	25.303	137.44	P	4.4	0.20	5170	4.6	0.72	0.22	P	3.45	1.05	13.7
12121570	2290.01	91.500	165.68	P	2.5	0.19	4977	4.6	0.70	0.07	SM	1.95	0.25	2.2
12154526	2004.01	56.188	146.39	P	1.9	0.20	5663	4.3	1.21	0.12	SM	2.54	0.37	15.4
12251650	621.01	17.762	138.68	P	20.2	2.61	5166	4.6	0.73	0.22	P	16.11	5.26	22.4
12253474	1947.01	6.423	135.56	P	1.3	0.06	6085	4.5	1.01	0.30	P	1.47	0.44	265.7
12253769	3310.01	20.551	141.07	C	1.3	0.09	5450	4.5	0.92	0.09	SM	1.29	0.16	31.7
12254792	1506.01	40.429	139.52	P	2.8	0.06	5831	4.5	0.88	0.26	P	2.71	0.82	15.3
12256520	2264.01	33.243	143.44	P	1.7	0.11	5559	4.4	1.00	0.30	P	1.89	0.58	23.2

Table 5.2 (cont'd): Properties of 836 eKOIs

KIC	KOI	$P$ days	$t_0$ days	Disp.	$p$ %	$\sigma(p)$	$T_{\text{eff}}$ K	$\log g$ cgs	$R_{\star}$ $R_{\odot}$	$\sigma(R_{\star})$	Prov.	$R_P$ $R_{\oplus}$	$\sigma(R_P)$	$F_P$ $F_{\oplus}$
12266636	1522.01	33.386	148.92	P	2.2	0.12	5801	4.4	0.99	0.30	P	2.41	0.73	25.7
12301181	2059.01	6.147	134.88	P	1.0	0.05	4999	4.6	0.74	0.07	SM	0.84	0.09	84.0
12302530	438.01	5.931	133.29	P	3.2	0.27	4478	4.7	0.63	0.06	SM	2.18	0.29	44.9
12306808		37.879	138.13	R	65.9	0.42	6055	4.5	0.96	0.29	P	68.73	20.62	22.0
12400538	1503.01	150.244	138.27	P	5.1	0.36	5598	4.5	0.96	0.10	SM	5.33	0.65	2.8
12403119	1478.01	76.135	199.49	P	5.5	0.11	5551	4.5	0.94	0.09	SM	5.58	0.57	6.4
12404305	486.01	22.183	147.31	P	2.7	0.16	5566	4.4	1.01	0.10	SM	2.96	0.34	41.1
12417486	622.01	155.042	213.51	P	7.1	0.13	5005	3.5	3.28	0.33	SM	25.33	2.58	16.3
12454461	2463.01	7.467	136.39	P	0.8	0.05	6027	4.3	1.26	0.13	SM	1.11	0.13	300.3
12505654	2353.01	5.187	135.01	P	2.1	0.20	5182	4.6	0.73	0.22	P	1.71	0.54	118.3
12508335	215.01	42.944	155.21	P	15.3	0.44	5802	4.4	1.02	0.31	P	17.10	5.15	19.4
12557713		7.215	132.51	R	29.1	2.62	4873	4.6	0.69	0.21	P	21.86	6.85	57.3
12644769	1611.01	41.078	132.66	VD	33.6	0.16	4198	4.7	0.54	0.16	P	19.94	5.98	2.2
12735740	3663.01	282.521	363.06	P	8.9	0.10	5576	4.4	0.93	0.09	SM	9.03	0.91	1.2
12735830	3311.01	31.829	134.58	P	1.9	0.28	4712	4.6	0.65	0.19	P	1.33	0.45	6.3
12834874	487.01	7.659	134.74	P	2.4	0.06	5666	4.5	0.88	0.26	P	2.26	0.68	131.5

Note. — For each of the 836 eKOIs, we list the target star identifier, ephemeris, false positive status, transit fit parameters, host star properties, and planet radius. KIC — *Kepler* Input Catalog [Brown et al. \(2011\)](#) identifier. KOI — *Kepler* team identifier, if eKOI appears in 13 September 2013 cumulative list of candidates from the NASA Exoplanet Archive [Akeson et al. \(2013\)](#). Disp. — disposition according to the false positive vetting described in 5.5. eKOIs may be designated as a false positives for any of the following reasons: ‘SE’ — secondary eclipse, ‘VD’ — variable depth transits, ‘TTV’ — large transit timing variations, ‘V’ — V-shaped transit, ‘C’ — centroid offset. If an eKOI passes all the vetting steps, it is considered a planet, ‘P.’  $p$  — planet to star radius ratio,  $R_P/R_{\star}$ . Prov. — provenience of stellar parameters: SpecMatch ‘SM’ or photometric ‘P’.

Table 5.3: Spectroscopic properties of 13 eKOIs (added in proof)

KIC	KOI	$P$ days	$t_0$ days	Disp.	$p$ %	$\sigma(p)$	$T_{\text{eff}}$ K	$\log g$ cgs	$R_{\star}$ $R_{\odot}$	$\sigma(R_{\star})$	Prov.	$R_P$ $R_{\oplus}$	$\sigma(R_P)$	$F_P$ $F_{\oplus}$
4478142		219.909	329.43	P	2.5	0.34	5648	4.3	1.06	0.11	SM	2.92	0.49	2.3
4820550	3823.01	202.121	292.04	P	5.7	0.65	5594	4.5	0.94	0.09	SM	5.79	0.88	1.8
6225454		89.338	218.54	P	2.4	0.58	4652	4.6	0.68	0.07	SM	1.73	0.46	1.6
6307083	2050.01	75.378	167.11	SE	1.7	0.09	5109	4.6	0.77	0.08	SM	1.43	0.16	3.4
7101828	455.01	47.878	145.35	VD	2.2	0.10	4328	4.7	0.55	0.05	SM	1.33	0.15	2.0
7866914	3971.01	366.020	182.66	SE	4.0	1.15	5713	4.3	1.06	0.11	SM	4.67	1.40	1.2
7877978	2760.01	56.573	146.59	P	2.5	0.35	4675	4.6	0.68	0.07	SM	1.87	0.32	3.0
8044608	3523.01	106.176	234.62	R	55.2	2.76	6056	4.4	1.12	0.11	SM	67.58	7.56	7.7
9447166	3296.01	62.868	166.04	P	1.9	0.26	4739	4.6	0.72	0.07	SM	1.48	0.25	2.9
10292238	3526.01	143.116	245.53	R	59.4	7.13	5957	4.4	1.09	0.11	SM	70.56	11.03	4.7
11305996	3256.01	55.699	152.72	C	2.0	0.31	4241	4.7	0.48	0.05	SM	1.03	0.19	1.4
11462341	2124.01	42.337	158.28	P	1.8	0.08	4282	4.7	0.54	0.05	SM	1.04	0.11	2.3
11769146		282.962	350.44	R	67.9	5.69	5787	4.5	0.95	0.10	SM	70.64	9.21	1.3

Note. — We obtained 13 additional spectra of long period eKOIs during peer-review. In this work, we used photometric properties for these 13 eKOIs, but we include them here for completeness. Column descriptions are the same as Table 5.2.

# 6

## Carbon and Oxygen in Nearby Stars: Keys to Protoplanetary Disk Chemistry

A version of this chapter was previously published in the *Astrophysical Journal* (Erik A. Petigura & Geoffrey W. Marcy, 2011, ApJ 735, 41).

We present carbon and oxygen abundances for 941 FGK stars—the largest such catalog to date. We find that planet-bearing systems are enriched in these elements. We self-consistently measure  $N_C/N_O$ , which is thought to play a key role in planet formation. We identify 46 stars with  $N_C/N_O \geq 1.00$  as potential hosts of carbon-dominated exoplanets. We measure a downward trend in [O/Fe] versus [Fe/H] and find distinct trends in the thin and thick disk, supporting the work of [Bensby et al. \(2004\)](#). Finally, we measure sub-solar  $N_C/N_O = 0.40_{-0.07}^{+0.11}$  for WASP-12, a surprising result as this star is host to a transiting hot Jupiter whose dayside atmosphere was recently reported to have  $N_C/N_O \geq 1$  by [Madhusudhan et al. \(2011\)](#). Our measurements are based on 15,000 high signal-to-noise spectra taken with the Keck 1 telescope as part of the California Planet Search. We derive abundances from the [OI] and CI absorption lines at  $\lambda = 6300$  and  $6587 \text{ \AA}$  using the SME spectral synthesizer.

### 6.1 Introduction

After primordial hydrogen and helium, carbon and oxygen are the most abundant elements in the cosmos. Life on earth is built upon the versatility of carbon's four valence electrons and is powered by metabolizing nutrients with oxygen.

The prevalence of carbon and oxygen gives them a prominent role in stellar interiors, opacities, and energy generation. As a result, studying their abundances helps to reveal the nucleosynthetic chemical evolution of galaxies.

The interstellar medium is thought to be enriched with oxygen by Type II supernovae. Taken with iron, which is produced in both Type Ia and Type II supernovae, oxygen provides a record of galactic chemical enrichment and star formation rate ([Bensby et al. 2004](#)). It

is well known that stars synthesize helium into carbon through the triple alpha reaction. However, it is still unclear which stars dominate carbon production in the galaxy. For a discussion of the possible sites of carbon synthesis see [Gustafsson et al. \(1999\)](#).

The ratio of carbon to oxygen ( $N_C/N_O$ ) is thought to play a critical role in the bulk properties of terrestrial extrasolar planets. [Kuchner & Seager \(2005\)](#) and [Bond et al. \(2010\)](#) predict that above a threshold ratio of  $N_C/N_O$  near unity, planets transition from silicate- to carbide-dominated compositions.

We present the oxygen and carbon abundances derived from the [OI] line at 6300 Å and the CI line at 6587 Å for 941 stars in the California Planet Search (CPS) catalog. We compute the abundances with the **Spectroscopy Made Easy** (SME) spectral synthesizer ([Valenti & Piskunov 1996](#)). Using SME, we self-consistently account for the NiI contamination in [OI] and report detailed Monte Carlo-based errors. Others have measured stellar carbon and oxygen before. [Edvardsson et al. \(1993\)](#) measured oxygen in 189 F and G dwarfs, and [Gustafsson et al. \(1999\)](#) measured carbon in 80 of these stars. More recent studies include, [Bensby et al. \(2005\)](#), [Luck & Heiter \(2006\)](#), and [Ramírez et al. \(2007\)](#). However, the sheer number (15,000) of CPS spectra give us a unique opportunity to measure the distributions of these important elements in a large sample.

## 6.2 Observations

### 6.2.1 Stellar Sample

The stellar sample is drawn from the Spectroscopic Properties of Cool Stars (SPOCS) catalog ([Valenti & Fischer 2005](#), hereafter VF05) and from the N2K (“Next 2000”) sample ([Fischer et al. 2005](#)). We include 533 N2K stars and 537 VF05 stars for a total of 1070 stars.

We adopt stellar atmospheric parameters for each star from VF05 and from the identical analysis for the N2K targets (D. Fischer 2008, private communication). These parameters are: effective temperature,  $T_{eff}$ ; gravity,  $\log g$ ; metallicity, [M/H]; rotational broadening,  $v \sin i$ ; macroturbulent broadening,  $v_{mac}$ ; microturbulent broadening,  $v_{mic}$ ; and abundances of Na, Si, Ti, Fe, and Ni. Metallicity includes all elements heavier than helium. A star’s abundance distribution is the solar abundance pattern from [Grevesse & Sauval \(1998\)](#) scaled by the star’s metallicity. Na, Si, Ti, Fe, and Ni abundances are computed independently from [M/H] and are allowed vary from scaled solar [M/H].

### 6.2.2 Spectra

Our spectra were taken with HIRES, the High Resolution Echelle Spectrograph ([Vogt et al. 1994](#)) between August, 2004 and April, 2010 on the Keck 1 Telescope. The spectra were originally obtained by the CPS to detect exoplanets. For a more complete description of the CPS and its goals, see [Marcy et al. \(2008\)](#). The CPS uses the same detector setup each observing run and employs the HIRES exposure meter ([Kibrick et al. 2006](#)) to set exposure times, ensuring consistent and high quality spectra across years of data collection.

The spectra have resolution  $R = 50,000$  and  $S/N \sim 200$  at 6300 and 6587 Å. This analysis deals with three classes of observations:

1. *Iodine cell in.* For the majority of its observations, the CPS passes starlight through an iodine cell (Marcy & Butler 1992), which imprints lines between 5000 and 6400 Å that serve as a wavelength fiducial. We discuss how we remove these lines and their effect on oxygen measurements in §6.3.4.
2. *Iodine cell out.* Calibration spectra taken without the iodine cell.
3. *Iodine reference.* At the beginning and end of each observing night, the CPS takes reference spectra of the iodine cell using an incandescent lamp.

## 6.3 Spectroscopic Analysis

### 6.3.1 Line Synthesis

We use the SME suite of routines to fine-tune line lists based on the solar spectrum, determine global stellar parameters, and measure carbon and oxygen. To generate a synthetic spectrum, SME first constructs a model atmosphere by interpolating between the Kurucz (1992) grid of model atmospheres. Then, SME solves the equations of radiative transfer assuming Local Thermodynamic Equilibrium (LTE). Finally, SME applies line-broadening to account for photospheric turbulence, stellar rotation, and instrument profile. For a more complete description of SME, please consult Valenti & Piskunov (1996) and VF05. We emphasize that SME solves molecular and ionization equilibrium for a core group (around 400) of species that includes CO (N. Piskunov 2011, private communication).

### 6.3.2 Atomic Parameters

Measuring stellar oxygen is notoriously difficult because of the limited number of indicators in visible wavelengths. The general consensus is that the weak, forbidden [OI] transition at 6300 Å is the best indicator because it is less sensitive to departures from local thermodynamic equilibrium than other indicators. In dwarf stars, this line suffers from a significant NiI blend, which is an isotopic splitting of  $^{58}\text{Ni}$  and  $^{60}\text{Ni}$  (Johansson et al. 2003). The NiI feature was first noted by Lambert (1978), but only recently included in abundance studies (Allende Prieto et al. 2001). Carbon is more generous to visual spectroscopists. We select the CI line at 6587 Å because it sits relatively far from neighboring lines and is in a wavelength region with weak iodine lines (see § 6.3.4).

Line lists are initially drawn from the Vienna Astrophysics Line Database (Piskunov et al. 1995). We tune line parameters by fitting the disk-integrated National Solar Observatory (NSO) solar spectrum of Kurucz et al. (1984) with the SME model of the solar atmosphere. Table 6.1 lists the atmospheric parameters adopted when modeling the sun. We fit a broad

spectral range from 6295 to 6305 Å surrounding the [OI] line and 6584 to 6591 Å surrounding the CI line. We adopt the solar abundances of [Grevesse & Sauval \(1998\)](#) except for O and Ni where we adopt  $\log \epsilon_{\text{O}}^1 = 8.70$  and  $\log \epsilon_{\text{Ni}} = 6.17$  ([Scott et al. 2009](#)) and  $\log \epsilon_{\text{C}} = 8.50$  ([Caffau et al. 2010](#)). We adjust line centers, van der Waals broadening parameters ( $\Gamma_6$ ), and oscillator strengths ( $\log gf$ ) so our synthetic spectra best match the NSO atlas. Table 6.2 shows the best fit atomic parameters after fitting the NSO solar atlas.

Given the high quality of the solar spectrum, solar abundances and line parameters are often measured using sophisticated three-dimensional, hydrodynamical, non-LTE codes. For this work, however, we are more interested in self-consistently determining line parameters using SME than from a more sophisticated solar model. As a result, the line parameters in Table 6.2 are not in tight agreement with the best laboratory measurements. For example, [Johansson et al. \(2003\)](#) measured  $\log gf = -2.11$  for the NiI blend in contrast to  $\log gf = -1.98$  in this work. The purpose of fitting the atomic parameters in the sun is to determine the best parameters given our atmospheric code and our adopted solar abundance distribution.

We show the fitted NSO spectrum for both wavelength regions in Figures 6.1 and 6.2. The shaded regions (6300.0-6300.6 and 6587.4-6587.8 Å) represent the fitting region. Only points in the fitting region are used in the  $\chi^2$  minimization routines (see § 6.3.5).

Figure 6.3 shows a close up view of the [OI]/NiI blend in the sun. To help the reader visualize the relative contributions of each line in the sun, we synthesize the oxygen and nickel lines individually. To compute the relative strength of [OI], we remove all Ni in our solar model and re-synthesize the spectrum in SME. To calculate the NiI contribution we remove all oxygen. Since the both lines are weak ( $< 5\%$  of continuum), the line profile for the [OI]/Ni blend is nearly the product of the individual [OI] and Ni lines. This would not be true in the case of deeper lines. In the sun, the [OI] and NiI contributions to the blend are comparable. In some stars, the blend is decidedly nickel-dominated, while in others, oxygen dominates.

Figure 6.4 shows the carbon indicator plotted on the same intensity scale as the oxygen detail shown in Figure 6.3. There is an unknown line on the red wing of the carbon indicator. We exclude the mystery line from the fitting region.

As a point of reference for the reader, we include stellar counterparts to Figures 6.3 and 6.4 in Figure 6.5. We show stars with low and high carbon and oxygen abundance along with the best fit SME spectrum.

### 6.3.3 Telluric Rejection

There are several telluric lines from O<sub>2</sub> and H<sub>2</sub>O in the vicinity of our indicators including the 6300.3 Å airglow (see Figures 6.1 and 6.2). These lines are produced in the rest frame of the Earth and contaminate different parts of a star's spectrum depending on the relative line of sight velocity between the Earth and the star. We compute this velocity directly from

---

<sup>1</sup> $\log \epsilon_X = \log_{10}(N_X/N_H) + 12$

Table 6.1: Adopted solar atmospheric parameters

Parameter	Value
$T_{\text{eff}}$	5770 K
$\log g$	4.44 (cgs)
$v_{\text{mic}}$	1.00 km/s
$v_{\text{mac}}$	3.60 km/s
$v \sin i$	1.60 km/s
$v_{\text{rad}}$	0.02 km/s

Note. — Adopted atmospheric parameters in the SME solar model

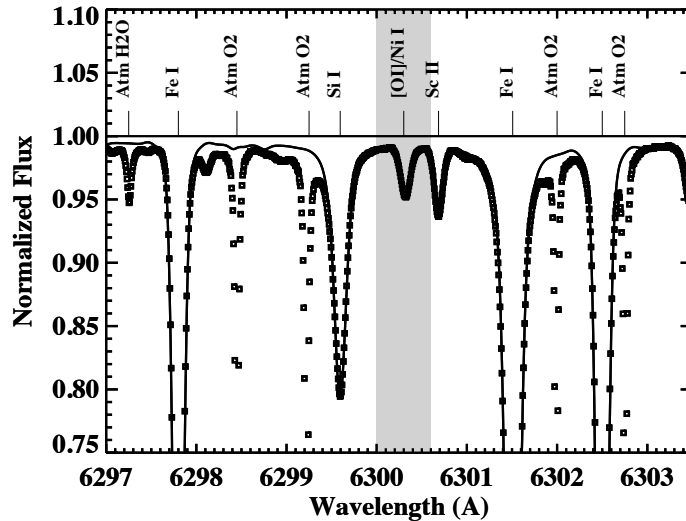


Figure 6.1: Solar spectrum in the vicinity of the [OI] line at 6300.312 Å. The points are from the NSO solar atlas, and the solid line is the SME fit. The shaded region marks the region that is included in the  $\chi^2$  fit to the [OI]/NiI blend.

Table 6.2: Atomic parameters from fitting the NSO atlas

Element	$\lambda$ ( $\text{\AA}$ )	$\log gf$	$\Gamma_6$
[OI] region			
Fe 1	6297.801	-2.766	-7.89
Si 1	6297.889	-2.899	-6.88
O 1	6300.312	-9.716	-8.89
Ni 1	6300.335	-1.983	-7.12
Sc 2	6300.685	-2.041	-8.01
Fe 1	6301.508	-0.793	-7.53
Fe 1	6302.501	-0.972	-7.99
CI region			
Ti 1	6585.249	-0.399	-7.56
Ni 1	6586.319	-2.775	-7.68
Fe 2	6586.672	-2.247	-7.76
C 1	6587.625	-1.086	-7.19
Si 1	6588.179	-3.082	-7.12

Note. — Best fit line center ( $\lambda$ ), oscillator strengths ( $\log gf$ ), and van der Waals broadening parameter ( $\Gamma_6$ ) for our [OI] and CI indicators and nearby lines. They are derived by fitting the NSO atlas.

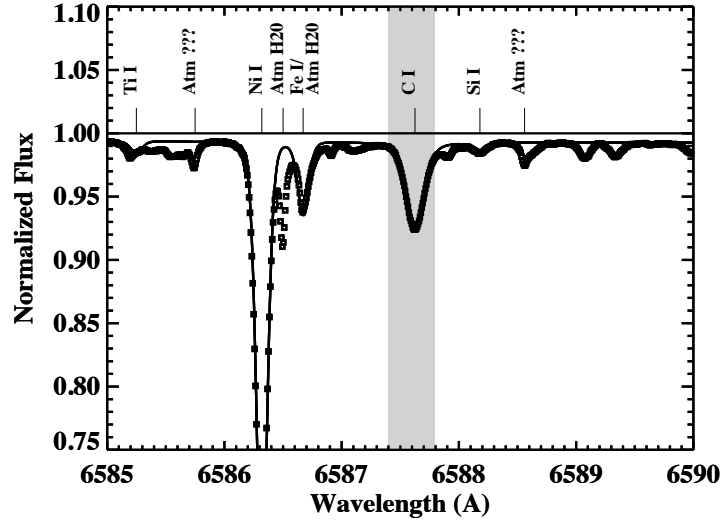


Figure 6.2: Solar spectrum in the vicinity of the CI line at 6587.625 Å. The points are from the NSO solar atlas, and the solid line is the SME fit. The shaded region marks the region that is included in the  $\chi^2$  fit to the CI line.

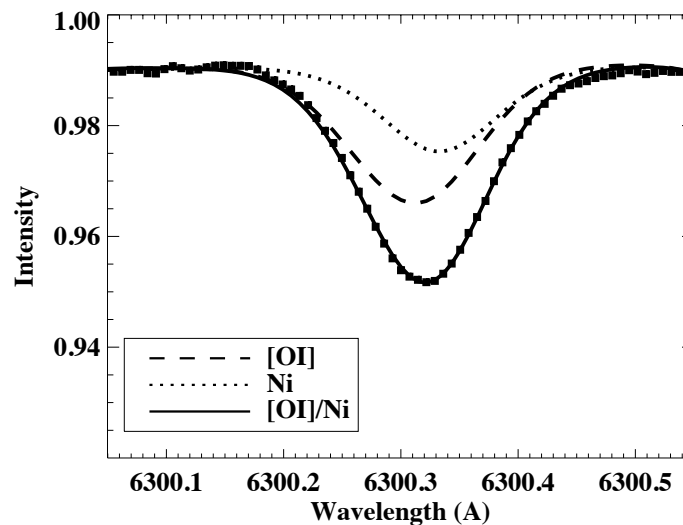


Figure 6.3: The [OI]/NiI blend in the NSO spectrum. The points are from the NSO solar atlas, and the solid line is the SME fit. The relative contribution of [OI] and Ni are shown by the dashed and dotted lines respectively.

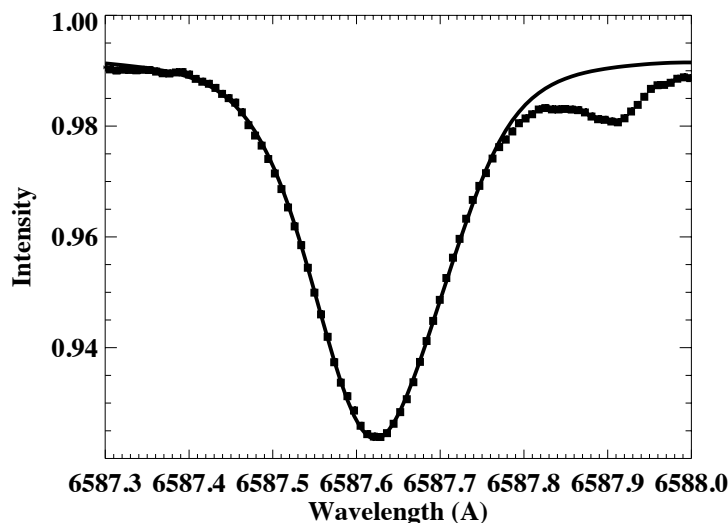


Figure 6.4: The CI line in the NSO spectrum. The points are the from NSO solar atlas, and the solid line is the SME fit. The fitting region for this line is 6587.4-6587.8 Å and excludes the unidentified feature at 6587.9.

the spectra, by cross-correlating the stellar spectra with the NSO solar atlas. Based on this velocity, we account for any shift in the location of the telluric line in the stellar rest frame.

If a telluric line enters the fitting region, we discard that observation. Figure 6.6 shows the [OI]/NiI blend from two different observations of HIP 92922: one where the blend is contaminated by a telluric absorption line and one where the blend is free from telluric contamination. We reject 53% of our [OI] spectra and 43% of our CI spectra because of telluric contamination. Telluric lines affect the [OI] region more strongly due to the airglow at 6300 Å.

### 6.3.4 Iodine Removal

The majority of the spectra in the CPS catalog were taken through the iodine cell. Iodine lines are  $\sim 0.5\%$  deep in the CI region—comparable to the photon noise. In the [OI] region, they are a  $\sim 5\%$  effect and must be removed. For a given iodine cell in observation, we locate the most recent iodine observation (usually at the beginning of the night). We account for any shift of the CCD between the two observations by cross-correlating spectral orders 8, 9, and 10 ( $\lambda = 5608 - 5895\text{Å}$ , where the iodine lines are strongest). After removing any shift, we divide the iodine cell in observations by the iodine reference observations. Figure 6.7 shows a stellar spectrum, an iodine spectrum, and the ratio of the two.

Dividing the iodine spectrum from an iodine cell in spectrum cannot be done to within photon statistics. On nights of good seeing, a star’s image may be narrower than the HIRES slit. The reference iodine spectra are produced with a lamp that fills the slit uniformly, so

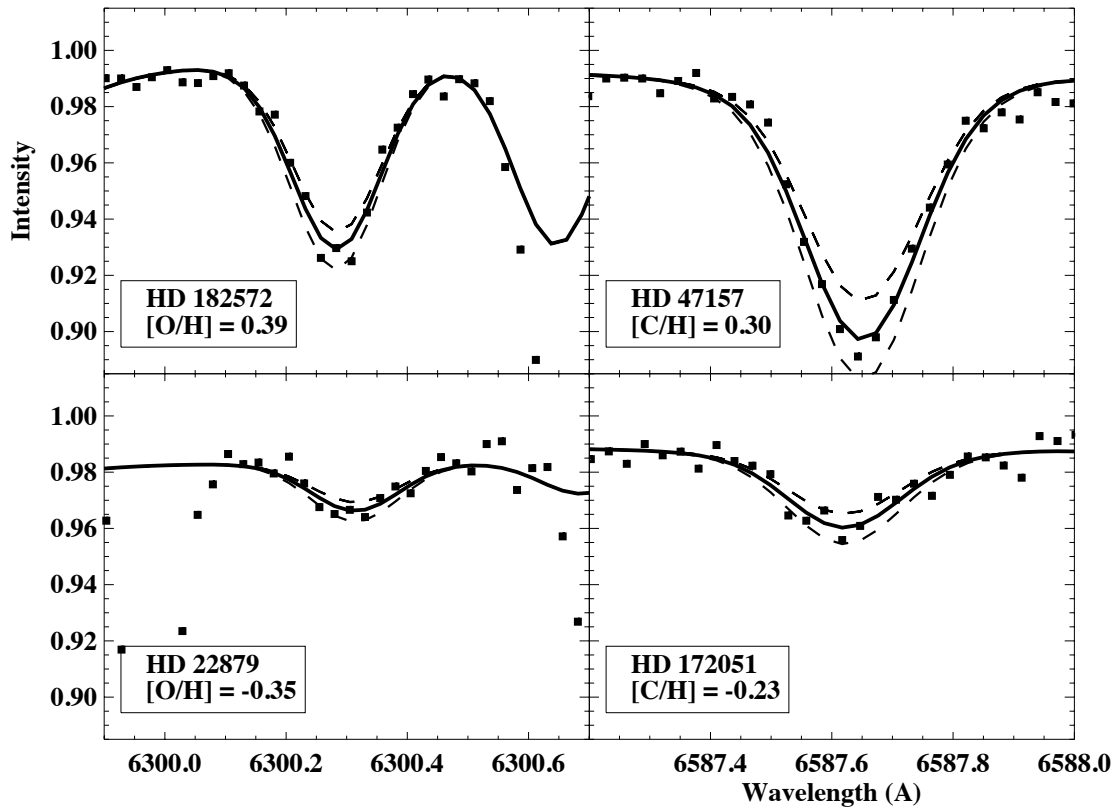


Figure 6.5: Sample spectra of stars with low and high carbon and oxygen abundances. The solid line shows the best fit SME spectrum. The dashed lines are the SME spectra with  $[X/H]$  increased and decreased by 0.1 dex  $\sim 25\%$  from the best fit value. The  $[OI]$  line in the HD 22879 spectrum sits between two telluric lines.

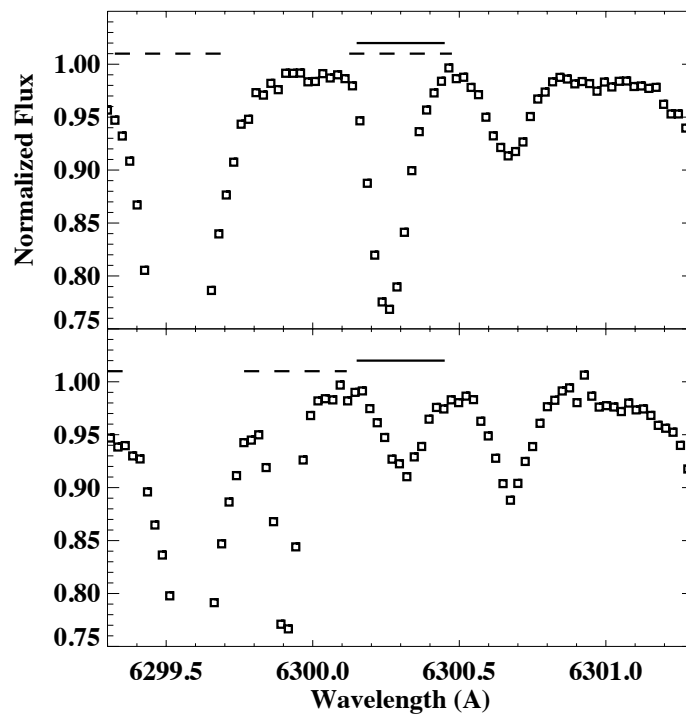


Figure 6.6: Two spectra of HIP 92922 in the star's rest frame. The [OI]/NiI region (marked with the solid line) in the upper panel is contaminated with an atmospheric O<sub>2</sub> (marked with a dashed line). The same telluric absorption line is shifted 0.3 Å blueward in the lower panel and does not contaminate the [OI]/NiI blend.

the iodine lines from the iodine cell in observations can be narrower than the reference iodine lines. The result is artifacts from the division at the  $\sim 1\%$  level. Iodine cell in spectra for a single star generally yield a larger spread in derived oxygen abundance compared to iodine cell out observations. However, when we plot oxygen abundances derived from iodine cell in observations against abundances from iodine cell out observations in Figure 6.8, we see no systematic trend.

### 6.3.5 Fitting Abundances

We converge on abundance by iterating three  $\chi^2$  minimization routines that fit the continuum, line center, and abundance. Only points within the fitting range are used to calculate the  $\chi^2$  statistic. Any point deviating from the fit by more than five times the photon noise is not included in calculating  $\chi^2$ . A short description of each routine is given below:

1. *Continuum.* Given the shallowness of our indicators, a small error in the continuum level will have a significant effect on the derived abundance. We refine the continuum value by registering the level of the spectrum so that  $\chi^2$  is minimized.
2. *Line center.* The wavelength zero point and dispersion is initially determined from a thorium lamp calibration taken each night and refined by cross-correlating the observed spectrum with the solar spectrum. We adjust the radial velocity of the model spectrum to minimize  $\chi^2$ .
3. *Abundance.* We begin with the solar oxygen abundance scaled by the star's metallicity. We refine this value by searching over 2 dex of abundance space and minimizing  $\chi^2$ .

We terminate the iteration when the fits arrive at a stable solution or when we exceed 10 iterations.

## 6.4 Results

### 6.4.1 Carbon and Oxygen Abundances

We report  $[\text{O}/\text{H}]^2$  and  $[\text{C}/\text{H}]$  for 694 and 704 stars respectively. These are subsamples of our initial 1070 star sample and arise after we apply the following global cuts:

1.  $v \sin i$ . In rapidly rotating stars, our indicators can be polluted by the wings of neighboring lines due to rotational broadening. When this happens, the abundances of our elements of interest become degenerate with that of the polluting line. This effect sets in earlier for the [OI] line, which sits shoulder to shoulder between SiI and ScII features. We do not report oxygen or carbon abundances for stars with  $v \sin i$  greater than 7 and 15 km/s respectively.

---

<sup>2</sup> $[\text{X}/\text{H}] = \log \epsilon_X - \log \epsilon_{\text{X},\odot}$

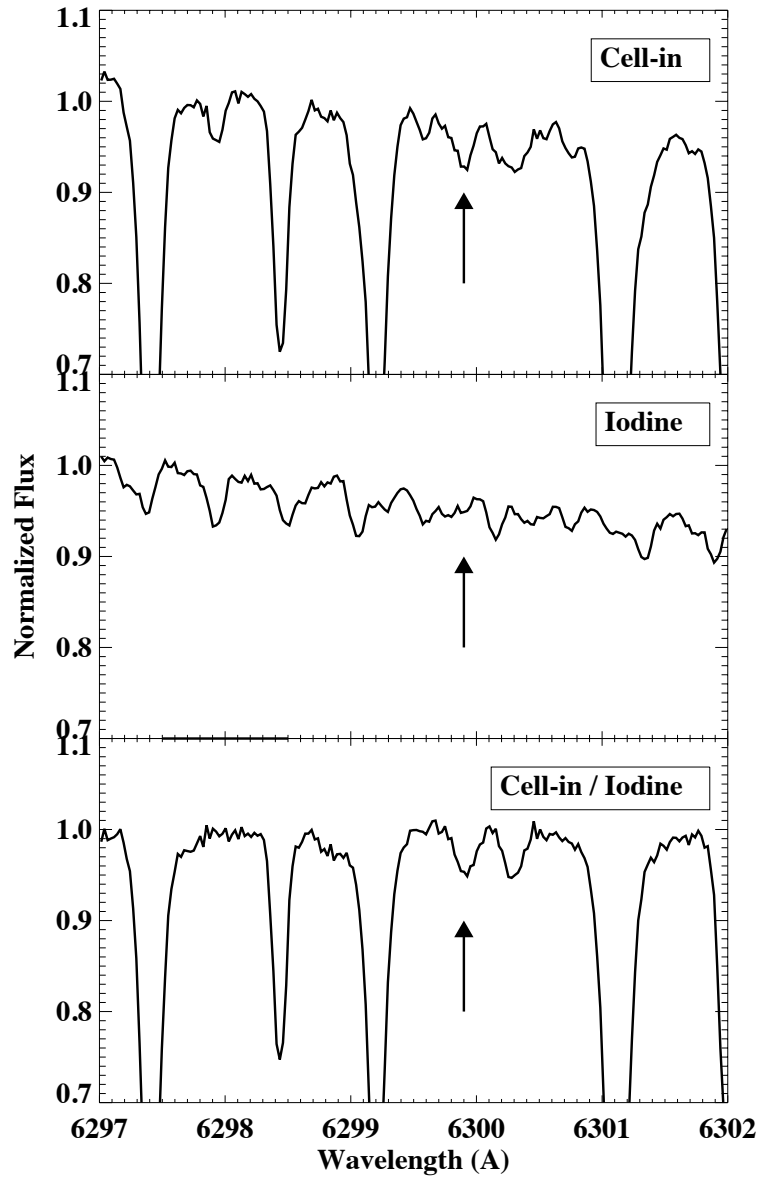


Figure 6.7: HD 148284 spectrum with iodine contamination (top), reference iodine observation (middle), and stellar spectrum divided by iodine spectrum (bottom). The arrow marks the [OI]/NiI blend. The iodine is removed to a level of  $\sim 1\%$  of the continuum intensity.

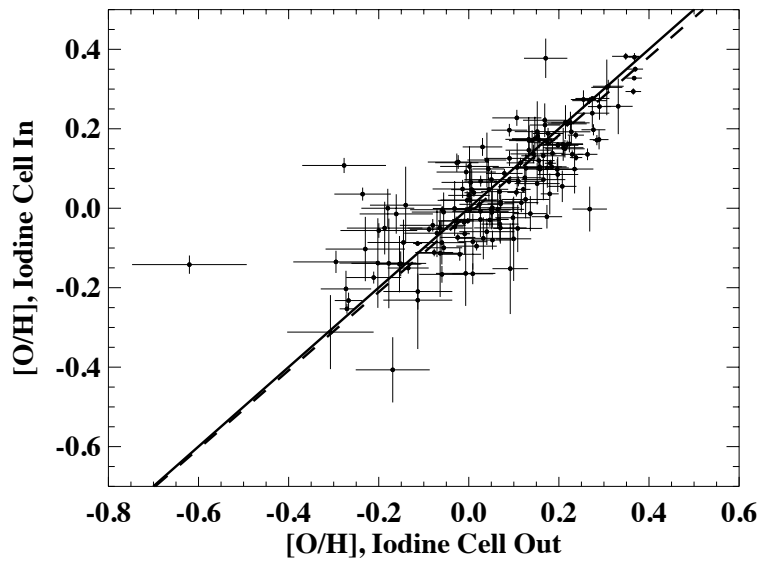


Figure 6.8: Comparison of oxygen abundances derived from spectra taken with the iodine cell in (vertical axis) to those taken with the iodine cell out (horizontal axis). The solid line corresponds to an equality of the two, while the dashed line shows the best fit to the points. Apparently the oxygen abundances derived from both types of spectra show no systematic difference, indicating that the removal of the iodine spectrum works without introducing a systematic error.

2.  $T_{\text{eff}}$ . The high excitation energy of the CI line (8.537 eV) means the line is very weak in cool stars. For example, at 5000K, the line depth in a solar analog is 1%. We do not report carbon abundances for stars cooler than 5300 K.
3. *Statistical scatter*. We choose to report abundances for stars where the scatter in derived abundance is less than 0.30 dex or, in other words, stars where our measurements are precise to a factor of 2. Our estimates of measurement precision are based on empirical scatter and a Monte Carlo analysis, which we describe in sections § 6.4.2 & § 6.4.3. While our measurement precision is based on a variety of factors including line depth and signal to noise, stars that fail this cut generally have sub-solar carbon and oxygen abundances.

With our large stellar sample, it is possible to detect and correct for systematic trends that would be invisible in smaller samples. Figure 6.9 shows carbon and oxygen abundances plotted against temperature. We believe that the Kurucz (1992) model atmospheres are most accurate for solar analogs and that errors in the atmosphere profile grows as we move away from  $T_{\text{eff}} = T_{\odot} = 5770$  K.

We model the systematic behavior of implied abundance with  $T_{\text{eff}}$  by fitting a cubic to the data. Simply subtracting out the cubic would artificially force the mean  $[X/H]$  to zero, but there is no reason why the mean disk abundance should be solar. Therefore, we let the solar abundance fix the constant term in the cubic by requiring the systematic correction be zero at 5770 K. This correction reaches 0.11 dex for oxygen and 0.15 dex for carbon. We have removed the temperature trend for all abundances quoted henceforth.

By removing abundance trends with  $T_{\text{eff}}$  for the sake of correcting errors in atmosphere models, we may have erased a real astrophysical trend of  $[X/H]$  with  $T_{\text{eff}}$ . For example, hotter stars are more massive and have shorter main sequence lifetimes than cool stars. Therefore, the hotter stars in our sample are on average younger and formed at a later time in the galactic chemical enrichment history. However, we chose to remove the  $T_{\text{eff}}$  trends because we believe uncertainties in atmospheric models are the dominant effect.

We report our temperature-corrected values for  $[O/H]$  and  $[C/H]$  with 85% and 15% confidence limits along with other stellar data in the Appendix. We summarize the statistical properties of derived abundances in Table 6.3 and show their distributions in Figure 6.10.

### 6.4.2 Random Errors

We use Monte Carlo bootstrapping to estimate random errors. We generate Monte Carlo spectra by scrambling the residuals from our fits and adding them back to the synthetic spectra. For each star we generate and refit 1000 Monte Carlo realizations of the spectrum. The resulting abundance distribution provides a good estimate of the true error distribution.

For some stars we have many independent spectra, allowing us to compute confidence limits of the oxygen abundances from them as an *empirical* measure of our internal errors. Figure 6.11 shows the length of the error bars computed empirically and from Monte Carlo for stars with more than 50 empirical fits. The error estimate from Monte Carlo tracks the

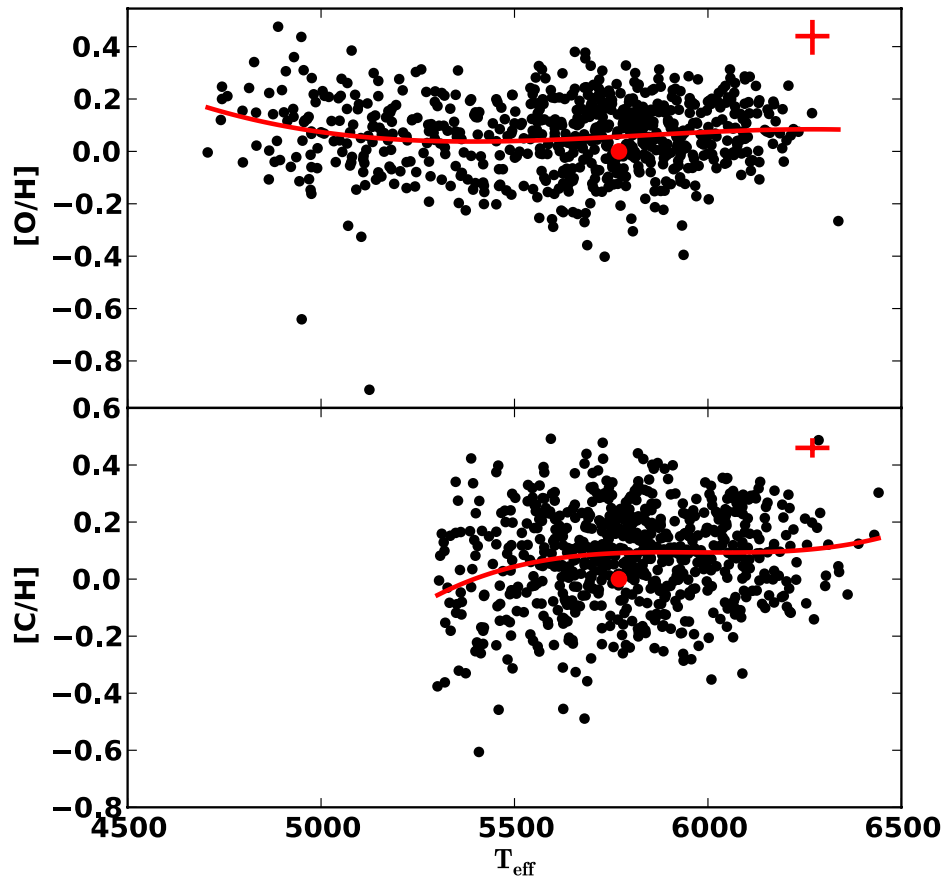


Figure 6.9: Plots showing systematic trends of  $[\text{O}/\text{H}]$  and  $[\text{C}/\text{H}]$  with temperature. The red line is the best fit cubic. Our correction for the  $T_{\text{eff}}$  trend is this cubic with the constant term chosen so that the correction is zero at  $T_{\text{eff}} = 5770$  K (large red dot). The crosses show the median errors.

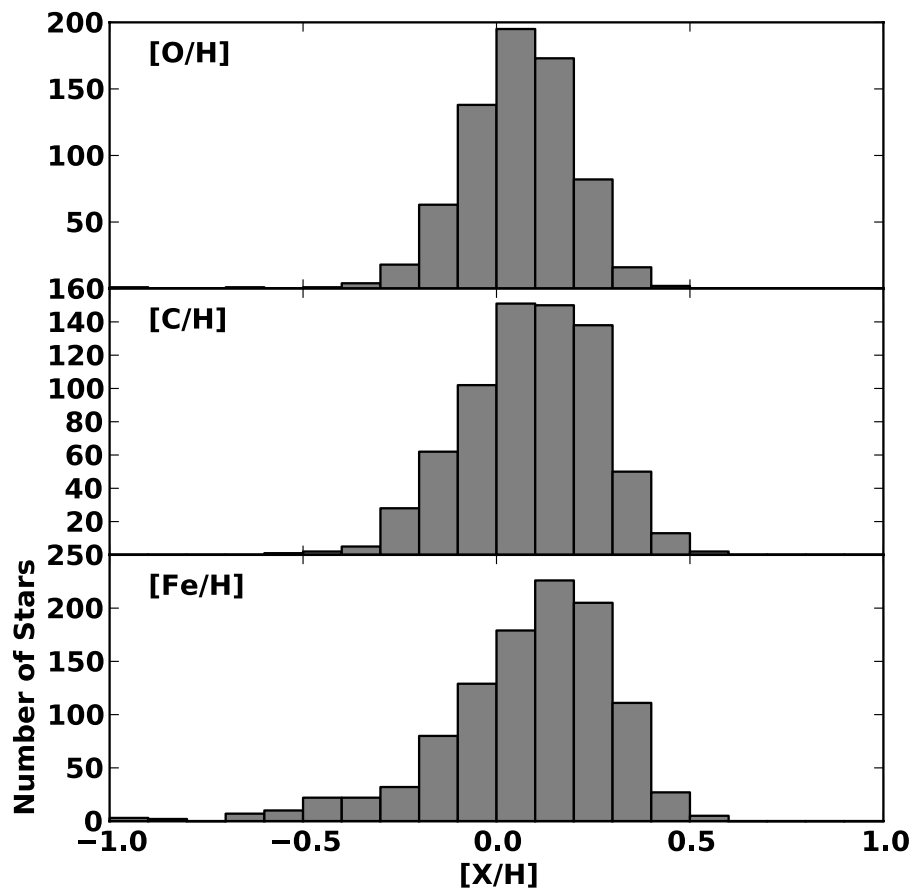


Figure 6.10: Distributions of [O/H], [C/H], and [Fe/H] for comparison.

Table 6.3: Summary of Derived Abundances.

	N	m (dex)	S (dex)	Min (dex)	Max (dex)
[O/H]	694	0.06	0.14	-0.91	0.43
[C/H]	704	0.09	0.17	-0.52	0.52
[Fe/H]	1070	0.07	0.27	-1.95	0.56

Note. — Here, N is the number of stars with determined abundances, m is the mean abundance, and S is the standard deviation of abundance distribution.

empirical scatter well, slightly overestimating it. This is due to systematic errors in our fits that appear as random errors when we scramble the residuals.

For stars with fewer than 20 observations, we adopt the Monte Carlo confidence intervals as our statistical error; for stars with 20 or more observations, we adopt the empirical confidence intervals. We diminish these errors by  $\sqrt{N_{obs}}$ . Futhuremore, we impose an error floor of 0.03 dex.

### 6.4.3 Nickel Systematics

Since we are deriving oxygen from a line that is blended with nickel, the errors in nickel abundance are covariant with errors in oxygen abundance. FV05 quote a uniform error of 0.03 dex for their nickel measurements. The amount that [OI] and NiI contribute to the blend is different for every star. Therefore, we evaluate the effect of the 0.03 dex error in nickel abundance on oxygen abundance on a star-by-star basis. We begin with a synthetic spectrum at our quoted oxygen abundance. We then refit the oxygen line to a spectrum with 0.03 dex more and 0.03 dex less nickel. These errors are added in quadrature to the statistical errors.

There are many other sources of systematic error in our abundance measurements such as inaccurate solar reference abundances, additional blends, and our assumption of LTE. However, these effects should be largely consistent between stars, so we expect them to contribute little to errors in our differential abundances.

### 6.4.4 Comparison with Literature

We compare our results with [Bensby et al. \(2005\)](#) and [Luck & Heiter \(2006\)](#). We report oxygen abundances for 16 stars analyzed by [Bensby et al. \(2005\)](#) and 67 stars analyzed

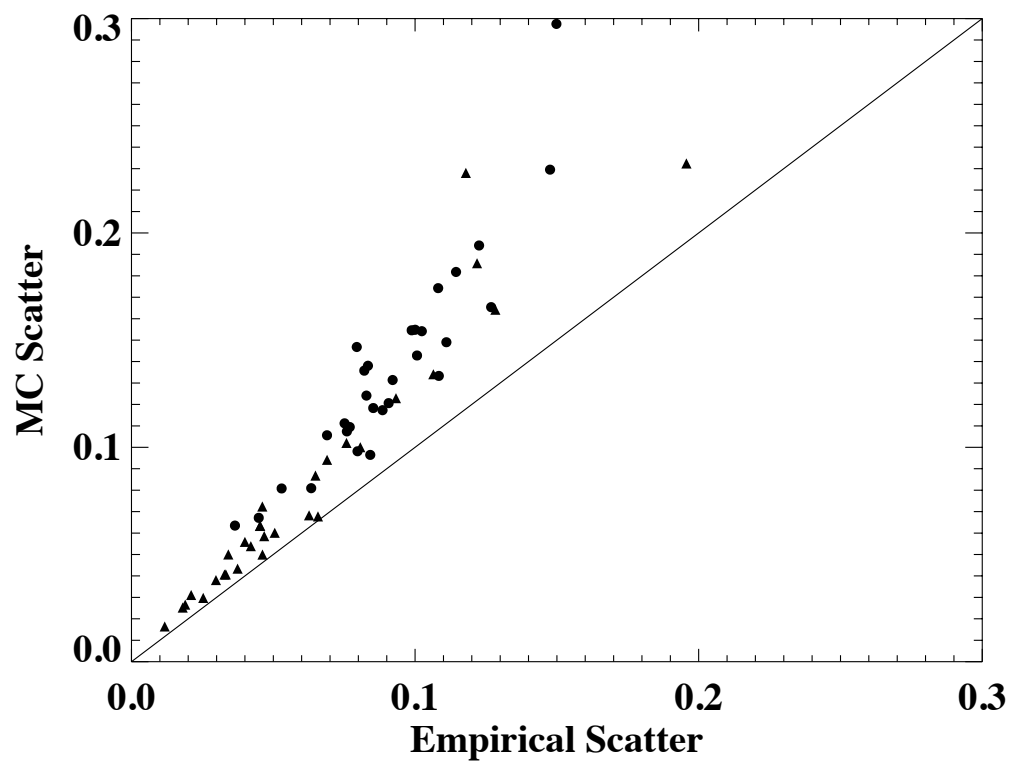


Figure 6.11: Scatter in MC simulations as a function of empirical scatter for stars with more than 50 observations. Oxygen and carbon measurements are represented by circles and triangles respectively. The solid line represents a 1:1 correlation.

by Luck & Heiter (2006). We plot the comparison in Figure 6.12. Our results track these comparison studies well. We recognize that the agreement is poorest for low values of  $[C/H]$ . This likely the result of less robust fits to stars with weaker carbon features.

The standard deviation of the differences in derived abundances is 0.08 dex for oxygen and 0.09 dex for carbon. Since Bensby et al. (2005) and Luck & Heiter (2006) use different instruments, spectral synthesizers, and fitting algorithms, it is unlikely there are common systematic errors. Therefore, the scatter in the differences can be interpreted as a measure of the typical combined statistical and systematic error. We cannot say how much of the observed scatter is due to our errors and those of the comparison studies.

### 6.4.5 Abundance Trends in the Thin and Thick Disks

The Milky Way is thought to be made up of three distinct star populations: The thin disk, thick disk, and the halo. Most of the stars in the local neighborhood belong to the thin disk, which has a scale height of 300 pc. The thick disk has a scale height of 1450 pc and is comprised of older, metal-poor stars.

Peek (2009) combined proper motion measurements from the *Hipparcos* catalog (ESA 1997) with radial velocity measurements from the Nidever et al. (2002), SPOCS, and N2K catalogs into three-dimensional space motions for 1025 of our 1070 program stars. Peek (2009) computed the probability of membership to each of the three populations in the manner of Bensby et al. (2003), Mishenina et al. (2004), and Reddy et al. (2006) for 900 of our 941 stars with measured carbon and oxygen. Our sample contains 847 thin disk stars, 16 thick disk stars, 12 halo stars, and 25 borderline stars (all three membership probabilities less than 0.7).

We plot  $[O/H]$  and  $[C/H]$  against  $[Fe/H]$  in Figure 6.13. We fit the trends with a line and list the best fit parameters in Table 6.4. If the scatter was purely statistical, we would expect our fits to have a reduced- $\sqrt{\chi^2} \sim 1$ . Our fits have reduced- $\sqrt{\chi^2} \sim 2$ , which suggests that some of the observed scatter is astrophysical. These main sequence stars have not begun to process heavy elements, so the ranges of C, O, and Fe ratios reflect the heterogeneous interstellar medium from which they formed.

We also plot  $[O/Fe]$  and  $[C/Fe]$  against  $[Fe/H]$  in Figure 6.14. The trends suggest that carbon and oxygen lagged behind iron production for much of the period of galactic chemical enrichment. These trends flatten out for high  $[Fe/H]$ . Due to the paucity of thick disk stars in our sample, we are cautious in interpreting its abundance trends. However, in the thick disk, oxygen seems to be enhanced relative to iron, a result also reported by Bensby et al. (2004). This enhancement in oxygen suggests that type II supernova played a more active role in enriching the thick disk.

### 6.4.6 Exoplanets

100 stars in our initial 1070 sample are known to host planets. Gonzalez (1997) measured relatively high stellar metallicity in the first four exoplanet host stars, and Santos et al.

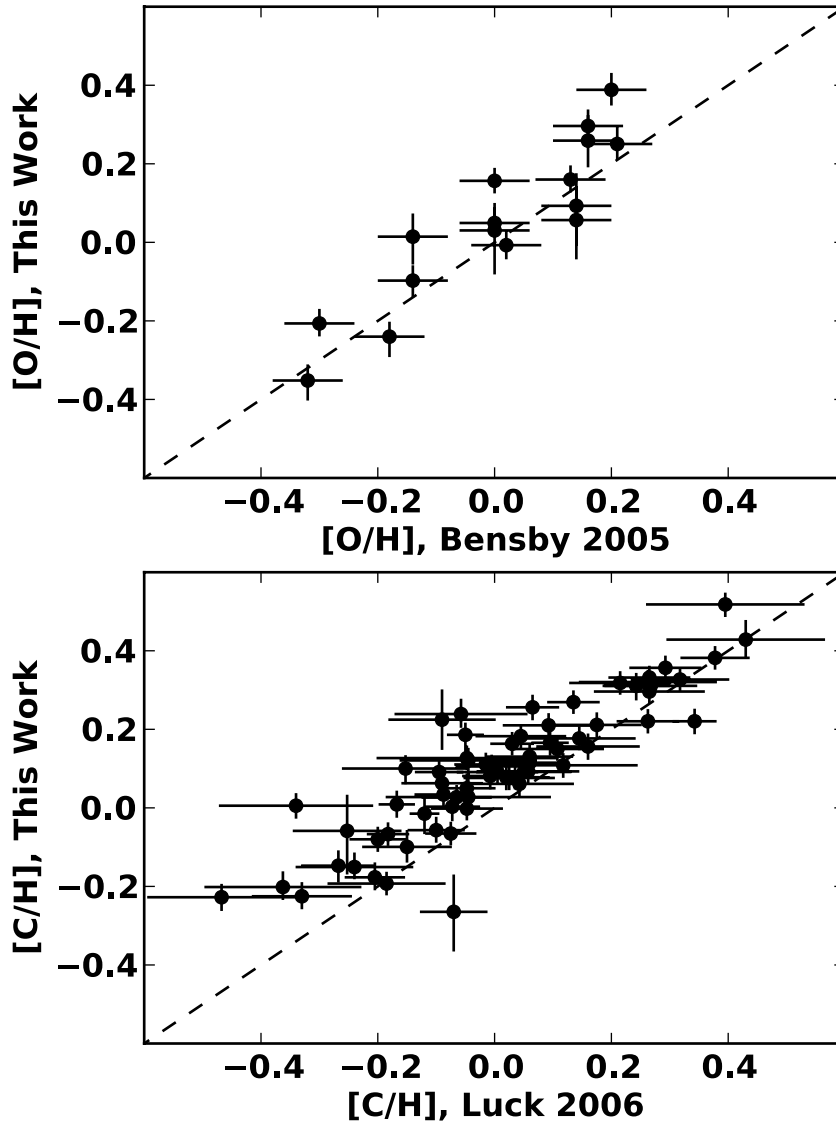


Figure 6.12: Comparison plots of abundances from this work against those of [Bensby et al. \(2005\)](#) and [Luck & Heiter \(2006\)](#). The line shows a 1:1 correlation. We note a systematic offset in the carbon comparison. This may stem from the fact that the two works use different indicators.

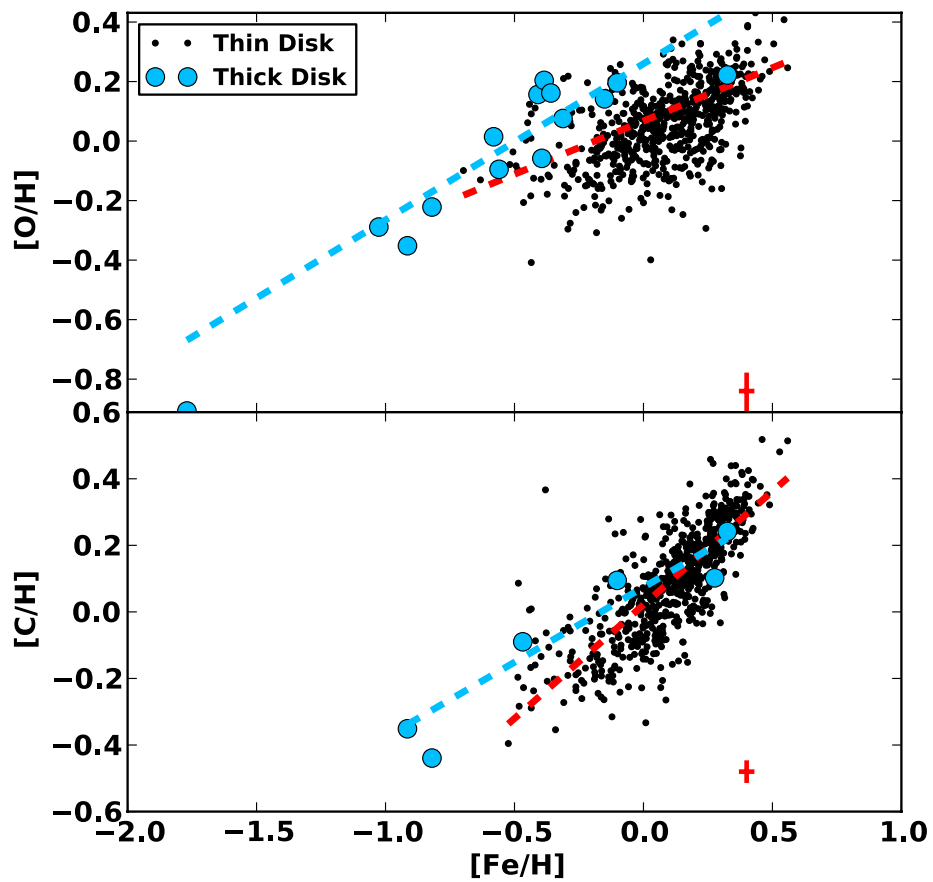


Figure 6.13: Carbon and oxygen abundance plotted against iron abundance. The black points are the thin disk stars; the blue points are the thick disk stars. The lines show the abundance ratios in 0.1 dex bins. The crosses show median uncertainties.

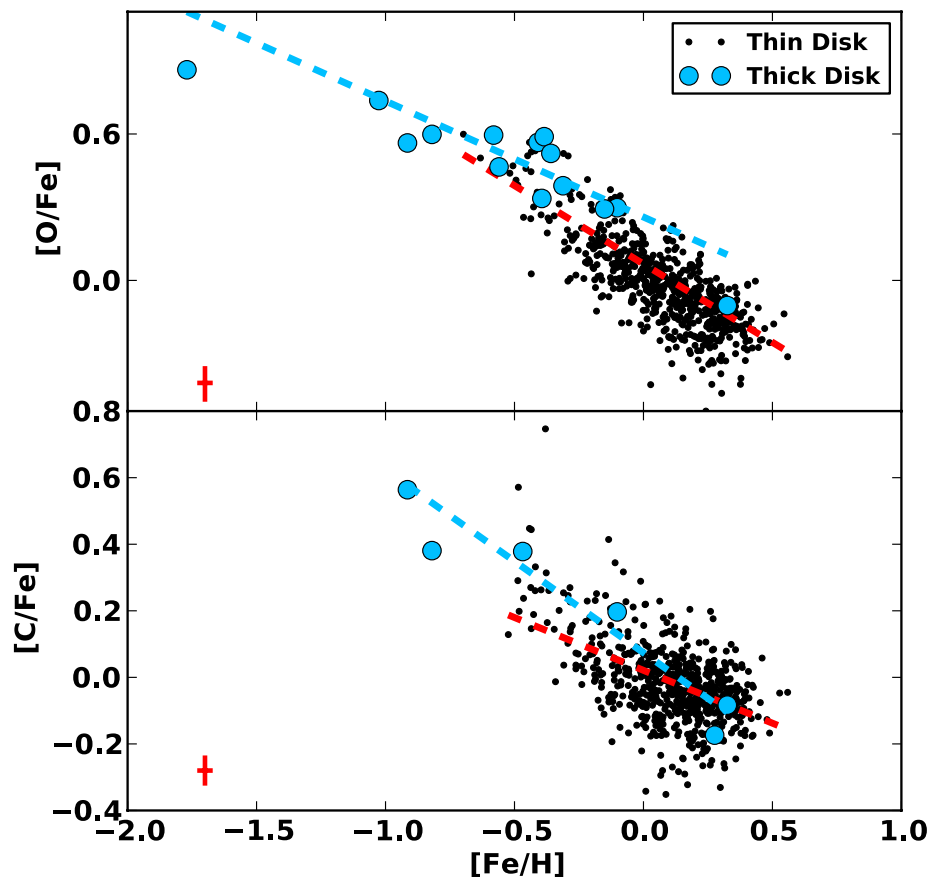


Figure 6.14: The ratios of carbon and oxygen to iron plotted against iron abundance. The black points are the thin disk stars; the blue points are the thin disk stars. The line shows the average ratios in 0.1 dex bins. The crosses show median uncertainties.

Table 6.4: Best fit parameters to abundance trends.

	Pop.	$m$	$b$	$\sqrt{\chi^2}$
[C/H]	thick	$0.450 \pm 0.074$	$0.074 \pm 0.035$	2.19
[C/H]	thin	$0.682 \pm 0.019$	$0.021 \pm 0.004$	2.52
[O/H]	thick	$0.525 \pm 0.081$	$0.260 \pm 0.047$	2.41
[O/H]	thin	$0.358 \pm 0.017$	$0.067 \pm 0.004$	1.66

Note. — We fit thin and thick disk abundance trends with the following function  $[X/H] = m [X/Fe] + b$ . The best fit parameters are listed above along with the reduced- $\sqrt{\chi^2}$ .

(2004) and Fischer & Valenti (2005) showed that the fraction of stars bearing planets increases rapidly above solar metallicity. In light of the correlation between C, O, and Fe, it is not surprising that hosts to exoplanets are enriched in carbon and oxygen relative to the comparison sample.

As shown in Table 6.5, the mean [O/H] of the planet host and comparison sample is 0.10 dex and 0.05 dex respectively. If we take the error on the mean abundance to be the standard deviation of derived abundances divided by the square root of the number of stars in each sample i.e.  $\sigma_{mean} = \frac{\text{Std. Dev.}}{\sqrt{N}}$ ,  $\sigma_{mean}$  for [O/H] is 0.01 dex. Carbon is also enriched in planet hosts where the mean [C/H] is 0.17 dex ( $\sigma_{mean} = 0.02$  dex) compared to 0.08 dex in the comparison sample with. For both carbon and oxygen, the mean abundance of the planet host sample is enriched by  $\sim 5\sigma$  compared to the non-host sample.

In Figure 6.15, we divide the stars into 0.1 dex bins in [X/H]. For each bin, we divide the number of planet-bearing stars by the total number of stars in the bin. As with iron, we observe an increase in planet occurrence rate as carbon and oxygen abundance increases. While there is a hint of a possible plateau or turnover at the highest abundance bins, these bins are dominated by small number statistics. The data are not inconsistent with a monotonic rise, within the errors. The possibility that very enriched systems inhibit planet formation is intriguing, and this parameter space warrants further exploration.

#### 6.4.7 $N_C/N_O$

We present the ratio of carbon to oxygen atoms,  $N_C/N_O$ <sup>3</sup> for 457 stars with reliable carbon and oxygen measurements as listed in the last column of Table 6.6 of the Appendix. Since we do not report carbon for stars cooler than 5300 K, our  $N_C/N_O$  measurements apply

<sup>3</sup> $N_C/N_O = 10^{\log \epsilon_C - \log \epsilon_O}$

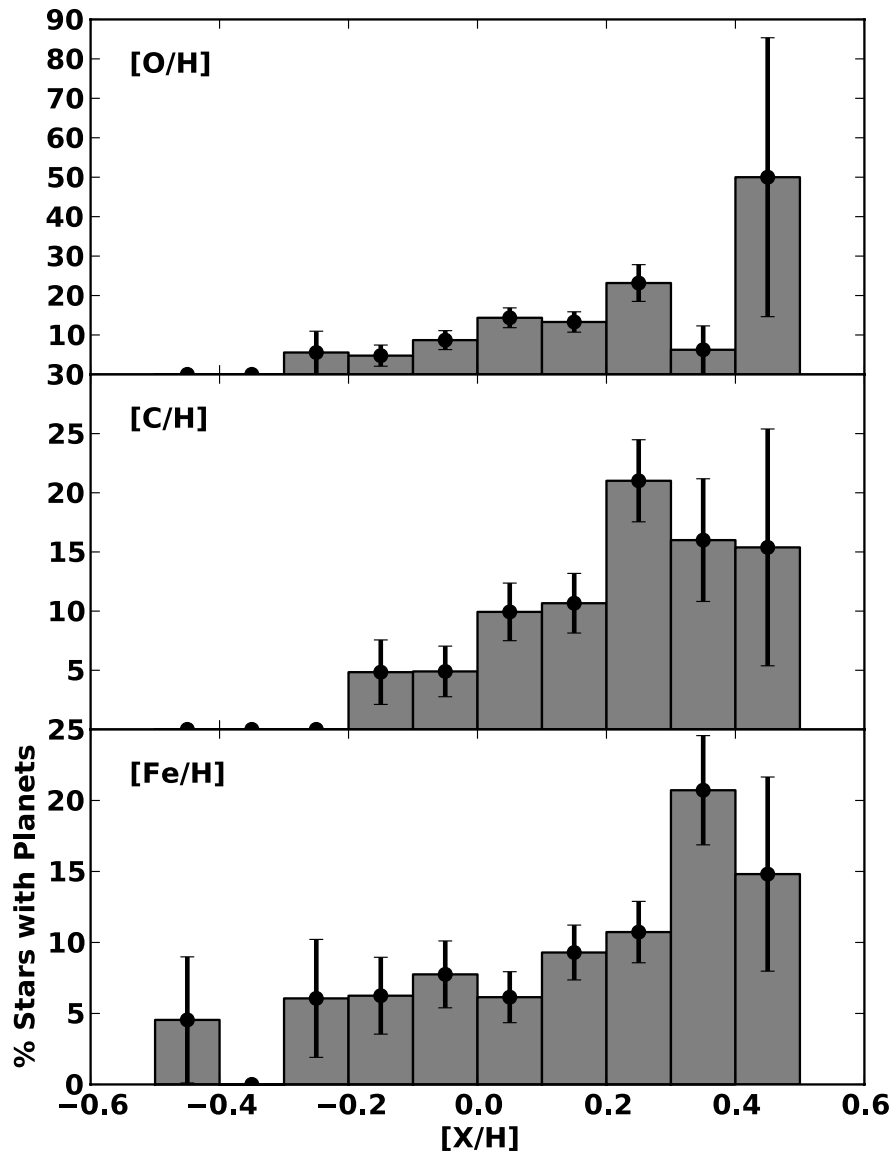


Figure 6.15: The percentage of stars with known planets for 0.1 dex bins in oxygen, carbon, and iron. The histograms are constructed from the 694, 704, and 1070 stars with reliable measurements of  $[O/H]$ ,  $[C/H]$ , and  $[Fe/H]$  respectively.

Table 6.5: Statistical abundance properties of stars with planets.

	Hosts				Non-Hosts			
	N	mean	Std. Dev.	$\sigma_{mean}$	N	mean	Std. Dev.	$\sigma_{mean}$
[O/H]	88	0.10	0.12	0.01	606	0.05	0.14	0.01
[C/H]	79	0.17	0.14	0.02	625	0.08	0.17	0.01
[Fe/H]	100	0.17	0.18	0.02	970	0.06	0.27	0.01

Note. — We list the number of stars, mean abundance (dex), standard deviation (dex), and error on the mean abundance (dex) for the host and non-host populations. The error on the mean abundance is computed by  $\sigma_{mean} = \frac{\text{Std. Dev.}}{\sqrt{N}}$ .

only to F and G spectral types. While there is a weak correlation between  $N_C/N_O$  and Fe at high [Fe/H], we note the large degree of scatter in  $N_C/N_O$ , which spans a wide range from 0.24 to 1.55.

We emphasize that our measurements of [C/H] and [O/H] are differential relative to solar and should be insensitive to revisions in the solar abundance distribution.  $N_C/N_O$  depends on our adopted solar abundances of oxygen (Scott et al. 2009) and carbon (Caffau et al. 2010). We believe the abundances of carbon and oxygen are known at the  $\sim 0.1$  dex level. Therefore, we expect revisions to the solar abundance distribution to systematically shift our  $N_C/N_O$  measurements by roughly  $\sim 10^{0.1}$  or  $\sim 25\%$

We measure 46 stars with  $N_C/N_O$  greater than 1.00. Given the size of our random errors as determined by the Monte Carlo analysis of § 6.4.2, very few of these stars are  $1\sigma$  detections of  $N_C/N_O > 1$ . However, since these errors are random, we believe our measurements accurately reflect the *distribution* of  $N_C/N_O$  in nearby disk stars. Neglecting the zero-point offsets discussed earlier, we measure  $N_C/N_O > 1$  for roughly 10% of nearby FG stars.

As noted by our anonymous reviewer, the CO molecule controls the equilibrium between carbon and oxygen in M dwarfs. It is believed that  $N_C/N_O > 1$  in M dwarfs results in an atmosphere rich in C<sub>2</sub>, while  $N_C/N_O < 1$  gives rise to TiO. We are unaware of M dwarfs with strong C<sub>2</sub> bands indicating  $N_C/N_O > 1$ . This suggests such a population is rare, assuming we understand the behavior of carbon-rich M dwarf atmospheres. We also note the additional complexities involved in modeling M star atmospheres. Abundance estimates in cool stars rely on opacity tables of H<sub>2</sub>O and other molecules that are not well understood at the temperatures probed by M star atmospheres. The fact that M stars are fully convective and have strong magnetic fields introduce additional complexities into model atmospheres.

Despite the uncertainties in accurately measuring  $N_C/N_O$ , we have characterized the distribution of  $N_C/N_O$  for an unprecedented number of FG stars. Furthermore, we have identified 46 stars have high  $N_C/N_O$ . Given the predictions regarding exotic planets that form in a carbon rich environment, these stars constitute important hosts for future work on

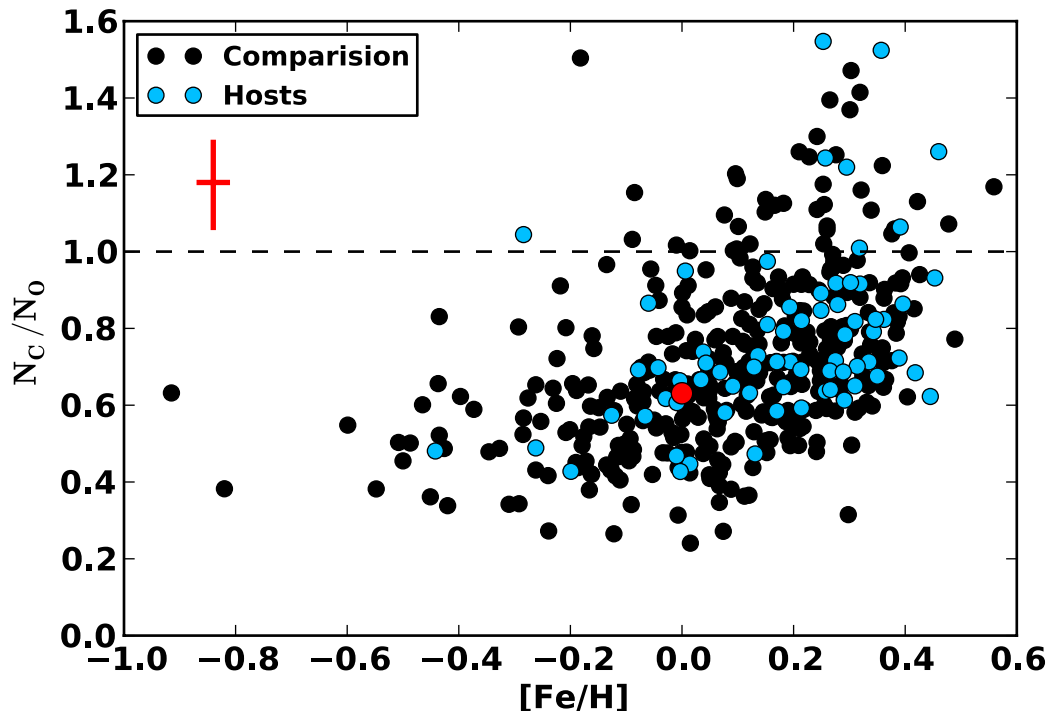


Figure 6.16:  $N_C/N_O$  as a function of iron abundance. The large red dot shows the solar values. The horizontal line shows equal carbon and oxygen.

their exoplanets and exozodiacal dust. Observations of dust with ALMA and JWST may be particularly valuable.

#### 6.4.8 WASP-12

WASP-12b, discovered by Hebb et al. (2009), is a transiting gas giant and a favorable target for atmosphere studies. Campo et al. (2011) and Croll et al. (2011) measured secondary eclipses of WASP-12b at wavelengths ranging from 1-8  $\mu\text{m}$ , which can be used to characterize the planet’s dayside emission spectrum. In a recent study, Madhusudhan et al. (2011) found that these measurements are best-described by atmosphere models with  $N_C/N_O \geq 1$  at 3 sigma significance.

We analyze WASP-12 identically to the 1070 star sample. With a V-mag of 11.69 (Hebb et al. 2009), WASP-12 is dimmest star in this work and our spectra have  $S/N \sim 50$ . However, we measured oxygen and carbon based on 9 and 7 spectra respectively. We find  $[O/H] = 0.29^{+0.06}_{-0.10}$ ,  $[C/H] = 0.10^{+0.04}_{-0.06}$ , and  $N_C/N_O = 0.40^{+0.11}_{-0.07}$  i.e., sub-solar.

If the composition of the host star truly reflects the material from which WASP-12b formed, our measurements suggest that WASP-12b does not have a carbon-dominated bulk

composition. It is possible that the planet acquired extra carbon at some point during its formation, or that the planet's nightside and/or interior are acting as a sink for oxygen, creating a carbon-rich dayside atmosphere while maintaining bulk  $N_C/N_O$  less than unity. In any case, this planet and its host star warrant further study.

## 6.5 Conclusion

We have presented oxygen and carbon abundances for 941 stars based on HIRES spectra gathered by the Keck telescope. We measure oxygen by fitting the reliable 6300 Å forbidden line with SME and self-consistently account for the significant nickel blend. Our carbon abundances are derived from the 6587 Å CI line. Our errors are based on a rigorous Monte Carlo treatment, and our measurements agree with values in the literature. Our sample is large enough to characterize and remove systematic trends due to  $T_{\text{eff}}$ . We see that carbon and oxygen are both enriched in stars with known planets. We see a significant number of stars with  $N_C/N_O$  exceeding unity, which supports the possibility that some stars host exotic carbon-rich planets. However, our measurement of sub-solar  $N_C/N_O$  for WASP-12, complicates the recent claim by [Madhusudhan et al. \(2011\)](#) that WASP-12b is a carbon world.

Table 6.6: Stellar Data.

Name <sup>a</sup> (HD)	$V^b$ (mag)	$d^b$ (pc)	$T^c$ (K)	$\log g^c$ (cgs)	Pop <sup>d</sup>	Host	[M/H] <sup>c,e</sup>	[Ni/H] <sup>c</sup>	$N_O$	[O/H] <sup>f</sup>	$N_C$	[C/H] <sup>f</sup>	C/O <sup>f</sup>
105	7.51	40	6126	4.65	dn	no	-0.02	0.02	0	...	4	$-0.04^{+0.04}_{-0.04}$	...
166	6.07	13	5577	4.58	dn	no	0.12	0.19	11	$-0.09^{+0.07}_{-0.08}$	7	$0.12^{+0.03}_{-0.04}$	$1.02^{+0.21}_{-0.19}$
377	7.59	39	5873	4.28	dn	no	0.11	0.12	0	...	10	$-0.09^{+0.03}_{-0.03}$	...
449	8.58	95	5860	4.40	dn	no	0.12	0.27	1	$0.23^{+0.07}_{-0.07}$	3	$0.38^{+0.03}_{-0.03}$	$0.90^{+0.16}_{-0.15}$
457	7.72	54	5897	4.07	dn	no	0.22	0.40	1	$0.10^{+0.08}_{-0.10}$	1	$0.35^{+0.03}_{-0.03}$	$1.11^{+0.26}_{-0.22}$
531B	8.65	50	5707	4.62	...	no	0.03	0.12	0	...	2	$-0.09^{+0.05}_{-0.06}$	...
691	7.95	34	5633	4.66	dn	no	0.20	0.31	0	...	2	$0.04^{+0.06}_{-0.05}$	...
804	8.18	51	5753	4.26	dn	no	-0.02	0.05	4	$-0.05^{+0.04}_{-0.05}$	0	...	...
1205	7.90	72	5848	4.29	...	no	0.15	0.36	10	$0.05^{+0.05}_{-0.07}$	6	$0.35^{+0.03}_{-0.03}$	$1.25^{+0.21}_{-0.17}$
1388	6.51	26	5952	4.42	dn	no	-0.04	0.04	1	$0.07^{+0.09}_{-0.11}$	3	$-0.05^{+0.04}_{-0.04}$	$0.48^{+0.13}_{-0.11}$
1461	6.47	23	5765	4.42	dn	yes	0.15	0.30	276	$0.06^{+0.05}_{-0.04}$	294	$0.16^{+0.03}_{-0.03}$	$0.79^{+0.09}_{-0.10}$
1497	8.19	70	5773	4.10	...	no	0.19	0.34	2	$-0.02^{+0.09}_{-0.07}$	1	$0.11^{+0.03}_{-0.03}$	$0.85^{+0.15}_{-0.19}$
1605	7.52	84	5079	3.76	...	no	0.18	0.27	13	$0.38^{+0.03}_{-0.03}$	0	...	...
2025	7.92	18	4865	4.61	dn	no	-0.27	-0.26	1	$-0.16^{+0.04}_{-0.04}$	0	...	...
2589	6.18	39	5120	3.96	dn	no	-0.12	0.02	2	$0.19^{+0.04}_{-0.04}$	0	...	...
3404	7.94	72	5405	4.01	dn	no	0.12	0.32	4	$0.15^{+0.05}_{-0.05}$	5	$0.20^{+0.03}_{-0.03}$	$0.71^{+0.10}_{-0.10}$
3545	8.57	...	4814	2.74	...	no	0.01	0.13	4	$0.17^{+0.03}_{-0.04}$	0	...	...
3578	9.71	92	6022	4.36	dn	no	-0.04	0.09	3	$-0.08^{+0.09}_{-0.14}$	3	$0.04^{+0.03}_{-0.03}$	$0.84^{+0.27}_{-0.19}$
3592	8.76	78	5904	4.39	dn	no	0.30	0.52	3	$0.15^{+0.07}_{-0.09}$	0	...	...
3651	5.88	11	5221	4.45	dn	yes	0.16	0.24	2	$0.07^{+0.08}_{-0.08}$	0	...	...
3684	7.35	91	6151	3.76	...	no	0.13	0.26	0	...	2	$0.18^{+0.03}_{-0.03}$	...
3795	6.14	28	5369	4.16	dk	no	-0.41	-0.46	1	$0.01^{+0.06}_{-0.07}$	0	...	...
4113	7.88	44	5753	4.33	...	yes	0.28	0.46	4	$-0.06^{+0.08}_{-0.10}$	4	$0.10^{+0.04}_{-0.04}$	$0.92^{+0.23}_{-0.19}$
4203	8.70	77	5702	4.36	dn	yes	0.33	0.55	3	$0.21^{+0.10}_{-0.11}$	9	$0.38^{+0.03}_{-0.03}$	$0.93^{+0.24}_{-0.24}$
4208	7.78	32	5600	4.52	dn	yes	-0.26	-0.23	1	$-0.28^{+0.19}_{-0.29}$	2	$-0.06^{+0.06}_{-0.05}$	$1.04^{+0.71}_{-0.49}$

Table 6.6 (cont'd): Stellar Data.

Name <sup>a</sup> (HD)	$V^b$ (mag)	$d^b$ (pc)	$T^c$ (K)	$\log g^c$ (cgs)	Pop <sup>d</sup>	Host	[M/H] <sup>c,e</sup>	[Ni/H] <sup>c</sup>	$N_O$	[O/H] <sup>f</sup>	$N_C$	[C/H] <sup>f</sup>	C/O <sup>f</sup>
4256	8.03	22	4930	4.80	dn	no	0.22	0.40	37	$0.33^{+0.04}_{-0.03}$	0	...	...
4307	6.15	31	5839	4.10	dn	no	-0.18	-0.14	33	$-0.03^{+0.03}_{-0.03}$	37	$-0.19^{+0.03}_{-0.03}$	$0.44^{+0.04}_{-0.04}$
4614	3.46	5	5941	4.44	dn	no	-0.17	-0.19	5	$-0.00^{+0.06}_{-0.06}$	39	$-0.15^{+0.04}_{-0.03}$	$0.45^{+0.07}_{-0.07}$
4628	5.74	7	4944	4.51	dn	no	-0.19	-0.22	53	$-0.14^{+0.04}_{-0.03}$	0	...	...
4747	7.15	18	5335	4.64	dn	no	-0.25	-0.21	12	$-0.11^{+0.05}_{-0.04}$	19	$-0.06^{+0.05}_{-0.05}$	$0.72^{+0.11}_{-0.12}$
4915	6.98	22	5650	4.58	dn	no	-0.18	-0.16	30	$-0.06^{+0.04}_{-0.04}$	39	$-0.20^{+0.03}_{-0.03}$	$0.45^{+0.05}_{-0.06}$
5133	7.15	14	4968	4.80	dn	no	-0.13	-0.03	2	$0.11^{+0.05}_{-0.04}$	0	...	...
5319	8.05	100	5053	3.58	dn	yes	0.16	0.24	36	$0.27^{+0.03}_{-0.03}$	0	...	...
5372	7.53	41	5877	4.40	dn	no	0.18	0.32	1	$0.16^{+0.08}_{-0.09}$	1	$0.20^{+0.03}_{-0.03}$	$0.68^{+0.15}_{-0.14}$
5470	8.36	67	5966	4.32	dn	no	0.20	0.34	2	$0.16^{+0.07}_{-0.09}$	3	$0.22^{+0.03}_{-0.03}$	$0.72^{+0.16}_{-0.12}$
5946	8.94	91	5577	4.00	dn	no	0.32	0.48	4	$0.14^{+0.06}_{-0.09}$	4	$0.40^{+0.03}_{-0.04}$	$1.16^{+0.26}_{-0.17}$
6512	8.15	47	5802	4.25	dn	no	0.09	0.23	1	$0.13^{+0.09}_{-0.11}$	2	$0.19^{+0.03}_{-0.04}$	$0.71^{+0.18}_{-0.15}$
6558	8.20	73	6086	4.26	dn	no	0.19	0.35	0	...	2	$0.28^{+0.03}_{-0.03}$	...
6697	8.03	59	5821	4.38	dn	no	0.23	0.46	1	$0.25^{+0.10}_{-0.12}$	2	$0.32^{+0.05}_{-0.04}$	$0.74^{+0.22}_{-0.19}$
6734	6.44	46	5067	3.81	dk	no	-0.28	-0.29	7	$0.16^{+0.03}_{-0.03}$	0	...	...
6963	7.66	26	5495	4.54	dn	no	-0.18	-0.17	0	...	2	$-0.26^{+0.09}_{-0.15}$	...
7510	7.63	58	5485	3.90	dn	no	0.13	0.26	0	...	1	$0.16^{+0.03}_{-0.03}$	...
7924	7.17	16	5177	4.58	dn	yes	-0.12	-0.14	151	$-0.05^{+0.04}_{-0.03}$	0	...	...
8038	8.41	52	5689	4.51	dn	no	0.11	0.23	0	...	2	$0.12^{+0.04}_{-0.04}$	...
8328	8.28	78	5817	4.19	dn	no	0.29	0.49	2	$0.17^{+0.06}_{-0.07}$	1	$0.32^{+0.03}_{-0.03}$	$0.88^{+0.16}_{-0.15}$
8446	8.16	74	5854	4.10	dn	no	0.22	0.42	4	$0.01^{+0.07}_{-0.08}$	1	$0.24^{+0.04}_{-0.04}$	$1.07^{+0.22}_{-0.20}$
8574	7.12	44	6050	4.21	dn	yes	-0.01	0.05	3	$0.02^{+0.08}_{-0.10}$	5	$0.00^{+0.03}_{-0.04}$	$0.61^{+0.16}_{-0.12}$
8648	7.38	39	5790	4.34	dn	no	0.14	0.26	3	$0.13^{+0.05}_{-0.06}$	1	$0.18^{+0.04}_{-0.04}$	$0.71^{+0.11}_{-0.11}$
8765	8.14	75	5590	4.24	dn	no	0.14	0.24	0	...	10	$0.25^{+0.03}_{-0.03}$	...
8828	7.96	29	5413	4.42	dn	no	-0.05	-0.10	6	$-0.00^{+0.05}_{-0.05}$	22	$-0.18^{+0.03}_{-0.03}$	$0.42^{+0.06}_{-0.06}$

Table 6.6 (cont'd): Stellar Data.

Name <sup>a</sup> (HD)	$V^b$ (mag)	$d^b$ (pc)	$T^c$ (K)	$\log g^c$ (cgs)	Pop <sup>d</sup>	Host	[M/H] <sup>c,e</sup>	[Ni/H] <sup>c</sup>	$N_O$	[O/H] <sup>f</sup>	$N_C$	[C/H] <sup>f</sup>	C/O <sup>f</sup>
8859	8.41	40	5505	4.41	dn	no	-0.06	-0.04	0	...	2	$-0.01^{+0.04}_{-0.04}$	...
8907	6.66	34	6204	4.36	dn	no	-0.07	-0.09	0	...	3	$-0.10^{+0.04}_{-0.05}$	...
9070	7.93	42	5657	4.36	dn	no	0.23	0.40	0	...	2	$0.23^{+0.03}_{-0.03}$	...
9081	8.13	83	5752	4.16	dn	no	0.22	0.43	1	$0.20^{+0.07}_{-0.08}$	1	$0.17^{+0.04}_{-0.04}$	$0.60^{+0.12}_{-0.11}$
9113	9.23	...	6286	4.29	...	no	0.35	0.62	0	...	2	$0.47^{+0.04}_{-0.03}$	...
9407	6.52	20	5657	4.49	dn	no	0.00	0.10	143	$0.07^{+0.04}_{-0.04}$	89	$0.08^{+0.03}_{-0.03}$	$0.65^{+0.07}_{-0.07}$
9472	7.63	33	5867	4.67	dn	no	-0.00	0.02	3	$0.06^{+0.08}_{-0.12}$	2	$-0.12^{+0.07}_{-0.07}$	$0.41^{+0.14}_{-0.10}$
9540	6.97	19	5462	4.56	dn	no	-0.04	-0.01	1	$0.00^{+0.07}_{-0.08}$	1	$-0.08^{+0.05}_{-0.06}$	$0.52^{+0.12}_{-0.10}$
9562	5.75	29	5939	4.13	dn	no	0.19	0.36	1	$0.06^{+0.09}_{-0.10}$	1	$0.16^{+0.03}_{-0.03}$	$0.79^{+0.19}_{-0.17}$
9826	4.10	13	6213	4.25	dn	yes	0.12	0.21	0	...	1	$0.11^{+0.03}_{-0.03}$	...
9986	6.77	25	5805	4.45	dn	no	0.05	0.13	4	$0.06^{+0.06}_{-0.07}$	11	$0.03^{+0.03}_{-0.03}$	$0.59^{+0.10}_{-0.09}$
10015	8.65	38	5236	4.25	dn	no	0.26	0.32	4	$0.14^{+0.06}_{-0.07}$	0	...	...
10145	7.70	36	5638	4.44	dn	no	0.00	0.03	0	...	4	$0.04^{+0.03}_{-0.03}$	...
10195	7.53	47	5998	4.27	dn	no	0.04	0.05	0	...	1	$0.06^{+0.05}_{-0.05}$	...
10353	8.48	51	5726	4.54	dn	no	-0.06	-0.09	0	...	4	$-0.22^{+0.04}_{-0.04}$	...
10442	7.84	...	5045	3.48	...	no	-0.01	0.12	7	$0.19^{+0.03}_{-0.03}$	0	...	...
10476	5.24	7	5181	4.53	dn	no	-0.07	-0.00	30	$0.02^{+0.04}_{-0.04}$	0	...	...
10697	6.27	32	5680	4.12	dn	yes	0.10	0.26	1	$0.07^{+0.07}_{-0.08}$	1	$0.12^{+0.04}_{-0.04}$	$0.71^{+0.15}_{-0.13}$
10700	3.49	3	5283	4.58	dn	no	-0.36	-0.41	142	$-0.08^{+0.03}_{-0.03}$	0	...	...
10780	5.63	9	5327	4.54	dn	no	-0.06	0.04	6	$0.10^{+0.05}_{-0.05}$	14	$0.10^{+0.03}_{-0.04}$	$0.64^{+0.09}_{-0.09}$
11020	8.98	38	5173	4.62	dn	no	-0.17	-0.15	1	$0.05^{+0.05}_{-0.06}$	0	...	...
11271	8.45	85	6095	4.33	dn	no	0.16	0.33	1	$0.16^{+0.06}_{-0.06}$	3	$0.16^{+0.03}_{-0.03}$	$0.64^{+0.10}_{-0.10}$
11506	7.51	53	6011	4.29	dn	yes	0.17	0.38	34	$-0.03^{+0.06}_{-0.07}$	33	$0.26^{+0.03}_{-0.03}$	$1.22^{+0.20}_{-0.19}$
11731	8.24	72	5845	4.26	dn	no	0.23	0.43	0	...	4	$0.31^{+0.03}_{-0.03}$	...
11791	8.86	109	5632	4.09	dn	no	0.07	0.12	3	$0.08^{+0.05}_{-0.04}$	1	$-0.06^{+0.07}_{-0.08}$	$0.46^{+0.10}_{-0.09}$

Table 6.6 (cont'd): Stellar Data.

Name <sup>a</sup> (HD)	$V^b$ (mag)	$d^b$ (pc)	$T^c$ (K)	$\log g^c$ (cgs)	Pop <sup>d</sup>	Host	[M/H] <sup>c,e</sup>	[Ni/H] <sup>c</sup>	$N_O$	[O/H] <sup>f</sup>	$N_C$	[C/H] <sup>f</sup>	C/O <sup>f</sup>
11850	7.85	33	5663	4.55	dn	no	0.04	0.07	5	$0.14^{+0.09}_{-0.11}$	3	$-0.08^{+0.04}_{-0.04}$	$0.38^{+0.10}_{-0.09}$
11997	9.19	40	4986	4.43	dn	no	0.14	0.12	2	$0.17^{+0.05}_{-0.05}$	0	...	...
12051	7.14	24	5495	4.62	dn	no	0.14	0.29	54	$0.23^{+0.04}_{-0.04}$	26	$0.25^{+0.03}_{-0.03}$	$0.65^{+0.08}_{-0.08}$
12165	8.85	91	5799	4.20	dn	no	0.04	0.10	0	...	4	$0.08^{+0.03}_{-0.04}$	...
12484	8.18	47	5951	4.60	dn	no	0.10	0.11	0	...	6	$-0.15^{+0.04}_{-0.10}$	...
12661	7.43	37	5743	4.42	dn	yes	0.31	0.50	12	$0.17^{+0.07}_{-0.08}$	7	$0.28^{+0.03}_{-0.03}$	$0.82^{+0.16}_{-0.14}$
12846	6.89	23	5626	4.42	dn	no	-0.20	-0.21	34	$-0.11^{+0.04}_{-0.04}$	68	$-0.12^{+0.03}_{-0.03}$	$0.62^{+0.07}_{-0.07}$
13043	6.88	36	5897	4.27	dn	no	0.06	0.17	0	...	68	$0.09^{+0.03}_{-0.03}$	...
13345	7.38	58	6052	4.04	...	no	0.18	0.33	1	$0.07^{+0.12}_{-0.14}$	1	$0.24^{+0.04}_{-0.03}$	$0.91^{+0.31}_{-0.26}$
13357	7.63	48	5696	4.47	dn	no	-0.02	0.01	1	$-0.19^{+0.08}_{-0.12}$	3	$0.01^{+0.03}_{-0.03}$	$1.02^{+0.29}_{-0.21}$
13361	8.23	74	5848	4.22	dn	no	0.18	0.35	0	...	1	$0.19^{+0.04}_{-0.04}$	...
13579	7.13	23	5211	4.59	dn	no	0.26	0.43	3	$0.24^{+0.07}_{-0.07}$	0	...	...
13584	8.36	98	5020	3.56	dn	no	-0.07	0.07	1	$0.19^{+0.04}_{-0.04}$	0	...	...
13612B	7.56	124	5741	4.50	dk/h	no	0.10	0.21	2	$0.09^{+0.08}_{-0.09}$	0	...	...
13773	8.67	116	6172	4.20	...	no	0.25	0.48	0	...	2	$0.31^{+0.03}_{-0.03}$	...
13931	7.61	45	5830	4.30	dn	yes	0.02	0.10	12	$0.07^{+0.05}_{-0.05}$	16	$0.10^{+0.03}_{-0.03}$	$0.67^{+0.09}_{-0.09}$
13999	8.33	79	5798	4.17	dn	no	-0.08	-0.07	2	$0.03^{+0.05}_{-0.05}$	1	$-0.24^{+0.10}_{-0.12}$	$0.34^{+0.10}_{-0.09}$
14223	9.52	...	5943	3.91	...	no	0.11	0.23	0	...	1	$0.23^{+0.04}_{-0.04}$	...
14374	8.48	39	5422	4.45	dn	no	-0.00	0.02	1	$-0.14^{+0.14}_{-0.19}$	3	$0.02^{+0.04}_{-0.10}$	$0.91^{+0.46}_{-0.30}$
14412	6.33	12	5374	4.69	dn	no	-0.45	-0.43	48	$-0.21^{+0.04}_{-0.03}$	58	$-0.23^{+0.03}_{-0.04}$	$0.60^{+0.07}_{-0.07}$
14655	8.13	101	5886	4.11	dn	no	0.11	0.27	28	$0.17^{+0.04}_{-0.04}$	36	$0.10^{+0.03}_{-0.03}$	$0.54^{+0.06}_{-0.06}$
15335	5.89	30	5891	4.07	dn	no	-0.20	-0.11	0	...	3	$-0.06^{+0.03}_{-0.03}$	...
15337	9.10	41	5919	4.14	...	no	0.09	0.29	1	$0.18^{+0.06}_{-0.07}$	0	...	...
16141	6.83	35	5794	4.22	dn	yes	0.09	0.22	8	$0.13^{+0.04}_{-0.05}$	7	$0.09^{+0.03}_{-0.03}$	$0.58^{+0.08}_{-0.07}$
16160	5.79	7	4866	4.66	dn	no	-0.00	-0.03	12	$0.17^{+0.04}_{-0.04}$	0	...	...

Table 6.6 (cont'd): Stellar Data.

Name <sup>a</sup> (HD)	$V^b$ (mag)	$d^b$ (pc)	$T^c$ (K)	$\log g^c$ (cgs)	Pop <sup>d</sup>	Host	[M/H] <sup>c,e</sup>	[Ni/H] <sup>c</sup>	$N_O$	[O/H] <sup>f</sup>	$N_C$	[C/H] <sup>f</sup>	C/O <sup>f</sup>
16249	9.78	103	5983	4.39	dn	no	0.08	0.18	3	$0.01^{+0.08}_{-0.10}$	3	$0.06^{+0.03}_{-0.03}$	$0.70^{+0.16}_{-0.14}$
16275	8.66	74	5839	4.39	dn	no	0.24	0.42	2	$0.13^{+0.09}_{-0.11}$	1	$0.23^{+0.03}_{-0.03}$	$0.79^{+0.21}_{-0.18}$
16287	8.10	24	5075	4.67	dn	no	0.08	0.26	1	$0.07^{+0.12}_{-0.20}$	0	...	...
16297	8.38	39	5516	4.65	...	no	0.02	0.09	1	$0.12^{+0.09}_{-0.13}$	0	...	...
16397	7.36	35	5788	4.50	dn/dk	no	-0.35	-0.41	2	$-0.13^{+0.06}_{-0.07}$	2	$-0.23^{+0.04}_{-0.04}$	$0.50^{+0.09}_{-0.08}$
16417	5.78	25	5817	4.17	dn	yes	0.07	0.21	0	...	18	$0.09^{+0.03}_{-0.03}$	...
16623	8.76	65	5819	4.49	dn/dk	no	-0.25	-0.35	1	$0.07^{+0.06}_{-0.08}$	2	$-0.18^{+0.04}_{-0.04}$	$0.36^{+0.08}_{-0.06}$
16760	8.70	50	5479	4.21	dn	yes	0.00	-0.03	14	$-0.13^{+0.06}_{-0.06}$	16	$-0.09^{+0.03}_{-0.03}$	$0.70^{+0.11}_{-0.11}$
17156	8.17	78	6019	4.22	dn	yes	0.14	0.31	16	$0.05^{+0.05}_{-0.04}$	38	$0.16^{+0.03}_{-0.03}$	$0.82^{+0.10}_{-0.11}$
17190	7.89	25	5142	4.40	dn	no	-0.10	-0.07	2	$-0.10^{+0.05}_{-0.05}$	0	...	...
17354	7.78	60	5950	4.35	dn	no	0.34	0.62	1	$0.27^{+0.07}_{-0.09}$	0	...	...
18143	7.52	22	5148	4.55	dn	no	0.21	0.34	27	$0.22^{+0.05}_{-0.05}$	0	...	...
18445	7.84	25	4894	4.57	dn	no	-0.07	-0.07	3	$-0.08^{+0.06}_{-0.07}$	0	...	...
18632	7.97	23	5088	4.42	dn	no	0.18	0.24	1	$0.21^{+0.09}_{-0.12}$	0	...	...
18702	8.11	32	5249	4.43	dn/dk	no	0.13	0.20	3	$0.14^{+0.06}_{-0.07}$	0	...	...
18747	8.16	85	5008	3.71	dn	no	-0.03	0.01	2	$0.05^{+0.04}_{-0.04}$	0	...	...
18803	6.62	21	5638	4.45	dn	no	0.09	0.19	32	$0.04^{+0.04}_{-0.04}$	62	$0.12^{+0.03}_{-0.03}$	$0.76^{+0.09}_{-0.09}$
18975	7.51	53	6337	4.35	dn	no	0.10	0.25	1	$-0.29^{+0.16}_{-0.29}$	1	$0.02^{+0.03}_{-0.03}$	$1.30^{+0.88}_{-0.48}$
18993	8.23	64	5805	4.30	...	no	0.13	0.25	2	$0.01^{+0.08}_{-0.17}$	2	$0.14^{+0.03}_{-0.03}$	$0.85^{+0.33}_{-0.17}$
19034	8.08	35	5470	4.63	dn	no	-0.30	-0.36	0	...	1	$0.09^{+0.04}_{-0.05}$	...
19056	8.87	81	5866	4.32	dn	no	0.15	0.34	3	$-0.00^{+0.07}_{-0.09}$	0	...	...
19308	7.36	42	5807	4.34	dn	no	0.11	0.23	1	$0.10^{+0.08}_{-0.10}$	3	$0.20^{+0.04}_{-0.03}$	$0.79^{+0.19}_{-0.17}$
19373	4.05	10	6032	4.31	dn	no	0.13	0.26	64	$0.15^{+0.04}_{-0.03}$	107	$0.12^{+0.03}_{-0.03}$	$0.58^{+0.06}_{-0.06}$
19467	6.97	31	5715	4.44	dn	no	-0.09	-0.06	3	$0.16^{+0.05}_{-0.04}$	3	$0.10^{+0.03}_{-0.03}$	$0.54^{+0.06}_{-0.08}$
19502	8.54	...	5870	4.34	...	no	0.34	0.66	1	$0.17^{+0.11}_{-0.13}$	1	$0.40^{+0.03}_{-0.03}$	$1.07^{+0.33}_{-0.29}$

Table 6.6 (cont'd): Stellar Data.

Name <sup>a</sup> (HD)	$V^b$ (mag)	$d^b$ (pc)	$T^c$ (K)	$\log g^c$ (cgs)	Pop <sup>d</sup>	Host	[M/H] <sup>c,e</sup>	[Ni/H] <sup>c</sup>	$N_O$	[O/H] <sup>f</sup>	$N_C$	[C/H] <sup>f</sup>	C/O <sup>f</sup>
19617	8.69	56	5600	4.18	dn	no	0.15	0.23	0	...	1	$0.15^{+0.04}_{-0.04}$	...
19638	8.16	100	5604	4.19	dn	no	0.11	0.37	0	...	1	$0.32^{+0.04}_{-0.04}$	...
19773	8.06	68	6192	4.30	dn	no	0.15	0.30	4	$-0.02^{+0.07}_{-0.07}$	4	$0.25^{+0.04}_{-0.04}$	$1.18^{+0.21}_{-0.21}$
19961	8.57	80	6050	4.46	dn	no	0.33	0.60	0	...	2	$0.35^{+0.03}_{-0.03}$	...
20155	7.88	93	6070	4.23	dn	no	0.17	0.37	1	$0.15^{+0.07}_{-0.08}$	2	$0.23^{+0.04}_{-0.07}$	$0.77^{+0.20}_{-0.15}$
20165	7.83	22	5110	4.49	dn	no	-0.04	0.03	2	$-0.02^{+0.06}_{-0.07}$	0	...	...
20439	7.78	46	6090	4.67	dn	no	0.21	0.39	0	...	8	$0.11^{+0.03}_{-0.04}$	...
20619	7.05	24	5703	4.54	dn	no	-0.18	-0.18	13	$-0.13^{+0.05}_{-0.05}$	30	$-0.03^{+0.03}_{-0.04}$	$0.80^{+0.11}_{-0.10}$
20670	7.68	77	5812	4.07	dn	no	0.20	0.42	1	$0.30^{+0.06}_{-0.07}$	3	$0.28^{+0.04}_{-0.04}$	$0.61^{+0.11}_{-0.10}$
20781	8.48	35	5279	4.50	dn	no	-0.04	-0.05	2	$0.09^{+0.09}_{-0.09}$	0	...	...
21313	8.18	71	5989	4.30	dn	no	0.14	0.30	1	$-0.03^{+0.14}_{-0.22}$	0	...	...
21316	8.68	82	6107	4.35	dn	no	0.08	0.17	3	$0.12^{+0.06}_{-0.09}$	0	...	...
21774	8.08	49	5764	4.39	dn	no	0.21	0.35	1	$0.26^{+0.06}_{-0.07}$	1	$0.23^{+0.03}_{-0.03}$	$0.59^{+0.10}_{-0.10}$
22072	6.14	42	5027	3.65	dn	no	-0.19	-0.17	3	$0.10^{+0.03}_{-0.03}$	0	...	...
22282	8.54	50	5475	4.50	dn	no	0.15	0.21	4	$0.14^{+0.08}_{-0.06}$	2	$0.30^{+0.03}_{-0.04}$	$0.90^{+0.16}_{-0.17}$
22670	9.07	59	5886	4.55	dn	no	-0.01	0.01	1	$-0.04^{+0.11}_{-0.15}$	3	$-0.13^{+0.04}_{-0.05}$	$0.51^{+0.19}_{-0.14}$
22879	6.68	24	5688	4.41	dk	no	-0.76	-0.87	11	$-0.35^{+0.04}_{-0.05}$	32	$-0.35^{+0.04}_{-0.04}$	$0.63^{+0.10}_{-0.08}$
23221	8.48	92	6052	4.36	dn	no	0.08	0.28	3	$0.18^{+0.05}_{-0.08}$	0	...	...
23249	3.52	9	5095	3.98	dn	no	0.04	0.22	20	$0.16^{+0.04}_{-0.03}$	0	...	...
23356	7.10	14	4991	4.59	dn	no	-0.07	-0.06	16	$-0.01^{+0.04}_{-0.04}$	0	...	...
23416	7.95	56	6133	4.18	dn	no	0.04	0.10	2	$-0.13^{+0.11}_{-0.19}$	1	$0.07^{+0.03}_{-0.03}$	$1.01^{+0.44}_{-0.26}$
23439	7.67	24	5070	4.71	dk	no	-0.72	-0.90	21	$-0.29^{+0.04}_{-0.03}$	0	...	...
24040	7.50	46	5853	4.36	dn	no	0.17	0.32	14	$0.15^{+0.04}_{-0.04}$	15	$0.18^{+0.03}_{-0.03}$	$0.67^{+0.08}_{-0.08}$
24213	6.77	39	6044	4.23	dn	no	0.06	0.15	2	$-0.07^{+0.10}_{-0.12}$	3	$0.02^{+0.03}_{-0.04}$	$0.78^{+0.22}_{-0.18}$
24238	7.84	21	4973	4.59	dn	no	-0.32	-0.39	20	$-0.04^{+0.03}_{-0.03}$	0	...	...

Table 6.6 (cont'd): Stellar Data.

Name <sup>a</sup> (HD)	$V^b$ (mag)	$d^b$ (pc)	$T^c$ (K)	$\log g^c$ (cgs)	Pop <sup>d</sup>	Host	[M/H] <sup>c,e</sup>	[Ni/H] <sup>c</sup>	$N_O$	[O/H] <sup>f</sup>	$N_C$	[C/H] <sup>f</sup>	C/O <sup>f</sup>
24341	7.87	65	5459	4.08	dn	no	-0.47	-0.47	0	...	2	$-0.40^{+0.05}_{-0.05}$	...
24365	7.89	111	5205	3.70	dn	no	-0.26	-0.18	2	$-0.06^{+0.04}_{-0.04}$	0	...	...
24496	6.81	20	5572	4.56	dn	no	-0.01	0.05	50	$0.00^{+0.04}_{-0.04}$	92	$0.02^{+0.03}_{-0.03}$	$0.66^{+0.07}_{-0.08}$
24505	8.05	72	5727	4.32	dn	no	0.07	0.19	2	$0.31^{+0.06}_{-0.05}$	5	$0.29^{+0.05}_{-0.03}$	$0.60^{+0.08}_{-0.10}$
24727	7.06	48	6211	4.10	dn	no	-0.12	-0.12	0	...	1	$-0.12^{+0.03}_{-0.04}$	...
24892	6.88	38	5363	4.12	dn	no	-0.25	-0.23	2	$0.07^{+0.04}_{-0.04}$	4	$-0.02^{+0.03}_{-0.09}$	$0.52^{+0.11}_{-0.06}$
25311	8.28	85	6282	4.22	dn	no	0.06	0.28	0	...	2	$0.16^{+0.04}_{-0.09}$	...
25445	9.00	83	5865	4.47	dn	no	0.01	0.08	0	...	3	$-0.01^{+0.04}_{-0.04}$	...
25565	9.20	42	5157	4.41	dn	no	0.08	0.11	2	$0.07^{+0.10}_{-0.07}$	0	...	...
25665	7.70	18	4936	4.51	dn	no	-0.06	0.02	12	$-0.05^{+0.04}_{-0.06}$	0	...	...
25682	8.32	45	5477	4.53	dn	no	0.07	0.12	0	...	1	$0.26^{+0.04}_{-0.03}$	...
25825	7.85	46	5941	4.38	dn	no	0.01	0.12	1	$0.01^{+0.13}_{-0.17}$	3	$0.06^{+0.07}_{-0.05}$	$0.72^{+0.30}_{-0.24}$
25894	8.55	64	5719	4.41	dn	no	0.24	0.38	0	...	3	$0.21^{+0.04}_{-0.03}$	...
26151	8.49	45	5348	4.47	dn	no	0.19	0.34	3	$0.23^{+0.06}_{-0.07}$	4	$0.46^{+0.04}_{-0.05}$	$1.06^{+0.22}_{-0.17}$
26257	7.64	65	5950	4.05	dn	no	0.04	0.12	0	...	3	$0.15^{+0.03}_{-0.04}$	...
26736	8.05	46	5870	4.51	dn	no	0.14	0.25	0	...	9	$0.03^{+0.03}_{-0.03}$	...
26756	8.45	45	5760	4.55	dn	no	0.14	0.24	0	...	2	$0.08^{+0.04}_{-0.04}$	...
26794	8.78	33	4909	4.74	dn	no	0.04	0.13	2	$0.27^{+0.05}_{-0.05}$	0	...	...
26965	4.43	5	5151	4.58	dn	no	-0.08	-0.16	31	$0.10^{+0.03}_{-0.03}$	0	...	...
26990	7.50	34	5748	4.39	dn	no	-0.01	-0.08	0	...	7	$-0.13^{+0.04}_{-0.04}$	...
27063	8.07	40	5696	4.36	dn	no	0.00	0.08	1	$0.05^{+0.07}_{-0.07}$	2	$0.02^{+0.04}_{-0.04}$	$0.58^{+0.11}_{-0.11}$
27149	7.53	45	5798	4.49	dn	no	0.16	0.23	0	...	2	$0.06^{+0.05}_{-0.06}$	...
27250	8.62	42	5606	4.53	dn	no	0.13	0.23	0	...	2	$0.08^{+0.04}_{-0.04}$	...
27282	8.47	47	5707	4.57	dn	no	0.18	0.28	3	$0.01^{+0.14}_{-0.18}$	7	$0.03^{+0.03}_{-0.03}$	$0.66^{+0.27}_{-0.22}$
27496	8.95	92	5575	4.16	dn	no	0.35	0.50	7	$0.19^{+0.06}_{-0.09}$	1	$0.42^{+0.04}_{-0.04}$	$1.06^{+0.22}_{-0.17}$

Table 6.6 (cont'd): Stellar Data.

Name <sup>a</sup> (HD)	$V^b$ (mag)	$d^b$ (pc)	$T^c$ (K)	$\log g^c$ (cgs)	Pop <sup>d</sup>	Host	[M/H] <sup>c,e</sup>	[Ni/H] <sup>c</sup>	$N_O$	[O/H] <sup>f</sup>	$N_C$	[C/H] <sup>f</sup>	C/O <sup>f</sup>
27530	8.16	61	5941	4.42	dn	no	0.14	0.31	6	$-0.14^{+0.09}_{-0.11}$	1	$0.16^{+0.03}_{-0.03}$	$1.25^{+0.34}_{-0.27}$
27732	8.84	48	5549	4.54	dn	no	0.09	0.20	0	...	3	$0.04^{+0.04}_{-0.07}$	...
27748	8.59	44	5621	4.38	dn	no	-0.18	-0.19	3	$-0.22^{+0.07}_{-0.08}$	0	...	...
28005	6.72	29	5819	4.38	dn	no	0.29	0.47	18	$0.17^{+0.06}_{-0.06}$	10	$0.31^{+0.03}_{-0.03}$	$0.88^{+0.13}_{-0.13}$
28097	7.67	87	6133	4.03	dn	no	-0.05	0.04	1	$-0.07^{+0.06}_{-0.07}$	5	$-0.01^{+0.03}_{-0.03}$	$0.72^{+0.13}_{-0.11}$
28099	8.10	46	5852	4.52	dn	no	0.14	0.27	0	...	3	$0.07^{+0.03}_{-0.04}$	...
28137	8.57	90	5513	3.89	dn	no	0.03	0.13	3	$0.02^{+0.07}_{-0.05}$	0	...	...
28187	7.79	41	5781	4.56	dn	no	-0.25	-0.31	1	$0.11^{+0.05}_{-0.06}$	2	$-0.16^{+0.05}_{-0.06}$	$0.34^{+0.06}_{-0.05}$
28192	8.06	51	5923	4.47	dn	no	0.09	0.17	2	$0.04^{+0.08}_{-0.10}$	2	$-0.00^{+0.04}_{-0.05}$	$0.56^{+0.14}_{-0.12}$
28291	8.62	49	5625	4.49	dn	no	0.18	0.24	0	...	3	$-0.03^{+0.04}_{-0.04}$	...
28462	9.08	40	5349	4.60	dn	no	0.19	0.26	0	...	2	$-0.00^{+0.07}_{-0.07}$	...
28593	8.59	45	5640	4.56	dn	no	0.20	0.26	0	...	2	$0.02^{+0.04}_{-0.04}$	...
28946	7.92	26	5321	4.55	dn	no	-0.16	-0.12	2	$0.01^{+0.07}_{-0.08}$	2	$-0.02^{+0.06}_{-0.06}$	$0.59^{+0.14}_{-0.12}$
28992	7.90	43	6004	4.55	dn	no	0.15	0.27	0	...	2	$0.07^{+0.04}_{-0.04}$	...
29461	7.96	48	5913	4.52	dn	no	0.20	0.29	2	$0.07^{+0.09}_{-0.09}$	1	$0.11^{+0.03}_{-0.03}$	$0.69^{+0.15}_{-0.15}$
29528	8.93	56	5524	4.50	dn/dk	no	0.17	0.19	0	...	1	$0.12^{+0.04}_{-0.04}$	...
29621	8.84	51	5604	4.26	dn	no	0.08	0.12	0	...	3	$0.06^{+0.04}_{-0.03}$	...
29818	8.77	48	5524	4.44	dn	no	-0.06	-0.09	3	$-0.12^{+0.07}_{-0.11}$	0	...	...
29883	8.00	22	4952	4.61	dn	no	-0.16	-0.14	18	$0.01^{+0.04}_{-0.03}$	0	...	...
29980	8.03	54	5924	4.46	dn	no	0.12	0.22	0	...	3	$0.09^{+0.04}_{-0.05}$	...
30246	8.30	51	5841	4.51	dn	no	0.17	0.25	0	...	2	$0.01^{+0.04}_{-0.04}$	...
30286	7.81	32	5603	4.39	dn	no	-0.06	-0.09	3	$-0.15^{+0.08}_{-0.09}$	0	...	...
30339	8.21	73	6074	4.37	dn	no	0.21	0.38	1	$0.01^{+0.13}_{-0.19}$	4	$0.26^{+0.03}_{-0.03}$	$1.12^{+0.49}_{-0.36}$
30572	8.50	75	6015	4.48	dn	no	0.25	0.41	2	$-0.05^{+0.14}_{-0.17}$	2	$0.17^{+0.03}_{-0.03}$	$1.05^{+0.41}_{-0.35}$
30649	6.94	29	5778	4.44	dn	no	-0.33	-0.40	1	$-0.10^{+0.07}_{-0.08}$	2	$-0.20^{+0.03}_{-0.04}$	$0.50^{+0.10}_{-0.09}$

Table 6.6 (cont'd): Stellar Data.

Name <sup>a</sup> (HD)	$V^b$ (mag)	$d^b$ (pc)	$T^c$ (K)	$\log g^c$ (cgs)	Pop <sup>d</sup>	Host	[M/H] <sup>c,e</sup>	[Ni/H] <sup>c</sup>	$N_O$	[O/H] <sup>f</sup>	$N_C$	[C/H] <sup>f</sup>	C/O <sup>f</sup>
30663	8.43	92	5997	4.32	dn	no	0.03	0.10	0	...	4	$-0.01^{+0.04}_{-0.03}$	...
30712	7.73	42	5614	4.50	dn	no	0.10	0.23	0	...	2	$0.19^{+0.04}_{-0.04}$	...
31018	7.64	92	5952	3.98	dn	no	0.10	0.27	7	$0.17^{+0.04}_{-0.05}$	9	$0.15^{+0.03}_{-0.03}$	$0.60^{+0.08}_{-0.07}$
31253	7.13	53	6065	4.10	dn	no	0.10	0.23	5	$0.07^{+0.05}_{-0.10}$	10	$0.12^{+0.03}_{-0.03}$	$0.71^{+0.17}_{-0.09}$
31412	7.02	35	6096	4.37	dn	no	0.04	0.10	7	$0.02^{+0.06}_{-0.07}$	4	$0.04^{+0.03}_{-0.03}$	$0.65^{+0.11}_{-0.10}$
31452	8.43	39	5212	4.42	dn	no	0.13	0.23	2	$0.08^{+0.07}_{-0.07}$	0	...	...
31560	8.13	17	4744	4.88	dn	no	0.01	0.23	2	$0.10^{+0.08}_{-0.08}$	0	...	...
31864	7.63	31	5403	4.38	dn	no	-0.20	-0.22	0	...	1	$-0.13^{+0.05}_{-0.06}$	...
31966	6.75	35	5781	4.22	dn	no	0.11	0.20	0	...	1	$0.05^{+0.04}_{-0.04}$	...
32147	6.22	8	4827	4.69	dn	no	0.30	0.43	54	$0.28^{+0.04}_{-0.03}$	0	...	...
32259	7.51	38	5881	4.43	dn	no	-0.09	-0.04	3	$0.00^{+0.11}_{-0.13}$	0	...	...
32673	7.79	80	5818	3.94	dn	no	0.18	0.37	1	$0.24^{+0.06}_{-0.07}$	0	...	...
32923	4.91	15	5694	4.20	dn	no	-0.13	-0.11	22	$0.14^{+0.04}_{-0.03}$	24	$-0.00^{+0.03}_{-0.03}$	$0.45^{+0.05}_{-0.05}$
32963	7.60	35	5763	4.43	dn	no	0.07	0.17	3	$-0.06^{+0.09}_{-0.13}$	0	...	...
33108	8.92	99	6130	4.34	dn	no	0.27	0.45	3	$-0.02^{+0.10}_{-0.11}$	0	...	...
33283	8.05	86	6038	4.26	dn	yes	0.26	0.53	12	$0.22^{+0.05}_{-0.05}$	27	$0.35^{+0.03}_{-0.03}$	$0.86^{+0.11}_{-0.11}$
33334	7.61	46	5596	4.26	dn	no	0.01	0.09	0	...	11	$0.11^{+0.03}_{-0.03}$	...
33636	7.00	28	5904	4.43	dn	yes	-0.12	-0.11	5	$-0.14^{+0.06}_{-0.10}$	8	$-0.18^{+0.04}_{-0.03}$	$0.57^{+0.13}_{-0.09}$
33822	8.12	55	5723	4.30	dn	no	0.26	0.41	0	...	3	$0.29^{+0.04}_{-0.04}$	...
34411	4.69	12	5911	4.37	dn	no	0.09	0.19	57	$0.09^{+0.04}_{-0.04}$	30	$0.09^{+0.03}_{-0.03}$	$0.63^{+0.07}_{-0.07}$
34445	7.31	45	5837	4.21	dn	yes	0.10	0.22	15	$0.09^{+0.05}_{-0.06}$	16	$0.15^{+0.03}_{-0.03}$	$0.73^{+0.12}_{-0.10}$
34575	7.09	29	5651	4.45	dn	no	0.25	0.39	3	$0.23^{+0.08}_{-0.07}$	4	$0.26^{+0.03}_{-0.03}$	$0.68^{+0.12}_{-0.14}$
34721	5.96	24	5999	4.25	dn	no	-0.08	-0.01	28	$-0.03^{+0.04}_{-0.04}$	18	$-0.04^{+0.03}_{-0.03}$	$0.61^{+0.07}_{-0.07}$
34745	7.00	37	6070	4.29	dn	no	-0.09	-0.08	1	$-0.02^{+0.10}_{-0.14}$	3	$-0.13^{+0.04}_{-0.04}$	$0.50^{+0.16}_{-0.12}$
34887	8.15	41	5458	4.30	h	no	0.21	0.44	0	...	9	$0.46^{+0.03}_{-0.03}$	...

Table 6.6 (cont'd): Stellar Data.

Name <sup>a</sup> (HD)	$V^b$ (mag)	$d^b$ (pc)	$T^c$ (K)	$\log g^c$ (cgs)	Pop <sup>d</sup>	Host	[M/H] <sup>c,e</sup>	[Ni/H] <sup>c</sup>	$N_O$	[O/H] <sup>f</sup>	$N_C$	[C/H] <sup>f</sup>	C/O <sup>f</sup>
34957	9.23	106	5964	4.56	dn	no	-0.16	-0.11	11	$-0.04^{+0.06}_{-0.08}$	20	$-0.20^{+0.03}_{-0.03}$	$0.44^{+0.09}_{-0.07}$
35627	7.49	58	6069	4.24	dn	no	-0.01	0.07	2	$0.12^{+0.07}_{-0.07}$	0	...	...
35974	7.18	58	5888	3.99	dn	no	-0.19	-0.12	1	$-0.16^{+0.08}_{-0.08}$	1	$-0.07^{+0.03}_{-0.03}$	$0.78^{+0.16}_{-0.15}$
36308	8.40	35	5612	4.82	dn	no	0.07	0.12	1	$0.03^{+0.11}_{-0.15}$	2	$-0.09^{+0.07}_{-0.08}$	$0.48^{+0.18}_{-0.14}$
36387	8.11	53	5928	4.33	dn	no	0.05	0.14	3	$-0.11^{+0.07}_{-0.09}$	3	$0.03^{+0.03}_{-0.03}$	$0.88^{+0.20}_{-0.16}$
37008	7.74	20	4975	4.55	dn	no	-0.31	-0.36	26	$-0.08^{+0.04}_{-0.03}$	0	...	...
37124	7.68	33	5500	4.60	dn	yes	-0.29	-0.32	9	$0.12^{+0.04}_{-0.04}$	18	$0.01^{+0.03}_{-0.03}$	$0.48^{+0.06}_{-0.06}$
37213	8.22	84	5453	4.04	dn	no	-0.42	-0.41	1	$-0.18^{+0.06}_{-0.07}$	1	$-0.17^{+0.05}_{-0.05}$	$0.66^{+0.13}_{-0.12}$
37216	7.85	27	5364	4.44	dn	no	-0.10	-0.07	1	$-0.06^{+0.08}_{-0.09}$	5	$0.03^{+0.05}_{-0.08}$	$0.78^{+0.22}_{-0.16}$
37394	6.21	12	5351	4.60	dn	no	0.16	0.22	3	$0.07^{+0.16}_{-0.09}$	6	$0.03^{+0.07}_{-0.04}$	$0.57^{+0.13}_{-0.23}$
37605	8.67	42	5317	4.22	dn	yes	0.29	0.36	1	$0.12^{+0.09}_{-0.10}$	5	$0.27^{+0.04}_{-0.04}$	$0.89^{+0.22}_{-0.21}$
37962	7.84	36	5651	4.41	dn	no	-0.18	-0.21	1	$-0.22^{+0.11}_{-0.13}$	2	$-0.21^{+0.05}_{-0.04}$	$0.64^{+0.20}_{-0.18}$
38230	7.34	20	5174	4.53	dn	no	-0.02	0.00	11	$0.16^{+0.04}_{-0.04}$	0	...	...
38400	8.20	73	6009	4.24	dn	no	0.08	0.23	0	...	1	$0.07^{+0.03}_{-0.03}$	...
38467	8.27	72	5790	4.22	dn	no	0.24	0.41	2	$0.12^{+0.06}_{-0.06}$	4	$0.22^{+0.04}_{-0.03}$	$0.80^{+0.13}_{-0.13}$
38529	5.95	42	5697	4.05	dn	yes	0.27	0.53	17	$0.33^{+0.04}_{-0.04}$	11	$0.33^{+0.03}_{-0.03}$	$0.62^{+0.08}_{-0.08}$
38801	8.26	99	5274	3.82	dn	yes	0.27	0.43	1	$0.05^{+0.08}_{-0.09}$	0	...	...
38858	5.97	15	5726	4.51	dn	no	-0.21	-0.19	65	$-0.15^{+0.04}_{-0.03}$	34	$-0.17^{+0.03}_{-0.03}$	$0.60^{+0.06}_{-0.07}$
38949	7.80	42	6051	4.55	dn	no	-0.12	-0.07	5	$-0.04^{+0.09}_{-0.11}$	7	$-0.10^{+0.04}_{-0.03}$	$0.54^{+0.14}_{-0.12}$
39094	7.89	66	5400	3.92	dn	no	0.19	0.32	5	$0.15^{+0.06}_{-0.06}$	9	$0.32^{+0.03}_{-0.03}$	$0.93^{+0.15}_{-0.15}$
39480	8.34	81	5999	4.34	dn	no	0.23	0.43	1	$0.04^{+0.10}_{-0.12}$	0	...	...
39715	8.84	26	4798	4.75	dn	no	-0.10	-0.01	1	$-0.12^{+0.09}_{-0.13}$	0	...	...
39796	8.05	71	5494	3.98	dn/dk	no	0.18	0.27	2	$0.10^{+0.05}_{-0.06}$	2	$0.12^{+0.03}_{-0.04}$	$0.66^{+0.11}_{-0.09}$
39833	7.65	46	5831	4.44	dn	no	0.11	0.20	2	$0.08^{+0.09}_{-0.08}$	3	$0.05^{+0.05}_{-0.04}$	$0.58^{+0.12}_{-0.14}$
39881	6.60	27	5718	4.42	dn	no	-0.05	-0.04	15	$0.24^{+0.04}_{-0.03}$	8	$0.08^{+0.03}_{-0.03}$	$0.43^{+0.05}_{-0.05}$

Table 6.6 (cont'd): Stellar Data.

Name <sup>a</sup> (HD)	$V^b$ (mag)	$d^b$ (pc)	$T^c$ (K)	$\log g^c$ (cgs)	Pop <sup>d</sup>	Host	[M/H] <sup>c,e</sup>	[Ni/H] <sup>c</sup>	$N_O$	[O/H] <sup>f</sup>	$N_C$	[C/H] <sup>f</sup>	C/O <sup>f</sup>
39997	8.48	103	6046	4.12	dn	no	0.01	0.13	0	...	1	$0.22^{+0.03}_{-0.03}$	...
40330	8.47	74	5965	4.25	dn	no	0.09	0.21	0	...	3	$0.11^{+0.03}_{-0.04}$	...
40397	6.99	23	5542	4.59	dk	no	-0.04	-0.02	18	$0.20^{+0.04}_{-0.04}$	51	$0.09^{+0.03}_{-0.03}$	$0.50^{+0.05}_{-0.05}$
40979	6.74	33	6089	4.30	dn	yes	0.12	0.22	0	...	5	$0.13^{+0.03}_{-0.03}$	...
41484	7.96	81	5993	4.13	dn	no	0.08	0.25	0	...	1	$0.16^{+0.03}_{-0.03}$	...
42182	8.45	29	5048	4.43	dn	no	0.08	0.08	1	$0.11^{+0.07}_{-0.08}$	0	...	...
42250	7.43	25	5396	4.60	dn	no	0.01	0.07	2	$0.16^{+0.05}_{-0.05}$	3	$0.23^{+0.05}_{-0.05}$	$0.74^{+0.13}_{-0.12}$
42618	6.85	23	5747	4.43	dn	no	-0.09	-0.05	0	...	1	$-0.16^{+0.04}_{-0.04}$	...
43296	8.90	98	6111	4.20	dn	no	0.24	0.44	0	...	3	$0.29^{+0.03}_{-0.03}$	...
43691	8.03	93	6120	4.18	h	yes	0.20	0.38	0	...	1	$0.29^{+0.03}_{-0.03}$	...
43745	6.05	39	6095	4.02	dn	no	0.06	0.19	1	$0.26^{+0.06}_{-0.07}$	2	$0.10^{+0.03}_{-0.03}$	$0.44^{+0.08}_{-0.07}$
43947	6.61	27	5933	4.37	dn	no	-0.28	-0.26	3	$-0.30^{+0.08}_{-0.10}$	4	$-0.19^{+0.04}_{-0.04}$	$0.80^{+0.19}_{-0.16}$
44420	7.63	41	5796	4.35	dn	no	0.28	0.44	3	$0.19^{+0.06}_{-0.07}$	3	$0.28^{+0.03}_{-0.03}$	$0.78^{+0.13}_{-0.12}$
44614	7.59	44	5733	4.14	dn	no	-0.01	0.13	1	$-0.40^{+0.19}_{-0.27}$	0	...	...
44663	8.11	68	6043	4.22	dn	no	-0.00	0.11	0	...	1	$0.14^{+0.03}_{-0.03}$	...
44985	7.01	32	5929	4.29	dn	no	-0.07	-0.06	1	$-0.13^{+0.07}_{-0.08}$	0	...	...
45067	5.88	33	6044	4.08	dn	no	-0.09	-0.01	3	$-0.03^{+0.07}_{-0.07}$	5	$-0.08^{+0.04}_{-0.03}$	$0.55^{+0.10}_{-0.10}$
45161	8.14	42	5672	4.36	dn	no	0.10	0.16	0	...	3	$0.03^{+0.04}_{-0.04}$	...
45184	6.37	22	5810	4.37	dn	no	0.03	0.07	27	$-0.01^{+0.04}_{-0.04}$	114	$-0.01^{+0.03}_{-0.03}$	$0.63^{+0.07}_{-0.07}$
45350	7.89	48	5616	4.33	dn	yes	0.26	0.34	8	$0.22^{+0.05}_{-0.05}$	6	$0.20^{+0.03}_{-0.03}$	$0.61^{+0.08}_{-0.08}$
45588	6.05	29	6168	4.29	dn	no	-0.02	0.07	3	$0.00^{+0.09}_{-0.17}$	1	$-0.01^{+0.03}_{-0.03}$	$0.62^{+0.25}_{-0.13}$
45652	8.10	36	5312	4.39	dn	yes	0.24	0.37	2	$-0.09^{+0.12}_{-0.19}$	4	$0.30^{+0.04}_{-0.04}$	$1.55^{+0.68}_{-0.46}$
46375	7.91	33	5285	4.53	dn	yes	0.20	0.36	1	$0.12^{+0.11}_{-0.14}$	0	...	...
47157	7.61	38	5733	4.43	dn	no	0.31	0.49	0	...	25	$0.30^{+0.03}_{-0.03}$	...
47309	7.60	42	5708	4.21	dn	no	0.03	0.10	3	$-0.10^{+0.07}_{-0.08}$	0	...	...

Table 6.6 (cont'd): Stellar Data.

Name <sup>a</sup> (HD)	$V^b$ (mag)	$d^b$ (pc)	$T^c$ (K)	$\log g^c$ (cgs)	Pop <sup>d</sup>	Host	[M/H] <sup>c,e</sup>	[Ni/H] <sup>c</sup>	$N_O$	[O/H] <sup>f</sup>	$N_C$	[C/H] <sup>f</sup>	C/O <sup>f</sup>
47752	8.08	17	4707	4.72	dn	no	-0.18	-0.07	5	$-0.12^{+0.05}_{-0.05}$	0	...	...
48682	5.24	16	6064	4.33	dn	no	0.09	0.16	0	...	6	$0.08^{+0.03}_{-0.03}$	...
48938	6.43	26	5937	4.31	dn	no	-0.39	-0.40	1	$-0.41^{+0.11}_{-0.17}$	1	$-0.29^{+0.04}_{-0.04}$	$0.83^{+0.33}_{-0.23}$
49674	8.10	40	5662	4.56	dn	yes	0.23	0.38	7	$0.11^{+0.08}_{-0.08}$	18	$0.12^{+0.03}_{-0.03}$	$0.65^{+0.13}_{-0.12}$
50281	6.58	8	4758	4.92	dn	no	-0.01	0.16	3	$0.12^{+0.07}_{-0.08}$	0	...	...
50499	7.21	47	6070	4.37	dn	yes	0.25	0.45	13	$0.24^{+0.05}_{-0.05}$	4	$0.29^{+0.03}_{-0.03}$	$0.71^{+0.10}_{-0.10}$
50554	6.84	31	5929	4.29	dn	yes	-0.07	-0.04	6	$-0.01^{+0.06}_{-0.08}$	8	$-0.06^{+0.03}_{-0.03}$	$0.57^{+0.11}_{-0.09}$
50639	7.05	39	6098	4.29	dn	no	-0.03	0.03	2	$0.09^{+0.13}_{-0.10}$	1	$0.01^{+0.04}_{-0.04}$	$0.53^{+0.13}_{-0.17}$
50692	5.74	17	5891	4.36	dn	no	-0.13	-0.10	14	$-0.02^{+0.04}_{-0.05}$	28	$-0.13^{+0.03}_{-0.03}$	$0.50^{+0.06}_{-0.06}$
50806	6.05	25	5683	4.35	dn/dk	no	0.07	0.17	2	$0.36^{+0.04}_{-0.04}$	1	$0.19^{+0.03}_{-0.03}$	$0.42^{+0.05}_{-0.05}$
51046	8.06	39	5622	4.45	dn	no	-0.03	0.04	0	...	5	$0.02^{+0.04}_{-0.04}$	...
51067A	7.15	37	5852	4.11	dn	no	-0.01	0.06	1	$-0.05^{+0.10}_{-0.15}$	1	$0.07^{+0.04}_{-0.03}$	$0.84^{+0.29}_{-0.21}$
51067B	8.24	33	5463	4.44	dn	no	0.14	0.20	1	$-0.11^{+0.15}_{-0.22}$	1	$-0.03^{+0.06}_{-0.06}$	$0.76^{+0.39}_{-0.28}$
51219	7.41	32	5642	4.46	dn	no	0.00	0.06	2	$-0.11^{+0.09}_{-0.14}$	1	$0.05^{+0.04}_{-0.04}$	$0.91^{+0.31}_{-0.21}$
51419	6.94	24	5637	4.46	dn	no	-0.33	-0.35	13	$-0.13^{+0.04}_{-0.05}$	14	$-0.13^{+0.03}_{-0.04}$	$0.62^{+0.09}_{-0.07}$
51813	8.66	58	6001	4.47	dn	no	0.11	0.21	2	$0.08^{+0.09}_{-0.11}$	0	...	...
52265	6.29	28	6076	4.26	dn	yes	0.16	0.27	20	$0.02^{+0.04}_{-0.04}$	10	$0.15^{+0.03}_{-0.03}$	$0.86^{+0.10}_{-0.10}$
52456	8.16	28	5109	4.37	dn	no	0.01	0.10	1	$-0.03^{+0.09}_{-0.11}$	0	...	...
52711	5.93	19	5889	4.41	dn	no	-0.10	-0.07	45	$-0.01^{+0.04}_{-0.03}$	72	$-0.07^{+0.03}_{-0.03}$	$0.55^{+0.06}_{-0.06}$
53532	8.25	43	5769	4.62	dn	no	0.12	0.19	0	...	5	$-0.02^{+0.03}_{-0.04}$	...
55696	7.95	73	6154	4.32	...	no	0.27	0.50	3	$0.13^{+0.08}_{-0.14}$	7	$0.26^{+0.03}_{-0.03}$	$0.85^{+0.28}_{-0.16}$
56274	7.74	33	5681	4.47	dn/dk	no	-0.50	-0.51	1	$-0.26^{+0.10}_{-0.14}$	1	$-0.48^{+0.06}_{-0.08}$	$0.38^{+0.14}_{-0.10}$
56303	7.34	41	5895	4.24	dn	no	0.13	0.21	2	$0.02^{+0.13}_{-0.15}$	2	$0.09^{+0.03}_{-0.03}$	$0.74^{+0.27}_{-0.23}$
56957	7.57	63	5874	4.30	dn	no	0.27	0.56	1	$0.30^{+0.06}_{-0.06}$	0	...	...
57204	7.99	83	5156	3.62	dn	no	0.06	0.21	1	$-0.09^{+0.08}_{-0.10}$	0	...	...

Table 6.6 (cont'd): Stellar Data.

Name <sup>a</sup> (HD)	$V^b$ (mag)	$d^b$ (pc)	$T^c$ (K)	$\log g^c$ (cgs)	Pop <sup>d</sup>	Host	[M/H] <sup>c,e</sup>	[Ni/H] <sup>c</sup>	$N_O$	[O/H] <sup>f</sup>	$N_C$	[C/H] <sup>f</sup>	C/O <sup>f</sup>
57813	8.64	40	5294	4.25	dn	no	0.28	0.29	4	$0.06^{+0.07}_{-0.08}$	0	...	...
58781	7.24	29	5604	4.46	dn	no	0.06	0.18	2	$0.10^{+0.10}_{-0.13}$	2	$0.14^{+0.04}_{-0.04}$	$0.69^{+0.21}_{-0.17}$
59062	8.15	46	5546	4.47	dn	no	0.23	0.40	0	...	1	$0.35^{+0.06}_{-0.05}$	...
60491	8.16	24	5091	4.63	dn	no	-0.26	-0.20	2	$-0.15^{+0.09}_{-0.19}$	0	...	...
60521	8.00	51	5929	4.43	dn	no	0.15	0.28	1	$-0.03^{+0.13}_{-0.21}$	1	$0.09^{+0.04}_{-0.03}$	$0.83^{+0.41}_{-0.26}$
61364	8.66	95	5718	4.04	dn	no	-0.03	-0.02	0	...	1	$-0.03^{+0.04}_{-0.04}$	...
61447	8.41	50	5592	4.33	...	no	0.18	0.32	0	...	2	$0.26^{+0.04}_{-0.04}$	...
61606	7.18	14	4964	4.71	dn	no	-0.05	0.07	1	$0.10^{+0.07}_{-0.09}$	0	...	...
62128	7.53	51	5800	4.25	dn	no	0.26	0.45	0	...	6	$0.29^{+0.03}_{-0.03}$	...
62694	9.07	89	5788	4.37	dn/dk	no	0.11	0.28	1	$0.11^{+0.10}_{-0.13}$	3	$0.23^{+0.03}_{-0.03}$	$0.85^{+0.26}_{-0.20}$
62857	8.51	53	5872	4.66	dn	no	0.19	0.32	2	$0.27^{+0.12}_{-0.17}$	2	$-0.03^{+0.04}_{-0.04}$	$0.31^{+0.13}_{-0.09}$
63754	6.54	51	6096	4.07	dn	no	0.13	0.30	2	$0.25^{+0.05}_{-0.05}$	1	$0.19^{+0.03}_{-0.03}$	$0.54^{+0.07}_{-0.08}$
64502	8.44	110	4913	3.52	dn	no	0.04	0.05	2	$0.08^{+0.04}_{-0.04}$	0	...	...
64942	8.37	48	5784	4.48	dn	no	-0.02	-0.02	5	$0.00^{+0.08}_{-0.12}$	3	$-0.12^{+0.05}_{-0.04}$	$0.48^{+0.14}_{-0.10}$
65080	8.21	53	5802	4.20	dn	no	-0.08	-0.07	3	$-0.26^{+0.08}_{-0.15}$	1	$0.00^{+0.04}_{-0.04}$	$1.15^{+0.42}_{-0.23}$
65277	8.05	17	4741	4.76	dn	no	-0.15	-0.10	12	$0.02^{+0.03}_{-0.04}$	0	...	...
65430	7.68	23	5183	4.55	dn	no	-0.04	-0.04	3	$0.17^{+0.05}_{-0.10}$	0	...	...
65583	6.97	16	5279	4.76	dn/dk	no	-0.48	-0.57	21	$-0.02^{+0.03}_{-0.04}$	0	...	...
66171	8.18	47	5711	4.41	dn	no	-0.28	-0.26	2	$-0.15^{+0.06}_{-0.07}$	0	...	...
66221	8.06	43	5547	4.26	dn	no	0.20	0.23	1	$0.09^{+0.07}_{-0.09}$	0	...	...
66428	8.25	55	5752	4.49	dn	yes	0.23	0.41	15	$0.18^{+0.05}_{-0.05}$	7	$0.30^{+0.03}_{-0.03}$	$0.82^{+0.12}_{-0.12}$
66485	8.43	44	5566	4.37	dn	no	-0.03	0.02	1	$0.02^{+0.09}_{-0.12}$	4	$0.08^{+0.04}_{-0.04}$	$0.71^{+0.20}_{-0.17}$
67346	7.62	69	6091	4.18	dn	no	0.24	0.48	0	...	1	$0.29^{+0.03}_{-0.03}$	...
67458	6.80	25	5838	4.45	dn	no	-0.18	-0.15	1	$-0.19^{+0.12}_{-0.17}$	1	$-0.18^{+0.03}_{-0.04}$	$0.64^{+0.26}_{-0.19}$
67767	5.73	41	5344	3.88	dn/dk	no	-0.05	0.07	3	$0.13^{+0.04}_{-0.04}$	0	...	...

Table 6.6 (cont'd): Stellar Data.

Name <sup>a</sup> (HD)	$V^b$ (mag)	$d^b$ (pc)	$T^c$ (K)	$\log g^c$ (cgs)	Pop <sup>d</sup>	Host	[M/H] <sup>c,e</sup>	[Ni/H] <sup>c</sup>	$N_O$	[O/H] <sup>f</sup>	$N_C$	[C/H] <sup>f</sup>	C/O <sup>f</sup>
68017	6.78	21	5552	4.65	dn	no	-0.30	-0.31	41	$0.09^{+0.03}_{-0.03}$	53	$0.01^{+0.03}_{-0.03}$	$0.52^{+0.05}_{-0.05}$
68168	7.34	33	5724	4.40	dn	no	0.10	0.20	1	$0.10^{+0.07}_{-0.09}$	10	$0.06^{+0.03}_{-0.03}$	$0.58^{+0.13}_{-0.11}$
68978	6.70	27	5919	4.43	dn	no	-0.00	0.07	2	$0.04^{+0.07}_{-0.07}$	1	$0.01^{+0.03}_{-0.04}$	$0.58^{+0.10}_{-0.10}$
68988	8.20	58	5960	4.41	dn	yes	0.30	0.47	0	...	2	$0.22^{+0.03}_{-0.03}$	...
69027	8.91	79	5535	4.98	dn	no	-0.52	-0.36	0	...	3	$0.37^{+0.05}_{-0.05}$	...
69056	7.72	37	5490	4.27	dn	no	0.06	0.16	0	...	1	$0.29^{+0.03}_{-0.04}$	...
69809	7.86	50	5817	4.30	dn	no	0.24	0.39	1	$0.12^{+0.06}_{-0.07}$	2	$0.30^{+0.03}_{-0.03}$	$0.97^{+0.18}_{-0.16}$
69830	5.95	12	5361	4.46	dn	yes	-0.08	-0.01	33	$-0.07^{+0.04}_{-0.04}$	74	$0.06^{+0.03}_{-0.03}$	$0.87^{+0.09}_{-0.11}$
69960	8.00	61	5690	4.21	dk	no	0.29	0.43	4	$0.22^{+0.05}_{-0.05}$	5	$0.24^{+0.03}_{-0.03}$	$0.66^{+0.09}_{-0.09}$
71067	8.66	66	6071	4.49	dn	no	0.01	0.04	0	...	1	$-0.07^{+0.04}_{-0.04}$	...
71334	7.81	38	5716	4.48	dn	no	-0.05	-0.00	0	...	3	$-0.04^{+0.04}_{-0.06}$	...
71479	7.17	41	5953	4.30	dn	no	0.18	0.33	2	$0.19^{+0.06}_{-0.07}$	1	$0.20^{+0.03}_{-0.03}$	$0.65^{+0.12}_{-0.10}$
71835	8.39	39	5488	4.58	h	no	-0.02	0.05	0	...	2	$-0.00^{+0.04}_{-0.05}$	...
71881	7.44	40	5822	4.29	dn	no	-0.02	0.05	1	$0.07^{+0.06}_{-0.06}$	2	$0.02^{+0.03}_{-0.03}$	$0.56^{+0.09}_{-0.08}$
72616	8.35	72	5803	4.08	dn	no	0.21	0.35	1	$0.15^{+0.07}_{-0.08}$	0	...	...
72659	7.46	51	5920	4.24	dn	yes	-0.03	0.06	12	$0.01^{+0.04}_{-0.04}$	10	$0.03^{+0.03}_{-0.03}$	$0.66^{+0.08}_{-0.07}$
72673	6.38	12	5243	4.67	dn	no	-0.33	-0.32	8	$-0.12^{+0.05}_{-0.05}$	0	...	...
73226	7.54	43	5873	4.36	dn	no	0.09	0.23	1	$0.14^{+0.06}_{-0.07}$	9	$0.18^{+0.03}_{-0.03}$	$0.68^{+0.13}_{-0.11}$
73256	8.08	36	5566	4.55	dn	yes	0.23	0.33	1	$0.01^{+0.11}_{-0.15}$	4	$0.17^{+0.04}_{-0.04}$	$0.92^{+0.32}_{-0.24}$
73534	8.23	96	4929	3.69	dn	yes	0.15	0.29	10	$0.10^{+0.04}_{-0.04}$	0	...	...
73667	7.61	18	4990	4.64	dn	no	-0.36	-0.44	16	$-0.08^{+0.04}_{-0.04}$	0	...	...
73933	7.88	58	6076	4.39	dn	no	0.03	0.16	0	...	1	$0.09^{+0.04}_{-0.04}$	...
73940	7.59	83	5685	4.00	dn	no	0.08	0.20	1	$0.25^{+0.04}_{-0.05}$	3	$0.20^{+0.03}_{-0.04}$	$0.56^{+0.08}_{-0.07}$
74156	7.61	64	6068	4.26	dn	yes	0.12	0.21	12	$0.20^{+0.04}_{-0.07}$	21	$0.08^{+0.03}_{-0.03}$	$0.47^{+0.09}_{-0.06}$
75576	8.27	85	5954	3.98	dn	no	0.14	0.19	0	...	1	$0.18^{+0.04}_{-0.04}$	...

Table 6.6 (cont'd): Stellar Data.

Name <sup>a</sup> (HD)	$V^b$ (mag)	$d^b$ (pc)	$T^c$ (K)	$\log g^c$ (cgs)	Pop <sup>d</sup>	Host	[M/H] <sup>c,e</sup>	[Ni/H] <sup>c</sup>	$N_O$	[O/H] <sup>f</sup>	$N_C$	[C/H] <sup>f</sup>	C/O <sup>f</sup>
75732	5.96	12	5235	4.45	dn	yes	0.25	0.45	143	$0.13^{+0.06}_{-0.06}$	0	...	...
75784	7.84	84	4904	3.60	dn	no	0.16	0.30	9	$0.11^{+0.04}_{-0.04}$	0	...	...
75898	8.03	80	6021	4.17	h	yes	0.23	0.38	12	$0.18^{+0.05}_{-0.05}$	20	$0.23^{+0.03}_{-0.03}$	$0.72^{+0.09}_{-0.10}$
76539	7.86	53	5727	4.25	dn	no	0.14	0.28	2	$0.16^{+0.06}_{-0.07}$	1	$0.12^{+0.04}_{-0.04}$	$0.58^{+0.11}_{-0.10}$
76617	8.17	90	5960	4.06	dn	no	0.14	0.25	1	$-0.08^{+0.15}_{-0.22}$	3	$0.22^{+0.03}_{-0.03}$	$1.26^{+0.66}_{-0.44}$
76780	7.63	33	5635	4.28	dn	no	0.10	0.20	3	$-0.06^{+0.07}_{-0.07}$	4	$0.19^{+0.04}_{-0.04}$	$1.12^{+0.20}_{-0.20}$
76909	7.84	47	5740	4.39	dn	no	0.34	0.51	1	$0.18^{+0.08}_{-0.09}$	2	$0.30^{+0.03}_{-0.03}$	$0.84^{+0.18}_{-0.17}$
76974	8.46	46	5597	4.49	dn	no	0.07	0.21	1	$-0.25^{+0.18}_{-0.21}$	0	...	...
77519	7.97	87	6269	4.32	dn	no	0.23	0.52	1	$0.12^{+0.15}_{-0.22}$	0	...	...
77803	8.60	66	5862	4.35	dn	no	0.05	0.13	3	$0.04^{+0.06}_{-0.07}$	0	...	...
78277	8.17	91	5764	4.00	dn	no	0.22	0.40	1	$-0.08^{+0.12}_{-0.15}$	0	...	...
78536	8.31	97	5925	4.33	dn	no	0.10	0.25	1	$0.15^{+0.06}_{-0.06}$	3	$0.10^{+0.03}_{-0.03}$	$0.56^{+0.09}_{-0.08}$
78538	8.15	43	5804	4.58	dn	no	-0.03	0.01	0	...	2	$-0.15^{+0.05}_{-0.04}$	...
78752	7.84	83	6038	4.05	dn	no	0.10	0.25	0	...	1	$0.18^{+0.04}_{-0.04}$	...
79282	8.30	56	5903	4.45	dn	no	0.09	0.18	0	...	3	$-0.03^{+0.04}_{-0.04}$	...
79498	8.05	48	5652	4.28	dn	no	0.10	0.27	1	$0.00^{+0.13}_{-0.16}$	0	...	...
80367	8.15	29	5098	4.51	dn	no	0.03	0.09	6	$0.18^{+0.04}_{-0.04}$	0	...	...
80606	9.06	58	5573	4.44	dn	yes	0.26	0.43	28	$0.21^{+0.05}_{-0.05}$	37	$0.31^{+0.03}_{-0.03}$	$0.79^{+0.11}_{-0.11}$
81324	8.42	106	5083	3.59	dn	no	0.05	0.18	3	$0.10^{+0.05}_{-0.05}$	0	...	...
81505	8.40	86	5788	4.41	dn	no	0.33	0.60	1	$0.33^{+0.09}_{-0.10}$	0	...	...
82460	8.40	46	5774	4.46	dn	no	-0.01	0.02	1	$-0.21^{+0.12}_{-0.18}$	3	$-0.08^{+0.03}_{-0.03}$	$0.86^{+0.36}_{-0.25}$
82905	8.91	90	5949	4.34	dn	no	0.09	0.20	0	...	3	$0.09^{+0.03}_{-0.04}$	...
82943	6.54	27	5997	4.42	dn	yes	0.20	0.37	27	$0.14^{+0.04}_{-0.05}$	29	$0.18^{+0.03}_{-0.03}$	$0.69^{+0.09}_{-0.08}$
83443	8.23	43	5453	4.49	dn	yes	0.27	0.52	2	$0.06^{+0.13}_{-0.17}$	4	$0.44^{+0.04}_{-0.04}$	$1.52^{+0.63}_{-0.48}$
83983	8.92	43	5294	4.48	dn	no	0.19	0.24	2	$0.06^{+0.08}_{-0.09}$	0	...	...

Table 6.6 (cont'd): Stellar Data.

Name <sup>a</sup> (HD)	$V^b$ (mag)	$d^b$ (pc)	$T^c$ (K)	$\log g^c$ (cgs)	Pop <sup>d</sup>	Host	[M/H] <sup>c,e</sup>	[Ni/H] <sup>c</sup>	$N_O$	[O/H] <sup>f</sup>	$N_C$	[C/H] <sup>f</sup>	C/O <sup>f</sup>
84117	4.93	14	6152	4.31	dn	no	-0.08	-0.04	23	$0.05^{+0.04}_{-0.03}$	37	$-0.00^{+0.03}_{-0.03}$	$0.56^{+0.06}_{-0.06}$
84501	8.26	92	5810	4.14	dn/dk	no	0.12	0.33	1	$0.26^{+0.06}_{-0.07}$	1	$0.14^{+0.04}_{-0.04}$	$0.48^{+0.08}_{-0.08}$
84703	7.88	63	5981	4.17	h	no	-0.07	0.06	1	$0.05^{+0.08}_{-0.11}$	0	...	...
84737	5.08	18	5960	4.24	dn	no	0.14	0.25	21	$0.17^{+0.04}_{-0.04}$	32	$0.13^{+0.03}_{-0.03}$	$0.57^{+0.06}_{-0.06}$
85301	7.74	32	5725	4.62	dn	no	0.12	0.21	4	$0.09^{+0.09}_{-0.15}$	14	$-0.00^{+0.03}_{-0.03}$	$0.51^{+0.18}_{-0.12}$
85689	7.71	45	6002	4.38	dn	no	-0.18	-0.12	8	$-0.20^{+0.07}_{-0.08}$	17	$-0.21^{+0.03}_{-0.03}$	$0.62^{+0.12}_{-0.11}$
86081	8.73	91	6028	4.29	dn	yes	0.15	0.34	6	$0.20^{+0.05}_{-0.05}$	28	$0.21^{+0.03}_{-0.03}$	$0.64^{+0.09}_{-0.08}$
86728	5.37	14	5700	4.29	dn	no	0.11	0.26	47	$0.04^{+0.05}_{-0.04}$	39	$0.18^{+0.03}_{-0.03}$	$0.87^{+0.10}_{-0.12}$
87001	8.96	75	5816	4.18	dn	no	0.11	0.23	3	$0.14^{+0.05}_{-0.10}$	3	$0.16^{+0.03}_{-0.03}$	$0.66^{+0.16}_{-0.10}$
87359	7.49	31	5676	4.49	dn	no	0.04	0.10	1	$0.02^{+0.06}_{-0.07}$	3	$-0.05^{+0.04}_{-0.04}$	$0.54^{+0.09}_{-0.09}$
87836	7.49	43	5774	4.32	dn	no	0.30	0.48	1	$0.22^{+0.06}_{-0.06}$	1	$0.25^{+0.03}_{-0.03}$	$0.67^{+0.11}_{-0.11}$
87883	7.56	18	4958	4.56	dn	yes	0.04	0.12	26	$0.09^{+0.04}_{-0.04}$	0	...	...
88072	7.55	37	5751	4.40	dn	no	-0.01	0.09	1	$-0.01^{+0.09}_{-0.11}$	0	...	...
88133	8.01	74	5494	4.23	dn/dk	yes	0.21	0.50	10	$0.23^{+0.05}_{-0.07}$	8	$0.35^{+0.03}_{-0.03}$	$0.82^{+0.15}_{-0.12}$
88218	6.14	30	5837	4.10	dn	no	-0.12	-0.09	1	$0.02^{+0.05}_{-0.06}$	0	...	...
88371	8.42	62	5630	4.50	dn	no	-0.14	-0.19	3	$0.21^{+0.05}_{-0.05}$	1	$-0.06^{+0.04}_{-0.04}$	$0.34^{+0.05}_{-0.05}$
88402	7.57	60	6009	4.21	dn	no	0.14	0.32	3	$0.01^{+0.11}_{-0.09}$	0	...	...
88656	9.08	43	5301	4.65	h	no	0.07	0.01	3	$0.19^{+0.05}_{-0.06}$	6	$-0.23^{+0.07}_{-0.10}$	$0.24^{+0.06}_{-0.05}$
88725	7.75	36	5581	4.54	dn	no	-0.55	-0.59	1	$-0.10^{+0.10}_{-0.11}$	0	...	...
88775	7.74	76	5830	4.14	dn	no	0.09	0.24	3	$0.14^{+0.07}_{-0.07}$	2	$0.05^{+0.03}_{-0.03}$	$0.51^{+0.09}_{-0.09}$
88986	6.46	32	5838	4.23	dn	no	0.03	0.14	1	$0.22^{+0.06}_{-0.06}$	1	$0.12^{+0.03}_{-0.03}$	$0.51^{+0.08}_{-0.08}$
89022	8.97	78	5850	4.36	dn	no	0.17	0.34	3	$-0.03^{+0.10}_{-0.15}$	0	...	...
89269	6.66	20	5586	4.44	dn	no	-0.18	-0.14	43	$-0.14^{+0.04}_{-0.04}$	27	$-0.13^{+0.03}_{-0.03}$	$0.66^{+0.08}_{-0.07}$
89391	7.94	120	4976	3.59	dn	no	-0.06	-0.00	9	$0.26^{+0.03}_{-0.03}$	0	...	...
89454	8.03	40	5681	4.41	...	no	0.11	0.16	0	...	2	$0.07^{+0.04}_{-0.04}$	...

Table 6.6 (cont'd): Stellar Data.

Name <sup>a</sup> (HD)	$V^b$ (mag)	$d^b$ (pc)	$T^c$ (K)	$\log g^c$ (cgs)	Pop <sup>d</sup>	Host	[M/H] <sup>c,e</sup>	[Ni/H] <sup>c</sup>	$N_O$	[O/H] <sup>f</sup>	$N_C$	[C/H] <sup>f</sup>	C/O <sup>f</sup>
89793	8.84	62	5678	4.41	dn	no	0.07	0.21	4	$-0.03^{+0.08}_{-0.09}$	3	$0.14^{+0.03}_{-0.04}$	$0.92^{+0.20}_{-0.18}$
90054	7.87	68	6131	4.26	dn/dk	no	0.28	0.47	1	$0.16^{+0.07}_{-0.07}$	3	$0.31^{+0.03}_{-0.03}$	$0.90^{+0.16}_{-0.16}$
90125	6.33	100	4928	3.16	dn	no	-0.13	-0.03	1	$0.13^{+0.04}_{-0.04}$	0	...	...
90156	6.92	22	5626	4.63	dn	no	-0.21	-0.17	6	$-0.06^{+0.05}_{-0.07}$	52	$-0.14^{+0.03}_{-0.03}$	$0.53^{+0.09}_{-0.07}$
90211	8.05	76	6160	4.19	h	no	0.20	0.34	1	$0.04^{+0.12}_{-0.17}$	0	...	...
90323	8.27	79	5970	4.12	dn	no	0.21	0.36	1	$0.09^{+0.09}_{-0.09}$	1	$0.28^{+0.03}_{-0.03}$	$0.96^{+0.22}_{-0.20}$
90383	8.80	80	5710	4.15	dn	no	0.20	0.34	3	$-0.06^{+0.09}_{-0.13}$	0	...	...
90681	7.83	45	5995	4.49	dn	no	0.24	0.40	0	...	3	$0.16^{+0.03}_{-0.03}$	...
90711	7.89	32	5466	4.50	dn	no	0.24	0.40	13	$0.18^{+0.06}_{-0.06}$	10	$0.29^{+0.03}_{-0.03}$	$0.81^{+0.13}_{-0.13}$
90722	7.88	50	5719	4.31	dn	no	0.29	0.46	2	$0.28^{+0.06}_{-0.06}$	1	$0.29^{+0.04}_{-0.04}$	$0.65^{+0.11}_{-0.10}$
90905	6.88	31	6148	4.57	dn	no	0.03	0.05	0	...	5	$-0.10^{+0.04}_{-0.04}$	...
91148	7.93	37	5615	4.43	dn	no	0.08	0.17	3	$-0.13^{+0.09}_{-0.11}$	1	$0.06^{+0.04}_{-0.04}$	$0.98^{+0.26}_{-0.21}$
91204	7.82	51	5914	4.29	dn	no	0.17	0.33	1	$0.27^{+0.06}_{-0.08}$	1	$0.20^{+0.03}_{-0.03}$	$0.54^{+0.11}_{-0.09}$
91275	8.68	50	5575	4.35	dn	no	-0.01	0.00	0	...	3	$-0.10^{+0.04}_{-0.05}$	...
91331	9.11	103	5935	4.35	dn	no	0.11	0.23	0	...	3	$0.08^{+0.04}_{-0.04}$	...
91348	8.63	89	5728	4.31	dn	no	0.39	0.67	0	...	3	$0.48^{+0.03}_{-0.03}$	...
91856	8.71	45	5379	4.31	dn	no	-0.00	0.03	3	$-0.09^{+0.08}_{-0.08}$	0	...	...
91876	8.22	93	6208	4.11	dn	no	0.19	0.39	3	$0.22^{+0.13}_{-0.14}$	4	$0.29^{+0.03}_{-0.04}$	$0.73^{+0.24}_{-0.22}$
91909	9.19	70	5669	4.38	dn	no	-0.12	-0.11	3	$-0.05^{+0.05}_{-0.06}$	3	$-0.09^{+0.04}_{-0.04}$	$0.59^{+0.09}_{-0.09}$
92194	8.62	48	5655	4.43	dn	no	0.10	0.16	0	...	2	$0.02^{+0.04}_{-0.04}$	...
92222A	9.40	...	5753	4.70	...	no	0.19	0.29	0	...	8	$-0.01^{+0.03}_{-0.04}$	...
92222B	9.30	...	5690	4.65	...	no	0.20	0.32	3	$-0.01^{+0.11}_{-0.12}$	4	$-0.02^{+0.04}_{-0.04}$	$0.61^{+0.19}_{-0.16}$
92320	8.38	41	5636	4.43	dn	no	-0.10	-0.07	0	...	3	$-0.08^{+0.04}_{-0.04}$	...
92788	7.31	32	5836	4.66	dn	yes	0.16	0.41	4	$0.11^{+0.10}_{-0.13}$	3	$0.31^{+0.03}_{-0.04}$	$1.01^{+0.32}_{-0.23}$
92855	7.28	35	6140	4.58	dn	no	-0.07	-0.03	0	...	5	$-0.09^{+0.04}_{-0.03}$	...

Table 6.6 (cont'd): Stellar Data.

Name <sup>a</sup> (HD)	$V^b$ (mag)	$d^b$ (pc)	$T^c$ (K)	$\log g^c$ (cgs)	Pop <sup>d</sup>	Host	[M/H] <sup>c,e</sup>	[Ni/H] <sup>c</sup>	$N_O$	[O/H] <sup>f</sup>	$N_C$	[C/H] <sup>f</sup>	C/O <sup>f</sup>
92885	8.11	74	6311	4.46	dn	no	0.09	0.30	0	...	3	$0.10^{+0.03}_{-0.03}$	...
92945	7.72	21	5183	4.76	dn	no	-0.12	0.08	1	$0.12^{+0.06}_{-0.07}$	0	...	...
93215	8.05	47	5798	4.46	dn	no	0.16	0.32	0	...	3	$0.14^{+0.04}_{-0.03}$	...
93664	7.80	90	6025	4.12	dn	no	0.17	0.30	1	$0.17^{+0.06}_{-0.07}$	3	$0.23^{+0.03}_{-0.03}$	$0.72^{+0.13}_{-0.11}$
93745	7.48	55	5918	4.12	dn	no	0.02	0.15	3	$0.05^{+0.05}_{-0.08}$	3	$0.10^{+0.03}_{-0.03}$	$0.71^{+0.13}_{-0.09}$
93849	7.86	74	6109	4.20	dn	no	0.17	0.31	1	$-0.06^{+0.09}_{-0.12}$	1	$0.28^{+0.03}_{-0.03}$	$1.39^{+0.39}_{-0.29}$
93932	7.53	52	5897	4.20	dn	no	0.05	0.15	1	$0.11^{+0.06}_{-0.08}$	1	$0.14^{+0.03}_{-0.04}$	$0.68^{+0.14}_{-0.11}$
94151	7.84	37	5592	4.43	dn	no	0.04	0.13	3	$0.13^{+0.06}_{-0.06}$	6	$0.08^{+0.03}_{-0.03}$	$0.56^{+0.09}_{-0.09}$
94292	7.75	76	5904	4.28	dn	no	0.06	0.20	2	$0.08^{+0.06}_{-0.07}$	3	$0.09^{+0.04}_{-0.03}$	$0.65^{+0.11}_{-0.10}$
94375	8.00	74	6076	4.02	dn	no	0.06	0.18	1	$0.00^{+0.10}_{-0.14}$	0	...	...
94383	8.35	70	6193	4.28	dn	no	0.05	0.17	3	$0.13^{+0.05}_{-0.10}$	0	...	...
95088	8.42	105	5179	3.85	...	no	0.17	0.33	10	$0.16^{+0.04}_{-0.06}$	0	...	...
95128	5.03	14	5882	4.38	dn	yes	0.02	0.12	14	$0.03^{+0.05}_{-0.05}$	8	$0.08^{+0.04}_{-0.03}$	$0.71^{+0.10}_{-0.10}$
95188	8.49	36	5482	4.65	dn	no	-0.03	-0.02	5	$0.08^{+0.07}_{-0.12}$	6	$-0.23^{+0.07}_{-0.07}$	$0.31^{+0.10}_{-0.07}$
95622	9.08	108	6084	4.26	dn	no	-0.16	-0.07	3	$0.02^{+0.07}_{-0.10}$	8	$-0.11^{+0.03}_{-0.03}$	$0.47^{+0.11}_{-0.08}$
96167	8.09	84	5820	4.18	dn	yes	0.28	0.53	17	$0.11^{+0.06}_{-0.06}$	30	$0.34^{+0.03}_{-0.03}$	$1.06^{+0.16}_{-0.16}$
96361	8.74	90	5736	4.11	dn	no	-0.02	0.03	1	$-0.03^{+0.05}_{-0.05}$	4	$0.07^{+0.03}_{-0.03}$	$0.78^{+0.11}_{-0.10}$
96529	8.85	77	5668	4.18	dn	no	0.19	0.26	4	$0.11^{+0.06}_{-0.07}$	4	$0.15^{+0.03}_{-0.03}$	$0.68^{+0.12}_{-0.10}$
96700	6.51	26	5865	4.41	dn	no	-0.17	-0.14	0	...	5	$-0.14^{+0.03}_{-0.04}$	...
96937	7.69	30	5393	4.39	dn	no	0.09	0.17	1	$-0.13^{+0.12}_{-0.15}$	0	...	...
97038	7.70	66	5789	4.36	dn	no	0.12	0.27	0	...	1	$0.18^{+0.04}_{-0.04}$	...
97343	7.05	21	5399	4.56	dn	no	-0.05	0.03	16	$0.17^{+0.04}_{-0.04}$	43	$0.17^{+0.03}_{-0.03}$	$0.64^{+0.08}_{-0.07}$
97645	7.88	63	6171	4.32	dn	no	0.19	0.38	3	$0.15^{+0.07}_{-0.08}$	3	$0.12^{+0.03}_{-0.04}$	$0.58^{+0.12}_{-0.11}$
97658	7.76	21	5148	4.65	dn	no	-0.27	-0.24	88	$-0.07^{+0.04}_{-0.03}$	0	...	...
97854	8.23	81	6211	4.45	dn	no	0.22	0.46	0	...	5	$0.24^{+0.03}_{-0.03}$	...

Table 6.6 (cont'd): Stellar Data.

Name <sup>a</sup> (HD)	$V^b$ (mag)	$d^b$ (pc)	$T^c$ (K)	$\log g^c$ (cgs)	Pop <sup>d</sup>	Host	[M/H] <sup>c,e</sup>	[Ni/H] <sup>c</sup>	$N_O$	[O/H] <sup>f</sup>	$N_C$	[C/H] <sup>f</sup>	C/O <sup>f</sup>
98281	7.29	21	5419	4.61	dn	no	-0.17	-0.17	51	$-0.03^{+0.04}_{-0.03}$	28	$-0.10^{+0.03}_{-0.03}$	$0.54^{+0.06}_{-0.06}$
98553	7.54	33	6009	4.69	dn	no	-0.31	-0.31	0	...	2	$-0.35^{+0.07}_{-0.19}$	...
98618	7.65	38	5812	4.42	dn	no	0.00	0.10	0	...	2	$0.04^{+0.03}_{-0.03}$	...
98630	8.08	101	6124	4.10	dn	no	0.25	0.49	3	$0.23^{+0.06}_{-0.09}$	6	$0.28^{+0.03}_{-0.03}$	$0.72^{+0.15}_{-0.11}$
98736	7.93	31	5291	4.32	dn	no	0.35	0.46	2	$0.09^{+0.11}_{-0.13}$	0	...	...
99109	9.10	60	5272	4.44	dn	yes	0.25	0.43	7	$0.24^{+0.06}_{-0.07}$	0	...	...
99491	6.49	17	5502	4.58	dn	no	0.23	0.42	85	$0.17^{+0.06}_{-0.05}$	67	$0.33^{+0.03}_{-0.03}$	$0.92^{+0.13}_{-0.13}$
99492	7.58	17	4955	4.77	dn	yes	0.24	0.43	53	$0.28^{+0.04}_{-0.04}$	0	...	...
100069	7.97	84	5929	4.07	dn	no	0.13	0.31	1	$0.22^{+0.06}_{-0.07}$	1	$0.11^{+0.03}_{-0.03}$	$0.50^{+0.08}_{-0.08}$
100180	6.27	23	5989	4.38	dn	no	-0.02	0.03	29	$0.01^{+0.04}_{-0.06}$	22	$0.03^{+0.03}_{-0.03}$	$0.67^{+0.11}_{-0.08}$
100623	5.96	9	5189	4.68	dn	no	-0.32	-0.32	9	$-0.11^{+0.05}_{-0.05}$	0	...	...
101165	9.18	97	6054	4.15	dn	no	-0.02	0.08	0	...	1	$0.05^{+0.04}_{-0.03}$	...
101348	7.82	81	5788	4.07	dn	no	0.31	0.52	0	...	1	$0.27^{+0.04}_{-0.04}$	...
101444	8.50	41	5319	4.43	dn	no	-0.05	-0.01	1	$0.23^{+0.06}_{-0.06}$	1	$0.23^{+0.06}_{-0.06}$	$0.64^{+0.13}_{-0.13}$
101472	7.41	38	6191	4.43	dn	no	-0.05	-0.07	0	...	4	$-0.07^{+0.03}_{-0.04}$	...
101501	5.31	9	5488	4.43	dn	no	-0.03	-0.04	1	$0.02^{+0.08}_{-0.10}$	1	$-0.10^{+0.04}_{-0.04}$	$0.48^{+0.12}_{-0.10}$
101675	9.00	84	5651	4.33	dn	no	0.14	0.26	2	$0.03^{+0.08}_{-0.11}$	4	$0.11^{+0.04}_{-0.04}$	$0.76^{+0.20}_{-0.16}$
101847	8.33	59	5924	4.44	dn	no	0.09	0.21	6	$-0.07^{+0.06}_{-0.08}$	8	$0.10^{+0.03}_{-0.03}$	$0.91^{+0.19}_{-0.15}$
101904	8.21	79	5868	4.09	dn	no	0.07	0.18	0	...	8	$0.11^{+0.03}_{-0.03}$	...
101959	6.97	32	6049	4.39	dn	no	-0.11	-0.12	4	$-0.06^{+0.08}_{-0.09}$	4	$-0.17^{+0.03}_{-0.04}$	$0.50^{+0.11}_{-0.10}$
102071	7.97	30	5279	4.53	dn	no	-0.07	0.08	2	$-0.18^{+0.12}_{-0.19}$	0	...	...
102158	8.06	52	5725	4.49	dk	no	-0.26	-0.33	0	...	2	$-0.09^{+0.04}_{-0.04}$	...
102283	8.30	104	6000	4.12	dn	no	0.22	0.38	1	$0.17^{+0.08}_{-0.09}$	0	...	...
102361	8.16	84	6290	4.45	dn	no	0.17	0.35	0	...	1	$0.22^{+0.03}_{-0.03}$	...
102365	4.89	9	5630	4.57	dn	no	-0.26	-0.25	17	$-0.01^{+0.04}_{-0.04}$	1	$-0.13^{+0.05}_{-0.05}$	$0.49^{+0.07}_{-0.07}$

Table 6.6 (cont'd): Stellar Data.

Name <sup>a</sup> (HD)	$V^b$ (mag)	$d^b$ (pc)	$T^c$ (K)	$\log g^c$ (cgs)	Pop <sup>d</sup>	Host	[M/H] <sup>c,e</sup>	[Ni/H] <sup>c</sup>	$N_O$	[O/H] <sup>f</sup>	$N_C$	[C/H] <sup>f</sup>	C/O <sup>f</sup>
103095	6.42	9	4950	4.66	h	no	-1.16	-1.39	3	$-0.67^{+0.07}_{-0.11}$	0	...	...
103417	8.80	51	5532	4.36	dn	no	0.18	0.31	0	...	4	$0.23^{+0.03}_{-0.04}$	...
103432	8.20	37	5641	4.52	dn	no	-0.10	-0.09	1	$-0.01^{+0.08}_{-0.11}$	2	$-0.19^{+0.05}_{-0.04}$	$0.42^{+0.11}_{-0.09}$
103459	7.60	62	5782	4.13	dn	no	0.22	0.40	5	$0.15^{+0.06}_{-0.06}$	11	$0.23^{+0.03}_{-0.03}$	$0.75^{+0.12}_{-0.11}$
103828	8.44	54	5701	4.28	dn	no	-0.02	0.04	1	$-0.12^{+0.07}_{-0.09}$	0	...	...
103829	9.24	89	5750	4.36	dn	no	0.03	0.20	0	...	2	$0.25^{+0.04}_{-0.04}$	...
103847	8.07	29	5320	4.63	dn	no	0.07	0.06	4	$0.03^{+0.08}_{-0.08}$	6	$-0.23^{+0.06}_{-0.06}$	$0.35^{+0.08}_{-0.08}$
103890	8.00	64	6203	4.29	dn	no	-0.06	0.06	1	$0.01^{+0.08}_{-0.10}$	2	$-0.01^{+0.03}_{-0.03}$	$0.59^{+0.14}_{-0.12}$
104067	7.92	20	4956	4.64	dn	no	0.04	0.14	18	$0.08^{+0.04}_{-0.04}$	0	...	...
104304	5.54	12	5565	4.56	dn	no	0.16	0.42	26	$0.17^{+0.05}_{-0.06}$	18	$0.36^{+0.03}_{-0.03}$	$0.96^{+0.15}_{-0.13}$
104389	8.45	59	5967	4.43	dn	no	-0.01	0.05	0	...	12	$-0.04^{+0.03}_{-0.03}$	...
104437	8.62	64	5743	4.35	dn	no	0.16	0.29	3	$0.04^{+0.08}_{-0.15}$	1	$0.14^{+0.04}_{-0.04}$	$0.81^{+0.28}_{-0.16}$
104556	6.64	55	5051	3.79	dk	no	-0.27	-0.27	3	$0.20^{+0.03}_{-0.03}$	0	...	...
104588	8.66	84	5781	4.21	dn	no	0.28	0.48	2	$0.16^{+0.06}_{-0.07}$	4	$0.21^{+0.05}_{-0.03}$	$0.71^{+0.13}_{-0.13}$
104800	9.21	62	5626	4.53	dk	no	-0.64	-0.75	3	$-0.22^{+0.15}_{-0.08}$	3	$-0.44^{+0.05}_{-0.06}$	$0.38^{+0.09}_{-0.14}$
105113	6.49	51	5922	3.97	dn	no	-0.11	-0.04	2	$0.01^{+0.05}_{-0.05}$	4	$-0.10^{+0.03}_{-0.03}$	$0.48^{+0.07}_{-0.07}$
105279	8.40	80	6008	4.43	dn	no	0.24	0.49	2	$0.16^{+0.09}_{-0.09}$	2	$0.32^{+0.03}_{-0.03}$	$0.92^{+0.20}_{-0.19}$
105304	9.63	41	4866	4.53	dn	no	-0.03	-0.02	5	$-0.05^{+0.07}_{-0.12}$	0	...	...
105631	7.46	24	5462	4.57	dn	no	0.14	0.23	68	$0.10^{+0.05}_{-0.04}$	86	$0.04^{+0.03}_{-0.03}$	$0.54^{+0.07}_{-0.07}$
105844	8.07	42	5453	4.31	dn	no	0.20	0.29	0	...	1	$0.23^{+0.04}_{-0.05}$	...
106088	8.37	106	5604	4.08	dn	no	0.35	0.57	1	$0.07^{+0.12}_{-0.14}$	5	$0.24^{+0.03}_{-0.03}$	$0.93^{+0.32}_{-0.26}$
106116	7.43	33	5681	4.42	dn	no	0.12	0.22	1	$0.13^{+0.06}_{-0.06}$	2	$0.06^{+0.03}_{-0.03}$	$0.53^{+0.09}_{-0.08}$
106156	7.92	30	5492	4.58	dn	no	0.19	0.30	1	$0.09^{+0.10}_{-0.11}$	2	$0.17^{+0.04}_{-0.04}$	$0.76^{+0.21}_{-0.19}$
106949	8.36	100	6071	3.98	dn	no	-0.07	0.02	1	$0.07^{+0.09}_{-0.10}$	1	$-0.11^{+0.03}_{-0.04}$	$0.42^{+0.11}_{-0.10}$
107087	8.04	82	6127	4.26	dn	no	0.11	0.29	0	...	1	$0.15^{+0.03}_{-0.03}$	...

Table 6.6 (cont'd): Stellar Data.

Name <sup>a</sup> (HD)	$V^b$ (mag)	$d^b$ (pc)	$T^c$ (K)	$\log g^c$ (cgs)	Pop <sup>d</sup>	Host	[M/H] <sup>c,e</sup>	[Ni/H] <sup>c</sup>	$N_O$	[O/H] <sup>f</sup>	$N_C$	[C/H] <sup>f</sup>	C/O <sup>f</sup>
107146	7.04	28	5882	4.47	dn	no	-0.05	-0.05	0	...	4	$-0.17^{+0.04}_{-0.04}$	...
107148	8.01	51	5797	4.45	dn	yes	0.27	0.42	9	$0.20^{+0.06}_{-0.06}$	18	$0.24^{+0.03}_{-0.03}$	$0.70^{+0.11}_{-0.11}$
107181	8.43	82	5674	4.14	dn	no	0.29	0.47	2	$0.17^{+0.06}_{-0.10}$	2	$0.24^{+0.04}_{-0.04}$	$0.74^{+0.19}_{-0.12}$
107211	8.38	67	5909	4.46	dn	no	0.33	0.58	1	$0.22^{+0.09}_{-0.10}$	4	$0.40^{+0.03}_{-0.04}$	$0.94^{+0.24}_{-0.20}$
108300	9.05	83	5884	4.28	...	no	0.02	0.15	1	$-0.06^{+0.09}_{-0.10}$	1	$0.14^{+0.04}_{-0.04}$	$1.00^{+0.25}_{-0.22}$
108874	8.76	68	5551	4.35	dn	yes	0.15	0.27	2	$0.20^{+0.06}_{-0.07}$	11	$0.21^{+0.03}_{-0.03}$	$0.65^{+0.11}_{-0.09}$
108916	8.49	55	5739	4.25	dn	no	0.08	0.21	1	$0.02^{+0.10}_{-0.12}$	1	$0.16^{+0.04}_{-0.04}$	$0.86^{+0.25}_{-0.21}$
108942	7.91	47	5802	4.40	dn	no	0.19	0.41	2	$0.14^{+0.08}_{-0.12}$	4	$0.29^{+0.03}_{-0.03}$	$0.89^{+0.26}_{-0.18}$
109202	8.12	65	6029	4.35	dn	no	0.20	0.38	0	...	3	$0.21^{+0.03}_{-0.04}$	...
109286	8.78	52	5663	4.43	dn	no	0.09	0.13	1	$-0.23^{+0.11}_{-0.14}$	0	...	...
109331	8.07	71	6186	4.23	dn	no	0.04	0.17	2	$0.04^{+0.14}_{-0.13}$	2	$0.09^{+0.03}_{-0.03}$	$0.71^{+0.22}_{-0.23}$
109358	4.24	8	5930	4.43	dn	no	-0.10	-0.11	38	$-0.02^{+0.03}_{-0.03}$	61	$-0.19^{+0.03}_{-0.03}$	$0.42^{+0.04}_{-0.04}$
109718	9.12	109	5899	4.09	dn	no	0.11	0.24	3	$0.10^{+0.06}_{-0.06}$	1	$0.06^{+0.03}_{-0.03}$	$0.58^{+0.09}_{-0.09}$
109749	8.08	59	5815	4.27	dn	yes	0.19	0.38	9	$-0.02^{+0.06}_{-0.07}$	10	$0.28^{+0.03}_{-0.03}$	$1.24^{+0.21}_{-0.19}$
109929	7.64	81	6065	4.12	dn	no	0.30	0.48	0	...	11	$0.31^{+0.03}_{-0.03}$	...
110044	8.99	41	5133	4.34	dn	no	0.02	0.02	3	$0.04^{+0.07}_{-0.15}$	0	...	...
110537	7.83	46	5752	4.40	dn	no	0.09	0.19	0	...	8	$0.11^{+0.03}_{-0.03}$	...
110745	8.68	84	6087	4.36	dn	no	0.03	0.16	1	$-0.03^{+0.15}_{-0.19}$	2	$0.08^{+0.03}_{-0.03}$	$0.81^{+0.36}_{-0.28}$
111031	6.87	30	5806	4.38	dn	no	0.26	0.40	4	$0.20^{+0.07}_{-0.08}$	11	$0.22^{+0.03}_{-0.03}$	$0.66^{+0.13}_{-0.11}$
111153	7.91	107	6430	4.06	dn	no	0.10	0.24	0	...	3	$0.11^{+0.03}_{-0.03}$	...
111395	6.29	17	5654	4.55	dn	no	0.06	0.12	0	...	1	$-0.01^{+0.05}_{-0.05}$	...
111515	8.13	33	5399	4.62	dn/dk	no	-0.43	-0.49	4	$-0.10^{+0.07}_{-0.07}$	5	$-0.16^{+0.07}_{-0.07}$	$0.55^{+0.13}_{-0.12}$
111528	8.25	95	5737	4.05	dn	no	0.06	0.21	1	$0.03^{+0.08}_{-0.09}$	1	$0.10^{+0.04}_{-0.04}$	$0.75^{+0.17}_{-0.15}$
111814	8.14	83	5725	4.07	dn	no	0.24	0.43	9	$0.11^{+0.05}_{-0.06}$	10	$0.19^{+0.03}_{-0.03}$	$0.77^{+0.11}_{-0.10}$
112019	7.69	47	6171	4.42	dn	no	-0.11	-0.02	0	...	2	$-0.09^{+0.03}_{-0.04}$	...

Table 6.6 (cont'd): Stellar Data.

Name <sup>a</sup> (HD)	$V^b$ (mag)	$d^b$ (pc)	$T^c$ (K)	$\log g^c$ (cgs)	Pop <sup>d</sup>	Host	[M/H] <sup>c,e</sup>	[Ni/H] <sup>c</sup>	$N_O$	[O/H] <sup>f</sup>	$N_C$	[C/H] <sup>f</sup>	C/O <sup>f</sup>
112257	7.80	41	5697	4.45	dn	no	0.02	0.06	4	$0.18^{+0.05}_{-0.05}$	1	$0.06^{+0.04}_{-0.04}$	$0.48^{+0.07}_{-0.07}$
112337	9.08	101	5704	4.26	dn	no	0.26	0.46	0	...	2	$0.33^{+0.03}_{-0.03}$	...
112415	8.75	58	5604	4.28	dn	no	0.33	0.47	3	$0.22^{+0.06}_{-0.15}$	1	$0.29^{+0.04}_{-0.04}$	$0.76^{+0.27}_{-0.13}$
113039	8.94	68	5831	4.35	dn	no	-0.04	0.04	1	$0.03^{+0.09}_{-0.12}$	0	...	...
113938	9.16	97	5866	4.14	dn	no	0.28	0.45	0	...	1	$0.26^{+0.04}_{-0.04}$	...
114174	6.78	26	5781	4.51	dn	no	0.03	0.13	2	$0.09^{+0.06}_{-0.08}$	0	...	...
114375	8.49	109	5048	3.56	dn	no	0.09	0.15	4	$0.03^{+0.06}_{-0.04}$	0	...	...
114613	4.85	20	5782	4.09	dn	no	0.15	0.35	0	...	26	$0.15^{+0.03}_{-0.03}$	...
114729	6.68	35	5821	4.14	dn	yes	-0.20	-0.22	2	$-0.08^{+0.05}_{-0.07}$	1	$-0.19^{+0.03}_{-0.03}$	$0.49^{+0.09}_{-0.06}$
114783	7.56	20	5135	4.53	dn	yes	0.10	0.18	12	$0.10^{+0.06}_{-0.05}$	0	...	...
114946	5.31	38	5114	3.54	dn	no	-0.29	-0.17	1	$-0.13^{+0.05}_{-0.06}$	0	...	...
115589	9.57	66	5259	4.55	dn	no	0.16	0.30	1	$0.33^{+0.05}_{-0.05}$	0	...	...
115617	4.74	8	5571	4.47	dn	yes	0.09	0.07	131	$0.08^{+0.04}_{-0.04}$	132	$0.09^{+0.03}_{-0.03}$	$0.65^{+0.07}_{-0.07}$
116321	7.81	97	6441	4.21	dn	no	0.20	0.44	0	...	8	$0.25^{+0.03}_{-0.03}$	...
116442	7.06	16	5182	4.56	dn	no	-0.30	-0.36	20	$-0.06^{+0.04}_{-0.03}$	0	...	...
116443	7.35	16	5038	4.58	dn	no	-0.29	-0.34	64	$-0.05^{+0.03}_{-0.03}$	0	...	...
117122	8.42	51	5640	4.32	dn	no	0.01	0.09	1	$-0.14^{+0.11}_{-0.16}$	7	$0.06^{+0.04}_{-0.03}$	$1.00^{+0.37}_{-0.26}$
117176	4.97	18	5545	4.07	dn	yes	-0.01	0.04	40	$0.14^{+0.03}_{-0.03}$	28	$0.01^{+0.04}_{-0.03}$	$0.47^{+0.05}_{-0.05}$
117207	7.26	33	5724	4.51	dn	yes	0.16	0.34	1	$0.20^{+0.09}_{-0.10}$	1	$0.20^{+0.03}_{-0.03}$	$0.64^{+0.15}_{-0.14}$
117378	7.64	39	6014	4.45	dn	no	-0.04	-0.02	0	...	1	$-0.12^{+0.04}_{-0.05}$	...
117497	8.76	78	6228	4.13	dn	no	-0.03	0.06	0	...	11	$-0.01^{+0.03}_{-0.03}$	...
118034	8.92	94	5859	4.23	dn	no	0.22	0.38	1	$0.11^{+0.08}_{-0.10}$	0	...	...
118914	8.89	73	5728	4.30	dn	no	0.17	0.25	1	$0.13^{+0.05}_{-0.06}$	1	$0.10^{+0.04}_{-0.03}$	$0.58^{+0.09}_{-0.09}$
119824	8.30	45	5739	4.41	dn	no	-0.08	-0.07	1	$-0.10^{+0.10}_{-0.15}$	0	...	...
120528	8.55	73	5617	4.05	dn	no	0.01	0.16	3	$0.01^{+0.06}_{-0.05}$	4	$0.24^{+0.03}_{-0.03}$	$1.07^{+0.15}_{-0.16}$

Table 6.6 (cont'd): Stellar Data.

Name <sup>a</sup> (HD)	$V^b$ (mag)	$d^b$ (pc)	$T^c$ (K)	$\log g^c$ (cgs)	Pop <sup>d</sup>	Host	[M/H] <sup>c,e</sup>	[Ni/H] <sup>c</sup>	$N_O$	[O/H] <sup>f</sup>	$N_C$	[C/H] <sup>f</sup>	C/O <sup>f</sup>
120666	8.87	76	5781	4.18	dn	no	0.14	0.27	3	$-0.02^{+0.06}_{-0.07}$	3	$0.15^{+0.03}_{-0.03}$	$0.93^{+0.16}_{-0.15}$
121320	7.89	33	5548	4.54	dn	no	-0.24	-0.24	2	$-0.13^{+0.09}_{-0.15}$	2	$-0.18^{+0.05}_{-0.05}$	$0.56^{+0.20}_{-0.13}$
121550	9.32	61	5305	4.46	dn	no	-0.03	0.04	9	$0.12^{+0.05}_{-0.05}$	32	$0.14^{+0.03}_{-0.03}$	$0.67^{+0.09}_{-0.09}$
121579	7.90	109	6389	4.14	dn	no	0.07	0.22	0	...	4	$0.09^{+0.03}_{-0.03}$	...
122255	8.64	93	6210	4.24	dn	no	-0.08	0.01	0	...	4	$-0.04^{+0.03}_{-0.03}$	...
122652	7.16	37	6093	4.25	dn	no	-0.01	0.02	1	$0.04^{+0.05}_{-0.06}$	3	$-0.04^{+0.03}_{-0.04}$	$0.52^{+0.09}_{-0.07}$
123265	8.35	38	5295	4.44	dn	no	0.17	0.28	4	$0.25^{+0.05}_{-0.05}$	0	...	...
123812	9.69	87	5202	4.53	dn	no	0.21	0.34	3	$0.29^{+0.06}_{-0.09}$	0	...	...
124106	7.93	23	5117	4.58	dn	no	-0.13	-0.11	4	$0.01^{+0.05}_{-0.06}$	0	...	...
124292	7.05	22	5501	4.65	dn	no	-0.10	-0.02	20	$-0.01^{+0.05}_{-0.04}$	27	$0.01^{+0.03}_{-0.03}$	$0.65^{+0.08}_{-0.09}$
125184	6.47	32	5691	4.16	dn	no	0.25	0.39	3	$0.25^{+0.05}_{-0.06}$	7	$0.22^{+0.03}_{-0.03}$	$0.59^{+0.09}_{-0.08}$
125455	7.58	20	5109	4.53	dn	no	-0.15	-0.13	9	$-0.08^{+0.05}_{-0.04}$	0	...	...
125612	8.31	52	5902	4.47	dn	yes	0.17	0.33	0	...	17	$0.11^{+0.03}_{-0.03}$	...
126053	6.25	17	5640	4.53	dn	no	-0.29	-0.29	7	$-0.08^{+0.05}_{-0.06}$	29	$-0.20^{+0.04}_{-0.03}$	$0.48^{+0.07}_{-0.07}$
126203	8.26	80	6101	4.19	dn	no	-0.05	0.04	1	$-0.03^{+0.13}_{-0.19}$	6	$0.06^{+0.03}_{-0.03}$	$0.77^{+0.34}_{-0.23}$
126614	8.81	68	5594	4.43	dn	no	0.46	0.69	11	$0.25^{+0.09}_{-0.09}$	24	$0.51^{+0.03}_{-0.03}$	$1.17^{+0.26}_{-0.24}$
126831	7.82	80	6183	3.95	dn	no	-0.12	-0.05	0	...	2	$0.01^{+0.03}_{-0.03}$	...
127334	6.36	23	5744	4.37	dn	no	0.22	0.36	8	$0.10^{+0.05}_{-0.05}$	38	$0.19^{+0.03}_{-0.03}$	$0.77^{+0.11}_{-0.10}$
129010	7.45	66	6052	4.01	dn	no	0.06	0.15	0	...	1	$0.09^{+0.03}_{-0.04}$	...
129191	8.19	54	5817	4.41	dn	no	0.22	0.36	0	...	2	$0.20^{+0.04}_{-0.03}$	...
129471	9.64	102	5688	4.46	dn	no	0.28	0.48	2	$0.16^{+0.12}_{-0.15}$	0	...	...
129814	7.52	41	5844	4.41	dn	no	-0.00	0.06	1	$0.12^{+0.06}_{-0.07}$	2	$0.07^{+0.03}_{-0.04}$	$0.56^{+0.10}_{-0.08}$
130087	7.52	55	6057	4.27	dn	no	0.24	0.41	1	$0.29^{+0.06}_{-0.06}$	1	$0.30^{+0.03}_{-0.03}$	$0.64^{+0.10}_{-0.09}$
130322	8.04	29	5308	4.41	dn	yes	-0.05	0.04	1	$0.05^{+0.06}_{-0.06}$	1	$0.22^{+0.08}_{-0.08}$	$0.95^{+0.21}_{-0.21}$
130672	7.65	75	6229	4.08	dn	no	-0.00	0.15	0	...	1	$0.05^{+0.03}_{-0.05}$	...

Table 6.6 (cont'd): Stellar Data.

Name <sup>a</sup> (HD)	$V^b$ (mag)	$d^b$ (pc)	$T^c$ (K)	$\log g^c$ (cgs)	Pop <sup>d</sup>	Host	[M/H] <sup>c,e</sup>	[Ni/H] <sup>c</sup>	$N_O$	[O/H] <sup>f</sup>	$N_C$	[C/H] <sup>f</sup>	C/O <sup>f</sup>
130992	7.81	16	4833	4.70	dn	no	-0.07	0.03	26	$-0.04^{+0.04}_{-0.03}$	0	...	...
131156	4.54	6	5570	4.65	dn	no	-0.07	-0.09	2	$-0.06^{+0.17}_{-0.13}$	3	$-0.06^{+0.09}_{-0.11}$	$0.64^{+0.25}_{-0.29}$
131183	7.89	56	5656	4.36	dn	no	0.09	0.20	3	$0.25^{+0.04}_{-0.05}$	7	$0.27^{+0.04}_{-0.04}$	$0.67^{+0.09}_{-0.09}$
131509	7.96	71	5112	3.84	dn	no	-0.15	-0.07	1	$-0.04^{+0.04}_{-0.05}$	0	...	...
131977	5.72	5	4744	4.76	dn	no	0.10	0.18	1	$0.15^{+0.06}_{-0.06}$	0	...	...
132130	7.91	67	5391	3.95	dn	no	0.09	0.21	0	...	1	$0.13^{+0.04}_{-0.05}$	...
132133	7.53	87	6154	4.00	dn	no	0.04	0.21	0	...	1	$0.09^{+0.03}_{-0.03}$	...
132142	7.77	23	5122	4.60	dn	no	-0.30	-0.32	6	$0.06^{+0.04}_{-0.04}$	0	...	...
132173	7.66	48	6254	4.50	dn	no	0.03	0.03	0	...	5	$-0.10^{+0.06}_{-0.04}$	...
133295	7.18	33	6089	4.43	dn	no	-0.02	-0.05	0	...	3	$-0.33^{+0.04}_{-0.05}$	...
134319	8.40	44	5662	4.52	dn	no	-0.12	-0.08	0	...	4	$-0.02^{+0.05}_{-0.07}$	...
134987	6.47	25	5750	4.35	dn	yes	0.24	0.41	15	$0.16^{+0.06}_{-0.05}$	20	$0.30^{+0.03}_{-0.03}$	$0.86^{+0.12}_{-0.13}$
135599	6.92	15	5221	4.46	dn	no	-0.09	-0.07	1	$-0.13^{+0.07}_{-0.08}$	0	...	...
135724	8.27	80	6107	4.37	dn	no	0.09	0.26	0	...	1	$0.07^{+0.03}_{-0.03}$	...
136352	5.65	14	5672	4.58	dn/dk	no	-0.23	-0.24	4	$0.03^{+0.07}_{-0.11}$	0	...	...
136442	6.34	36	4889	3.91	dn	no	0.30	0.51	32	$0.43^{+0.03}_{-0.03}$	0	...	...
136618	7.99	105	5935	4.02	dn	no	0.25	0.47	0	...	1	$0.26^{+0.04}_{-0.03}$	...
136713	7.97	21	4981	4.62	dn	no	0.15	0.32	60	$0.20^{+0.04}_{-0.04}$	0	...	...
136925	7.91	46	5717	4.50	dn	no	-0.14	-0.18	1	$0.22^{+0.05}_{-0.06}$	1	$-0.05^{+0.04}_{-0.04}$	$0.34^{+0.06}_{-0.05}$
137631	7.80	100	6251	3.88	dn	no	0.12	0.29	0	...	1	$0.20^{+0.04}_{-0.04}$	...
137778	7.57	20	5185	4.60	dn	no	0.18	0.32	3	$0.08^{+0.10}_{-0.13}$	0	...	...
137985	8.59	98	5856	4.35	dn	no	0.33	0.59	4	$0.15^{+0.08}_{-0.11}$	3	$0.40^{+0.03}_{-0.04}$	$1.13^{+0.30}_{-0.23}$
138004	7.48	32	5742	4.49	dn	no	-0.13	-0.06	3	$-0.09^{+0.09}_{-0.11}$	6	$0.12^{+0.04}_{-0.04}$	$1.03^{+0.27}_{-0.23}$
138278	8.36	107	5990	4.12	dn	no	0.21	0.39	3	$0.03^{+0.08}_{-0.09}$	1	$0.23^{+0.04}_{-0.03}$	$0.99^{+0.21}_{-0.20}$
138549	7.96	33	5534	4.43	dn	no	-0.02	0.08	3	$0.01^{+0.07}_{-0.08}$	1	$0.16^{+0.03}_{-0.03}$	$0.89^{+0.18}_{-0.17}$

Table 6.6 (cont'd): Stellar Data.

Name <sup>a</sup> (HD)	$V^b$ (mag)	$d^b$ (pc)	$T^c$ (K)	$\log g^c$ (cgs)	Pop <sup>d</sup>	Host	[M/H] <sup>c,e</sup>	[Ni/H] <sup>c</sup>	$N_O$	[O/H] <sup>f</sup>	$N_C$	[C/H] <sup>f</sup>	C/O <sup>f</sup>
138600	7.62	87	5904	3.79	dn	no	-0.07	0.06	6	$-0.02^{+0.05}_{-0.07}$	7	$0.11^{+0.03}_{-0.03}$	$0.84^{+0.14}_{-0.11}$
138776	8.74	66	5681	4.31	dn	no	0.32	0.51	1	$0.25^{+0.07}_{-0.09}$	2	$0.41^{+0.03}_{-0.03}$	$0.92^{+0.20}_{-0.17}$
139457	7.07	47	5957	3.99	dn	no	-0.42	-0.47	0	...	3	$-0.28^{+0.03}_{-0.03}$	...
139813	7.30	21	5491	4.71	dn	no	0.07	0.11	0	...	4	$-0.15^{+0.07}_{-0.06}$	...
139879	7.96	55	6060	4.22	dn	no	0.25	0.38	1	$0.18^{+0.07}_{-0.08}$	1	$0.28^{+0.04}_{-0.03}$	$0.80^{+0.16}_{-0.14}$
139907	8.65	79	5916	4.28	dn	no	0.29	0.48	3	$0.23^{+0.08}_{-0.07}$	5	$0.30^{+0.04}_{-0.03}$	$0.74^{+0.13}_{-0.16}$
140296	8.69	72	5894	4.37	dn	no	-0.02	0.04	1	$-0.02^{+0.11}_{-0.16}$	1	$-0.03^{+0.04}_{-0.04}$	$0.63^{+0.23}_{-0.17}$
140538A	5.86	14	5653	4.44	dn	no	0.06	0.11	108	$-0.09^{+0.05}_{-0.04}$	34	$-0.08^{+0.03}_{-0.03}$	$0.64^{+0.08}_{-0.08}$
140913	8.06	47	6048	4.57	dn	no	0.07	0.12	0	...	1	$0.19^{+0.03}_{-0.04}$	...
141004	4.42	11	5936	4.30	dn	no	0.09	0.10	0	...	1	$-0.26^{+0.10}_{-0.10}$	...
141085	8.70	107	5833	4.31	...	no	0.24	0.55	0	...	1	$0.42^{+0.05}_{-0.04}$	...
141186	8.77	73	6305	3.99	dn	no	0.07	0.18	0	...	3	$-0.01^{+0.03}_{-0.04}$	...
141937	7.25	33	5847	4.42	dn	yes	0.11	0.18	10	$0.05^{+0.05}_{-0.07}$	7	$0.09^{+0.04}_{-0.04}$	$0.70^{+0.12}_{-0.10}$
142229	8.08	40	5930	4.50	dn	no	0.01	0.03	0	...	1	$0.01^{+0.03}_{-0.04}$	...
142267	6.07	17	5756	4.48	dn	no	-0.38	-0.40	11	$-0.12^{+0.05}_{-0.05}$	7	$-0.24^{+0.03}_{-0.04}$	$0.49^{+0.07}_{-0.07}$
143006	10.21	...	5875	4.23	...	no	0.08	0.18	0	...	13	$-0.04^{+0.04}_{-0.04}$	...
143174	8.65	59	5864	4.25	dn	no	0.09	0.15	34	$-0.13^{+0.04}_{-0.04}$	5	$-0.01^{+0.03}_{-0.03}$	$0.83^{+0.10}_{-0.10}$
143332	8.00	100	6089	3.78	dn	no	0.18	0.29	0	...	2	$0.25^{+0.06}_{-0.04}$	...
143761	5.39	17	5823	4.37	dn	yes	-0.14	-0.13	23	$0.09^{+0.03}_{-0.03}$	20	$-0.08^{+0.03}_{-0.03}$	$0.43^{+0.05}_{-0.05}$
144585	6.32	28	5854	4.33	dn	no	0.25	0.43	0	...	16	$0.26^{+0.03}_{-0.03}$	...
144988	7.16	72	5862	3.86	dn	no	-0.20	-0.14	1	$-0.16^{+0.07}_{-0.08}$	1	$-0.24^{+0.04}_{-0.04}$	$0.52^{+0.10}_{-0.09}$
145229	7.45	33	5885	4.37	dn	no	-0.16	-0.20	1	$-0.23^{+0.14}_{-0.15}$	1	$-0.26^{+0.05}_{-0.05}$	$0.60^{+0.22}_{-0.20}$
145331	8.36	65	5683	4.50	dn	no	0.28	0.51	1	$0.38^{+0.08}_{-0.09}$	0	...	...
145675	6.61	18	5388	4.52	dn	yes	0.41	0.57	14	$0.22^{+0.09}_{-0.11}$	78	$0.52^{+0.03}_{-0.03}$	$1.26^{+0.32}_{-0.27}$
145809	6.68	39	5780	4.16	dn	no	-0.21	-0.21	2	$0.10^{+0.04}_{-0.05}$	1	$-0.26^{+0.04}_{-0.04}$	$0.27^{+0.04}_{-0.03}$

Table 6.6 (cont'd): Stellar Data.

Name <sup>a</sup> (HD)	V <sup>b</sup> (mag)	d <sup>b</sup> (pc)	T <sup>c</sup> (K)	log g <sup>c</sup> (cgs)	Pop <sup>d</sup>	Host	[M/H] <sup>c,e</sup>	[Ni/H] <sup>c</sup>	N <sub>O</sub>	[O/H] <sup>f</sup>	N <sub>C</sub>	[C/H] <sup>f</sup>	C/O <sup>f</sup>
145934	8.49	...	4899	3.19	...	no	-0.01	0.18	2	0.19 <sup>+0.04</sup> <sub>-0.04</sub>	0	...	...
145958B	7.38	...	5388	4.57	...	no	-0.06	0.02	37	0.00 <sup>+0.04</sup> <sub>-0.04</sub>	11	0.07 <sup>+0.03</sup> <sub>-0.04</sub>	0.73 <sup>+0.09</sup> <sub>-0.09</sub>
146050	7.97	59	5729	4.38	dn	no	0.28	0.53	4	0.23 <sup>+0.06</sup> <sub>-0.07</sub>	3	0.42 <sup>+0.04</sup> <sub>-0.05</sub>	1.00 <sup>+0.18</sup> <sub>-0.17</sub>
146233	5.49	14	5791	4.41	dn	no	0.04	0.10	91	0.01 <sup>+0.04</sup> <sub>-0.04</sub>	32	0.03 <sup>+0.03</sup> <sub>-0.03</sub>	0.67 <sup>+0.07</sup> <sub>-0.07</sub>
146434	8.14	78	5974	4.73	dn	no	0.09	0.22	1	0.26 <sup>+0.10</sup> <sub>-0.15</sub>	1	0.15 <sup>+0.04</sup> <sub>-0.04</sub>	0.49 <sup>+0.17</sup> <sub>-0.12</sub>
146775	7.68	41	5806	4.33	dn	no	-0.08	-0.03	0	...	1	0.04 <sup>+0.03</sup> <sub>-0.04</sub>	...
147062	7.59	65	6045	4.24	dn	no	0.19	0.41	1	0.23 <sup>+0.07</sup> <sub>-0.07</sub>	1	0.24 <sup>+0.03</sup> <sub>-0.03</sub>	0.65 <sup>+0.11</sup> <sub>-0.11</sub>
147231	7.83	40	5636	4.51	dn	no	0.03	0.07	0	...	1	0.11 <sup>+0.03</sup> <sub>-0.04</sub>	...
147776	8.40	21	4880	4.72	dn	no	-0.26	-0.28	1	-0.09 <sup>+0.05</sup> <sub>-0.06</sub>	0	...	...
147887	7.99	79	5972	4.34	dn	no	0.08	0.26	1	0.09 <sup>+0.10</sup> <sub>-0.12</sub>	0	...	...
148238	8.94	82	5858	4.30	dn	no	0.05	0.10	1	0.09 <sup>+0.08</sup> <sub>-0.09</sub>	1	-0.01 <sup>+0.04</sup> <sub>-0.04</sub>	0.49 <sup>+0.11</sup> <sub>-0.10</sub>
148284	9.01	83	5605	4.06	dn	no	0.11	0.26	10	0.13 <sup>+0.04</sup> <sub>-0.04</sub>	7	0.23 <sup>+0.04</sup> <sub>-0.03</sub>	0.79 <sup>+0.10</sup> <sub>-0.10</sub>
148428	7.57	65	5838	4.33	dn	no	0.24	0.53	0	...	1	0.24 <sup>+0.03</sup> <sub>-0.04</sub>	...
149026	8.15	78	6195	4.41	dn	yes	0.23	0.48	0	...	30	0.21 <sup>+0.03</sup> <sub>-0.03</sub>	...
149143	7.89	63	6058	4.45	dn	yes	0.25	0.51	15	0.26 <sup>+0.05</sup> <sub>-0.05</sub>	23	0.29 <sup>+0.03</sup> <sub>-0.03</sub>	0.68 <sup>+0.09</sup> <sub>-0.09</sub>
149661	5.77	9	5277	4.57	dn	no	0.05	0.10	1	0.12 <sup>+0.07</sup> <sub>-0.08</sub>	0	...	...
149724	7.85	55	5738	4.29	dn	no	0.36	0.53	0	...	1	0.35 <sup>+0.04</sup> <sub>-0.03</sub>	...
149750	8.58	80	5781	4.02	dn	no	0.14	0.27	3	-0.09 <sup>+0.12</sup> <sub>-0.09</sub>	4	0.16 <sup>+0.04</sup> <sub>-0.04</sub>	1.14 <sup>+0.25</sup> <sub>-0.33</sub>
149760	8.82	102	5743	4.36	dn	no	0.34	0.57	1	0.17 <sup>+0.13</sup> <sub>-0.18</sub>	0	...	...
149806	7.09	20	5359	4.54	dn	no	0.17	0.30	26	0.09 <sup>+0.06</sup> <sub>-0.06</sub>	18	0.14 <sup>+0.03</sup> <sub>-0.03</sub>	0.71 <sup>+0.11</sup> <sub>-0.11</sub>
150237	8.66	71	5852	4.18	dn	no	0.12	0.20	2	-0.09 <sup>+0.13</sup> <sub>-0.14</sub>	1	-0.13 <sup>+0.08</sup> <sub>-0.09</sub>	0.57 <sup>+0.22</sup> <sub>-0.20</sub>
150433	7.21	29	5649	4.56	dn	no	-0.22	-0.25	0	...	1	-0.06 <sup>+0.03</sup> <sub>-0.05</sub>	...
150437	7.84	55	5811	4.30	dn	no	0.28	0.45	1	-0.03 <sup>+0.10</sup> <sub>-0.10</sub>	1	0.31 <sup>+0.04</sup> <sub>-0.03</sub>	1.37 <sup>+0.35</sup> <sub>-0.33</sub>
150554	7.67	44	6010	4.29	dn	no	-0.01	0.02	0	...	4	-0.03 <sup>+0.04</sup> <sub>-0.03</sub>	...
150698	6.72	47	5878	4.12	dn	no	0.16	0.33	1	0.24 <sup>+0.05</sup> <sub>-0.05</sub>	2	0.14 <sup>+0.03</sup> <sub>-0.03</sub>	0.50 <sup>+0.07</sup> <sub>-0.07</sub>

Table 6.6 (cont'd): Stellar Data.

Name <sup>a</sup> (HD)	$V^b$ (mag)	$d^b$ (pc)	$T^c$ (K)	$\log g^c$ (cgs)	Pop <sup>d</sup>	Host	[M/H] <sup>c,e</sup>	[Ni/H] <sup>c</sup>	$N_O$	[O/H] <sup>f</sup>	$N_C$	[C/H] <sup>f</sup>	C/O <sup>f</sup>
150936	8.76	79	5691	4.31	dn	no	0.23	0.34	0	...	1	$0.19^{+0.03}_{-0.03}$	...
151504	8.08	39	5416	4.36	dn/dk	no	0.10	0.14	0	...	4	$0.25^{+0.04}_{-0.08}$	...
151541	7.56	24	5332	4.57	dn	no	-0.18	-0.14	0	...	38	$0.04^{+0.03}_{-0.03}$	...
151995	8.85	26	4832	4.72	dn	no	0.00	0.08	1	$0.09^{+0.06}_{-0.06}$	0	...	...
152125	8.92	66	5625	4.24	dn	no	0.08	0.19	7	$-0.07^{+0.08}_{-0.07}$	4	$0.17^{+0.04}_{-0.04}$	$1.10^{+0.20}_{-0.22}$
152792	6.81	47	5698	4.03	dn	no	-0.28	-0.26	0	...	3	$-0.27^{+0.03}_{-0.03}$	...
153378	8.06	82	5928	4.14	dn	no	0.08	0.30	0	...	8	$0.15^{+0.03}_{-0.03}$	...
153458	7.98	43	5907	4.59	dn	no	0.11	0.18	3	$0.20^{+0.07}_{-0.07}$	1	$0.10^{+0.04}_{-0.04}$	$0.51^{+0.09}_{-0.10}$
154088	6.59	18	5409	4.46	dn	no	0.28	0.42	121	$0.17^{+0.06}_{-0.05}$	57	$0.36^{+0.03}_{-0.03}$	$0.98^{+0.14}_{-0.15}$
154144	8.18	74	6050	4.15	dn	no	0.19	0.36	0	...	17	$0.28^{+0.03}_{-0.03}$	...
154325	8.51	66	5803	4.22	dn	no	0.07	0.22	5	$-0.02^{+0.05}_{-0.07}$	3	$0.16^{+0.03}_{-0.03}$	$0.96^{+0.17}_{-0.13}$
154656	8.53	42	5348	4.47	dn	no	-0.04	-0.09	4	$0.09^{+0.07}_{-0.07}$	1	$0.28^{+0.07}_{-0.08}$	$0.97^{+0.23}_{-0.21}$
154697	7.83	33	5577	4.41	...	no	0.05	0.15	0	...	1	$0.14^{+0.05}_{-0.05}$	...
154994	9.50	67	5481	4.44	dn	no	0.07	0.16	0	...	5	$0.14^{+0.04}_{-0.05}$	...
155415	8.29	86	6135	4.23	dn	no	0.24	0.47	0	...	1	$0.34^{+0.03}_{-0.03}$	...
155968	8.41	53	5726	4.42	dn	no	0.09	0.22	0	...	1	$0.17^{+0.04}_{-0.03}$	...
156079	7.53	56	5888	4.24	dn	no	0.23	0.44	1	$0.14^{+0.09}_{-0.10}$	1	$0.38^{+0.04}_{-0.04}$	$1.11^{+0.28}_{-0.25}$
156365	6.59	47	5856	4.09	dn	no	0.24	0.42	0	...	1	$0.30^{+0.04}_{-0.03}$	...
156549	7.91	90	6269	4.20	dn	no	0.11	0.34	0	...	3	$0.18^{+0.04}_{-0.03}$	...
157172	7.84	33	5490	4.53	dn	no	0.14	0.24	0	...	1	$0.08^{+0.04}_{-0.03}$	...
157214	5.38	14	5697	4.50	dk	no	-0.15	-0.24	6	$0.16^{+0.06}_{-0.10}$	0	...	...
157299	8.16	92	5855	4.15	dn/dk	no	0.16	0.34	1	$0.23^{+0.08}_{-0.09}$	1	$0.19^{+0.03}_{-0.04}$	$0.59^{+0.14}_{-0.11}$
157338	6.92	32	5961	4.28	dn	no	-0.09	-0.04	9	$-0.03^{+0.04}_{-0.04}$	17	$-0.04^{+0.03}_{-0.03}$	$0.62^{+0.08}_{-0.07}$
157347	6.28	19	5714	4.50	dn	no	0.03	0.12	56	$0.05^{+0.04}_{-0.04}$	49	$0.07^{+0.03}_{-0.03}$	$0.66^{+0.07}_{-0.07}$
158210	8.02	59	6108	4.40	dn	no	0.14	0.29	0	...	2	$0.04^{+0.03}_{-0.03}$	...

Table 6.6 (cont'd): Stellar Data.

Name <sup>a</sup> (HD)	$V^b$ (mag)	$d^b$ (pc)	$T^c$ (K)	$\log g^c$ (cgs)	Pop <sup>d</sup>	Host	[M/H] <sup>c,e</sup>	[Ni/H] <sup>c</sup>	$N_O$	[O/H] <sup>f</sup>	$N_C$	[C/H] <sup>f</sup>	C/O <sup>f</sup>
159222	6.52	23	5743	4.26	dn	no	0.09	0.18	4	$-0.13^{+0.07}_{-0.10}$	4	$0.14^{+0.03}_{-0.03}$	$1.19^{+0.29}_{-0.21}$
159868	7.24	52	5623	4.05	dn	yes	-0.00	0.07	9	$0.05^{+0.04}_{-0.06}$	21	$-0.12^{+0.03}_{-0.03}$	$0.43^{+0.06}_{-0.05}$
160693	8.39	54	5820	4.51	h	no	-0.35	-0.44	2	$-0.06^{+0.06}_{-0.07}$	1	$-0.20^{+0.04}_{-0.04}$	$0.45^{+0.08}_{-0.08}$
161424	7.62	78	5749	4.04	dn	no	0.18	0.37	1	$0.20^{+0.07}_{-0.07}$	0	...	...
161479	8.14	46	5747	4.54	dn	no	0.23	0.42	1	$0.22^{+0.07}_{-0.08}$	3	$0.30^{+0.13}_{-0.06}$	$0.75^{+0.17}_{-0.25}$
161797	3.42	8	5597	4.10	dn	no	0.24	0.40	5	$0.22^{+0.06}_{-0.06}$	22	$0.32^{+0.03}_{-0.03}$	$0.80^{+0.12}_{-0.13}$
161848	8.91	38	5075	4.59	dk	no	-0.26	-0.28	1	$-0.06^{+0.06}_{-0.07}$	0	...	...
161897	7.60	28	5623	4.58	dn	no	0.03	0.06	2	$0.11^{+0.07}_{-0.08}$	3	$0.07^{+0.06}_{-0.06}$	$0.57^{+0.13}_{-0.12}$
162232	8.59	74	5534	4.42	dn	no	0.12	0.25	0	...	1	$0.31^{+0.03}_{-0.03}$	...
162808	8.39	62	5982	4.36	dn	no	0.11	0.21	2	$0.13^{+0.12}_{-0.12}$	1	$0.10^{+0.04}_{-0.04}$	$0.59^{+0.18}_{-0.18}$
163153	6.92	44	5744	4.35	dn	no	0.31	0.59	11	$0.23^{+0.07}_{-0.07}$	6	$0.32^{+0.06}_{-0.04}$	$0.77^{+0.15}_{-0.16}$
163489	7.83	21	5004	3.13	...	no	0.04	0.36	12	$0.21^{+0.03}_{-0.04}$	0	...	...
163607	8.00	69	5519	3.91	dn	no	0.16	0.28	0	...	27	$0.20^{+0.03}_{-0.03}$	...
164330	7.72	83	5878	4.39	dn	no	0.18	0.43	2	$-0.16^{+0.13}_{-0.18}$	4	$0.21^{+0.03}_{-0.04}$	$1.47^{+0.62}_{-0.45}$
164507	6.28	45	5647	3.93	dn	no	0.11	0.26	1	$0.22^{+0.05}_{-0.06}$	2	$0.12^{+0.04}_{-0.06}$	$0.49^{+0.09}_{-0.07}$
164509	8.10	51	5945	4.42	dn	no	0.14	0.29	15	$0.00^{+0.06}_{-0.06}$	18	$0.10^{+0.03}_{-0.03}$	$0.79^{+0.12}_{-0.12}$
164595	7.07	28	5745	4.50	dn	no	-0.06	-0.00	1	$-0.03^{+0.08}_{-0.10}$	2	$0.01^{+0.03}_{-0.03}$	$0.69^{+0.17}_{-0.14}$
164922	7.01	21	5385	4.51	dn	yes	0.17	0.23	75	$0.21^{+0.04}_{-0.04}$	48	$0.26^{+0.03}_{-0.03}$	$0.71^{+0.08}_{-0.09}$
165269	7.29	62	6047	4.09	dn	no	0.20	0.38	0	...	1	$0.35^{+0.03}_{-0.03}$	...
165672	7.77	43	5892	4.43	dn	no	0.10	0.24	0	...	1	$0.16^{+0.03}_{-0.03}$	...
166435	6.84	25	5843	4.44	dn	no	0.01	-0.01	0	...	1	$-0.09^{+0.05}_{-0.04}$	...
166620	6.38	11	5000	4.47	dn	no	-0.05	-0.11	22	$0.06^{+0.04}_{-0.03}$	0	...	...
167389	7.38	33	5911	4.47	dn	no	0.01	0.02	1	$-0.08^{+0.11}_{-0.14}$	2	$-0.01^{+0.04}_{-0.06}$	$0.74^{+0.25}_{-0.19}$
167665	6.36	29	6115	4.22	dn	no	-0.14	-0.12	4	$-0.06^{+0.09}_{-0.12}$	1	$-0.04^{+0.05}_{-0.04}$	$0.65^{+0.19}_{-0.16}$
168009	6.30	22	5767	4.31	dn	no	-0.02	0.08	2	$-0.12^{+0.09}_{-0.11}$	2	$-0.14^{+0.07}_{-0.07}$	$0.61^{+0.18}_{-0.16}$

Table 6.6 (cont'd): Stellar Data.

Name <sup>a</sup> (HD)	$V^b$ (mag)	$d^b$ (pc)	$T^c$ (K)	$\log g^c$ (cgs)	Pop <sup>d</sup>	Host	[M/H] <sup>c,e</sup>	[Ni/H] <sup>c</sup>	$N_O$	[O/H] <sup>f</sup>	$N_C$	[C/H] <sup>f</sup>	C/O <sup>f</sup>
168443	6.92	37	5580	4.25	dn	yes	0.03	0.16	11	$0.29^{+0.04}_{-0.04}$	9	$0.26^{+0.03}_{-0.03}$	$0.58^{+0.07}_{-0.07}$
168723	3.23	18	4975	3.29	dn	no	-0.17	-0.01	1	$0.04^{+0.04}_{-0.04}$	0	...	...
168746	7.95	43	5564	4.52	dn	yes	-0.01	0.01	1	$0.20^{+0.05}_{-0.06}$	1	$0.24^{+0.04}_{-0.04}$	$0.69^{+0.11}_{-0.10}$
169830	5.90	36	6221	4.06	dn	yes	0.08	0.17	4	$0.06^{+0.05}_{-0.05}$	12	$0.17^{+0.03}_{-0.03}$	$0.81^{+0.11}_{-0.10}$
170174	8.31	...	5245	3.11	...	no	0.09	0.32	1	$0.32^{+0.04}_{-0.04}$	0	...	...
170469	8.21	64	5811	4.39	dn	yes	0.24	0.43	1	$-0.00^{+0.13}_{-0.18}$	0	...	...
170512	7.77	57	6147	4.35	dn	no	0.14	0.32	6	$0.06^{+0.07}_{-0.11}$	2	$0.21^{+0.05}_{-0.07}$	$0.90^{+0.28}_{-0.18}$
170657	6.81	13	5103	4.61	dn	no	-0.15	-0.14	1	$0.05^{+0.06}_{-0.06}$	0	...	...
171067	7.20	25	5643	4.50	dn	no	-0.03	0.02	1	$0.05^{+0.09}_{-0.10}$	0	...	...
171238	8.61	44	5460	4.50	dn	yes	0.15	0.29	1	$-0.11^{+0.15}_{-0.26}$	0	...	...
171665	7.43	30	5651	4.48	dn	no	-0.05	0.01	1	$-0.10^{+0.09}_{-0.11}$	2	$0.04^{+0.05}_{-0.13}$	$0.87^{+0.34}_{-0.22}$
171918	7.98	57	5775	4.28	dn	no	0.18	0.31	1	$-0.02^{+0.10}_{-0.13}$	0	...	...
171999	8.34	37	5312	4.42	dn	no	0.18	0.29	1	$0.24^{+0.09}_{-0.11}$	0	...	...
172051	5.85	12	5564	4.50	dn	no	-0.23	-0.22	33	$-0.24^{+0.04}_{-0.05}$	25	$-0.23^{+0.04}_{-0.03}$	$0.65^{+0.09}_{-0.08}$
172310	8.44	35	5414	4.60	dn	no	-0.37	-0.35	0	...	2	$-0.09^{+0.10}_{-0.09}$	...
172513	7.95	33	5531	4.51	dn	no	-0.02	0.03	0	...	1	$-0.01^{+0.04}_{-0.06}$	...
174719	7.51	28	5492	4.38	dn	no	-0.17	-0.18	1	$-0.15^{+0.12}_{-0.18}$	2	$0.01^{+0.04}_{-0.05}$	$0.91^{+0.40}_{-0.27}$
175425	7.90	52	5728	4.08	dn	no	0.11	0.16	0	...	1	$0.10^{+0.04}_{-0.04}$	...
175441	8.32	89	6103	4.08	dn	no	0.19	0.36	3	$0.03^{+0.06}_{-0.09}$	3	$0.21^{+0.03}_{-0.03}$	$0.95^{+0.21}_{-0.16}$
175541	8.02	127	5055	3.52	dn	yes	-0.23	-0.04	32	$-0.01^{+0.03}_{-0.03}$	0	...	...
176377	6.80	23	5788	4.40	dn	no	-0.23	-0.25	19	$-0.10^{+0.04}_{-0.04}$	0	...	...
176414	7.70	82	6256	3.90	dn	no	0.01	0.08	0	...	2	$0.11^{+0.04}_{-0.04}$	...
176982	8.36	95	5524	3.96	dn	no	-0.14	-0.04	1	$0.07^{+0.05}_{-0.06}$	3	$-0.08^{+0.04}_{-0.04}$	$0.46^{+0.08}_{-0.07}$
177033	9.92	46	4876	4.71	dn	no	-0.05	-0.05	1	$0.09^{+0.07}_{-0.08}$	0	...	...
177274	8.35	88	6135	4.21	dn	no	0.13	0.29	0	...	7	$0.09^{+0.04}_{-0.03}$	...

Table 6.6 (cont'd): Stellar Data.

Name <sup>a</sup> (HD)	$V^b$ (mag)	$d^b$ (pc)	$T^c$ (K)	$\log g^c$ (cgs)	Pop <sup>d</sup>	Host	[M/H] <sup>c,e</sup>	[Ni/H] <sup>c</sup>	$N_O$	[O/H] <sup>f</sup>	$N_C$	[C/H] <sup>f</sup>	C/O <sup>f</sup>
177830	7.18	59	4949	4.03	dn	yes	0.33	0.69	4	$0.41^{+0.05}_{-0.05}$	0	...	...
178911B	7.97	46	5668	4.55	dn	yes	0.25	0.38	7	$0.20^{+0.06}_{-0.06}$	0	...	...
179079	7.95	63	5701	4.17	dn	yes	0.21	0.38	46	$0.18^{+0.04}_{-0.04}$	33	$0.28^{+0.03}_{-0.03}$	$0.78^{+0.09}_{-0.09}$
179957	6.75	...	5676	4.34	...	no	0.00	0.06	4	$0.02^{+0.07}_{-0.10}$	0	...	...
179958	6.57	...	5760	4.39	...	no	0.05	0.12	8	$-0.03^{+0.07}_{-0.08}$	0	...	...
180684	7.02	58	6090	4.07	dn	no	0.00	0.09	1	$0.05^{+0.09}_{-0.12}$	2	$0.04^{+0.03}_{-0.03}$	$0.62^{+0.17}_{-0.13}$
181234	8.59	48	5354	4.47	dn	no	0.33	0.45	2	$0.33^{+0.06}_{-0.07}$	1	$0.39^{+0.06}_{-0.06}$	$0.73^{+0.15}_{-0.14}$
181253	7.51	75	6202	4.04	dn	no	0.11	0.23	0	...	6	$0.15^{+0.03}_{-0.03}$	...
182407	7.77	95	6022	4.02	dn	no	0.08	0.20	3	$0.09^{+0.07}_{-0.10}$	2	$0.10^{+0.03}_{-0.03}$	$0.65^{+0.15}_{-0.12}$
182488	6.37	15	5453	4.67	dn	no	0.12	0.28	17	$0.22^{+0.05}_{-0.06}$	38	$0.19^{+0.03}_{-0.03}$	$0.59^{+0.09}_{-0.08}$
182572	5.17	15	5656	4.32	dn	no	0.36	0.51	39	$0.39^{+0.04}_{-0.04}$	35	$0.38^{+0.03}_{-0.03}$	$0.62^{+0.07}_{-0.08}$
183162	8.06	67	6015	4.30	dn	no	0.06	0.22	0	...	1	$0.12^{+0.04}_{-0.04}$	...
183263	7.86	52	5936	4.40	dn	yes	0.21	0.41	14	$0.07^{+0.06}_{-0.08}$	1	$0.23^{+0.03}_{-0.03}$	$0.92^{+0.18}_{-0.14}$
183650	6.95	36	5713	4.24	dn	no	0.28	0.44	1	$0.15^{+0.10}_{-0.14}$	4	$0.31^{+0.03}_{-0.03}$	$0.91^{+0.31}_{-0.22}$
183658	7.27	34	5798	4.42	dn	no	0.04	0.13	7	$0.07^{+0.05}_{-0.05}$	3	$0.08^{+0.03}_{-0.03}$	$0.64^{+0.09}_{-0.09}$
183870	7.53	18	5067	4.69	dn	no	-0.05	0.03	2	$0.02^{+0.07}_{-0.09}$	0	...	...
185144	4.67	5	5246	4.53	dn	no	-0.15	-0.14	421	$-0.06^{+0.04}_{-0.03}$	0	...	...
185295	8.65	...	5223	3.83	...	no	-0.15	-0.05	1	$0.05^{+0.04}_{-0.05}$	0	...	...
186408	5.99	21	5781	4.34	dn	no	0.08	0.18	37	$0.09^{+0.04}_{-0.04}$	24	$0.11^{+0.03}_{-0.03}$	$0.66^{+0.07}_{-0.08}$
186427	6.25	21	5674	4.36	dn	yes	0.02	0.12	40	$0.04^{+0.04}_{-0.04}$	26	$0.11^{+0.03}_{-0.03}$	$0.74^{+0.08}_{-0.09}$
187123	7.83	47	5815	4.36	dn	yes	0.10	0.21	15	$0.08^{+0.05}_{-0.05}$	18	$0.08^{+0.03}_{-0.03}$	$0.63^{+0.09}_{-0.09}$
187237	6.87	26	5831	4.49	dn	no	0.05	0.10	3	$0.04^{+0.07}_{-0.08}$	1	$-0.17^{+0.06}_{-0.06}$	$0.39^{+0.09}_{-0.09}$
187897	7.14	33	5835	4.30	dn	no	0.08	0.12	2	$-0.02^{+0.08}_{-0.10}$	1	$0.02^{+0.05}_{-0.05}$	$0.69^{+0.18}_{-0.14}$
187923	6.16	27	5726	4.28	dn	no	-0.08	-0.05	87	$0.19^{+0.03}_{-0.03}$	76	$0.03^{+0.03}_{-0.03}$	$0.43^{+0.04}_{-0.04}$
188015	8.24	52	5746	4.45	dn	yes	0.28	0.41	3	$0.19^{+0.07}_{-0.07}$	9	$0.22^{+0.03}_{-0.03}$	$0.69^{+0.12}_{-0.12}$

Table 6.6 (cont'd): Stellar Data.

Name <sup>a</sup> (HD)	$V^b$ (mag)	$d^b$ (pc)	$T^c$ (K)	$\log g^c$ (cgs)	Pop <sup>d</sup>	Host	[M/H] <sup>c,e</sup>	[Ni/H] <sup>c</sup>	$N_O$	[O/H] <sup>f</sup>	$N_C$	[C/H] <sup>f</sup>	C/O <sup>f</sup>
188268	8.78	47	5132	4.39	dn	no	0.14	0.22	2	$0.13^{+0.10}_{-0.14}$	0	...	...
188298	8.46	53	5766	4.51	dn	no	0.00	0.07	1	$0.08^{+0.12}_{-0.14}$	0	...	...
188311	8.93	42	5068	4.42	dn	no	0.12	0.20	1	$0.26^{+0.06}_{-0.07}$	0	...	...
188512	3.71	13	5163	3.79	dn	no	-0.18	-0.07	12	$0.01^{+0.04}_{-0.04}$	0	...	...
189625	7.34	34	5822	4.43	dn	no	0.14	0.25	0	...	1	$0.13^{+0.04}_{-0.04}$	...
189627	8.11	68	6150	4.26	dn	no	0.19	0.37	0	...	1	$0.25^{+0.03}_{-0.03}$	...
190067	7.15	19	5356	4.61	dn	no	-0.30	-0.29	61	$-0.18^{+0.04}_{-0.04}$	79	$-0.21^{+0.03}_{-0.03}$	$0.59^{+0.07}_{-0.07}$
190228	7.30	62	5348	3.98	dn	yes	-0.25	-0.15	3	$-0.04^{+0.04}_{-0.05}$	0	...	...
190360	5.73	15	5552	4.38	dn/dk	yes	0.18	0.31	34	$0.25^{+0.04}_{-0.04}$	5	$0.29^{+0.03}_{-0.04}$	$0.69^{+0.09}_{-0.09}$
190404	7.28	15	4973	4.64	dn/dk	no	-0.44	-0.52	2	$-0.17^{+0.05}_{-0.05}$	0	...	...
190406	5.80	17	5932	4.45	dn	no	0.02	0.09	26	$0.04^{+0.04}_{-0.04}$	42	$0.07^{+0.03}_{-0.03}$	$0.66^{+0.08}_{-0.07}$
190594	8.35	43	5334	4.39	dn	no	0.06	0.10	13	$0.18^{+0.04}_{-0.04}$	2	$0.28^{+0.04}_{-0.04}$	$0.79^{+0.11}_{-0.10}$
190821	8.30	100	5853	4.09	dn	no	0.12	0.29	3	$0.14^{+0.07}_{-0.11}$	11	$0.16^{+0.03}_{-0.03}$	$0.65^{+0.17}_{-0.12}$
190931	9.63	62	5405	4.61	dn	no	0.06	0.10	5	$0.08^{+0.07}_{-0.07}$	5	$-0.16^{+0.05}_{-0.05}$	$0.36^{+0.07}_{-0.07}$
191408	5.32	6	4922	4.58	dk	no	-0.34	-0.45	69	$-0.09^{+0.04}_{-0.03}$	0	...	...
191785	7.34	20	5140	4.60	dk	no	-0.10	-0.04	15	$0.14^{+0.04}_{-0.04}$	0	...	...
192020	7.96	23	5194	4.57	...	no	-0.01	0.01	1	$0.19^{+0.07}_{-0.08}$	0	...	...
192148	8.53	58	5626	4.33	dn	no	0.17	0.25	1	$-0.12^{+0.12}_{-0.15}$	1	$0.13^{+0.04}_{-0.04}$	$1.13^{+0.39}_{-0.32}$
192263	7.79	19	4975	4.60	dn	yes	-0.07	0.06	1	$0.05^{+0.07}_{-0.08}$	0	...	...
192310	5.73	8	5080	4.55	dn	no	0.00	0.10	42	$-0.02^{+0.04}_{-0.04}$	0	...	...
192343	8.01	65	5839	4.34	dn	no	0.18	0.35	0	...	2	$0.20^{+0.03}_{-0.03}$	...
192344	7.71	62	5772	4.22	dn	no	0.20	0.37	0	...	3	$0.18^{+0.03}_{-0.03}$	...
193690	9.37	64	5559	4.45	dn	no	0.18	0.32	12	$0.13^{+0.06}_{-0.07}$	10	$0.21^{+0.03}_{-0.03}$	$0.76^{+0.13}_{-0.11}$
193795	8.50	71	5878	4.36	dn	no	0.12	0.26	0	...	3	$0.19^{+0.03}_{-0.03}$	...
193901	8.65	43	5408	4.14	h	no	-1.19	-1.38	0	...	3	$-0.52^{+0.08}_{-0.14}$	...

Table 6.6 (cont'd): Stellar Data.

Name <sup>a</sup> (HD)	$V^b$ (mag)	$d^b$ (pc)	$T^c$ (K)	$\log g^c$ (cgs)	Pop <sup>d</sup>	Host	[M/H] <sup>c,e</sup>	[Ni/H] <sup>c</sup>	$N_O$	[O/H] <sup>f</sup>	$N_C$	[C/H] <sup>f</sup>	C/O <sup>f</sup>
194080	7.71	92	5982	3.70	dn	no	-0.06	-0.02	0	...	2	$0.07^{+0.03}_{-0.03}$	...
194913	7.96	93	5797	4.07	dn	no	0.15	0.33	0	...	3	$0.18^{+0.03}_{-0.03}$	...
195019	6.87	37	5788	4.22	dn/dk	yes	0.00	0.11	6	$0.02^{+0.06}_{-0.08}$	4	$0.06^{+0.04}_{-0.04}$	$0.69^{+0.13}_{-0.11}$
195564	5.66	24	5699	4.16	dn	no	0.01	0.14	12	$0.19^{+0.04}_{-0.04}$	20	$0.09^{+0.03}_{-0.03}$	$0.50^{+0.06}_{-0.06}$
196124	8.91	30	4886	4.54	dn	no	-0.04	-0.10	21	$-0.01^{+0.04}_{-0.05}$	0	...	...
196201	8.50	38	5460	4.57	dn	no	-0.15	-0.10	1	$-0.05^{+0.10}_{-0.15}$	0	...	...
196761	6.36	14	5419	4.54	dn	no	-0.25	-0.24	16	$-0.10^{+0.05}_{-0.06}$	12	$-0.15^{+0.04}_{-0.04}$	$0.57^{+0.10}_{-0.08}$
196850	6.76	26	5790	4.37	dn	no	-0.11	-0.05	78	$0.03^{+0.03}_{-0.03}$	85	$-0.10^{+0.03}_{-0.03}$	$0.47^{+0.05}_{-0.05}$
197076	6.43	20	5823	4.47	dn	no	-0.09	-0.05	47	$-0.08^{+0.04}_{-0.04}$	33	$-0.17^{+0.03}_{-0.03}$	$0.51^{+0.06}_{-0.06}$
198387	6.29	41	5151	3.84	dn	no	-0.12	-0.01	6	$0.10^{+0.04}_{-0.05}$	0	...	...
198483	7.67	51	6084	4.46	dn	no	0.20	0.36	1	$0.12^{+0.12}_{-0.15}$	1	$0.27^{+0.04}_{-0.03}$	$0.90^{+0.33}_{-0.27}$
198683	8.06	82	6169	4.27	dn	no	0.18	0.35	1	$0.16^{+0.09}_{-0.11}$	0	...	...
198802	6.38	45	5767	3.96	dn	no	-0.02	0.10	2	$0.14^{+0.05}_{-0.05}$	3	$0.02^{+0.03}_{-0.03}$	$0.47^{+0.06}_{-0.06}$
199019	8.23	34	5560	4.60	dn	no	0.01	0.00	4	$0.16^{+0.07}_{-0.07}$	5	$-0.21^{+0.06}_{-0.06}$	$0.27^{+0.06}_{-0.06}$
199100	7.78	58	5661	4.18	dn	no	0.34	0.54	1	$0.17^{+0.09}_{-0.10}$	0	...	...
199476	7.81	29	5470	4.61	dn	no	-0.30	-0.33	10	$-0.05^{+0.04}_{-0.07}$	0	...	...
199683	8.18	77	6008	4.15	dn	no	0.00	0.17	0	...	1	$0.03^{+0.04}_{-0.04}$	...
199960	6.21	26	5962	4.31	dn	no	0.24	0.41	1	$0.09^{+0.08}_{-0.10}$	3	$0.24^{+0.03}_{-0.03}$	$0.88^{+0.22}_{-0.18}$
200156	8.76	96	6361	4.04	dn	no	-0.18	-0.15	0	...	1	$-0.08^{+0.03}_{-0.03}$	...
200538	7.72	55	6037	4.34	dn	no	0.07	0.19	1	$0.10^{+0.08}_{-0.10}$	1	$0.12^{+0.03}_{-0.03}$	$0.65^{+0.16}_{-0.13}$
200565	8.39	63	5684	4.37	dn	no	-0.10	-0.04	1	$-0.23^{+0.13}_{-0.19}$	2	$-0.05^{+0.04}_{-0.04}$	$0.95^{+0.42}_{-0.29}$
200968	7.12	17	5221	4.61	dn	no	0.03	0.11	1	$-0.03^{+0.10}_{-0.14}$	0	...	...
201219	8.01	35	5653	4.57	dn	no	0.09	0.19	2	$0.11^{+0.11}_{-0.18}$	4	$0.08^{+0.04}_{-0.05}$	$0.58^{+0.25}_{-0.16}$
201989	7.38	29	5749	4.58	dn	no	0.05	0.16	0	...	2	$0.09^{+0.04}_{-0.04}$	...
202751	8.15	19	4797	4.71	dn	no	-0.09	-0.06	6	$0.08^{+0.04}_{-0.04}$	0	...	...

Table 6.6 (cont'd): Stellar Data.

Name <sup>a</sup> (HD)	$V^b$ (mag)	$d^b$ (pc)	$T^c$ (K)	$\log g^c$ (cgs)	Pop <sup>d</sup>	Host	[M/H] <sup>c,e</sup>	[Ni/H] <sup>c</sup>	$N_O$	[O/H] <sup>f</sup>	$N_C$	[C/H] <sup>f</sup>	C/O <sup>f</sup>
202917	8.65	45	5617	4.39	dn	no	0.03	0.03	0	...	2	$-0.01^{+0.05}_{-0.06}$	...
204277	6.72	33	6196	4.37	dn	no	-0.05	-0.04	4	$-0.07^{+0.10}_{-0.15}$	4	$-0.07^{+0.04}_{-0.04}$	$0.63^{+0.23}_{-0.16}$
205351	8.41	70	5892	4.20	dn	no	0.08	0.20	2	$-0.12^{+0.09}_{-0.12}$	0	...	...
205353	8.18	62	5967	4.39	dn	no	0.05	0.18	1	$-0.15^{+0.13}_{-0.18}$	1	$0.02^{+0.04}_{-0.04}$	$0.93^{+0.39}_{-0.29}$
205855	8.62	36	5163	4.38	dn	no	0.06	0.06	17	$0.08^{+0.04}_{-0.05}$	0	...	...
206116	7.61	54	6133	4.35	dn	no	0.18	0.38	2	$0.17^{+0.08}_{-0.07}$	3	$0.14^{+0.03}_{-0.03}$	$0.58^{+0.11}_{-0.12}$
206374	7.45	26	5587	4.52	dn	no	-0.08	-0.06	1	$0.04^{+0.08}_{-0.10}$	1	$-0.14^{+0.06}_{-0.07}$	$0.42^{+0.12}_{-0.09}$
206387	8.27	54	5852	4.50	dn	no	0.15	0.22	0	...	2	$-0.04^{+0.04}_{-0.04}$	...
206658	7.85	47	5852	4.33	dn	no	0.08	0.21	13	$0.09^{+0.04}_{-0.05}$	33	$0.12^{+0.03}_{-0.03}$	$0.67^{+0.09}_{-0.08}$
207583	8.28	38	5558	4.55	dn	no	0.04	0.09	1	$0.10^{+0.12}_{-0.14}$	2	$-0.05^{+0.04}_{-0.05}$	$0.45^{+0.15}_{-0.13}$
207832	8.78	55	5740	4.50	dn	no	0.14	0.25	17	$0.02^{+0.06}_{-0.06}$	25	$0.05^{+0.03}_{-0.03}$	$0.67^{+0.10}_{-0.10}$
207874	8.19	31	5148	4.50	dn	no	0.10	0.17	1	$0.27^{+0.06}_{-0.06}$	0	...	...
208313	7.73	20	5033	4.54	dn	no	-0.08	0.00	11	$0.03^{+0.05}_{-0.05}$	0	...	...
209203	7.54	47	6214	4.40	dn	no	-0.07	-0.04	3	$0.03^{+0.05}_{-0.06}$	3	$-0.13^{+0.03}_{-0.06}$	$0.44^{+0.09}_{-0.06}$
209340	8.51	93	5970	4.03	dn	no	0.04	0.15	2	$-0.19^{+0.11}_{-0.09}$	1	$0.09^{+0.04}_{-0.04}$	$1.20^{+0.26}_{-0.32}$
209393	7.96	33	5541	4.38	dn	no	-0.15	-0.19	1	$0.06^{+0.07}_{-0.08}$	6	$-0.16^{+0.04}_{-0.06}$	$0.38^{+0.09}_{-0.07}$
209458	7.65	47	6099	4.38	dn	yes	0.02	0.04	10	$0.08^{+0.05}_{-0.05}$	20	$-0.07^{+0.03}_{-0.03}$	$0.45^{+0.06}_{-0.06}$
209706	7.80	68	6274	3.24	dn/dk	no	-0.49	-0.26	0	...	3	$-0.16^{+0.04}_{-0.04}$	...
210277	6.54	21	5555	4.50	dn	yes	0.20	0.29	51	$0.30^{+0.04}_{-0.04}$	25	$0.27^{+0.03}_{-0.03}$	$0.59^{+0.07}_{-0.07}$
210302	4.94	18	6339	4.16	dn	no	0.08	0.10	0	...	15	$0.00^{+0.03}_{-0.03}$	...
210312	8.63	55	5760	4.47	dn	no	0.18	0.37	0	...	1	$0.20^{+0.04}_{-0.04}$	...
210320	8.64	57	5563	4.41	dn	no	0.08	0.22	1	$0.34^{+0.05}_{-0.06}$	0	...	...
210323	8.43	52	5804	4.39	dn	no	-0.12	-0.12	0	...	4	$-0.06^{+0.04}_{-0.04}$	...
210460	6.18	55	5658	3.95	dn	no	-0.22	-0.14	3	$0.06^{+0.04}_{-0.04}$	1	$-0.32^{+0.04}_{-0.04}$	$0.27^{+0.03}_{-0.03}$
211038	6.55	38	5009	3.88	dn	no	-0.13	-0.12	1	$0.20^{+0.04}_{-0.04}$	0	...	...

Table 6.6 (cont'd): Stellar Data.

Name <sup>a</sup> (HD)	$V^b$ (mag)	$d^b$ (pc)	$T^c$ (K)	$\log g^c$ (cgs)	Pop <sup>d</sup>	Host	[M/H] <sup>c,e</sup>	[Ni/H] <sup>c</sup>	$N_O$	[O/H] <sup>f</sup>	$N_C$	[C/H] <sup>f</sup>	C/O <sup>f</sup>
211080	7.82	81	5820	4.19	dn	no	0.28	0.49	0	...	2	$0.22^{+0.03}_{-0.03}$	...
211567	9.07	70	5711	4.11	dn	no	0.03	0.13	1	$-0.07^{+0.10}_{-0.11}$	1	$0.11^{+0.04}_{-0.04}$	$0.95^{+0.26}_{-0.23}$
211810	8.59	61	5519	4.21	dn	no	0.08	0.13	10	$0.12^{+0.04}_{-0.04}$	7	$0.16^{+0.03}_{-0.03}$	$0.68^{+0.09}_{-0.08}$
212291	7.91	32	5602	4.56	dn	no	-0.10	-0.11	26	$-0.08^{+0.04}_{-0.04}$	27	$-0.21^{+0.03}_{-0.03}$	$0.47^{+0.05}_{-0.06}$
212315	7.60	107	6303	4.27	dn	no	-0.03	0.14	0	...	2	$-0.04^{+0.05}_{-0.09}$	...
212585	8.03	45	5836	4.43	...	no	0.08	0.20	0	...	5	$0.13^{+0.03}_{-0.03}$	...
212735	8.23	51	5556	4.13	dn	no	0.23	0.37	1	$0.08^{+0.08}_{-0.10}$	1	$0.29^{+0.04}_{-0.04}$	$1.02^{+0.24}_{-0.20}$
212801	7.68	79	5456	3.98	dn	no	0.03	0.14	1	$0.21^{+0.05}_{-0.06}$	1	$-0.03^{+0.05}_{-0.05}$	$0.37^{+0.07}_{-0.06}$
213066	7.71	79	6004	4.11	dn	no	0.33	0.55	1	$0.18^{+0.09}_{-0.11}$	2	$0.30^{+0.03}_{-0.03}$	$0.83^{+0.22}_{-0.17}$
213472	8.17	64	5799	4.30	dn/dk	no	0.14	0.21	0	...	1	$0.02^{+0.04}_{-0.04}$	...
213519	7.68	43	5832	4.44	dn	no	-0.01	0.08	1	$0.17^{+0.06}_{-0.07}$	1	$0.01^{+0.03}_{-0.04}$	$0.45^{+0.08}_{-0.07}$
214759	7.41	26	5434	4.44	dn	no	0.14	0.28	7	$0.08^{+0.06}_{-0.07}$	3	$0.22^{+0.04}_{-0.04}$	$0.88^{+0.17}_{-0.15}$
214823	8.06	97	5924	3.87	dn	no	0.04	0.14	8	$0.02^{+0.06}_{-0.07}$	5	$0.10^{+0.03}_{-0.03}$	$0.77^{+0.14}_{-0.12}$
215032	8.74	70	5973	4.46	dn	no	0.07	0.18	0	...	4	$0.06^{+0.04}_{-0.04}$	...
215578	7.51	...	5136	3.37	...	no	0.14	0.49	2	$0.30^{+0.05}_{-0.05}$	0	...	...
215625	7.92	53	6073	4.18	dn	no	-0.00	0.10	0	...	1	$0.07^{+0.03}_{-0.03}$	...
216083	8.52	104	6010	3.87	dn	no	0.28	0.49	4	$0.18^{+0.05}_{-0.07}$	2	$0.28^{+0.03}_{-0.04}$	$0.79^{+0.15}_{-0.11}$
216175	7.92	57	6111	4.46	...	no	0.11	0.21	4	$-0.10^{+0.09}_{-0.13}$	0	...	...
216259	8.29	21	4969	4.81	dn	no	-0.47	-0.57	39	$-0.13^{+0.03}_{-0.03}$	0	...	...
216275	7.22	31	5863	4.38	dn	no	-0.14	-0.15	1	$-0.22^{+0.15}_{-0.23}$	4	$-0.15^{+0.04}_{-0.04}$	$0.75^{+0.40}_{-0.27}$
216772	8.44	84	6146	4.18	dn	no	0.12	0.26	0	...	1	$0.02^{+0.04}_{-0.03}$	...
216783	7.87	79	6078	3.89	dn	no	0.14	0.24	0	...	1	$0.23^{+0.04}_{-0.03}$	...
217014	5.45	15	5787	4.45	dn	yes	0.15	0.31	0	...	10	$0.21^{+0.03}_{-0.03}$	...
217107	6.17	19	5704	4.54	dn	yes	0.27	0.47	13	$0.26^{+0.07}_{-0.07}$	27	$0.32^{+0.03}_{-0.03}$	$0.72^{+0.12}_{-0.12}$
217165	7.67	43	5936	4.39	dn	no	-0.03	0.05	3	$0.05^{+0.07}_{-0.08}$	7	$0.02^{+0.03}_{-0.03}$	$0.58^{+0.12}_{-0.10}$

Table 6.6 (cont'd): Stellar Data.

Name <sup>a</sup> (HD)	$V^b$ (mag)	$d^b$ (pc)	$T^c$ (K)	$\log g^c$ (cgs)	Pop <sup>d</sup>	Host	[M/H] <sup>c,e</sup>	[Ni/H] <sup>c</sup>	$N_O$	[O/H] <sup>f</sup>	$N_C$	[C/H] <sup>f</sup>	C/O <sup>f</sup>
217523	7.86	59	5806	3.86	dn	no	-0.20	-0.17	1	$-0.31^{+0.09}_{-0.15}$	4	$0.07^{+0.03}_{-0.04}$	$1.50^{+0.54}_{-0.34}$
217850	8.52	61	5547	4.24	dn	no	0.29	0.40	6	$0.23^{+0.05}_{-0.06}$	17	$0.32^{+0.03}_{-0.03}$	$0.77^{+0.11}_{-0.10}$
217877	6.68	30	5953	4.29	dn	no	-0.10	-0.05	2	$0.13^{+0.06}_{-0.07}$	3	$-0.06^{+0.03}_{-0.03}$	$0.41^{+0.07}_{-0.06}$
218133	7.10	37	5923	4.22	dn	no	-0.08	0.01	5	$-0.05^{+0.09}_{-0.07}$	2	$-0.00^{+0.03}_{-0.03}$	$0.70^{+0.12}_{-0.15}$
218168	8.12	48	5879	4.39	dn	no	-0.05	-0.04	0	...	2	$-0.09^{+0.03}_{-0.03}$	...
218209	7.49	29	5585	4.60	dn	no	-0.31	-0.37	2	$0.00^{+0.07}_{-0.09}$	0	...	...
218445	8.84	93	5787	4.23	dn	no	0.24	0.42	3	$0.16^{+0.06}_{-0.05}$	4	$0.21^{+0.03}_{-0.03}$	$0.71^{+0.10}_{-0.12}$
218868	6.98	23	5540	4.45	dn	no	0.19	0.31	0	...	18	$0.10^{+0.03}_{-0.03}$	...
219428	8.26	60	6103	4.56	dn	no	0.12	0.27	0	...	10	$0.11^{+0.03}_{-0.03}$	...
219538	8.07	24	5078	4.50	dn	no	-0.05	0.00	12	$-0.05^{+0.05}_{-0.05}$	0	...	...
219542	7.62	55	5710	4.44	...	no	0.10	0.22	2	$0.09^{+0.09}_{-0.10}$	2	$0.09^{+0.03}_{-0.03}$	$0.62^{+0.15}_{-0.14}$
219770	8.31	103	6108	4.25	dn	no	0.18	0.38	1	$0.26^{+0.07}_{-0.10}$	1	$0.16^{+0.03}_{-0.03}$	$0.50^{+0.12}_{-0.09}$
219781	8.38	51	5604	4.25	dn	no	0.12	0.23	1	$0.08^{+0.06}_{-0.07}$	2	$0.16^{+0.04}_{-0.04}$	$0.76^{+0.15}_{-0.13}$
219828	8.04	81	5761	4.04	dn	yes	0.12	0.24	2	$-0.03^{+0.06}_{-0.07}$	5	$0.16^{+0.03}_{-0.03}$	$0.97^{+0.17}_{-0.16}$
219834B	5.19	0	5168	4.59	...	no	0.15	0.29	18	$0.14^{+0.05}_{-0.06}$	0	...	...
220339	7.80	19	4975	4.53	dn	no	-0.24	-0.27	27	$-0.19^{+0.04}_{-0.03}$	0	...	...
220908	7.60	74	6158	4.05	dn	no	-0.03	0.04	1	$0.12^{+0.08}_{-0.08}$	1	$-0.06^{+0.04}_{-0.03}$	$0.42^{+0.08}_{-0.08}$
221149	8.27	108	5999	4.06	dn	no	0.18	0.39	0	...	2	$0.18^{+0.05}_{-0.04}$	...
221354	6.76	16	5133	4.38	dn	no	-0.01	0.08	32	$0.10^{+0.04}_{-0.04}$	0	...	...
221356	6.50	26	5976	4.31	dn	no	-0.16	-0.21	2	$-0.07^{+0.09}_{-0.08}$	1	$-0.24^{+0.04}_{-0.04}$	$0.43^{+0.09}_{-0.09}$
221561	8.06	91	6175	4.29	dn	no	0.01	0.17	1	$0.09^{+0.09}_{-0.11}$	0	...	...
222035	8.28	101	5621	3.98	dn	no	0.22	0.36	1	$0.12^{+0.06}_{-0.07}$	1	$0.16^{+0.04}_{-0.04}$	$0.70^{+0.12}_{-0.11}$
222038	8.41	61	5581	4.12	dn	no	0.21	0.34	0	...	1	$0.27^{+0.04}_{-0.04}$	...
222335	7.18	18	5231	4.54	dn	no	-0.16	-0.13	4	$-0.02^{+0.04}_{-0.04}$	0	...	...
222391	7.56	80	6127	4.02	dn	no	0.06	0.20	3	$0.12^{+0.09}_{-0.07}$	3	$0.09^{+0.04}_{-0.04}$	$0.58^{+0.11}_{-0.13}$

Table 6.6 (cont'd): Stellar Data.

Name <sup>a</sup> (HD)	$V^b$ (mag)	$d^b$ (pc)	$T^c$ (K)	$\log g^c$ (cgs)	Pop <sup>d</sup>	Host	[M/H] <sup>c,e</sup>	[Ni/H] <sup>c</sup>	$N_O$	[O/H] <sup>f</sup>	$N_C$	[C/H] <sup>f</sup>	C/O <sup>f</sup>
222582	7.68	41	5727	4.34	dn	yes	-0.02	0.05	5	$0.06^{+0.05}_{-0.05}$	5	$0.05^{+0.04}_{-0.04}$	$0.62^{+0.10}_{-0.09}$
222697	8.65	43	5361	4.41	dn	no	0.05	0.18	0	...	2	$0.27^{+0.07}_{-0.11}$	...
222986	8.81	72	5949	4.45	dn	no	0.20	0.29	11	$-0.08^{+0.07}_{-0.09}$	10	$-0.00^{+0.03}_{-0.03}$	$0.75^{+0.16}_{-0.13}$
223205	9.59	62	5294	4.36	dn	no	0.02	-0.01	3	$0.21^{+0.04}_{-0.05}$	0	...	...
223315	8.78	53	5606	4.34	dn	no	0.28	0.39	0	...	2	$0.19^{+0.03}_{-0.03}$	...
223498	8.34	48	5628	4.58	dn	no	0.14	0.27	0	...	1	$0.19^{+0.04}_{-0.04}$	...
223691	7.86	69	5506	4.08	dn	no	-0.20	-0.11	1	$-0.00^{+0.04}_{-0.05}$	3	$-0.07^{+0.04}_{-0.06}$	$0.54^{+0.09}_{-0.07}$
224449	8.95	61	5695	4.40	dn	no	0.11	0.25	0	...	2	$0.23^{+0.04}_{-0.04}$	...
224601	8.66	104	6234	4.02	dn	no	0.04	0.15	1	$0.05^{+0.09}_{-0.11}$	0	...	...
224693	8.23	94	6047	4.26	dn	yes	0.24	0.47	24	$0.17^{+0.04}_{-0.04}$	17	$0.20^{+0.03}_{-0.03}$	$0.68^{+0.08}_{-0.09}$
225118	8.24	39	5559	4.52	dn	no	0.20	0.33	8	$-0.16^{+0.10}_{-0.13}$	1	$0.02^{+0.05}_{-0.07}$	$0.95^{+0.33}_{-0.24}$
225261	7.82	25	5265	4.59	dn	no	-0.31	-0.35	2	$0.01^{+0.05}_{-0.05}$	0	...	...
230999	9.67	99	5665	4.53	dn/dk	no	0.15	0.18	2	$0.05^{+0.08}_{-0.12}$	0	...	...
231157	10.22	102	5541	4.38	dn/dk	no	0.04	0.11	1	$0.26^{+0.06}_{-0.06}$	0	...	...
232301	8.83	78	6171	4.42	dn	no	0.06	0.17	0	...	4	$0.02^{+0.03}_{-0.05}$	...
233165	9.19	94	6038	4.12	dn	no	-0.06	0.06	0	...	3	$0.15^{+0.04}_{-0.04}$	...
233641	9.24	96	6086	4.09	dn	no	-0.18	-0.09	2	$-0.11^{+0.07}_{-0.11}$	1	$-0.14^{+0.03}_{-0.03}$	$0.60^{+0.16}_{-0.11}$
234314	9.31	107	5571	4.12	dn	no	0.16	0.25	2	$0.33^{+0.04}_{-0.05}$	5	$0.23^{+0.03}_{-0.03}$	$0.51^{+0.06}_{-0.06}$
238008	8.87	106	6090	4.26	dn	no	0.21	0.44	2	$0.10^{+0.09}_{-0.11}$	3	$0.23^{+0.03}_{-0.04}$	$0.84^{+0.22}_{-0.19}$
238069	9.17	106	5904	4.25	dn	no	0.19	0.41	0	...	4	$0.29^{+0.03}_{-0.03}$	...
244992	9.10	70	5916	4.46	dn	no	-0.01	0.02	3	$-0.08^{+0.09}_{-0.15}$	5	$-0.08^{+0.04}_{-0.04}$	$0.62^{+0.22}_{-0.13}$
256714	8.82	66	5719	4.26	dn	no	0.24	0.40	3	$-0.07^{+0.09}_{-0.10}$	0	...	...
278253	9.09	95	6022	4.27	dn	no	0.18	0.36	3	$0.04^{+0.07}_{-0.09}$	0	...	...
281309	9.19	79	5819	4.33	dn	no	-0.03	-0.02	0	...	3	$-0.04^{+0.04}_{-0.04}$	...
283704	9.19	58	5509	4.48	dn	no	0.15	0.23	0	...	2	$0.02^{+0.04}_{-0.04}$	...

Table 6.6 (cont'd): Stellar Data.

Name <sup>a</sup> (HD)	$V^b$ (mag)	$d^b$ (pc)	$T^c$ (K)	$\log g^c$ (cgs)	Pop <sup>d</sup>	Host	[M/H] <sup>c,e</sup>	[Ni/H] <sup>c</sup>	$N_O$	[O/H] <sup>f</sup>	$N_C$	[C/H] <sup>f</sup>	C/O <sup>f</sup>
355183	9.43	110	5940	4.02	dn	no	0.08	0.17	10	$-0.00^{+0.04}_{-0.06}$	20	$0.09^{+0.03}_{-0.03}$	$0.77^{+0.11}_{-0.09}$
BD-103166	10.00	...	5393	4.68	...	yes	0.27	0.47	0	...	2	$0.43^{+0.05}_{-0.05}$	...
GANYMEDE	-26.73	0	5770	4.44	dn	yes	0.00	0.00	5	$0.01^{+0.07}_{-0.05}$	5	$0.02^{+0.03}_{-0.03}$	$0.65^{+0.09}_{-0.11}$
HIP1780	9.09	92	5747	4.20	dn	no	0.11	0.25	3	$-0.03^{+0.07}_{-0.08}$	2	$0.21^{+0.03}_{-0.03}$	$1.10^{+0.23}_{-0.19}$
HIP5938	7.55	26	5421	4.46	dn	no	-0.02	0.04	2	$-0.11^{+0.08}_{-0.10}$	3	$0.02^{+0.04}_{-0.04}$	$0.86^{+0.22}_{-0.18}$
HIP6276	8.43	35	5421	4.56	dn	no	-0.01	0.03	2	$-0.18^{+0.11}_{-0.17}$	3	$-0.09^{+0.06}_{-0.07}$	$0.78^{+0.34}_{-0.23}$
HIP6778	8.74	106	5843	4.14	dn	no	0.19	0.35	3	$-0.02^{+0.08}_{-0.08}$	2	$0.14^{+0.04}_{-0.04}$	$0.91^{+0.18}_{-0.18}$
HIP7728	9.04	68	5573	4.25	dn	no	-0.00	0.06	0	...	3	$0.07^{+0.04}_{-0.04}$	...
HIP7924	8.60	54	5444	4.30	dn	no	0.17	0.25	3	$0.13^{+0.09}_{-0.11}$	3	$0.12^{+0.04}_{-0.04}$	$0.63^{+0.17}_{-0.14}$
HIP10449	9.08	61	5625	4.67	h	no	-0.81	-0.91	0	...	2	$-0.29^{+0.09}_{-0.12}$	...
HIP13447	8.41	74	5819	4.31	dn	no	0.20	0.49	0	...	2	$0.44^{+0.04}_{-0.03}$	...
HIP14113	9.50	102	5753	4.33	dn	no	0.28	0.46	3	$-0.01^{+0.09}_{-0.09}$	1	$0.34^{+0.03}_{-0.03}$	$1.41^{+0.32}_{-0.30}$
HIP14809	8.51	49	5788	4.44	dn	no	-0.04	-0.05	0	...	1	$-0.05^{+0.05}_{-0.05}$	...
HIP14810	8.52	52	5570	4.40	dn	yes	0.24	0.39	45	$0.13^{+0.05}_{-0.05}$	42	$0.26^{+0.03}_{-0.03}$	$0.85^{+0.12}_{-0.12}$
HIP19946	9.91	77	5719	4.22	dk	no	-0.13	-0.19	3	$0.08^{+0.07}_{-0.06}$	0	...	...
HIP20705	9.53	90	6032	4.45	dn	no	-0.02	-0.01	0	...	4	$-0.14^{+0.03}_{-0.04}$	...
HIP21091	8.70	67	5782	4.37	dn	no	0.02	0.03	1	$-0.07^{+0.13}_{-0.17}$	3	$-0.07^{+0.03}_{-0.04}$	$0.62^{+0.25}_{-0.19}$
HIP24141	9.46	109	6065	4.32	dn	no	-0.30	-0.23	1	$-0.03^{+0.10}_{-0.13}$	1	$-0.21^{+0.05}_{-0.05}$	$0.42^{+0.13}_{-0.11}$
HIP26080	8.76	70	6089	4.45	dn	no	0.09	0.19	0	...	3	$-0.00^{+0.03}_{-0.03}$	...
HIP27793	8.79	51	5699	4.58	dn	no	0.12	0.21	1	$-0.04^{+0.13}_{-0.21}$	5	$0.01^{+0.06}_{-0.04}$	$0.71^{+0.34}_{-0.23}$
HIP31546	9.95	79	5757	4.57	dn	no	0.26	0.37	0	...	3	$0.05^{+0.04}_{-0.04}$	...
HIP32132	9.23	82	5732	4.55	dn	no	-0.01	0.09	1	$0.10^{+0.11}_{-0.17}$	5	$0.05^{+0.04}_{-0.04}$	$0.56^{+0.22}_{-0.15}$
HIP32892	8.94	93	5686	4.24	dn	no	0.15	0.39	0	...	3	$0.45^{+0.03}_{-0.04}$	...
HIP42731	8.86	104	5811	4.18	dn	no	0.08	0.23	3	$-0.01^{+0.07}_{-0.07}$	0	...	...
HIP43151	9.23	77	5885	4.34	dn	no	-0.20	-0.21	0	...	3	$-0.16^{+0.04}_{-0.05}$	...

Table 6.6 (cont'd): Stellar Data.

Name <sup>a</sup> (HD)	$V^b$ (mag)	$d^b$ (pc)	$T^c$ (K)	$\log g^c$ (cgs)	Pop <sup>d</sup>	Host	[M/H] <sup>c,e</sup>	[Ni/H] <sup>c</sup>	$N_O$	[O/H] <sup>f</sup>	$N_C$	[C/H] <sup>f</sup>	C/O <sup>f</sup>
HIP47455	9.08	85	6105	4.43	dn	no	0.27	0.49	3	$0.16^{+0.07}_{-0.07}$	2	$0.28^{+0.04}_{-0.04}$	$0.82^{+0.15}_{-0.15}$
HIP54498	8.94	77	5833	4.46	dn	no	0.03	0.16	0	...	4	$0.12^{+0.03}_{-0.04}$	...
HIP55368	9.15	101	6067	4.43	dn	no	0.01	0.08	3	$-0.04^{+0.10}_{-0.14}$	1	$-0.08^{+0.04}_{-0.04}$	$0.57^{+0.19}_{-0.14}$
HIP68461	8.93	79	5716	4.17	dn	no	0.33	0.52	1	$0.10^{+0.07}_{-0.08}$	1	$0.38^{+0.04}_{-0.04}$	$1.22^{+0.25}_{-0.24}$
HIP73302	8.80	43	5288	4.38	dn	no	-0.03	-0.10	1	$0.11^{+0.07}_{-0.08}$	0	...	...
HIP89215	10.37	58	5104	4.85	h	no	-0.82	-0.98	1	$-0.33^{+0.12}_{-0.17}$	0	...	...
HIP90075	8.58	79	5882	4.37	dn	no	0.20	0.30	1	$-0.01^{+0.10}_{-0.15}$	1	$0.06^{+0.04}_{-0.04}$	$0.73^{+0.26}_{-0.19}$
HIP92922	9.12	99	5624	4.16	dn	no	0.31	0.47	2	$0.31^{+0.06}_{-0.07}$	0	...	...
HIP100040	8.37	86	5577	4.29	dn/dk	no	0.12	0.28	0	...	2	$0.31^{+0.03}_{-0.03}$	...
HIP103269	10.28	70	5125	4.29	dk	no	-1.72	-2.00	2	$-0.91^{+0.10}_{-0.13}$	0	...	...
HIP105904	8.27	94	5993	4.22	dn	no	0.26	0.49	0	...	1	$0.34^{+0.03}_{-0.03}$	...
HIP108056	9.15	104	6169	4.43	dk	no	0.16	0.31	0	...	2	$0.10^{+0.05}_{-0.04}$	...
HIP113207	8.88	98	5637	4.07	dn	no	0.22	0.35	0	...	1	$0.25^{+0.04}_{-0.04}$	...
HIP114914	7.60	54	5708	4.19	dn	no	-0.00	0.11	1	$0.08^{+0.08}_{-0.10}$	1	$0.12^{+0.03}_{-0.04}$	$0.69^{+0.18}_{-0.13}$
HIP115525	9.75	105	5804	4.26	dn	no	0.03	0.14	3	$0.14^{+0.06}_{-0.08}$	3	$0.20^{+0.04}_{-0.04}$	$0.74^{+0.15}_{-0.12}$
HIP117386	9.81	81	5657	4.46	dn	no	-0.40	-0.33	0	...	3	$-0.11^{+0.04}_{-0.04}$	...
WASP12	11.69	...	6272	4.37	...	yes	0.27	0.17	9	$0.29^{+0.06}_{-0.10}$	7	$0.10^{+0.04}_{-0.06}$	$0.40^{+0.11}_{-0.07}$

<sup>a</sup>Names are HD numbers unless otherwise indicated.

<sup>b</sup>Johnson  $V$ -magnitude and distance from the Hip catalog; where stars were not in the Hip catalog,  $d$  and  $V$  are from the Geneva-Copenhagen Catalog (Nordström et al. 2004);  $d$  and  $V$  are taken from SIMBAD as a last resort.

<sup>c</sup>Stellar parameters from VF05 and D. Fischer.

<sup>d</sup>Membership identification taken from Peek (2009)

<sup>e</sup>[M/H] is computed from all elements heavier than He.

<sup>f</sup>We have corrected these abundances a for a systematic trend in temperature (see § 6.4.1).

## 7

# SpecMatch: Accurate Stellar Characterization with Optical Spectra

## 7.1 Introduction

The ability to extract fundamental stellar parameters from spectra is essential in understanding a wide range of astrophysical phenomena, from exoplanet host star characterization to the study of galactic stellar kinematics and chemical enrichment history. Recently, research in extrasolar planets has spawned a renewed interest in the fundamental properties (e.g. masses, radii, effective temperatures, ages) of stars, particularly for M-dwarfs (Boyajian et al. 2012; Mann et al. 2013). New observational techniques such as asteroseismology using space-based photometers like *Kepler* (Huber et al. 2013; Chaplin et al. 2014) and interferometric measurements of stellar radii (Boyajian et al. 2012, 2013; von Braun et al. 2014) are providing new empirical touchstones that serve to improve spectroscopic methods.

The observation, analysis, and interpretation of exoplanets is closely linked to the fundamental properties of their host stars. In some cases, the presence of an extrasolar planet can improve our knowledge of the host star beyond that from spectroscopy or photometry alone. For example, the transit profile can constrain mean stellar density,  $\rho_*$ . Torres et al. (2012) used transit-constrained  $\rho_*$  to refine host star properties beyond existing spectroscopic analyses. In most cases, however, knowledge of planetary properties like planet mass, size, and equilibrium temperature is limited by our knowledge of stellar mass, radius, and effective temperature.

In this paper, we present a new technique called SpecMatch that extracts the following properties from high-resolution optical spectra: effective temperatures,  $T_{\text{eff}}$ ; surface gravities,  $\log g$ ; metallicities,  $[\text{Fe}/\text{H}]$ ; and projected rotational velocities,  $v \sin i$ . Throughout this paper,  $T_{\text{eff}}$  is measured in Kelvin;  $\log g$  is  $\log_{10}(g) = GM_*/R_*^2$ , measured in cgs units; metallicity is  $[\text{Fe}/\text{H}] = \log_{10}(n_{\text{Fe}}/n_{\text{H}}) - \log_{10}(n_{\text{Fe},\odot}/n_{\text{H},\odot})$ , where  $n_{\text{Fe}}$  and  $n_{\text{H}}$  are the number densities of iron and hydrogen, respectively; and  $v \sin i$  is measured in  $\text{km s}^{-1}$ .

Here, we briefly review the processes that connect an observed stellar spectrum to the physical properties of the star (for a more thorough review, see Gray 2005). Stellar effective

temperature, surface gravity, metallicity, and rotation all affect the depths and detailed shapes of spectral lines. The dependence is perhaps the most straightforward; stars with higher  $[\text{Fe}/\text{H}]$ , have deeper iron lines. The energy level populations of absorber species is set by the Boltzmann equation for neutral species, and by the Saha equation for ionized species. Both the Boltzmann and Saha equations have an exponential sensitivity to temperature. Thus the relative strength of different lines having different excitation potentials is a good diagnostic of temperature.

Surface gravity is much harder to measure. The Saha equation has a linear dependence on the local electron pressure which is a probe of the surface gravity. One diagnostic of  $\log g$  is the relative strength of lines corresponding to different ionization states of the same element. Fe I and Fe II are often used. Another approach involves modeling the wings of so-called “pressure-sensitive” lines like Na I D doublet, Ca II H&K, Mg I b triplet, and Ca I at 4227 Å. However, modeling in detail how, as an example, the Mg I b line profile changes with differing surface gravities is challenging, especially considering the covariant effects of temperature and Mg abundance. Temperature, surface gravity and metallicity all influence a star’s spectrum in different, but non-orthogonal ways. Measurements of  $T_{\text{eff}}$ ,  $\log g$ ,  $[\text{Fe}/\text{H}]$  are often complicated by covariances between all three parameters.

Lastly, rotation broadens spectral lines due to the Doppler effect. Lines formed at the receding limb of the star are red-shifted and blue shifted if they are formed on the approaching limb. Rotation is relatively easy to measure in the case of moderate stellar rotation ( $v \sin i \gtrsim 5 \text{ km s}^{-1}$ ) by fitting the profiles of unsaturated lines. For slowly rotating stars, rotational broadening becomes sub-dominant compared to other broadening terms like, macroturbulence, microturbulence, thermal broadening, pressure broadening, and the instrumental profile of the spectrometer.

Determining  $T_{\text{eff}}$ ,  $\log g$ ,  $[\text{Fe}/\text{H}]$ , and  $v \sin i$  for planet-hosting stars has a wide variety of applications. Combining spectroscopic  $T_{\text{eff}}$ ,  $\log g$ , and  $[\text{Fe}/\text{H}]$  with isochrone-fitting offers dramatic improvements over photometrically determined stellar masses, radii, and luminosities, which result in more precise planet masses, radii, and equilibrium temperatures. For example, photometric radii from the *Kepler* Input Catalog are uncertain at the  $\sim 35\%$  level (Brown et al. 2011; Batalha et al. 2013; Burke et al. 2014) while spectroscopically-derived radii have uncertainties ranging from 1–10%, depending on the type of star (Valenti & Fischer 2005). Correlations between planet occurrence and stellar metallicity probe the connection between planet formation efficiency and the composition of the protoplanetary disk. Projected rotational velocity can constrain the inclination of the stellar spin axis (and star-planet spin orbit alignment) if the star’s equatorial velocity is known (by, for example, rotation modulation).

Previous spectroscopic studies of nearby stars often enjoy high SNR spectra. For example, Valenti & Fischer (2005) measured  $T_{\text{eff}}$ ,  $\log g$ ,  $[\text{Fe}/\text{H}]$ , and  $v \sin i$  for 1040 stars using spectra where  $\text{SNR} > 100/\text{pixel}$ . While SpecMatch is a general purpose tool, it was designed to measure spectroscopic properties of faint *Kepler* stars with the HIRES spectrometer (Vogt et al. 1994) on the Keck I telescope. At 1 kpc, a typical distance to a *Kepler* target star, a solar analog has  $V = 14.7$ . Obtaining a spectrum with  $\text{SNR} = 100/\text{pixel}$  would take

2.5 hours and is not feasible for large samples of stars. We designed SpecMatch in order to yield reliable stellar parameters when  $\text{SNR} \lesssim 40/\text{pixel}$ .

This chapter is organized as follows: In Section 7.2 we describe how we condition observed spectra and extract spectroscopic parameters. In Section 7.3 we assess the reliability of SpecMatch parameters. We present a detailed Monte Carlo study of the precision SpecMatch as a function of spectral SNR and assess systematic uncertainties by analyzing spectra of touchstone stars from the literature. We summarize our results in Section 7.4, and expand on several compelling applications of SpecMatch.

## 7.2 SpecMatch

In brief, SpecMatch works by comparing an observed high-resolution optical spectrum to a library of synthetic model spectra from [Coelho et al. \(2005\)](#) (C05, hereafter) that span a range of  $T_{\text{eff}}$ ,  $\log g$ , and  $[\text{Fe}/\text{H}]$ . In its current implementation, SpecMatch accepts spectra taken with HIRES on the Keck I telescope. However, SpecMatch can be easily adapted to work with other high resolution optical spectrometers. In this section we describe how we condition observed spectra and extract stellar parameters.

### 7.2.1 Reduction and Calibration of Target Spectra

We remove the blaze function by dividing the target spectrum by the spectrum of a rapidly rotating B star. The California Planet Search ([Marcy et al. 2008](#)) routinely takes spectra of rapidly rotating B stars which have nearly featureless spectra that, when observed with HIRES, provide a good description of the shape of the blaze function. We divide the target spectrum by the average of 20 B stars having weak stellar absorption lines. The resulting spectra still show variations at the few percent level due to differences in slit illumination and changes optics of HIRES. A low-order polynomial is fit to the 95 percentile level of the spectrum to remove residual curvature.

After normalizing out the continuum, we place the star’s spectrum onto its rest wavelength scale. We cross-correlate chunks of the target spectrum with a model template spectrum, taken from the C05 library of synthetic spectra. We use one of six model spectra with parameters listed in 7.3 as our wavelength standard. We cross-correlate a segment<sup>1</sup> of the target star spectrum with each of the 6 models and select the model spectrum with the highest cross-correlation peak as the wavelength standard.

For each of the 16 orders, we cross-correlate seven segments of 1000 pixels wide.<sup>2</sup> Each of these seven segments gives an apparent velocity shift. Taking all the orders together, we

<sup>1</sup>The middle chip on HIRES has 16 orders. We label the orders starting from zero, i.e. 0, 1, ... 15, from bluest to reddest. Order number 2 is used to select the model spectrum acting as wavelength standard.

<sup>2</sup>A shift of one HIRES pixel is equivalent to a velocity displacement of  $\sim 1.3 \text{ km s}^{-1}$ . The seven segments are evenly-spaced, starting at pixel number 0, 500, 1000, 1500, 2000, 2500, and 3000.

construct  $\delta\mathbf{v}$ , a matrix of velocity shifts:

$$\delta\mathbf{v} = \begin{pmatrix} \delta v_{1,1} & \dots & \delta v_{1,7} \\ \vdots & \ddots & \vdots \\ \delta v_{16,1} & \dots & \delta v_{16,7} \end{pmatrix},$$

where  $\delta v_{i,j}$  corresponds to the velocity shift of segment  $j$  in order  $i$ . We compute the average shift (with sigma clipping) over each of the columns of  $\delta\mathbf{v}$  and fit a linear relationship to derive  $\delta v$  as a function of pixel number. This average velocity shift is applied to all orders to place the target spectrum on its rest wavelength scale.

### 7.2.2 Comparison to Library Spectra

We compare the target spectrum to a suite of model spectra from the C05 library. C05 modeled spectra over a grid in  $T_{\text{eff}}$ ,  $\log g$ ,  $[\text{Fe}/\text{H}]$ , and  $[\alpha/\text{Fe}]$ . SpecMatch uses a subset of C05 model spectra having solar  $[\alpha/\text{Fe}]$ , and  $T_{\text{eff}}$ ,  $\log g$ , and  $[\text{Fe}/\text{H}]$  listed in Table 7.1. The SpecMatch library consists of a  $15 \times 9 \times 7$  regular grid of C05 model spectra. C05 used model atmospheres from [Castelli & Kurucz \(2003\)](#). Line lists came from [Barbuy et al. \(2003\)](#) and [Meléndez & Barbuy \(1999\)](#). Oscillator strengths were taken from the NIST database ([Reader et al. 2002](#)), other works (see references in C05), as well as empirically by fitting line profiles to the solar spectrum. Damping constants ( $\gamma$ ) for strong neutral lines were taken from [Anstee & O’Mara \(1995\)](#); [Barklem & O’Mara \(1997\)](#); and [Barklem et al. \(1998, 2000\)](#). Damping constants for other lines were fit manually to the solar spectrum or assumed to have an interaction constant of  $C_6 = 0.3 \times 10^{-31}$ . C05 synthesized model spectra over  $\lambda = 3000\text{--}18,000 \text{ \AA}$  with  $0.02 \text{ \AA}$  sampling using the PFANT radiative transfer code ([Spite 1967](#); [Cayrel et al. 1991](#); [Barbuy et al. 2003](#)). C05 used the following prescription for microturbulence:

$$v_t = \begin{cases} 1.0 \text{ km s}^{-1} & : \log g \geq 3.0 \\ 1.8 \text{ km s}^{-1} & : 1.5 \leq \log g \leq 3.0 \\ 2.5 \text{ km s}^{-1} & : \log g \leq 1.0 \end{cases}$$

Each target-model comparison involves subtracting the model spectrum from the observed spectrum. We filter the residuals and remove trends longer than 400 pixels ( $\sim 8.6 \text{ \AA}$ ) before computing  $\chi^2$ . This high-pass filtering ensures that well-matched models are not penalized on account of low-frequency noise (due to imperfect continuum fitting).

The comparisons are performed independently on different segments of stellar spectra. We found by trial and error that the five spectral regions listed in Table 7.2 produced parameters that were in close agreement with touchstone stars from [Huber et al. \(2013\)](#) (with asteroseismic constraints) and from [Torres et al. \(2012\)](#) (with transit-constrained  $\rho_\star$ ). We also identified, by inspection, certain lines that poorly matched observed spectra and constructed a mask to exclude these regions from the computation of  $\chi_f^2$ . Figures 7.12–7.16 show the five spectral regions for a KOI-1, a star with nearly Solar parameters<sup>3</sup> The

<sup>3</sup>  $T_{\text{eff}} = 5850 \text{ K}$ ,  $\log g = 4.46$ , and  $[\text{Fe}/\text{H}] = -0.15 \text{ dex}$  ([Huber et al. 2013](#))

Table 7.1: Parameters for Model Spectra in C05 Library

Parameter	Library Values
$T_{\text{eff}}$	3500–7000 K, steps of 250 K
$\log g$	1.0–5.0 (cgs), steps of 0.5 dex.
[Fe/H]	{−2.0, −1.5, −1.0, −0.5, +0.0, +0.2, +0.5} dex
[ $\alpha$ /Fe]	0.0 dex

Table 7.2: SpecMatch Wavelength Segments

$\lambda_{\text{min}}$ (Å)	$\lambda_{\text{max}}$ (Å)	HIRES Order
5200	5280	3
5360	5440	5
5530	5610	7
6100	6190	13
6210	6260	14

masked regions are grayed out. The SpecMatch spectral segments are characterized by having relatively few saturated and overlapping lines. One aspect that makes SpecMatch suitable for low SNR spectra is that it uses a wide region (380 Å) of optical spectrum. As a point of comparison the VF05 analysis used  $\approx 170$  Å.

One surprise was that the HIRES order containing the Mg I b triplet produced  $\log g$  values in poor agreement with asteroseismology. The Mg I b line is a so-called “pressure sensitive” line and is often used as a  $\log g$  diagnostic. While the wings of the line are, in principle, good probes of stellar surface gravity, we excluded them because of the observed tension with asteroseismology. There may be issues with the C05 treatment of these lines or that strong covariances with  $T_{\text{eff}}$  or magnesium abundance (which may not scale with [Fe/H]) are complicating the fit to the Mg I b lines.

The C05 model spectra incorporate natural, thermal, collisional, and microturbulent broadening. Since the model spectra do not account for broadening due to rotation, macroturbulence, or the instrumental profile, lines in the C05 models are narrower than observed spectra. During each target-model comparison we convolve the model spectrum with a standard rotational broadening kernel (see p. 374 of [Gray 1992](#)) to account for additional broadening.  $v \sin i$  is allowed to float as a free parameter. Note that  $v \sin i$  is acting as a stand-in for other broadening terms besides rotation like macroturbulence and the instrumental profile. In a later polishing step (Section 7.2.5), macroturbulence and the instrumental profile are treated individually. The instrumental profile is determined empirically for each spectrum using telluric lines, following a procedure described in Section 7.2.4.

### 7.2.3 Stellar Parameters from Linear Combinations of Spectra

We zero in on a best-fit  $T_{\text{eff}}$ ,  $\log g$ , and  $[\text{Fe}/\text{H}]$  by taking linear combinations of  $m$  model spectra that have lowest  $\chi_f^2$ , when compared to the target spectrum. This linear combination can be represented as,  $\mathbf{MA}$ , where,  $\mathbf{M}$  is an  $n \times m$  matrix of best-match model spectra and  $\mathbf{A}$  is a  $m \times 1$  matrix of coefficients. We solve for the set of positive coefficients that minimize  $\chi^2$  using a non-negative least-squares solver,<sup>4</sup> i.e.

$$\operatorname{argmin}_{\mathbf{A}} \|\mathbf{MA} - \mathbf{S}\|_2 \text{ for } \mathbf{A} \geq 0.$$

By trial and error, we found that using  $m = 8$  model spectra to construct  $\mathbf{M}$  gave the fitter adequate flexibility while keeping the number of free parameters manageable. We arrive at the target star's  $T_{\text{eff}}$ ,  $\log g$ , and  $[\text{Fe}/\text{H}]$  by taking an average of the  $T_{\text{eff}}$ ,  $\log g$ , and  $[\text{Fe}/\text{H}]$  associated with each of the best  $m$  models, weighted by  $\mathbf{A}$ . This averaging is done for each of the stellar parameters associated with each wavelength segment. The  $T_{\text{eff}}$ ,  $\log g$ , and  $[\text{Fe}/\text{H}]$  determined from each segment are averaged again to determine a single set of  $T_{\text{eff}}$ ,  $\log g$ , and  $[\text{Fe}/\text{H}]$  for the target star spectrum.

### 7.2.4 Measuring the Instrumental Profile with Telluric Lines

Properly treating the width of the instrumental profile is especially important for  $v \sin i$  work. If our model of the instrumental profile is too narrow, SpecMatch will increase  $v \sin i$  in order to correctly match the width of absorption lines. While telluric lines are broadened by turbulence in the Earth's atmosphere to  $\sim 100 \text{ m s}^{-1}$ , telluric lines remain narrow compared to the instrumental profile of HIRES (several  $\text{km s}^{-1}$ ) and are good diagnostics its width. For each target spectrum, fit the  $\text{O}_2$  B-X band of telluric lines with a comb of Gaussians:

$$I(\lambda) = 1 - \sum_i a_i e^{-\frac{1}{2} \left( \frac{\lambda - \lambda_{c,i}}{\sigma_{\text{IP}}} \right)^2}, \quad (7.1)$$

where  $a_i$  and  $\lambda_i$  specifies line depths and centers respectively and  $\sigma_{\text{IP}}$  sets the width of the Gaussians. In the fit,  $\sigma_{\text{IP}}$  is allowed to float as a free parameter. Figure 7.1 shows the fit to the telluric lines HD 209458 spectrum, a high SNR spectrum ( $\text{SNR} \sim 160/\text{pixel}$ ). We show the fits to the KOI-2 spectrum in Figure 7.2 with  $\text{SNR} \sim 45/\text{pixel}$ .

The width of the instrumental profile,  $\sigma_{\text{IP}}$ , depends on seeing, the HIRES slit width, and the performance and focus of the spectrometer optics. We illustrate this variability in PSF-width in Figure 7.3, where we show the measured line widths, for 43 spectra of stars from the Albrecht et al. (2012) Rossiter-McLaughlin sample (see Section 7.3.2) organized by HIRES decker. The wider deckers, B5 and C2, have a sky projected width of  $0.861''$  and larger  $\sigma_{\text{IP}}$ , than the B1 and B3 deckers ( $0.574''$  projected width). For different observations with the same decker, the instrumental profile width varies by  $\sim 0.4$  pixels =  $0.5 \text{ km s}^{-1}$ . Thus, adopting a single instrumental profile width would produce errors in  $v \sin i$  as large as  $\sim 0.5 \text{ km s}^{-1}$ , hampering the measurement of small  $v \sin i$ .

<sup>4</sup>As implemented in `scipy.optimize.nnls` algorithm from Lawson C., Hanson R.J., (1987) Solving Least Squares Problems, SIAM

Table 7.3: Parameters of Template Spectra Used for Wavelength Calibration

$T_{\text{eff}}$ (K)	$\log g$ (cgs)	[Fe/H] (dex)
4000	5.0	0.0
4500	5.0	0.0
5000	4.5	0.0
5500	4.5	0.0
6000	4.5	0.0
6500	4.0	0.0

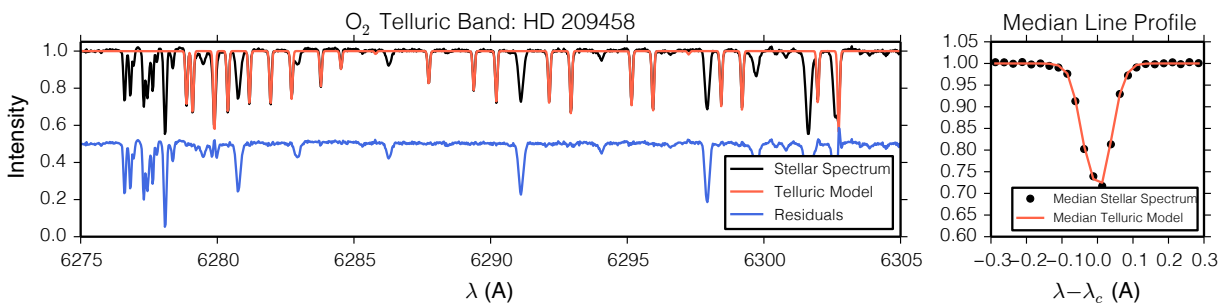


Figure 7.1: Left panel—Spectrum of HD 209458 around the  $\text{O}_2$  telluric band (black line). We fit the telluric lines with a comb of Gaussians (red line). Residuals are shown in blue. Right panel—median intensity (computed for  $0.025 \text{ \AA}$  bins) of the HD 209458 spectrum (black) and telluric model (red) within  $0.3 \text{ \AA}$  of the telluric line centers. The observed and model telluric line profiles have the same width. Since the telluric lines are not broadened by the thermal and convective velocities in the star’s photosphere, they are a good diagnostic for the instrumental profile of HIRES. For HD 209458, the best fit  $\sigma_{\text{IP}} = 1.41$  HIRES pixels. In subsequent modeling of the HD 209458 spectrum, we describe the instrumental profile as a Gaussian with  $\sigma_{\text{IP}} = 1.41$  pixels.

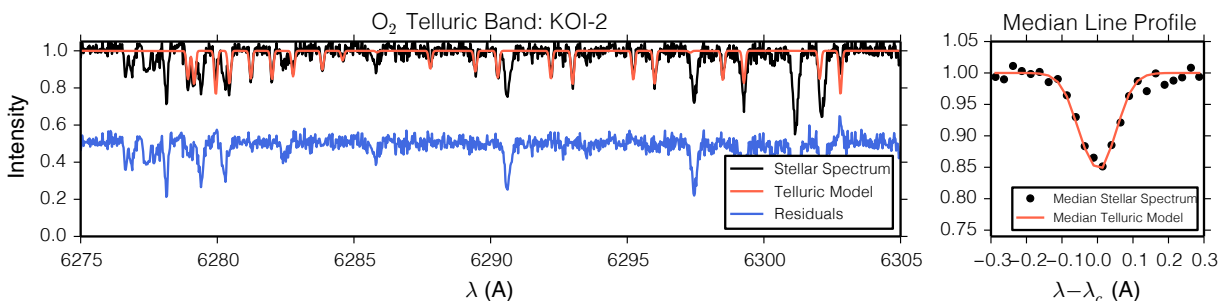


Figure 7.2: Same as Figure 7.1, except for KOI-2. This spectrum has  $\text{SNR} = 45/\text{pixel}$ . This spectrum was taken using the wider C2 decker thus the instrumental profile is broader,  $\sigma_{\text{IP}} = 1.87$  pixels.

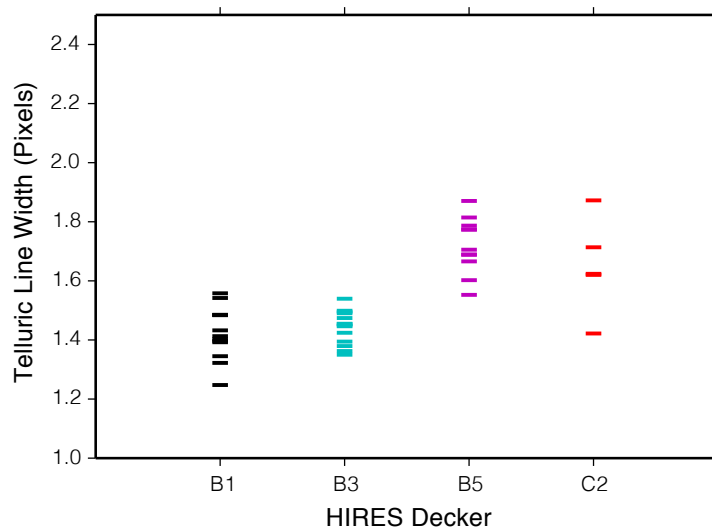


Figure 7.3: Width of telluric lines in spectra of stars from the Albrecht et al. (2012) sample for different HIRES deckers. On average, the wider B5 and C2 deckers have broader instrumental profiles (hence broader telluric lines) than the narrower B1 and B3 deckers. For any single decker, however,  $\sigma_{\text{IP}}$ , the measured width of the telluric lines (see Equation 7.1), varies by  $\sim 0.4$  pixels =  $0.5 \text{ km s}^{-1}$ . Thus adopting a single instrumental profile width would introduce errors in  $v \sin i$  as large as  $0.5 \text{ km s}^{-1}$ .

### 7.2.5 Polishing the Parameters by Forward Modeling

The linear combination approach gives good initial guesses for the parameters. We refine these parameters using a forward modeling approach. Here, we synthesize model spectra with an arbitrary  $T_{\text{eff}}$ ,  $\log g$ ,  $[\text{Fe}/\text{H}]$ ,  $v \sin i$ , and instrumental profile according to the following three steps:

1. We select the eight model spectra with parameters that enclose the desired set of  $T_{\text{eff}}$ ,  $\log g$ , and  $[\text{Fe}/\text{H}]$  in a box in the 3D space of  $T_{\text{eff}}$ ,  $\log g$ , and  $[\text{Fe}/\text{H}]$ . We synthesize an intermediate spectrum within this box using trilinear interpolation.
2. We then account for rotation and macroturbulence (parametrized by  $\xi$ ) by constructing a combined rotational-macroturbulent profile (equation 17 of [Hirano et al. 2011](#)) and convolving it with the spectrum from step 1. For stars with moderate  $v \sin i$  and  $\xi$ , it is possible to solve for  $v \sin i$  and  $\xi$  independently, with very high SNR and very high spectral resolution. For our CKS spectra there is a large degeneracy between  $v \sin i$  and  $\xi$ , so we adopt the following relationship from [Valenti & Fischer \(2005\)](#):

$$\xi = 3.98 + \left( \frac{T_{\text{eff}} - 5700 \text{ K}}{650 \text{ K}} \right) \text{ km s}^{-1}$$

3. We convolve the spectrum from step 2 with a Gaussian to model the effects of the HIRES instrumental profile, which is determined from telluric lines, as described in Section 7.2.4.

After synthesizing the model spectrum, we re-compute  $\chi_f^2$  according to the procedure outlined in Section 7.2.3. We refine the parameters determined during the linear combination step (Section 7.2.3) by varying  $T_{\text{eff}}$ ,  $\log g$ ,  $[\text{Fe}/\text{H}]$ , and  $v \sin i$  in search of the best match. We converge on the best match using a Levenberg-Marquardt algorithm. As an example, we show the spectrum of KOI-1 along with the best-fitting model spectrum in Figures 7.12–7.16.

### 7.2.6 Calibrating Effective Temperature and Metallicity to Valenti & Fischer (2005)

While spectroscopy routinely achieves effective temperature precision of  $< 100$  K, zero-point and temperature-dependent offsets persist at the  $\sim 100$  K level. These offsets are observed when comparing effective temperatures based on photometry and spectroscopy and when comparing effective temperatures based on different spectroscopic techniques ([Casagrande et al. 2010](#)). Further work is needed to anchor the spectroscopic effective temperatures to the absolute effective temperatures from  $L_\star$  and  $R_\star$ .

[Valenti & Fischer \(2005\)](#), VF05 hereafter, used the ‘‘Spectroscopy Made Easy’’ (SME) spectrum synthesis code ([Valenti & Piskunov 1996](#)) to measure stellar properties for 1040 nearby FGK stars. We choose to anchor SpecMatch effective temperatures to the VF05 scale

because the VF05 catalog is an important touchstone in the literature. We analyzed spectra of 352 stars from the VF05 catalog using SpecMatch. We use these shared stars to link the SpecMatch effective temperatures to the SME scale. In Figure 7.4, we show the difference between SpecMatch and VF05 effective temperatures,  $\Delta T_{\text{eff}}$ . We fit these differences using a linear relationship,

$$\Delta T_{\text{eff}} = c_0 \left( \frac{T_{\text{eff}} - 5770 \text{ K}}{100 \text{ K}} \right) + c_1,$$

where  $c_0 = -4.23$  and  $c_1 = -7.6$  K. Subsequent effective temperatures presented in this work have been calibrated against this relationship.

The VF05 catalog is also an important with respect to planet-metallicity work. Using the VF05 catalog, Fischer & Valenti (2005) firmly established the correlation between Jovian planet occurrence and host star metallicity. We elect to anchor SpecMatch [Fe/H] to the VF05 scale in order to facilitate comparisons between the two studies. Figure 7.5 shows the difference between SpecMatch and VF05 metallicities,  $\Delta[\text{Fe}/\text{H}]$ . We fit these differences using a linear relationship,

$$\Delta[\text{Fe}/\text{H}] = c_0 \left( \frac{[\text{Fe}/\text{H}]}{0.1 \text{ dex}} \right) + c_1,$$

where  $c_0 = 0.0065$  and  $c_1 = -0.015$  dex are the best fit coefficients. Subsequent metallicities presented in this work have been calibrated according to this relationship.

### 7.2.7 Calibrating Surface Gravities to Huber et al. (2013)

Huber et al. (2013) (H13, hereafter) published stellar parameters of 77 *Kepler* planet hosts where asteroseismic modes were detected. Analysis of power spectra of *Kepler* short cadence photometry revealed solar-like oscillations in these 77 stars. H13 measured the large frequency separation,  $\delta\nu$ , which depends on  $M_\star$  and  $R_\star$ , and  $\nu_{\text{max}}$ , which depends on  $M_\star$ ,  $R_\star$ , and  $T_{\text{eff}}$ —2 equations and three unknowns. Starting with an initial temperature from spectroscopy, H13 solved for  $M_\star$  and  $R_\star$  and hence  $\log g$ .  $\log g$  was then fixed in the spectroscopic analysis and  $T_{\text{eff}}$  and [Fe/H] were re-derived from modeling spectra.  $T_{\text{eff}}$  was fed back into the asteroseismic equations iteratively until convergence.

Because asteroseismology offers exquisite  $\log g$  precision for bright stars<sup>5</sup> we use 75 stars<sup>6</sup> from the H13 sample to calibrate SpecMatch surface gravities in the following two regions of the HR diagram:

1. For stars with  $\log g = 3.5\text{--}5.0$  (cgs) and  $T_{\text{eff}} = 5700\text{--}6500$  K, we note a weak dependence of  $\Delta \log g = \log g$  (SM)  $- \log g$  (H13) on  $T_{\text{eff}}$  and [Fe/H], which is shown in the top

<sup>5</sup>The median  $\log g$  uncertainty from H13 is 0.025 dex.

<sup>6</sup>Two stars were omitted from our comparison: KOI-1054 and KOI-2481. KOI-1054 is a very evolved star and had a challenging seismic detection (D. Huber, private communication). The spectroscopic input parameters for KOI-2481 we based on a single low SNR spectrum and resulted in a poor fit during the SPC analysis.

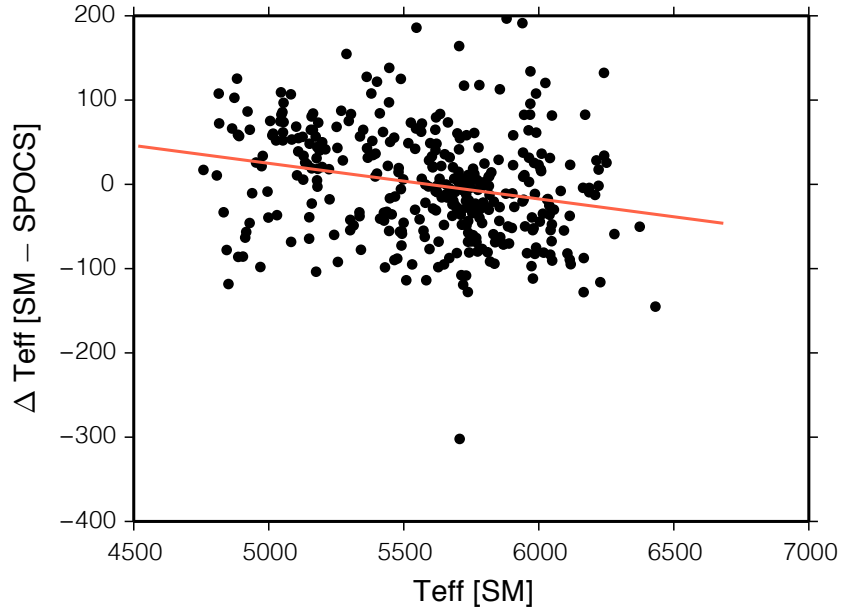


Figure 7.4: Difference in effective temperatures from SpecMatch and Valenti & Fischer (2005),  $\Delta T_{\text{eff}} = T_{\text{eff}}[\text{SM}] - T_{\text{eff}}[\text{VF05}]$ . We have fit a straight line to these points. Subsequent effective temperatures presented in this work have had this trend removed.

row of Figure 7.6. We calibrate the dependence of  $\log g$  on  $T_{\text{eff}}$  and  $[\text{Fe}/\text{H}]$ , by fitting a plane:

$$\Delta \log g = c_0 \left( \frac{T_{\text{eff}} - 5770 \text{ K}}{100 \text{ K}} \right) + c_1 \left( \frac{[\text{Fe}/\text{H}]}{0.1 \text{ dex}} \right) + c_2,$$

where  $c_0 = 0.040$ ,  $c_1 = 0.025$ ,  $c_2 = -0.084$  dex. The bottom panels of Figure 7.6 shows the difference between the calibrated SpecMatch and H13 surface gravities as a function of  $T_{\text{eff}}$  and  $[\text{Fe}/\text{H}]$ . The calibration decreased the  $\log g$  dispersion from 0.106 dex to 0.067 dex.

2. For stars with  $\log g = 1.0\text{--}4.0$  (cgs) and  $T_{\text{eff}} = 4000\text{--}5500$  K, we subtract 0.014 dex from SpecMatch surface gravities to place them on the H13 scale.

All subsequent surface gravities presented in this work have been calibrated against H13, according to the above method.

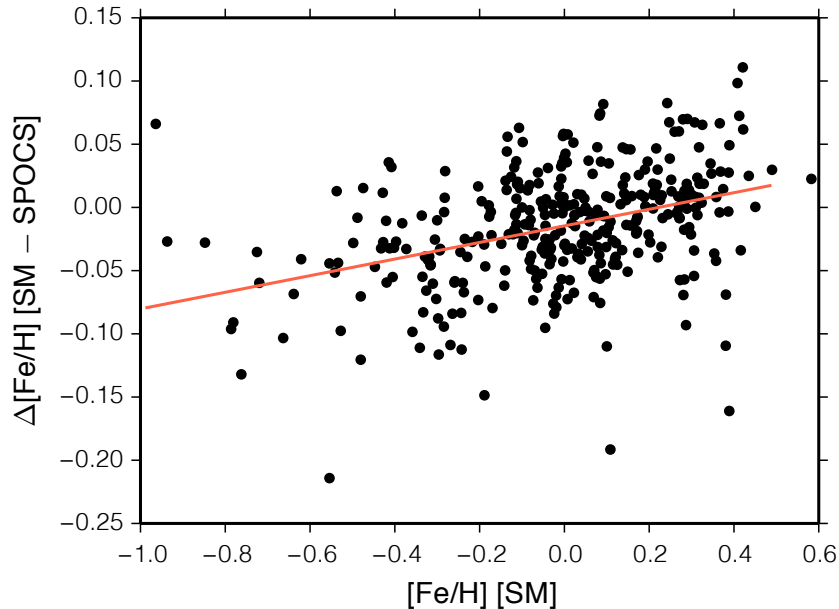


Figure 7.5: Difference in metallicities from SpecMatch and Valenti & Fischer (2005),  $\Delta[\text{Fe}/\text{H}] = [\text{Fe}/\text{H}][\text{SM}] - T_{\text{eff}}[\text{VF05}]$ . We have fit a straight line to these points. Subsequent metallicities presented in this work have had this trend removed.

## 7.3 Reliability of SpecMatch Parameters

### 7.3.1 Photon-Limited Errors

We explored how photon noise affects our derived parameters using a Monte Carlo approach. Starting with 10 high SNR spectra from the VF05 catalog ( $\text{SNR}/\text{pixel} \sim 150$ ), we injected noise to simulate lower SNR spectra. Spectra were degraded to  $\text{SNR}/\text{pixel}$  of 80, 40, 20, and 10. To understand the degree to which pixel-to-pixel fluctuations affect  $T_{\text{eff}}$ ,  $\log g$ , and  $[\text{Fe}/\text{H}]$ , we generated 20 realizations of each stellar spectrum at each SNR level ( $20 \times 10 \times 4 = 800$  total realizations). We adopted the standard deviation of the best fit values of  $T_{\text{eff}}$ ,  $\log g$ , and  $[\text{Fe}/\text{H}]$  for the 20 realizations as the error associated with Poisson fluctuations for each spectrum at each SNR level. Figure 7.7 shows the standard deviation of best fit  $T_{\text{eff}}$ ,  $\log g$ , and  $[\text{Fe}/\text{H}]$  for each star at each SNR level. Scatter in the derived parameters grows with decreasing SNR. Poisson errors tend to be larger for hotter stars since they have fewer lines in the SpecMatch spectral regions. We list the median photon-limited error for  $T_{\text{eff}}$ ,  $\log g$ , and  $[\text{Fe}/\text{H}]$  for different SNR levels in Table 7.4. At  $\text{SNR}/\text{pixel} = 40$ , photon-limited errors are 14 K in  $T_{\text{eff}}$ , 0.03 dex in  $\log g$ , and 0.012 dex in  $[\text{Fe}/\text{H}]$ , and as we will show in Section 7.3.2, photon-limited errors are second order compared to systematic uncertainties.

Photon-limited errors have the biggest impact on the PSF-fitting component of SpecMatch,

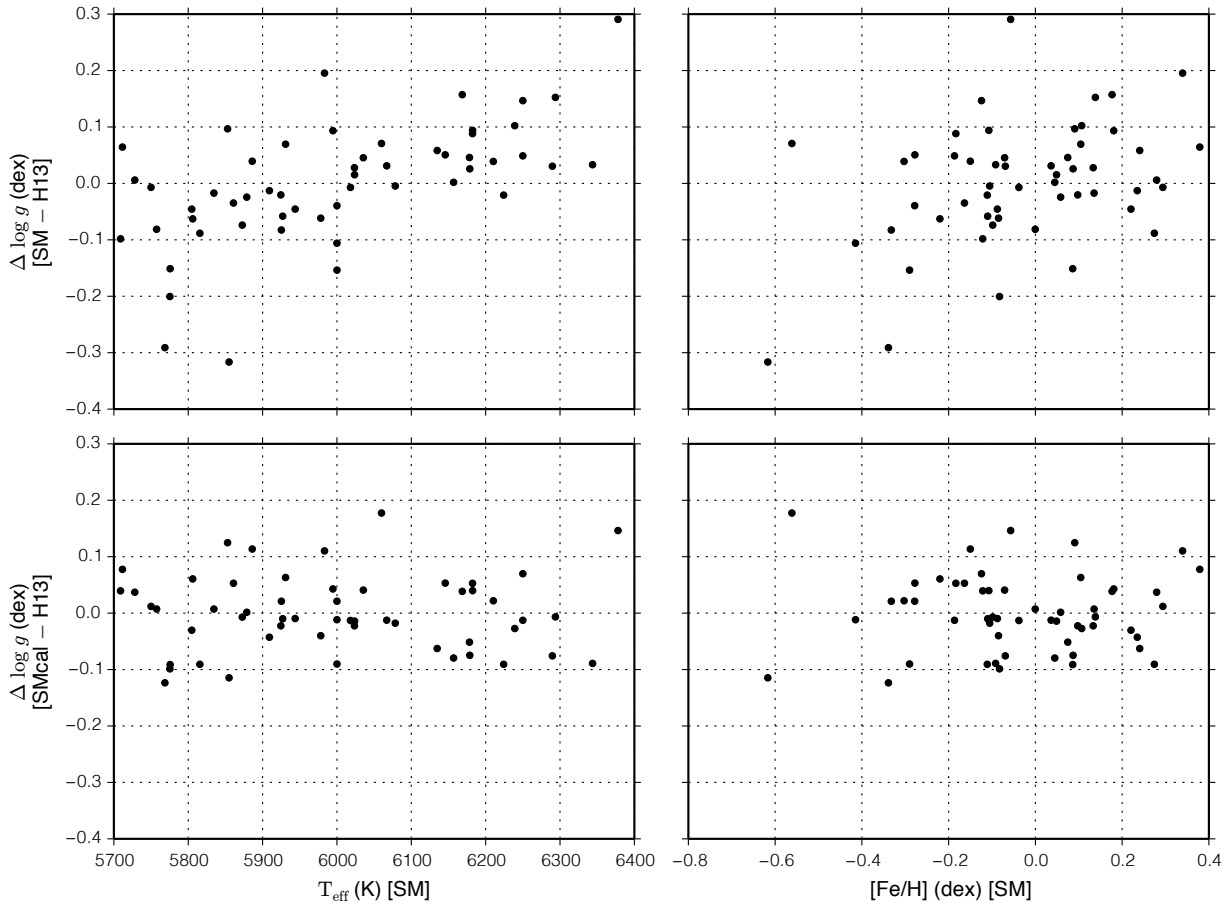


Figure 7.6: Top row: differences between SpecMatch and H13 surface gravities,  $\Delta \log g$ , as a function of SpecMatch  $T_{\text{eff}}$  and  $[\text{Fe}/\text{H}]$ . The stars shown have H13 parameters within the following range:  $\log g = 3.5\text{--}5.0$  (cgs) and  $T_{\text{eff}} = 5700\text{--}6500$  K. SpecMatch tends to yield higher surface gravities than H13 for high temperature and high metallicity stars. We calibrate the SpecMatch surface gravities to the H13 scale by fitting a plane to  $\Delta \log g(T_{\text{eff}}, [\text{Fe}/\text{H}])$  and subtracting this relationship from the SpecMatch  $\log g$  values. Bottom row: difference between calibrated SpecMatch and H13 surface gravities. Trends in  $\Delta \log g$  have been removed, and scatter in  $\Delta \log g$  is smaller using calibrated SpecMatch  $\log g$ —0.067 dex versus 0.106 dex.

described in Section 7.2.5. The HIRES PSF is determined empirically by fitting telluric lines in a  $\sim 20$  Å spectral segment with a comb of Gaussians. Due to the small number of telluric lines, pixel-to-pixel fluctuations have a large effect on the measured PSF width. One could imagine implementing a prior on the PSF width for the case of low SNR spectra. SpecMatch could likely maintain low statistical errors, even for low SNR spectra at the expense of more uncertain  $v \sin i$  values.

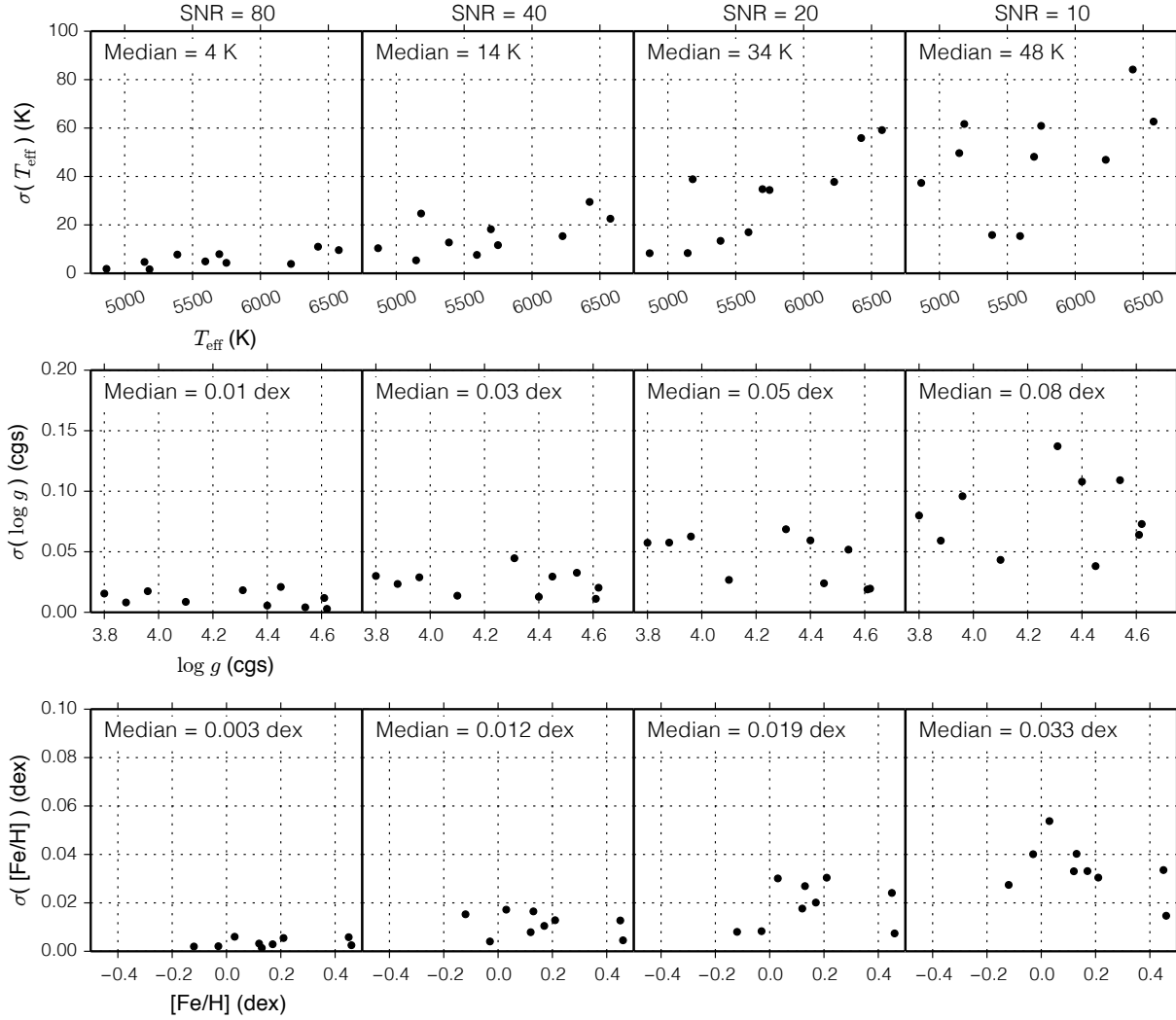


Figure 7.7: The scatter in best fit  $T_{\text{eff}}$ ,  $\log g$ , and  $[\text{Fe}/\text{H}]$  among the 20 Monte Carlo realizations for each of the 10 diagnostic stars at 4 different SNR levels: SNR/pixel = 80, 40, 20, and 10. For example, the top left panel shows the standard deviation of the best fit temperatures computed from 20 SNR/pixel = 80 realizations for 10 diagnostic stars. The median standard deviation in temperature for all 10 stars 4 K. The SNR levels in columns 1, 2, 3, and 4 are 80, 40, 20, and 10, respectively. As SNR declines, the scatter in the SpecMatch-derived parameters increases for the Monte Carlo simulated spectra. This scatter is representative of photon-limited errors at different SNR levels. At SNR/pixel = 40, slightly below the typical SNR/pixel = 45 for CKS, photon-limited errors are 14 K in  $T_{\text{eff}}$ , 0.03 dex in  $\log g$ , and 0.012 dex in  $[\text{Fe}/\text{H}]$ , and is second order compared to expected systematic uncertainties. Note that the statistical error in  $T_{\text{eff}}$  is larger hotter  $T_{\text{eff}}$  stars. At higher  $T_{\text{eff}}$ , there are fewer lines, so pixel-by-pixel errors have more of an impact on the derived best fit parameters.

Table 7.4: Median photon-limited errors as a function of SNR

SNR	Median Scatter		
	$T_{\text{eff}}$ (K)	$\log g$ (dex)	[Fe/H] (dex)
10	48	0.076	0.033
20	34	0.055	0.019
40	14	0.026	0.012
80	4	0.010	0.003

### 7.3.2 Systematic Errors

We assessed these systematic errors by analyzing spectra of touchstone stars from [Huber et al. \(2013\)](#), [Torres et al. \(2012\)](#), [Albrecht et al. \(2012\)](#), and [Valenti & Fischer \(2005\)](#).

#### Comparison with Huber et al. (2013)

As discussed in Section 7.2.7, asteroseismology offers high precision surface gravity measurements that are largely independent of stellar spectra. We compared SpecMatch and H13 parameters for 75 stars and list these parameters in Table 7.6. We show the agreement between the two methods graphically in Figure 7.8. Dispersion (RMS) about the 1-to-1 line is 64 K in  $T_{\text{eff}}$ , 0.087 dex in  $\log g$ , and 0.09 dex in [Fe/H]. If the star with the highest discrepancy in  $\Delta \log g$  is excluded, the dispersion in  $\log g$  decreases to 0.075 dex.

Assuming the H13 parameters represent the ground truth, this dispersion is an upper limit to SpecMatch errors. Solar-type oscillations are detectable with *Kepler* short cadence photometry for stars solar-type and earlier, along with evolved stars. For regions of the HR diagram sampled by [Huber et al. \(2013\)](#),<sup>7</sup> we adopt  $\sigma(\log g) = 0.08$  dex as our uncertainty in surface gravity. Due to the nature of asteroseismic observations, we cannot use asteroseismology to assess the integrity of SpecMatch surface gravities for main sequence stars earlier than  $\sim$ G2. However, because the agreement to [Huber et al. \(2013\)](#) was 0.10 dex before any calibration, we adopt  $\sigma(\log g) = 0.10$  dex errors in surface gravity for stars with  $T_{\text{eff}} < 5700$  K.

#### Comparison to Torres et al. (2012)

An additional sample of comparison stars comes from the work of [Torres et al. \(2012\)](#) (T12, hereafter). T12 measured  $T_{\text{eff}}$ ,  $\log g$ , and [Fe/H] for 56 stars with transiting planets. T12 measured these parameters spectroscopically using three different techniques: SME ([Valenti & Piskunov 1996](#); [Valenti & Fischer 2005](#)); SPC ([Buchhave et al. 2012](#)), and MOOG ([Snedden 1973](#)). When making comparisons, we use the SME parameters. Because these stars host transiting planets, mean stellar density,  $\rho_*$ , may be extracted from the transit light

<sup>7</sup>  $T_{\text{eff}} = 5700\text{--}6500$  K;  $\log g = 3.5\text{--}5.0$  and  $T_{\text{eff}} = 4000\text{--}5700$  K;  $\log g = 1.0\text{--}4.0$

curve. Surface gravities with the additional constraint of  $\rho_*$  from transit fitting may be more accurate than surface gravities based on spectroscopy alone. However, as shown in Figure 8 in H13 and Figure 3 from [Sliski & Kipping \(2014\)](#),  $\rho_*$  from transit-fitting can disagree at the  $> 50\%$ -level compared to  $\rho_*$  from asteroseismology. When fitting a transit profile, strong degeneracies exist between impact parameter and  $\rho_*$ , and H13 found that disagreements in  $\rho_*$  were largest for high impact parameters.

Using SpecMatch, we measured  $T_{\text{eff}}$ ,  $\log g$ , and  $[\text{Fe}/\text{H}]$  for 43 main-sequence stars from the T12 analysis having  $T_{\text{eff}} = 4700\text{--}6700$  K. We list the SpecMatch and T12 parameters in Table 7.7. We show a graphical comparison in Figure 7.9. Dispersion about the 1-to-1 line is 89 K in  $T_{\text{eff}}$ , 0.077 dex in  $\log g$ , and 0.11 dex in  $[\text{Fe}/\text{H}]$ . The fact that surface gravities agree to 0.077 dex, even when main sequence stars with  $T_{\text{eff}} < 5700$  K are included, supports our adoption of  $\sigma(\log g) = 0.10$  for stars cooler than 5700 K.

We note a systematic trend in  $[\text{Fe}/\text{H}]$ , where above 0.2 dex, SpecMatch produces iron values that are higher compared to T12. Also, we note a systematic trend in the  $T_{\text{eff}}$ , below  $\sim 6000$  K, SpecMatch runs hot compared to T12, while above  $\sim 6000$  K, SpecMatch runs cool. However, we are not able to tell whether these systematics are due to errors in the C05 models, the SpecMatch fitting procedure, or the joint SME/ $\rho_*$  analysis of [Torres et al. \(2012\)](#).

### Comparison to Albrecht et al. (2012)

Stellar rotation broadens stellar lines by an amount equal to twice the projected rotational velocity of the star, or  $v \sin i$ . Although often treated as a nuisance parameter,  $v \sin i$  contains information about a star’s spin axis (when combined with  $v_{\text{eq}}$ ) and a star’s suitability to precise RV followup. Measuring accurate  $v \sin i$  when  $v \sin i$  is small ( $< 5 \text{ km s}^{-1}$ ) is notoriously difficult because rotational broadening competes with other broadening mechanisms like microturbulence, macroturbulence, and the instrumental profile of the spectrometer.

We adopt stars from [Albrecht et al. \(2012\)](#) (A12 hereafter) as touchstones to assess the accuracy of SpecMatch-based  $v \sin i$ . Stars with RM measurements offer a robust calibration sample for  $v \sin i$ , given that the amplitude of the anomalous Doppler shift during transit depends on  $v \sin i$ . A12 compiled RM measurements from 53 stars, from which we select 43 stars with  $v \sin i$  uncertainties of less than  $2 \text{ km s}^{-1}$  as a calibration sample for our  $v \sin i$  values. We list the decker, measured instrumental profile width, and  $v \sin i$  measurements from SpecMatch A12  $v \sin i$  for each of these stars in Table 7.9.

Figure 7.10 compares SpecMatch  $v \sin i$  with the RM-based  $v \sin i$  from A12. There is good  $v \sin i$  agreement down to  $v \sin i$  of  $\sim 1 \text{ km s}^{-1}$ . Below  $2 \text{ km s}^{-1}$ ,  $v \sin i$  is so small compared to other broadening terms that we do not consider SpecMatch  $v \sin i$  values reliable. SpecMatch yields  $\sigma(v \sin i) = 1 \text{ km s}^{-1}$  down to  $v \sin i = 2 \text{ km s}^{-1}$ . For lower rotational velocity, we adopt an upper limit on stellar  $v \sin i$  at  $2 \text{ km s}^{-1}$ .

### Comparison to Valenti and Fischer (2005)

As discussed in Section 7.2.6, we ran SpecMatch on 352 stars from the VF05 catalog. We list the VF05 and SpecMatch parameters in Table 7.8, and compare the two parameters graphically in Figure 7.11. VF05 list two  $\log g$  values: a “spectroscopic  $\log g$ ,” based solely on the SME analysis and a “isochrone  $\log g$ ,” which incorporates constraints on  $\log g$  based on  $R_*$  (determined from  $T_{\text{eff}}$  and absolute magnitudes) and Yonsei-Yale isochrones. We choose to compare our  $\log g$  values to the “spectroscopic  $\log g$ ” because SpecMatch does not impose any constraints based on isochrones. Dispersion about the 1-to-1 line is 66 K in  $T_{\text{eff}}$ , 0.161 dex in  $\log g$ , and 0.04 dex in  $[\text{Fe}/\text{H}]$  (recall that  $T_{\text{eff}}$  and  $[\text{Fe}/\text{H}]$  have been calibrated to the VF05 scale).

We use the scatter in the differences between SpecMatch and VF05 effective temperatures and metallicities to assess our systematic uncertainties in these parameters. If systematics effects are independent during the SpecMatch and VF05 fitting, the scatter in  $\Delta T_{\text{eff}}$  and  $\Delta[\text{Fe}/\text{H}]$  represent systematic errors in  $T_{\text{eff}}$  and  $\log g$  for both analyses, added in quadrature. We adopt  $\sigma(T_{\text{eff}}) = 60$  K and  $\sigma([\text{Fe}/\text{H}]) = 0.04$  which makes the conservative assumption that the VF parameters contribute negligibly to the errors. Zero-point offsets remain a concern given that both techniques relied on optical spectra and model atmospheres with similar provenience. SME used Kurucz (1992) atmospheres and SpecMatch uses Castelli & Kurucz (2003) atmospheres. However, SpecMatch and SME used different line lists and spectral regions.

The differences in  $\log g$  between SpecMatch and VF05 were the highest of any of the comparison samples. That we see lower dispersion and no systematic offset comparing SpecMatch to H13 and T12, which incorporate additional constraints on  $\log g$  from asteroseismology and transit light curves suggests lower  $\log g$  precision in VF05. In the SME analysis of VF05, the measured  $\log g$  was largely driven by the model fit to the wings of the Mg I b lines. Modeling these lines requires careful treatment of the continuum and the effects of pressure broadening, which could be hampering the  $\log g$  precision of SME. Recall that SpecMatch  $T_{\text{eff}}$  and  $\log g$  have been placed on the SPOCS scale (see Section 7.2.6) but that for most stars the correction is smaller than 60 K and 0.04 dex.

### 7.3.3 Summary

We have assessed systematic errors present in SpecMatch parameters through comparisons to well-characterized stars from the literature. We summarize these errors in Table 7.5 for different domains of  $T_{\text{eff}}$ ,  $\log g$ , and  $[\text{Fe}/\text{H}]$ .

## 7.4 Conclusions

We developed new tool, SpecMatch, that can reliably extract stellar parameters from high-resolution optical spectra. We have assessed the systematic errors associated with SpecMatch parameters by analyzing high SNR spectra of well-characterized touchstone stars

Table 7.5: SpecMatch Systematic Uncertainties

Region			Systematic Uncertainty			
$T_{\text{eff}}$ (K)	$\log g$ (dex)	[Fe/H] (dex)	$T_{\text{eff}}$ (K)	$\log g$ (dex)	[Fe/H] (dex)	$v \sin i$ (km s <sup>-1</sup> )
5700–6500	3.5–5.0	–1.0–0.5	60	0.08	0.04	1.0
4700–5700	1.0–4.0	–1.0–0.5	60	0.08	0.04	1.0
4700–5700	4.0–5.0	–1.0–0.5	60	0.10	0.04	1.0

Note. — We have not assessed the reliability of SpecMatch outside of the tabulated ranges of  $T_{\text{eff}}$ ,  $\log g$ , and [Fe/H] due to a lack of literature stars. Parameters outside of these ranges are uncertain by unknown amounts. When SpecMatch returns  $v \sin i < 2 \text{ km s}^{-1}$ , we treat the measurement as an upper limit of  $2 \text{ km s}^{-1}$ .

from Huber et al. (2013), Torres et al. (2012), Albrecht et al. (2012), and Valenti & Fischer (2005). These errors are summarized in Table 7.5. The fact that SpecMatch uses a robust model template fitting procedure involving a large spectral region (380 Å) results in reliable parameters even for low SNR spectra. As we showed in Section 7.3.1, photon-limited uncertainties become comparable to systematic uncertainties at SNR/pixel = 10. Such a spectrum requires 100× less integration time than the SNR/pixel = 100 spectra often used for stellar parametrization. This corresponds to a reduction from 2.5 hours to 1.5 minutes of integration time for a  $V = 14.7$  star, typical of *Kepler* planet hosts, observed with HIRES on Keck I.

SpecMatch is a powerful tool for the characterization of large samples of planet-bearing stars from *Kepler*. Here, we elaborate on some of the science applications for SpecMatch as applied to *Kepler* planet-hosting stars. SpecMatch can be used to improve the radii of large samples of *Kepler* planets. With *Kepler*, the planet to star radius ratio,  $R_P/R_*$ , which depends on the transit depth to first order, is typically measured with high precision.<sup>8</sup> Stellar radii based on photometry in the Kepler Input Catalog (Brown et al. 2011) are uncertain at the ~35% level (Batalha et al. 2013; Burke et al. 2014). Thus, our knowledge of the sizes of *Kepler* planets is limited by stellar radius uncertainties. One of the key results of the *Kepler* mission is the distribution of planet sizes (Howard et al. 2012; Fressin et al. 2013; Petigura et al. 2013b) which provides important constraints for planet formation models. If the underlying radius distribution contains sharp features that would indicate an important size scale for planet formation are blurred by photometric radius errors. Combining SpecMatch-derived parameters with Dartmouth isochrones (Dotter et al. 2008) yields stellar radii good to ≈ 5%, for solar analog stars. By improving stellar radii, SpecMatch will reveal smaller details in the planet radius distribution.

SpecMatch can help probe the connection planet formation and the composition of pro-

<sup>8</sup>The median  $\sigma(R_P/R_*)$  in the Batalha et al. (2013) KOI catalog list is 5.4%.

toplanetary disks. Among nearby stars, there is a well-established correlation between giant planet occurrence and host star metallicity (Gonzalez 1997; Santos et al. 2004; Fischer & Valenti 2005). Higher metallicity stars are thought to have more massive protoplanetary disks which appear to form giant planets more efficiently. However, planets the size of Neptune and smaller are found around stars with a wide range of metallicities, both in the solar neighborhood (Mayor et al. 2011) and in the *Kepler* field (Buchhave et al. 2012).

Finally, for transiting planets detected by *Kepler*,  $v \sin i$  can be combined with the stars equatorial velocity (derived from photometric rotational modulation) to derive the inclination of the star's spin axis with respect to the Earth. Transiting planets have orbital inclinations very close to  $90^\circ$ . The  $1 \text{ km s}^{-1}$  precision of SpecMatch  $v \sin i$  measurements, can probe star-planet spin-orbit misalignment for planets that are too small and stars that are too faint for current Rossiter-McLaughlin techniques.

## Acknowledgements

We thank Andrew Mann, Kelsey Clubb, Tabettha Boyajian, John Brewer, Daniel Huber, and Marc Pinsonneault for enlightening conversations that improved this manuscript. We thank the many observers who took and reduced the spectra used in this work including Geoffrey Marcy, Andrew Howard, John Johnson, Howard Isaacson, Lauren Weiss, Lea Hirsch, Benjamin Fulton, and Evan Sinukoff. We wish to acknowledge the staff of the Keck Observatory for their outstanding support of the Keck Telescope and HIRES spectrometer. We extend special thanks to those of Hawai'ian ancestry on whose sacred mountain of Mauna Kea we are privileged to be guests. Without their generous hospitality, the Keck observations presented herein would not have been possible. This research used resources of the National Energy Research Scientific Computing Center, which is supported by the Office of Science of the U.S. Department of Energy under Contract No. DE-AC02-05CH11231. This work made use of NASA's Astrophysics Data System Bibliographic Services as well as the NumPy (Oliphant 2007), SciPy (Jones et al. 2001–), h5py (Collette 2008), IPython (Pérez & Granger 2007), and Matplotlib (Hunter 2007) Python modules.

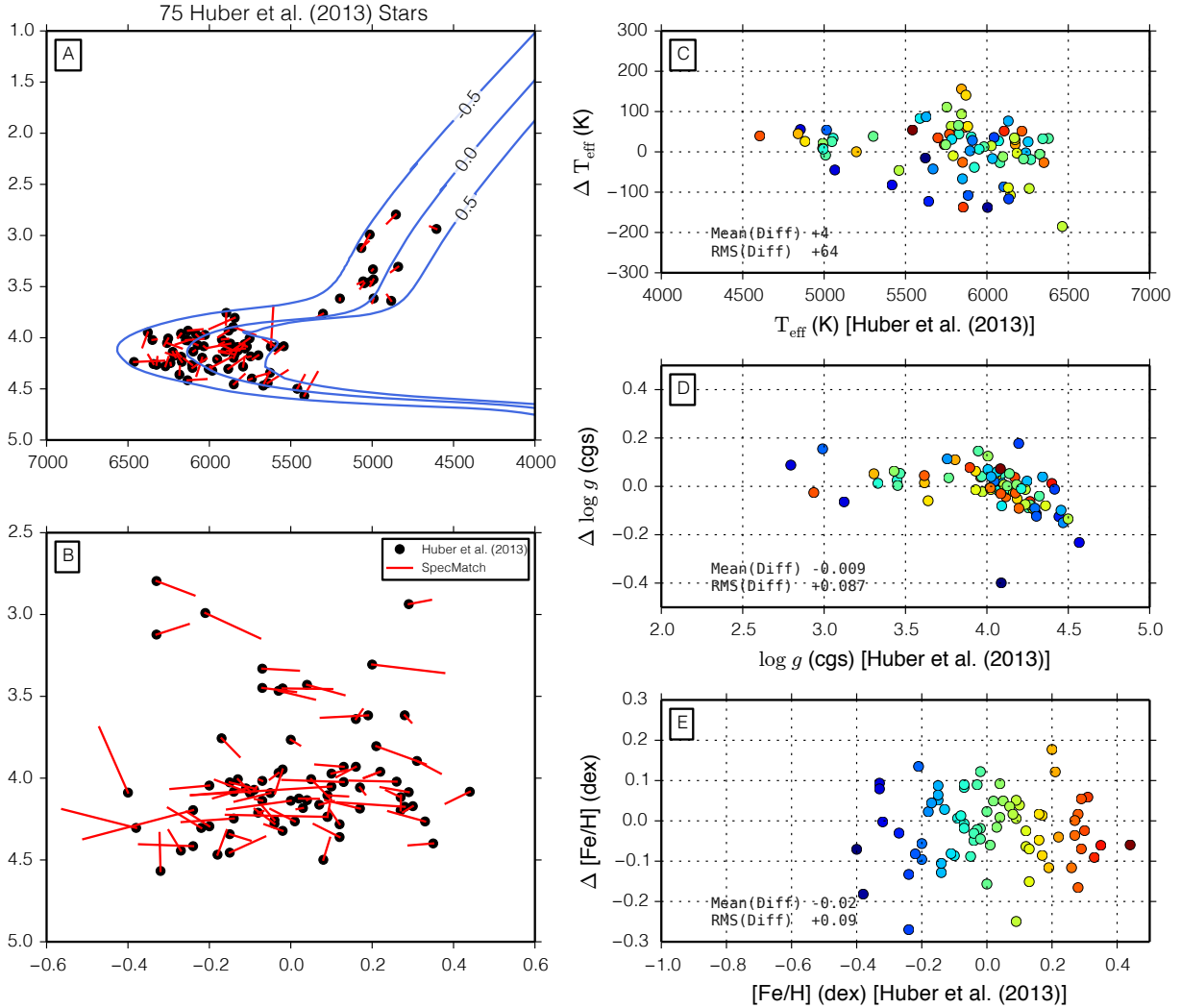


Figure 7.8: Comparison of stellar parameters of 75 stars from the [Huber et al. \(2013\)](#) asteroseismic analysis and SpecMatch. Panel A—black points show  $T_{\text{eff}}$  and  $\log g$  from [Huber et al. \(2013\)](#) and red lines point to the SpecMatch values. Shorter lines correspond to tighter agreement. We show several 5 Gyr Dartmouth isochrones ([Dotter et al. 2008](#)) having  $[\text{Fe}/\text{H}]$  of  $-0.5, 0.0,$  and  $0.5$  dex to indicate the range of  $T_{\text{eff}}$  and  $\log g$  values allowed by stellar evolution models. Panel B—same as panel A, except showing  $\log g$  and  $[\text{Fe}/\text{H}]$ . Panel C—differences in  $T_{\text{eff}}$  between SpecMatch and [Huber et al. \(2013\)](#), i.e.  $\Delta T_{\text{eff}} = T_{\text{eff}}(\text{SM}) - T_{\text{eff}}(\text{H13})$ , as a function of  $T_{\text{eff}}$  (H13). Points are colored according to [Huber et al. \(2013\)](#) metallicity (see panel E for the mapping between color and metallicity). Panels D and E—same as panel C, except showing  $\log g$  and  $[\text{Fe}/\text{H}]$ , respectively. Dispersion (RMS) in  $\Delta T_{\text{eff}}$ ,  $\Delta \log g$ ,  $\Delta [\text{Fe}/\text{H}]$  is 64 K, 0.087 (cgs), 0.09 (dex), respectively. If the largest outlier in  $\Delta \log g$  is excluded the dispersion decreases to 0.075 dex

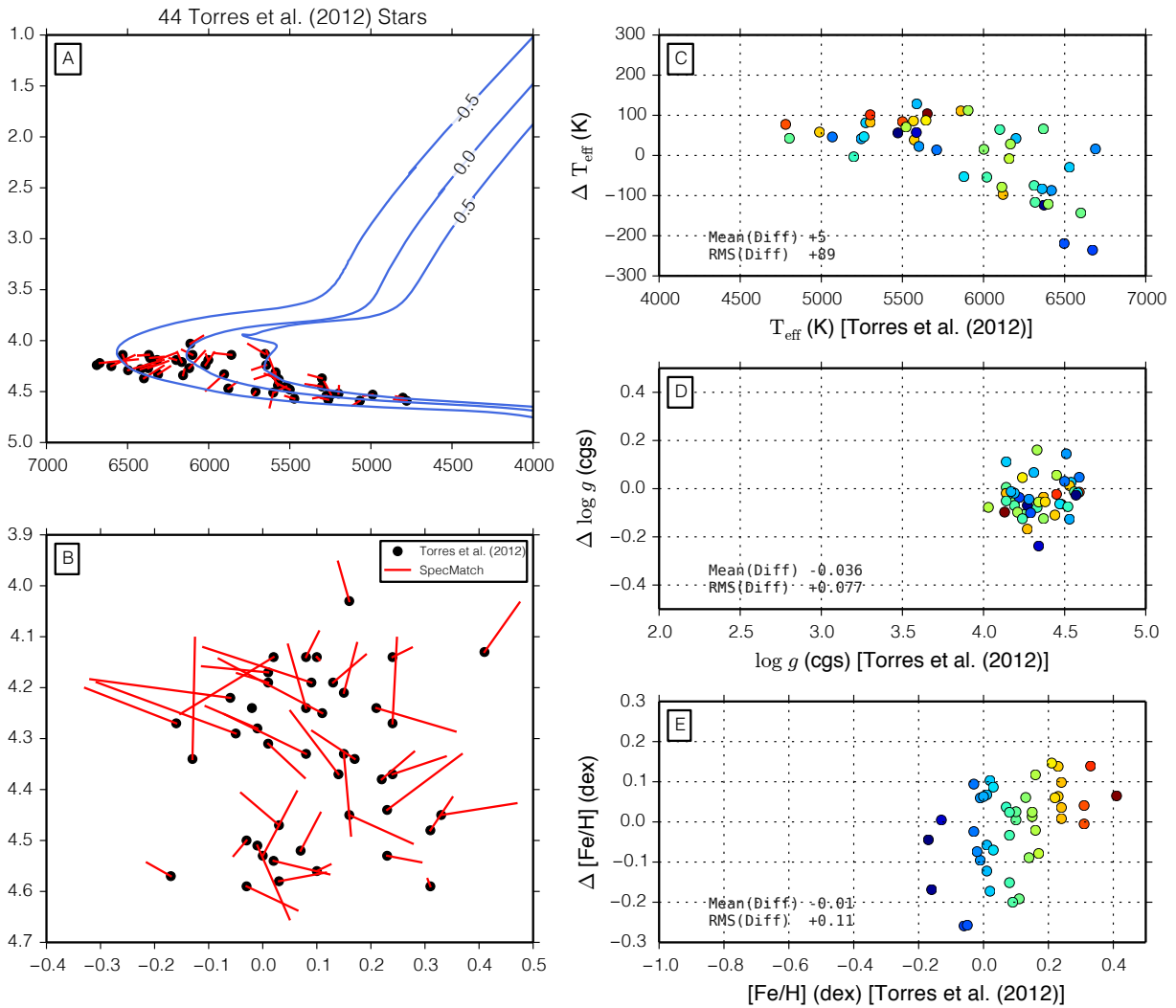


Figure 7.9: Same as Figure 7.8, except comparing SpecMatch parameters to the Torres et al. (2012) sample. Dispersion in  $\Delta T_{\text{eff}}$ ,  $\Delta \log g$ ,  $\Delta [\text{Fe}/\text{H}]$  is 89 K, 0.077 (cgs), 0.11 (dex), respectively.

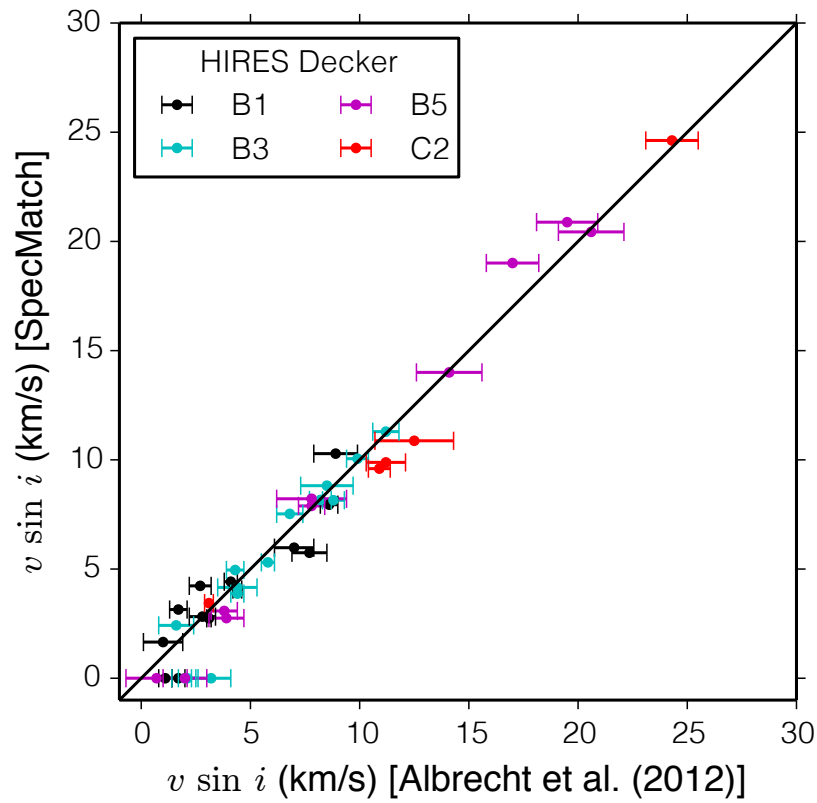


Figure 7.10: SpecMatch  $v \sin i$  versus Albrecht et al. (2012)  $v \sin i$  for stars where the uncertainty on the Albrecht et al. (2012)  $v \sin i$  (shown as horizontal bars) was less than  $2 \text{ km s}^{-1}$ .

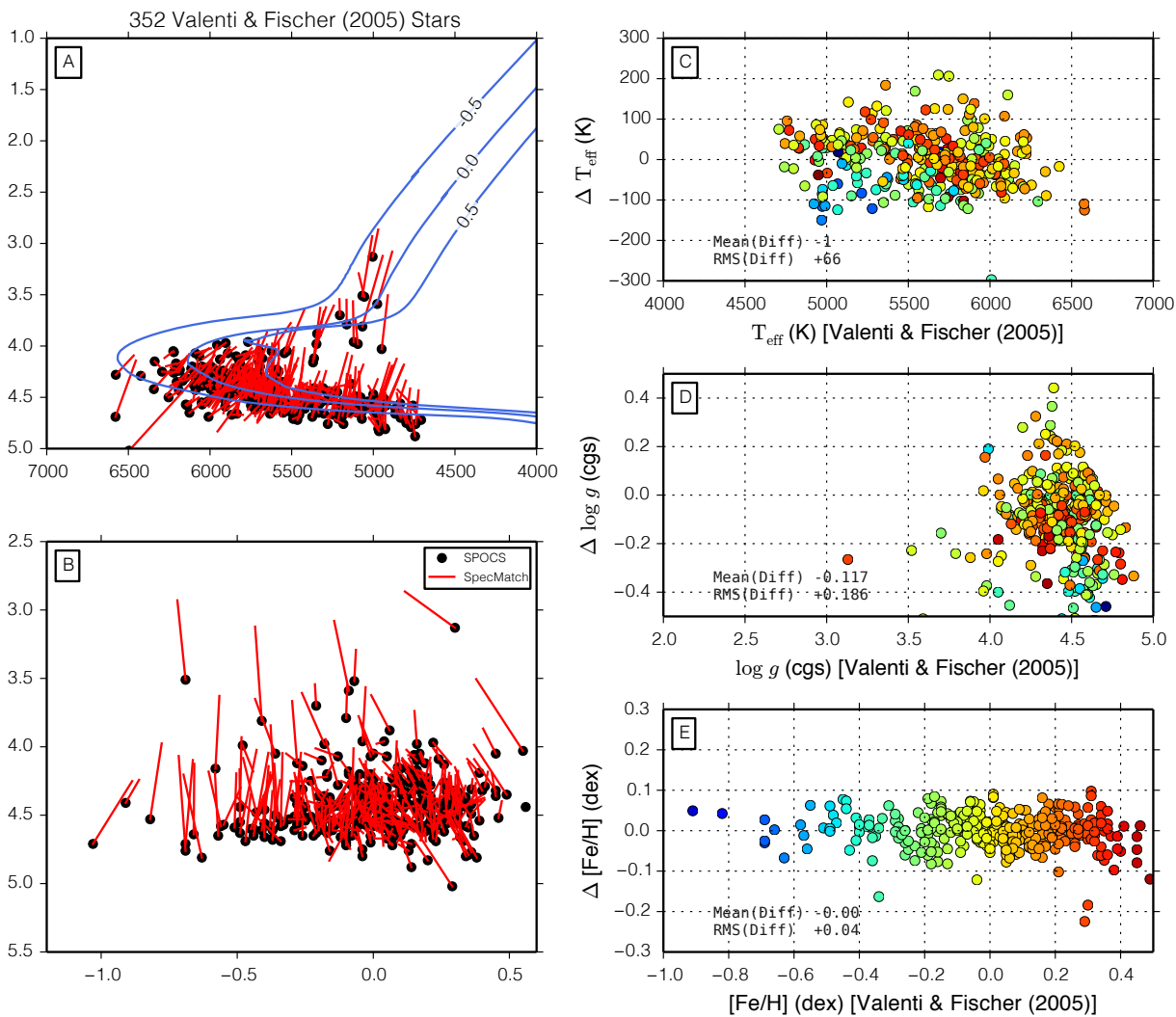


Figure 7.11: Same as Figure 7.8, but showing comparison between SpecMatch and SPOCS (Valenti & Fischer 2005). Dispersion in  $\Delta T_{\text{eff}}$ ,  $\Delta \log g$ ,  $\Delta [\text{Fe}/\text{H}]$  is 66 K, 0.161 (cgs), 0.04 (dex), respectively.

## 7.5 Appendix

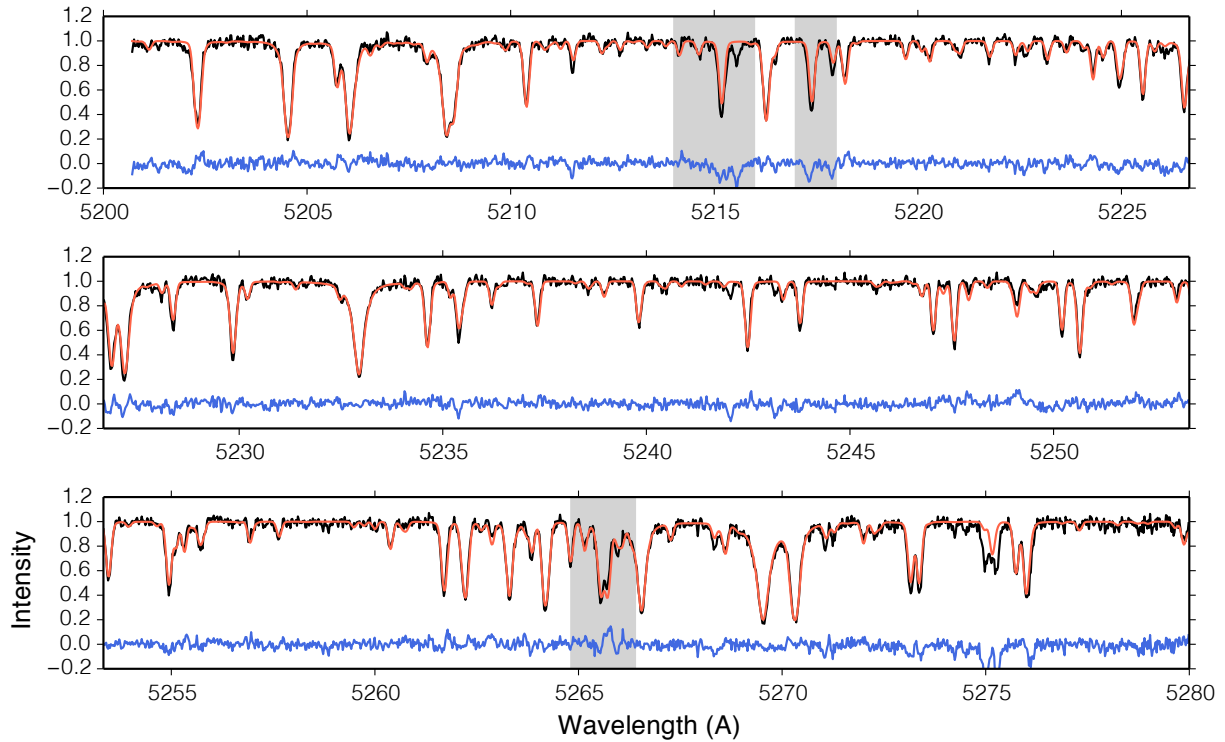


Figure 7.12: Spectrum of KOI-1 (black) with best fit model spectrum (red) and residuals (blue). The wavelength region 5200–5280 Å is broken into three segments. The gray regions are excluded from  $\chi^2$ . Line depths and line widths generally well-matched, with a few exceptions. For example at 5275 Å, several lines seem to be missing from the model. [Huber et al. \(2013\)](#) determined the properties of KOI-1 and found that it was a close solar analog:  $T_{\text{eff}} = 5850$  K,  $\log g = 4.46$  (cgs), and  $[\text{Fe}/\text{H}] = -0.15$  dex.

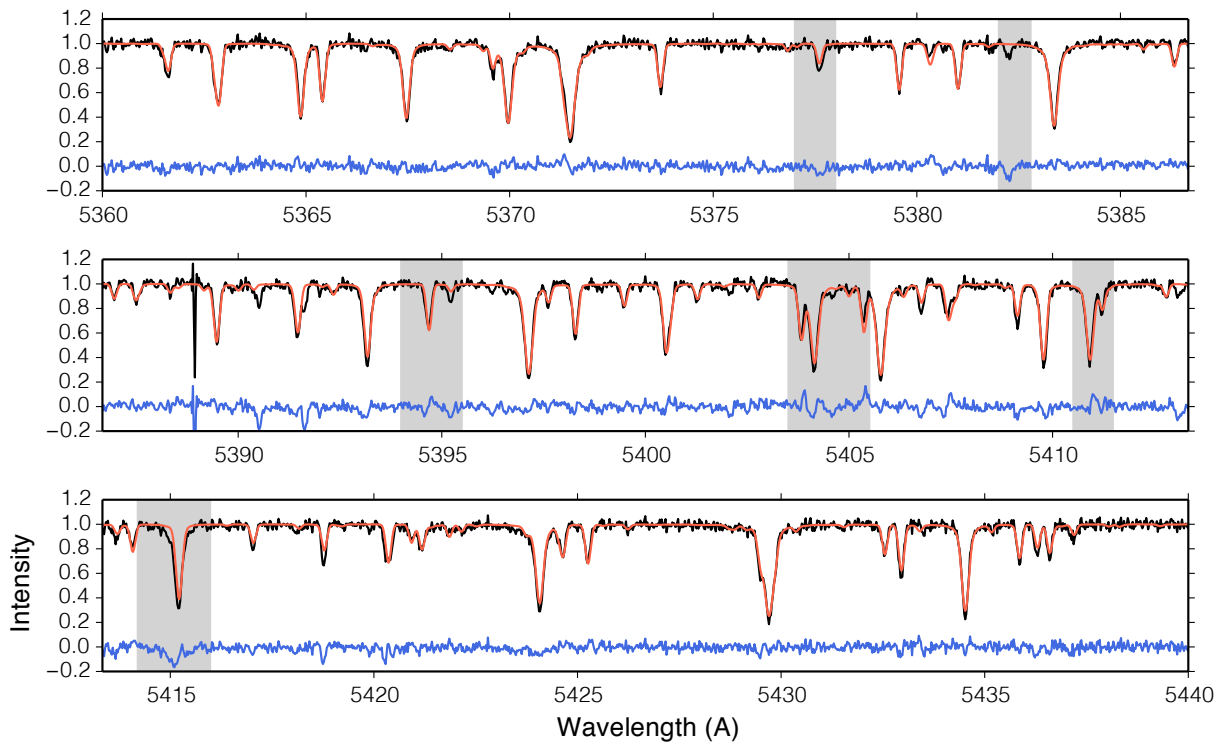


Figure 7.13: Same as Figure 7.12 except for wavelength region beginning at 5360 Å.

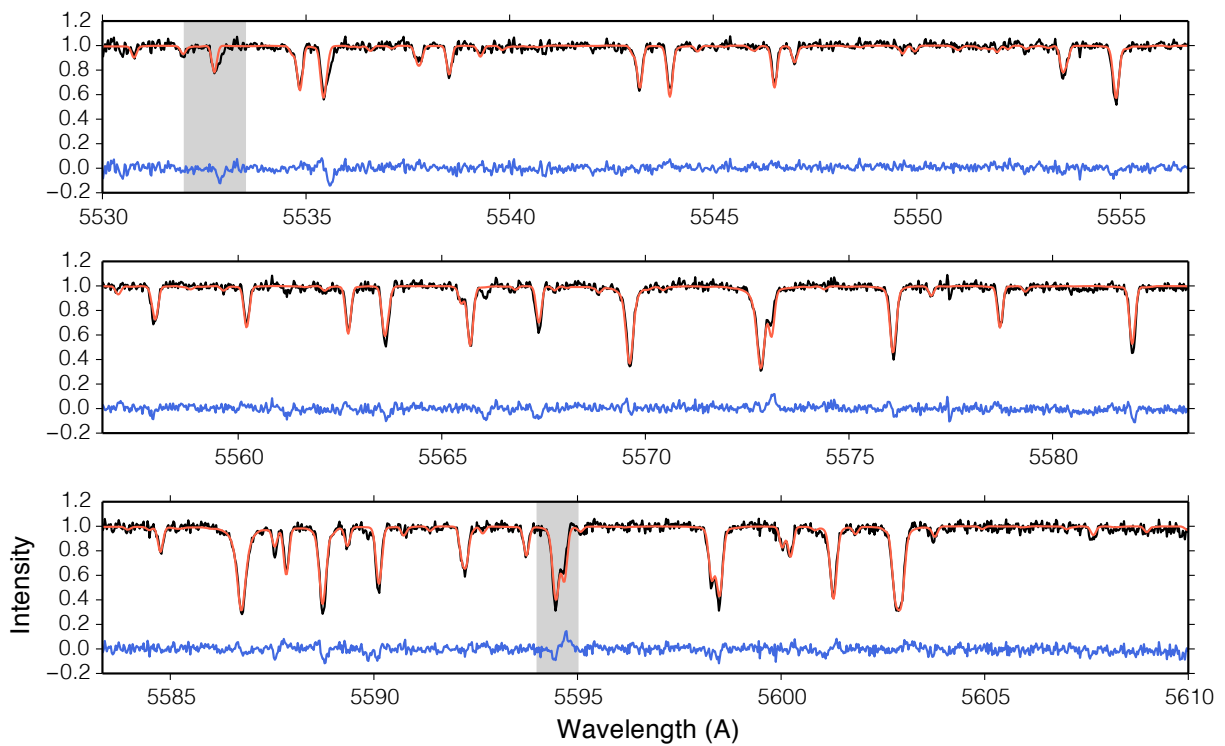


Figure 7.14: Same as Figure 7.12 except for wavelength region beginning at 5530 Å.

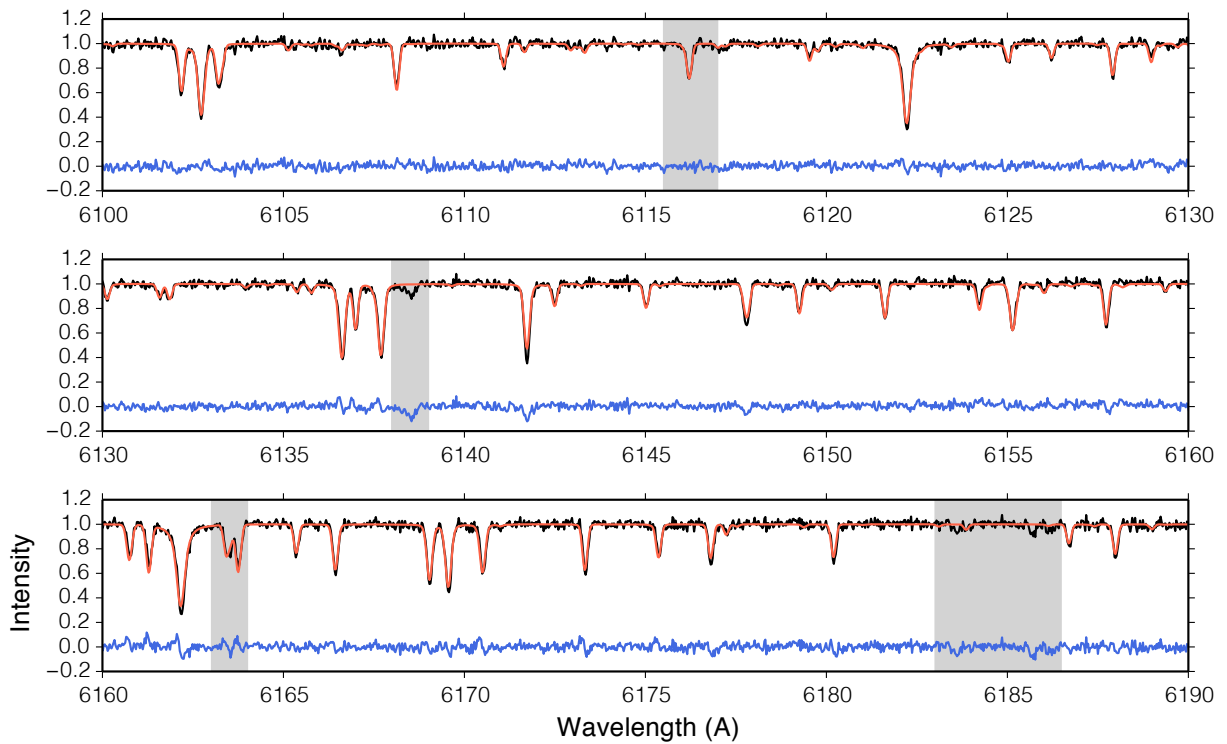


Figure 7.15: Same as Figure 7.12 except for wavelength region beginning at 6100 Å.

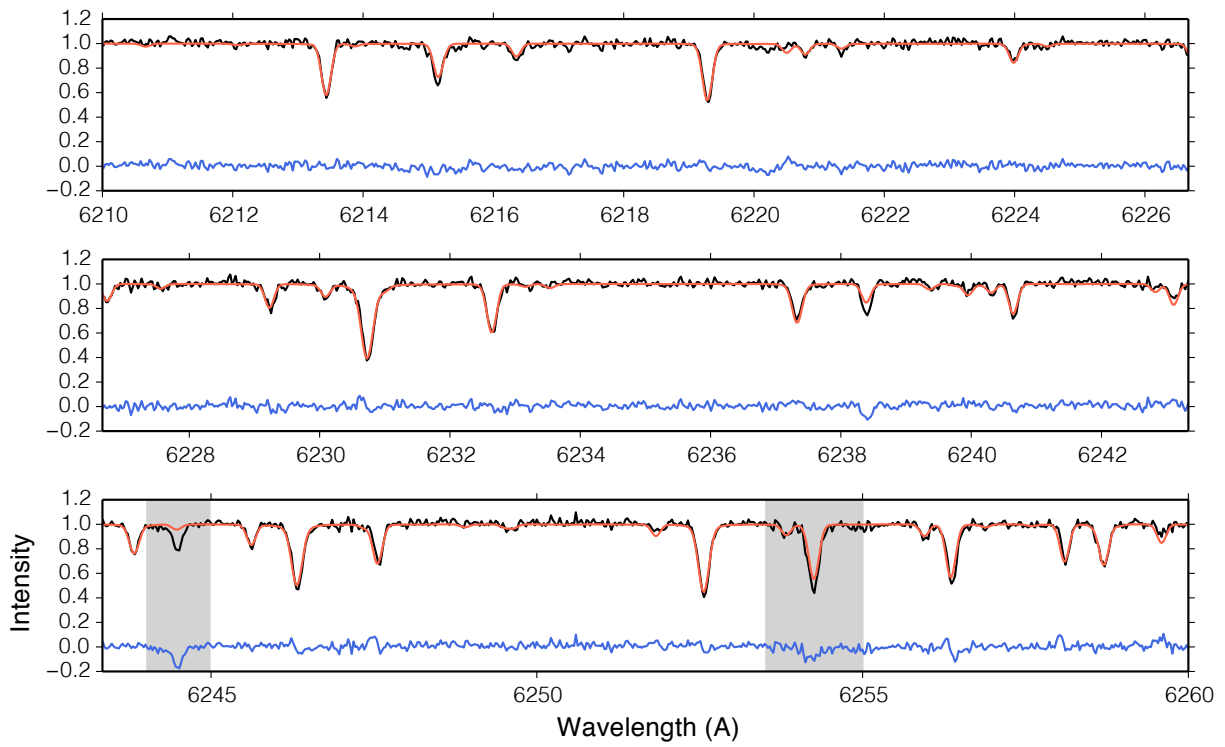


Figure 7.16: Same as Figure 7.12 except for wavelength region beginning at 6210 Å.

Table 7.6: SpecMatch/ Huber et al. (2013) Comparison

Name	$T_{\text{eff}}$			$\log g$			[Fe/H]			$v \sin i$
	SM	H13	$\Delta$	SM	H13	$\Delta$	SM	H13	$\Delta$	
CK00001	5783	5850	-66	4.36	4.46	-0.10	-0.06	-0.15	0.09	0.0
CK00002	6323	6350	-26	4.01	4.02	-0.01	0.14	0.26	-0.12	4.4
CK00005	5864	5753	111	4.13	4.01	0.12	0.10	0.05	0.05	8.5
CK00007	5844	5781	63	4.11	4.10	0.01	0.14	0.09	0.05	1.9
CK00041	5890	5825	65	4.13	4.12	0.00	0.07	0.02	0.05	3.4
CK00042	6319	6325	-5	4.19	4.26	-0.08	-0.05	0.01	-0.06	12.9
CK00064	5340	5302	38	3.80	3.77	0.04	0.02	-0.00	0.02	0.9
CK00069	5626	5669	-42	4.32	4.47	-0.15	-0.16	-0.18	0.02	0.0
CK00072	5713	5627	86	4.38	4.34	0.04	-0.10	-0.15	0.05	0.9
CK00075	5898	5896	2	3.87	3.76	0.11	-0.13	-0.17	0.04	4.7
CK00085	6203	6169	34	4.16	4.24	-0.07	0.10	0.09	0.01	8.4
CK00087	5519	5642	-122	4.32	4.44	-0.13	-0.30	-0.27	-0.03	0.0
CK00097	6041	6027	14	3.95	3.97	-0.02	0.14	0.10	0.04	2.5
CK00098	6411	6378	33	4.09	3.95	0.15	-0.04	-0.02	-0.02	8.7
CK00107	5922	5862	60	4.07	4.12	-0.04	0.23	0.27	-0.04	3.2
CK00108	5938	5845	93	4.14	4.16	-0.02	0.11	0.07	0.04	3.1
CK00113	5597	5543	54	4.16	4.08	0.07	0.38	0.44	-0.06	0.0
CK00117	5825	5851	-25	4.11	4.20	-0.09	0.27	0.27	0.00	2.0
CK00118	5764	5747	17	4.19	4.18	0.01	0.01	0.03	-0.02	1.5
CK00119	5716	5854	-137	3.97	3.89	0.08	0.37	0.31	0.06	0.0
CK00122	5733	5699	34	4.21	4.17	0.04	0.28	0.30	-0.02	0.0
CK00123	5958	5952	6	4.20	4.21	-0.01	-0.07	-0.08	0.01	2.4
CK00168	5872	5828	44	4.14	4.09	0.05	-0.14	-0.05	-0.09	1.5
CK00244	6250	6270	-19	4.19	4.28	-0.09	-0.09	-0.04	-0.05	9.5
CK00245	5334	5417	-82	4.34	4.57	-0.23	-0.32	-0.32	-0.00	0.0
CK00246	5783	5793	-9	4.19	4.28	-0.09	0.10	0.12	-0.02	0.0
CK00257	6180	6184	-3	4.28	4.36	-0.08	0.06	0.12	-0.06	7.3
CK00260	6236	6239	-2	4.27	4.25	0.02	-0.27	-0.14	-0.13	8.6
CK00262	6207	6225	-17	4.19	4.14	0.05	-0.16	-0.00	-0.16	9.9
CK00263	5815	5784	31	4.12	4.06	0.06	-0.19	-0.11	-0.08	1.6
CK00268	6375	6343	32	4.17	4.26	-0.09	-0.07	-0.04	-0.03	8.5
CK00269	6277	6463	-185	4.22	4.24	-0.01	-0.16	0.09	-0.25	11.6
CK00270	5671	5588	83	4.01	4.09	-0.08	-0.19	-0.10	-0.09	2.9
CK00271	6157	6106	51	4.20	4.26	-0.06	0.24	0.33	-0.09	6.2
CK00273	5756	5739	17	4.41	4.40	0.01	0.29	0.35	-0.06	0.8
CK00274	6099	6072	27	4.05	4.07	-0.02	-0.08	-0.09	0.01	6.2
CK00275	5813	5770	43	4.06	4.09	-0.03	0.22	0.29	-0.07	2.4
CK00276	5994	5982	12	4.28	4.32	-0.04	-0.06	-0.02	-0.04	0.0
CK00277	5939	5911	28	4.07	4.05	0.02	-0.30	-0.20	-0.10	3.9
CK00279	6266	6215	51	4.15	4.17	-0.03	0.11	0.28	-0.17	13.0

Table 7.6 (cont'd): SpecMatch/ Huber et al. (2013) Comparison

Name	$T_{\text{eff}}$			$\log g$			[Fe/H]			$v \sin i$
	SM	H13	$\Delta$	SM	H13	$\Delta$	SM	H13	$\Delta$	SM
CK00280	6017	6134	-116	4.40	4.42	-0.01	-0.37	-0.24	-0.13	2.0
CK00281	5606	5622	-15	3.69	4.09	-0.40	-0.47	-0.40	-0.07	0.0
CK00282	5776	5884	-107	4.18	4.30	-0.12	-0.30	-0.22	-0.08	0.0
CK00285	6011	5871	140	4.10	4.06	0.04	0.18	0.17	0.01	3.0
CK00288	6192	6174	18	4.00	3.96	0.04	0.18	0.22	-0.04	7.5
CK00319	5945	5882	63	3.99	3.93	0.06	0.11	0.16	-0.05	4.8
CK00370	6036	6144	-107	4.01	4.02	-0.01	-0.02	0.13	-0.15	6.4
CK00371	5198	5198	0	3.63	3.62	0.01	0.07	0.19	-0.12	0.0
CK00623	5866	6004	-137	4.19	4.30	-0.11	-0.56	-0.38	-0.18	0.0
CK00674	4908	4883	25	3.58	3.64	-0.06	0.18	0.16	0.02	1.9
CK00974	6277	6253	24	4.08	4.01	0.07	-0.10	-0.13	0.03	7.6
CK00975	6207	6131	76	4.07	4.03	0.04	-0.09	-0.15	0.06	7.3
CK00981	5021	5066	-44	3.06	3.12	-0.06	-0.25	-0.33	0.08	1.3
CK01019	5000	5009	-8	3.46	3.45	0.00	0.10	-0.02	0.12	0.6
CK01221	4999	4991	8	3.66	3.62	0.04	0.30	0.28	0.02	1.3
CK01222	5088	5055	33	3.47	3.45	0.03	0.01	-0.07	0.08	1.4
CK01230	5069	5015	54	3.15	2.99	0.16	-0.08	-0.21	0.13	3.2
CK01241	4885	4840	45	3.36	3.31	0.05	0.38	0.20	0.18	0.0
CK01282	6017	6034	-16	4.10	4.08	0.02	-0.25	-0.14	-0.11	5.8
CK01299	5001	4995	6	3.34	3.33	0.01	0.02	-0.07	0.09	1.4
CK01314	5073	5048	25	3.52	3.47	0.05	0.06	-0.03	0.09	1.4
CK01537	6169	6260	-90	4.10	4.05	0.05	-0.24	0.10	-0.34	5.7
CK01612	6017	6104	-86	4.20	4.29	-0.09	-0.26	-0.20	-0.06	3.1
CK01613	6079	6044	35	4.37	4.20	0.18	-0.51	-0.24	-0.27	9.0
CK01618	6203	6173	30	4.13	4.19	-0.05	0.08	0.17	-0.09	9.7
CK01621	6054	6081	-26	4.01	3.97	0.04	-0.05	-0.03	-0.02	5.5
CK01890	6087	6099	-11	4.12	4.13	-0.01	0.05	0.04	0.01	6.9
CK01894	5013	4992	21	3.49	3.43	0.06	0.13	0.04	0.09	1.7
CK01924	5999	5844	155	3.91	3.80	0.11	0.33	0.21	0.12	4.9
CK01925	5414	5460	-45	4.36	4.50	-0.13	0.10	0.08	0.02	0.0
CK01930	5884	5923	-38	4.01	4.02	-0.01	-0.08	-0.07	-0.01	4.0
CK01962	5941	5904	37	4.13	4.14	-0.01	-0.09	-0.07	-0.02	3.8
CK02133	4644	4605	39	2.91	2.94	-0.03	0.34	0.29	0.05	3.6
CK02545	6042	6131	-88	3.92	3.93	-0.01	0.06	0.13	-0.07	6.6
CK02640	4909	4854	55	2.88	2.80	0.09	-0.24	-0.33	0.09	2.3

Note. —

Table 7.7: SpecMatch/ Torres et al. (2012) Comparison

Name	$T_{\text{eff}}$			$\log g$			[Fe/H]			$v \sin i$
	SM	T12	$\Delta$	SM	T12	$\Delta$	SM	T12	$\Delta$	SM
CoRoT-2	5624	5602	22	4.65	4.51	0.14	0.05	-0.01	0.06	9.6
CoRoT-7	5355	5274	81	4.57	4.54	0.03	0.12	0.02	0.10	0.0
HAT-P-11	4857	4780	77	4.58	4.59	-0.01	0.30	0.31	-0.01	1.4
HAT-P-13	5756	5653	103	4.03	4.13	-0.10	0.47	0.41	0.06	3.2
HAT-P-14	6456	6600	-143	4.14	4.25	-0.11	-0.08	0.11	-0.19	8.3
HAT-P-15	5654	5568	86	4.33	4.38	-0.05	0.28	0.22	0.06	0.0
HAT-P-16	6149	6158	-8	4.28	4.34	-0.06	0.09	0.17	-0.08	3.1
HAT-P-17	5287	5246	41	4.40	4.53	-0.13	0.06	0.00	0.06	0.0
HAT-P-18	4845	4803	42	4.55	4.56	-0.01	0.13	0.10	0.03	0.0
HAT-P-19	5047	4989	58	4.54	4.53	0.01	0.29	0.23	0.06	1.6
HAT-P-21	5716	5588	128	4.38	4.31	0.07	0.08	0.01	0.07	3.6
HAT-P-22	5384	5302	82	4.34	4.37	-0.03	0.34	0.24	0.10	0.6
HAT-P-23	6017	5905	112	4.49	4.33	0.16	0.16	0.15	0.01	8.3
HAT-P-24	6249	6373	-123	4.20	4.27	-0.07	-0.33	-0.16	-0.17	10.5
HAT-P-25	5584	5500	84	4.42	4.48	-0.06	0.35	0.31	0.04	0.0
HAT-P-4	5970	5860	110	4.12	4.14	-0.02	0.28	0.24	0.04	5.7
HAT-P-6	6436	6672	-235	4.18	4.22	-0.04	-0.32	-0.06	-0.26	8.2
HAT-P-8	6242	6200	42	4.17	4.19	-0.02	-0.05	0.01	-0.06	11.5
HD 147506	6435	6369	66	4.15	4.14	0.01	0.10	0.10	0.00	20.6
HD 149026	6022	6120	-97	4.10	4.27	-0.17	0.25	0.24	0.01	6.3
HD 17156	6017	6002	15	4.14	4.19	-0.05	0.19	0.13	0.06	4.5
HD 189733	5114	5068	46	4.64	4.59	0.05	0.06	-0.03	0.09	3.0
HD 80606	5611	5573	38	4.33	4.44	-0.11	0.37	0.23	0.14	0.0
Kepler-10	5643	5586	57	4.10	4.34	-0.24	-0.13	-0.13	0.00	0.0
Kepler-6	5732	5645	87	4.29	4.24	0.05	0.36	0.21	0.15	1.4
Kepler-7	6034	6113	-78	3.95	4.03	-0.08	0.14	0.16	-0.02	2.7
Kepler-8	6201	6318	-116	4.12	4.19	-0.07	-0.11	0.09	-0.20	10.4
TRES-1	5309	5263	46	4.56	4.58	-0.02	0.12	0.03	0.09	0.0
TRES-2	5826	5879	-52	4.41	4.47	-0.06	-0.04	0.03	-0.07	0.0
TRES-3	5528	5472	56	4.54	4.57	-0.03	-0.21	-0.17	-0.04	0.0
WASP-1	6194	6166	28	4.11	4.21	-0.10	0.17	0.15	0.02	1.5
WASP-12	6164	6100	64	4.09	4.14	-0.05	0.10	0.08	0.02	3.1
WASP-13	5965	6020	-54	4.12	4.24	-0.12	0.05	0.08	-0.03	3.9
WASP-14	6277	6497	-219	4.19	4.29	-0.10	-0.31	-0.05	-0.26	3.1
WASP-17	6500	6530	-29	4.25	4.14	0.11	-0.15	0.02	-0.17	10.1
WASP-18	6277	6399	-121	4.25	4.37	-0.12	0.05	0.14	-0.09	11.3
WASP-19	5592	5522	70	4.51	4.45	0.06	0.28	0.16	0.12	4.5
WASP-2	5196	5200	-3	4.45	4.52	-0.07	0.11	0.07	0.04	0.0
WASP-3	6331	6419	-87	4.24	4.28	-0.04	-0.11	-0.01	-0.10	14.1
XO-1	5724	5711	13	4.53	4.50	0.03	-0.05	-0.03	-0.02	0.0

Table 7.7 (cont'd): SpecMatch/ Torres et al. (2012) Comparison

Name	$T_{\text{eff}}$			$\log g$			[Fe/H]			$v \sin i$
	SM	T12	$\Delta$	SM	T12	$\Delta$	SM	T12	$\Delta$	SM
XO-2	5403	5302	101	4.43	4.45	-0.02	0.47	0.33	0.14	1.6
XO-3	6706	6690	16		4.24		-0.09	-0.02	-0.07	19.1
XO-4	6277	6361	-83	4.16	4.17	-0.01	-0.11	0.01	-0.12	8.2

Note. — For WASP-8,  $v \sin i$  was misprinted as  $20 \pm 0.6 \text{ km s}^{-1}$ , instead of  $2.0 \pm 0.6 \text{ km s}^{-1}$  in the original reference (Queloz 2010).

Table 7.8: SpecMatch/ Valenti &amp; Fischer (2005) Comparison

Name	$T_{\text{eff}}$			$\log g$			[Fe/H]			$v \sin i$
	SM	VF05	$\Delta$	SM	VF05	$\Delta$	SM	VF05	$\Delta$	
100180	6024	5989	35	4.38	4.38	0.00	0.01	-0.01	0.02	2.5
100623	5131	5189	-57	4.37	4.68	-0.31	-0.36	-0.37	0.01	0.3
101259	5006	5067	-60	2.93	3.51	-0.58	-0.72	-0.69	-0.03	0.8
10145	5673	5638	35	4.34	4.44	-0.10	0.01	-0.01	0.02	1.2
101472	6211	6191	20	4.45	4.43	0.02	-0.06	-0.03	-0.03	5.0
101959	6049	6049	0	4.39	4.39	-0.00	-0.11	-0.11	0.00	3.0
102071	5392	5279	113	4.47	4.53	-0.06	0.09	0.01	0.08	0.0
102365	5633	5630	3	4.25	4.57	-0.32	-0.30	-0.33	0.03	0.0
104067	4991	4956	35	4.61	4.65	-0.04	0.10	0.10	0.00	2.0
104304	5593	5565	28	4.34	4.56	-0.22	0.31	0.27	0.04	0.0
10476	5254	5181	73	4.52	4.53	-0.01	0.01	-0.04	0.05	0.1
104800	5619	5626	-6	3.98	4.53	-0.55	-0.78	-0.82	0.04	0.1
105	6061	6126	-64	4.57	4.65	-0.08	0.02	0.08	-0.06	14.6
105631	5476	5462	14	4.60	4.57	0.03	0.22	0.20	0.02	2.0
106156	5493	5492	1	4.51	4.58	-0.07	0.25	0.23	0.02	0.0
10697	5690	5680	10	4.04	4.12	-0.08	0.17	0.19	-0.02	1.8
107146	5918	5882	36	4.66	4.47	0.19	0.00	-0.03	0.03	4.4
107148	5773	5797	-23	4.29	4.45	-0.16	0.30	0.31	-0.01	0.0
10780	5403	5327	76	4.55	4.54	0.01	0.09	0.03	0.06	0.0
108874	5636	5551	85	4.39	4.35	0.04	0.25	0.18	0.07	0.5
109358	5846	5930	-83	4.40	4.44	-0.04	-0.24	-0.16	-0.08	0.3
110537	5764	5752	12	4.36	4.40	-0.04	0.11	0.12	-0.01	0.3
111031	5744	5806	-61	4.25	4.38	-0.13	0.27	0.28	-0.01	1.0
112257	5630	5697	-66	4.10	4.45	-0.35	-0.03	-0.03	0.00	0.2
114174	5738	5781	-42	4.34	4.51	-0.17	0.07	0.07	-0.00	0.1
114613	5744	5782	-37	4.02	4.09	-0.07	0.23	0.24	-0.01	1.4
114729	5718	5821	-102	4.05	4.14	-0.09	-0.32	-0.26	-0.06	0.1
114783	5161	5135	26	4.54	4.53	0.01	0.14	0.12	0.02	0.0
115617	5604	5571	33	4.35	4.47	-0.12	-0.00	0.05	-0.05	0.4
116442	5140	5182	-41	4.29	4.56	-0.27	-0.39	-0.40	0.01	1.0
116443	4973	5038	-64	4.32	4.58	-0.26	-0.37	-0.38	0.01	0.8
117176	5495	5545	-49	3.82	4.07	-0.25	-0.05	-0.01	-0.04	0.2
117207	5701	5724	-22	4.32	4.51	-0.19	0.26	0.27	-0.01	0.0
11850	5709	5663	46	4.73	4.55	0.18	0.11	0.09	0.02	5.1
12051	5485	5495	-9	4.43	4.62	-0.19	0.23	0.26	-0.03	1.0
121320	5488	5548	-59	4.32	4.54	-0.22	-0.30	-0.25	-0.05	0.4
122064	4852	4757	95	4.42	4.58	-0.16	0.17	0.18	-0.01	1.5
122652	6138	6093	45	4.33	4.24	0.09	-0.01	-0.00	-0.01	2.9
124106	5156	5117	39	4.61	4.58	0.03	-0.07	-0.10	0.03	0.5
124115	6453	6579	-125	4.14	4.69	-0.55	0.26	0.23	0.03	30.5

Table 7.8 (cont'd): SpecMatch/ Valenti &amp; Fischer (2005) Comparison

Name	$T_{\text{eff}}$			$\log g$			[Fe/H]			$v \sin i$
	SM	VF05	$\Delta$	SM	VF05	$\Delta$	SM	VF05	$\Delta$	
124292	5439	5501	-61	4.28	4.65	-0.37	-0.06	-0.08	0.02	0.2
125455	5115	5109	6	4.39	4.53	-0.14	-0.11	-0.18	0.07	0.2
126053	5577	5640	-62	4.12	4.52	-0.40	-0.36	-0.35	-0.01	0.0
12661	5736	5743	-6	4.27	4.42	-0.15	0.38	0.36	0.02	0.1
126614	5591	5594	-2		4.44			0.56		1.8
127334	5718	5744	-25	4.27	4.37	-0.10	0.27	0.27	-0.00	0.0
128311	5027	4965	62	4.70	4.83	-0.13	0.15	0.20	-0.05	3.1
12846	5634	5626	8	4.23	4.42	-0.19	-0.25	-0.28	0.03	0.1
129191	5803	5817	-13	4.31	4.41	-0.10	0.25	0.24	0.01	0.7
129333	5824	5845	-20	4.68	4.47	0.21	0.09	0.16	-0.07	16.7
130322	5440	5308	132	4.52	4.41	0.11	0.10	0.01	0.09	0.1
13043	5864	5897	-32	4.18	4.27	-0.09	0.07	0.09	-0.02	1.3
130992	4860	4833	27	4.60	4.70	-0.10	-0.02	-0.01	-0.01	0.9
132142	5107	5122	-14	4.21	4.60	-0.39	-0.37	-0.45	0.08	0.0
132173	6190	6254	-63	4.44	4.50	-0.06	-0.03	0.05	-0.08	9.6
133295	6101	6089	12	4.52	4.43	0.09	-0.01	0.01	-0.02	9.6
134319	5787	5662	125	4.72	4.52	0.20	0.04	0.03	0.01	10.2
134987	5736	5750	-13	4.23	4.35	-0.12	0.28	0.28	0.00	1.5
13579	5240	5211	29	4.59	4.59	-0.00	0.35	0.35	-0.00	0.1
136352	5595	5672	-76	4.05	4.58	-0.53	-0.33	-0.34	0.01	0.8
136713	5032	4981	51	4.56	4.62	-0.06	0.23	0.22	0.01	0.8
136925	5683	5717	-33	4.04	4.51	-0.47	-0.27	-0.29	0.02	0.0
138004	5745	5742	3	4.39	4.49	-0.10	-0.09	-0.09	0.00	1.3
1388	5913	5952	-38	4.30	4.42	-0.12	-0.02	-0.00	-0.02	2.3
13931	5827	5830	-2	4.22	4.30	-0.08	0.03	0.03	0.00	1.4
139323	5145	5099	46	4.52	4.65	-0.13	0.36	0.37	-0.01	0.1
139457	5999	5957	42	4.18	3.99	0.19	-0.44	-0.48	0.04	0.5
139813	5449	5491	-41	4.68	4.71	-0.03	0.09	0.14	-0.05	5.2
140913	6021	6048	-26	4.56	4.57	-0.01	0.08	0.13	-0.05	7.9
141004	5898	5936	-37	4.20	4.30	-0.10	0.01	0.05	-0.04	1.3
141937	5918	5847	71	4.45	4.42	0.03	0.14	0.13	0.01	0.1
142267	5671	5756	-84	4.08	4.48	-0.40	-0.48	-0.43	-0.05	0.8
143761	5748	5823	-74	4.17	4.36	-0.19	-0.23	-0.20	-0.03	0.3
14412	5325	5374	-48	4.35	4.69	-0.34	-0.45	-0.47	0.02	0.3
144579	5130	5214	-83	4.10	4.71	-0.61	-0.66	-0.69	0.03	0.6
144585	5843	5854	-10	4.18	4.33	-0.15	0.31	0.31	0.00	0.7
145229	5983	5885	98	4.66	4.37	0.29	-0.16	-0.16	-0.00	3.2
145675	5392	5388	4	4.40	4.52	-0.12	0.47	0.46	0.01	0.1
1461	5743	5765	-21	4.34	4.41	-0.07	0.19	0.18	0.01	1.3
146233	5773	5791	-17	4.38	4.41	-0.03	0.05	0.03	0.02	0.0

Table 7.8 (cont'd): SpecMatch/ Valenti &amp; Fischer (2005) Comparison

Name	$T_{\text{eff}}$			$\log g$			[Fe/H]			$v \sin i$
	SM	VF05	$\Delta$	SM	VF05	$\Delta$	SM	VF05	$\Delta$	SM
149724	5763	5738	25	4.18	4.29	-0.11	0.42	0.41	0.01	1.8
149806	5387	5359	28	4.50	4.54	-0.04	0.27	0.21	0.06	0.1
150554	6060	6010	50	4.35	4.29	0.06	0.01	0.00	0.01	2.0
151541	5374	5332	42	4.47	4.57	-0.10	-0.11	-0.19	0.08	0.1
152391	5543	5479	64	4.66	4.57	0.09	0.06	0.04	0.02	2.9
152555	6068	5967	101	4.57	4.46	0.11	0.10	0.05	0.05	16.8
15335	5842	5891	-48	4.01	4.07	-0.06	-0.21	-0.13	-0.08	3.5
153458	5848	5907	-58	4.50	4.59	-0.09	0.13	0.16	-0.03	0.0
154088	5459	5409	50	4.39	4.46	-0.07	0.32	0.31	0.01	0.7
154345	5513	5468	45	4.51	4.54	-0.03	-0.06	-0.10	0.04	0.1
157214	5582	5697	-114	3.84	4.50	-0.66	-0.38	-0.36	-0.02	0.8
157338	5979	5961	18	4.25	4.28	-0.03	-0.12	-0.08	-0.04	2.1
157347	5693	5714	-20	4.29	4.50	-0.21	0.01	0.03	-0.02	0.0
158633	5227	5302	-74	4.36	4.66	-0.30	-0.40	-0.40	-0.00	0.1
159222	5867	5743	124	4.36	4.26	0.10	0.12	0.10	0.02	2.4
159868	5505	5623	-117	3.78	4.05	-0.27	-0.05	-0.00	-0.05	2.2
16141	5805	5794	11	4.21	4.22	-0.01	0.16	0.17	-0.01	0.8
16160	4800	4866	-65	4.34	4.66	-0.32	-0.09	-0.12	0.03	0.7
161897	5621	5623	-1	4.49	4.58	-0.09	0.04	0.03	0.01	0.1
163153	5651	5744	-92	3.99	4.35	-0.36	0.37	0.49	-0.12	1.8
163489	4970	5004	-33	2.86	3.13	-0.27	0.12	0.30	-0.18	3.4
16417	5763	5817	-53	4.08	4.17	-0.09	0.11	0.13	-0.02	2.1
164922	5386	5385	1	4.34	4.51	-0.17	0.14	0.17	-0.03	0.9
166	5618	5577	41	4.68	4.58	0.10	0.18	0.18	-0.00	3.4
166620	5029	5000	29	4.39	4.47	-0.08	-0.15	-0.18	0.03	0.0
167665	6066	6115	-48	4.22	4.22	0.00	-0.21	-0.17	-0.04	4.2
168009	5779	5767	12	4.30	4.31	-0.01	0.01	-0.00	0.01	1.6
168443	5579	5580	0	3.96	4.25	-0.29	0.09	0.08	0.01	0.1
168746	5487	5564	-76	4.01	4.52	-0.51	-0.07	-0.08	0.01	1.1
16895	6254	6344	-89	4.26	4.42	-0.16	-0.00	0.06	-0.06	8.4
169830	6234	6221	13	4.06	4.06	0.00	0.13	0.15	-0.02	3.5
170469	5789	5811	-21	4.21	4.39	-0.18	0.30	0.30	0.00	2.6
170493	4842	4770	72	4.55	4.79	-0.24	0.28	0.35	-0.07	0.2
170657	5132	5103	29	4.62	4.61	0.01	-0.11	-0.15	0.04	0.0
172051	5471	5564	-92	4.19	4.50	-0.31	-0.29	-0.26	-0.03	0.4
175541	5089	5055	34	3.29	3.52	-0.23	-0.06	-0.07	0.01	2.0
176377	5772	5788	-15	4.47	4.40	0.07	-0.28	-0.27	-0.01	0.1
177153	6026	5993	33	4.26	4.20	0.06	-0.05	-0.05	-0.00	3.0
177830	4910	4949	-38	3.51	4.03	-0.52	0.38	0.55	-0.17	2.4
178911B	5658	5668	-9	4.45	4.55	-0.10	0.29	0.28	0.01	0.7

Table 7.8 (cont'd): SpecMatch/ Valenti &amp; Fischer (2005) Comparison

Name	$T_{\text{eff}}$			$\log g$			[Fe/H]			$v \sin i$
	SM	VF05	$\Delta$	SM	VF05	$\Delta$	SM	VF05	$\Delta$	
179949	6188	6168	20	4.32	4.34	-0.02	0.15	0.14	0.01	6.7
179957	5674	5676	-1	4.16	4.34	-0.18	0.00	-0.02	0.02	0.1
179958	5747	5760	-12	4.30	4.39	-0.09	0.05	0.04	0.01	0.1
180684	5994	6090	-95	4.02	4.07	-0.05	-0.01	0.05	-0.06	6.1
18143	5181	5148	33	4.48	4.55	-0.07	0.27	0.28	-0.01	0.4
182488	5404	5453	-48	4.36	4.67	-0.31	0.20	0.22	-0.02	0.6
182572	5642	5656	-13	4.12	4.32	-0.20	0.35	0.40	-0.05	2.0
183263	5922	5936	-13	4.22	4.40	-0.18	0.28	0.30	-0.02	1.9
185144	5261	5246	15	4.47	4.53	-0.06	-0.20	-0.19	-0.01	0.2
186408	5782	5781	1	4.26	4.34	-0.08	0.10	0.10	0.00	2.2
186427	5738	5674	64	4.33	4.35	-0.02	0.08	0.04	0.04	0.1
187123	5801	5815	-13	4.34	4.36	-0.02	0.11	0.12	-0.01	1.0
187897	5985	5835	150	4.51	4.30	0.21	0.15	0.10	0.05	4.0
187923	5701	5726	-24	3.94	4.28	-0.34	-0.18	-0.13	-0.05	0.9
188015	5759	5746	13	4.38	4.44	-0.06	0.29	0.29	0.00	1.4
18803	5703	5638	65	4.43	4.45	-0.02	0.16	0.11	0.05	0.1
188512	5164	5163	1	3.55	3.79	-0.24	-0.10	-0.10	0.00	0.1
190067	5289	5356	-66	4.24	4.61	-0.37	-0.34	-0.37	0.03	0.6
190228	5241	5348	-106	3.61	3.98	-0.37	-0.26	-0.18	-0.08	1.7
19034	5420	5470	-49	4.02	4.63	-0.61	-0.43	-0.49	0.06	0.9
190360	5617	5552	65	4.24	4.38	-0.14	0.25	0.21	0.04	1.0
190404	4857	4973	-115	4.12	4.64	-0.52	-0.66	-0.66	0.00	0.0
190406	5979	5932	47	4.44	4.45	-0.01	0.06	0.05	0.01	2.0
191408	4812	4922	-109	4.18	4.58	-0.40	-0.61	-0.56	-0.05	0.9
191785	5140	5140	0	4.29	4.60	-0.31	-0.08	-0.15	0.07	0.8
192263	5060	4975	85	4.65	4.60	0.05	0.06	0.05	0.01	0.8
192310	5146	5080	66	4.54	4.55	-0.01	0.07	0.02	0.05	0.3
19308	5826	5807	19	4.30	4.34	-0.04	0.15	0.13	0.02	1.4
19373	5994	6032	-37	4.19	4.31	-0.12	0.13	0.16	-0.03	3.2
19467	5725	5715	10	4.25	4.44	-0.19	-0.09	-0.15	0.06	0.1
195019	5760	5788	-27	4.19	4.23	-0.04	0.05	0.07	-0.02	0.2
195564	5694	5699	-4	4.02	4.16	-0.14	0.09	0.10	-0.01	0.4
196201	5419	5460	-40	4.37	4.57	-0.20	-0.16	-0.14	-0.02	0.3
196761	5434	5419	15	4.36	4.54	-0.18	-0.29	-0.28	-0.01	0.1
196850	5794	5790	4	4.35	4.37	-0.02	-0.09	-0.11	0.02	1.2
196885	6239	6185	54	4.21	4.23	-0.02	0.21	0.20	0.01	7.4
198802	5751	5767	-15	3.98	3.96	0.02	0.01	0.04	-0.03	2.4
199019	5565	5560	5	4.68	4.60	0.08	0.05	0.07	-0.02	5.8
199476	5430	5470	-39	4.19	4.61	-0.42	-0.38	-0.41	0.03	0.2
19994	6127	6188	-60	4.08	4.24	-0.16	0.21	0.19	0.02	8.7

Table 7.8 (cont'd): SpecMatch/ Valenti &amp; Fischer (2005) Comparison

Name	$T_{\text{eff}}$			$\log g$			[Fe/H]			$v \sin i$
	SM	VF05	$\Delta$	SM	VF05	$\Delta$	SM	VF05	$\Delta$	SM
199960	5958	5962	-3	4.22	4.31	-0.09	0.28	0.27	0.01	1.8
200565	5892	5684	208	4.61	4.37	0.24	0.01	-0.06	0.07	7.2
200968	5283	5221	62	4.70	4.61	0.09	0.09	0.11	-0.02	1.1
201219	5712	5653	59	4.66	4.57	0.09	0.18	0.15	0.03	1.5
20165	5166	5110	56	4.56	4.49	0.07	0.02	-0.03	0.05	0.5
201989	5768	5749	19	4.62	4.58	0.04	0.15	0.12	0.03	3.9
2025	4901	4865	36	4.59	4.61	-0.02	-0.25	-0.29	0.04	0.5
202751	4774	4797	-22	4.41	4.70	-0.29	-0.09	-0.10	0.01	0.7
202917	5640	5617	23	4.62	4.39	0.23	0.10	0.11	-0.01	14.0
204277	6211	6196	15	4.41	4.37	0.04	-0.04	-0.02	-0.02	4.9
20619	5687	5703	-15	4.40	4.54	-0.14	-0.20	-0.21	0.01	0.2
206332	5997	6033	-35	4.19	4.33	-0.14	0.28	0.27	0.01	1.5
206374	5607	5587	20	4.48	4.52	-0.04	-0.03	-0.05	0.02	0.2
20675	6467	6577	-109	4.09	4.28	-0.19	0.11	0.21	-0.10	17.9
206860	6028	5974	54	4.59	4.47	0.12	-0.01	-0.02	0.01	9.7
208313	5080	5033	47	4.54	4.54	0.00	0.02	-0.04	0.06	0.1
209253	6268	6109	159	4.48	4.20	0.28	-0.04	-0.09	0.05	16.4
209393	5709	5541	168	4.75	4.38	0.37	-0.09	-0.17	0.08	3.6
209458	6036	6099	-62	4.29	4.38	-0.09	-0.02	0.01	-0.03	4.2
21019	5423	5529	-105	3.65	4.05	-0.40	-0.43	-0.36	-0.07	0.9
210277	5459	5555	-95	4.12	4.49	-0.37	0.21	0.21	0.00	0.8
210302	6309	6339	-29	4.20	4.15	0.05	0.07	0.09	-0.02	14.0
211080	5788	5820	-31	4.09	4.19	-0.10	0.34	0.39	-0.05	2.2
211681	5736	5839	-102	4.09	4.32	-0.23	0.37	0.45	-0.08	2.8
212291	5579	5602	-22	4.39	4.56	-0.17	-0.12	-0.12	-0.00	0.1
213519	5775	5832	-56	4.33	4.44	-0.11	-0.02	-0.00	-0.02	0.1
216259	4819	4969	-149	4.20	4.81	-0.61	-0.70	-0.63	-0.07	0.1
216275	5960	5863	97	4.45	4.38	0.07	-0.12	-0.16	0.04	1.7
217014	5791	5787	4	4.30	4.45	-0.15	0.21	0.20	0.01	0.1
217107	5683	5704	-20	4.30	4.54	-0.24	0.38	0.39	-0.01	0.0
217165	5961	5936	25	4.39	4.39	-0.00	0.03	0.01	0.02	1.7
218566	4925	4927	-1	4.46	4.81	-0.35	0.28	0.38	-0.10	0.1
218868	5620	5540	80	4.52	4.45	0.07	0.28	0.21	0.07	0.0
219134	4893	4835	58	4.54	4.56	-0.02	0.09	0.12	-0.03	0.8
219538	5140	5078	62	4.58	4.50	0.08	0.01	-0.04	0.05	0.1
219834B	5193	5168	25	4.50	4.59	-0.09	0.23	0.22	0.01	0.1
220339	5003	4975	28	4.53	4.53	-0.00	-0.25	-0.31	0.06	0.1
22049	5159	5146	13	4.69	4.57	0.12	-0.01	-0.03	0.02	0.7
221354	5274	5133	141	4.41	4.37	0.04	0.09	0.01	0.08	0.2
221356	6016	5976	40	4.40	4.31	0.09	-0.26	-0.26	0.00	1.8

Table 7.8 (cont'd): SpecMatch/ Valenti &amp; Fischer (2005) Comparison

Name	$T_{\text{eff}}$			$\log g$			[Fe/H]			$v \sin i$
	SM	VF05	$\Delta$	SM	VF05	$\Delta$	SM	VF05	$\Delta$	SM
222368	6136	6204	-67	4.11	4.18	-0.07	-0.12	-0.09	-0.03	6.4
222582	5744	5727	17	4.30	4.34	-0.04	0.01	-0.03	0.04	0.1
222697	5545	5361	184	4.63	4.41	0.22	0.24	0.16	0.08	1.9
223315	5728	5606	122	4.50	4.34	0.16	0.36	0.30	0.06	0.1
223498	5572	5628	-55	4.32	4.58	-0.26	0.20	0.23	-0.03	0.1
22484	5971	6038	-66	4.09	4.21	-0.12	-0.05	-0.02	-0.03	3.2
22879	5707	5688	19	4.24	4.41	-0.17	-0.86	-0.91	0.05	0.0
23249	5109	5095	14	3.74	3.98	-0.24	0.15	0.16	-0.01	1.4
23356	5029	4991	38	4.63	4.59	0.04	-0.04	-0.06	0.02	0.3
23439	5088	5070	18	4.25	4.71	-0.46	-0.89	-1.03	0.14	0.0
23596	6042	5904	138	4.13	3.97	0.16	0.29	0.22	0.07	3.5
24040	5781	5853	-71	4.18	4.36	-0.18	0.18	0.21	-0.03	1.6
24238	4887	4973	-85	4.19	4.59	-0.40	-0.50	-0.51	0.01	0.0
24365	5207	5205	2	3.54	3.70	-0.16	-0.21	-0.21	-0.00	0.1
24496	5539	5572	-32	4.40	4.56	-0.16	0.01	0.01	-0.00	0.2
24892	5302	5363	-60	3.67	4.12	-0.45	-0.30	-0.28	-0.02	0.1
25665	5022	4936	86	4.60	4.51	0.09	0.03	-0.03	0.06	0.3
2589	5124	5120	4	3.56	3.96	-0.40	-0.03	-0.04	0.01	1.0
26151	5439	5348	91	4.47	4.47	-0.00	0.32	0.26	0.06	0.0
26965	5061	5151	-89	4.18	4.57	-0.39	-0.27	-0.28	0.01	0.0
26990	5954	5748	206	4.83	4.39	0.44	-0.16	-0.04	-0.12	5.6
28005	5758	5819	-60	4.18	4.38	-0.20	0.31	0.32	-0.01	2.6
283	5084	5094	-9	4.30	4.57	-0.27	-0.49	-0.55	0.06	0.0
28946	5354	5321	33	4.47	4.55	-0.08	-0.10	-0.15	0.05	0.2
29461	5915	5913	2	4.56	4.52	0.04	0.24	0.25	-0.01	0.1
29883	4947	4952	-4	4.45	4.61	-0.16	-0.18	-0.18	0.00	0.3
30649	5700	5778	-77	3.93	4.44	-0.51	-0.48	-0.49	0.01	1.0
30652	6406	6424	-17	4.27	4.29	-0.02	0.02	0.03	-0.01	17.2
31253	6006	6065	-58	4.02	4.10	-0.08	0.12	0.16	-0.04	3.0
31412	6067	6096	-28	4.31	4.37	-0.06	0.03	0.05	-0.02	1.1
31560	4783	4744	39	4.55	4.88	-0.33	0.08	0.14	-0.06	2.7
32147	4856	4827	29	4.46	4.69	-0.23	0.27	0.33	-0.06	1.0
32923	5706	5694	12	4.12	4.20	-0.08	-0.15	-0.17	0.02	0.1
32963	5720	5763	-42	4.31	4.43	-0.12	0.08	0.08	0.00	0.0
33636	5956	5904	52	4.44	4.43	0.01	-0.09	-0.13	0.04	2.3
34411	5829	5911	-81	4.15	4.37	-0.22	0.08	0.12	-0.04	0.1
34445	5818	5837	-18	4.18	4.21	-0.03	0.12	0.14	-0.02	1.2
34721	5964	5999	-34	4.19	4.25	-0.06	-0.08	-0.07	-0.01	2.7
35850	6102	6496	-393	4.33	5.02	-0.69	0.07	0.29	-0.22	52.6
3651	5292	5221	71	4.48	4.45	0.03	0.20	0.16	0.04	0.1

Table 7.8 (cont'd): SpecMatch/ Valenti &amp; Fischer (2005) Comparison

Name	$T_{\text{eff}}$			$\log g$			[Fe/H]			$v \sin i$
	SM	VF05	$\Delta$	SM	VF05	$\Delta$	SM	VF05	$\Delta$	
37006	5598	5549	49	4.66	4.58	0.08	0.04	0.02	0.02	3.6
37008	4901	4975	-73	4.16	4.55	-0.39	-0.49	-0.49	-0.00	0.2
37124	5540	5500	40	4.19	4.60	-0.41	-0.37	-0.44	0.07	0.0
37216	5484	5364	120	4.62	4.44	0.18	0.02	-0.05	0.07	0.1
37394	5377	5351	26	4.69	4.60	0.09	0.19	0.19	0.00	1.6
3765	5063	5032	31	4.53	4.59	-0.06	0.17	0.18	-0.01	0.0
377	5984	5873	111	4.60	4.28	0.32	0.16	0.15	0.01	14.3
3795	5324	5369	-44	3.63	4.16	-0.53	-0.57	-0.58	0.01	0.1
38230	5161	5174	-12	4.27	4.53	-0.26	-0.04	-0.08	0.04	0.1
38529	5651	5697	-45	3.87	4.05	-0.18	0.40	0.45	-0.05	3.7
3861	6247	6223	24	4.27	4.26	0.01	0.07	0.08	-0.01	1.6
38858	5629	5726	-96	4.19	4.51	-0.32	-0.27	-0.23	-0.04	0.7
38949	6052	6051	1	4.53	4.55	-0.02	-0.05	-0.05	-0.00	6.6
39587	6006	5882	124	4.59	4.34	0.25	0.01	-0.01	0.02	8.8
39715	4833	4798	35	4.59	4.75	-0.16	-0.06	-0.04	-0.02	2.0
39881	5723	5718	5	4.24	4.42	-0.18	-0.09	-0.13	0.04	1.2
40397	5481	5542	-60	4.18	4.59	-0.41	-0.08	-0.10	0.02	0.2
40979	6196	6089	107	4.35	4.30	0.05	0.22	0.17	0.05	6.9
4203	5708	5702	6	4.19	4.36	-0.17	0.44	0.45	-0.01	1.5
4208	5557	5600	-42	4.22	4.52	-0.30	-0.28	-0.28	-0.00	1.0
4256	4980	4930	50	4.52	4.80	-0.28	0.28	0.34	-0.06	0.0
42618	5716	5747	-30	4.42	4.43	-0.01	-0.09	-0.11	0.02	0.3
4307	5725	5839	-113	4.05	4.10	-0.05	-0.25	-0.19	-0.06	1.7
43947	5956	5933	23	4.37	4.37	-0.00	-0.29	-0.29	-0.00	0.5
44420	5744	5796	-51	4.21	4.35	-0.14	0.28	0.29	-0.01	0.1
45184	5834	5810	24	4.40	4.37	0.03	0.04	0.04	-0.00	0.1
45350	5654	5616	38	4.28	4.32	-0.04	0.31	0.29	0.02	1.0
4614	5881	5941	-59	4.38	4.44	-0.06	-0.28	-0.25	-0.03	0.1
4628	4951	4944	7	4.43	4.51	-0.08	-0.28	-0.27	-0.01	0.1
46375	5339	5285	54	4.47	4.53	-0.06	0.30	0.24	0.06	0.1
47157	5784	5733	51	4.35	4.43	-0.08	0.40	0.34	0.06	1.6
4747	5357	5335	22	4.53	4.65	-0.12	-0.18	-0.22	0.04	0.1
47752	4781	4707	74	4.57	4.72	-0.15	-0.10	-0.10	0.00	2.1
48682	6057	6064	-6	4.27	4.33	-0.06	0.08	0.12	-0.04	4.3
4915	5620	5650	-29	4.38	4.57	-0.19	-0.19	-0.19	0.00	0.9
49674	5686	5662	24	4.48	4.56	-0.08	0.34	0.31	0.03	0.1
50499	5989	6070	-80	4.15	4.37	-0.22	0.30	0.34	-0.04	4.3
50554	6007	5929	78	4.34	4.29	0.05	-0.02	-0.07	0.05	2.7
50639	6062	6098	-35	4.25	4.29	-0.04	-0.03	-0.02	-0.01	4.2
50692	5819	5891	-71	4.30	4.36	-0.06	-0.21	-0.18	-0.03	0.1

Table 7.8 (cont'd): SpecMatch/ Valenti &amp; Fischer (2005) Comparison

Name	$T_{\text{eff}}$			$\log g$			[Fe/H]			$v \sin i$
	SM	VF05	$\Delta$	SM	VF05	$\Delta$	SM	VF05	$\Delta$	
5133	5019	4968	51	4.66	4.80	-0.14	-0.06	-0.04	-0.02	1.2
51419	5609	5637	-27	4.14	4.46	-0.32	-0.38	-0.40	0.02	0.1
52265	6058	6076	-17	4.18	4.26	-0.08	0.17	0.19	-0.02	4.2
52711	5890	5889	1	4.37	4.41	-0.04	-0.10	-0.10	0.00	1.9
53665	6278	6225	53	4.12	4.05	0.07	0.18	0.17	0.01	8.2
60491	5137	5091	46	4.70	4.63	0.07	-0.15	-0.17	0.02	3.3
61606	5023	4964	59	4.71	4.71	-0.00	0.06	0.07	-0.01	0.3
65277	4722	4741	-18	4.43	4.76	-0.33	-0.21	-0.16	-0.05	1.4
65430	5162	5183	-20	4.33	4.55	-0.22	-0.08	-0.12	0.04	0.9
6558	6075	6086	-10	4.13	4.26	-0.13	0.27	0.26	0.01	6.0
65583	5157	5279	-121	4.07	4.76	-0.69	-0.72	-0.69	-0.03	0.4
66428	5754	5752	2	4.34	4.49	-0.15	0.29	0.31	-0.02	0.7
6734	4942	5067	-124	3.12	3.81	-0.69	-0.43	-0.41	-0.02	1.6
67767	5289	5344	-54	3.62	3.88	-0.26	-0.01	0.06	-0.07	1.6
68017	5489	5552	-62	4.04	4.65	-0.61	-0.39	-0.44	0.05	0.0
68168	5735	5724	11	4.39	4.40	-0.01	0.12	0.12	-0.00	0.1
68988	5954	5960	-5	4.28	4.41	-0.13	0.34	0.32	0.02	2.4
691	5625	5633	-7	4.68	4.66	0.02	0.29	0.32	-0.03	5.0
6963	5566	5495	71	4.59	4.54	0.05	-0.10	-0.15	0.05	0.1
69809	5824	5817	7	4.20	4.30	-0.10	0.26	0.27	-0.01	1.2
69830	5416	5361	55	4.37	4.46	-0.09	0.01	-0.06	0.07	0.1
69897	6190	6294	-103	4.25	4.25	0.00	-0.30	-0.23	-0.07	4.4
70843	6269	6208	61	4.20	4.17	0.03	0.19	0.16	0.03	4.1
71881	5862	5822	40	4.28	4.29	-0.01	-0.03	-0.05	0.02	0.2
72659	5868	5920	-51	4.13	4.24	-0.11	-0.03	-0.00	-0.03	1.5
72673	5209	5243	-33	4.40	4.67	-0.27	-0.36	-0.37	0.01	0.2
73667	4875	4990	-114	4.19	4.65	-0.46	-0.58	-0.57	-0.01	0.4
74156	6002	6068	-65	4.15	4.26	-0.11	0.09	0.13	-0.04	3.9
75732	5352	5235	117	4.37	4.45	-0.08	0.41	0.31	0.10	0.1
76218	5442	5465	-22	4.65	4.72	-0.07	0.04	0.07	-0.03	3.1
78366	5990	6014	-23	4.50	4.54	-0.04	0.05	0.08	-0.03	2.3
7924	5180	5177	3	4.52	4.58	-0.06	-0.15	-0.15	0.00	0.1
80606	5622	5573	49	4.34	4.44	-0.10	0.38	0.34	0.04	0.1
82943	6002	5997	5	4.34	4.42	-0.08	0.27	0.27	0.00	0.9
83443	5523	5453	70	4.39	4.49	-0.10	0.41	0.36	0.05	0.0
84117	6136	6152	-15	4.25	4.31	-0.06	-0.08	-0.07	-0.01	5.4
84737	5902	5960	-57	4.09	4.24	-0.15	0.13	0.17	-0.04	1.4
85301	5723	5725	-1	4.68	4.62	0.06	0.17	0.19	-0.02	5.8
8574	6033	6050	-16	4.19	4.20	-0.01	-0.02	-0.01	-0.01	4.1
86728	5768	5700	68	4.29	4.29	0.00	0.21	0.20	0.01	2.1

Table 7.8 (cont'd): SpecMatch/ Valenti &amp; Fischer (2005) Comparison

Name	$T_{\text{eff}}$			$\log g$			[Fe/H]			$v \sin i$
	SM	VF05	$\Delta$	SM	VF05	$\Delta$	SM	VF05	$\Delta$	SM
87359	5663	5676	-12	4.38	4.49	-0.11	0.07	0.06	0.01	0.2
87424	5105	5069	36	4.68	4.64	0.04	-0.06	-0.07	0.01	2.9
8765	5666	5590	76	4.39	4.23	0.16	0.22	0.19	0.03	0.4
87836	5807	5774	33	4.24	4.31	-0.07	0.36	0.36	0.00	1.4
87883	5032	4958	74	4.59	4.56	0.03	0.11	0.07	0.04	0.0
88986	5776	5838	-61	4.11	4.23	-0.12	0.04	0.09	-0.05	2.1
8907	6248	6204	44	4.39	4.35	0.04	-0.03	-0.02	-0.01	13.3
89269	5607	5586	21	4.32	4.44	-0.12	-0.17	-0.20	0.03	0.1
89391	4884	4976	-91	3.08	3.59	-0.51	-0.14	-0.09	-0.05	2.2
90156	5528	5626	-97	4.26	4.63	-0.37	-0.26	-0.21	-0.05	0.2
90711	5475	5466	9	4.39	4.50	-0.11	0.31	0.30	0.01	1.4
90905	6114	6148	-33	4.53	4.57	-0.04	0.03	0.07	-0.04	9.0
92788	5798	5836	-37	4.39	4.66	-0.27	0.32	0.32	-0.00	1.1
92855	6068	6140	-71	4.50	4.58	-0.08	-0.04	-0.00	-0.04	11.2
92945	5236	5183	53	4.71	4.76	-0.05	0.09	0.13	-0.04	5.1
9407	5659	5657	2	4.29	4.48	-0.19	0.04	0.02	0.02	0.0
9472	5798	5867	-68	4.67	4.67	0.00	0.00	0.05	-0.05	0.7
95128	5866	5882	-15	4.27	4.38	-0.11	0.02	0.04	-0.02	1.8
95188	5462	5482	-19	4.61	4.65	-0.04	-0.03	-0.01	-0.02	4.2
9562	5879	5939	-59	4.01	4.13	-0.12	0.22	0.26	-0.04	4.2
96700	5743	5865	-121	4.27	4.41	-0.14	-0.23	-0.18	-0.05	0.1
97334	5977	5898	79	4.59	4.42	0.17	0.14	0.09	0.05	5.5
97343	5443	5399	44	4.37	4.56	-0.19	0.01	-0.04	0.05	0.0
97658	5171	5148	23	4.53	4.65	-0.12	-0.26	-0.26	-0.00	0.0
9826	6140	6213	-72	4.10	4.25	-0.15	0.11	0.15	-0.04	9.4
98281	5330	5419	-88	4.25	4.61	-0.36	-0.23	-0.20	-0.03	0.1
98553	5711	6009	-297	4.36	4.69	-0.33	-0.50	-0.34	-0.16	0.5
99109	5370	5272	98	4.40	4.44	-0.04	0.40	0.31	0.09	0.5
99491	5563	5502	61	4.51	4.58	-0.07	0.36	0.34	0.02	0.5
99492	4988	4955	33	4.54	4.77	-0.23	0.30	0.36	-0.06	0.1
9986	5823	5805	18	4.46	4.45	0.01	0.09	0.08	0.01	1.1

Note. —

Table 7.9: SpecMatch/ [Albrecht et al. \(2012\)](#) Comparison

Name	Decker	$\sigma_{IP}$	$v \sin i$	
			SM	A12
HAT-P-1	B5	1.69	3.8	3.2
HAT-P-11	B1	1.40	1.0	1.8
HAT-P-13	B1	1.40	1.7	3.4
HAT-P-14	B3	1.36	8.2	8.3
HAT-P-16	B5	1.87	3.9	3.0
HAT-P-2	B5	1.71	19.5	21.1
HAT-P-23	B5	1.67	7.8	8.3
HAT-P-24	C2	1.42	11.2	10.0
HAT-P-30	C2	1.62	3.1	3.7
HAT-P-32	B5	1.77	20.6	21.0
HAT-P-34	C2	1.62	24.3	25.0
HAT-P-4	B3	1.45	5.8	5.4
HAT-P-6	B5	1.55	7.8	8.0
HAT-P-7	B1	1.32	2.7	4.4
HAT-P-8	B5	1.45	14.5	11.5
HAT-P-9	C2	1.71	12.5	11.0
HD-149026	B1	1.25	7.7	6.2
HD-17156	B1	1.43	4.1	4.5
HD-189733	B1	1.49	3.1	3.0
HD-209458	B1	1.41	4.4	4.2
HD-80606	B1	1.35	1.7	0.0
KOI-13	B5	1.67	65.0	81.5
Kepler-8	B1	1.48	8.9	10.4
TrES-1	B1	1.54	1.1	0.0
TrES-2	B5	1.69	2.0	0.0
TrES-4	B3	1.35	8.5	8.9
WASP-1	B5	1.79	0.7	0.5
WASP-12	B3	1.38	1.6	2.2
WASP-14	B1	1.39	2.8	2.6
WASP-15	B3	1.45	4.3	5.1
WASP-16	B3	1.49	3.2	0.0
WASP-17	B3	1.50	9.9	10.0
WASP-18	B3	1.50	11.2	11.4
WASP-19	B3	1.54	4.4	4.3
WASP-22	B3	1.45	4.4	4.0
WASP-24	B1	1.56	7.0	6.0
WASP-3	B5	1.60	14.1	14.2
WASP-31	B3	1.39	6.8	7.6
WASP-33	B5	1.77	86.0	84.9
WASP-38	B1	1.48	8.6	8.1

Table 7.9 (cont'd): SpecMatch/ [Albrecht et al. \(2012\)](#) Comparison

Name	Decker	$\sigma_{IP}$	$v \sin i$	
			SM	A12
WASP-4	B3	1.47	2.1	0.0
WASP-7	B5	1.85	14.0	18.1
WASP-8	B3	1.42	2.0	0.0
XO-3	B5	1.81	17.0	19.1
XO-4	B3	1.45	8.8	8.2

Note. — For WASP-8,  $v \sin i$  was misprinted as  $20 \pm 0.6 \text{ km s}^{-1}$ , instead of  $2.0 \pm 0.6 \text{ km s}^{-1}$  in the original reference (Queloz 2010).

# Bibliography

- Adams, E. R., Seager, S., & Elkins-Tanton, L. 2008, *ApJ*, 673, 1160
- Akeson, R. L., Chen, X., Ciardi, D., et al. 2013, *PASP*, 125, 989
- Albrecht, S., Winn, J. N., Johnson, J. A., et al. 2012, *ApJ*, 757, 18
- Allende Prieto, C., Lambert, D. L., & Asplund, M. 2001, *ApJ*, 556, L63
- Alonso, R., Brown, T. M., Torres, G., et al. 2004, *ApJ*, 613, L153
- Anstee, S. D., & O'Mara, B. J. 1995, *MNRAS*, 276, 859
- Bakos, G. Á., Noyes, R. W., Kovács, G., et al. 2007, *ApJ*, 656, 552
- Barbuy, B., Perrin, M.-N., Katz, D., et al. 2003, *A&A*, 404, 661
- Barklem, P. S., & O'Mara, B. J. 1997, *MNRAS*, 290, 102
- Barklem, P. S., O'Mara, B. J., & Ross, J. E. 1998, *MNRAS*, 296, 1057
- Barklem, P. S., Piskunov, N., & O'Mara, B. J. 2000, *A&AS*, 142, 467
- Batalha, N. M., Borucki, W. J., Bryson, S. T., et al. 2011, *ApJ*, 729, 27
- Batalha, N. M., Rowe, J. F., Bryson, S. T., et al. 2012, *arXiv*, 1202, 5852
- Batalha, N. M., Rowe, J. F., Bryson, S. T., et al. 2013, *ApJS*, 204, 24
- Beugé, C., & Nesvorný, D. 2013, *ApJ*, 763, 12
- Bensby, T., Feltzing, S., & Lundström, I. 2003, *A&A*, 410, 527
- . 2004, *A&A*, 415, 155
- Bensby, T., Feltzing, S., Lundström, I., & Ilyin, I. 2005, *A&A*, 433, 185
- Billings, L. 2013, *Five Billion Years of Solitude: The Search for Life Among the Stars (Current)*
- Bond, J. C., Laretta, D. S., & O'Brien, D. P. 2010, in *IAU Symposium, Vol. 265, IAU Symposium*, ed. K. Cunha, M. Spite, & B. Barbuy, 399
- Bonfils, X., Delfosse, X., Udry, S., et al. 2013, *A&A*, 549, A109
- Borucki, W. J., & Summers, A. L. 1984, *Icarus*, 58, 121
- Borucki, W. J., Koch, D. G., Lissauer, J. J., et al. 2003, in *Society of Photo-Optical Instrumentation Engineers (SPIE) Conference Series, Vol. 4854, Future EUV/UV and Visible Space Astrophysics Missions and Instrumentation.*, ed. J. C. Blades & O. H. W. Siegmund, 129
- Borucki, W. J., Koch, D., Basri, G., et al. 2010, *Science*, 327, 977
- Borucki, W. J., Koch, D. G., Basri, G., et al. 2011, *ApJ*, 728, 117
- Borucki, W. J., Koch, D. G., Basri, G., et al. 2011, *ApJ*, 736, 19
- Boyajian, T. S., von Braun, K., van Belle, G., et al. 2012, *ApJ*, 757, 112

- . 2013, [ApJ](#), **771**, 40
- Brown, T. M., Charbonneau, D., Gilliland, R. L., Noyes, R. W., & Burrows, A. 2001, [ApJ](#), **552**, 699
- Brown, T. M., Latham, D. W., Everett, M. E., & Esquerdo, G. A. 2011, [AJ](#), **142**, 112
- Bryson, S. T., Jenkins, J. M., Gilliland, R. L., et al. 2013, [PASP](#), **125**, 889
- Buchhave, L. A., Latham, D. W., Johansen, A., et al. 2012, [Nature](#), **486**, 375
- Burke, C. J., Bryson, S. T., Mullally, F., et al. 2014, [ApJS](#), **210**, 19
- Butler, R. P., & Marcy, G. W. 1996, [ApJ](#), **464**, L153
- Caffau, E., Ludwig, H., Bonifacio, P., et al. 2010, [A&A](#), **514**, A92
- Campbell, B. 1983, [PASP](#), **95**, 577
- Campo, C. J., Harrington, J., Hardy, R. A., et al. 2011, [ApJ](#), **727**, 125
- Casagrande, L., Ramírez, I., Meléndez, J., Bessell, M., & Asplund, M. 2010, [A&A](#), **512**, A54
- Castelli, F., & Kurucz, R. L. 2003, in IAU Symposium, Vol. 210, Modelling of Stellar Atmospheres, ed. N. Piskunov, W. W. Weiss, & D. F. Gray, 20P
- Cayrel, R., Perrin, M.-N., Barbuy, B., & Buser, R. 1991, [A&A](#), **247**, 108
- Chaplin, W. J., Basu, S., Huber, D., et al. 2014, [ApJS](#), **210**, 1
- Charbonneau, D., Brown, T. M., Latham, D. W., & Mayor, M. 2000, [ApJ](#), **529**, L45
- Chiang, E., & Laughlin, G. 2012, ArXiv e-prints, [arXiv:1211.1673 \[astro-ph.EP\]](#)
- Christiansen, J., Science Office, K., & Science Operations Center, K. 2012, in AAS/Division for Planetary Sciences Meeting Abstracts, Vol. 44, AAS/Division for Planetary Sciences Meeting Abstracts, 113.01
- Christiansen, J. L., Van Cleve, J. E., Jenkins, J. M., et al. 2011, Kepler Data Characteristics Handbook (KSCI-19040-002)
- Coelho, P., Barbuy, B., Meléndez, J., Schiavon, R. P., & Castilho, B. V. 2005, [A&A](#), **443**, 735
- Collette, A. 2008, HDF5 for Python
- Croll, B., Lafreniere, D., Albert, L., et al. 2011, [AJ](#), **141**, 30
- Cumming, A., Butler, R. P., Marcy, G. W., et al. 2008, [PASP](#), **120**, 531
- Demarque, P., Woo, J.-H., Kim, Y.-C., & Yi, S. K. 2004, [ApJS](#), **155**, 667
- Dong, S., & Zhu, Z. 2012, ArXiv e-prints, [arXiv:1212.4853 \[astro-ph.EP\]](#)
- Dotter, A., Chaboyer, B., Jevremović, D., et al. 2008, [ApJS](#), **178**, 89
- Doyle, L. R., Carter, J. A., Fabrycky, D. C., et al. 2011, [Science](#), **333**, 1602
- Dressing, C. D., & Charbonneau, D. 2013, [ApJ](#), **767**, 95
- Edvardsson, B., Andersen, J., Gustafsson, B., et al. 1993, [A&A](#), **275**, 101
- ESA. 1997, VizieR Online Data Catalog, 1239, 0
- Fang, J., & Margot, J.-L. 2012, [ApJ](#), **761**, 92
- Fischer, D. A., & Valenti, J. 2005, [ApJ](#), **622**, 1102
- Fischer, D. A., Laughlin, G., Butler, P., et al. 2005, [ApJ](#), **620**, 481
- Fischer, D. A., Schwamb, M. E., Schawinski, K., et al. 2011, [Monthly Notices of the Royal Astronomical Society](#), **419**, 2900
- Fraquelli, D., & Thompson, S. E. 2012, Kepler Archive Manual (KDMC-10008-004)
- Fressin, F., Torres, G., Rowe, J. F., et al. 2012, [Nature](#), **482**, 195

- Fressin, F., Torres, G., Charbonneau, D., et al. 2013, [ApJ](#), 766, 81
- Gonzalez, G. 1997, *MNRAS*, 285, 403
- Gray, D. F. 1992, The observation and analysis of stellar photospheres.
- . 2005, The Observation and Analysis of Stellar Photospheres
- Grevesse, N., & Sauval, A. J. 1998, [Space Science Reviews](#), 85, 161
- Gustafsson, B., Karlsson, T., Olsson, E., Edvardsson, B., & Ryde, N. 1999, *A&A*, 342, 426
- Haisch, Jr., K. E., Lada, E. A., & Lada, C. J. 2001, [ApJ](#), 553, L153
- Han, E., Wang, S. X., Wright, J. T., et al. 2014, [PASP](#), 126, 827
- Hansen, B. M. S., & Murray, N. 2012, [ApJ](#), 751, 158
- Hebb, L., Collier-Cameron, A., Loeillet, B., et al. 2009, [ApJ](#), 693, 1920
- Henry, G. W., Marcy, G. W., Butler, R. P., & Vogt, S. S. 2000, [ApJ](#), 529, L41
- Hirano, T., Suto, Y., Winn, J. N., et al. 2011, [ApJ](#), 742, 69
- Howard, A. W., Marcy, G. W., Johnson, J. A., et al. 2010, *Science*, 330, 653
- Howard, A. W., Marcy, G. W., Bryson, S. T., et al. 2012, [ApJS](#), 201, 15
- Huang, X., Bakos, G. Á., & Hartman, J. D. 2012, [arXiv](#), astro-ph.EP
- Huber, D., Chaplin, W. J., Christensen-Dalsgaard, J., et al. 2013, [ApJ](#), 767, 127
- Hunter, J. D. 2007, *Computing In Science & Engineering*, 9, 90
- Ida, S., & Lin, D. N. C. 2008, [ApJ](#), 685, 584
- . 2010, [ApJ](#), 719, 810
- Ida, S., Lin, D. N. C., & Nagasawa, M. 2013, [ApJ](#), 775, 42
- Jenkins, J. M., Caldwell, D. A., Chandrasekaran, H., et al. 2010a, [ApJ](#), 713, L87
- Jenkins, J. M., Chandrasekaran, H., McCauliff, S. D., et al. 2010b, in *Society of Photo-Optical Instrumentation Engineers (SPIE) Conference Series*, Vol. 7740
- Johansson, S., Litzén, U., Lundberg, H., & Zhang, Z. 2003, [ApJ](#), 584, L107
- Jones, E., Oliphant, T., Peterson, P., et al. 2001–, SciPy: Open source scientific tools for Python
- Kasting, J. F., Whitmire, D. P., & Reynolds, R. T. 1993, *Icarus*, 101, 108
- Koch, D. G., Borucki, W. J., Basri, G., et al. 2010, [ApJ](#), 713, L79
- Kopparapu, R. K. 2013, [ApJ](#), 767, L8
- Kopparapu, R. K., Ramirez, R., Kasting, J. F., et al. 2013, [ApJ](#), 765, 131
- Kovács, G., Bakos, G., & Noyes, R. W. 2005, [Monthly Notices of the Royal Astronomical Society](#), 356, 557
- Kovács, G., Zucker, S., & Mazeh, T. 2002, *A&A*, 391, 369
- Kuchner, M. J., & Seager, S. 2005, ArXiv Astrophysics e-prints, [arXiv:astro-ph/0504214](#)
- Kurucz, R. L. 1992, in *IAU Symposium*, Vol. 149, The Stellar Populations of Galaxies, ed. B. Barbuy & A. Renzini, 225
- Kurucz, R. L., Furenlid, I., Brault, J., & Testerman, L. 1984, Solar flux atlas from 296 to 1300 nm, ed. Kurucz, R. L., Furenlid, I., Brault, J., & Testerman, L.
- Lambert, D. L. 1978, *MNRAS*, 182, 249
- Latham, D. W. 1985, in *Stellar Radial Velocities*, ed. A. G. D. Philip & D. W. Latham, 21
- Latham, D. W., Stefanik, R. P., Mazeh, T., Mayor, M., & Burki, G. 1989, *Nature*, 339, 38
- Levy, E. H., & Lunine, J. I., eds. 1993, *Growth of planets from planetesimals*, ed. E. H. Levy

- & J. I. Lunine, 1061
- Lintott, C., Schwamb, M. E., Sharzer, C., et al. 2012, [eprint arXiv:1202.6007](#)
- Lissauer, J. J., Fabrycky, D. C., Ford, E. B., et al. 2011, *Nature*, **469**, 53
- Lissauer, J. J., Ragozzine, D., Fabrycky, D. C., et al. 2011, *ApJS*, **197**, 8
- Lissauer, J. J., Marcy, G. W., Rowe, J. F., et al. 2012, *ApJ*, **750**, 112
- Luck, R. E., & Heiter, U. 2006, *AJ*, **131**, 3069
- Madhusudhan, N., Harrington, J., Stevenson, K. B., et al. 2011, *Nature*, **469**, 64
- Mandel, K., & Agol, E. 2002, *ApJ*, **580**, L171
- Mann, A. W., Gaidos, E., & Ansdell, M. 2013, *ApJ*, **779**, 188
- Marcy, G., Butler, R. P., Fischer, D., et al. 2005, *Progress of Theoretical Physics Supplement*, **158**, 24
- Marcy, G. W. 1983, in *Bulletin of the American Astronomical Society*, Vol. 15, *Bulletin of the American Astronomical Society*, 947
- Marcy, G. W., & Butler, R. P. 1992, *PASP*, **104**, 270
- . 1996, *ApJ*, **464**, L147
- Marcy, G. W., Butler, R. P., Vogt, S. S., et al. 2008, *Exoplanet properties from Lick, Keck and AAT*
- Mayor, M., & Maurice, E. 1985, in *Stellar Radial Velocities*, ed. A. G. D. Philip & D. W. Latham, 299
- Mayor, M., & Queloz, D. 1995, *Nature*, **378**, 355
- Mayor, M., Marmier, M., Lovis, C., et al. 2011, *ArXiv e-prints*, [arXiv:1109.2497 \[astro-ph.EP\]](#)
- McCullough, P. R., Stys, J. E., Valenti, J. A., et al. 2005, *PASP*, **117**, 783
- Meléndez, J., & Barbuy, B. 1999, *ApJS*, **124**, 527
- Mishenina, T. V., Soubiran, C., Kovtyukh, V. V., & Korotin, S. A. 2004, *A&A*, **418**, 551
- Mordasini, C., Alibert, Y., Georgy, C., et al. 2012, *A&A*, **547**, A112
- Morton, T. D. 2012, *ApJ*, **761**, 6
- Morton, T. D., & Johnson, J. A. 2011, *ApJ*, **738**, 170
- Muirhead, P. S., Johnson, J. A., Apps, K., et al. 2012, *ApJ*, **747**, 144
- Nidever, D. L., Marcy, G. W., Butler, R. P., Fischer, D. A., & Vogt, S. S. 2002, *ApJS*, **141**, 503
- Nordström, B., Mayor, M., Andersen, J., et al. 2004, *The Messenger*, **118**, 61
- Ofir, A., & Dreizler, S. 2012, [arXiv](#), *astro-ph.EP*
- Oliphant, T. E. 2007, *Computing in Science Engineering*, **9**, 10
- Peek, K. 2009, PhD thesis, University of California, Berkeley
- Pérez, F., & Granger, B. E. 2007, *Comput. Sci. Eng.*, **9**, 21
- Petigura, E. A., Howard, A. W., & Marcy, G. W. 2013a, *Proceedings of the National Academy of Science*, **110**, 19273
- Petigura, E. A., & Marcy, G. W. 2012, *PASP*, **124**, 1073
- Petigura, E. A., Marcy, G. W., & Howard, A. W. 2013b, *ApJ*, **770**, 69
- Pierrehumbert, R., & Gaidos, E. 2011, *ApJ*, **734**, L13
- Pinsonneault, M. H., An, D., Molenda-Żakowicz, J., et al. 2012, *ApJS*, **199**, 30
- Piskunov, N. E., Kupka, F., Ryabchikova, T. A., Weiss, W. W., & Jeffery, C. S. 1995, *A&AS*,

- 112, 525
- Pollacco, D. L., Skillen, I., Collier Cameron, A., et al. 2006, *PASP*, **118**, 1407
- Pollack, J. B., Hubickyj, O., Bodenheimer, P., et al. 1996, *Icarus*, **124**, 62
- Raghavan, D., McAlister, H. A., Henry, T. J., et al. 2010, *ApJS*, **190**, 1
- Ramírez, I., Allende Prieto, C., & Lambert, D. L. 2007, *A&A*, **465**, 271
- Rasmussen, C. E., & Williams, C. K. I. 2006, *Gaussian Processes for Machine Learning* (MIT Press)
- Reader, J., Wiese, W. L., Martin, W. C., Musgrove, A., & Fuhr, J. R. 2002, 80
- Reddy, B. E., Lambert, D. L., & Allende Prieto, C. 2006, *MNRAS*, **367**, 1329
- Santos, N. C., Israelian, G., & Mayor, M. 2004, *A&A*, **415**, 1153
- Scott, P., Asplund, M., Grevesse, N., & Sauval, A. J. 2009, *ApJ*, **691**, L119
- Seager, S. 2013, *Science*, **340**, 577
- Seager, S., & Lissauer, J. J. 2010, *Introduction to Exoplanets*, ed. S. Seager, 3
- Sliski, D. H., & Kipping, D. M. 2014, ArXiv e-prints, [arXiv:1401.1207 \[astro-ph.EP\]](https://arxiv.org/abs/1401.1207)
- Smith, J. C., Stumpe, M. C., Van Cleve, J. E., et al. 2012, *PASP*, **124**, 1000
- Snedden, C. A. 1973, PhD thesis, The University Of Texas At Austin
- Spite, M. 1967, *Annales d'Astrophysique*, **30**, 211
- Staelin, D. H. 1969, in *Proceedings of the IEEE*, National Radio Astronomy Observatory, Charlottesville, VA, USA, 724
- Struve, O. 1952, *The Observatory*, **72**, 199
- Stumpe, M. C., Smith, J. C., Van Cleve, J. E., et al. 2012, *PASP*, **124**, 985
- Tamuz, O., Mazeh, T., & Zucker, S. 2005, *Monthly Notices of the Royal Astronomical Society*, **356**, 1466
- Tenenbaum, P., Bryson, S. T., Chandrasekaran, H., et al. 2010, *Software and Cyberinfrastructure for Astronomy*. Edited by Radziwill, 7740, 16
- Torres, G., Fischer, D. A., Sozzetti, A., et al. 2012, *ApJ*, **757**, 161
- Torres, G., Fressin, F., Batalha, N. M., et al. 2011, *ApJ*, **727**, 24
- Traub, W. A. 2012, *ApJ*, **745**, 20
- Twicken, J. D., Chandrasekaran, H., Jenkins, J. M., et al. 2010, in *Society of Photo-Optical Instrumentation Engineers (SPIE) Conference Series*, Vol. 7740
- Udalski, A., Paczynski, B., Zebrun, K., et al. 2002, *Acta Astron.*, **52**, 1
- Valenti, J. A., & Fischer, D. A. 2005, *ApJS*, **159**, 141
- Valenti, J. A., & Piskunov, N. 1996, *A&AS*, **118**, 595
- Van Cleve, J. E., & Caldwell, D. A. 2009, *Kepler Instrument Handbook (KSCI-19033-001)*
- Vogt, S. S., Allen, S. L., Bigelow, B. C., et al. 1994, in *Society of Photo-Optical Instrumentation Engineers (SPIE) Conference Series*, Vol. 2198, *Instrumentation in Astronomy VIII*, ed. D. L. Crawford & E. R. Craine, 362
- von Braun, K., Boyajian, T. S., van Belle, G. T., et al. 2014, *MNRAS*, **438**, 2413
- Weiss, L. M., Marcy, G. W., Rowe, J. F., et al. 2013, *ApJ*, **768**, 14
- Winn, J. N. 2010, *Exoplanet Transits and Occultations*, ed. S. Seager, 55
- Wolszczan, A., & Frail, D. A. 1992, *Nature*, **355**, 145
- Yi, S., Demarque, P., Kim, Y.-C., et al. 2001, *ApJS*, **136**, 417

---

Youdin, A. N. 2011, [ApJ](#), 742, 38

Zsom, A., Seager, S., de Wit, J., & Stamenkovic, V. 2013, ArXiv e-prints, [arXiv:1304.3714](#)  
[\[astro-ph.EP\]](#)